

12

AD-A178 314

AFWAL-TR-84-3089
Volume II



**AEROSPACE STRUCTURES TECHNOLOGY
DAMPING DESIGN GUIDE
VOLUME II — DESIGN GUIDE**

J. SOOVEKE
LOCKHEED CALIFORNIA COMPANY
P.O. BOX 551
BURBANK, CALIFORNIA 91520

M.L. DRAKE
UNIVERSITY OF DAYTON RESEARCH INSTITUTE
300 COLLEGE PARK AVENUE
DAYTON, OHIO 45469

DECEMBER 1985

Final Report for Period September 1981 — July 1984

Approved for Public Release; Distribution is Unlimited

DTIC FILE COPY

DTIC
ELECTE
MAR 30 1987
S E D

FLIGHT DYNAMICS LABORATORY
AIR FORCE WRIGHT AERONAUTICAL LABORATORIES
AIR FORCE SYSTEMS COMMAND
WRIGHT-PATTERSON AIR FORCE BASE, OHIO 45433

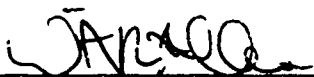
87

NOTICE

When Government drawings, specifications, or other data are used for any purpose other than in connection with a definitely related Government procurement operation, the United States Government thereby incurs no responsibility nor any obligation whatsoever; and the fact that the government may have formulated, furnished, or in any way supplied the said drawings, specifications, or other data, is not to be regarded by implication or otherwise as in any manner licensing the holder or any other person or corporation, or conveying any rights or permission to manufacture, use, or sell any patented invention that may in any way be related thereto.

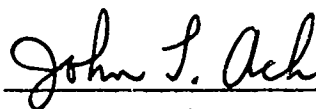
This report has been reviewed by the Office of Public Affairs (ASD/PA) and is releasable to the National Technical Information Service (NTIS). At NTIS, it will be available to the general public, including foreign nations.

This technical report has been reviewed and is approved for publication.



Vincent R. Miller
Project Engineer

FOR THE COMMANDER



John T. Ach, Actg Chief
Structural Vibrations Branch
Structures & Dynamics Division



ROBERT M. BADER
Acting Chief
Structures & Dynamics Division

"If your address has changed, if you wish to be removed from our mailing list, or if the addressee is no longer employed by your organization please notify AFWAL/FIBGD, W-PAFB, OH 45433 to help us maintain a current mailing list".

Copies of this report should not be returned unless return is required by security considerations, contractual obligations, or notice on a specific document.

REPORT DOCUMENTATION PAGE

1a. REPORT SECURITY CLASSIFICATION UNCLASSIFIED			1b. RESTRICTIVE MARKINGS				
2a. SECURITY CLASSIFICATION AUTHORITY			3. DISTRIBUTION/AVAILABILITY OF REPORT Approved for Public Release; Distribution is unlimited				
2b. DECLASSIFICATION/DOWNGRADING SCHEDULE							
4. PERFORMING ORGANIZATION REPORT NUMBER(S)			5. MONITORING ORGANIZATION REPORT NUMBER(S) AFWAL-TR-84-3089, Vol. II				
6a. NAME OF PERFORMING ORGANIZATION Lockhead-California Company		6b. OFFICE SYMBOL (If applicable)		7a. NAME OF MONITORING ORGANIZATION Air Force Wright Aeronautical Laboratories Flight Dynamics Laboratory (AFWAL/FIBGD)			
6c. ADDRESS (City, State and ZIP Code) P. O. Box 551 Burbank, California 91520			7b. ADDRESS (City, State and ZIP Code) Wright-Patterson AFB, Ohio 45433				
8a. NAME OF FUNDING/SPONSORING ORGANIZATION Flight Dynamics Laboratory		8b. OFFICE SYMBOL (If applicable) AFWAL/FIBGD		9. PROCUREMENT INSTRUMENT IDENTIFICATION NUMBER F33615-81-C-3213			
8c. ADDRESS (City, State and ZIP Code) Wright-Patterson AFB, Ohio 45433			10. SOURCE OF FUNDING NOS.				
11. TITLE (Include Security Classification) (see reverse)			PROGRAM ELEMENT NO. 62201F		PROJECT NO. 2401	TASK NO. 01	WORK UNIT NO. 50
12. PERSONAL AUTHOR(S) Soovere, J., Drake, M.L.							
13a. TYPE OF REPORT Final		13b. TIME COVERED FROM Sept. '81 TO Jul. '84		14. DATE OF REPORT (Yr., Mo., Day) December 1985		15. PAGE COUNT 520	
16. SUPPLEMENTARY NOTATION							
17. COSATI CODES			18. SUBJECT TERMS (Continue on reverse if necessary and identify by block number)				
FIELD	GROUP	SUB. GR.	Vibration problems, vibration environments, structural vibration response equations, (see reverse) →				
01	03						
22	02						
19. ABSTRACT (Continue on reverse if necessary and identify by block number)							
This volume represents the basic design guide for the application of viscoelastic damping to primarily aerospace structures. Simplified design equations for the vibration response of structures and for the free layer, constrained layer and tuned damper damping applications are presented. These equations are to be used with the damping material data in Volume III to develop the required design. For more complex structures, the above analysis should be supplemented by finite element analysis also discussed in this volume. The other topics included in this volume are the factors contributing to vibration problems in aerospace type structures including a summary of the vibration environments; a discussion of the design approach including when each of the three damping treatments should be used; examples on the use of the design equations, design examples and case histories of successful applications viscoelastic damping, and a discussion of other practical design considerations; a summary of the damping in aerospace materials and structures; and finally, a summary of material properties for typical aerospace metals and composite materials. <i>Keywords:</i>							
20. DISTRIBUTION/AVAILABILITY OF ABSTRACT UNCLASSIFIED/UNLIMITED <input checked="" type="checkbox"/> SAME AS RPT <input type="checkbox"/> DTIC USERS <input type="checkbox"/>				21. ABSTRACT SECURITY CLASSIFICATION UNCLASSIFIED			
22a. NAME OF RESPONSIBLE INDIVIDUAL Vince Miller			22b. TELEPHONE NUMBER (Include Area Code) 513-255-5066		22c. OFFICE SYMBOL AFWAL/FIBGD		

UNCLASSIFIED

SECURITY CLASSIFICATION OF THIS PAGE (When Data Entered)

Block 11: Title:

Aerospace Structures Technology Damping Design Guide Volume II - Design Guide

Block 18: Subject Terms:

viscoelastic damping design approach, viscoelastic damping design equations, example problems, viscoelastic damping design applications, case histories, other design considerations, damping in composites, damping in metals, damping in aerospace structures, metal material properties, ~~composite material properties~~, conversion tables.



UNCLASSIFIED

SECURITY CLASSIFICATION OF THIS PAGE (When Data Entered)

FOREWORD

This report was prepared jointly by the Lockheed-California Company, Burbank, California and the University of Dayton Research Institute, Dayton, Ohio for the Structural Integrity Branch, Flight Dynamics Laboratory, Air Force Wright Aeronautical Laboratory, Wright-Patterson Air Force Base, Ohio under contract F33615-81-C-3213, "Aerospace Structures Technology Damping Design Guide." Mr. V. R. Miller of the Structural Integrity Branch was the Project Engineer. Dr. J. Soovere of the Lockheed-California Company was the overall Program Manager and Mr. M. L. Drake was the Program Manager for the University of Dayton. The authors wish to acknowledge the contribution to this report provided by Mr. M. Bouchard, Dr. M. Soni, Mr. M. F. Kluesener, Mr. R. Nash, Mr. R. Dominic, Mr. P. Graf, and Mr. D. M. Hopkins from the University of Dayton, and by Mr. M. A. Gamon from Lockheed-California Company.

This report consists of three volumes. Volume I provides a summary of the current technology in the application of viscoelastic damping, Volume II is the design guide for viscoelastic damping applications, and Volume III contains the damping material data for use with Volume II.

The damping material data in Volume III are presented in a simplified format, suitable for use by designers. All of the damping material data are believed to be accurate, but no guarantee of accuracy or completeness is made. No responsibility is assumed for changes in these data due to batch-to-batch variation in the commercially manufactured damping materials. The damping material data should be verified independently under the proposed operating conditions, for each damping material, prior to its use.

Accession For	
NTIS GRA&I	<input checked="" type="checkbox"/>
DTIC TAB	<input checked="" type="checkbox"/>
Unannounced	<input type="checkbox"/>
Justification	
By _____	
Distribution/ _____	
Availability Codes	
Dist	Avail and/or Special
A-1	6



TABLE OF CONTENTS

<u>Section</u>		<u>Page</u>
	FOREWORD	iii
	LIST OF FIGURES	xi
	LIST OF TABLES	xxiv
1	INTRODUCTION	1-1
2	VIBRATION PROBLEMS AND ENVIRONMENTS	2-1
2.1	INTRODUCTION	2-1
2.2	GENERAL DISCUSSION OF FACTORS CONTRIBUTING TO VIBRATION PROBLEMS	2-1
2.3	VIBRATION ENVIRONMENTS	2-6
2.3.1	Jet and Rocket Noise	2-6
2.3.2	Structural Vibration in Aircraft and Rockets	2-16
2.3.3	Aerodynamic Fluctuating Pressure Environments	2-23
2.3.4	Flow Induced Cavity Oscillations	2-29
2.3.5	Flow Impingement	2-31
2.3.6	Fan Noise in Engine Inlet Ducts	2-34
2.3.7	Propeller Noise	2-36
2.3.8	Overpressure from Gunfire	2-38
2.4	SOUND PRESSURE LEVEL CONVERSIONS	2-38
	REFERENCES	2-47
3	STRUCTURAL VIBRATION RESPONSE EQUATIONS	3-1
3.1	INTRODUCTION	3-1
3.2	SPRING-MASS-DAMPER SYSTEM	3-2
3.2.1	Single Spring-Mass-Damper System	3-2
3.3	BEAMS	3-17
3.3.1	Natural Frequencies and Mode Shapes	3-17
3.3.2	Response to Harmonic Excitation	3-21
3.3.3	Response to Random Excitation	3-25
3.4	FLAT PLATES	3-27
3.4.1	Natural Frequencies and Mode Shapes	3-27

TABLE OF CONTENTS (Continued)

<u>Section</u>		<u>Page</u>
3.4.2	Response to Harmonic Excitation	3-39
3.4.3	Response to Random Excitation	3-40
3.5	CURVED PLATES	3-43
3.5.1	Natural Frequencies	3-45
3.5.2	Response to Harmonic Excitation	3-46
3.5.3	Response to Random Excitation	3-46
3.6	HONEYCOMB PLATES	3-48
3.6.1	Natural Frequencies	3-48
3.6.2	Response to Harmonic Excitation	3-52
3.6.3	Response to Random Excitation	3-52
3.7	CYLINDRICAL SHELLS	3-55
3.8	NON-CYLINDRICAL SHELLS	3-68
	REFERENCES	3-70
4	DAMPING DESIGNS AND DESIGN APPROACH	4-1
4.1	SELECTION OF DAMPING CONCEPT	4-1
4.1.1	Free-Layer Damping	4-1
4.1.2	Constrained Layer Damping	4-2
4.2	TUNED DAMPERS	4-7
4.3	GENERAL APPROACH TO DAMPING DESIGN	4-13
4.3.1	Dynamic Problem Identification	4-13
4.3.2	Dynamic Characteristics of Structure	4-14
4.3.3	Environmental Definition	4-15
4.3.4	Required Damping Increase	4-17
4.3.5	Damping Materials and Application Design	4-18
4.4	SUMMARY	4-20
	REFERENCES	4-23
5.	DESIGN METHODS	5-1
5.1	SIMPLIFIED DESIGN EQUATIONS	5-1
5.1.1	Cantilever Beam with Free-Layer Damping on One Side	5-2

TABLE OF CONTENTS (Continued)

<u>Section</u>		<u>Page</u>
5.1.2	Simply Supported Beam with Free-Layer Damping on One Side	5-9
5.1.3	Clamped Beam with Free-Layer Damping on One Side	5-11
5.1.4	Free Beam with Free-Layer Damping on One Side	5-12
5.1.5	Clamped-Pinned Beam with Free-Layer Damping on One Side	5-13
5.1.6	Cantilever Beam with Free-Layer Damping on Both Sides	5-13
5.1.7	Simply Supported Beam with Free-Layer Damping on Both Sides	5-17
5.1.8	Clamped Beam with Free-Layer Damping on Both Sides	5-22
5.1.9	Free Beam with Free-Layer Damping on Both Sides	5-23
5.1.10	Clamped-Pinned Beam with Free-Layer Damping on Both Sides	5-23
5.1.11	Cantilever Beam with a Single Constrained Layer Damping System	5-24
5.1.12	Simply Supported Beam with a Single Constrained Layer Damping System Applied	5-28
5.1.13	Clamped Beam with a Single Constrained Layer Damping System Applied	5-36
5.1.14	Free Beam with a Single Constrained Damping System Applied	5-37
5.1.15	Clamped-Pinned Beam with a Single Constrained Layer Damping System Applied	5-37
5.1.16	Simply Supported Plate with a Single Constrained Layer Damping System Applied	5-38
5.2	FINITE ELEMENT DESIGN EQUATIONS	5-48
5.2.1	Integration of Finite Element Modeling into the Design Process	5-48
5.2.2	A Note on Finite Element Discretization of Layered Damping Designs	5-59
	REFERENCES	5-77
6	EXAMPLE PROBLEM, DESIGN EXAMPLES, AND CASE HISTORIES	6-1
6.1	EXAMPLE PROBLEM	6-1

TABLE OF CONTENTS (Continued)

<u>Section</u>		<u>Page</u>
6.1.1	A Solution to a Noise and Vibration Problem	6-1
6.2	DESIGN EXAMPLES	6-18
6.2.1	A Damped Cantilever Beam	6-18
6.2.2	Turbine Ground Power Component Design Example	6-24
6.2.3	F-15 Wedder Fairing Damper	6-29
6.2.4	TF-47 Engine Inlet Extension Damper	6-35
6.2.5	GSTA-1 Shield Damper	6-41
6.2.6	RF-33-P3 Turbojet Engine Component Design Example	6-44
6.2.7	Radar Antenna Tuned Damper Design Example	6-49
6.2.8	Laser Component (King Mirror) Design Example	6-58
6.2.9	Aerolastic Flutter Design Example	6-68
6.3	CASE HISTORIES	6-75
6.3.1	B-52 DPU 82/A Pitot-Static Tube Damper	6-75
6.3.2	A-10 Craft Fuselage Damper	6-77
6.3.3	B-747 Upper Deck Noise Suppression Damper	7-79
6.3.4	Distribution Manifold Damper	6-88
6.3.5	Engine Mount Ring Tuned Dampers	6-90
6.3.6	Design of a Damped Acoustic Enclosure	6-94
6.3.7	Printed Wiring Board Damper No. 1	6-98
6.3.8	Printed Wiring Board Damper No. 2	6-99
6.3.9	Vibration Damping Compound as a Means to Reduce Steel Noise Barrier Cost	6-102
6.3.10	Damping to Eliminate Rocket "Pogo" Problem	6-105
6.3.11	Damping for Rapid Transit Structures	6-106
6.3.12	Damping for a Diesel Engine Oil Pan	6-110
6.3.13	Jet Engine Inlet Vane Damper	6-119
6.3.14	Skin Stringer Structure Dampers	6-124
6.3.15	Mirror Mount Dampers	6-126
6.3.16	Composite Beam Damper	6-130

TABLE OF CONTENTS (Continued)

<u>Section</u>		<u>Page</u>
6.3.17	Floor Damping	6-130
6.3.18	Turbine Engine Exhaust Stack Damper	6-138
6.3.19	High Temperature Damper for an Afterburner Liner	6-141
6.3.20	Noise Damper for the HH-53C Helicopter	6-146
6.3.21	Turbine Blade High Cycle Fatigue Control Methods	6-153
6.3.22	Exducer-Turbine Assembly Damper	6-158
6.3.23	Shear Damper for Micro-Inch Deflections	6-167
	REFERENCES	6-170
7	OTHER DESIGN CONSIDERATIONS	7-1
7.1	INTRODUCTION	7-1
7.2	NATURE OF DAMPING MATERIALS	7-1
7.3	ENVIRONMENTAL CONSIDERATIONS	7-3
7.4	STRUCTURAL ASPECTS	7-4
	REFERENCES	7-9
8	SUMMARY OF DAMPING IN AEROSPACE MATERIALS AND STRUCTURES	8-1
8.1	MATERIAL DAMPING IN AEROSPACE METALS AND COMPOSITES	8-2
8.1.1	Material Damping in Metals	8-2
8.1.2	Material Damping in Composites with Epoxy or Polyester Matrix	8-2
8.1.3	Metal Matrix Composites	8-3
8.2	DAMPING IN STIFFENED HONEYCOMB AND STIFFENED MULTI-BAY COMPOSITE AND METAL PANELS	8-12
8.2.1	Nature of Damping	8-12
8.2.2	Damping Levels	8-17
8.2.3	Method for Predicting the Damping of Skin-Stringer Type Panels	8-17
8.2.4	Effect of Axial and Shear In-Plane Loads on Stiffened Panels Damping	8-23
8.2.5	Effect of Fluid Loading on Stiffened Panels Damping	8-23
8.3	DAMPING IN STIFFENED SHELLS	8-23
8.4	DAMPING IN SPACECRAFT AND ROCKETS	8-23

TABLE OF CONTENTS (Continued)

<u>Section</u>		<u>Page</u>
8.5	DAMPING IN JET ENGINE COMPONENTS	8-30
8.6	DAMPING IN PRINTED CIRCUIT BOARDS	8-30
	REFERENCES	8-34
9	MATERIAL DATA FOR COMPOSITES AND METALS, U.S./METRIC CONVERSION TABLES	9-1
	REFERENCES	9-7

LIST OF FIGURES

<u>Figure</u>		<u>Page</u>
2.1	Vibratory stress reduction obtained with additive damping on existing hardware.	2-7
2.2	Total acoustic power for jet flows compared to revised Lighthill parameter L_a .	2-8
2.3	Correction factor to overall sound pressure level due to exhaust temperature.	2-10
2.4	Typical spectrum shape for rocket and turbojet noise.	2-11
2.5	Typical contours of equal overall sound pressure level in dB for a turbojet and rocket.	2-12
2.6	Typical rise in jet engine noise on aircraft structure over the past two decades.	2-14
2.7	Comparison of model and full scale noise contours on B-52 wing depicting noise reduction in dB achieved with a noise suppressor.	2-15
2.8	Comparison of noise levels measured, with a scale model and during liftoff, at the cargo bay door center aft location on the space shuttle.	2-15
2.9	Sound-pressure-level contours for the B-58 in the 300 to 600 Hz octave band.	2-17
2.10	Acceleration levels on B-58 airplane plotted against pressure levels in 300 to 600 Hz octave band.	2-17
2.11	Comparison of predicted and measured acceleration power spectral density on rear fuselage of a large military transport aircraft.	2-19
2.12	Accelerations on structure adjacent to rocket engines during liftoff.	2-20
2.13	Accelerations on upper half of the rocket structure during liftoff.	2-21
2.14	Accelerations on upper half of the rocket structure near maximum dynamic pressure.	2-22
2.15	Typical narrowband acceleration power spectral density measured on a Titan I missile.	2-23
2.16	Typical overall fluctuating pressure levels on various locations on a rocket.	2-24
2.17	Efficiency of boundary layer pressure fluctuations relative to rocket noise in exciting structural vibration.	2-26

LIST OF FIGURES (Continued)

<u>Figure</u>		<u>Page</u>
2.18	Comparison of model and flight data, in third-octave levels, produced by pressure fluctuations at the cargo bay door center aft location on the space shuttle.	2-28
2.19	Comparison of model and flight power spectral density data for pressure fluctuation on C-141 faring aft of perforated spoilers.	2-28
2.20	Typical measured sound pressure level in an unsuppressed cavity due to high speed flow over aperture obtained by model tests in wind tunnel.	2-30
2.21	Overall fluctuating pressure levels measured on the surface of an externally blown triple flap model.	2-32
2.22	Typical p_{rms}/q ratios measured on externally blown double flap model.	2-33
2.23	Third-octave normalized spectra for externally blown double flap model.	2-33
2.24	Root-mean-square acceleration level on outer flap as a function of jet mach number.	2-34
2.25	Typical narrowband spectra of intake duct fanblade noise at both subsonic and supersonic blade tip speeds.	2-36
2.26	Typical sound pressure levels measured in engine inlet ducts.	2-37
2.27	Reference sound pressure level produced by a four bladed propeller as function of shaft horse power.	2-39
2.28	Conversion of sound pressure level in dB to sound pressure in psi rms or N/m^2 .	2-41
2.29	Number of decibels to be subtracted from sound pressure level reading to convert octave, 1/3 octave and narrow band (7%) to spectrum level in decibels.	2-44
2.30	Free stream dynamic pressure, standard atmosphere.	2-46
3.1	Single spring-mass-damper system.	3-2
3.2	Symmetric mode shapes for fully clamped square plate.	3-29
3.3	Nomograph for calculating fundamental mode natural frequency of rectangular panels.	3-30
3.4	A periodic skin stringer structure.	3-33

LIST OF FIGURES (Continued)

<u>Figure</u>		<u>Page</u>
3.5	Finite skin-stringer structure with different boundary conditions.	3-33
3.6	$a/b = 1.5$, $m=1$, Group 1.	3-35
3.7	$a/b = 1.5$, $m=2$, Group 1.	3-35
3.8	$a/b = 2.0$, $m=1$, Group 1.	3-36
3.9	$a/b = 2.0$, $m=2$, Group 1.	3-36
3.10	$a/b = 2.5$, $m=1$, Group 1.	3-37
3.11	$a/b = 2.5$, $m=2$, Group 2.	3-37
3.12	Open circular cylinder geometry.	3-44
3.13	Nomograph for calculating frequency ratio for shallow open circular cylindrical shells.	3-47
3.14	Typical honeycomb panel construction and geometry.	3-49
3.15	Nomograph for fundamental mode response frequency of a flat rectangular honeycomb sandwich panel.	3-50
3.16	Comparison of predicted and measured fundamental mode natural frequency of stiffened aluminum honeycomb panels.	3-53
3.17	Plot of $\alpha_1, \gamma_1, \delta_1, \eta_1$, and θ_1 for moderately deep open circular cylindrical shells.	3-56
3.18	Closed circular cylindrical shell geometry.	3-59
3.19	Radial vibration frequencies $R/h = 20$. No external pressure ($q_1 = 0$).	3-61
3.20	Radial vibration frequencies $R/h = 50$. No external pressure ($q_1 = 0$).	3-62
3.21	Radial vibration frequencies $R/h = 100$. No external pressure ($q_1 = 0$).	6-63
3.22	Radial vibration frequencies $R/h = 500$. No external pressure ($q_1 = 0$).	3-64
3.23	Radial vibration frequencies $R/h = 1000$. No external pressure ($q_1 = 0$).	3-65
3.24	Radial vibration frequencies $R/h = 2000$. No external pressure ($q_1 = 0$).	3-66
3.25	Radial vibration frequencies $R/h = 5000$. No external pressure ($q_1 = 0$).	3-67
3.26	Axisymmetric frequency parameters of clamped-free conical shells for various s_1/s_2 ratios.	3-69

LIST OF FIGURES (Continued)

<u>Figure</u>		<u>Page</u>
4.1	Typical free-layer damping treatment.	4-3
4.2	Optimum temperature range for free-layer treatment.	4-3
4.3	Multiple free-layer broadening effect.	4-4
4.4	Constrained layer damping treatment.	4-4
4.5	Optimum temperature range for constrained layer treatment.	4-6
4.6	Multiple constrained layer broadening effect.	4-6
4.7	Response of a single degree-of-freedom system with a dynamic absorber.	4-8
4.8	Idealized tuned damper.	4-9
4.9	Effect of tuned damper.	4-10
4.10	Effects of a tuned damper on different types of structures.	4-11
4.11	E and η versus temperature for typical elastomer.	4-12
4.12	Statistical temperature data.	4-16
4.13	Basic flow chart.	4-21
4.14	Reduced temperature nomogram.	4-22
5.1	Finite element analysis in damping design procedure.	5-49
5.2	Engine exhaust duct.	5-52
5.3	Finite element model.	5-53
5.4	Mode shapes of engine exhaust duct (perspective view).	5-55
5.5	Mode shapes of engine exhaust duct (end-on view).	5-56
5.6	Engine exhaust duct: effect of damping treatment on the amplitude-frequency response of the Second Mode of Forced Vibrations.	5-57
5.7	Detailed model with damping layer and constraining layer.	5-58
5.8	Finite element model of a cantilever plate.	5-60
5.9	Cross section of plate 1 damping system.	5-61
5.10	Analytical and experimental results for plate 1, 2nd bending mode.	5-63
5.11	Cross section of plate 2 damping system.	5-64
5.12	Experimental and analytical results for plate 2, 2nd bending mode.	5-65

LIST OF FIGURES (Continued)

<u>Figure</u>		<u>Page</u>
5.13	Experimental and analytical results for plate 2, 1st torsional mode.	5-66
5.14	Plate 1 modeling scheme using membrane elements.	5-69
5.15	FEA results comparing all solid model to membrane model.	5-70
5.16	Equivalent solid beam test specimen.	5-72
5.17	Plate 2 modeling scheme using the equivalent solid element approach.	5-73
5.18	Analytical results comparing the all solid model to the equivalent solid model for the second bending mode.	5-74
5.19	Analytical results comparing the all solid model to the equivalent solid model for plate 2 first torsion mode.	5-75
6.1.1	Motor and mounting bracket.	6-4
6.1.2	Computer representation of impact test geometry.	6-7
6.1.3	Typical impact response of motor.	6-7
6.1.4	Mode shape at 1150 Hz of motor housing (top view).	6-8
6.1.5	Mode shape at 1150 Hz of mounting bracket.	6-8
6.1.6	Loss factor versus temperature for 4th order analysis and finite element analysis.	6-10
6.1.7	Damped system response.	6-12
6.1.8	Carpet plot from which damping was chosen.	6-13
6.1.9	Impact locations for damping wrap evaluation (Note: point B is on the lip of the motor housing bracket).	6-14
6.1.10	Point 29 frequency response; damped and undamped.	6-15
6.1.11	Point 29 frequency response; undamped 10 mil, 20 mil, and 30 mil stainless steel constraining layers.	6-16
6.2.1.1	Illustration of damped system.	6-19
6.2.1.2	Loss factor versus temperature for ISD 112, ISD 113, MN, and M damping materials.	6-20
6.2.1.3	Predicted damped system response for both the ISD 113 and MN damping materials.	6-23
6.2.1.4	Comparison of predicted and measured beam composite loss factor.	6-23

LIST OF FIGURES (Continued)

<u>Figure</u>	<u>Page</u>
6.2.2.1 Damped system response data.	6-27
6.2.2.2 Final damper design.	6-28
6.2.3.1 Rudder and fairing.	6-30
6.2.3.2 Undamped fairing response.	6-30
6.2.3.3 Fairing mode shape at 213 Hz.	6-31
6.2.3.4 Fairing mode shape at 509 Hz.	6-31
6.2.3.5 Final damping configuration.	6-32
6.2.3.6 Damped system response.	6-33
6.2.3.7 Comparison of damped and undamped response.	6-34
6.2.4.1 TF-41 inlet extension.	6-35
6.2.4.2 Typical measured undamped frequency response of the inlet extension.	6-37
6.2.4.3 Damping design.	6-37
6.2.4.4 Predicted damped system response.	6-38
6.2.4.5 Measured inlet extension loss factor.	6-39
6.2.4.6 Fiber glass wrapped response.	6-39
6.2.4.6 Response of damped extension.	6-40
6.2.5.1 OSTA-1 shelf.	6-42
6.2.5.2 Typical carpet plot.	6-42
6.2.5.3 Loss factor versus temperature for shelf with 0.08 inch thick ISD 110 and 0.12 inch graphite constraining layer.	6-43
6.2.6.1 TF-33-P3 IGV case damping wrap configuration.	6-46
6.2.6.2 TF-33-P3 IGV vane loss factor for the range 1 - 5 kHz versus case temperature.	6-48
6.2.6.3 TF-33-P3 IGV outer shroud loss factor for the range 1 - 5 kHz versus case temperature.	6-48
6.2.7.1 Radar antenna.	6-50
6.2.7.2 Relative locations of cannon, pickups, and antenna.	6-51
6.2.7.3 Typical response spectra for undamped antenna.	6-51
6.2.7.4 Damping properties of panacril-BJ with 25 PHR carbon.	6-54
6.2.7.5 Final geometry of prototype.	6-55
6.2.7.6 Graphs of amplification factor against temperature for antenna with prototype 8 attached.	6-56

LIST OF FIGURES (Continued)

<u>Figure</u>	<u>Page</u>
6.2.8.1 Annular reference mirror on the bench.	6-59
6.2.8.2 Top and side view of flute element model of the ring mirror.	6-61
6.2.8.3 Modal deformation plot of ring mirror at 135 Hz.	6-61
6.2.8.4 Schematic drawing of the damped strap.	6-62
6.2.8.5 Modal deformation plot of ring mirror with damped strap at 172.6 Hz.	6-63
6.2.8.6 Material properties for 3M, type 112 viscoelastic.	6-65
6.2.8.7 Schematic of measured mode shapes of ring mirror.	6-66
6.2.8.8 Schematic drawing of the damped strap.	6-66
6.2.9.1 Plan and cross-sectional views of intermodule plate in holding fixture for experimental modal testing (not to scale).	6-69
6.2.9.2 First out-of-phase mode at 2140 Hz.	6-69
6.2.9.3 Plan and cross-sectional views of intermodule plate with O-ring in holding fixture for experimental modal analysis (not to scale).	6-71
6.2.9.4 NASTRAN model of undamped plate.	6-71
6.2.9.5 NASTRAN model of plate with O-ring damper.	6-72
6.2.9.6 Damping properties of O-ring (Dow Corning LS-63) material.	6-72
6.2.9.7 Properties of the intermodule plate with single O-ring damper.	6-74
6.3.1.1 Instrumented pitot-static tube mounted to aircraft.	6-76
6.3.1.2 View of pitot-static tube mount inside aircraft.	6-76
6.3.1.3 Typical response plot obtained from flight test data.	6-78
6.3.1.4 Exploded view of damping fix assembly to control fatigue failures of the B-52H AIMS TRU pitot tube.	6-78
6.3.2.1 Internal view of test specimen.	6-80
6.3.2.2 Undamped transfer function.	6-80
6.3.2.3 Structure mode shapes.	6-81
6.3.2.4 Configuration of damping treatments applied.	6-82
6.3.2.5 Placement of tuned dampers.	6-82
6.3.3.1 Fuselage skin panel structure.	6-85

LIST OF FIGURES (Continued)

<u>Figure</u>	<u>Page</u>
6.3.3.2 Comparison of skin panel response and cabin sound pressure.	6-85
6.3.3.3 Skin panel mode shapes.	6-86
6.3.3.4 Damping treatment configuration.	6-86
6.3.3.5 Thickness deformation in stiff constrained layer dampers.	6-87
6.3.3.6 Effect of beam damping system on structure frequency response.	6-87
6.3.3.7 Effect of beam damping system on cabin noise levels.	6-88
6.3.4.1 Section of distribution manifold.	6-89
6.3.5.1 Mount ring.	6-92
6.3.5.2 Engine illustration.	6-92
6.3.5.3 Typical undamped acceleration response of mount ring to 0.5 g's input.	6-93
6.3.5.4 Sketch of mount ring illustrating how and where the tuned viscoelastic damper units are attached.	6-95
6.3.5.5 Typical damped acceleration response of mount ring to 0.5 g's input.	6-96
6.3.6.1 Acoustic cover, measured noise reduction comparison to predicted values, with acoustic liner (OA external SPL = 150 dB).	6-98
6.3.7.1 Worst PWB response to Y-sweep.	6-100
6.3.8.1 Effect of edge strip on sine vibration response.	6-101
6.3.9.1 Profile of the panel tested (WRT-168, ARMC0, Canada).	6-103
6.3.9.2 Reduction of highway noise transmitted through a barrier with and without damping compound (Aquaplas).	6-104
6.3.10.1 Radial distortion of tank with and without added damping.	6-107
6.3.10.2 Comparison of dynamic pressure in liquid with and without added damping.	6-107
6.3.11.1 Impact sound octave band level as a function of prestress.	6-109
6.3.11.2 Model composite concrete-steel bridge girder.	6-109
6.3.11.3 Full scale composite concrete-steel bridge girder.	6-110
6.3.12.1 Variation of the noise and vibration of the oil pan with frequency for a typical operating condition.	6-112
6.3.12.2 Driving point frequency response on the left side of the undamped oil pan.	6-113

LIST OF FIGURES (Continued)

<u>Figure</u>	<u>Page</u>
6.3.12.3 Mode shape of vibration of the oil pan at 467 Hz.	6-113
6.3.12.4 Variation of the damping properties of a high temperature damping material.	6-114
6.3.12.5 Predicted values for damped oil pan.	6-115
6.3.12.6 Comparison of the damped and undamped oil pan response at 210°F.	6-116
6.3.12.7 Effects of damping on reducing the oil pan noise for a typical operating condition.	6-117
6.3.12.8 Effects of damping and reducing the oil pan vibration for a typical operating condition.	6-118
6.3.13.1 Frequency and rpm of peak stresses.	6-120
6.3.13.2 TF-30 IGV damper wrap.	6-122
6.3.13.3 Loss factor and percentage of time at temperature for the damped and undamped TF-30 IGV case vane.	6-123
6.3.14.1 Skin-stringer panel.	6-125
6.3.14.2 Typical skin-stringer structural response.	6-125
6.3.14.3 Close-up of dampers used for tests.	6-127
6.3.14.4 Joint designs of sonic fatigue test specimens with polyurethane cone.	6-127
6.3.14.5 Typical response of control panel, sinusoidal sweep test.	6-128
6.3.14.6 Typical response of viscoelastic panel, sinusoidal sweep test.	6-128
6.3.15.1 Torsionally compliant main mount.	6-129
6.3.15.2 Comparison of measured and predicted loss factor and frequency.	6-129
6.3.16.1 Graphite/epoxy test beams.	6-131
6.3.16.2 Variation of loss factor with temperature of graphite/epoxy beam.	6-131
6.3.17.1 Schematic of floor test specimens.	6-133
6.3.17.2 Additive damping configurations for flexible steel specimen.	6-133
6.3.17.3 Relatively stiff steel floor additive damping configurations.	6-135
6.3.17.4 Comparison of low bending stiffness specimen transfer function magnitudes undamped to free-layer damped at cabinet base near input.	6-135

LIST OF FIGURES (Continued)

<u>Figure</u>	<u>Page</u>
6.3.17.5 Comparison of low bending stiffness specimen transfer function magnitude free-layer damped to combined free-layer and constrained layer damped at cabinet base near input.	6-136
6.3.17.6 Comparison of low bending stiffness specimen transfer function magnitude undamped to constrained layer damped at cabinet base near input.	6-136
6.3.17.7 Comparison of high bending stiffness specimen transfer function magnitude undamped to constrained layer damped at cabinet base furthest from input.	6-137
6.3.17.8 Comparison of high bending stiffness specimen transfer function magnitude undamped to spaced constrained layer damped at cabinet base furthest from input.	6-137
6.3.18.1 Driving point 1 frequency response of undamped exhaust extension.	6-139
6.3.18.2 Driving point 2 frequency response of undamped exhaust extension.	6-139
6.3.18.3 Equivalent damping properties of the room temperature damping treatment.	6-140
6.3.18.4 Damping properties of Corning glass no. 8363.	6-140
6.3.18.5 Driving point 1 frequency response of the damped exhaust extension.	6-142
6.3.18.6 Driving point 2 frequency response of the damped exhaust extension.	6-142
6.3.18.7 Driving point frequency response of the damped exhaust extension showing 100% and 85% coverage.	6-143
6.3.19.1 Front two sections of the J-85 afterburner liner.	6-144
6.3.19.2 Enamel number 21 as fired, modes 2 and 3.	6-145
6.3.20.1 Sideview of HH-53 helicopter.	6-147
6.3.20.2 Eight percent bandwidth sound pressure level data.	6-147
6.3.20.3 Isometric view of center cabin structure where damping was applied.	6-149
6.3.20.4 Variations of the loss factor with temperature and frequency.	6-149
6.3.20.5 Variations of the real part of shear modulus with temperature and frequency.	6-150
6.3.20.6 Layered damping treatment.	6-150

LIST OF FIGURES (Continued)

<u>Figure</u>	<u>Page</u>
6.3.20.7 System loss factor of a clamped-clamped beam with multiple layer damping treatments.	6-151
6.3.20.8 Acceleration - 100% OGE hover.	6-151
6.3.20.9 Microphone data - 100% OGE hover.	6-152
6.3.20.10 Typical ground vibration test spectra.	6-153
6.3.21.1 Typical turbine blade. (Note: Half blade damping coatings applied.)	6-154
6.3.21.2 Transfer function taken at point 4 on blade.	6-155
6.3.21.3 First bending mode, 746 Hz, deformed mode shape superimposed on undeformed mode shape.	6-155
6.3.21.4 First torsional mode, 824 Hz, deformed mode shape superimposed on undeformed mode shape.	6-156
6.3.21.5 Loss factor measurement for undamped blades.	6-156
6.3.21.6 Results of damping material 8463 tested in all five damping configurations.	6-158
6.3.21.7 Damping coatings after spin testing.	6-159
6.3.22.1 Exducer turbine assembly with electromechanical shaker attached.	6-161
6.3.22.2 Tip vibration response of an exducer blade for the undamped C-5 cooling turbine.	6-161
6.3.22.3 Tip vibration response of a turbine blade for the undamped C-5 cooling turbine.	6-162
6.3.22.4 Configuration of viscoelastic damping treatment placed between exducer and turbine section of C-5 cooling turbine.	6-162
6.3.22.5 Tip vibration response of an exducer blade of the C-5 cooling turbine damped with the midspan wire damper.	6-163
6.3.22.6 Tip vibration response of a turbine blade of the C-5 cooling turbine with the midspan wire damper.	6-163
6.3.22.7 Tip vibration response of an exducer blade of the C-5 cooling turbine damped with a viscoelastic treatment between exducer and turbine.	6-164
6.3.22.8 Tip vibration response of a turbine blade of the C-5 cooling turbine damped with a viscoelastic damping treatment between exducer and turbine.	6-164

LIST OF FIGURES (Continued)

<u>Figure</u>	<u>Page</u>
6.3.22.9 Modal loss factor versus temperature for three configurations of the C-5 cooling turbine.	6-165
6.3.22.10 Modal loss factor versus temperature for three configurations of the C-5 cooling turbine.	6-165
6.3.23.1 Undamped and damped response.	6-169
6.3.23.2 Damping design.	6-169
7.1 Variation of loss factor with shear strain for silicone rubber.	7-3
7.2 Variation of test beam loss factor with temperature.	7-6
7.3 Variation of test beam frequency with temperature.	7-6
7.4 Composite constraining layer stress variation with damping compound shear modulus.	7-7
7.5 Variation of constraining layer normalized axial strain as a function of the shear parameter Kl , over its semi-span.	7-8
8.1 Variation of the material damping in metals with dynamic stress amplitude.	8-4
8.2 Variation of the material damping with dynamic stress amplitude in metals.	8-5
8.3 Typical damping ratio for various alloys at a stress level equal to one tenth of the yield stress as function of the elastic modulus.	8-6
8.4 Variation of viscous damping ratio with fiber volume in early beam tests.	8-8
8.5 Measured Young's modulus and damping for graphite/epoxy composite at ambient temperature.	8-8
8.6 Measured damping in free-free Kevlar honeycomb panels and beams.	8-9
8.7 The behavior of graphite/epoxy composite, as a function of temperature.	8-10
8.8 Actual measured variation of fundamental mode damping with frequency for stiffened honeycomb panels.	8-13
8.9 Variation of the measured damping in the fundamental mode of riveted and bonded multi-bay skin-stringer aluminum panels with frequency.	8-15

LIST OF FIGURES (Continued)

<u>Figure</u>		<u>Page</u>
8.10	Comparison of theoretically predicted and measured viscous damping ratios of blade stiffened mini-sandwich graphite/epoxy panel.	8-16
8.11	Comparison of theoretically predicted and measured viscous damping ratios for fundamental mode of stiffened composite honeycomb panels.	8-16
8.12	Comparison of measured and predicted damping in the fundamental mode of riveted and bonded multi-bay skin-stringer aluminum panels.	8-21
8.13	Comparison of measured and predicted damping of riveted multi-bay aluminum panels with predictions for higher mode damping.	8-22
8.14	Variation of damping with Jack load for J-stiffened mini-sandwich panel.	8-24
8.15	Variation of the J-stiffened mini-sandwich panel resonant frequencies with Jack load.	8-25
8.16	Damping measured on a welded stiffened steel structure in air and immersed in water.	8-26
8.17	Damping measured on bare stiffened shells and a trimmed stiffened shell as a function of frequency.	8-27
8.18	Comparison of typical damping levels measured on the ground and in orbit.	8-28
8.19	Typical damping levels measured during Galileo spacecraft modal tests.	8-29
8.20	Damping schedule for Titan launch vehicle.	8-29
8.21	Equivalent viscous damping ratios measured during space shuttle ascent vehicle Stage 1 vibration test.	8-31

LIST OF TABLES

<u>Table</u>		<u>Page</u>
2.1	Equations for Fluctuating Pressures, Convection Velocities and Spectra	2-25
2.2	Center and Approximate Band Frequencies for Standard Set of Octave and One-Third-Octave Bands Covering the Audio Frequency Range	2-42
3.1	List of Symbols	3-3
3.2	Summary of Frequency Response Functions for Linear SDOF System	3-15
3.3	Eigenvalues for Uniform Beams with Classical Boundary Conditions	3-18
3.4	Mode Shape Equations for Uniform Beams with Classical Boundary Conditions	3-18
3.5	Mode Shapes for Uniform Beams with Classical Boundary Conditions	3-19
3.6	Natural Frequencies for Beams with Rotationally Flexible Edges	3-20
3.7	I^* Versus \bar{Q} for Pinned End, Torsional Spring End Conditions	3-21
3.8	Mode Shapes for Pinned End, Torsional Spring End Conditions	3-22
3.9	Natural Frequencies of Massless Beams with Concentrated Mass Loads	3-22
3.10	Natural Frequencies of Massive Beams with Concentrated Mass Loads	3-22
3.11	Generalized Mass and Generalized Force for Uniform Loading of Beams, Fundamental Mode	3-25
3.12	Frequency Parameter for Flat Plates, Fundamental Mode	3-28
3.13	Natural Frequencies of Thin Flat Plates of Uniform Thickness	3-32
3.14	Mode Parameters for Stiffened Panels	3-38
3.15	Generalized Mass and Generalized Force for Uniform Pressure Loading of Rectangular Plates, Fundamental Mode	3-40
5.1	Eigenvalues of Cantilever Beam	5-3
5.2	Computer Listing for Program FLSID	5-6
5.3	User's Guide for Calculation of Bare and Composite Frequencies and System Loss Factor for Cantilever Beam Coated on One Side	5-7

LIST OF TABLES (Continued)

<u>Table</u>	<u>Page</u>
5.4	Symbols for Program FISID (Cantilever Beam Coated on One Side) 5-8
5.5	Eigenvalues of Simply Supported Beam 5-9
5.6	Eigenvalues of a Clamped Beam 5-12
5.7	Eigenvalues of a Free Beam 5-12
5.8	Eigenvalues of a Clamped-Pinned Beam 5-13
5.9	Eigenvalues of Cantilever Beam 5-14
5.10	Computer Listing for Program F2SID 5-18
5.11	User's Guide for Calculation of Bare and Composite Frequencies for Cantilever Beam Coated on Both Sides 5-19
5.12	Symbols for Program F2SID 5-20
5.13	Eigenvalues of a Simply Supported Beam 5-17
5.14	Eigenvalues of a Clamped Beam 5-22
5.15	Eigenvalues of a Free Beam 5-23
5.16	Eigenvalues of a Clamped-Pinned Beam 5-24
5.17	Eigenvalues of a Cantilever Beam 5-25
5.18	Computer Listing for Program PREDY 5-29
5.19	User's Guide for Calculation of System Loss Factor For a Beam with a Constrained Damping Layer System Applied 5-31
5.20	Symbols for Program PREDY 5-33
5.21	Eigenvalues of Simply Supported Beam 5-34
5.22	Eigenvalues of a Clamped Beam 5-36
5.23	Eigenvalues of a Free Beam 5-37
5.24	Eigenvalues of a Clamped-Pinned Beam 5-37
5.25	Eigenvalues of a Simply-Supported PLATE 5-39
5.26	Computer Listing for Program PLATE 5-43
5.27	User's Guide for Calculation of System Loss Factor for a Plate with a Constrained Damping Layer System Applied 5-45
5.28	Symbols for Program PLATE 5-47
5.29	Symbols for Section 5 5-76
6.2.1.1	Complex Modulus Data for ISD112, ISD113, MN, and M Damping Materials 6-21

LIST OF TABLES (Continued)

<u>Table</u>	<u>Page</u>
6.2.1.2 Input Data and Computed Results for Damped System for Both ISD 113 and MN Damping Materials	6-22
6.2.1.3 Predicted and Measured Frequency and Loss Factor for Cantilever Beam with MN Damping Material	6-22
6.2.2.1 Wrap Application Procedure	6-29
6.2.8.1 Frequency and Loss Parameters of Ring Mirror	6-64
6.3.1.1 Laboratory Test Data	6-79
6.3.2.1 Types of Damping Treatments and the Part of Structure which it is Applied	6-83
6.3.2.2 Treatment Number and Peak Transfer Function Results	6-83
6.3.4.1 Undamped Modal Frequencies Amplification Factors	6-91
6.3.4.2 Damped Modal Frequencies and Amplification Factors	6-91
6.3.8.1 Summary of Prediction and Measurement Article A	6-101
6.3.9.1 Transmission Loss (TL) of the Sample With and Without Damping Compound (Aquaplas)	6-103
6.3.20.1 Narrow Band Acceleration and Acoustic Levels of Flight 3 Compared with Flight 2	6-152
8.1 Typical Material Damping Levels in Metals	8-3
8.2 Typical Damping Values in Unidirectional Composites with Axial Fibers	8-7
8.3 Effect of Resin Damping on the Damping of Chopped Aligned Graphite Fiber Composite	8-10
8.4 Material Damping in Metal Matrix Composites	8-11
8.5 Fundamental Mode Viscous Damping Ratio for Metal and Composite Stiffened Panel Type Structures	8-18
8.6 Measured Damping Values for Engine Components	8-32
8.7 Typical Range of Measured Printed Circuit Board Damping Values	8-33
9.1 Typical Room Temperature Composite Material Properties	9-2
9.2 Typical Room Temperature Material Properties for Metals	9-3
9.3 Metric Units and Symbols	9-4
9.4 U.S.-To-Metric Conversion	9-5
9.5 Commonly Used Prefixes and Their Symbols	9-6
9.6 Greek Alphabet	9-6

SECTION 1

INTRODUCTION

This volume is the user-oriented damping design guide. It is intended to be used, together with the damping material data in Volume III, for purposes of developing viscoelastic damping applications that will reduce resonant vibrations to acceptable levels. The design of these viscoelastic applications requires a prior knowledge of vibration analysis. A brief introduction to vibration and vibration analysis is given in Section 2 for completeness together with references for further reading.

Since it is very difficult in general to anticipate vibration problems, a brief overview of circumstances which could lead to vibration problems is given in Section 3. A brief guide to the selection of the three primary viscoelastic damping treatments is contained in Section 4 together with the general approach to developing a damping treatment. The design equations and computer programs, useful in conducting preliminary analysis are given in Section 5. A discussion on the use of finite element analysis for more complex design problems is also included in Section 5.

An example problem, worked examples and case histories of successful applications of viscoelastic damping technology are given in Section 6. These worked examples are intended to illustrate the use of the design equations. The case histories are intended to indicate the broad range of application of this technology.

Other design considerations are discussed briefly in Section 7. The data in Section 8 represent a summary of typical damping levels in structures. These damping levels should be used as a guide when developing the viscoelastic damping application, for the structure under consideration, in the absence of measured damping data. Section 9 contains useful material and elastic properties for typical aerospace materials, including advanced composites. A list of metric units and symbols, a U.S.-to-metric conversion table, a list of common prefixes and the Greek alphabet are also included in Section 9.

SECTION 2

VIBRATION PROBLEMS AND ENVIRONMENTS

2.1 INTRODUCTION

Technological advances made over the past few decades, both in analytical methods and in the application of new materials, have resulted in the development of more efficient aerospace structures, as reflected in the lower weight of these structures. These advances have often been made in the face of increases in the level of the vibration environment brought on by the quest for higher performance. The design of space structures, for example, is dominated by their dynamic response to vibration environments. The net result is that greater attention is now being focused on vibration related problems. The even greater demands being placed on technology, especially space technology, requires that resonant vibration problems be solved during the design phase.

2.2 GENERAL DISCUSSION OF FACTORS CONTRIBUTING TO VIBRATION PROBLEMS

It is not easy to identify all of the vibration problems during the design phase. Sometimes vibration problems are encountered because of inaccuracies in or difficulties with modelling the structure. More often than not, vibration problems can be attributed to parameters in the analytical process that are difficult to establish during the design phase. Instead, estimates based on prior experience are often used that cannot be verified, until tests are conducted on the actual hardware. Even with the testing, it may be difficult to simulate the actual vibration environments encountered in service.

An example of such a problem area is the nonlinear dynamic behavior of many current unmanned satellites. As the excitation is progressively increased, bolted joints, including those supporting appendages, begin to

slip at different excitation levels. The result is a progressive lowering of the resonant frequencies accompanied by a progressive increase in the damping of the modes, the latter due to increasing frictional energy loss in the joints, as more joints begin to slip. During launch, and later at maximum dynamic pressure, the satellite within the rocket will be subjected to multiaxial random vibrations, superimposed on an increasing rocket acceleration force. Solutions to this type of a problem require a lot of testing to identify all of the potentially critical modes and the use of procedures in which the structural model is adjusted analytically to improve the match with the measured vibration response. Even this difficult problem can be overcome as witnessed by many successful launches. However failures do occur occasionally.

Similar nonlinear behavior has also been encountered, to a much lesser extent, in ground vibration testing of aircraft conducted as part of a flutter study. However, flutter, or flow induced structural instability, is basically a linear vibration problem. Another example, where similar nonlinear structural vibration response could be encountered in the future, includes the large truss type space structures when assembled with clip-on types of joints. The damping in these structures would be determined by the friction losses generated in these joints. With rigid joints, the vibration response would be linear but the damping would become very small, comparable to the basic material damping, if other means of increasing the damping are not used. Most other vibration problems are confined to smaller structures that usually do not require such complicated analysis.

The vibration amplitudes at resonance and therefore the dynamic stresses within the structure are limited only by the level of the damping in each of the modes. Of all the parameters affecting the vibration response of structures, only damping has defied theoretical definition and must be determined entirely by measurement. Generally, the damping in structures is due to energy loss from such mechanisms as material damping, acoustic radiation, gas pumping in joints, joint friction and structureborne energy loss to the surrounding structure. For space structures, the energy loss is confined to material damping and joint friction, and for some local modes, also to transmission to the surrounding structure.

The wide range of energy loss mechanisms, their general unpredictability, and data reduction errors in measuring the damping are considered to be responsible for the large scatter observed in the measured damping data. This large scatter in the damping data is also considered to be one of the main sources of error in vibration response prediction. Structures with low damping are especially prone to vibration problems.

In general, integrally stiffened graphite/epoxy panels, integrally stiffened metal panels and welded structures such as engine inlet guide vanes are typical structures that may exhibit very low damping, since the damping is due primarily to material damping and acoustic radiation. Recently, acoustic radiation has been shown to contribute more to stiffened panel damping than originally thought. Consequently, care must be taken in selecting the dimensions of the bays in multibay test panels since dimensions can affect the acoustic radiation. Acoustic edge conditions are also important in these panel tests.

The remaining parameter to be considered is the vibration environments. These environments can be divided into two classes. The first involves environments that do not produce damage but nevertheless may produce vibration problems. For example, turbulent boundary layer excitation of fuselage structure is the main source of interior noise problems in jet aircraft. Also, cooling flow through special lenses represents another source of unwanted low level excitation. In general, vibration problems can be expected to occur when specifications call for either unusually low vibration levels or extremely high pointing accuracies. The other class of vibration environments contains sufficient excitation energy at one or more of the structural resonances to drive the structure, or equipment attached to the structure, beyond its design requirements or capability to sustain such an environment. Examples of such environments are:

- jet engine and rocket exhaust noise and associated structureborne vibration
- fan blade generated noise in engine intake ducts

- pressure fluctuations produced by separated flow on wing surfaces during high Q maneuvers and shock wave induced flow separation
- pressure fluctuations aft of protrusions such as dive brakes and spoilers and due to base flow
- jet exhaust and wake impingement
- shock wave oscillation
- flow induced cavity noise
- propeller noise and propeller tip wakes
- blast pressure from armaments

Therefore, one of the more important steps in preventing vibration problems involves establishing the actual environment that the structure or equipment is exposed to. Included in the definition of such an environment are: the total excitation energy expressed in terms of the overall or root mean square (rms) excitation level; the distribution of this energy over the frequency range expressed in terms of the spectrum or power spectral density (PSD); the distribution of the energy over the surface of the structure or within the structure in successive frequency bands; the directivity relative to the structure; the normalized narrowband cross correlation characteristics which determines the degree to which the excitation couples with the vibration modes of the structure; and the duration. With random excitation, the power spectral density of the excitation at the structural resonant frequencies is more useful for calculating the structural response than knowledge of only the overall level, unless empirical data have been developed based on that parameter alone. The overall level does, however, provide an indication as to the severity of the environment.

A lot of effort has been expended over the many decades to develop much of the above data for the vibration environments encountered in the aerospace industry. In spite of all these efforts, accurate estimate of the actual

vibration environment can only be obtained by measurement on or within the actual structure. Since random processes are involved many measurements are required to establish suitable confidence limits to the measured data. Consequently, errors in these environments are another factor contributing to vibration problems. In the absence of test data, the vibration environments to be used in the design and testing can be found in military standards such as MIL-STD-810D.

Evaluation of the capability of any structure to withstand a particular level of dynamic stress requires the availability of appropriate fatigue data for such structure. These fatigue data can only be obtained by testing. In sonic fatigue, these data take the form of random rms stress or strain curves plotted as a function of average cycles to failure, for each of the critical components in the structure. Again since random processes are involved, the random fatigue curves must be based on sufficient data points to establish confidence limits. Often the random fatigue data are not available and must be derived from corresponding sinusoidal reverse bending data.

Any method developed for predicting the dynamic response of structures to the above environments must take account of the scatter in all of the previously described parameters. Often, a compromise must be made between an acceptable risk of failure and weight penalty. Any resonant vibration problems that are encountered can, in general, be solved by beefing up the structure to increase its stiffness, changing the structural stiffness to detune the resonant vibration mode, or by increasing the damping of the structure, either actively or passively. Any critical equipment mounted to structure can be vibration isolated, actively or passively, to reduce the vibration input. On rare occasions, it may also be possible to reduce the vibration environment such as the flow induced acoustic cavity modes by the use of spoilers or the buzz saw noise in engine intake ducts by perforated liners

Viscoelastic (passive) add-on damping has been used to solve vibration problems in structures where it has been difficult to change the basic design. The reduction in the resonant vibration stresses achieved by this means has often exceeded that possible by increasing the stiffness of the structure (Figure 2.1), for the same weight penalty. Integrally designed damping offers even greater potential for reducing the vibration stresses, with much lower weight penalties. The cost of this technology will also be minimized if applied at the design stage.

2.3 VIBRATION ENVIRONMENTS

This section contains a brief summary of typical vibration environments encountered in the aerospace industry. The purpose is to provide an indication of the nature and severity of such environments. More information about these environments are contained in References [2.1] to [2.5] and methods for estimating these environments are given in References [2.6] to [2.18]. These environments are expressed in terms of decibels (dB), rms pressure or the dynamic pressure. The relationship between these parameters are given in Section 2.4.

2.3.1 Jet and Rocket Noise

Rockets in general produce much greater acoustic power than turbojet engines because of their much higher exhaust velocities. The maximum overall sound pressure level (OASPL) L_w dB produced by the rockets, turbojets and model jets is plotted [2.1] in Figure 2.2 as a function of the modified Lighthill's parameter L_a given by

$$L_a = \frac{\rho A V^8}{\rho_0 c^5} \quad (2.1)$$

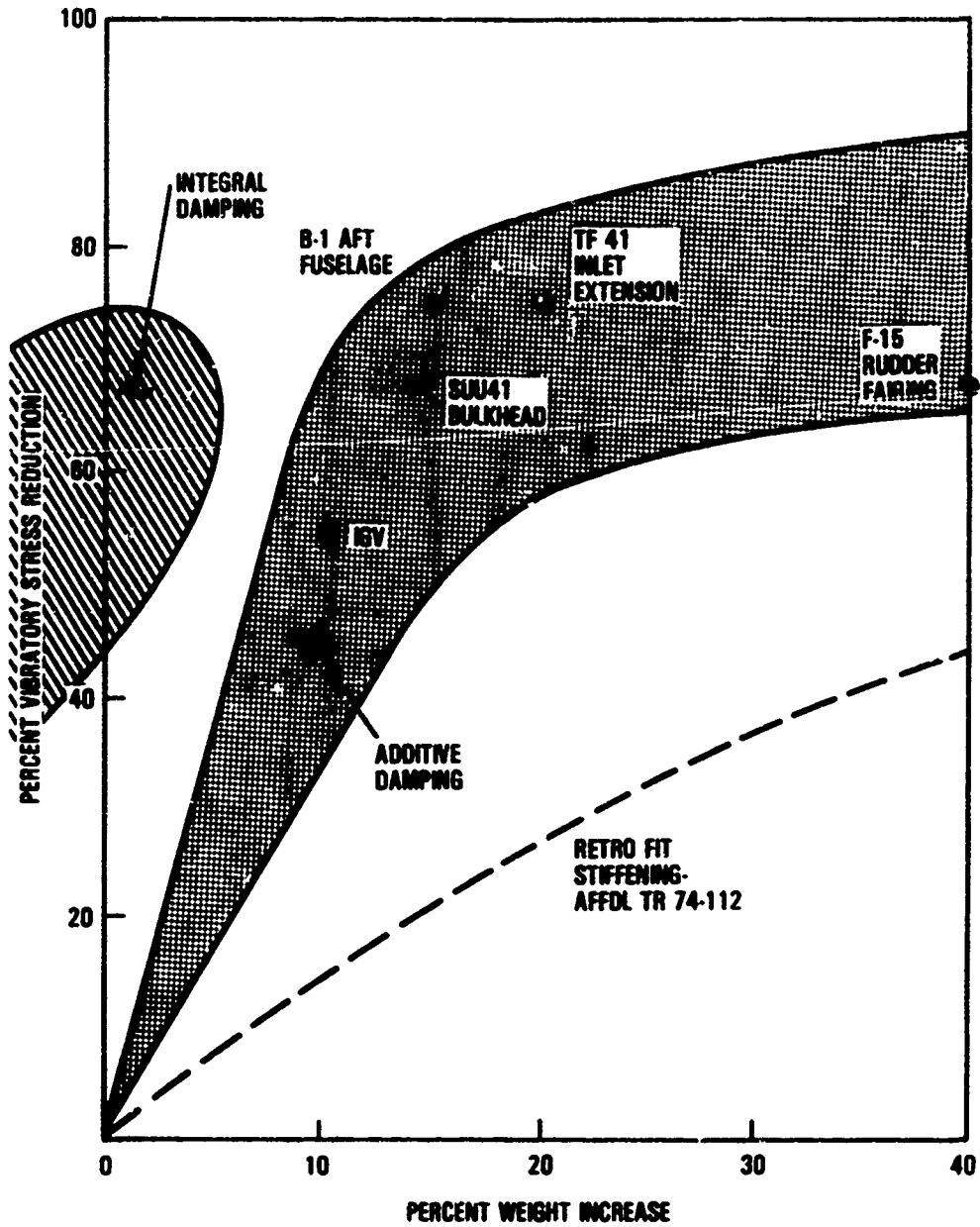


Figure 2.1. Vibratory stress reduction obtained with additive damping on existing hardware.

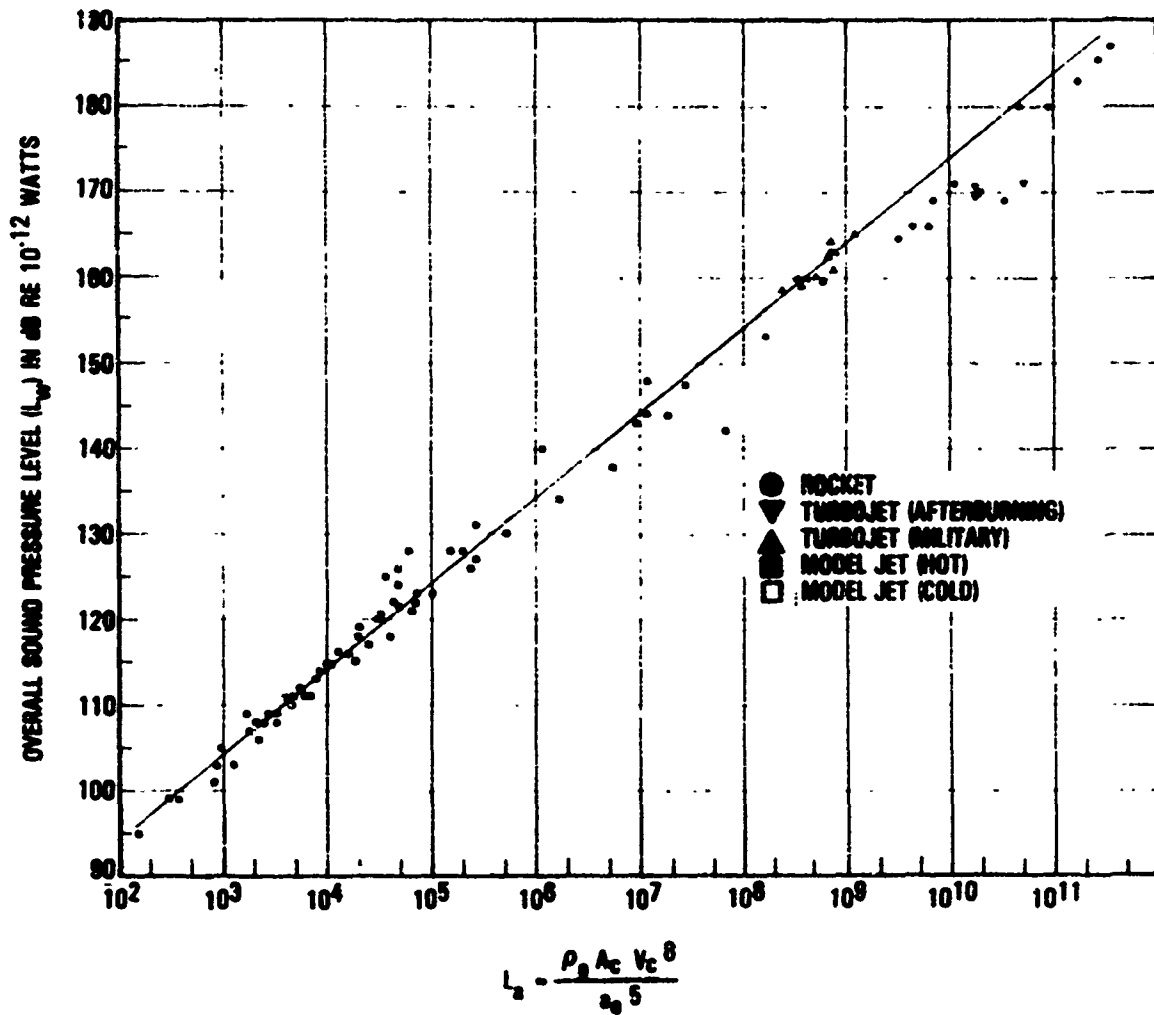


Figure 2.2. Total acoustic power for jet flows compared to revised Lighthill parameter L_a .

where

A_c is the characteristic jet or rocket area ($=\pi D_c^2/4$)

V_c is the characteristic jet or rocket velocity

a_o is the ambient speed of sound in the surrounding air

ρ_o is the ambient density of the surrounding air

The characteristic velocity, V_c , is equal to the speed of sound, a , in the throat of the exhaust nozzle, for sonic and supersonic flow velocities, at a flow temperature T . The characteristic diameter, D_c , of the rocket exhaust flow is given by

$$D_c = D \left[\left(\frac{2}{\gamma+1} \right)^{\gamma/\gamma-1} \frac{p}{p_o} \right]^{1/2} \quad (2.2)$$

where D is the diameter of the throat for rockets and the jet exhaust diameter for turbojets, γ is the ratio of specific heats for the exhaust flow, p is the total pressure at the rocket throat and p_o is the atmospheric pressure.

The maximum overall sound pressure level L_w of these jets can be expressed by the relationship [2.1]

$$L_w = 10 \log_{10} \left\{ 5 \cdot 10^{-5} \cdot L_a \cdot F(T) \right\} \quad (2.3)$$

where $F(T)$ is a correction factor for temperature, illustrated in Figure 2.3, that was introduced [2.1] to produce a better fit of the rocket data in Figure 2.2 to the theory. The typical spectrum shape of the rocket and turbojet noise, at the maximum noise level, is illustrated in Figure 2.4. All of the test data collapse onto a single curve when plotted against a Strouhal number S given by

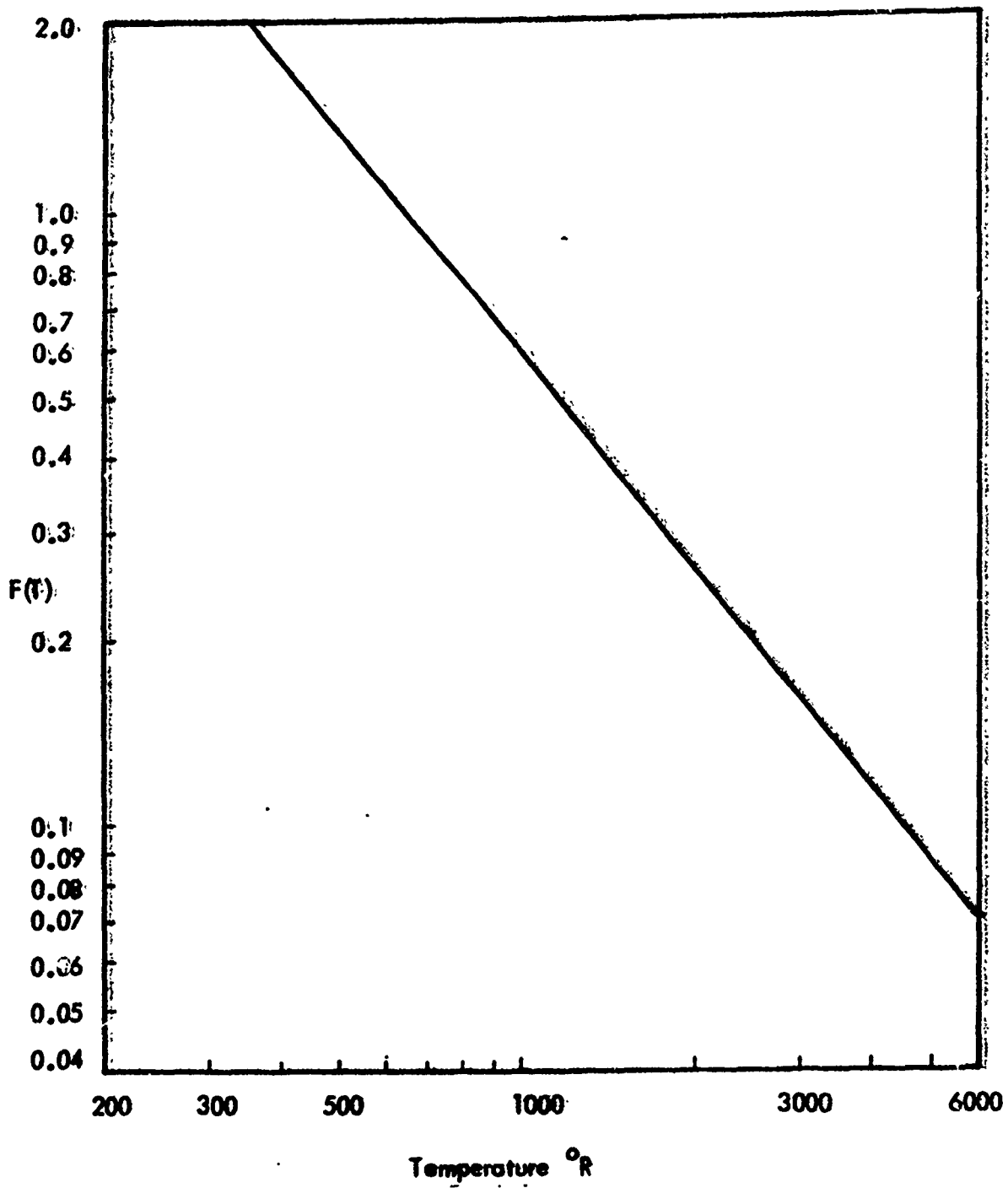


Figure 2.3. Correction factor to overall sound pressure level due to exhaust temperature.

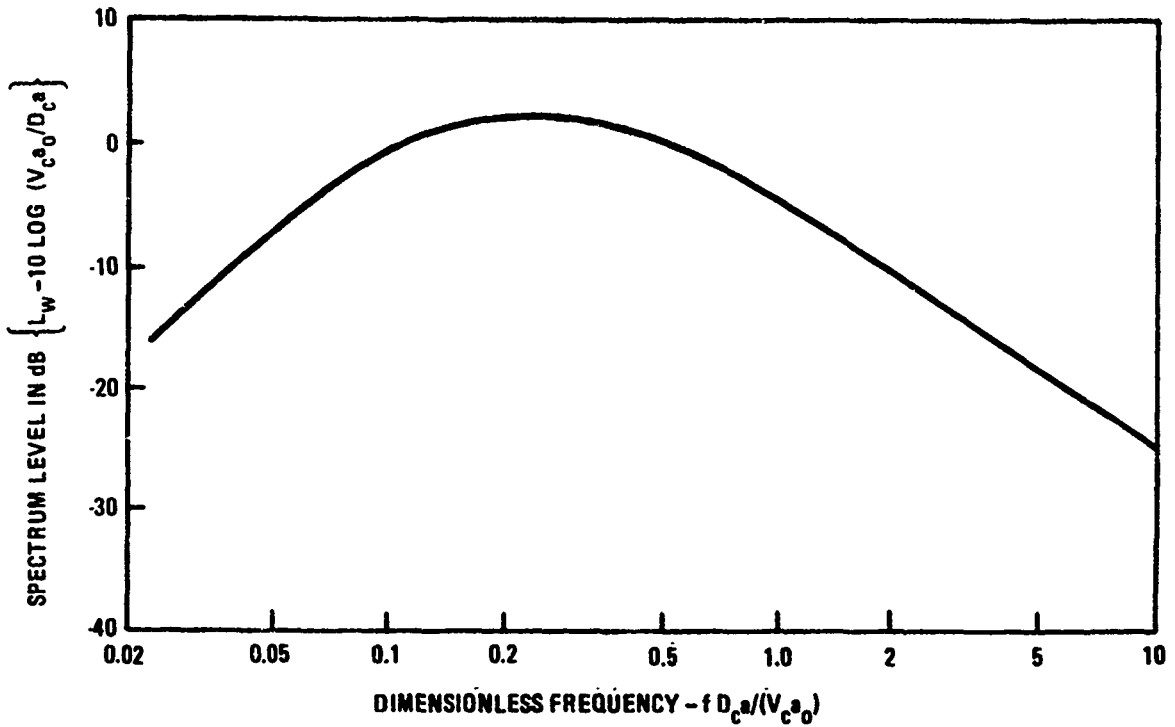


Figure 2.4. Typical spectrum shape for rocket and turbojet noise.

$$S = \frac{f D_{c0}}{V_{c0}} \quad (2.4)$$

where f is the frequency.

The acoustic power that the structure is exposed to is usually less than the maximum OASPL produced by the engines, especially for rockets. This result is due to the directivity of the noise radiation patterns [2.1] as illustrated by the free-field equal-level noise contours in Figure 2.5. The highest sound pressure levels occur downstream of the exhaust nozzle. Also, an uninterrupted jet flow of at least 10 to 30 diameters downstream is required for jet and rocket engines, respectively, to develop the maximum noise levels.

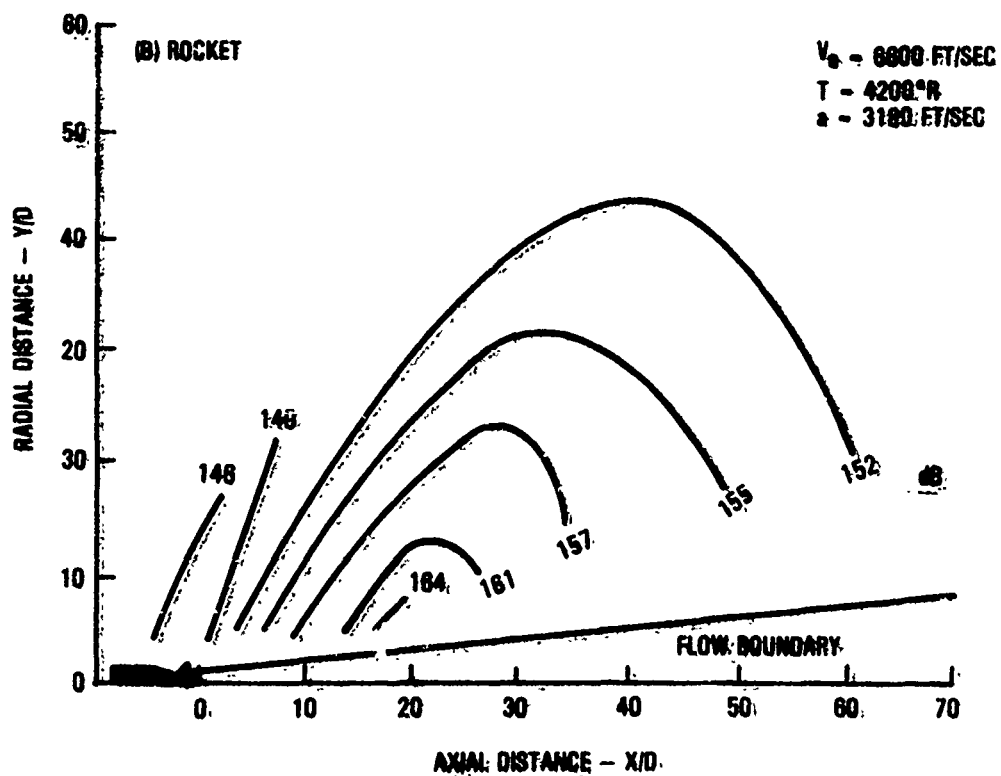
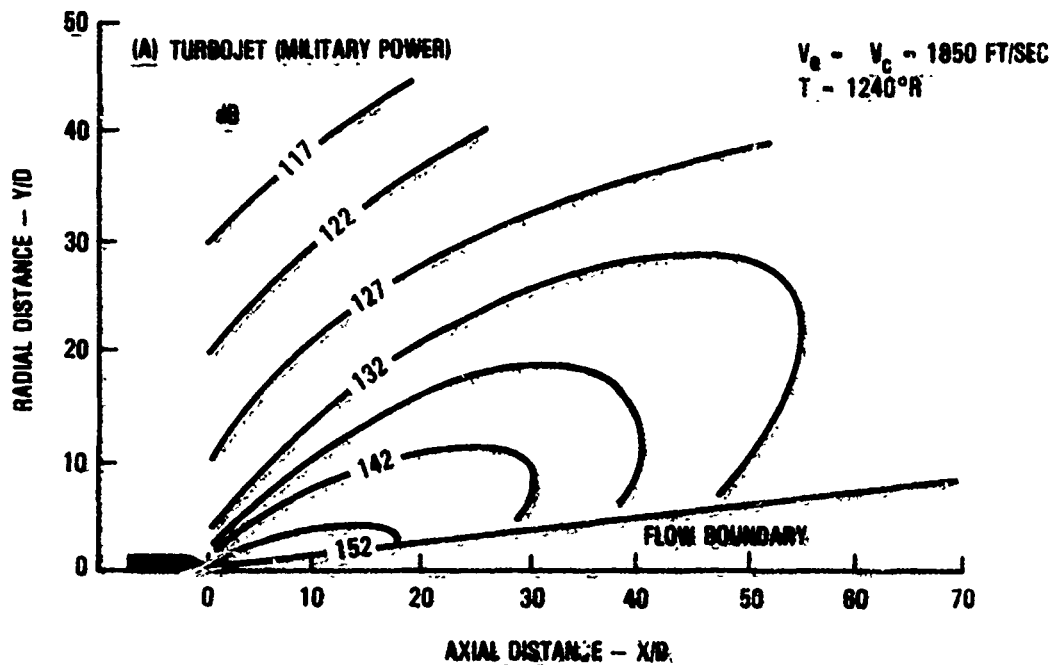


Figure 2.5. Typical contours of equal overall sound pressure level in dB for a turbojet and rocket.

The presence of aircraft structure affects the noise contours and could increase the noise level by as much as 6 dB over the free field level depending on the directivity of the noise propagation relative to the structural surfaces. The rise in the maximum overall sound pressure level on aircraft surfaces [2.19], over the past two decades, is illustrated in Figure 2.6 together with an estimate for the threshold noise level for acoustic fatigue damage. The presence of the ground, especially for vertical takeoff aircraft [2.8] and the launch pad configuration [2.1, 2.9] will also affect the noise level contours, often substantially increasing the noise level on the structure.

Near-field noise adjacent to the exhaust flow boundary (Figure 2.5) is responsible for producing many of the sonic fatigue failures encountered on aircraft. The spectrum shape of the jet noise is a function of frequency and the location of the measuring point relative to the jet nozzle exit. The exponent of the characteristic velocity in equation 2.1 can vary substantially [2.6, 2.7 and 2.18] from its theoretical value of 8 in this region. For these reasons, the noise levels on the surfaces of the structure are usually measured in octave frequency or third-octave bands using a scale model of the aircraft [2.20] or space vehicles [2.21] in which the geometry and the exhaust conditions have been accurately reproduced. Typical accuracy that can be achieved by the use of models is illustrated in Figure 2.7 for a B-52 aircraft [2.20], in this instance depicting reduction in noise level achieved with a noise suppressor, and in Figure 2.8 for the cargo bay door on the space shuttle [2.21]. Model data are generally used for preliminary design of the structure. Such data are, usually, supplemented, at a later date, by noise measurements on actual aircraft or spacecraft to verify the design levels.

The maximum OASPL is developed by the jet and rocket engines during takeoff and launch, respectively, although substantial noise levels can be also produced by the use of reverse thrust during landing, on different parts of the aircraft structure. The design duration at maximum takeoff and reverse thrust power could be hundreds of hours over the life of the aircraft, whereas the duration is measured in seconds for rockets.

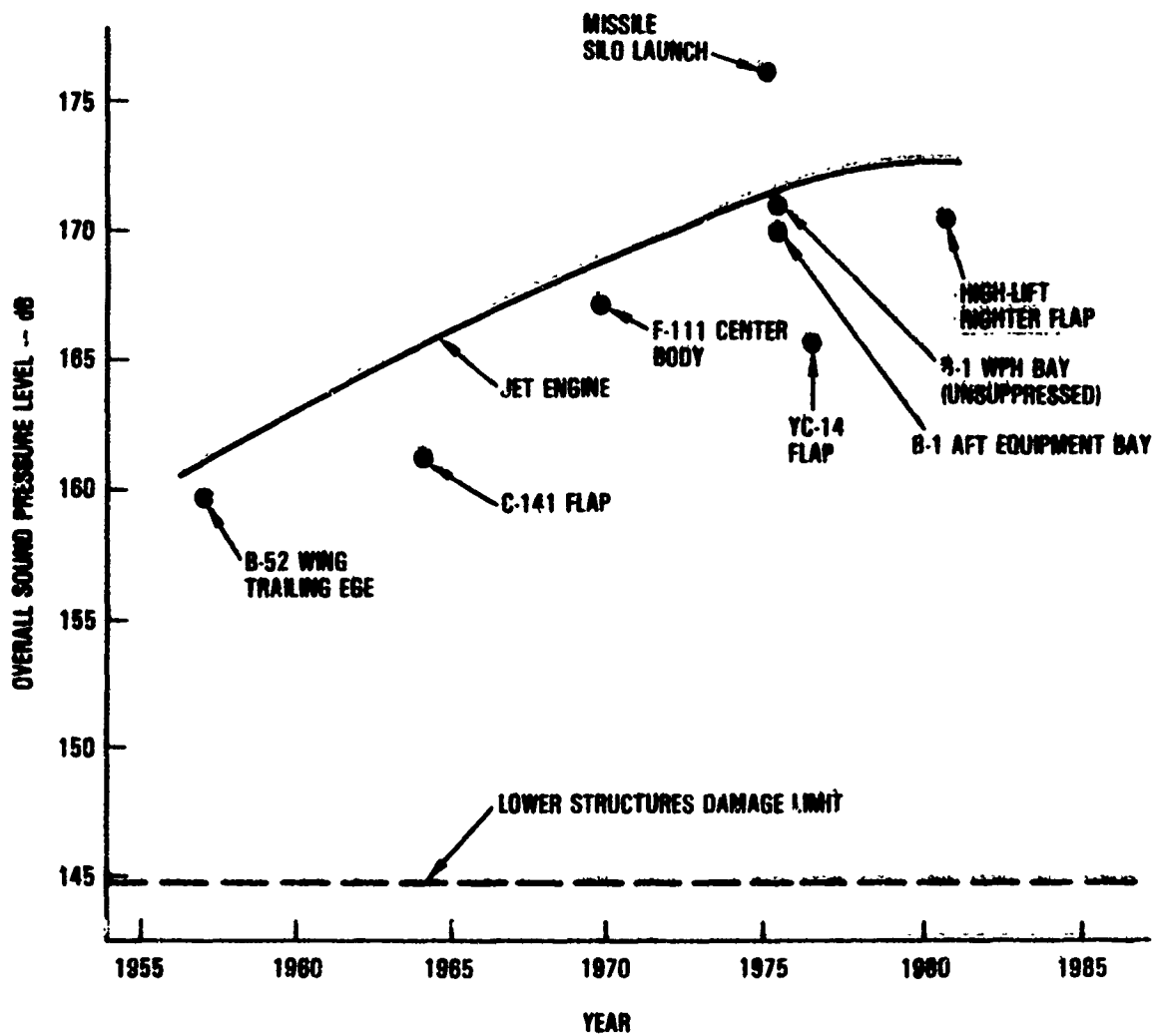


Figure 2.6. Typical rise in jet engine noise on aircraft structure over the past two decades.

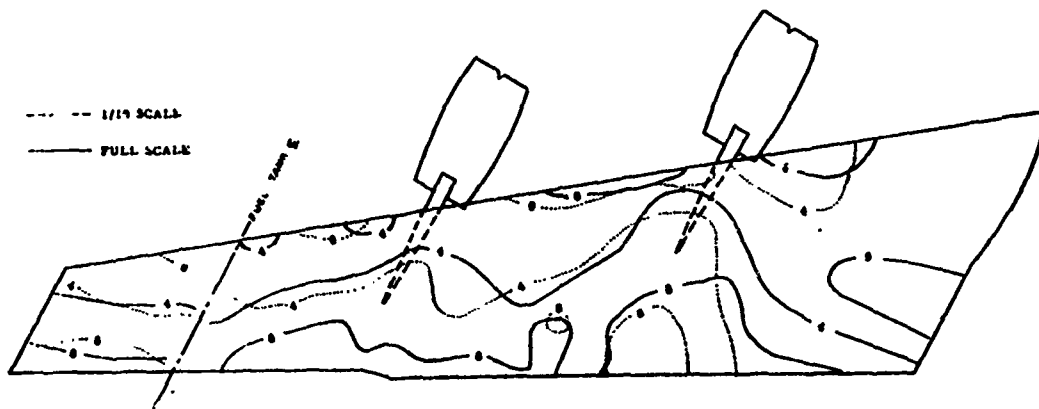


Figure 2.7. Comparison of model and full scale noise contours on B-52 wing depicting noise reduction in dB achieved with a noise suppressor.

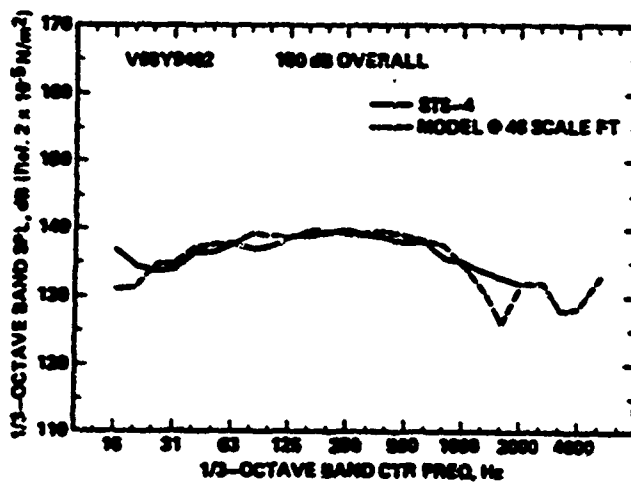


Figure 2.8. Comparison of noise levels measured, with a scale model and during liftoff, at the cargo bay door center aft location on the space shuttle.

2.3.2 Structural Vibration in Aircraft and Rockets

The jet and rocket noise produces vibrations in the structure of the aircraft and rocket, respectively, that can affect the reliability of equipment or payload mounted in these structures. In general, the takeoff noise environment produces the highest vibration levels in the equipment mounted within the aircraft structure. Similarly the launch, which includes both the liftoff and the region of maximum dynamic pressure during ascent, represents the most critical vibration environment for the payload of most rockets, including the space shuttle. However, the highest aeroacoustic loads on the space shuttle are actually encountered during reentry [2.21]. The vibration levels are obtained by measurement during ground and flight tests on aircraft and during captive engine firing or launch with rockets. For design purposes the vibration levels are estimated based on prior vibration measurements on similar vehicles. The various methods used in predicting these vibration levels are discussed in References [2.5], [2.13], [2.14] and [2.15]. In the absence of such data, the equipment mounted in these structures is required to meet test specifications such as those in MIL-STD-810D.

The first measurement of vibration levels was made by Mahaffey and Smith [2.22] on aircraft such as the B-58. The noise levels on the surface of the aircraft and the vibration levels on the structure were measured in octave bands such as illustrated in Figures 2.9 and 2.10, respectively. The noise levels in Figure 2.9 are expressed in dBs while the acceleration levels in Figure 2.10 are expressed in zero to peak g's, where g represents the acceleration due to gravity, since only sinusoidal qualification tests were performed in those days on equipment. The measured rms accelerations were multiplied by a factor of 3.3 in the conversion to zero-to-peak accelerations. The vibration levels correlate well with the sound pressure levels.

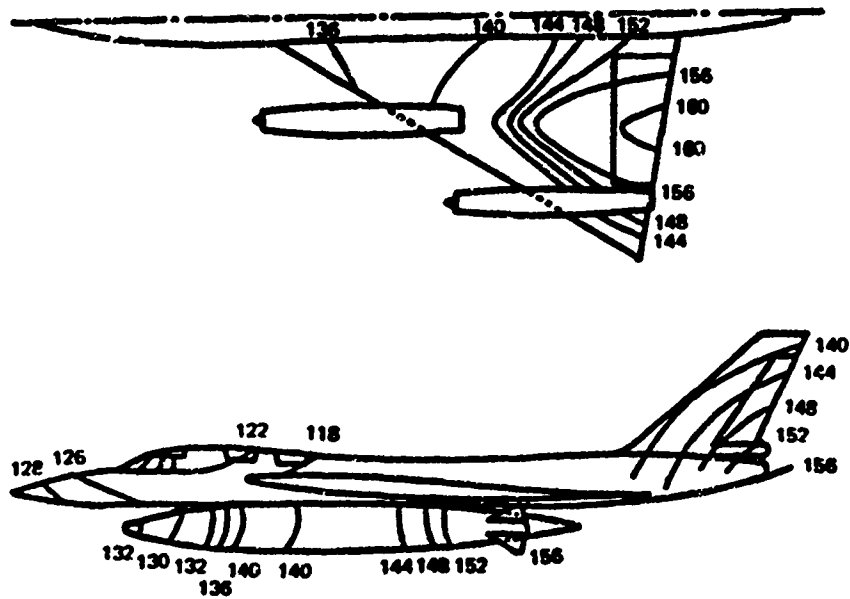


Figure 2.9. Sound-pressure-level contours for the B-58 in the 300 to 600 Hz octave band.

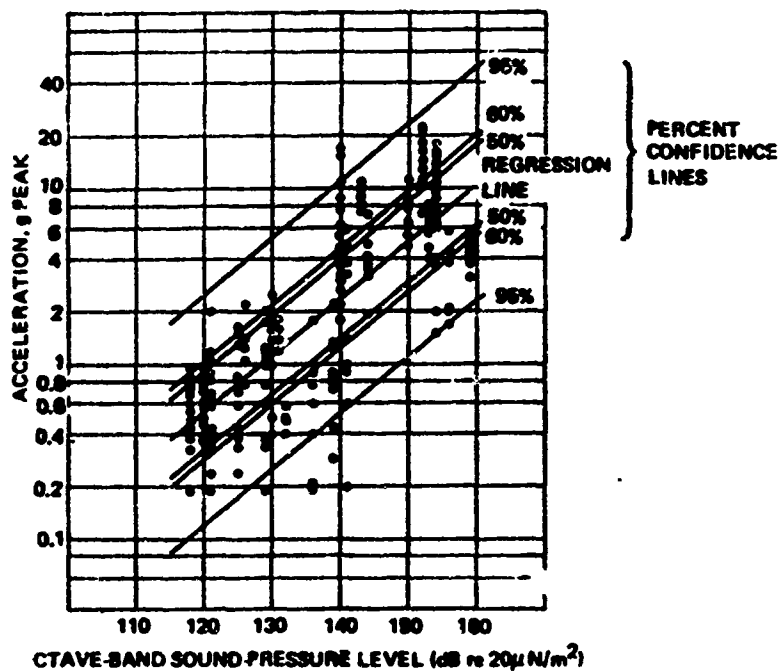


Figure 2.10. Acceleration levels on B-58 airplane plotted against pressure levels in 300 to 600 Hz octave band.

Currently, because random vibration qualification testing capability has been developed, it is customary to present the vibration data in terms of the acceleration power spectral density, expressed in g rms squared per Hertz. It is also customary to divide the aircraft into zones based on the noise level on the structure and combine the vibration measurements within each zone. A typical acceleration power spectral density, measured within the rear fuselage zone of a large military transport aircraft during takeoff is illustrated in Figure 2.11. Also included in the figure are predicted confidence limits based on extrapolated vibration data from other similar class of aircraft.

The highest vibration levels in rockets are encountered in the structure closest to the engines during liftoff [2.1, 2.3]. The payload usually experiences the lowest vibration levels during liftoff [2.3] since it is usually mounted on top of the rocket, furthest from the rocket engine. The payload is subjected to significant acceleration levels also during ascent due to aerodynamic pressure fluctuations which, generally, reach a peak during maximum dynamic pressure [2.1, 2.3]. These results are illustrated in Figures 2.12 through 2.14 which summarize some of the earliest vibration data [2.1] measured on rockets. The acceleration levels in the payload area are a function of the rocket launch weight, being lower for the heavier rockets. Currently, the acceleration measured on rocket structure is presented in the form of narrowband power spectral density in $(g_{\text{rms}})^2/\text{Hz}$ as a function of frequency, as illustrated in Figure 2.15 with data obtained from a Titan I missile.

Both vertical and lateral accelerations are encountered simultaneously on rocket structure [2.3] during both liftoff and at maximum dynamic pressure. The overall vibration levels on the space shuttle cargo bay area are typically in the region of 12 to 15 g's rms. Multistage rockets are also subjected to separation transients which can be quite significant in magnitude [2.3].

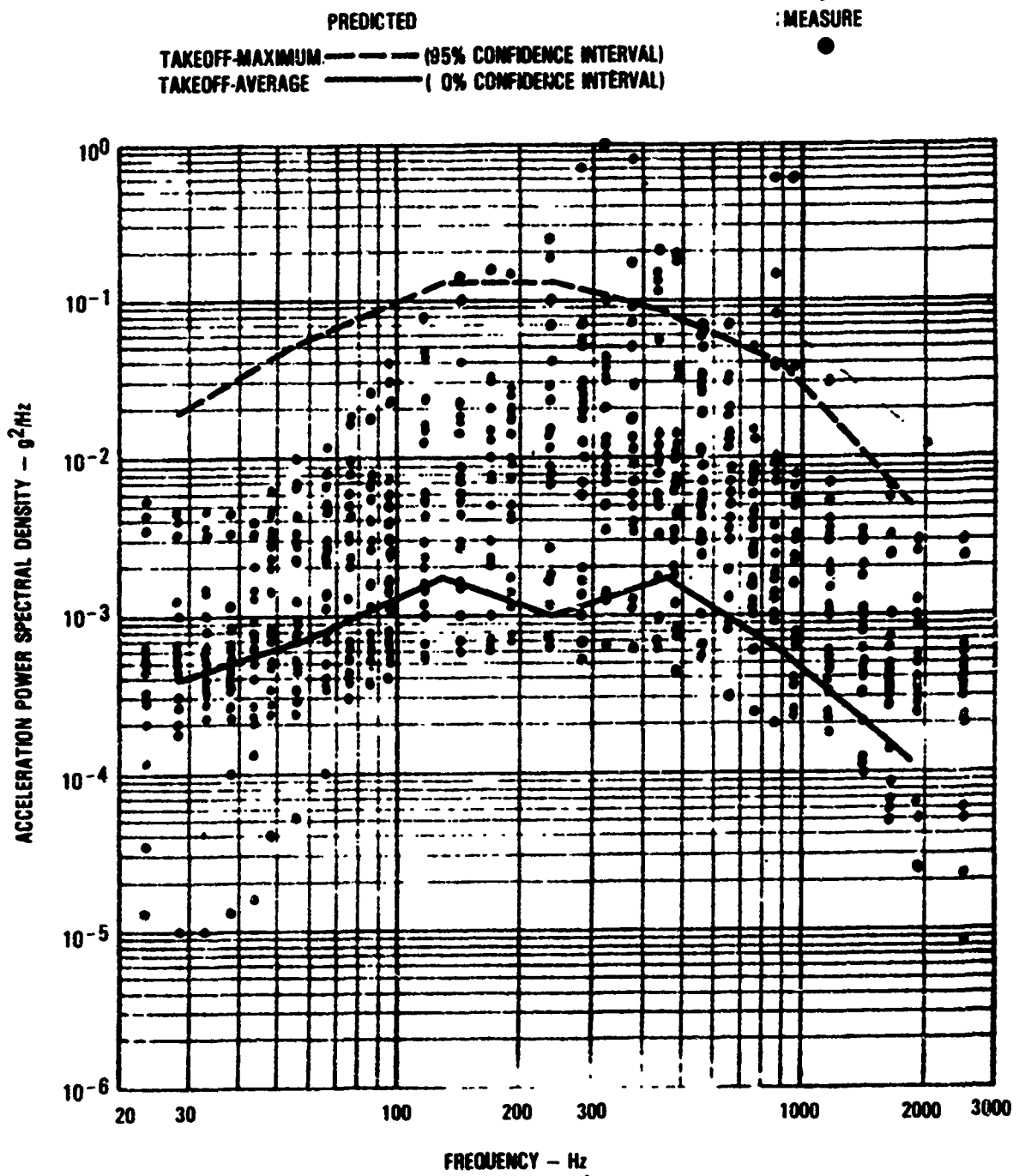


Figure 2.11. Comparison of predicted and measured acceleration power spectral density on rear fuselage of a large military transport aircraft.

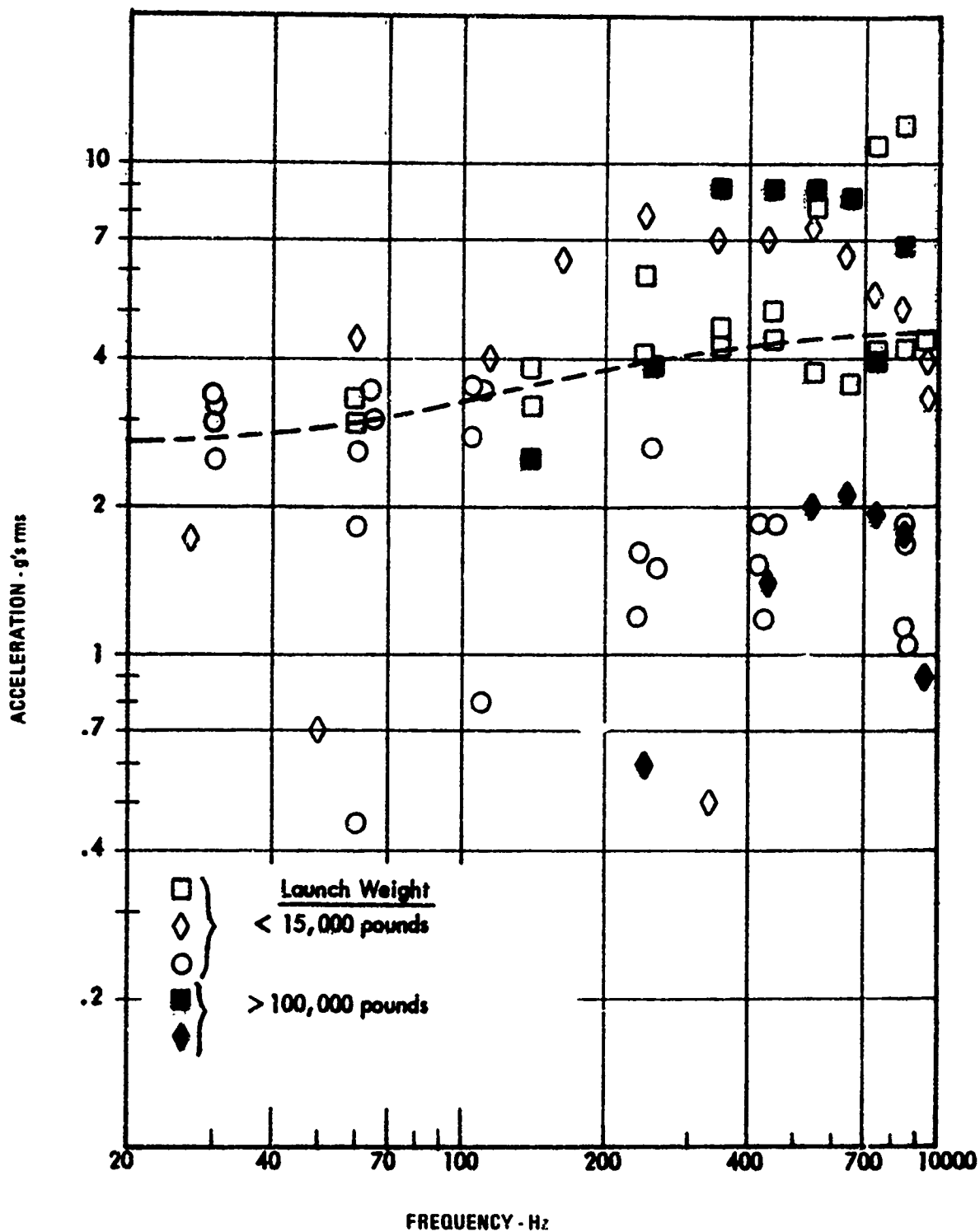


Figure 2.12. Accelerations on structure adjacent to rocket engines during liftoff.

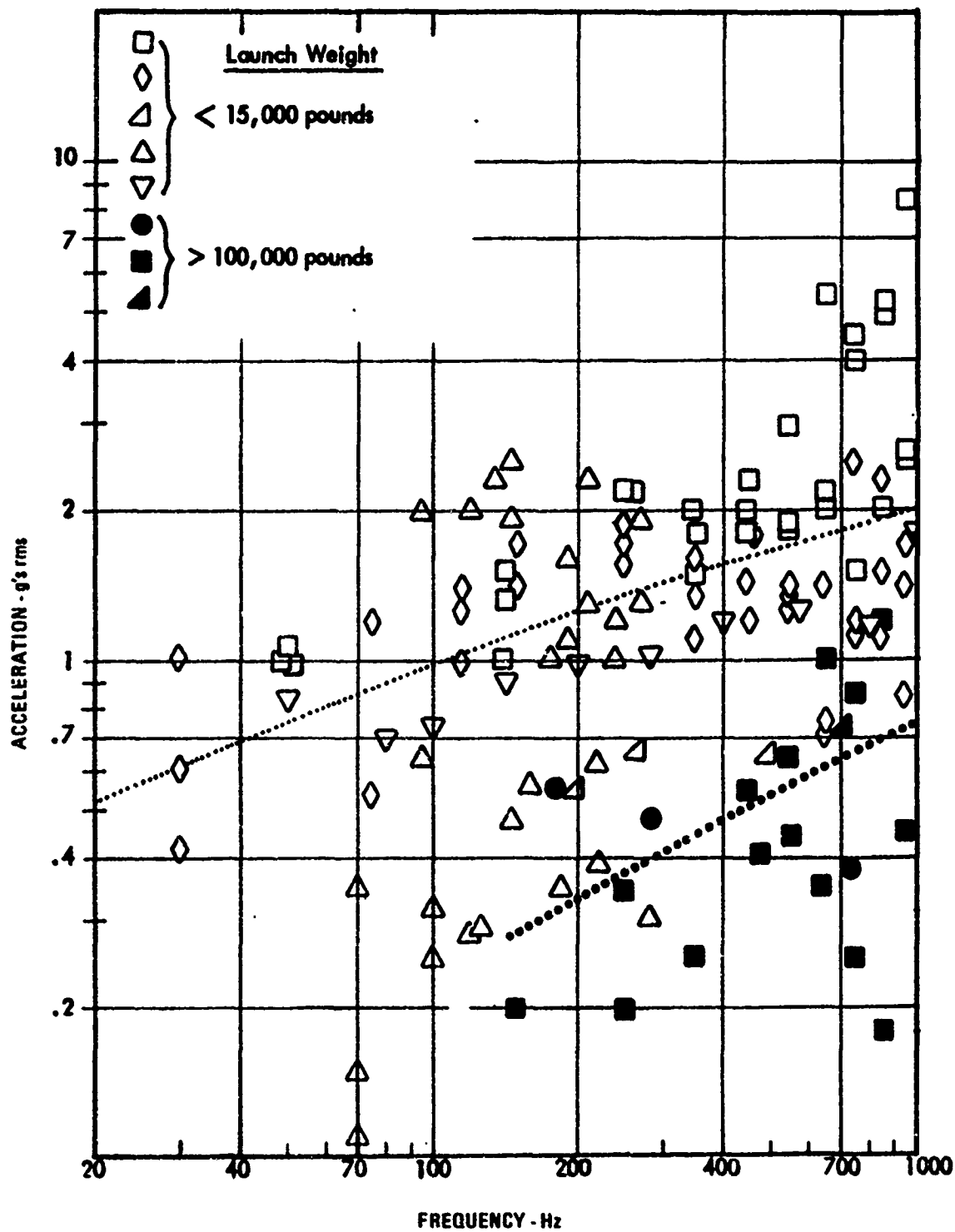


Figure 2.13. Accelerations on upper half of the rocket structure during liftoff.

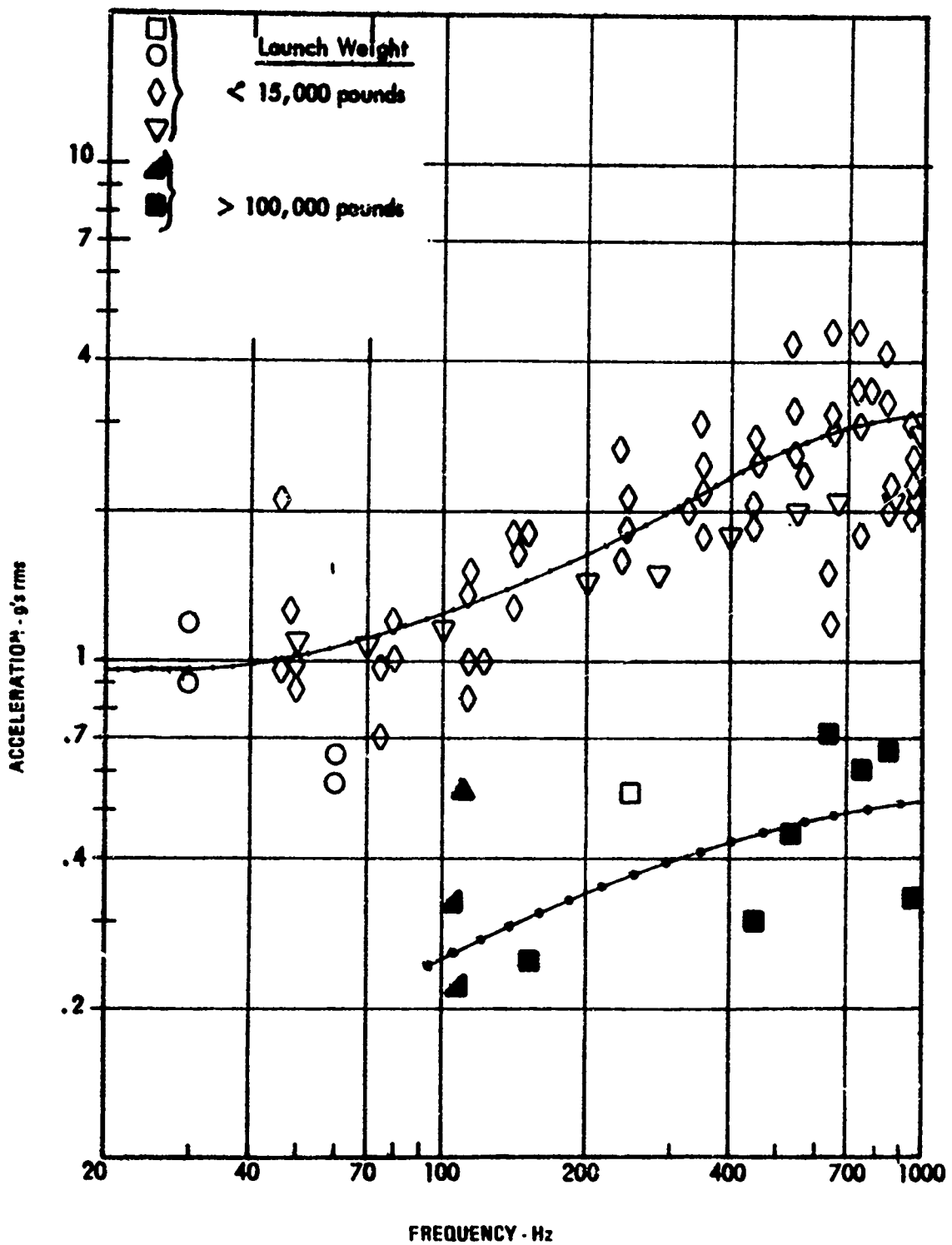


Figure 2.14. Accelerations on upper half of the rocket structure near maximum dynamic pressure.

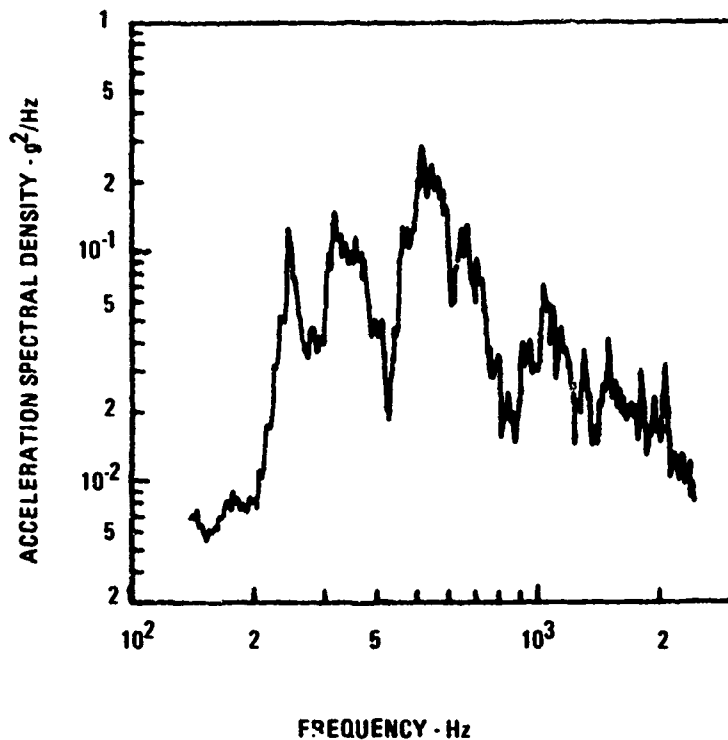


Figure 2.15. Typical narrowband acceleration power spectral density measured on a Titan I missile.

2.3.3 Aerodynamic Fluctuating Pressure Environments

Aircraft and rockets are subjected to a range of fluctuating pressure environments during flight and ascent, respectively. The highest levels are usually encountered at maximum dynamic pressure q . A summary of these environments [2.2] and typical levels encountered on various parts of a large rocket are contained in Figure 2.16. The fluctuating pressures are expressed in terms of P_{rms}/q where p_{rms} represents the root mean square (rms) of the fluctuating pressure and q is the dynamic pressure. The P_{rms}/q values applicable to aircraft, together with the corresponding power spectral densities and convection velocities [2.7], are summarized in Table 2.1. Since the aircraft surfaces are generally much smoother than rocket surfaces, the p_{rms}/q ratio for the attached turbulent boundary layer (TBL) on aircraft is typically around 0.006 at low Mach numbers. For separated flow at a Mach number of 0.9, the p_{rms}/q ratio is around 0.1. This ratio, at the above Mach number and an

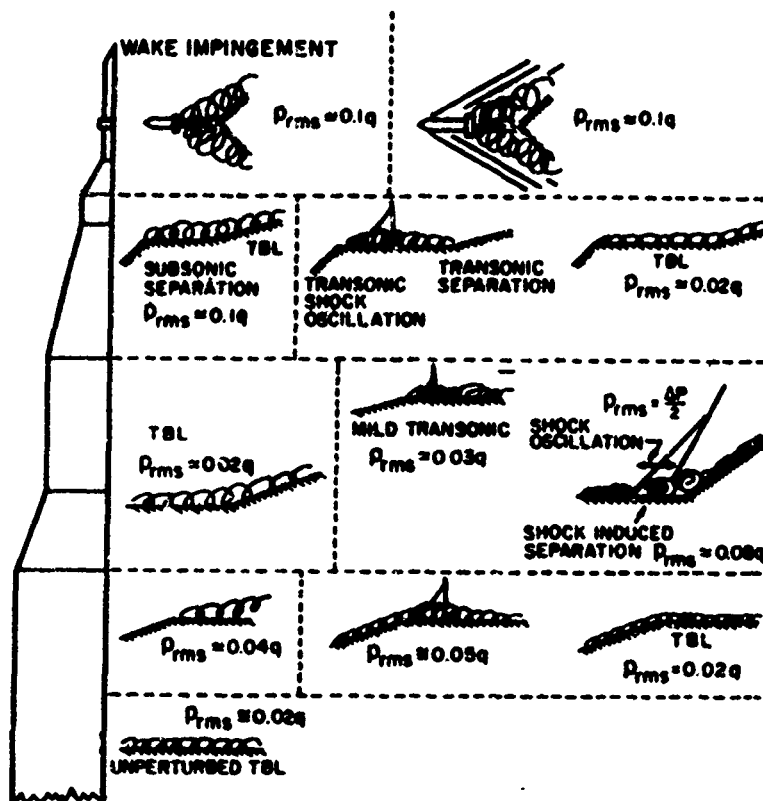
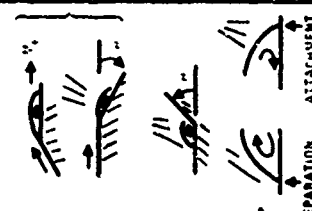


Figure 2.16. Typical overall fluctuating pressure levels on various locations on a rocket.

altitude of 10,000 feet (3050 m), translates into an overall sound pressure level of 166 dB. High q maneuvers, involving large angles of attack, could produce flow separation over the wings with excitation levels high enough to produce failures in the lightly loaded wing panels near the wing tips.

In general, the fluctuating pressures do not excite panel type structures as efficiently [2.14] as an acoustic progressive wave, travelling in the flow direction, at and below the panel fundamental mode frequency, f_n (Figure 2.17). As a rule-of-thumb, 5 dB can be subtracted from the fluctuating pressure level at this frequency to obtain the equivalent acoustic excitation level. The opposite is true at higher frequencies, where the pressure fluctuations excite the higher order panel modes with greater efficiency (Figure 2.14). This behavior is due to differences [2.6] in both

TABLE 2.1. EQUATIONS FOR FLUCTUATING PRESSURES, CONVECTION VELOCITIES AND SPECTRA

TYPE OF FLUCTUATING PRESSURE	P_{rms}/q	POWER SPECTRAL DENSITY - $S(f)$	CONVECTION VELOCITY
ATTACHED TURBULENT BOUNDARY LAYER (TBL)	$\frac{0.006}{1 + 0.14 M^2}$ $M < 5$ 0.0013 $M > 5$	$\frac{2}{\pi} \frac{P_{rms}^2 \hat{c}^*}{U} \left[1 + \left(\frac{2\pi f \hat{c}^*}{U} \right)^2 \right]^{-1}$ $M < 1$ $\frac{2}{\pi} \frac{P_{rms}^2 \hat{c}^*}{U} \left[1 + \left(\frac{4\pi f \hat{c}^* \cdot 0.9}{U} \right)^2 \right]^{-2}$ $M > 1$	$U_c = U \left[0.675 + 0.3e^{-0.11u\hat{c}/U} - 0.25e^{-0.38\epsilon/\hat{c}} \right]$
TRANSITIONAL TBL	$\frac{0.006}{1 + 0.013 M^2}$	$\frac{2}{\pi} \frac{P_{rms}^2 \delta_t}{U} \left[1 + \left(\frac{2\pi f \delta_t}{U} \right)^2 \right]^{-1}$	$0.7 U_c$ (above)
SEPARATED FLOW 	$\frac{0.045}{1 + M_e^2}$ 0.022 $\frac{0.14}{1 + 0.5 M_u^2}$	$\frac{5.9 P_{rms} \delta_t}{U_u} \left[1 + \left(\frac{0.17 f U_u}{\delta_u} \right)^2 \right]^{-2.15}$	$U_c = U_u \left[0.6 + \log \left\{ \frac{f x_s}{U_u} \right\} \right]$

P_{rms} = root mean square pressure
 q = free stream dynamic pressure
 M = free stream Mach number
 U = free stream flow speed
 U_c = convection velocity
 δ = boundary layer thickness ($\approx 8\delta^*$)
 δ^* = boundary layer displacement thickness
 δ_t = $\delta^* (1 + 0.013 M^2)$
 f = frequency - Hz
 $\omega = 2\pi f$
 ξ = Separation distance in streamwise direction
 M_e = Downstream Mach Number
 M_u = Upstream Mach Number
 δ_u = Upstream boundary layer thickness
 U_u = Upstream flow velocity

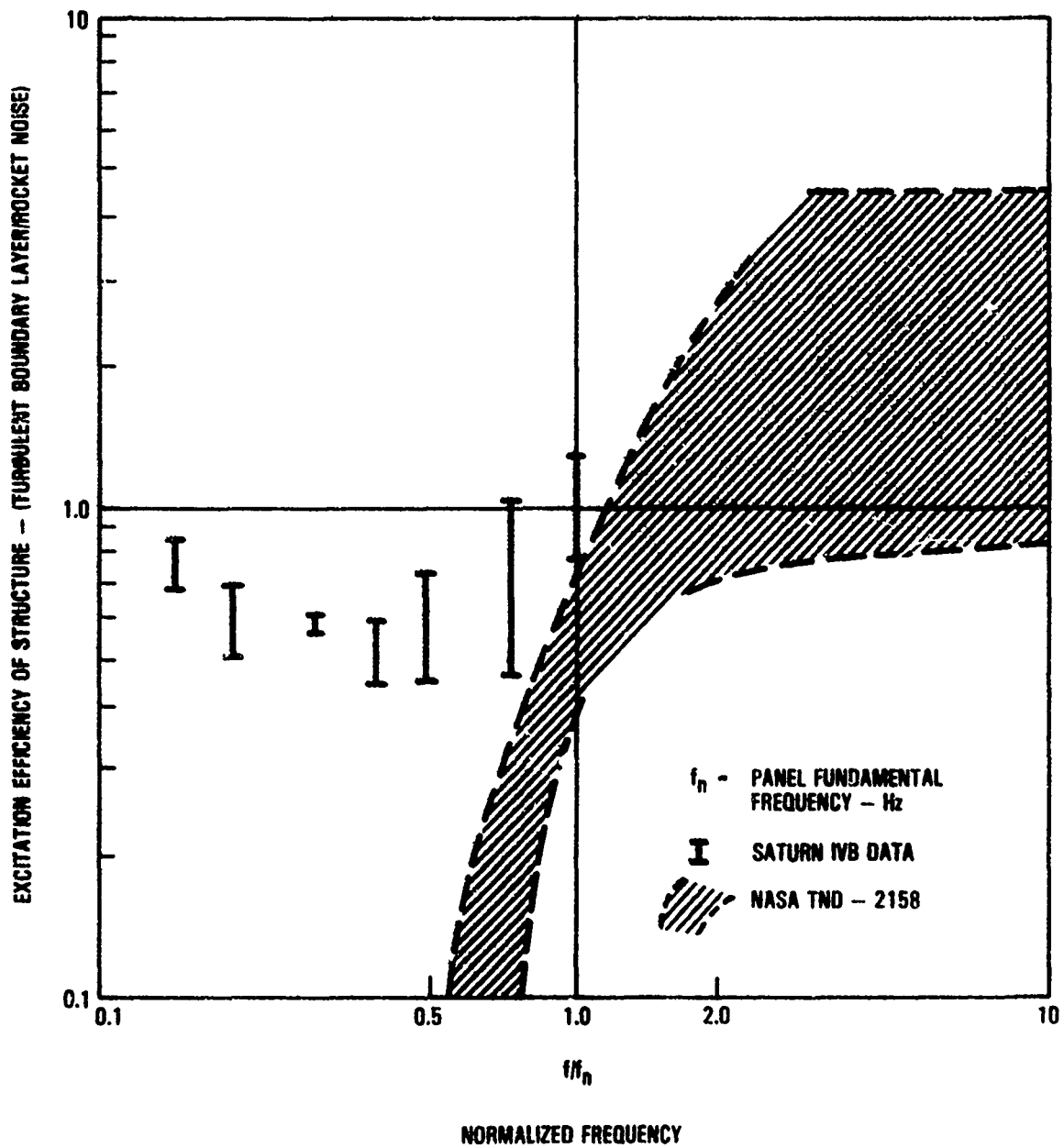


Figure 2.17. Efficiency of boundary layer pressure fluctuations relative to rocket noise in exciting structural vibration.

the spectral decay of the narrowband cross-correlation functions and the convection velocity between the flow induced pressure fluctuations and the rocket/jet noise. The flow induced pressure fluctuations propagate at 0.6 to 0.9 times the free stream velocity for attached flow in comparison to the local speed of sound for the acoustic excitation.

The pressure fluctuations are often measured during the design phase by means of accurate scale models in wind tunnels [2.21, 2.23]. The model pressure fluctuations, in general, provide a very good estimate of the pressure fluctuations measured on the actual structure during flight, as illustrated in Figure 2.18 for the space shuttle, and in Figure 2.19 for a C-141 aircraft with perforated spoiler deflected flow [2.24].

The region of flow separation behind blunt bodies, dive brakes, flow spoilers and the blunt body termination in rockets and reentry vehicles is known as base flow. The rms fluctuating pressure level p_{rms} , acting on the base structure due to the base flow, can be calculated [2.7] in terms of the base static pressure p_b and the Mach number M_b of the adjacent flow just outside the wake, from the following equation

$$\frac{p_{rms}}{p_b} = \frac{0.01 M_b^2}{1 + 0.04 M_b^2} \quad (2.5)$$

The following relationships are assumed in the above equation

$$q_{\infty} \approx q_b = \frac{1}{2} \rho V_b^2 \approx \frac{1}{2} \rho p_b M_b^2 \quad (2.6)$$

where q_{∞} is the free stream dynamic pressure which is assumed to be equal to the base dynamic pressure q_b , and V_b is the velocity of the flow just outside the wake. The corresponding power spectral density $S(f)$ of the base excitation can be calculated from

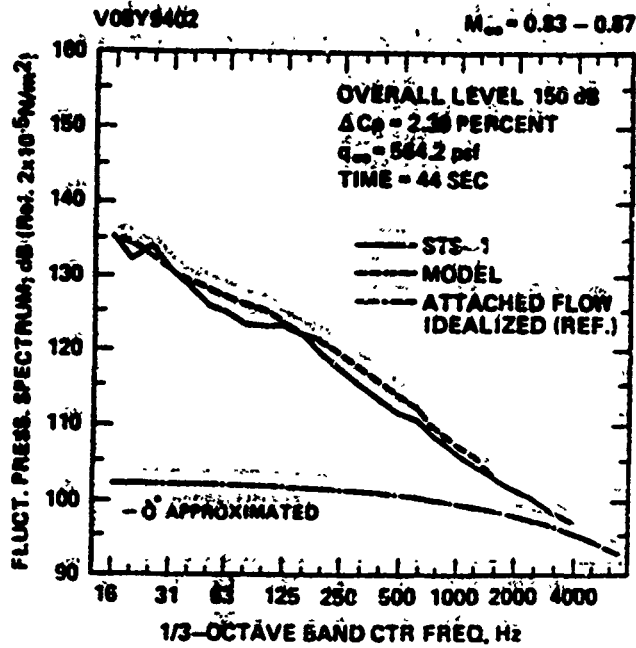


Figure 2.18. Comparison of model and flight data, in third-octave levels, produced by pressure fluctuations at the cargo bay door center aft location on the space shuttle.

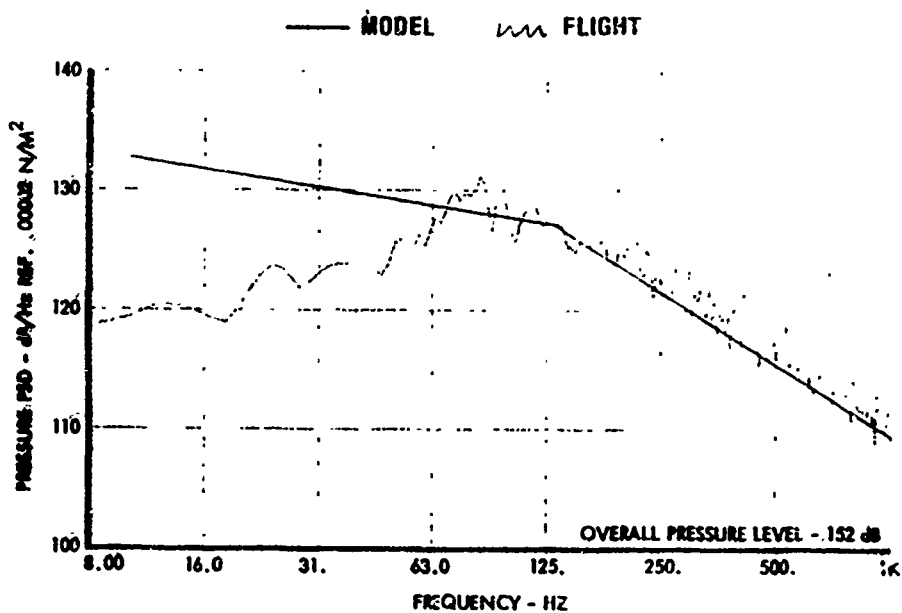


Figure 2.19. Comparison of model and flight power spectral density data for pressure fluctuation on C-141 faring aft of perforated spoilers.

$$\frac{S(f)V_b}{p_{rms}^2 D} = \frac{2}{1 + \left(\frac{\pi f D}{V_b}\right)^2} \quad (2.7)$$

where D is the diameter of the blunt base.

2.3.4 Flow Induced Cavity Oscillations

High-speed flow over cavities in aircraft and rockets surfaces produces a high level acoustic environment within the cavity consisting of discrete frequency spikes superimposed on lower level broadband noise (Figure 2.20). These discrete frequencies, which are the acoustic resonant modes of the cavity, have produced sonic fatigue failures in the structure surrounding the cavity. For shallow cavities, with length to width (L/D) ratios greater than 2, the frequencies of these acoustic modes can be predicted with reasonable accuracy [2.6] by the following equation

$$f_n = \frac{U}{L} \left[\frac{(n - 0.25) M}{\left(1 + \frac{\gamma - 1}{2} M^2\right)^{1/2}} + 1.75 \right] \quad n=1,2,3,\dots \quad (2.8)$$

where f_n is the frequency of the nth mode, U and M represent the free stream velocity and Mach number, respectively, L is the cavity length and γ (=1.4) is the ratio of specific heats of air. For deep cavities ($L/D < 2$), the following equation can be used to predict the frequencies of the first three modes.

$$f_n = \left(\frac{2n-1}{4}\right) \left(\frac{c}{D}\right) \quad n = 1,2,3 \quad (2.9)$$

where c is the speed of sound in the air and D is the cavity width.

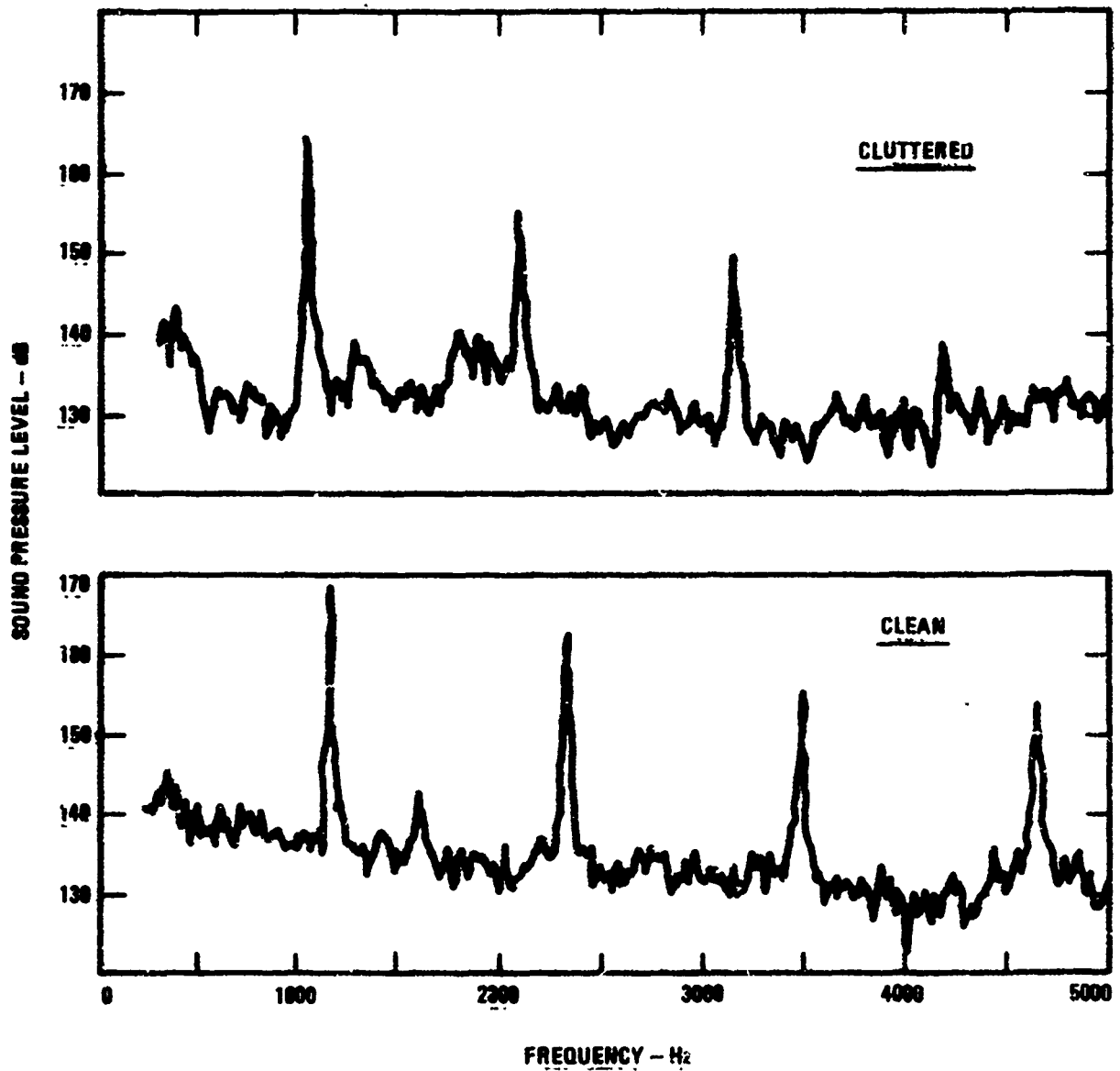


Figure 2.20. Typical measured sound pressure level in an unsuppressed cavity due to high speed flow over aperture obtained by model tests in wind tunnel.

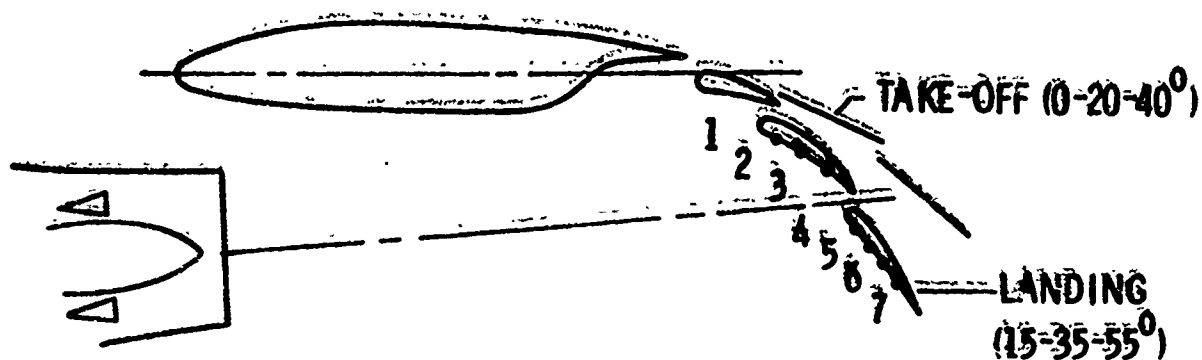
The noise levels vary with both position within the cavity and altitude, in addition to the above flow parameters. Methods for predicting these levels are contained in References [2.7] and [2.11]. These methods are basically empirical in nature. Consequently, the best method of obtaining the actual levels is to measure them either by means of scale model tests in a wind tunnel or on the actual hardware during flight tests. The noise levels in Figure 2.20 were obtained by such model tests [2.11] using both an empty (clean) cavity and one that included model missile clusters (cluttered) within the cavity.

The discrete frequency modes can be suppressed by the use of a variety of devices [2.10, 2.11] including perforated spoilers [2.23], usually at the expense of increasing the broadband noise. The model tests also provide a means of investigating the effectiveness of such devices [2.11].

2.3.5 Flow Impingement

High fluctuating pressure levels are generated when the jet exhaust impinges on a control surface edge or a flap. Typical fluctuating pressure levels, measured on the surface of externally blown three [2.6] and two flap [2.25] models directly behind the jet exhaust are summarized in Figures 2.21 and 2.22 respectively. The fluctuating pressure levels are expressed in dB's in Figure 2.21 and in terms of p_{rms} divided by the dynamic pressure q in Figure 2.22. The p_{rms}/q ratio of 0.066 to 0.126, directly in line with the jet exhaust, is comparable to that measured on rockets due to flow impingement (Figure 2.16).

The one-third-octave band spectra corresponding to the levels in Figure 2.22 are illustrated in Figure 2.23. The one-third-octave band fluctuating sound pressure levels have been normalized through division by the square of the dynamic pressure, and plotted against the nondimensional Strouhal number $D f/U$ where D is the bypass jet diameter, f is the frequency and U is core jet flow velocity. The above measurements were made for jet flow Mach numbers between 0.52 and 1.09. Significant acceleration levels can also be encountered on the flaps as illustrated in Figure 2.24 where the acceleration, in terms of g_{rms} , is plotted against jet flow Mach number.



Transducer	OAFPL in dB at Mach number of -									
	0.33	0.45	0.51	0.57	0.59	0.33	0.44	0.49	0.55	0.59
	Take-off flaps (0°-20°-40°)					Landing flaps (15°-35°-55°)				
1	149	155	156	158	159	150	156	158	160	162
2	151	157	159	160	161	148	154	156	159	160
3	152	158	60	162	163	148	153	155	157	159
4	149	154	156	159	160	146	152	153	156	157
5	145	150	152	155	156	147	152	154	156	156
6	143	148	150	152	153	148	154	155	156	157
7	144	149	151	---	154	148	153	155	157	157

Figure 2.21. Overall fluctuating pressure levels measured on the surface of an externally blown triple flap model.

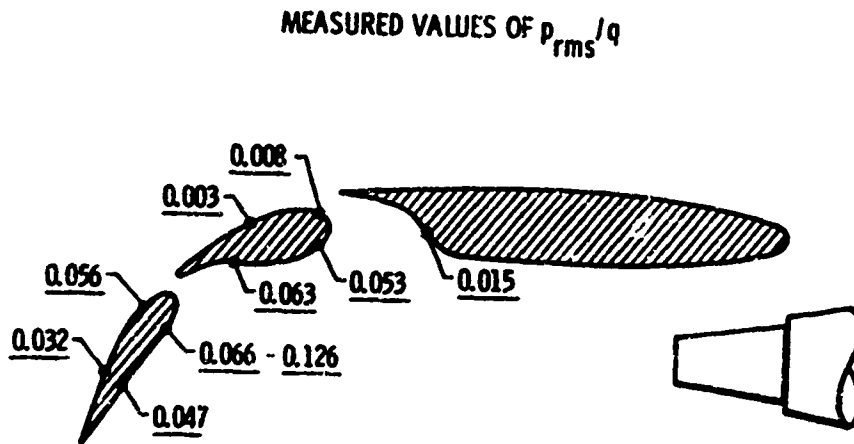


Figure 2.22. Typical p_{rms}/q ratios measured on externally blown double flap model.

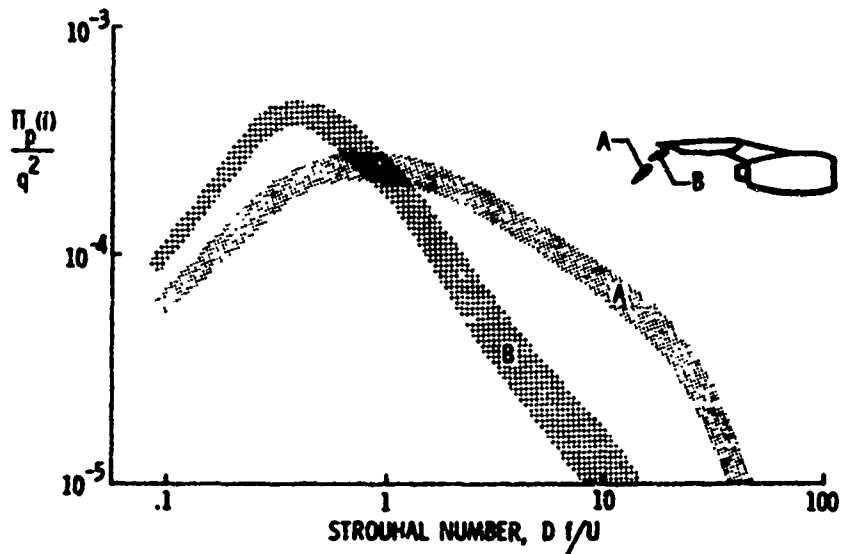


Figure 2.23. Third-octave normalized spectra for externally blown double flap model.

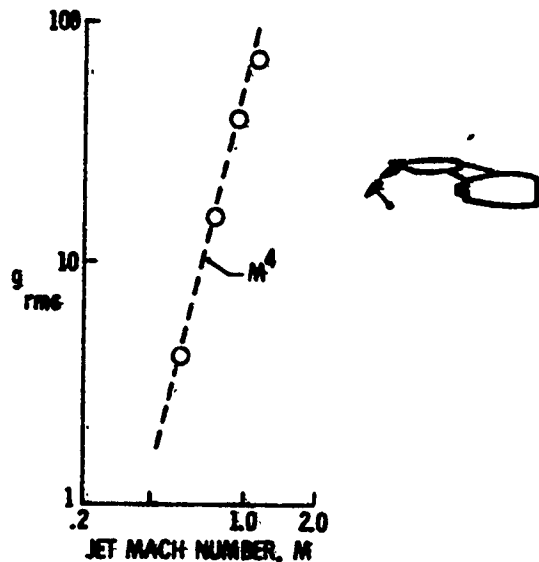


Figure 2.24. Root-mean-square acceleration level on outer flap as a function of jet mach number.

Upper surface blowing can produce overall fluctuating pressure levels on the adjacent fuselage structure of up to 160 dB. The levels on the curved flap can reach as high as 165 dB behind spoilers. These levels are discussed in more detail in References [2.6] and [2.12].

2.3.6 Fan Noise in Engine Inlet Ducts

The advent of the high by-pass ratio turbo-fan engine has been accompanied by a rapid rise in the noise level produced by the fan inside the engine intake duct. The intake duct noise has reached an intensity sufficient to produce failures in the intake duct structure. The noise field within the duct tends to be quite complex involving both duct acoustics and the pressure pulses generated by the blades.

The intake duct noise environment is a function of the fan diameter, the fan RPM, the fan blade tip Mach number and the density of the air. At low fan

speeds, the acoustic energy is concentrated at the fundamental blade passage frequency and its higher harmonics, as illustrated [2.18] in Figure 2.25 for a TF-34 engine, 8.3 inches (211 mm) from the fan face. The corresponding noise field acting on the duct structure, can be visualized as the sum of lobed circumferential pressure patterns, containing a predominant single positive and negative lobe per blade. These lobes are in phase throughout the length of the duct and rotate at the fan RPM. The intensity of the noise field decays rapidly with distance from the fan face.

When the blade tip speed exceeds Mach 1, shock waves with large crest factors are generated near the leading edge of the blades. The small differences in the geometry in each of the blades, produce shocks of unequal strengths. The stronger shocks travel faster than the weaker shocks which results in a progressively irregular circumferential pressure pattern, spiralling upstream at the fan RPM. The angle of the spiral increases with blade tip Mach number. The acoustic pressure falls off initially, within one blade chord with the inverse of the distance from the fan face raised to the power of one half and thereafter as the inverse of the distance. In long ducts a further change in the decay rate has been observed.

The spectral content in the fan noise is characterized by discrete frequency spikes at multiples of the individual blade rotational frequency, commonly referred to as buzz-saw. Figure 2.25. Once the blade tip speed exceeds Mach 1, propagation becomes possible at frequencies below the fundamental blade passage frequency. Each of the buzz-saw components has its own critical blade tip Mach number which must be exceeded if propagation is to take place.

The spectral content of the fan noise is dependent not only on the fan RPM but also on the variation of the speed of sound with temperature and, therefore, with altitude. The propagation of the first few buzz-saw components is only possible at altitude. Because of the differences in blade geometry from engine to engine, no two engines will have the same spectral content in the fan noise. If the blade tolerances can be improved, the spectrum level of the buzz-saw components will be considerably reduced and the noise energy will be concentrated more at the blade passage frequency and its higher harmonics.

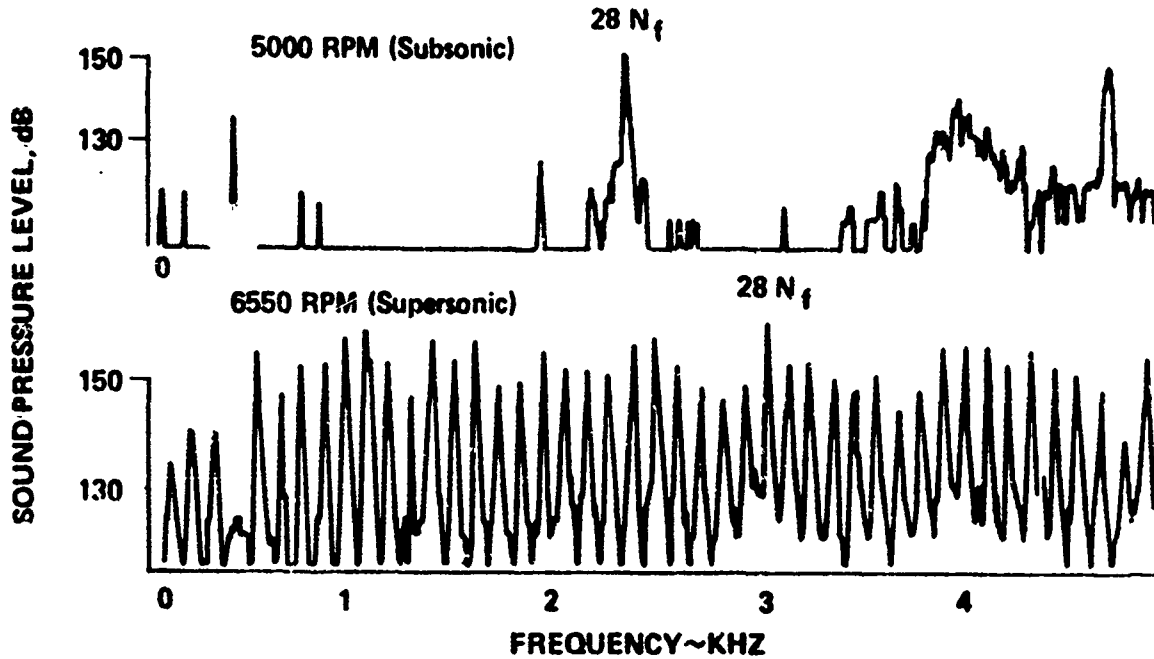


Figure 2.25. Typical narrowband spectra of intake duct fanblade noise at both subsonic and supersonic blade tip speeds.

Typical levels, measured [2.18] at various locations on the surface of the intake duct with flush mounted microphones, are illustrated in Figure 2.26 as a function of the fan revolutions per minute (RPM). The peak noise level occurs just below maximum fan RPM. The highest sound pressure level is encountered just ahead of the fan face. Since the closest measurement in Figure 2.26 of 175 dB OASPL was taken 5.625 inches (159 mm) from the fan face, it can be anticipated that the sound pressure level closer to the fan face can exceed 180 dB.

2.3.7 Propeller Noise

Propeller noise represents a significant source of discrete frequency excitation to the aircraft structure. Since most propellers operate at subsonic blade tip speeds, the acoustic energy is concentrated at the blade passage frequency (number of blades multiplied by the number of revolutions per second) and its higher harmonics. The highest noise levels are encountered at

SYMBOLS TYPICAL		KULITE No. 6, TF-34 IN TEST CELL
		KULITE No. 1, 18.08 INCHES AHEAD OF FAN BLADES
		KULITE No. 2, 8.31 INCHES AHEAD OF FAN BLADES
		KULITE No. 7, 8.31 INCHES AHEAD OF FAN BLADES
		TF-34 IN TEST CELL, BLADE PASSAGE FREQ. ($28N_f$)
		TF-34 IN TEST CELL, OVERALL LEVELS
		A-7 DATA OVERALL LEVELS 5-5/8 IN. FWD OF FAN

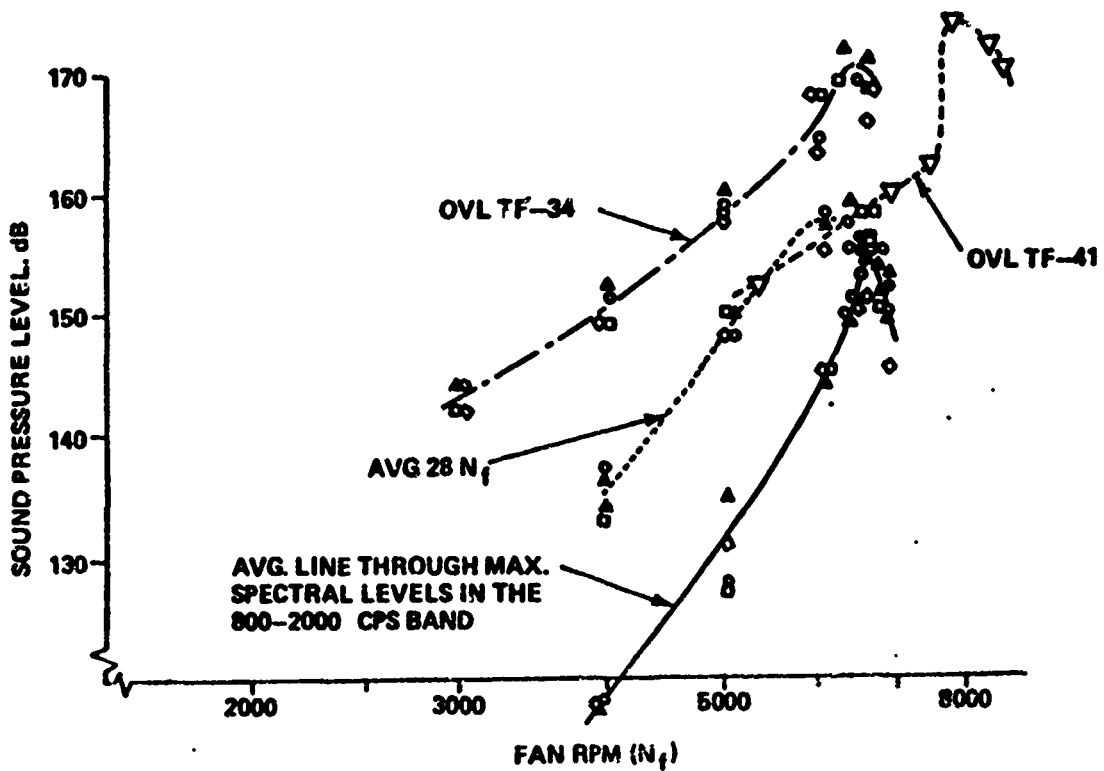


Figure 2.26. Typical sound pressure levels measured in engine inlet ducts.

the blade passage frequency which is typically around 68 Hz for a large four-engined transport aircraft with constant speed four-bladed propellers.

Methods for predicting the propeller noise are summarized in Reference [2.18]. The propeller noise level on the aircraft fuselage structure is a function of the shaft horse power (Figure 2.27), the number of propeller blades, blade tip Mach number, separation distance from the fuselage to blade tip, pressure "doubling" effect of the structure and distance from the propeller plane since the maximum noise levels are encountered in the propeller plane. Each of the above parameters produces a correction factor [2.18] that needs to be applied to the basic noise level in Figure 2.27.

Advanced sculptured propeller blades, with up to eight blades per propeller, are currently being studied for potential use on aircraft flying at speeds approaching Mach 0.8. Of all the potential configurations, contra rotating pusher propellers with sculptured blades appears to be attractive from many design considerations. However, this configuration is expected [2.26] to produce the highest noise levels on the structure. Noise levels of 165 dB in the vicinity of the propeller plane and unique pressure distribution patterns along the fuselage will probably be encountered. The highest noise levels may be in fact encountered during flight at cruising altitude, where the blade tips reach the highest Mach number, rather than at takeoff.

2.3.8 Over-pressure from Gunfire

The over-pressure produced by gunfire is a source of structural excitation in the vicinity of the nozzle. The magnitude of the loading depends on the weapon characteristics. Methods for estimating the vibration environment produced by the gunfire is given in References [2.6] and [2.7].

2.4 SOUND PRESSURE LEVEL CONVERSIONS

The overall sound pressure level, the level in octave and one-third-octave bands and the level in a narrow band spectrum, which is not divided by the analysis bandwidth, are usually expressed in dB. The narrow band spectrum is used to present the data when both discrete frequency and broadband random noise are present in the spectrum. Alternatively, when the noise is broadband

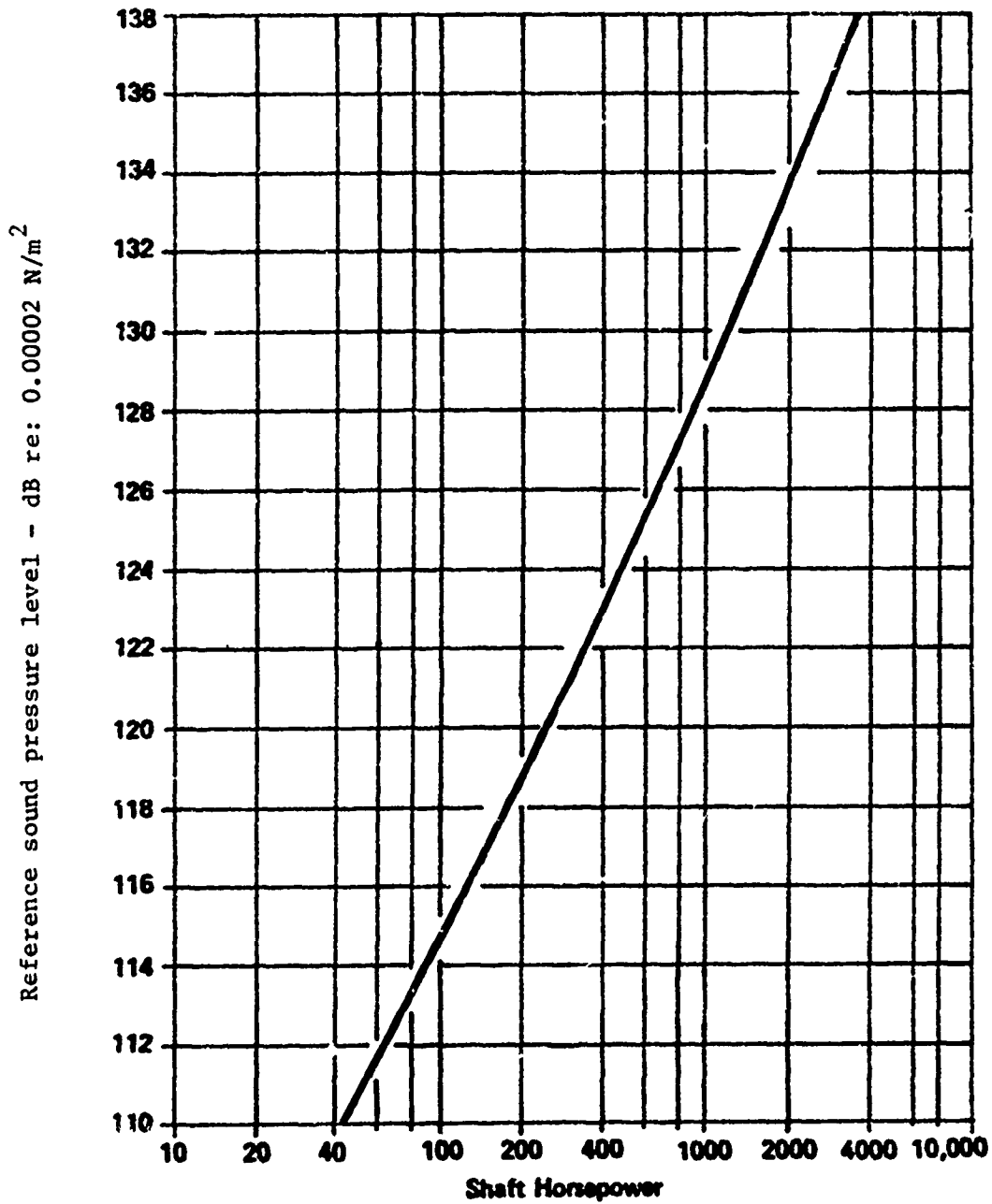


Figure 2.27. Reference sound pressure level produced by a four bladed propeller as function of shaft horse power.

random, the noise can be presented in the form of power spectral density (PSD) expressed in dB/Hz. The PSD is obtained by means of narrow band analysis in which the sound pressure level in each band is divided by the analysis bandwidth.

In order to apply these noise levels, it is often necessary to convert the noise levels from dB or dB/Hz into rms sound pressure or rms sound pressure squared per Hertz, respectively. This conversion can be accomplished by the use of Figure 2.28. For example, an overall sound pressure level of 170.75 dB converts into an rms pressure level of 1 psi or $6.9 \times 10^3 \text{ N/m}^2$. The equations for these conversions are

$$\text{SPL dB} = 20 \left\{ \text{LOG}_{10} p_{\text{rms}} \right\} + 170.75 \quad (2.10)$$

when p_{rms} is expressed in psi, and

$$\text{SPL dR} = 20 \left\{ \text{LOG}_{10} p_{\text{rms}} \right\} + 93.98 \quad (2.11)$$

when p_{rms} is expressed in N/m^2 .

In order to convert the PSD of 130.75 dB/Hz into sound pressure in psi^2/Hz , first convert 130.75 dB into psi rms and square this number. Therefore 130.75 dB/Hz is equivalent to $(.01)^2 \text{ psi}^2/\text{Hz} = .0001 \text{ psi}^2/\text{Hz}$.

Often the sound pressure level is expressed in octave or one-third-octave bands. A standard set of these bands are summarized in Table 2.2. These bands are defined by the following relationships:

- Octave band:

center frequency	f
upper frequency limit	$f \sqrt{2}$
lower frequency limit	$f \sqrt{2}/2$
bandwidth - Δf	$f \sqrt{2}/2$

- One-third-octave band

center frequency	f
upper frequency limit	$f(2)^{1/6}$

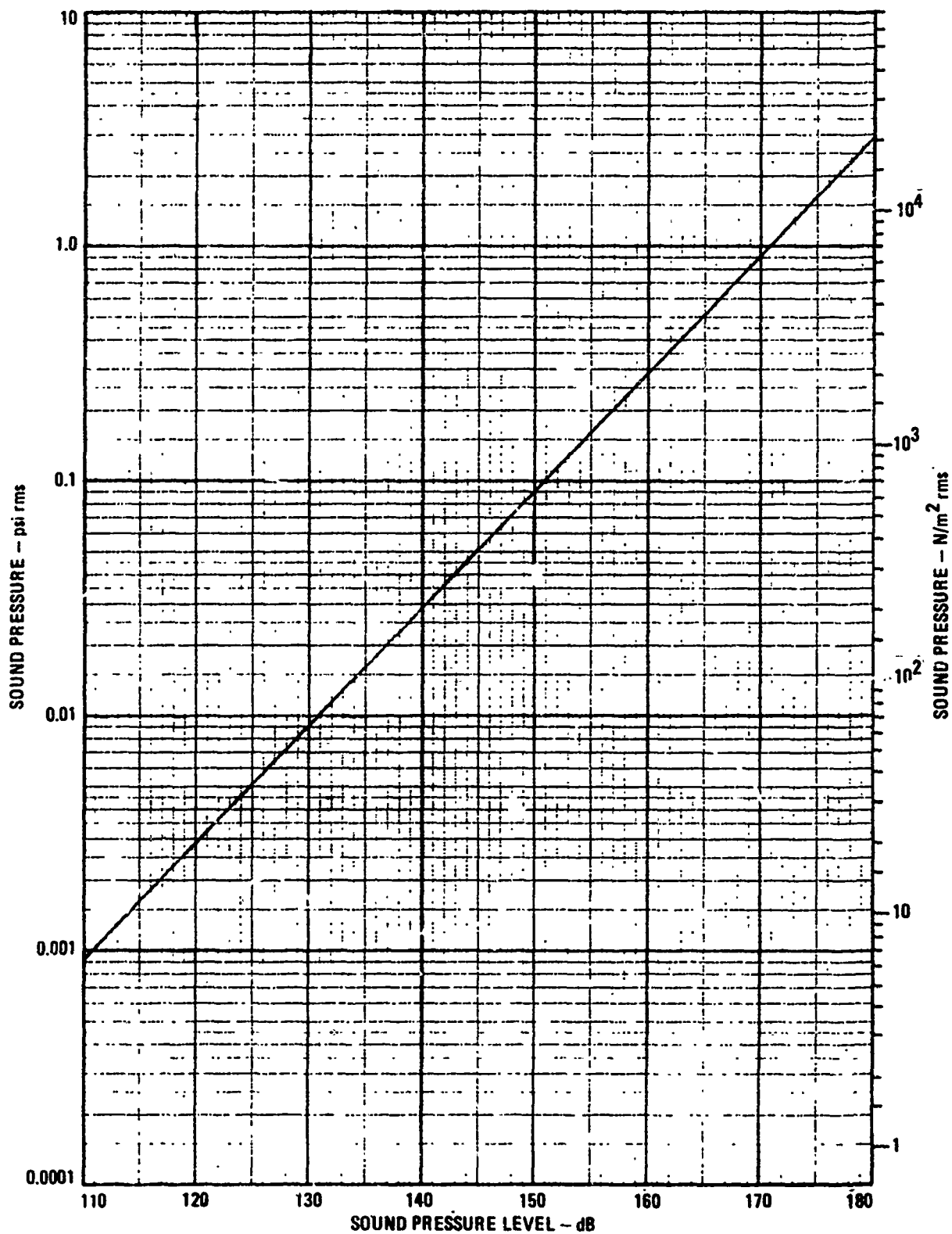


Figure 2.28. Conversion of sound pressure level in dB to sound pressure in psi rms or N/m².

TABLE 2.2. CENTER AND APPROXIMATE BAND FREQUENCIES FOR STANDARD SET OF OCTAVE AND ONE-THIRD-OCTAVE BANDS COVERING THE AUDIO FREQUENCY RANGE

Frequency, Hz					
Octave			One-third octave		
Lower band limit	Center	Upper band limit	Lower band limit	Center	Upper band limit
11	16	22	14.1	16	17.8
			17.8	20	22.4
			22.4	25	28.2
22	31.5	44	28.2	31.5	35.5
			35.5	40	44.7
			44.7	50	56.2
44	63	88	56.2	63	70.8
			70.8	80	89.1
			89.1	100	112
88	125	177	112	125	141
			141	160	178
			178	200	224
177	250	355	224	250	282
			282	315	355
			355	400	447
355	500	710	447	500	562
			562	630	708
			708	800	891
710	1,000	1,420	891	1,000	1,122
			1,122	1,250	1,413
			1,413	1,600	1,778
1,420	2,000	2,840	1,778	2,000	2,239
			2,239	2,500	2,818
			2,818	3,150	3,548
2,840	4,000	5,680	3,548	4,000	4,467
			4,467	5,000	5,623
			5,623	6,300	7,079
5,680	8,000	11,360	7,079	8,000	8,913
			8,913	10,000	11,220
			11,220	12,500	14,130
11,360	16,000	22,720	14,130	16,000	17,780
			17,780	20,000	22,390

$$\begin{array}{ll} \text{lower frequency limit} & f(2)^{-1/6} \\ \text{bandwidth} - \Delta f & f\{(2)^{1/6} - (2)^{-1/6}\} \end{array}$$

The octave or the one-third-octave levels, $\bar{G}(f)$, in dB, can be converted into average power spectral density, $G(f)$, in $p_{\text{rms}}^2/\text{Hz}$, by

- (1) converting $\bar{G}(f)$ into sound pressure $p_{\text{rms}}(f)$ using Figure 2.28
- (2) then $G(f)$ in $p_{\text{rms}}^2/\text{Hz}$ is simply

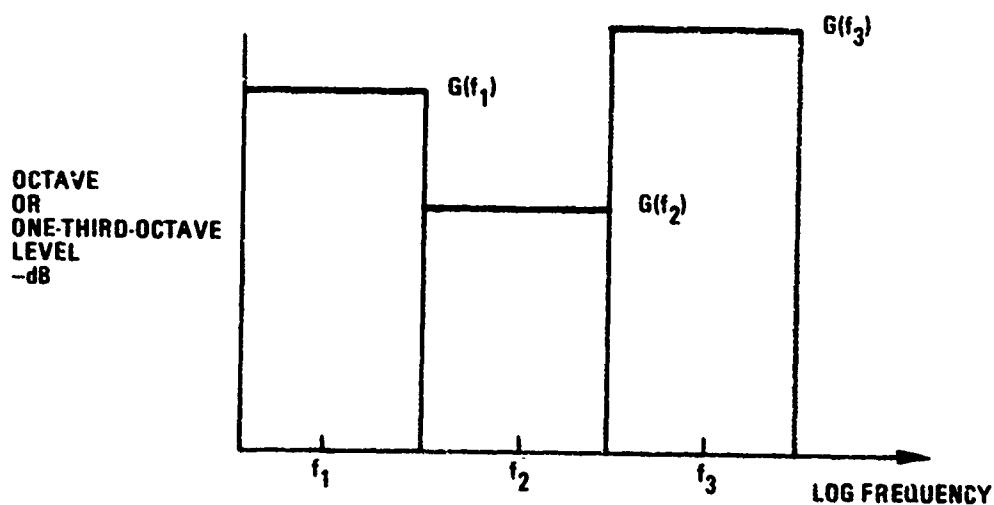
$$G(f) = p_{\text{rms}}^2(f)/\Delta f \quad (2.12)$$

where Δf is the octave or one-third-octave bandwidth. Alternatively, the octave or one-third-octave level in dB can be converted to average power spectral density $\hat{G}(f)$ in dB/Hz by the following relationship

$$\hat{G}(f) = \bar{G}(f) - 10 \text{ LOG}_{10} \Delta f \quad (2.13)$$

The $10 \text{ LOG}_{10} \Delta f$ term can also be obtained from Figure 2.29.

The octave and one-third-octave levels can be converted to overall sound pressure levels by the following procedure:



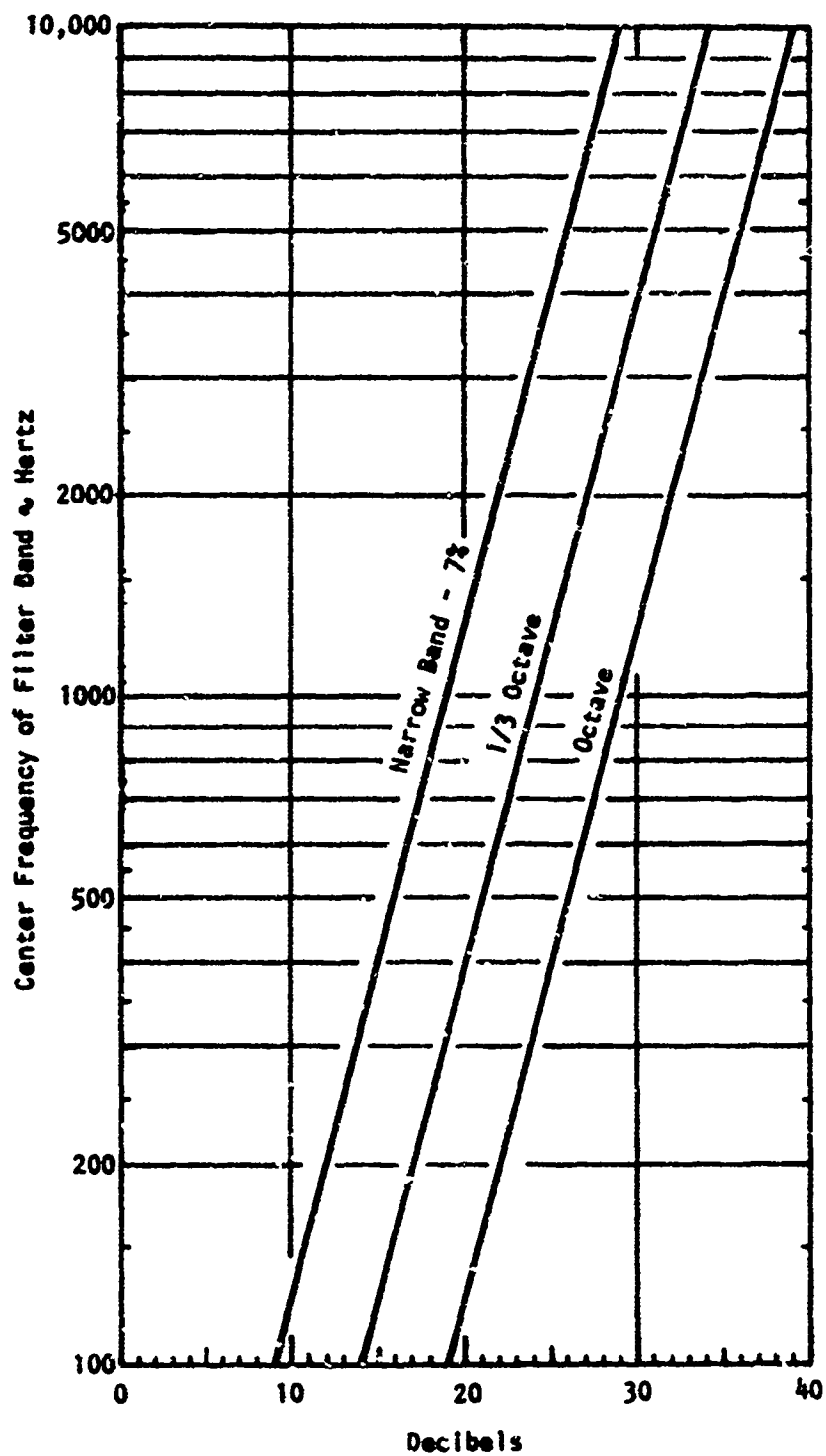
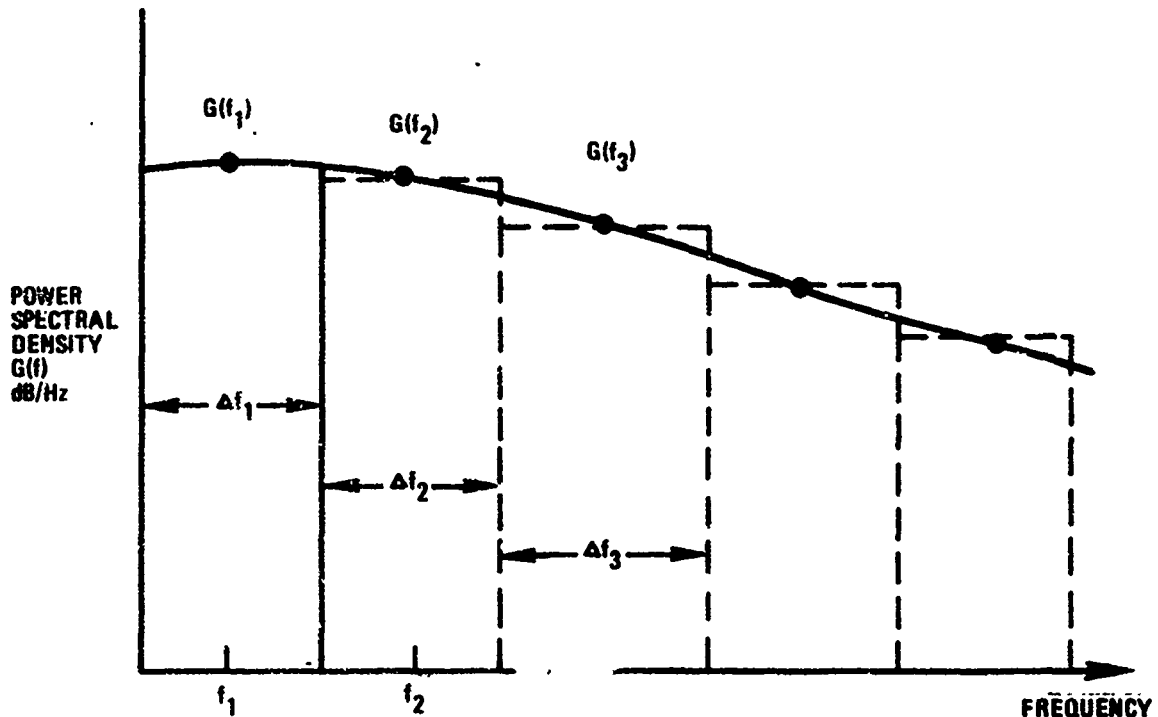


Figure 2.29. Number of decibels to be subtracted from sound pressure level reading to convert octave, 1/3 octave and narrow band (7%) to spectrum level in decibels.

- (1) Convert octave or one-third-octave levels $\bar{G}(f_1)$, $\bar{G}(f_2)$, $\bar{G}(f_3)$, ... to p_{rms} levels, that is $p(f_1)$, $p(f_2)$, $p(f_3)$, ... using Figure 2.28
- (2) The OASPL in dB = $10 \text{ LOG}_{10}(p^2(f_1) + p^2(f_2) + p^2(f_3) + \dots)$

The overall sound pressure level in dB can be calculated from the power spectral density $G(f)$ in dB/Hz by the following procedure:



- (1) Select suitably small bandwidths Δf_1 , Δf_2 , Δf_3 , ... with center frequencies f_1 , f_2 , f_3 , ... such that spectrum does not vary too much within the band.
- (2) Convert each corresponding PSD levels $G(f_1)$, $G(f_2)$, $G(f_3)$, ... into p_{rms} , that is $p(f_1)$, $p(f_2)$, $p(f_3)$, ... using Figure 2.28.
- (3) The OASPL in dB = $10 \text{ LOG}_{10}(p^2(f_1) \cdot \Delta f_1 + p^2(f_2) \cdot \Delta f_2 + p^2(f_3) \cdot \Delta f_3 + \dots)$

Aerodynamically produced fluctuating pressures are often expressed in terms of p_{rms}/q , where q is the dynamic pressure. The dynamic pressure for a standard atmosphere is given in Figure 2.30 as a function of both altitude and Mach number. Using the dynamic pressure from Figure 2.30, and knowing the p_{rms}/q ratio, the root mean square fluctuating pressure, p_{rms} , can be readily calculated.

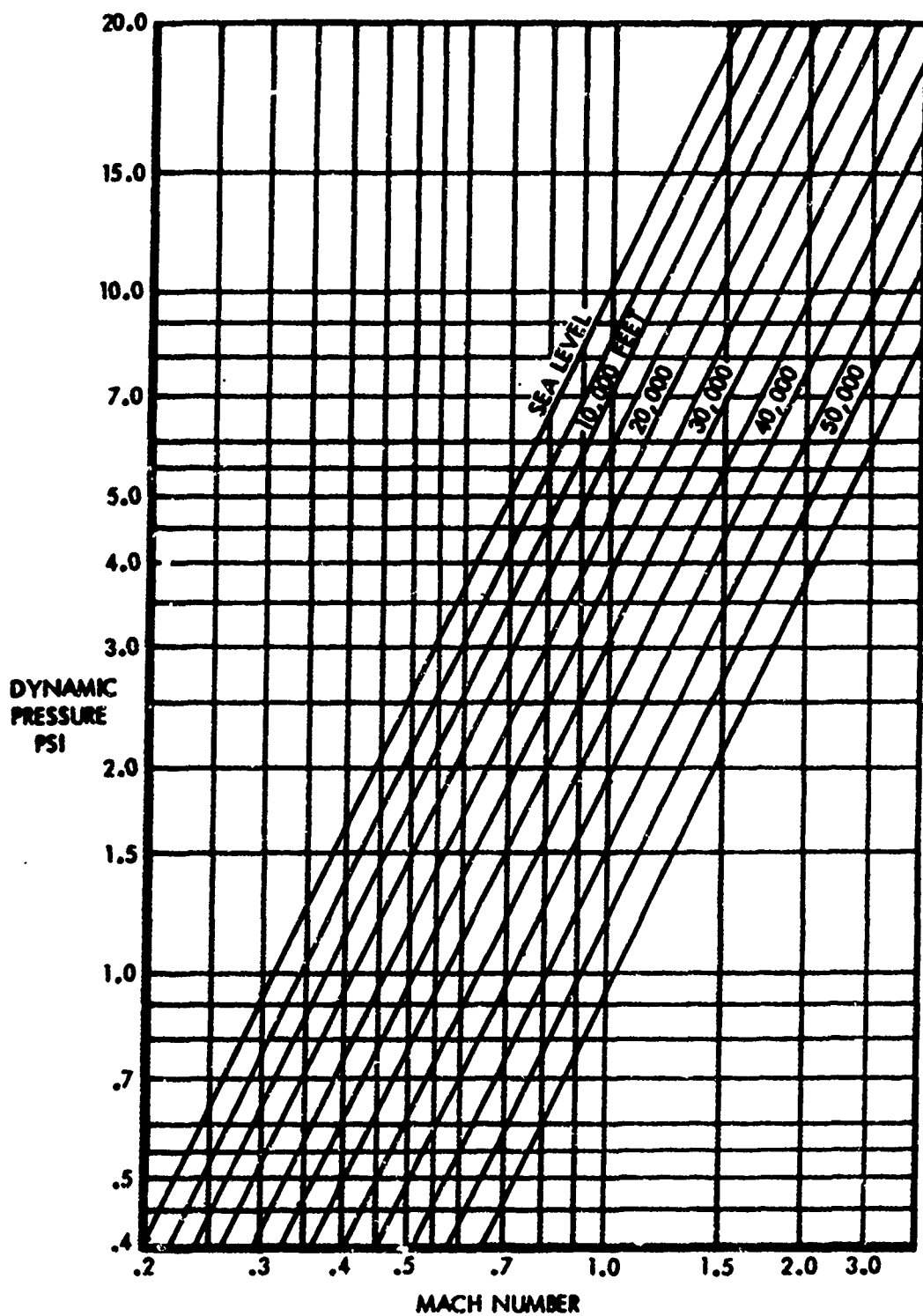


Figure 2.30. Free stream dynamic pressure, standard atmosphere.

REFERENCES

- 2.1 Eldred, K., Roberts, W. and White, R., "Structural Vibrations in Space Vehicles", WADD Technical Report 61-62, December 1961.
- 2.2 Lyon, R.H. "Random Noise and Vibration in Space Vehicles", SVM-1, 1967.
- 2.3 Meltzer, E.C., "Compilation of Shock and Vibration Flight Data from Eight Thor-Related Vehicles" NASA CR-196, March 1965.
- 2.4 Clevenson, S.A., "Lunar Orbiter Flight Vibration Data and Comparisons with Environmental Specifications", NASA TN D-6006, September 1970.
- 2.5 Klein, G.H. and Piersol, A.G., "Development of Vibration Test Specifications for Spacecraft Applications", NASA CR-234, May 1965.
- 2.6 Ungar, E.E., Wilby, J.F. and Bliss, D.B., "A Guide for Estimation of Aeroacoustic Loads on Flight Vehicle Surfaces", AFFDL-TR-76-91, Volume 1, February 1977.
- 2.7 Ungar, E.E., Wilby, J.F. and Bliss, D.B., "A Review of Methods for Estimation of Aeroacoustic Loads on Flight Vehicles Surfaces", AFFDL-TR-76-91, Volume 11, February 1977.
- 2.8 Sutherland, L.C. and Brown, D., "Prediction Methods for Near Field Noise Environments of VSTOL Aircraft", AFFDL-TR-71-180, May 1972.
- 2.9 Potter, R.C., and Crocker, M.J., "Acoustic Prediction Methods for Rocket Engines, Including the Effects of Clustered Engines and Deflected Flow", NASA CR-566, October 1966.
- 2.10 Shaw, L.L., "Suppression of Aerodynamically Induced Cavity Pressure Oscillations", AFFDL-TR-79-3119, November 1979.
- 2.11 Bartel, H.W. and Mc Avoy, J.M., "Cavity Oscillations in Cruise Missile Carrier Aircraft", AFWAL-TR-81-3036, June 1981.
- 2.12 Doherty, C.S. and Butzel, L.M., "STOL Aircraft Structural Vibration Prediction Methods," AFFDL-TR-79-3111, Volumes I and II, August 1979.
- 2.13 Himmelblau, H., Fuller, C.M., and Scharton T.D., "Assessment of Space Vehicle Aeroacoustic - Vibration Prediction, Design and Testing."
- 2.14 Barnoski, R.L., Piersol, A.G., et al, "Summary of Random Vibration Prediction Procedures", NASA CR-1302, April 1969.

- 2.15 Bartel, H.W. and Schneider, C.W., "A Method for Predicting Acoustically Induced Vibration in Transport Aircraft", AFFDL-TR-74-74, Appendix 1, September 1974.
- 2.16 Bartel, H.W. and Schneider, C.W., "Acoustically Induced Vibration in Transport Category Aircraft", AFFDL-TR-74-74, September 1974.
- 2.17 Chaump, L.E., Lanzon, J.H. and Minnich, H.R., "Vibration Response of Ballistic Re-Entry Vehicles", AFFDL-TR-72-140, Volumes 1 and 11, April 1973.
- 2.18 Rudder, F.F. and Plumblee, H.E., "Sonic Fatigue Design Guide for Military Aircraft", AFFDL-TR-74-112, May 1975.
- 2.19 Wolfe, H.F. and Holehouse, I., "Durability of Bonded Structures Subjected to Acoustic Loads", AGARD-R-701, December 1981.
- 2.20 Morgan, W.V., Sutherland, L.C. and Young, K.J., "The Use of Acoustic Scale Models for Investigating Near Field Noise of Jets and Rocket Engines", WADD Technical Report 61-178, April 1961.
- 2.21 Dougherty, N.S. and Guest, S.H., "A Correlation of Scale Model and Flight Aeroacoustic Data for the Space Shuttle Vehicle", Paper AIAA-84-2351, AIAA/NASA 9th Aeroacoustic Conference, Williamsburg, Virginia, October 15-17, 1984.
- 2.22 Mahaffey, P. T. and Smith, K.W., "Methods for Predicting Environmental Vibration Levels in Jet Powered Vehicles", Noise Control, Vol. 6, No. 4, July 1960.
- 2.23 Buell, D.A., "An Experimental Investigation of the Airflow Over a Cavity with Antiresonance Devices", NASA TND-6205, 1971.
- 2.24 La Barge, W.L., "Experimental Evaluation of the Sonic Fatigue Resistance of Structure of a Modified C-141 Airplane Structure", Contract Report Prepared by Lockheed-California Company for NASA AMES under Contract NAS 2-7644, October 1973.
- 2.25 Lansing, D.L., Drischler, J.A., Brown, T.J. and Mixson, J.S., "Dynamic Loading of Aircraft Surfaces Due to Exhaust Impingement", AGARD-CP-113, May 1973.
- 2.26 Block, P. J. W., "The Effects of Installation on Single- and Counter-Rotation Propeller Noise", Paper AIAA-84-2263 presented at AIAA/NASA 9th Aeroacoustics Conference, in Williamsburg, Virginia, October 15-17, 1984.

SECTION 3

STRUCTURAL VIBRATION RESPONSE EQUATIONS

3.1 INTRODUCTION

The purpose of this section is to provide a list of equations describing the vibration response of simple structures for quick reference purposes. These equations include expressions for the natural frequency, the mode shape and the vibration response to harmonic and random excitation, taken from existing literature. Graphic representation is also used in some instances. The types of structures included in this list are the damped spring mass system, beams, plates and shells. The intention is to provide equations compatible with the equations available in Section 5, for use in the preliminary design of damping treatments.

There are many References [3.1, 3.2, 3.3] for describing the vibration response of beams, plates and shells. The intention is not to include all of the equations contained in even these few references. The equations in this section have been selected on the basis of simplicity and include approximations to more accurate but also more complex equations. Even complex structures can be analyzed by simple equations or even modeled by lumped mass-spring systems. For example, the edge conditions for flat and curved plates, stiffened by open section stringers and frames, fall somewhere between simply supported and fully fixed for the fundamental stringer torsion mode, but tend toward the simply support edge conditions for the higher modes. Thus the simply supported plate analysis provides a reasonable approximation to this stiffened plate. A fixed plate analysis can be performed to provide the upper bound. A more accurate result can be obtained by applying an empirically derived correction factor to the simply supported plate equation [3.4, 3.5]. The curved plate analysis can be reduced to a flat plate analysis provided certain terms are added to account for the effects of curvature [3.6]. Thus considerable design effort can be avoided by bounding the problem through the use of simplified analysis before embarking on a more detailed analysis.

All of the equations in this section are expressed in terms of the viscous damping ratio, ζ , which is the ratio of the viscous damping coefficient, C , to the critical viscous damping coefficient, C_c . The loss factor, η , is also used in vibration analysis. The relationship between ζ and η is simply

$$\eta = 2\zeta \quad (3.1)$$

The viscous damping ratio is also assumed to be small compared to unity. This assumption is valid for most aerospace structures. Linear structural response is assumed throughout this section. Table 3.1 is a list of the symbols used in this section.

3.2 SPRING-MASS-DAMPER SYSTEM

3.2.1 Single Spring-Mass-Damper System

The single spring-mass-damper system is also known as the single degree-of-freedom (SDOF) system, and is illustrated in Figure 3.1. This section describes the free and forced response of the linear SDOF system, the latter due to both harmonic and random excitation, at the mass and at the base.

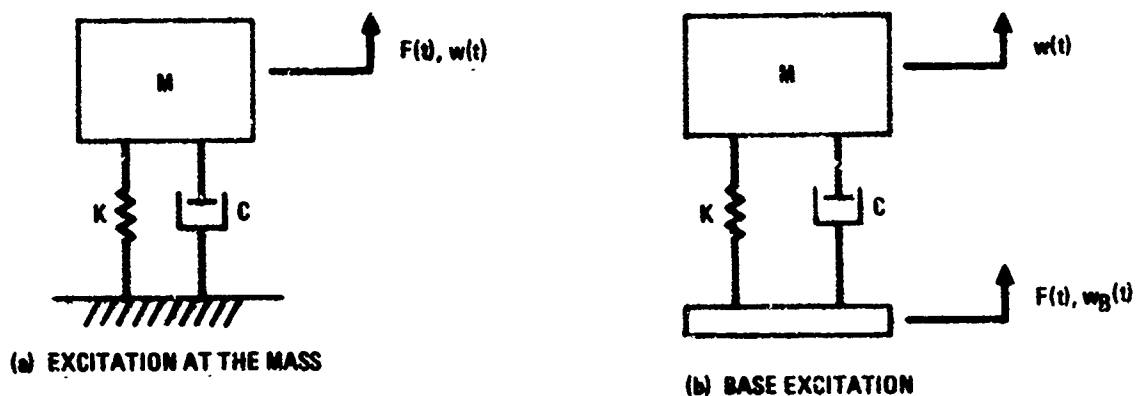


Figure 3.1 Single spring-mass-damper system.

TABLE 3.1 LIST OF SYMBOLS

SYMBOL	DEFINITION	LOCATION*
a	Plate length	3.30, 3.35-3.48, F3.3, T3.15
a	Length of straight side of open circular cylindrical shell	3.49-3.55, 3.66
a	Diameter of circular plate or side of square plate	T3.13
a	Overall length of honeycomb panel	3.57, 3.58, 3.60
A	Aspect ratio (a/b)	T3.12
\bar{A}	Beam cross-sectional area	3.15, 3.25, T3.11
b	Plate width	3.28, 3.30, 3.35-3.48, F3.3, T3.15
b	Stringer pitch for stiffened panel structure	3.31, F3.4
b	Arc length of open circular cylindrical shell	3.51-3.55, 3.66, F3.2
b	Overall width of honeycomb panel	3.56-3.58, 3.60, 3.65
b_1	Honeycomb panel inner face sheet width	3.62, 3.64
B	Frequency parameter. Equal to $P/\sqrt{12}$	T3.13
B_1	Numerator of transmissibility, T	T3.2
B_2	Denominator of transmissibility, T	T3.2
c	Speed of sound in air	3.60
C	Damping coefficient for linear SDOF system	T3.2
D	Flexural rigidity	3.28, 3.29, 3.35-3.42, 3.51

* x.xx Equation, Tx.xx Table, Fx.xx Figure

TABLE 3.1. LIST OF SYMBOLS (CONTINUED)

SYMBOL	DEFINITION	LOCATION*
D	Flexural rigidity per unit width of the skin plate, $Et^3/12(1-\nu^2)$	3.33
D	Stiffness parameter	3.67
E	Young's modulus	3.15, 3.16, 3.29, 3.32, 3.51-3.53, 3.55, 3.58, 3.63, 3.68, T3.9, T3.10, T3.13, F3.3
E^*	$E(1 - \nu^2)$	3.66
E	Young's modulus of the face sheets	3.63, 3.64
E_p	Young's modulus of the closeout plan	3.64
E_s	Young's modulus of stringer material	3.33
f	Frequency of harmonic driving excitation	3.7, 3.8, 3.10-3.12, 3.19, 3.20, T3.2
f_{CC}^n	Natural frequency for clamped-clamped beam	T3.6, T3.8
f_{CF}^n	Natural frequency for clamped-fixed beam	T3.6, T3.8
f_{CS}^n	Natural frequency for clamped-simple beam	T3.6, T3.8
f_{SF}^n	Natural frequency for simple-fixed beam	T3.6
f_{SS}^n	Natural frequency for simple-simple beam	T3.6
f_n	Natural frequency	3.2, 3.7, 3.8, 3.10, 3.11, 3.15, 3.25, 3.27, 3.28, 3.31, T3.6, T3.15

* x.xx Equation, Tx.xx Table, Fx.xx Figure

TABLE 3.1. LIST OF SYMBOLS (CONTINUED)

SYMBOL	DEFINITION	LOCATION*
f_r	Natural frequency of r^{th} normal mode	3.19, 3.20
f_{11}	Fundamental mode natural frequency of plate	F3.3
F	Driving force for forced vibration	3.7
\bar{F}	Dimensionless frequency parameter	3.28, T3.8, T3.12
F_o	Load per unit length for uniformly loaded beam	T3.11
$F(\star)$, $F(\xi)$	Force per unit length	3.24
G	Shear modulus of honeycomb panel core	3.63
G_B	Power spectral density of base displacement	3.14
G_F	Power spectral density of applied force	3.13, 3.25
$G_F(f)$	Power spectral density of applied force	3.12
G_p	Power spectral density of pressure excitation	3.60
$G_p(f_{11})$	Power spectral density of applied pressure loading, at frequency corresponding to fundamental mode of plate	3.35-3.42, 3.55
G_s	Shear modulus of stringer material	3.33
$G_w(f)$	Power spectral density of the response	3.12
h	Plate thickness	3.29, 3.35-3.42, 3.51-3.55, 3.66, F3.3, T3.13
h	Honeycomb panel core thickness	3.56, 3.58-3.60, 3.63, 3.64, F3.14
h^*	Rise of open circular cylindrical shell	F3.12
$H(f)$	Transfer function	3.12

* x.xx Equation, Tx.xx Table, Fx.xx Figure

TABLE 3.1. LIST OF SYMBOLS (CONTINUED)

SYMBOL	DEFINITION	LOCATION*
I	Area moment of inertia of beam cross section	3.15, 3.16, T3.9, T3.10
I_s	Polar moment of inertia of stringer cross section about point or skin directly beneath shear center of stringer	3.33
J_s	St. Venant constant of uniform torsion for stringer cross section	3.33
K	Spring stiffness for linear SDOF system	3.2, 3.7, T3.2
K	Frequency parameter	3.31
K	Frequency constant for honeycomb panels	3.56, T3.15
K_r	Generalized stiffness for r^{th} normal mode	3.19, 3.22
K_R	Stringer non-dimensional torsional stiffness	3.33
l	Beam length	3.15, 3.25, T3.9-T3.11
l	Length of solid honeycomb panel edge	3.65
L_r	Generalized force for r^{th} normal mode	3.19, T3.11, T3.15
m	Mass of concentrated mass on a beam	T3.9, T3.10
m	Concentrated mass on center of massless circular plate	T3.13
m	Number of half-waves across frame pitch for stiffened panel structure	F3.6-F3.11
m	Number of axial half-waves for cylindrical shell	F3.19
m_b	Total mass of beam	T3.10
M	Mass of linear SDOF system	3.2, 3.13, T3.2
\tilde{M}	Honeycomb panel mass per unit area	3.58-3.60

* x.xx Equation, Tx.xx Table, Fx.xx Figure

TABLE 3.1. LIST OF SYMBOLS (CONTINUED)

SYMBOL	DEFINITION	LOCATION*
MF	Magnification factor for forced vibration of linear SDOF system. Ratio of dynamic displacement to static displacement	3.7
M_1	Mode parameter for first group of natural frequencies for stiffened panel structure	3.14
M_r	Generalized mass for r^{th} normal mode	3.22, T3.11, T3.15
n	Number of circumferential waves for cylindrical shell	F3.19
n	Mode number (parallel to y axis)	3.61, 3.65
N	Number of panels for stiffened panel structure	3.34, T3.14
p	Uniform normal pressure on cylindrical shell, positive inward	3.67
P_0	Uniform pressure loading	T3.15
P	Axial load on shell boundary per unit distance	3.67
PTS	Pinned-end condition with torsional spring	T3.7
q_1	Non-dimensional pressure parameter	3.67
q_{10}	Value of q_1 for buckling due to external pressure	3.67
q_2	Non-dimensional axial load parameter	3.67
q_{20}	Value of q_2 for buckling due to axial load	3.67
q_{r0}	Amplitude of $q_r(t)$	3.19
$q_r(t)$	Generalized displacement of r^{th} normal mode	3.19, 3.21, 3.34
\bar{Q}	Beam end condition parameter	T3.6, T3.7
r	Mode number	T3.14

* x.xx Equation, Tx.xx Table, Fx.xx Figure

TABLE 3.1. LIST OF SYMBOLS (CONTINUED)

SYMBOL	DEFINITION	LOCATION [*]
$r(x,y)$	Mode shape of plate as function of position	3.30
R	Radius of cylindrical shell	3.49, 3.51-3.54, F3.12
s	Width of the solid panel edges	3.57
t	Thickness of plate	T3.13
z	Skin thickness, stiffened panel structure	3.31
t	Thickness of inner and outer face sheets	3.58-3.60, 36.3, 3.64, F3.14, 3.56
t	Time	3.3, 3.9, 3.21
t_{ad}	Adhesive film thickness	3.59
t_p	Thickness of closeout plan	3.64
T	Transmissibility. For linear SDOF system, T is the ratio of output (mass motion) to input (base motion) where both quantities are harmonic displacement, velocity or acceleration	3.9
T	Beam end torsional spring constant	3.16
T^*	Nondimensional beam end torsional spring stiffness	3.16
V	Velocity factor	3.31, 3.32
w_0	Initial displacement of mass for subsequent free decay	3.3, 3.6, 3.7
w_B	Amplitude of harmonic base displacement excitation	3.9
w_n	Modal intensity for the n^{th} bending mode	3.65
$w_1(x)$	Fundamental beam mode shape	T3.11

* x.xx Equation, Tx.xx Table, Fx.xx Figure

TABLE 3.1. LIST OF SYMBOLS (CONTINUED)

SYMBOL	DEFINITION	LOCATION*
$W(x,t)$	Beam displacement	3.21
$W(\xi)$	Beam mode shape	T3.4, T3.8
$w_r(x),$ $w_r(\xi)$	r^{th} mode shape	3.21
\bar{w}^2	Mean-square displacement	3.12-3.14
$\bar{w}^2(x)$	Mean-square displacement of a beam	3.25
$w(\xi,t)$	Mode shape	3.21
x	Distance along beam	T3.11
α	Vertex half-angle for conical shell	F3.26
β	Eigenvalue for the beam	3.15, T3.3 T3.4, T3.8
γ	Parameter used to calculate $w(\xi)$	T3.4, T3.8
γ	Density parameter	3.68
Γ_s	Warping constant of stringer cross section with respect to the point on skin directly below shear center of stringer	3.33
δ_r	Viscous damping ratio	3.60
ϵ_{ycl}	Inner face sheet strain at honeycomb panel center	3.60
ζ	Damping ratio, actual damping divided by critical damping	3.3-3.5, 3.7, 3.8, 3.10, 3.11, 3.13, 3.14, 3.25, 3.27 T3.2
ζ_r	Damping ratio for r^{th} normal mode	3.19 3.20
ζ_{11}	Damping ratio for the fundamental mode	3.35-3.42, 3.55

* x.xx Equation, Tx.xx Table, Fx.xx Figure

TABLE 3.1. LIST OF SYMBOLS (CONTINUED)

SYMBOL	DEFINITION	LOCATION*
μ	Plate mass per unit area	3.28
$\mu(x)$	Mass per unit length	3.24
ν	Poisson's ratio	3.29, 3.36-3.38, 3.44, 3.45, 3.58 3.66, 3.68, F3 3, T3.4, T3.13
ξ	Nondimensional distance along beam	T3.8, T3.4
ρ	Material density	3.15, 3.25, 3.32 3.35-3.42, 3.51-3.53, 3.55, 3.66, 3.68, T3.11, T3.13, T3.15
ρ_{ad}	Adhesive film density	3.59
ρ_c	Honeycomb panel core density	3.59
ρ_f	Honeycomb panel face sheet density	3.59
ρ_s	Density of stringer material	3.33
σ_0	Stress at point of interest	3.27
$\overline{\sigma^2}$	Mean-square stress	3.27
ϕ	Phase angle defining lag of free decay response relative to a pure cosine curve	3.3, 3.4, 3.7, 3.8
ϕ	Included arc angle of open circular cylindrical shell	3.49, 3.50, F3.12
χ	Angle of beveled edge of honeycomb core	3.62, 3.64, F3.14
ψ	Phase angle between input and response for SDOF system	3.9, 3.11

* x.xx Equation, Tx.xx Table, Fx.xx Figure

TABLE 3.1. LIST OF SYMBOLS (CONTINUED)

SYMBOL	DEFINITION	LOCATION*
ω_d	Frequency of free decay for damped SDOF system	3.5
ω_n	Natural circular frequency of undamped SDOF system ($\omega_n = 2\pi f_n$)	3.2, 3.3, 3.5, 3.13, T3.14, T3.9, T3.10
ω_n	Natural frequency of thin flat plate	T3.13
ω_o	Natural frequency of unloaded cylinder	3.67
ω_r	Natural circular frequency of the r^{th} mode	3.22

* x.xx Equation, Tx.xx Table, Fx.xx Figure

The natural frequency, f_n , of the SDOF system is given by

$$f_n = \frac{1}{2\pi} \sqrt{\frac{K}{M}} = \frac{\omega_n}{2\pi} \quad (3.2)$$

where the terms are defined in Table 3.1.

3.2.1.1 Free Decay

If the mass is displaced from rest by a distance, w_0 , and then released, the resulting free decay of the system is given by

$$\begin{aligned} w(t) &= w_0 e^{-\zeta \omega_n t} \left\{ \cos \left(\sqrt{1-\zeta^2} \omega_n t \right) + \frac{\zeta}{\sqrt{1-\zeta^2}} \sin \left(\sqrt{1-\zeta^2} \omega_n t \right) \right\} \\ &= \frac{w_0 e^{-\zeta \omega_n t}}{\sqrt{1-\zeta^2}} \cos (\omega_d t - \phi) \end{aligned} \quad (3.3)$$

where

$$\tan \phi = \frac{\zeta}{\sqrt{1-\zeta^2}} \quad (3.4)$$

$$\omega_d = \omega_n \sqrt{1-\zeta^2} \quad (3.5)$$

3.2.1.2 Forced Vibration - Sinusoidal Excitation

If the mass in Figure 3.1a is driven by a harmonic force $F \cos \omega t$, the mass displacement response is given by

$$w(t) = w_0 \cos (\omega t - \phi) \quad (3.6)$$

where

$$\frac{w_0 K}{F} = \frac{1}{\sqrt{\left\{ 1 - \left(\frac{f}{f_n} \right)^2 \right\}^2 + 4\zeta^2 \left(\frac{f}{f_n} \right)^2}} = MF \quad (3.7)$$

and

$$\tan \phi = \frac{2\zeta \left(\frac{f}{f_n} \right)}{1 - \left(\frac{f}{f_n} \right)^2} \quad (3.8)$$

MF represents the nondimensional amplitude of the vibration or the magnification factor. It has the value of unity at zero excitation frequency ($f=0$). At the resonant frequency, the nondimensional vibration amplitude becomes

$$\frac{w_0 K}{F} = \frac{1}{2\zeta \sqrt{1 - \zeta^2}} \approx \frac{1}{2\zeta} = Q$$

In the above equation, Q is called the amplification factor or the quality factor. This factor represents the ratio of the dynamic displacement at resonance to the static displacement.

If the base in Figure 3.1b is driven by a harmonic displacement, $w_B \cos \omega t$, then the mass displacement response is given by

$$w(t) = T w_B \cos (\omega t - \psi) \quad (3.9)$$

where T is the nondimensional transmissibility given by

$$T = \left\{ \frac{1 + 4\zeta^2 \left(\frac{f}{f_n}\right)^2}{\left[1 - \left(\frac{f}{f_n}\right)^2\right]^2 + 4\zeta^2 \left(\frac{f}{f_n}\right)^2} \right\}^{1/2} \quad (3.10)$$

The phase angle ψ is calculated from

$$\tan \psi = \frac{2\zeta \left(\frac{f}{f_n}\right)^3}{1 - \left(\frac{f}{f_n}\right)^2 + 4\zeta^2 \left(\frac{f}{f_n}\right)^2} \quad (3.11)$$

Table 3.2, taken from Reference [3.7], summarizes the magnitude of the frequency response functions, $H(f)$, relating all possible combinations of input and output for the linear SDOF system. In Table 3.2, the magnification factor, MF, in equation 3.7 is given by $1/B_2$, while the transmissibility in equation 3.10 is B_1/B_2 . Results are included for both absolute motions and relative motions of the mass with respect to the base.

3.2.1.3 Forced Vibration - Random Excitation

If a linear SDOF system is driven by a random excitation, then the response is random and is not defined in terms of an explicit function of time. The statistical properties of the response are related to those of the input excitation. In particular, the mean square of the response can be calculated from the integral of the power spectral density of the response

$$\bar{w}^2 = \int_0^{\infty} G_w(f) df = \int_0^{\infty} |H(f)|^2 G_F(f) df \quad (3.12)$$

TABLE 3.2. SUMMARY OF FREQUENCY RESPONSE FUNCTIONS FOR LINEAR SDOF SYSTEM

Values for the Response Function $H(f)$ of a Linear SDOF System as a Function of the Input and Output Parameters		Base Motion Input			Force Input at Mass
		Displacement	Velocity	Acceleration	Force (i.e. displacement units) $F(t)/K$ in.
		$w_B(t)$ in.	$\dot{w}_B(t)$ in./sec.	$\ddot{w}_B(t)$ in./sec. ²	
In terms of displacement output, in.	Absolute displacement $w(t)$	$\frac{B_1}{B_2}$	$\frac{B_1}{2\pi f B_2}$	$\frac{B_1}{4\pi^2 f^2 B_2}$	$\frac{1}{B_2}$
	Relative displacement $w(t) - w_B(t)$	$\frac{f^2}{f_n^2 B_2}$	$\frac{f}{2\pi f_n^2 B_2}$	$\frac{1}{4\pi^2 f_n^2 B_2}$	
In terms of velocity output, in./sec.	Absolute velocity $\dot{w}(t)$	$\frac{2\pi f B_1}{B_2}$	$\frac{B_1}{B_2}$	$\frac{B_1}{2\pi f B_2}$	$\frac{2\pi f}{B_2}$
	Relative velocity $\dot{w}(t) - \dot{w}_B(t)$	$\frac{2\pi f^3}{f_n^2 B_2}$	$\frac{f^2}{f_n^2 B_2}$	$\frac{f}{2\pi f_n^2 B_2}$	
In terms of acceleration output, in./sec. ²	Absolute acceleration $\ddot{w}(t)$	$\frac{4\pi^2 f^2 B_1}{B_2}$	$\frac{2\pi f B_1}{B_2}$	$\frac{B_1}{B_2}$	$\frac{4\pi^2 f^2}{B_2}$
	Relative acceleration $\ddot{w}(t) - \ddot{w}_B(t)$	$\frac{4\pi^2 f^4}{f_n^2 B_2}$	$\frac{2\pi f^3}{f_n^2 B_2}$	$\frac{f^2}{f_n^2 B_2}$	

$$B_1 = \sqrt{1 + [2\zeta(f/f_n)]^2}$$

$$B_2 = \sqrt{[1 - (f/f_n)^2]^2 + [2\zeta(f/f_n)]^2}$$

$$f_n = \frac{1}{2\pi} \sqrt{\frac{K}{M}}$$

$$\zeta = \frac{C}{2\sqrt{KM}}$$

where

$H(f)$ = frequency response function of linear SDOF system

$G_F(f)$ = the single sided power spectral density of the input

$G_{\ddot{w}}(f)$ = the single sided power spectral density of the response

Equation 3.12 has been evaluated for certain types of input power spectral densities and for various $H(f)$ relating the different input/output combinations for a linear SDOF system. The results are rather complex, and are described in detail in Reference [3.8]. The two primary cases of interest are shown here. In each case, the output response is mass displacement, and the input power spectrum is constant for all frequencies. The two inputs considered are applied force at the mass and displacement input at the base. The mean square mass displacement response is given by

$$\bar{w}^2 = \frac{G_F}{8\zeta M^2 \omega_n^3} \quad (\text{force applied at mass}) \quad (3.13)$$

$$\bar{w}^2 = \frac{\omega_n (1 + 4\zeta^2) G_B}{8\zeta} \quad (\text{displacement input at base}) \quad (3.14)$$

where G_F and G_B represent the constant power spectral density of the force and the base displacement, respectively.

Equation 3.14 is actually more general, in that it can be used for any mass response due to the corresponding base motion input. If G_B is taken as the power spectrum of base acceleration, velocity or displacement, then \bar{w}^2 is the corresponding mean square response of the mass acceleration, velocity or displacement.

3.3 BEAMS

3.3.1 Natural Frequencies and Mode Shapes

For beams with uniformly distributed mass, constant cross-sectional area and classical boundary conditions, the resonant frequencies and mode shapes are given in Reference [3.1]. The natural frequency for any mode of the beam is given by the general equation

$$f_n = \frac{\beta^2}{2\pi l^2} \sqrt{\frac{EI}{\rho \bar{A}}} \quad (3.15)$$

where

β = Eigenvalue for the mode

l = Beam length

E = Young's modulus

I = Area moment of inertia of beam cross section

ρ = Material density

\bar{A} = Beam cross-sectional area

Table 3.3 lists the eigenvalues, β , for the first 10 modes for 6 classical boundary conditions. An eigenvalue of zero corresponds to a rigid body mode for the free-free beam. Table 3.4 contains the corresponding equations for the mode shapes, $w(\xi)$, where $\xi = x/l$ is the nondimensional distance along the beam and the parameter, Y , used in the mode shape equations.

The end conditions are obtained at $\xi = 0$ and $\xi = 1$. The mode shapes, $w(\xi)$, in Table 3.4 are illustrated for the first 5 modes in Table 3.5, taken from Reference [3.9]. The parameter, A , in Table 3.5 corresponds to β^2 in equation 3.15. The hinged edges, listed in Tables 3.3 through 3.5, are the same as simply supported or pinned edges and the clamped edges are the same as fixed edges.

TABLE 3.3. EIGENVALUES FOR UNIFORM BEAMS WITH CLASSICAL BOUNDARY CONDITIONS

Mode	β for Beam with Following End Conditions:					
	Free-Free	Clamped-Free	Clamped-Clamped	Hinged-Hinged	Clamped-Hinged	Hinged-Free
1	0.0	1.875	4.730	3.142	3.927	0.0
2	4.730	4.694	7.853	6.283	7.069	3.927
3	7.853	7.855	10.996	9.425	10.210	7.069
4	10.996	10.996	14.137	12.566	13.352	10.210
5	14.173	14.137	17.274	15.708	16.493	13.352
6	17.274	17.279	20.420	18.850	19.635	16.493
7	20.420	20.420	23.562	21.991	22.777	19.635
8	23.562	23.562	26.703	25.133	25.918	22.777
9	26.703	26.704	29.845	28.274	29.060	25.918
10	29.845	29.845	32.987	31.416	32.201	29.060

TABLE 3.4. MODE SHAPE EQUATIONS FOR UNIFORM BEAMS WITH CLASSICAL BOUNDARY CONDITIONS

End Conditions	$w(\xi)$	γ
Free-Free	$\sin \beta \xi + \sinh \beta \xi + \gamma (\cos \beta \xi + \cosh \beta \xi)$	$\frac{\sin \beta - \sinh \beta}{\cosh \beta - \cos \beta}$
Clamped-Free	$\sin \beta \xi - \sinh \beta \xi - \gamma (\cos \beta \xi - \cosh \beta \xi)$	$\frac{\sin \beta + \sinh \beta}{\cos \beta + \cosh \beta}$
Clamped-Clamped	$\sinh \beta \xi - \sin \beta \xi + \gamma (\cosh \beta \xi - \cos \beta \xi)$	$\frac{\sinh \beta - \sin \beta}{\cos \beta - \cosh \beta}$
Hinged-Hinged	$\sin \beta \xi$	---
Clamped-Hinged	$\sinh \beta \xi - \sin \beta \xi + \gamma (\cosh \beta \xi - \cos \beta \xi)$	$\frac{\sinh \beta - \sin \beta}{\cos \beta - \cosh \beta}$
Hinged-Free	$\sin \beta \xi + \gamma \sinh \beta \xi$	$\frac{\sin \beta}{\sinh \beta}$

TABLE 3.5. MODE SHAPES FOR UNIFORM BEAMS WITH CLASSICAL BOUNDARY CONDITIONS

FIXED-FREE (CANTILEVER)	A: 3.52	A: 22.4	A: 61.7	A: 121.0	A: 200.0
HINGED-HINGED (SIMPLE)	A: 9.87	A: 39.5	A: 88.9	A: 158	A: 247
FIXED-FIXED (BUILT-IN)	A: 22.4	A: 61.7	A: 121	A: 200	A: 298
FREE-FREE	A: 22.4	A: 61.7	A: 121	A: 200	A: 298
FIXED-HINGED	A: 15.4	A: 50.0	A: 104	A: 178	A: 272
HINGED-FREE	A: 15.4	A: 50.0	A: 104	A: 178	A: 272

Nonclassical end conditions are discussed in Reference [3.1]; the results are too complex to fully tabulate here. The nonclassical end condition of most practical concern is a pinned end condition with a torsional spring. The results for this end condition, denoted herein as PTS, lie between those for clamped and simple end conditions. The first mode natural frequency can be calculated from the equations shown in Table 3.6 for the three end conditions shown.

The various frequencies f_{SP} , f_{CP} , etc., in Table 3.6 are calculated from the classical boundary condition results using equation 3.15 and Table 3.3. The parameter, Q , in Table 3.6 is a nondimensional measure of how far the PTS end condition has advanced from the simple to the clamped extremes. It is a

TABLE 3.6. NATURAL FREQUENCIES FOR BEAMS WITH ROTATIONALLY FLEXIBLE EDGES

END CONDITIONS	EQUATION FOR NATURAL FREQUENCY
Free - PTS	$f_n = f_{SF_n} + \bar{Q} (f_{CF_n} - f_{SF_n})$
Hinged - PTS	$f_n = f_{SS_n} + \bar{Q} (f_{CS_n} - f_{SS_n})$
Clamped - PTS	$f_n = f_{CS_n} + \bar{Q} (f_{CC_n} - f_{CS_n})$

function of the nondimensional torsion spring stiffness, T^* , which is calculated as

$$T^* = \frac{T\ell}{EI} \quad (3.16)$$

where

T^* = Torsional spring constant, in-pounds/radian

ℓ = Beam length, inches

E = Young's modulus, pounds/in²

I = Area moment of inertia of beam cross section, in⁴

Values of T^* versus \bar{Q} are shown in Table 3.7 for the 3 PTS end conditions being considered. The T^* vs \bar{Q} values in Table 3.7 are applicable only to the first mode; data for the first 10 modes are presented in Reference [3.1]. The procedure is to first calculate T^* from equation 3.16 and then to determine \bar{Q} by interpolation from Table 3.7. \bar{Q} is then used in the equations in Table 3.6 to calculate the fundamental mode natural frequency.

TABLE 3.7. T^* VERSUS \bar{Q} FOR BEAMS WITH ROTATIONALLY FLEXIBLE EDGES

\bar{Q}	T^* for End Condition		
	Free - PTS	Hinged - PTS	Clamped - PTS
0.05	0.0103	0.2924	0.3462
0.10	0.0416	0.6180	0.7306
0.20	0.1715	1.393	1.643
0.30	0.4065	2.392	2.813
0.40	0.7813	3.723	4.369
0.50	1.364	5.587	5.541
0.60	2.294	8.380	9.787
0.70	3.903	13.030	15.18
0.80	7.189	22.31	25.94
0.90	17.15	50.12	58.14

The mode shapes for these end conditions can be calculated from the equations in Table 3.8. The parameter, β , must first be calculated based on the natural frequency, f_n , (Table 3.6) and the β and natural frequency for the classical end condition cases as shown in Table 3.8. Once β is calculated, the mode shapes are readily available from the equations in Table 3.8.

For beams with concentrated mass loads, the natural frequencies are shown in Tables 3.9 (massless beams) and 3.10 (massive beams). These results are from Reference [3.9].

3.3.2 Response to Harmonic Excitation

The dynamic response of a beam to harmonic excitation is calculated as the summation of the responses in each normal mode. Equations 3.6 through 3.8 from Section 3.2 can be used to calculate the contribution of each normal mode. The equations take the following form:

$$q_r(t) = q_{r0} \cos(\omega_r t - \phi_r) \quad (3.18)$$

TABLE 3.8. MODE SHAPES FOR PINNED END, TORSIONAL SPRING END CONDITIONS

End Conditions	$w(\xi)$	γ	β
Free-PTS	$-(\sin \beta \xi + \sinh \beta \xi) + \gamma (\cos \beta \xi + \cosh \beta \xi)$	$\frac{\sin \beta + \sinh \beta}{\cos \beta + \cosh \beta}$	$\beta_{CF} \sqrt{\frac{f_n}{f_{CFn}}}$
Hinged-PTS	$\sin \beta \xi - \gamma \sinh \beta \xi$	$\frac{-\sin \beta}{\sinh \beta}$	$\beta_{CS} \sqrt{\frac{f_n}{f_{CSn}}}$
Clamped-PTS	$\sinh \beta \xi - \sin \beta \xi + \gamma (\cosh \beta \xi - \cos \beta \xi)$	$\frac{\sin \beta - \sinh \beta}{\cosh \beta - \cos \beta}$	$\beta_{CC} \sqrt{\frac{f_n}{f_{CCn}}}$

TABLE 3.9. NATURAL FREQUENCIES OF MASSLESS BEAMS WITH CONCENTRATED MASS LOADS

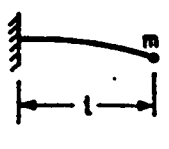
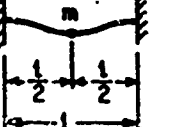
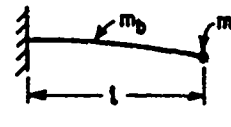
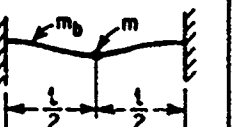
FIXED-FREE END LOAD	HINGED-HINGED CENTER LOAD	HINGED-HINGED OFF-CENTER LOAD	FIXED-FIXED CENTER LOAD	FIXED-FIXED OFF-CENTER LOAD
				
$f_n = \frac{1}{2\pi} \sqrt{\frac{3EI}{ml^3}}$	$f_n = \frac{2}{\pi} \sqrt{\frac{3EI}{ml^3}}$	$f_n = \frac{1}{2l_1 l_2} \sqrt{\frac{3EI l}{m}}$	$f_n = \frac{4}{\pi} \sqrt{\frac{3EI}{ml^3}}$	$f_n = \frac{1}{l_1 l_2} \sqrt{\frac{3EI l^3}{ml_1 l_2}}$

TABLE 3.10. NATURAL FREQUENCIES OF MASSIVE BEAMS WITH CONCENTRATED MASS LOADS

FIXED-FREE END LOAD	HINGED-HINGED CENTER LOAD	FIXED-FIXED CENTER LOAD
		
$f_n = \frac{1}{2\pi} \sqrt{\frac{3EI}{l^3(m+0.3m_b)}}$	$f_n = \frac{1}{2\pi} \sqrt{\frac{4EI}{l^3(m+0.5m_b)}}$	$f_n = \frac{7}{\pi} \sqrt{\frac{EI}{l^3(m+0.375m_b)}}$

where

$$q_{ro} = \frac{L_r}{K_r \left[\left\{ 1 - \left(\frac{f}{f_r} \right)^2 \right\}^2 + 4\zeta_r^2 \left(\frac{f}{f_r} \right)^2 \right]^{1/2}} \quad (3.19)$$

and

$$\tan \phi_r = \frac{2\zeta_r \left(\frac{f}{f_r} \right)}{1 - \left(\frac{f}{f_r} \right)^2} \quad (3.20)$$

Subscript r refers to the r^{th} normal mode. The terms in the above equation are:

$q_r(t)$ = Generalized displacement for r^{th} normal mode, inches

q_{ro} = Amplitude of $q_r(t)$

ϕ_r = Phase angle for r^{th} normal mode

K_r = Generalized stiffness for r^{th} normal mode

L_r = Generalized force for r^{th} normal mode,

f = Natural frequency

f_r = Natural frequency of r^{th} normal mode,

ζ_r = Damping ratio for r^{th} normal mode

The actual displacement of the beam, $w(x,t)$, is given by

$$w(x,t) = \sum_{r=1}^N w_r(x) q_r(t) = \sum_{r=1}^N w_r(\xi) q_r(t) \quad (3.21)$$

where $w_r(\xi)$ is the r^{th} mode shape (Table 3.4), and N is the total number of normal modes being considered. Equations 3.18 through 3.21 are general enough to cover any spatial distribution of harmonic loading applied to a beam, and any beam end conditions. In order to actually use equation 3.19, the generalized stiffness, K_r , and force, L_r , must be calculated. The general expressions for these are

$$K_r = \omega_r^2 M_r \quad (3.22)$$

$$M_r = \int_0^l w_r^2(x) \mu(x) dx = l \int_0^1 w_r^2(\xi) \mu(\xi) d\xi \quad (3.23)$$

$$L_r = \int_0^l w_r(x) F(x) dx = l \int_0^1 w_r(\xi) F(\xi) d\xi \quad (3.24)$$

where $\mu(x)$ and $F(x)$ are variable mass per unit length and force per unit length, respectively, and M_r is the generalized mass. The mass per unit length is constant for a uniform beam. The force per unit length can also be assumed to be constant. The integrations can still be quite involved since the mode shape, $w_r(\xi)$, and those in Table 3.4 can be rather complex.

For clamped-clamped and clamped-free end conditions, the shape of the first normal mode can be approximated with (1-cosine) functions. These approximate mode shapes can be readily integrated to obtain the generalized mass. The results are shown in Table 3.11, along with the results for simply supported end conditions, for which the mode shape is a simple sine wave. Also shown in Table 3.11 is the generalized force for the first mode of a beam with uniform loading, F_0 . Table 3.11 shows the generalized mass normalized to the mass of the beam, ρA , and the generalized force normalized to the total applied load $F_0 l$.

TABLE 3.11. GENERALIZED MASS AND GENERALIZED FORCE FOR UNIFORM LOADING OF BEAMS, FUNDAMENTAL MODE

End Condition	$w_1(x)$ First Mode Shape	$\frac{M}{\rho A l}$	$\frac{L}{F_0 l}$ for Uniform Loading
Hinged-Hinged	$\sin \frac{\pi x}{l}$	0.5	0.6366
Clamped-Clamped	$\frac{1}{2} (1 - \cos \frac{2\pi x}{l})$	0.375	0.5
Clamped-Free	$(1 - \cos \frac{\pi x}{2l})$	0.2268	0.3634

If a point load is applied to the beam, then the generalized force is the product of the mode shape $w(x)$ at the point of application times the amplitude of the force. The modes in Table 3.11 are all normalized to maximum value of 1.0, so if the point load is applied at the point of maximum modal deflection, then the generalized force is equal to the applied force. This situation is true if the load is applied in the center of the simply supported and clamped-clamped beams and at the free end of the clamped-free beam.

3.3.3 Response to Random Excitation

The methods used to develop equation 3.13 for the mean-square response to random excitation for a SDOF system can be applied to the beam problem. If only the fundamental mode is considered, then the mean-square displacement response of a beam is given by

$$\bar{w}^2(x) = \frac{\gamma(x) G_F}{64\pi^3 \zeta_n^3 (\rho A l)^2} \quad (3.25)$$

where

$$\gamma(x) = w_1^2(x) \left(\frac{L_F}{F_0 l} \right)^2 \left(\frac{M_F}{\rho \bar{A} l} \right)^{-2}$$

- $w_1(x)$ = Fundamental mode shape (Table 3.11)
 $\rho \bar{A} l$ = Mass of beam
 G_F = Power spectral density of total applied force
 ζ = Damping ratio for fundamental mode
 f_n = Natural frequency for fundamental mode

Note that the mean-square displacement is a function of the distance along the beam, x , since γ is a function of x through the mode shape, $w_1(x)$. The above equations are applicable to both point loading and uniformly distributed loading. The input power spectral density, G_0 , is assumed to be constant with frequency and in phase at all points along the beam.

An alternative expression developed by Miles (Reference [3.10]) relates the mean-square stress due to random, uniform pressure loading to the stress produced by a uniform static pressure loading. Miles' equation is

$$\bar{\sigma}^2 = \frac{\pi}{4 \zeta} f_n G_p \sigma_0^2 \quad (3.27)$$

where

$\bar{\sigma}^2$ = Mean square stress

f_n = Fundamental mode natural frequency

G_p = Constant power spectral density of applied pressure

σ_o = Stress at point of interest due to uniform static pressure of unit magnitude

The applied "pressure" in this case has units (pounds/in), meaning load per unit distance along the beam. The stresses $\bar{\sigma}^2$ and σ_o^2 in equation 3.27 can be replaced by displacements \bar{w}^2 and w_o^2 , where w_o is the displacement due to uniform static pressure distribution. The same is true for any consistent pair of responses, such as shear or bending moment.

3.4 FLAT PLATES

3.4.1 Natural Frequencies and Mode Shapes

Reference [3.2] contains an extensive tabulation of the available data concerning natural frequencies and mode shapes for flat plates. Results are presented here for rectangular plates with all edges simply supported and all edges clamped. Fundamental mode frequencies for all other edge conditions, except those with two or more free edges, lie within the results for the two extremes presented here.

The fundamental equation for the natural frequency of a flat plate is

$$f_n = \frac{\bar{F}}{2\pi b^2} \sqrt{\frac{D}{\mu}} \quad (3.28)$$

where

\bar{F} = Dimensionless frequency parameter

D = Flexural rigidity

b = Plate width

μ = Plate mass per unit area

The flexural rigidity is given by

$$D = \frac{Eh^3}{12(1-\nu^2)} \quad (3.29)$$

where

E = Young's modulus

h = Plate thickness

ν = Poisson's ratio

Equations for the frequency parameter, \bar{F} , are given in Table 3.12. A is the plate aspect ratio, a/b, where b is the width and a the length. The aspect ratio can be greater or less than 1. Table 3.12 also shows the frequency parameter for a square plate, A=1. The two edge conditions result in a frequency range of almost 2:1.

TABLE 3.12. FREQUENCY PARAMETER FOR FLAT PLATES, FUNDAMENTAL MODE

Edge Condition	Equation for \bar{F}	Value of \bar{F} for Square Plate
Simply-supported	$\pi^2 \left(1 + \frac{1}{A^2} \right)$	19.7392
Clamped	$12 \sqrt{\frac{7}{2} \left(1 + \frac{4}{7A^2} + \frac{1}{A^4} \right)}$	36.0000

For a plate with simply supported edge conditions, the fundamental mode shape is

$$r(x,y) = \sin \frac{\pi x}{a} \sin \frac{\pi y}{b} \quad (3.30)$$

where a and b are plate length and width. The mode shapes for fully clamped plates are not given by straightforward analytical expressions. Figure 3.2, taken from Reference [3.4], shows the first 6 symmetric mode shapes for a square plate. For rectangular plates in the range $0.5 \leq a/b \leq 2.0$, the variation from the mode shapes shown in Figure 3.2 is minor. The fundamental mode shown in Figure 3.2 (X_0, Y_0) can be approximated by a (1-cosine) shaped curve.

Figure 3.3, taken from Reference [3.7], presents a nomograph for calculating the fundamental mode natural frequency for isotropic rectangular plates. Results are given for both clamped and simply supported edges.

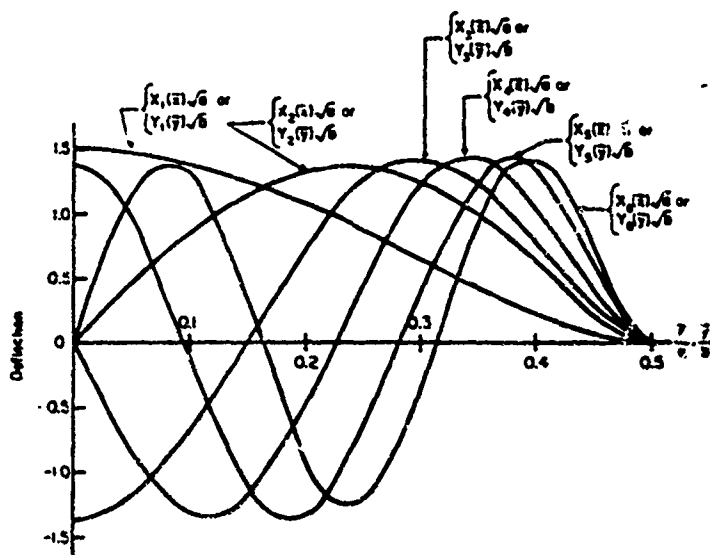


Figure 3.2. Symmetric mode shapes for fully clamped square plate.

Design Equations

Supported Edges $f_{11} = 9.452 \cdot 10^4 h (1/a^2 + 1/b^2)$

Clamped Edges $f_{11} = 1.178 \cdot 10^5 h (3.307/a^4 + 3.307/b^4 + 2/a^2 b^2)^{1/2}$

$E/(1-\nu) = 11.26 \times 10^6$

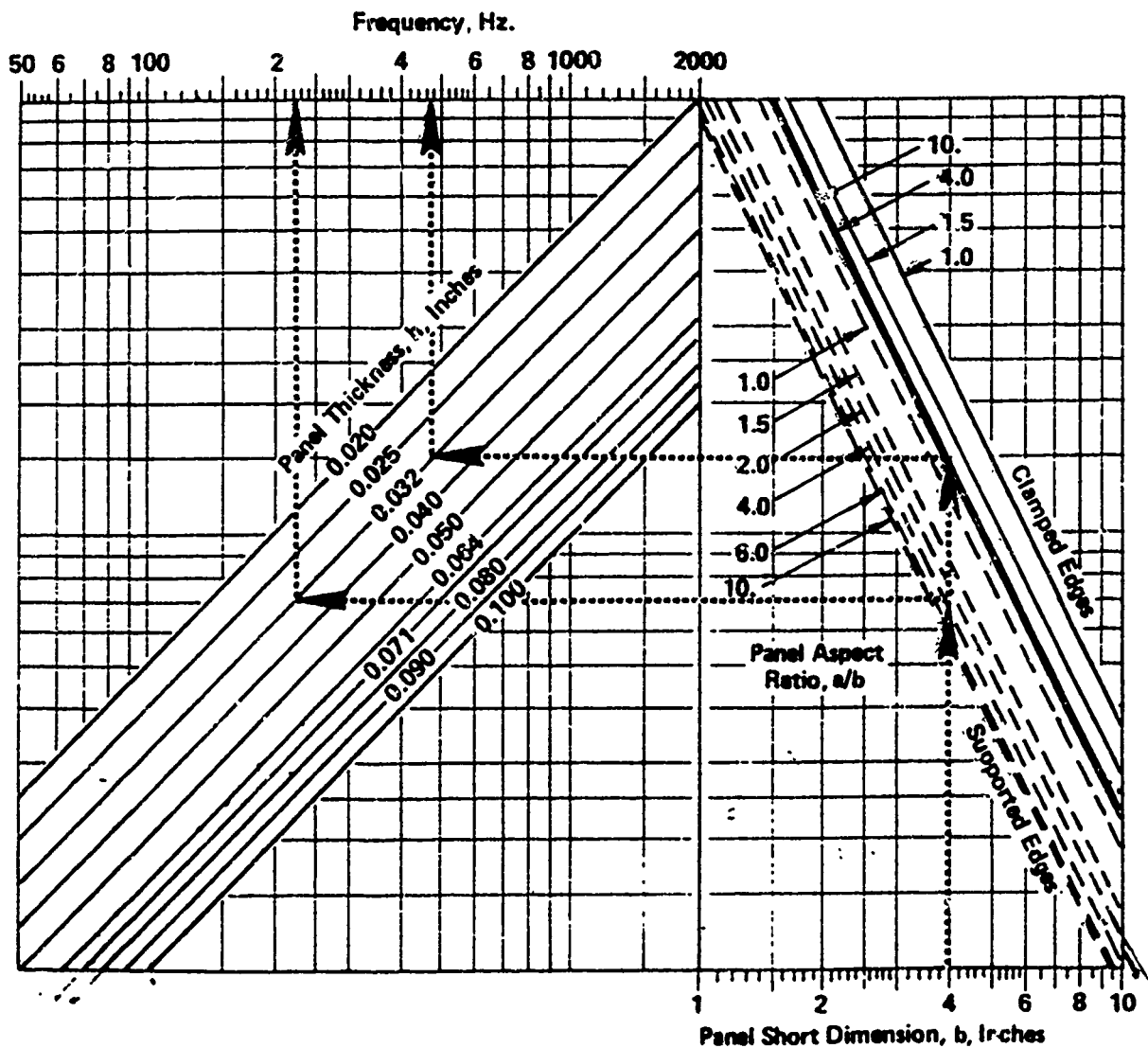


Figure 3.3. Nomograph for calculating fundamental mode natural frequency of rectangular panels.

Natural frequencies for circular and square plates with other edge conditions are shown in Table 3.13, taken from Reference [3.9]. The frequency parameter B in Table 3.13 is equal to \bar{F} in equation 3.28 divided by 12.

References [3.6] and [3.12] present methods for calculating the natural frequencies of stiffened panels typical of aircraft construction. In Reference [3.6], Szechenyi introduces the concept of "bending wavelength equivalencing factors," which lead to relatively simple approximate methods for calculating the natural frequencies of stiffened and curved panel structures. The following data is from Reference [3.12]. Figure 3.4 shows the typical stringer-frame stiffened panel structure considered, while Figure 3.5 describes the stringer torsional stiffness end conditions analyzed.

The natural frequencies of such multi-span structures occur in groups, the number of frequencies in each group being equal to the number of spans. For a panel having a large number of spans the lowest natural frequency in any group is generally associated with a mode in which the stringers twist and the highest natural frequency in that group is associated with a mode in which the stringers tend to bend without twisting. The mode shapes alternate between symmetric and anti-symmetric as frequency increases.

In developing the following procedure, the frame torsional stiffness has been neglected and the frame bending stiffness has been assumed to be infinite. The skin edges at the frames are thus assumed to be simply-supported. The natural frequencies are only slightly influenced by the stringer bending stiffness and therefore this stiffness has been assumed to be infinity.

These results can be used to predict the first group of natural frequencies of skin-stringer structures with four different end conditions. The results are presented for varying degrees of stringer torsional stiffness, for three different aspect ratios (a/b) and for two different values of n , the number of half-waves across the frame pitch.

TABLE 3.13. NATURAL FREQUENCIES OF THIN FLAT PLATES OF UNIFORM THICKNESS

$$\omega_n = B \sqrt{\frac{E t^3}{\rho a^4 (1-\nu^2)}} \text{ RAD/SEC}$$

E = YOUNG'S MODULUS, LB / IN.²
 t = THICKNESS OF PLATE, IN.
 ρ = MASS DENSITY, LB-SEC²/IN.⁴
 a = DIAMETER OF CIRCULAR PLATE OR SIDE OF SQUARE PLATE, IN.
 ν = POISSON'S RATIO

SHAPE OF PLATE	DIAGRAM	EDGE CONDITIONS	VALUE OF C FOR MODE:								
			1	2	3	4	5	6	7	8	
CIRCULAR		CLAMPED AT EDGE	11.84	24.61	40.41	46.14	103.12				
CIRCULAR		FREE	6.09	10.53	14.19	23.80	40.88	44.68	61.38	69.44	
CIRCULAR		CLAMPED AT CENTER	4.35	24.26	70.39	138.85					
CIRCULAR		SIMPLY SUPPORTED AT EDGE	5.90								
SQUARE		ONE EDGE CLAMPED-THREE EDGES FREE	1.01	2.47	6.20	7.94	9.01				
SQUARE		ALL EDGES CLAMPED	10.40	21.21	31.29	38.04	38.22	47.73			
SQUARE		TWO EDGES CLAMPED-TWO EDGES FREE	2.01	6.96	7.74	13.89	18.25				
SQUARE		ALL EDGES FREE	4.07	5.94	6.91	10.39	17.80	18.85			
SQUARE		ONE EDGE CLAMPED-THREE EDGES SIMPLY SUPPORTED	6.83	14.94	16.95	24.89	28.99	32.71			
SQUARE		TWO EDGES CLAMPED-TWO EDGES SIMPLY SUPPORTED	8.37	15.82	20.03	27.34	29.54	37.31			
SQUARE		ALL EDGES SIMPLY SUPPORTED	5.70	14.26	22.82	28.52	37.08	48.49			

MASSLESS CIRCULAR PLATE WITH CONCENTRATED CENTER MASS

CLAMPED EDGES



$$\omega_n = 4.09 \sqrt{\frac{Eh^3}{m a^2 (1-\nu^2)}}$$

SIMPLY SUPPORTED EDGES



$$\omega_n = 4.09 \sqrt{\frac{Eh^3}{m a^2 (1-\nu)(3+\nu)}}$$

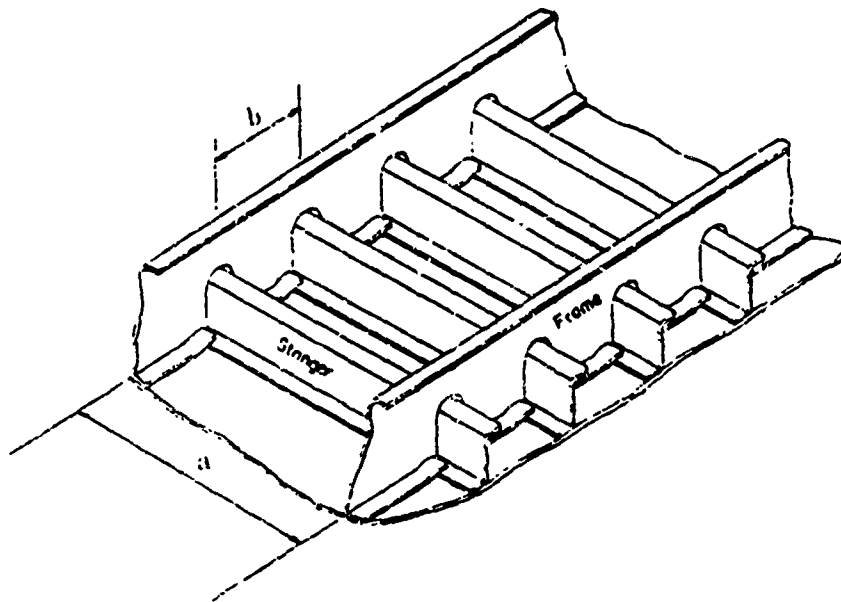


Figure 3.4. A periodic skin stringer structure.

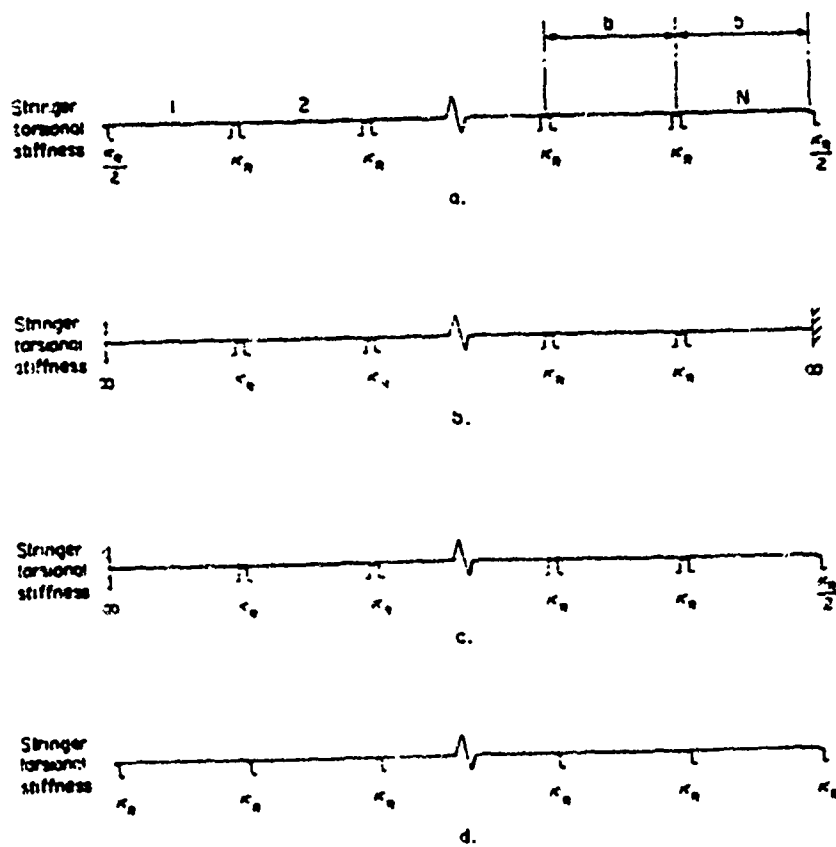


Figure 3.5. Finite skin-stringer structure with different boundary conditions.

The natural frequency is calculated from

$$f_n = \frac{VKt}{b^2} \quad (3.31)$$

where

- V = Velocity factor
- K = Frequency parameter
- t = Skin thickness
- b = Stringer pitch (Figure 3.4)

The velocity factor is given by

$$V = \frac{\left(\frac{E}{\rho}\right)^{1/2}}{200,000} \quad (3.32)$$

where E and ρ are Young's Modulus and material density, respectively. V is approximately 1.0 for all common structural metallic materials.

The frequency parameter K is obtained from Figures 3.6 through 3.11. The following parameters are required to obtain K from these plots:

- a/b = Aspect ratio (Figure 3.4)
- n = Number of half waves across frame pitch (n = 1 or 2)
- M₁ = Mode parameter for first group of natural frequencies
- K_R = Non-dimensional torsional stiffness of stringer

M₁ is obtained from Table 3.14. N is the number of spans and r is the mode number (r = 1, 2, . . . , N). The stringer nondimensional torsional stiffness is given by

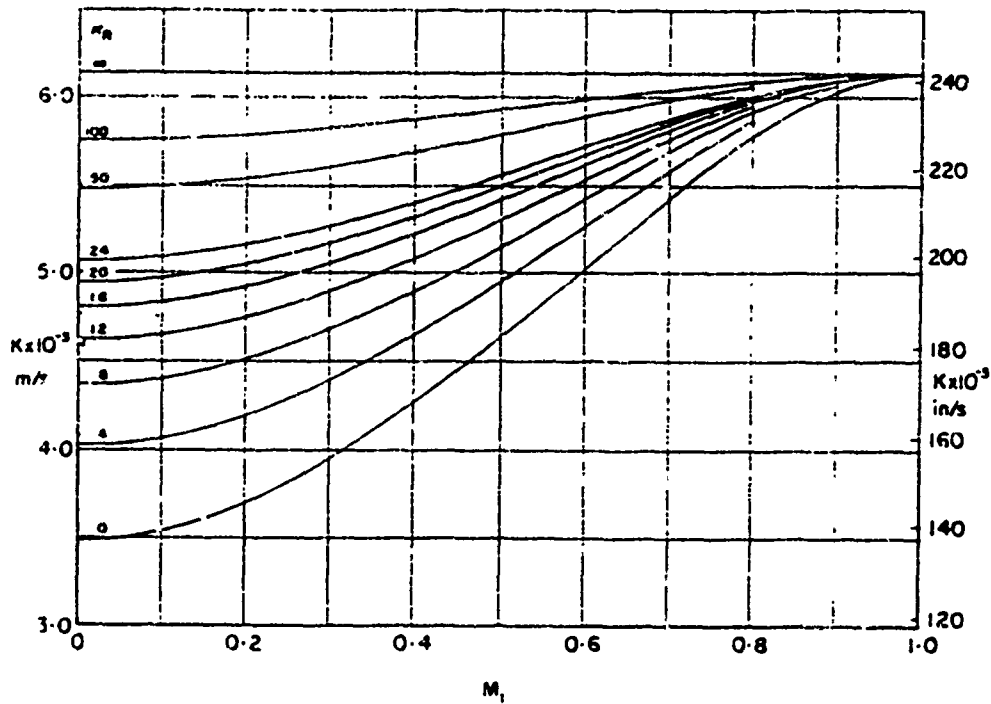


Figure 3.6. $a/b = 1.5$, $m=1$, Group 1.

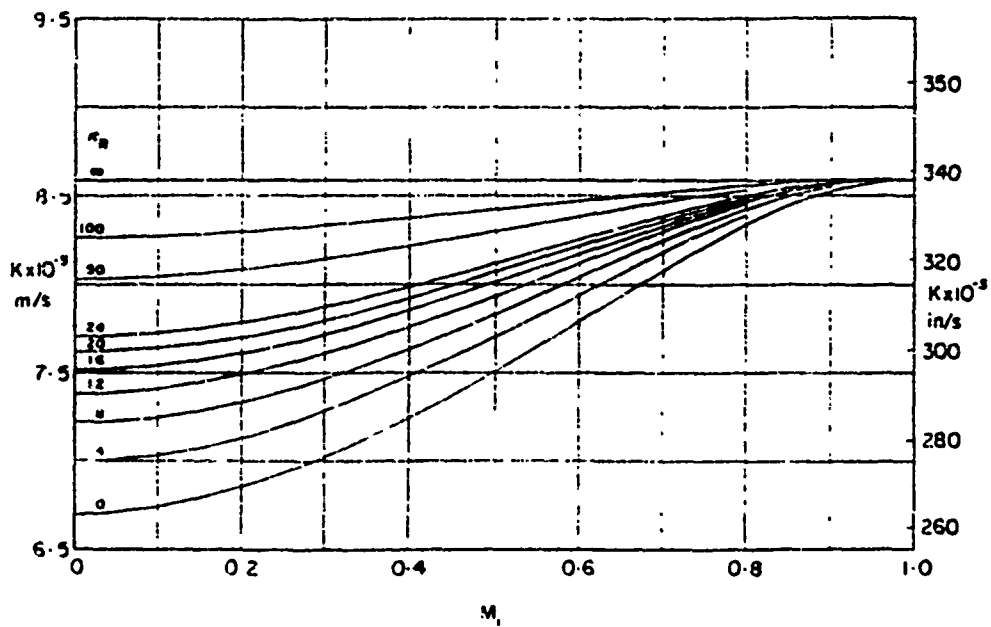


Figure 3.7. $a/b = 1.5$, $m=2$, Group 1.

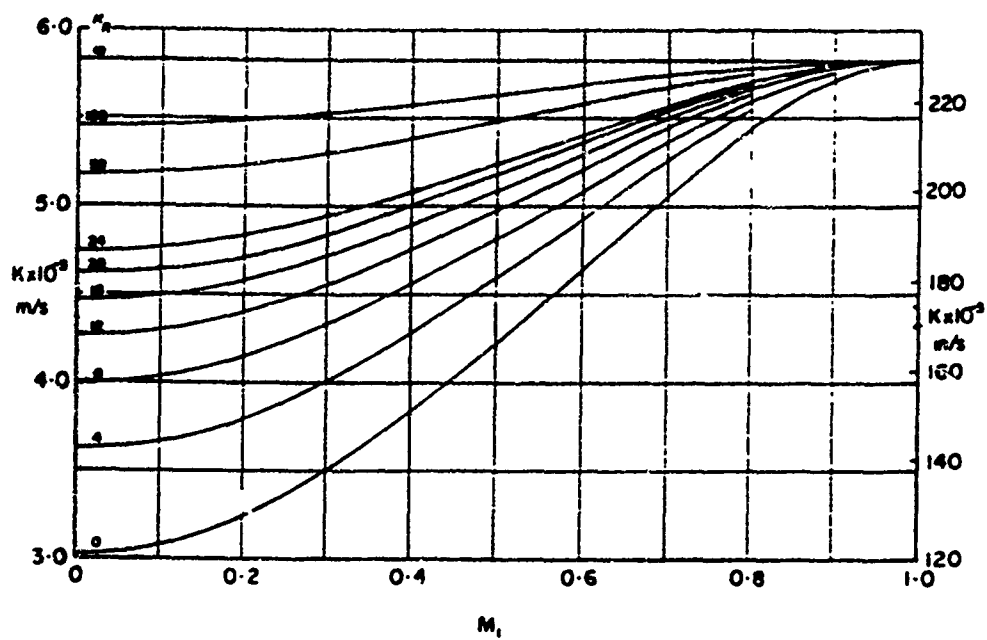


Figure 3.8. $a/b = 2.0$, $m=1$, Group 1.

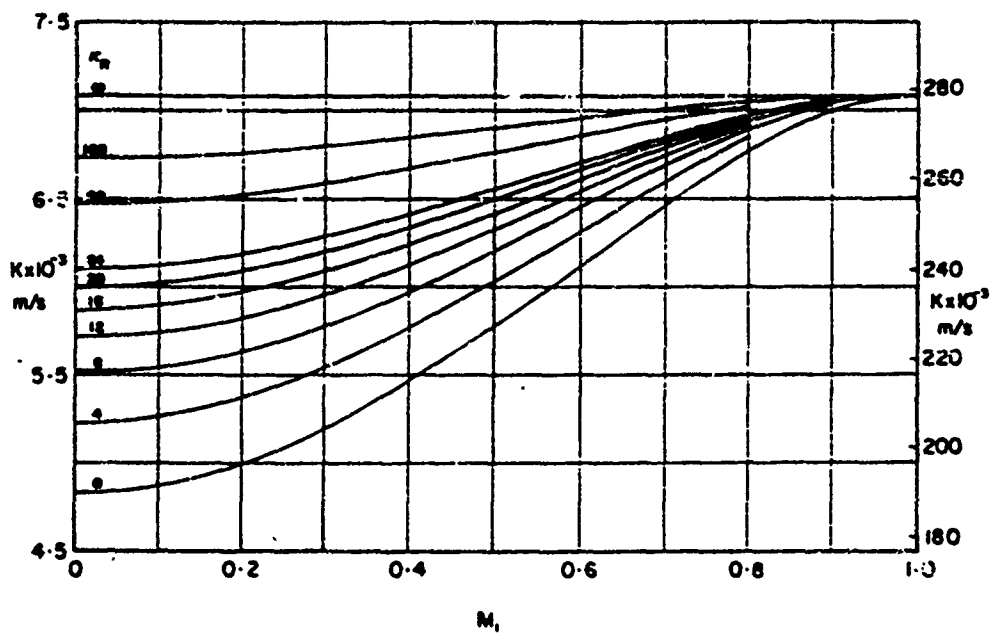


Figure 3.9. $a/b = 2.0$, $m=2$, Group 1.

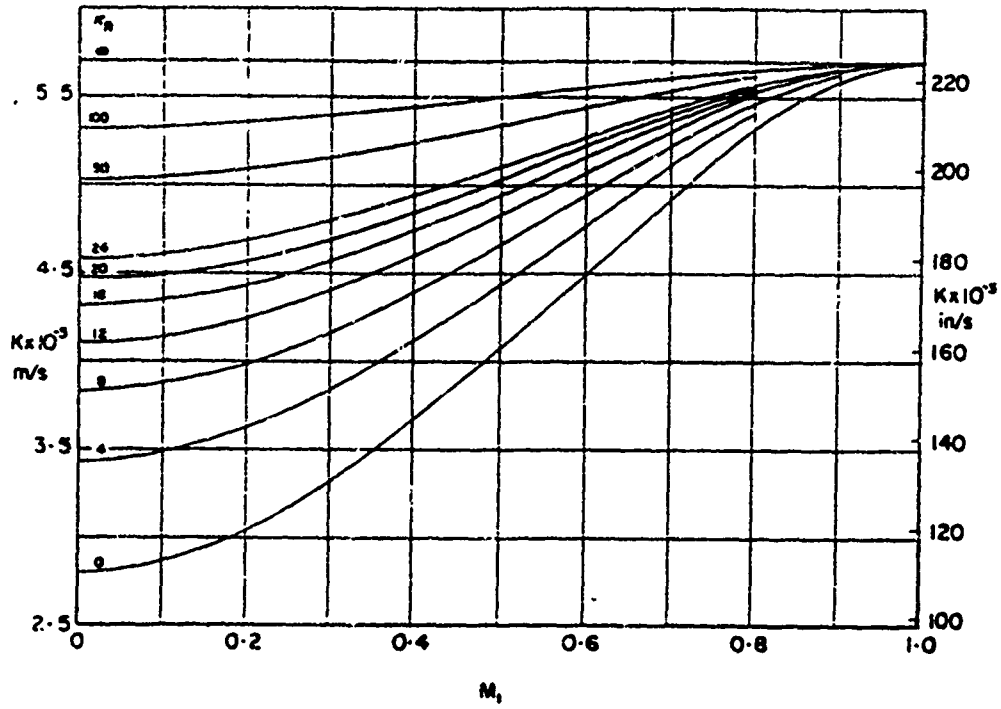


Figure 3.10. $a/b = 2.5$, $m=1$, Group 1.

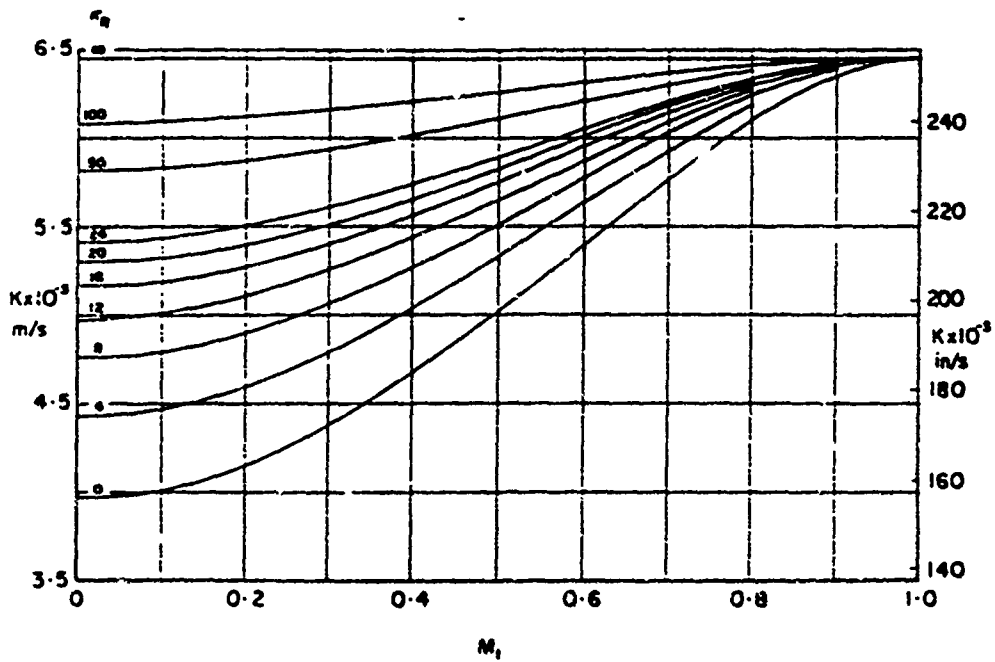


Figure 3.11. $a/b = 2.5$, $m=2$, Group 2.

TABLE 3.14. MODE PARAMETERS FOR STIFFENED PANELS

End Conditions as in	H_1 ($1 \leq r \leq N$)
Figure 3-5a	$\frac{r-1}{N}$
Figure 3-5b	$\frac{r}{N}$
Figure 3-5c	$\frac{2r-1}{2N}$
Figure 3-5d	*
*For structures with end conditions as in Figure 3.5d, K is approximately equal to the arithmetic average of the values of K obtained from the first two rows in the above table.	

$$K_R = \left\{ E_s \Gamma_s \left(\frac{m\pi}{a} \right)^4 + G_s J_s \left(\frac{m\pi}{a} \right)^2 - \rho_s I_s (2 f_\eta)^2 \right\} \times \frac{b}{D} \times \quad (3.33)$$

where

- E_s = Young's modulus of stringer material
- Γ_s = Warping constant of stringer cross section with respect to the point on skin directly beneath shear center of stringer
- G_s = Shear modulus of stringer material
- J_s = St. Venant constant of uniform torsion for stringer cross section
- ρ_s = Density of stringer material

I_s = Polar moment of inertia of stringer cross section about a point on skin directly beneath shear center of stringer

D = Flexural rigidity per unit width of the skin plate, $Et^3/12(1-\nu^2)$

Since f_η in equation 3.33 is unknown, it must be estimated initially. A value of 100 Hz is reasonable for commonly used skin-stringer structures.

Alternatively, f_η can be taken as the fundamental natural frequency of an individual panel with fully-fixed edges. Although an iteration procedure is required to coverage on the frequencies, the first estimate is typically within 4 percent of the final iterated value.

3.4.2 Response to Harmonic Excitation

The response of a plate to harmonic excitation is treated in the same manner as for a beam (Section 3.3.2). Equations 3.18 through 3.20 are applicable to a plate, and equation 3.21 takes the form

$$w(x,y,t) = \sum_{r=1}^N w_r(x,y) q_r(t) \quad (3.34)$$

where

$w_r(x,y)$ = Mode shape for r^{th} mode

$q_r(t)$ = Generalized displacement for r^{th} mode

The integration to obtain the generalized mass and force is now performed over the surface area of the panel as discussed in Section 4.3, Volume I, of this design guide. The generalized mass and generalized force for simply supported (all sides) and clamped (all sides) rectangular plates are shown in Table 3.15. The values shown are applicable to the fundamental mode. The generalized force is for a uniform pressure loading of p_0 over the entire plate. For a point load at the center of the plate, the generalized force is equal to the applied force.

TABLE 3.15. GENERALIZED MASS AND GENERALIZED FORCE FOR UNIFORM PRESSURE LOADING OF RECTANGULAR PLATES, FUNDAMENTAL MODE

End Condition	First Mode Shape	$\frac{M_r}{\rho \epsilon b}$	$\frac{L_r}{p_o ab}$
Simply Supported	$\sin \frac{\pi x}{a} \sin \frac{\pi y}{b}$	0.25	0.4053
Clamped	$\frac{1}{4} \left(1 - \cos \frac{2\pi x}{a}\right) \left(1 - \cos \frac{2\pi y}{b}\right)$	0.1406	0.2500

3.4.3 Response to Random Excitation

The basic normal mode theory commonly used to obtain the response of a plate to random excitation and simplification of the theory are discussed in Section 4.3, Volume I, of this design guide. A comprehensive discussion of the response of plates to random excitation is also contained in Reference [3.7]. The following equations, taken from Reference [3.7], apply to uniform pressure loading of a rectangular plate. Results are shown for simply supported and clamped edge conditions (all edges). For a simply supported plate, the mean square displacement is given by

$$\bar{w}^2(x,y,t) = \frac{32a^3b^3}{\pi^{10} \sqrt{\rho h D^3}} \cdot \frac{G_p(f_{11}) \sin^2(\pi x/a) \sin^2(\pi y/b)}{\zeta_{11} [(b/a) + (a/b)]^3} \quad (3.35)$$

where

- a = Plate length (x direction)
- b = Plate width (y direction)
- $G_p(f_{11})$ = Power spectral density of applied pressure loading, at frequency corresponding to fundamental mode of plate
- ρ = Plate material density
- h = Plate thickness

D = Flexural rigidity (equation 3.29)

ζ_{11} = Damping ratio for fundamental mode

Subscript 11 refers to the fundamental mode. The mean square tensile and shear stresses in the panel are given by

$$\bar{\sigma}_x^2(x,y,t) = \frac{1152ab}{\pi^6 h^4} \sqrt{D/\rho h} \frac{G_p(f_{11}) [(b/a) + \nu (a/b)]^2}{\zeta_{11} [(b/a) + (a/b)]^3} \sin^2(\pi x/a) \sin^2(\pi y/b) \quad (3.36)$$

$$\bar{\sigma}_y^2(x,y,t) = \frac{1152ab}{\pi^6 h^4} \sqrt{D/\rho h} \frac{G_p(f_{11}) [\nu (b/a) + (a/b)]^2}{\zeta_{11} [(b/a) + (a/b)]^3} \sin^2(\pi x/a) \sin^2(\pi y/b) \quad (3.37)$$

$$\bar{\tau}_{xy}^2(x,y,t) = \frac{1152ab}{\pi^6 h^4} \sqrt{D/\rho h} (1-\nu)^2 \frac{G_p(f_{11}) \cos^2(\pi x/a) \cos^2(\pi y/b)}{\zeta_{11} [(b/a) + (a/b)]^3} \quad (3.38)$$

where ν = Poisson's ratio. The maximum tensile stresses occur in the center of the plate ($x = a/2$, $y = b/2$). The maximum shear stress occurs at the four corners of the plate ($x = 0$ and a , $y = 0$ and b).

For a plate with all edges clamped, the mean square deflection and stresses are given by

$$\bar{w}^2(x,y,t) = \frac{3.1992 \cdot 10^{-5} a^3 b^3 G_p(f_{11}) X_1^2(x) Y_1^2(y)}{\sqrt{\rho h D^3} \zeta_{11} [3.307(b/a)^2 + 3.307(a/b)^2 + 2]^{3/2}} \quad (3.39)$$

$$\frac{\sigma_x^2}{x}(x,y,t) = 1.152 \cdot 10^{-3} \frac{ab\sqrt{D/\rho h} G_p(\xi_{11}) S_{x11}^2(x,y)}{h^4 \zeta_{11} [3.307(b/a)^2 + 3.307(a/b)^2 + 2]^{3/2}} \quad (3.40)$$

$$\frac{\sigma_y^2}{y}(x,y,t) = 1.152 \cdot 10^{-3} \frac{ab\sqrt{D/\rho h} G_p(\xi_{11}) S_{y11}^2(x,y)}{h^4 \zeta_{11} [3.307(b/a)^2 + 3.307(a/b)^2 + 2]^{3/2}} \quad (3.41)$$

$$\tau_{xy}^2(x,y,t) = 0.57650 \frac{ab\sqrt{D/\rho h} (1-\nu)^2 G_p(\xi_{11}) (X_1'(x) Y_1'(y))^2}{h^4 \zeta_{11} [3.307(b/a)^2 + 3.307(a/b)^2 + 2]^{3/2}} \quad (3.42)$$

The additional terms in the above equations are given by the following equations:

Center of Plate:

$$X_1^2(a/2) Y_1^2(b/2) = 6.36160 \quad (3.43)$$

$$S_{x11}^2(a/2, b/2) = 1865.8 [(b/a) + \nu(a/b)]^2 \quad (3.44)$$

$$S_{y11}^2(a/2, b/2) = 1865.8 [\nu(b/a) + (a/b)]^2 \quad (3.45)$$

Approximate Location of Maximum Shear

$$(X_1'(0.22a) Y_1'(0.22b))^2 = 1.14389 \quad (3.46)$$

Edge of Plate:

$$S_{x11}^2(0, b/2) = 5050.1 (b/a)^2 \quad (3.47)$$

$$S_{y11}^2(a/2,0) = 5050.1(a/b)^2 \quad (3.48)$$

3.5 CURVED PLATES

Curved plates are shells for which the radius of curvature is large compared to the panel length or width. Figure 3-12, from Reference [3.7], illustrates the geometry used in this section to describe open cylindrical circular shells, or curved plates.

The criterion for a shallow open circular cylindrical shell is that the rise h^* is less than $1/5$ of the smaller side, measured in the plane of its supports. The smaller side is either a or $b^* = 2R \sin(\phi/2)$. Therefore, a shallow open circular cylindrical shell is one for which the following geometric constraints are satisfied:

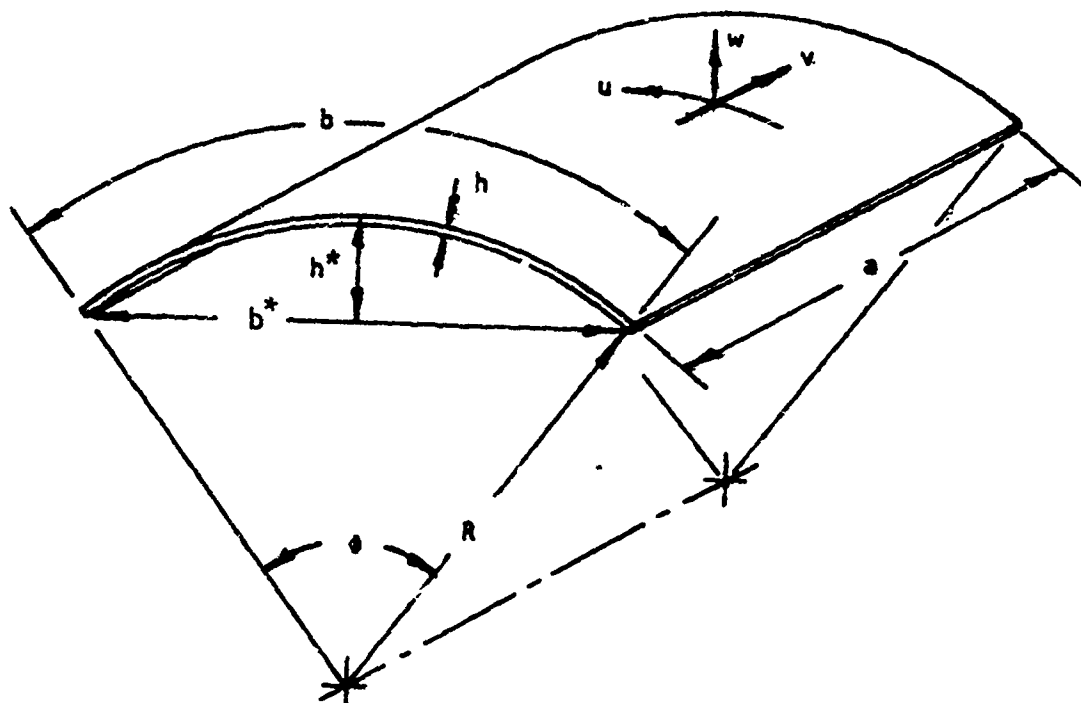
$$[1 - \cos(\phi/2)] \frac{R}{a} \leq 0.20 \quad (3.49)$$

if a is the shorter dimension, and

$$\frac{[1 - \cos(\phi/2)]}{\sin(\phi/2)} \leq 0.40 \quad (3.50)$$

if b^* is the shorter dimension (see Figure 3.12).

Reference [3.3] contains a comprehensive summary of the literature on shells, with extensive tabulation of analytical and experimental results. Reference [3.7] contains a briefer discussion of the results of primary interest. The results in this section are taken from Reference [3.7]. For a more in-depth understanding of shell theory, Reference [3.3] is the essential reference. For open circular cylindrical shells that do not satisfy equations 3.49 and 3.50, refer to Section 3.7.



ARC LENGTH: $b = R\phi$

SPAN: $b^* = 2R \sin(\phi/2)$

RISE: $h^* = R[1 - \cos(\phi/2)]$

Figure 3.12. Open circular cylinder geometry.

3.5.1 Natural Frequencies

The fundamental mode natural frequency for an open shallow circular cylindrical shell (Figure 3.12), with all edges simply supported, is

$$f_{11}^2 = \frac{\pi^2 D}{4\rho h a^2 b^2} \left[\frac{b}{a} + \frac{a}{b} \right]^2 + \frac{E}{4\pi^2 \rho R^2 \left[1 + \left(\frac{a}{b} \right)^2 \right]^2} \quad (3.51)$$

and the equation for all edges clamped is

$$f_{11}^2 = \frac{14.051 E h^2}{4\pi^2 \rho a^2 b^2} [3.307(b/a)^2 + 3.307(a/b)^2 + 2] + \frac{E}{4\pi^2 \rho R^2} \left\{ \frac{1.0685(b/a)^2 + 0.6692(a/b)^2 + 7.3243}{(b/a)^2 + (a/b)^2 + 9.4419} \right\} \quad (3.52)$$

In each case, the first term corresponds to the result for a flat plate, and the second term represents the correction for shell curvature.

Plumlee [3.4] developed an expression for the fundamental mode frequency of a shallow open cylindrical shell with all edges clamped using an approach similar to Sewall [3.11]. Both Plumlee and Sewall noted that experimental results for the lower order modes, especially the fundamental mode frequency, fell between the cases of all edges simply supported and all edges clamped. Plumlee empirically determined constants for the fundamental mode frequency expression to obtain, for $\nu = 0.32$,

$$f_{11}^2 = \frac{14.051 E h^2}{4\pi^2 \rho a^2 b^2} [3.307(b/a)^2 + 3.307(a/b)^2 + 2.0] + \frac{0.2788 E}{4\pi^2 \rho R^2} \quad (3.53)$$

The 0.2788, in the second term of equation, 3.53 is less than the corresponding, bracketed expression in the second term of equation 3.52. The latter expression varies from 0.678 to 1.043 as b/a varies from 0.1 to 10.0. Equation 3.53 is considered more accurate for clamped edge conditions than equation 3.52. A nomograph corresponding to equation 3.53 is shown in Figure 3.13, from Reference [3.7]. Figure 3.3 can be used to calculate the flat plate natural frequency required to convert the frequency ratio from Figure 3.13 to an actual frequency.

3.5.2 Response to Harmonic Excitation

Figure 3.13 can also be used to estimate the response of curved plates to sinusoidal excitation. The methods of Section 3.4.2 are first applied to calculate the flat plate response to harmonic excitation. Then Figure 3.13 is used to calculate the ratio σ_c/σ_∞ , where σ_∞ is the stress for a flat plate.

3.5.3 Response to Random Excitation

Reference [3.4] contains the derivation of an expression for the ratio of the root-mean-square stress response at the center of the straight edge of the shell in the circumferential direction to obtain

$$\frac{(\sigma_y)_{\text{curved}}}{(\sigma_y)_{\text{flat}}} = \left[1 + \frac{0.006a^2b^2}{h^2R^2 \left[\left(\frac{b}{a}\right)^2 + \left(\frac{a}{b}\right)^2 + 0.604 \right]} \right]^{-3/4} \\ \times \left[1 + \frac{0.453b^2}{Rh} \left(\frac{\left(\frac{b}{a}\right)^2 + 0.034}{\left(\frac{b}{a}\right)^4 + 9.62 \left(\frac{b}{a}\right)^2 + 1} \right) \right] \quad (3.54)$$

The stress $(\sigma_y)_{\text{flat}}$ is obtained from Section 3.4.3 using equations 3.41 and 3.42 to obtain

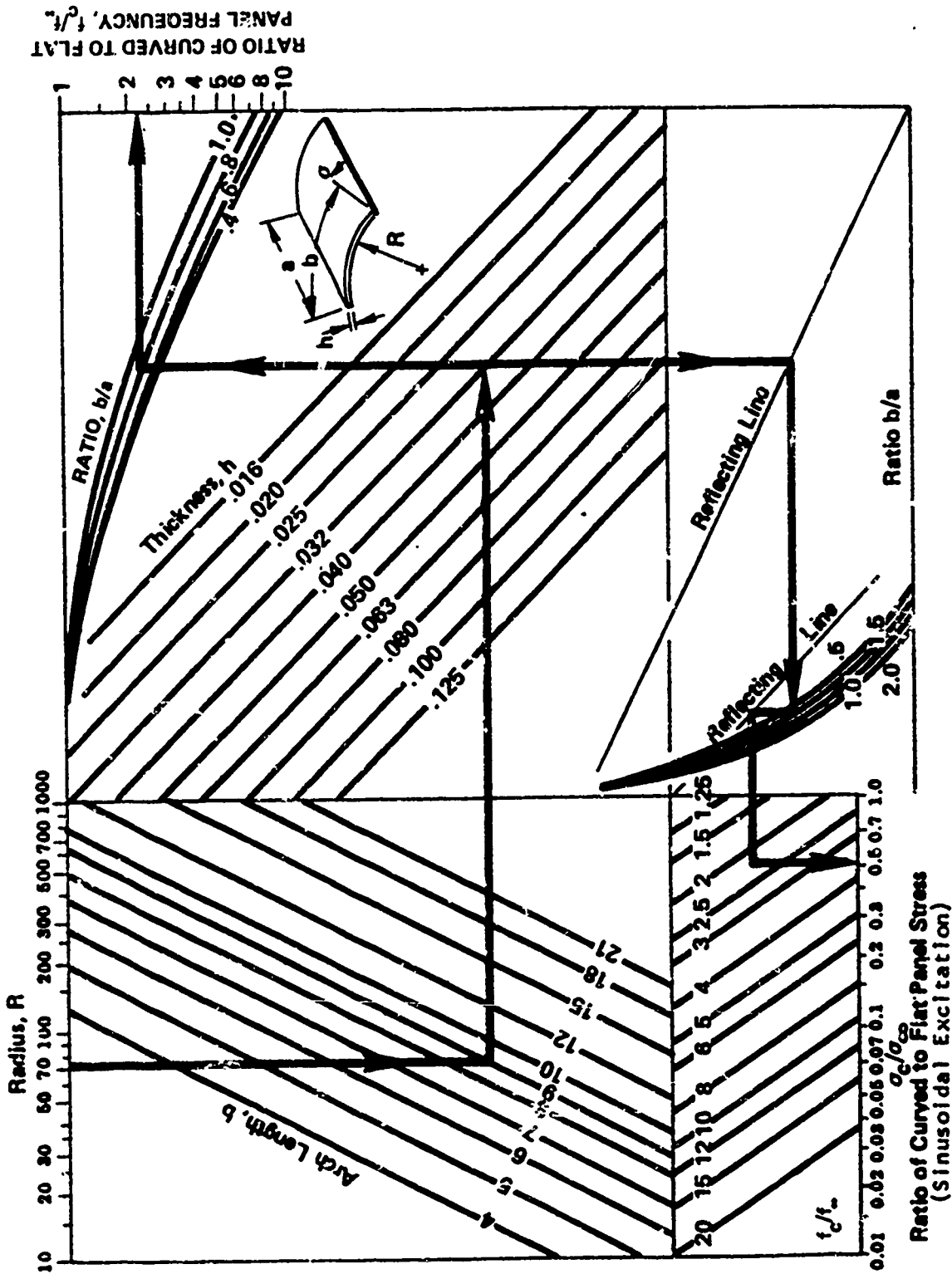


Figure 3.13. Nomograph for calculating frequency ratio for shallow open circular cylindrical shells.

$$(\sigma_y)_{\text{flat}}^2 = \frac{1.7726a^3 \sqrt{E/\rho} G_p(f_{11})}{bh^3 \zeta_{11} [3.307(b/a)^2 + 3.307(a/b)^2 + 2]^{3/2}} \quad (3.55)$$

In using the results of equations 3.54 and 3.55 it has been assumed that the pressure spectrum level is constant for the frequency range including the flat panel and the curved panel response frequency. In addition it has been assumed that $\nu = 0.32$.

3.6 HONEYCOMB PLATES

3.6.1 Natural Frequencies

An empirical equation is developed in Reference [3.7] for the fundamental mode natural frequency of a honeycomb sandwich panel. The empirical constants are based on sonic fatigue tests of 30 honeycomb panels. Figure 3.14 illustrates the construction and geometry for a typical honeycomb sandwich panel.

From Reference [3.7], the fundamental mode natural frequency, in Hz, is given by

$$f_{11} = K (h+t)/b^2 \quad (3.56)$$

where b is the panel width measured as shown in Figure 3.14. K is a function of panel aspect ratio and is given in Figure 3.15. The analysis assumes that the panel response is linear and that the flexural rigidity comes entirely from the facing sheets. The core density is assumed to be equal to or greater than 2.0 pounds/ft³.

Sweers in Reference [3.14] has shown that the natural frequencies of rigidly mounted honeycomb panel modes could be predicted, with reasonable accuracy, using equivalent simply supported honeycomb panel theory in which the honeycomb core is assumed to be infinitely stiff in shear. These honeycomb panels are also assumed to be simply supported at the base of the

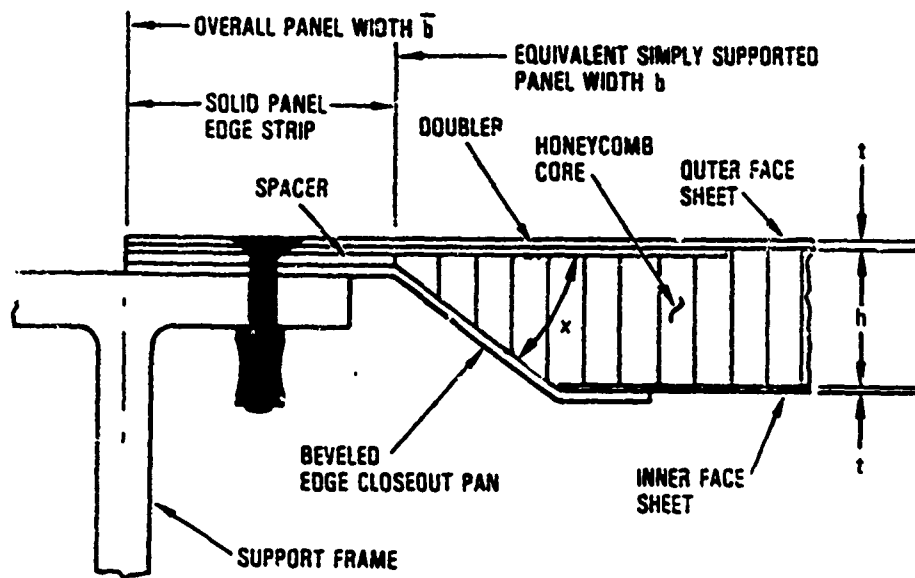


Figure 3.14. Typical honeycomb panel construction and geometry

$$\text{FREQUENCY} = f_{11} = K(h + t) b^2, \text{ Hz}$$

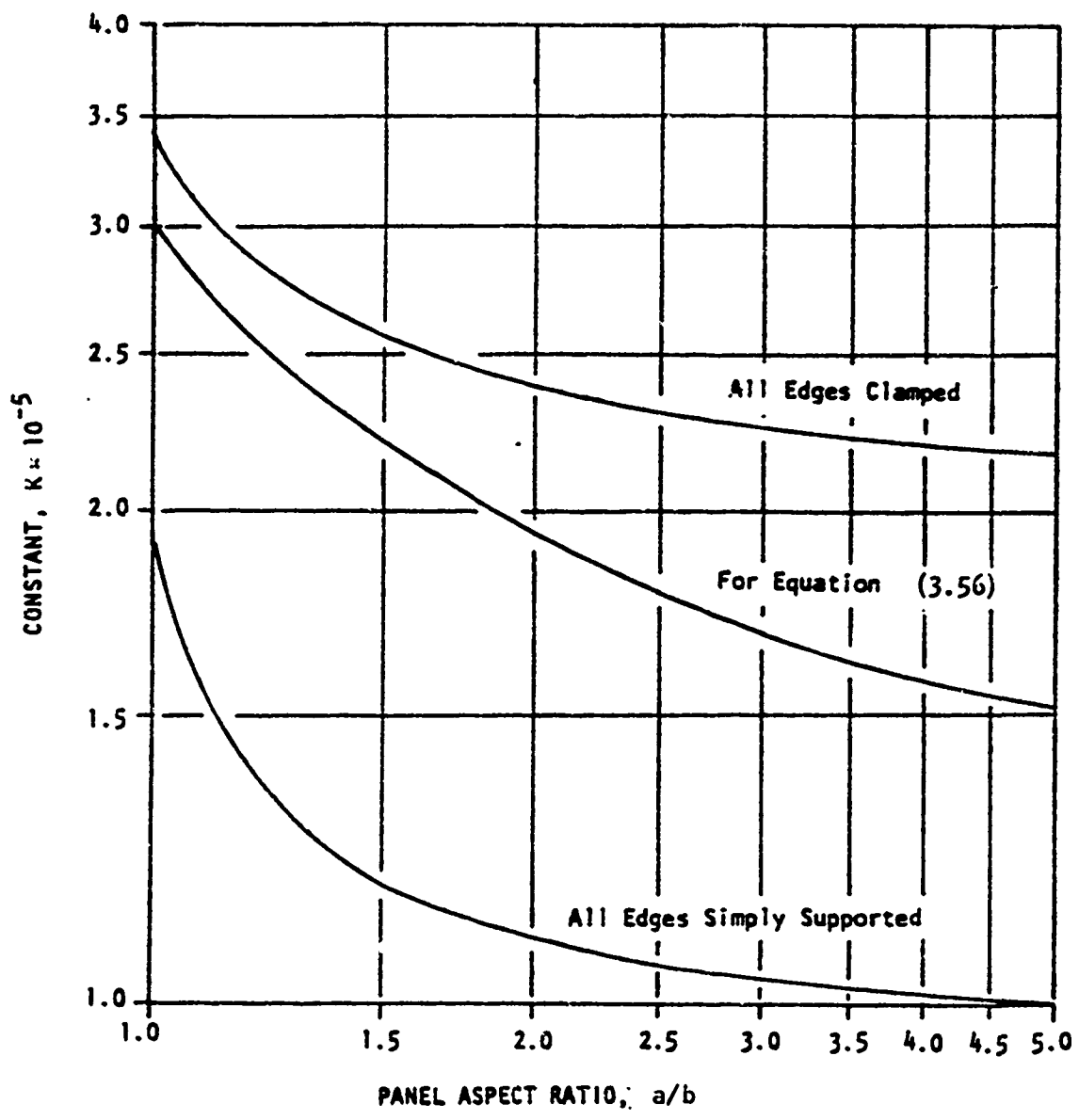


Figure 3.15. Nomograph for fundamental mode response frequency of a flat rectangular honeycomb sandwich panel.

beveled edges (Figure 3.14). The length, a , and width, b , of such an equivalent simply supported honeycomb panel are related to the overall length, \bar{a} , and width, \bar{b} , by

$$\begin{aligned} a &= \bar{a} - 2s \\ b &= \bar{b} - 2s \end{aligned} \quad (3.57)$$

where s is the width of the solid panel edges. The expression for the r^{th} (or m, n^{th}) mode natural frequency of the equivalent simply supported honeycomb panel, with isotropic face sheets and a honeycomb core that is infinitely stiff in shear, is given by

$$f_r = \frac{\pi}{2} (h + t) \left\{ \left(\frac{m}{a} \right)^2 + \left(\frac{n}{b} \right)^2 \right\} \left\{ \frac{Et}{2(1 - \nu^2)\tilde{M}} \right\}^{1/2} \quad (3.58)$$

where \tilde{M} , the mass per unit area, is

$$\tilde{M} = 2\rho_f t + \rho_c h + 2\rho_{ad} t_{ad} \quad (3.59)$$

and

- ρ_f = Face sheet material density
- t = Face sheet thickness
- E = Young's modulus for face sheet
- ν = Poisson's ratio for face sheet
- ρ_c = Honeycomb core density
- h = Honeycomb core thickness
- ρ_{ad} = Adhesive film density
- t_{ad} = Adhesive film thickness

The fundamental mode natural frequencies predicted by equation 3.58 appear to be in good agreement with the measured frequencies, for a wide range of honeycomb panels as illustrated in Figure 3.16 from Reference [3.13]. The use of the empirically derived equivalent simply supported mode shapes has both simplified the theory and enabled existing expressions for the generalized force of acoustically excited simply supported panels to be used in the subsequent analysis.

3.6.2 Response to Harmonic Excitation

The methods described in Section 3.4.2 for flat plates can be applied to honeycomb sandwich panels. Use equivalent simply supported panel dimensions a and b , and simply supported edge conditions in Table 3.15 to determine the generalized force and mass.

3.6.3 Response to Random Excitation

In Reference [3.13], Soovere develops an expression for the inner face sheet strain at the center of a honeycomb panel in response to random pressure excitation. The rotation of the beveled edges is shown to introduce a linear membrane strain into the inner face sheet, in the symmetric modes of honeycomb panels with stiff lateral edge supports, superimposed on the bending strain. This combined strain is highest in the fundamental mode with a theoretical maximum inner to outer face sheet strain ratio approaching 2.3. Since the predominant response to random acoustic loading is obtained in the fundamental mode, the theory explains why face sheet acoustic fatigue failures occur predominantly in the inner face sheet of rigidly mounted honeycomb panels.

The following equation is developed in Reference [3.13] for the inner face sheet strain at the panel center, due to random acoustic pressure excitation:

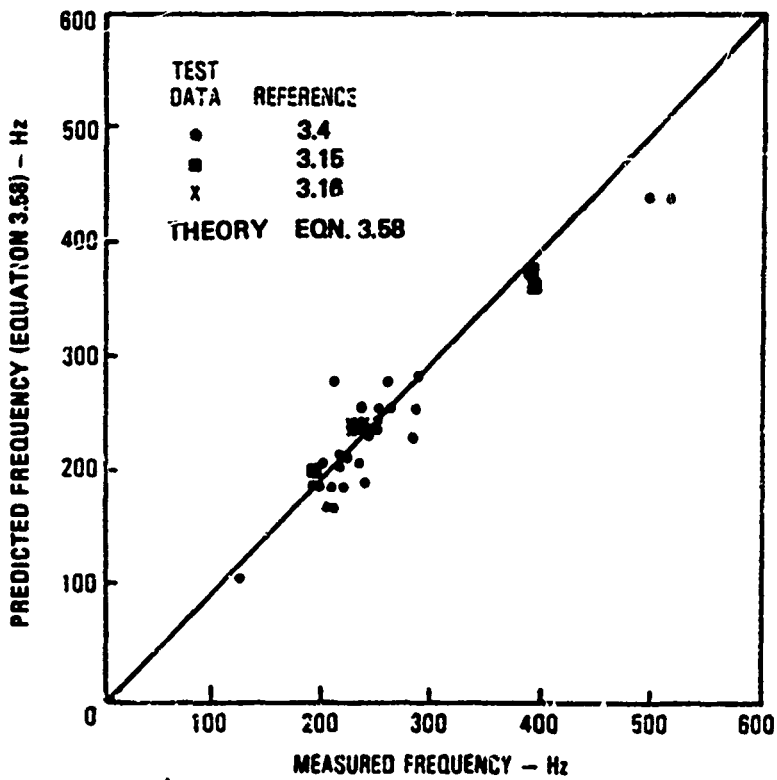


Figure 3.16. Comparison of predicted and measured fundamental mode natural frequency of stiffened aluminum honeycomb panels.

$$\epsilon_{ycl} = \frac{\bar{B}_y}{\kappa^2} \frac{h + 2t}{b^2 H} \left(\frac{G_p}{\delta_r} \right)^{1/2} \frac{1}{f_r^{3/2}} \frac{\left(1 + \cos \left\{ \frac{2\pi f_r a}{c} \right\} \right)^{1/2}}{\left(1 - \left(\frac{2f_r a}{c} \right)^2 \right)} \quad (3.60)$$

where

$$\bar{B}_y = \frac{1}{1.4} \left[1 + \frac{4\epsilon_{Mc}}{n\kappa\epsilon_{Mi}} \right] \quad (3.61)$$

and $\epsilon_{Mc}/\epsilon_{Mi}$ is given by

$$\frac{\epsilon_{Mc}}{\epsilon_{Mi}} = \left\{ 1 - \left[\cos^2 \chi + \frac{K' b_i}{2} \left\{ \frac{\cosh (K' b_i / 2) - 1}{\sinh (K' b_i / 2)} \right\} \right] \frac{\gamma_B}{\psi_A} \right\} \quad (3.62)$$

The new terms introduced in the above equations are:

- ϵ_{ycl} = Inner face sheet strain at panel center
- G_p = Power spectral density of pressure excitation
- δ_r = Viscous damping ratio
- f_r = Fundamental mode natural frequency (from equation 3.58)
- c = Speed of sound in air
- χ = Angle of beveled edge of honeycomb core
- b_i = Inner face sheet width

K' , γ_B and ψ_A are given by

$$K' = \left\{ \frac{G}{E t h} \right\}^{1/2} \quad (3.63)$$

$$\gamma_B = \frac{\psi_A}{\cos^2 \chi + \frac{E t_p b_1 \cos^2 \chi \sin \chi}{2E t_h} + \frac{K' b_1}{2} \left\{ \frac{\cosh (K' b_1 / 2) - 1}{\sinh (K' b_1 / 2)} \right\}} \quad (3.64)$$

$$\psi_A = \frac{n\pi}{b} w_n \cos \frac{n\pi l}{b} \quad (3.65)$$

where G is the shear modulus of the core and subscript p refers to the closeout pan (Figure 3.14). In equation 3.65, w_n is the modal intensity for the n^{th} bending mode.

3.7 CYLINDRICAL SHELLS

Reference [3.7] presents data for moderately deep open circular cylindrical shells, which are too deep to qualify as shallow shells as defined in Section 3.5. For the fundamental mode of a moderately deep open circular cylindrical shell with all edges clamped the expression for the frequency is

$$f_{11}^2 = \frac{E^*/\rho}{4\pi^2 R^2} + \frac{(E^*/\rho)h}{48\pi^2 a^2 b^2} \left\{ 500.6 \left(\frac{b}{a}\right)^2 + \frac{\alpha_1^4 \eta_1}{\theta_1} \left(\frac{a}{b}\right)^2 + 24.605 \frac{\alpha_1^2}{\theta_1} [\delta_1 - \nu(\gamma_1 + \delta_1)] \right\} \quad (3.66)$$

where the quantities α_1 , γ_1 , δ_1 , η_1 , θ_1 are functions of the included angle of the cylindrical shell (see Figure 3.4) and are presented in Figure 3.17.

Reference [3.3] presents more general results considering both higher order modes and other boundary conditions.

For closed or complete cylindrical shells, Reference [3.17] presents curves which can be used to calculate the natural frequencies. The geometry used in Reference [3.17] is shown in Figure 3.18. For freely supported

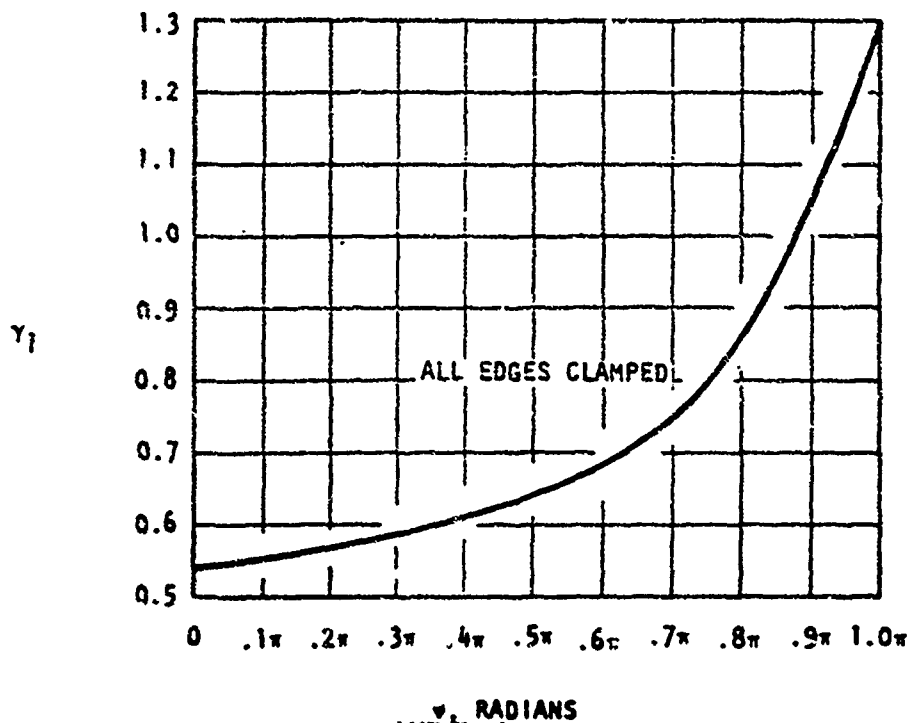
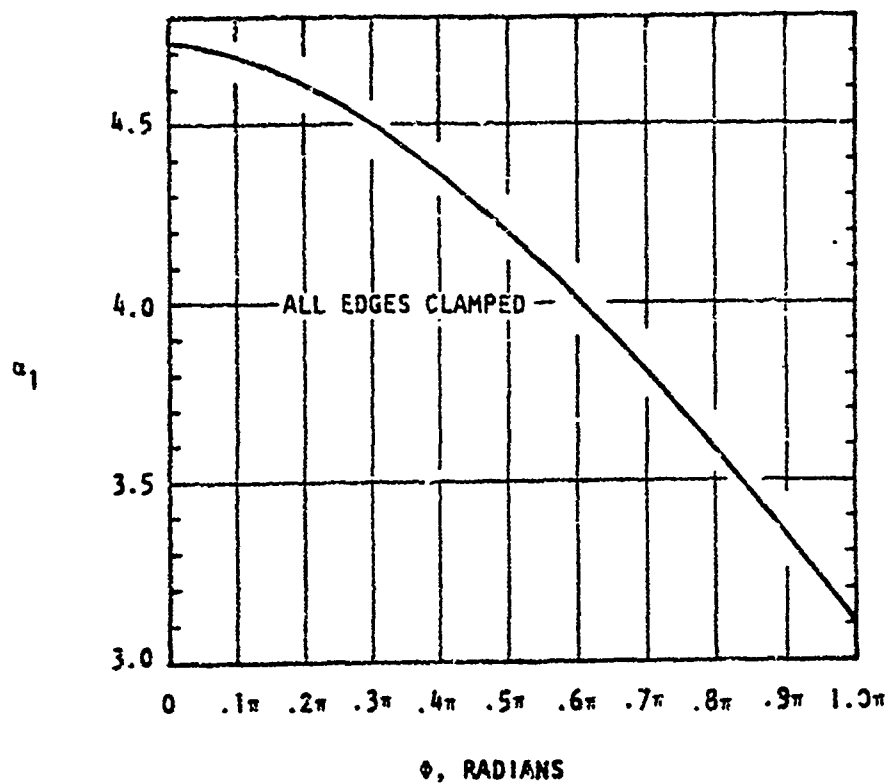


Figure 3.17. Plot of α_1 , γ_1 , δ_1 , η_1 , and θ_1 for moderately deep open circular cylindrical shells. (continued)

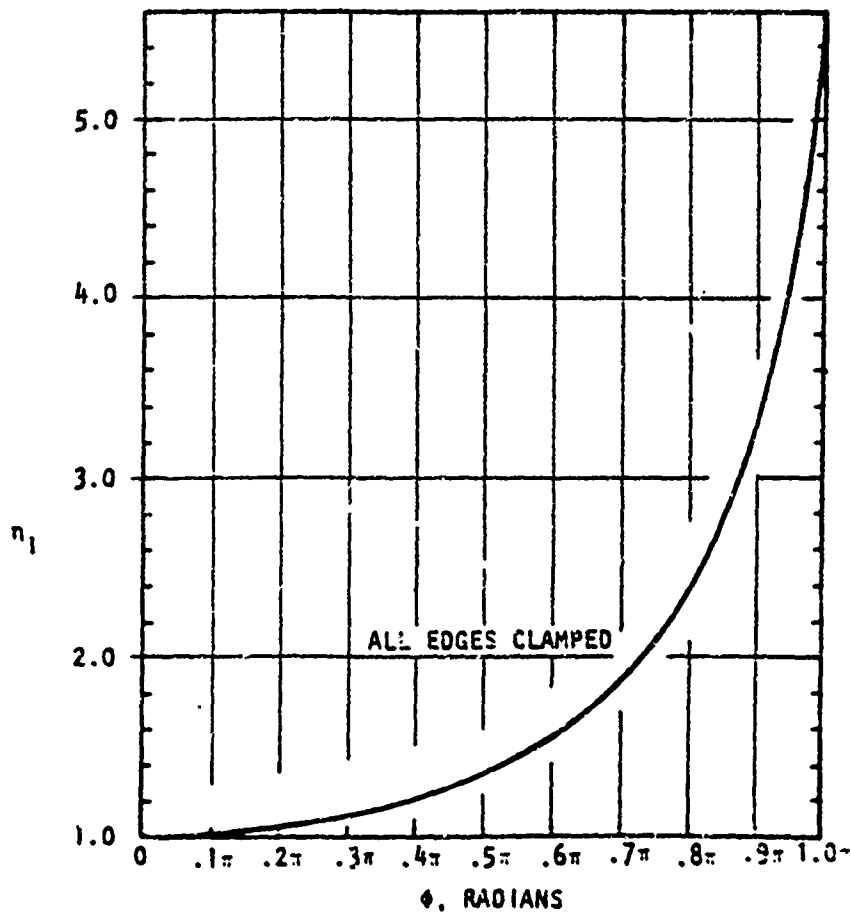
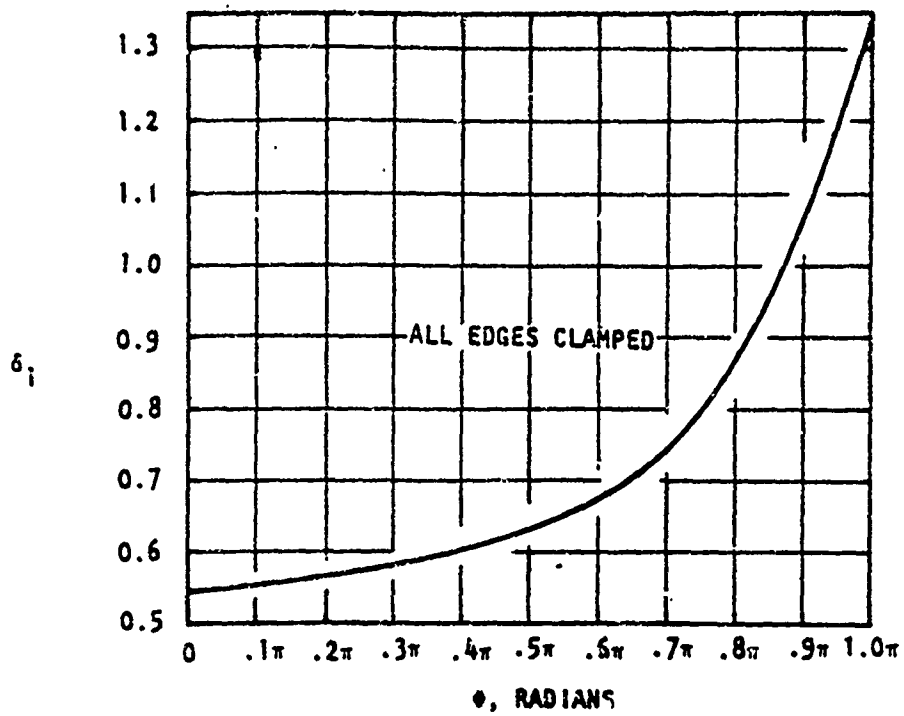


Figure 3.17. Plot of α_i , γ_i , δ_i , η_i , and θ for moderately deep open circular cylindrical shells. (continued)

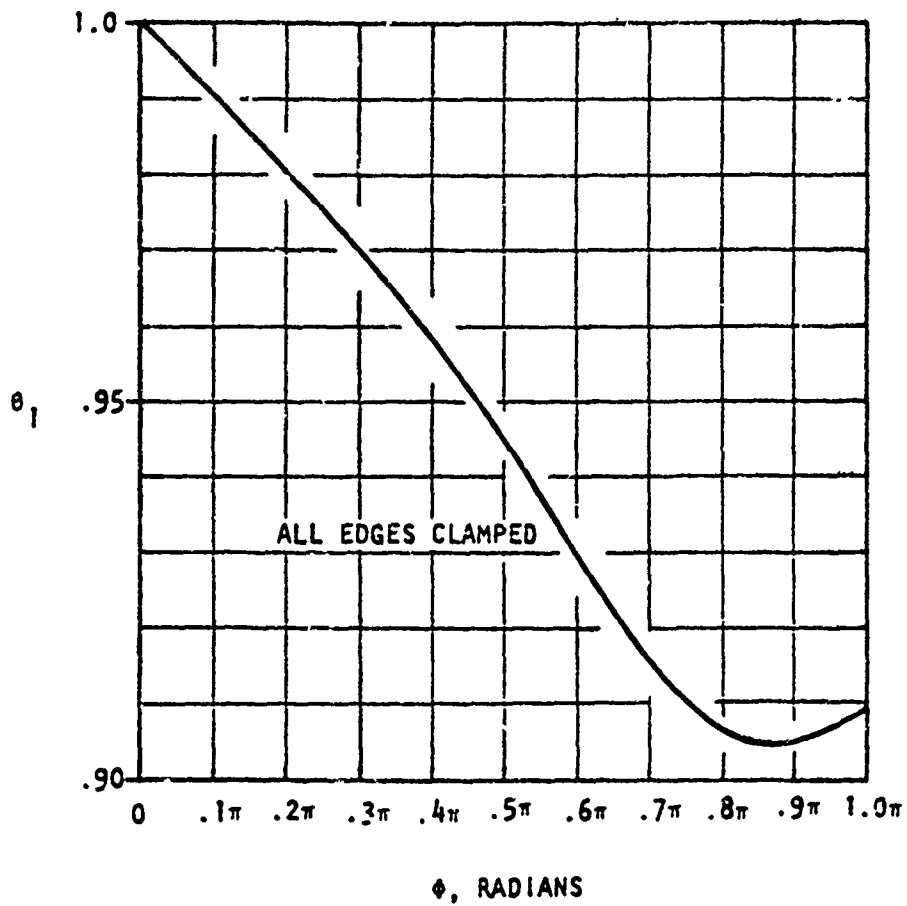


Figure 3.17. Plot of α_1 , γ_1 , δ_1 , η_1 , and θ_1 for moderately deep open circular cylindrical shells. (concluded)

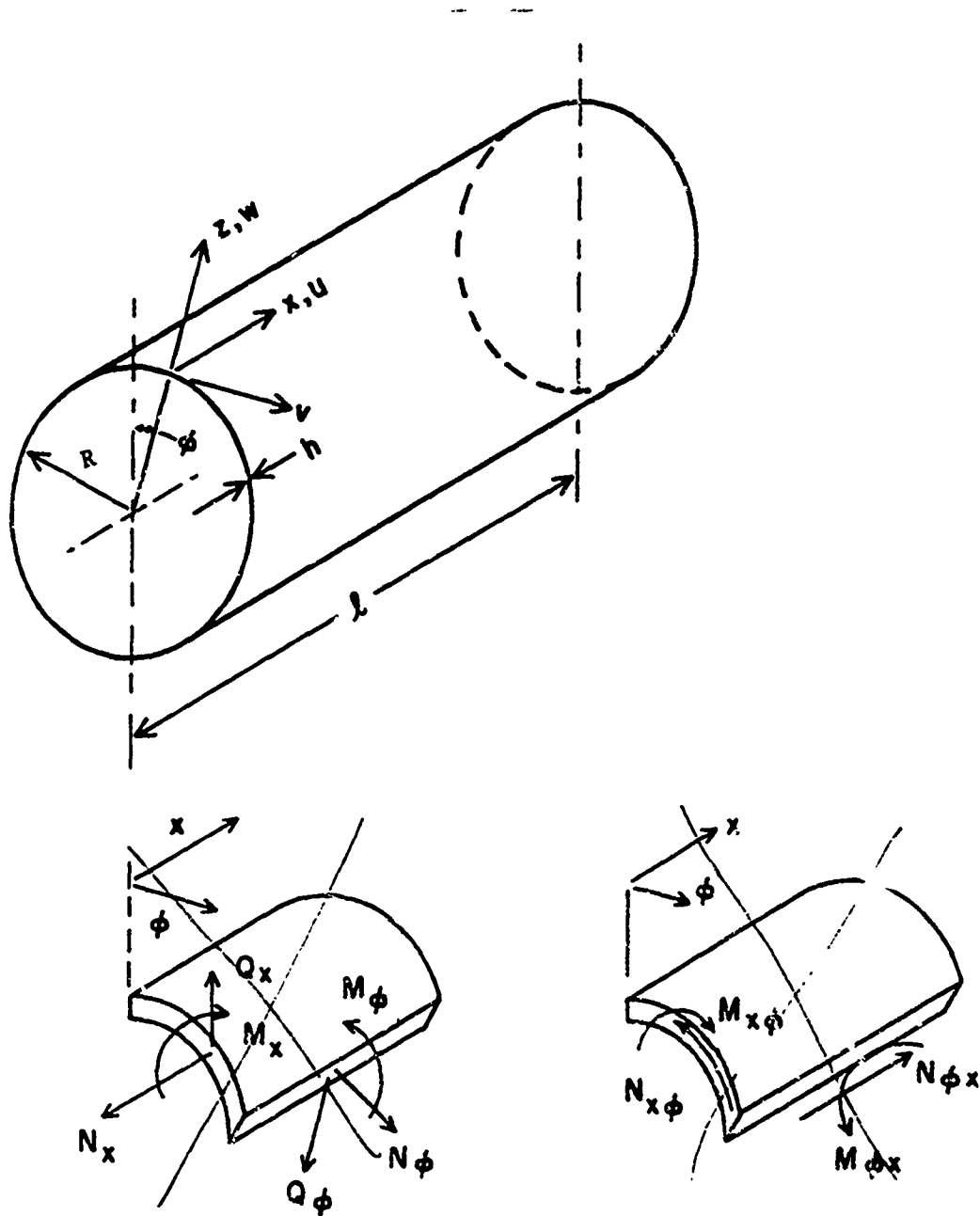


Figure 3.18. Closed circular cylindrical shell geometry.

cylinders subjected to both axial loads and a pressure loading, the natural frequency can be calculated from

$$\omega^2 = \omega_0^2 \left(1 - \frac{q_2}{q_{20}} - \frac{q_1}{q_{10}} \right) \quad (3.67)$$

where

- ω = Natural frequency for loaded cylinder
- ω_0 = Natural frequency for unloaded cylinder
- q_2 = P/D Non-dimensional axial load parameter
- q_{20} = Value of q_2 for buckling due to axial load
- q_1 = Pa/D Non-dimensional pressure parameter (positive for external pressure)
- q_{10} = Value of q_1 for buckling due to external pressure
- P = Axial load on shell boundary (positive in compression)
- D = $Eh/(1-\nu^2)$ Stiffness parameter
- p = Uniform normal pressure (positive inward)
- R = Radius of cylinder

Equation 3.67 shows that the natural frequency decreases for compressive axial loading and externally applied pressure.

The unloaded natural frequency, ω_0 , can be obtained from Figures 3.19 through 3.25, taken from Reference [3.17]. Each figure is for a different value of R/h , the shell radius divided by skin thickness. The natural frequency is a function of the number of circumferential waves, n , and the number of axial half-waves, m . The parameter γ is given by

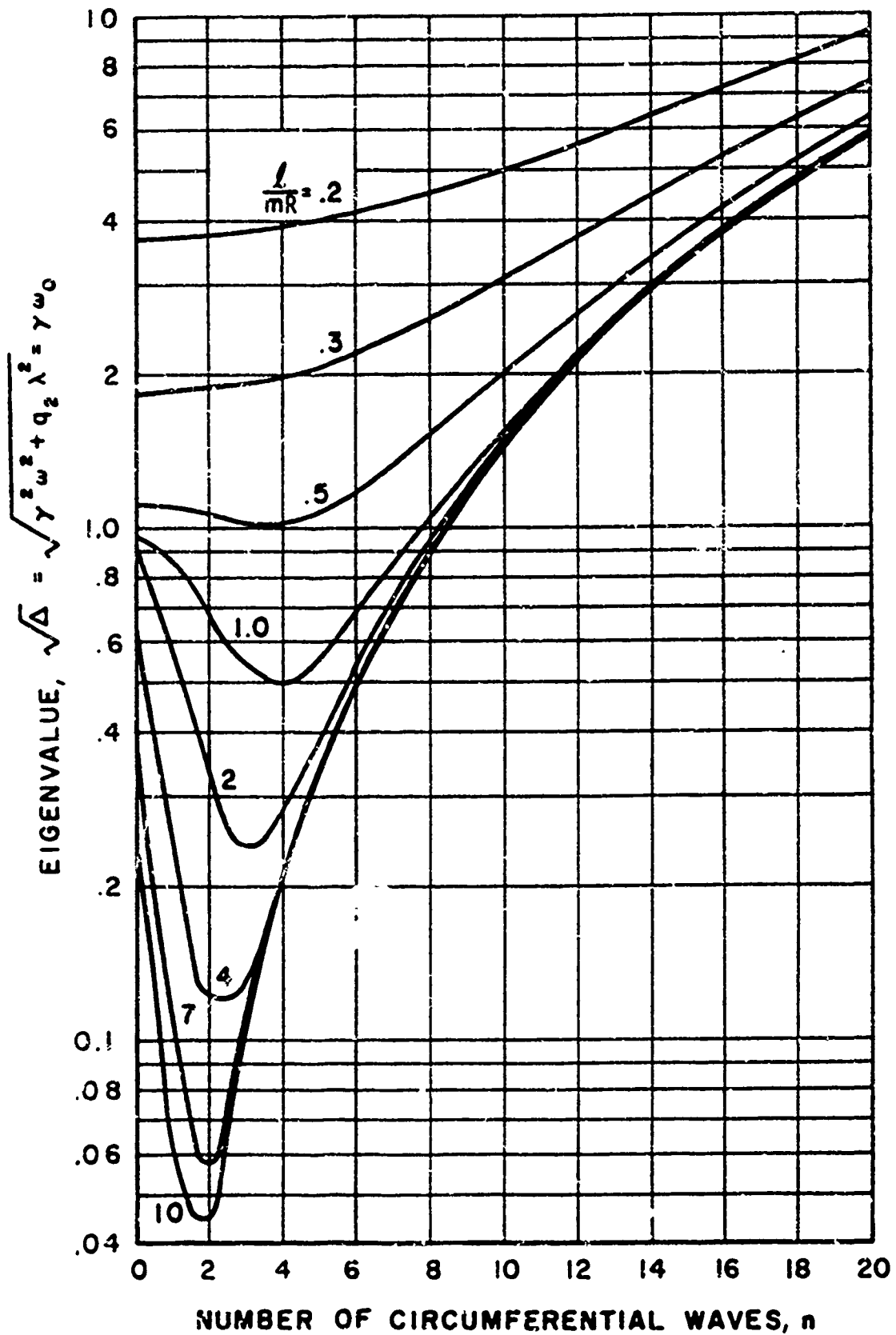


Figure 3.19. Radial vibration frequencies $R/h = 20$. No external pressure ($q_1 = 0$).

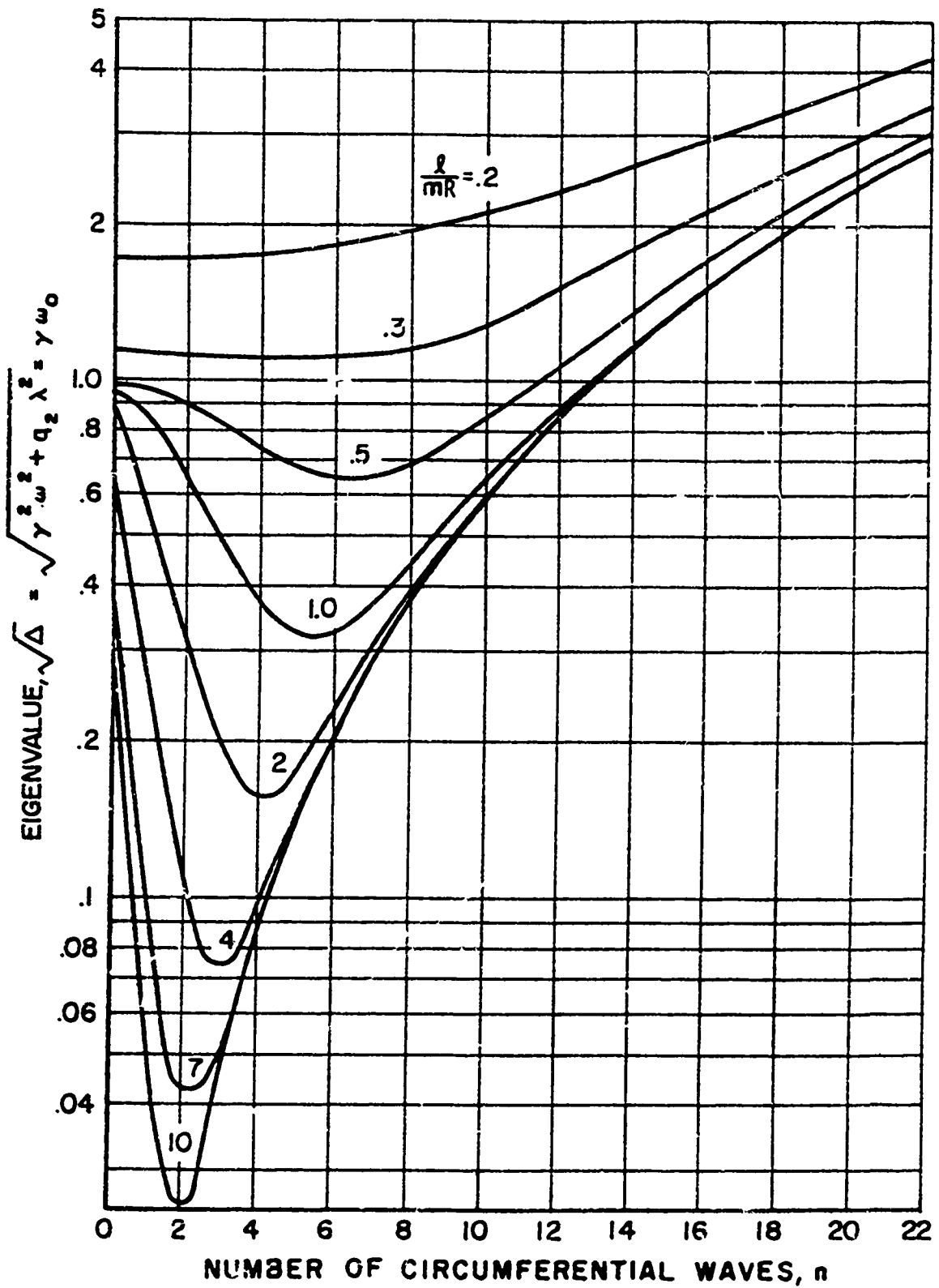


Figure 3.20. Radial vibration frequencies $R/h = 50$. No external pressure ($q_1 = 0$).

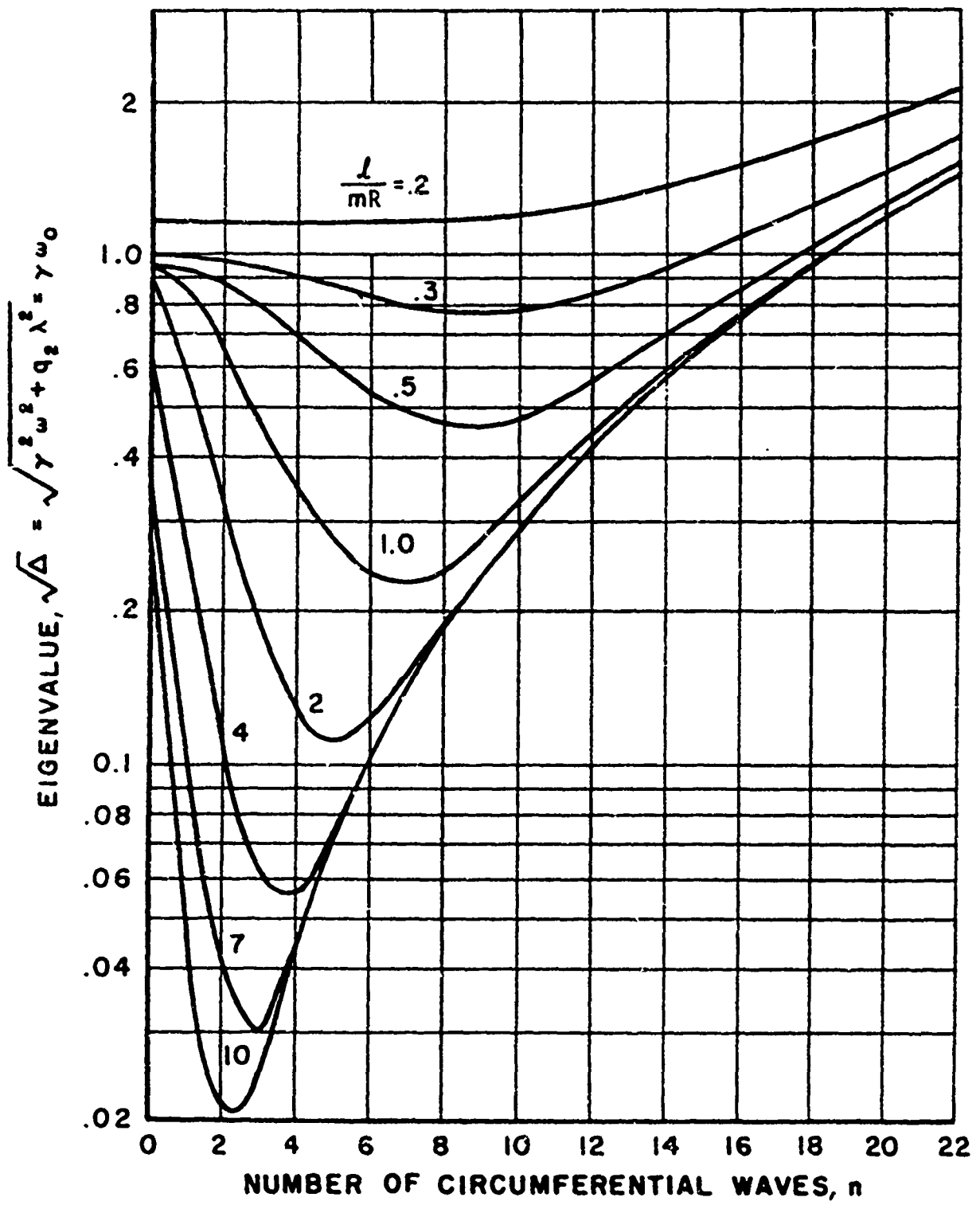


Figure 3.21. Radial vibration frequencies $R/h = 100$. No external pressure ($q_1 = 0$).

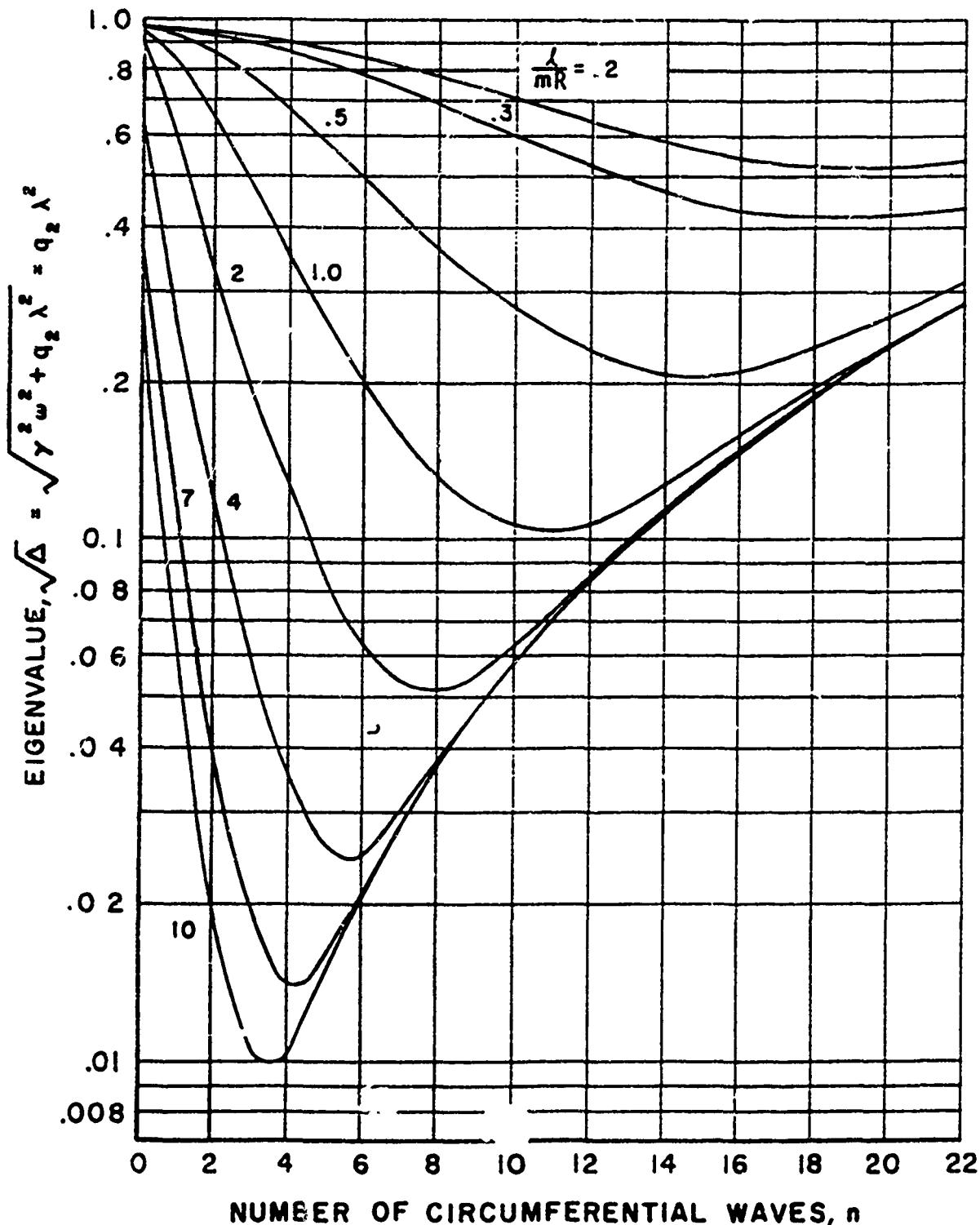


Figure 3.22. Radial vibration frequencies $R/h = 500$. No external pressure ($q_1 = 0$).

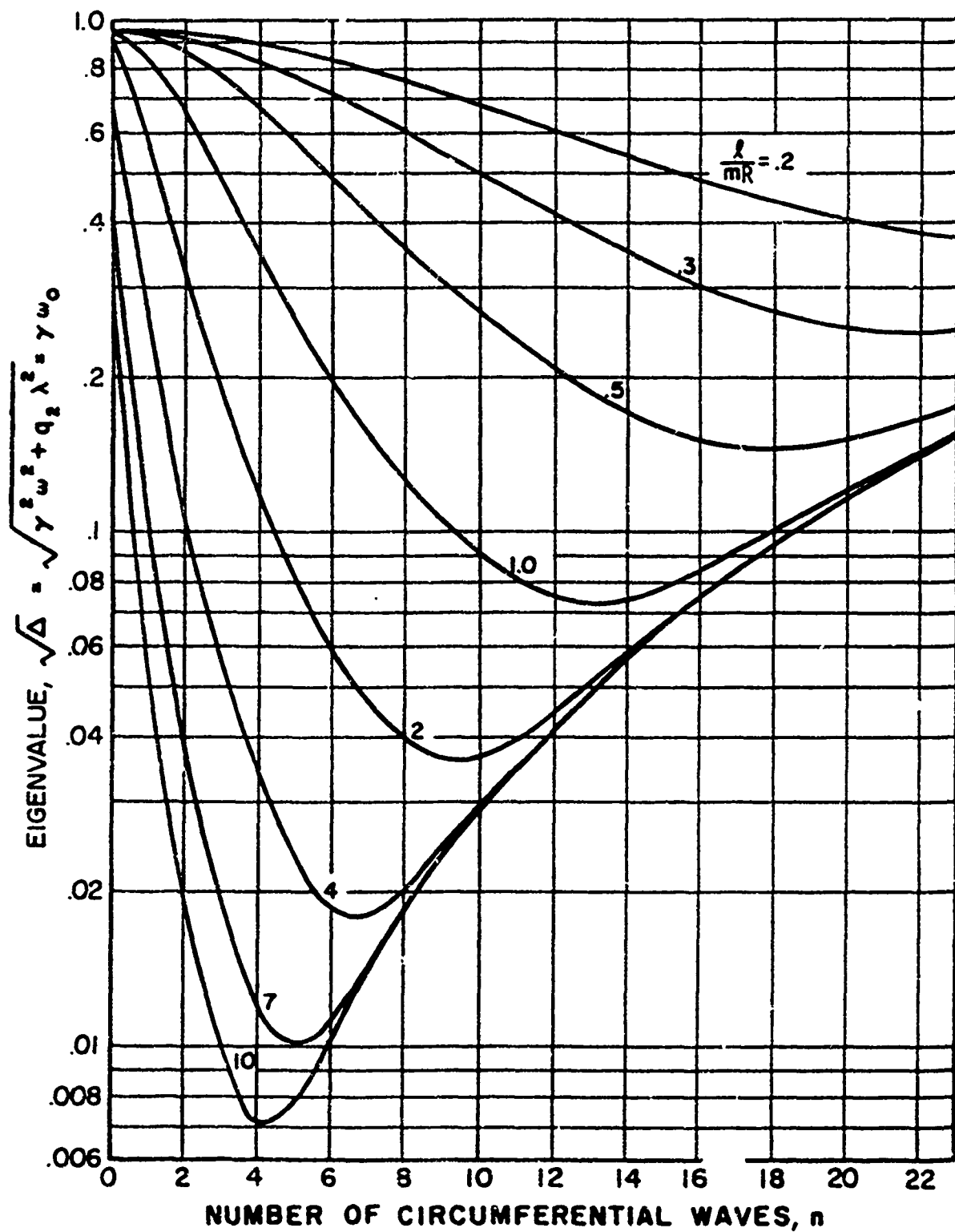


Figure 3.23. Radial vibration frequencies $R/h = 1000$. No external pressure ($q_1 = 0$).

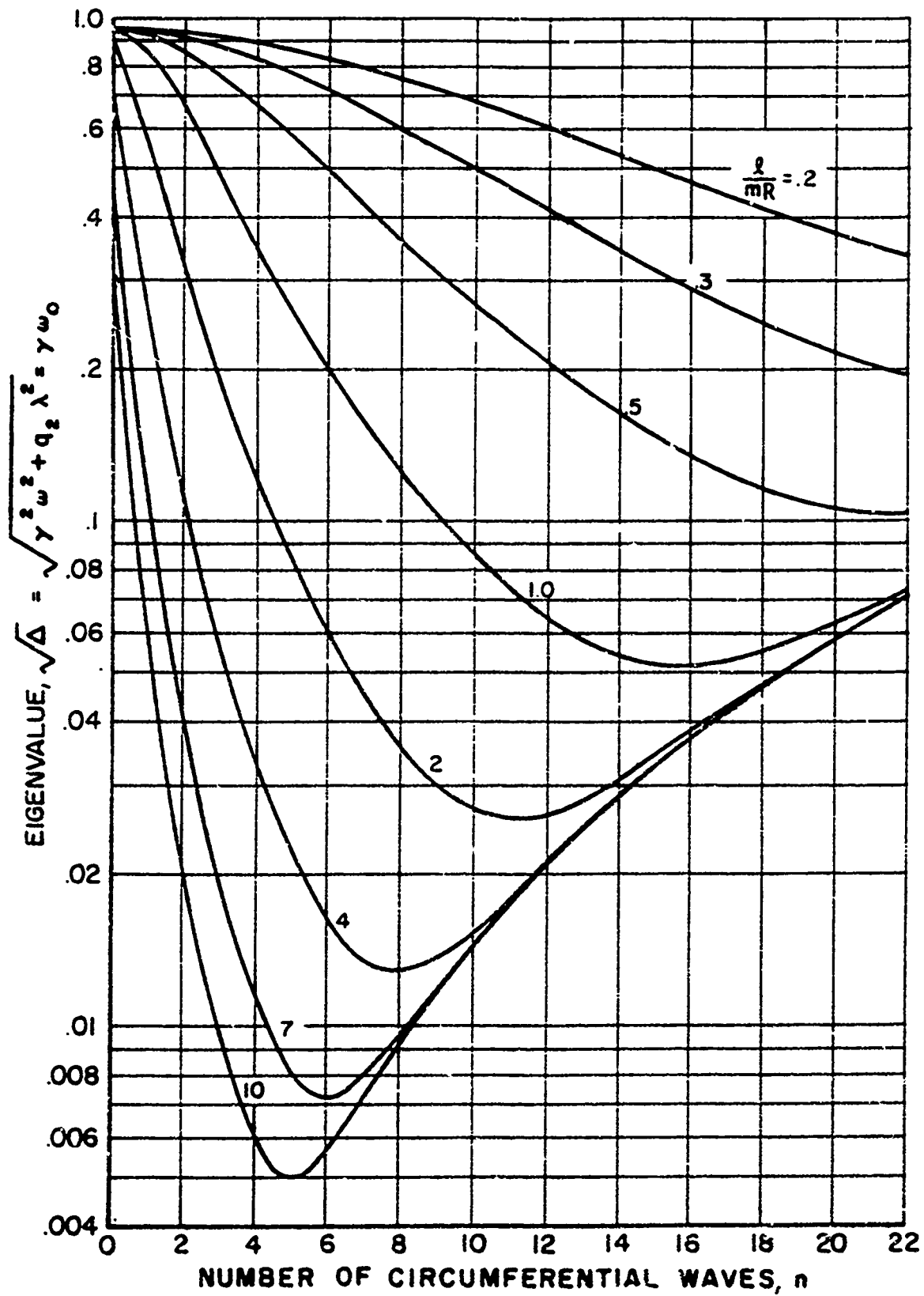


Figure 3.24. Radial vibration frequencies $R/h = 2000$. No external pressure ($q_1 = 0$).

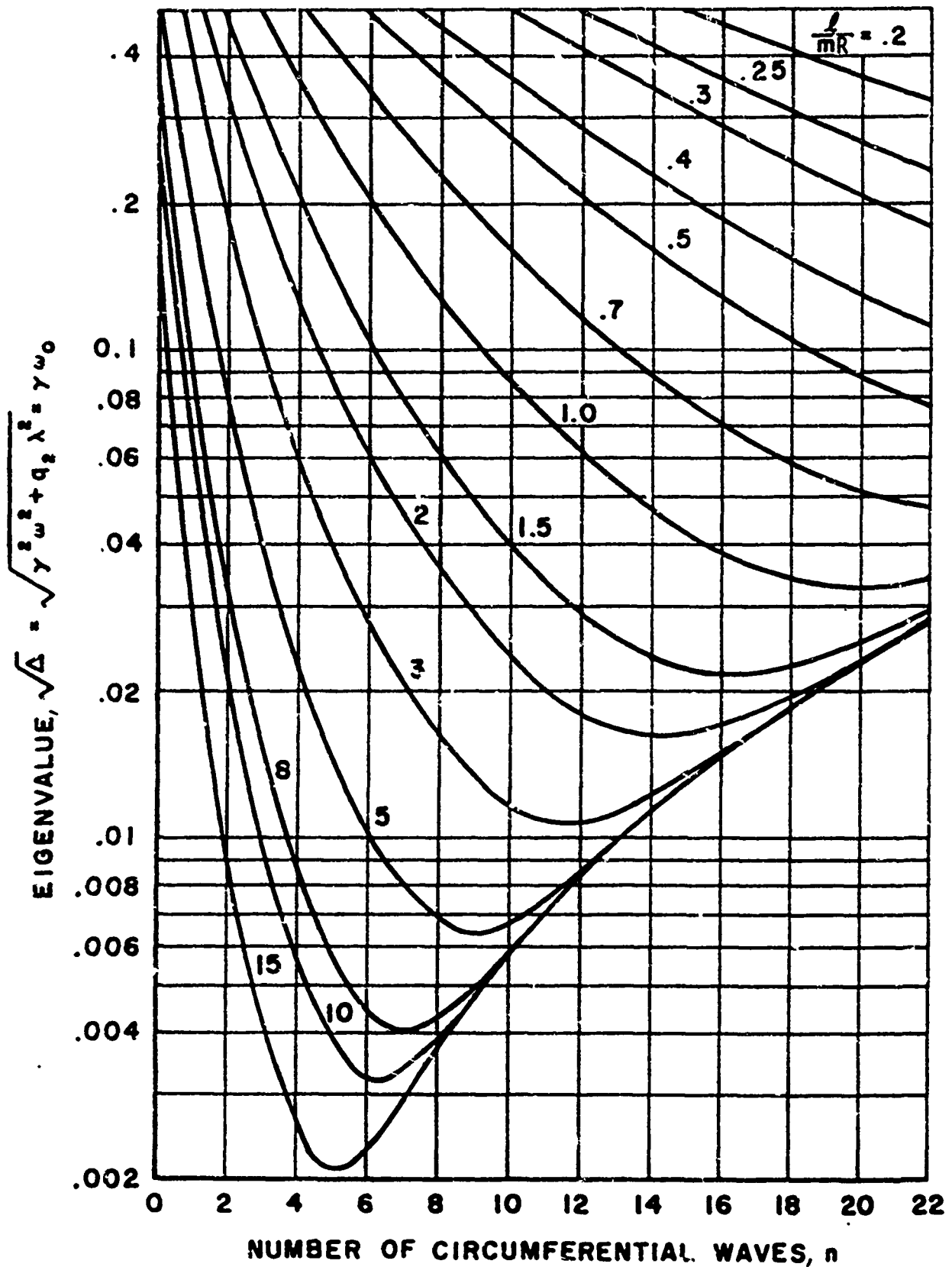


Figure 3-25. Radial vibration frequencies $R/h = 5000$. No external pressure ($q_1 = 0$).

$$2 = \frac{\rho R^2 (1-\nu^2)}{E} \quad (3.68)$$

and has units of seconds. E, ρ and ν are Young's modulus, density and Poisson's ratio of the shell skin.

3.8 NON-CYLINDRICAL SHELLS

Non-cylindrical shells include conical sections and general shells of revolution, the most common being spherical. Reference [3.3] discusses conical shells and presents the curves shown in Figure 3.26 for calculating the fundamental frequency for a frustrum of a cone with the small end clamped and large end free.

In Figure 3.26, the following definitions apply

- ω = Fundamental mode natural frequency
- r_2 = Radius at large end of cone
- ρ = Material density
- E = Young's modulus
- ν = Poisson's ratio
- h = Shell skin thickness
- α = Vertex half-angle

Results for other conical shell end conditions are presented in Reference [3.3], but are not simplified to the extent of Figure 3.26.

For shells of revolution, Reference [3.3], contains an extensive bibliography in Chapter 6, particularly for spherical shells. Other shells of revolution (ellipsoidal, paraboloidal, toroidal) have fewer references than spherical.

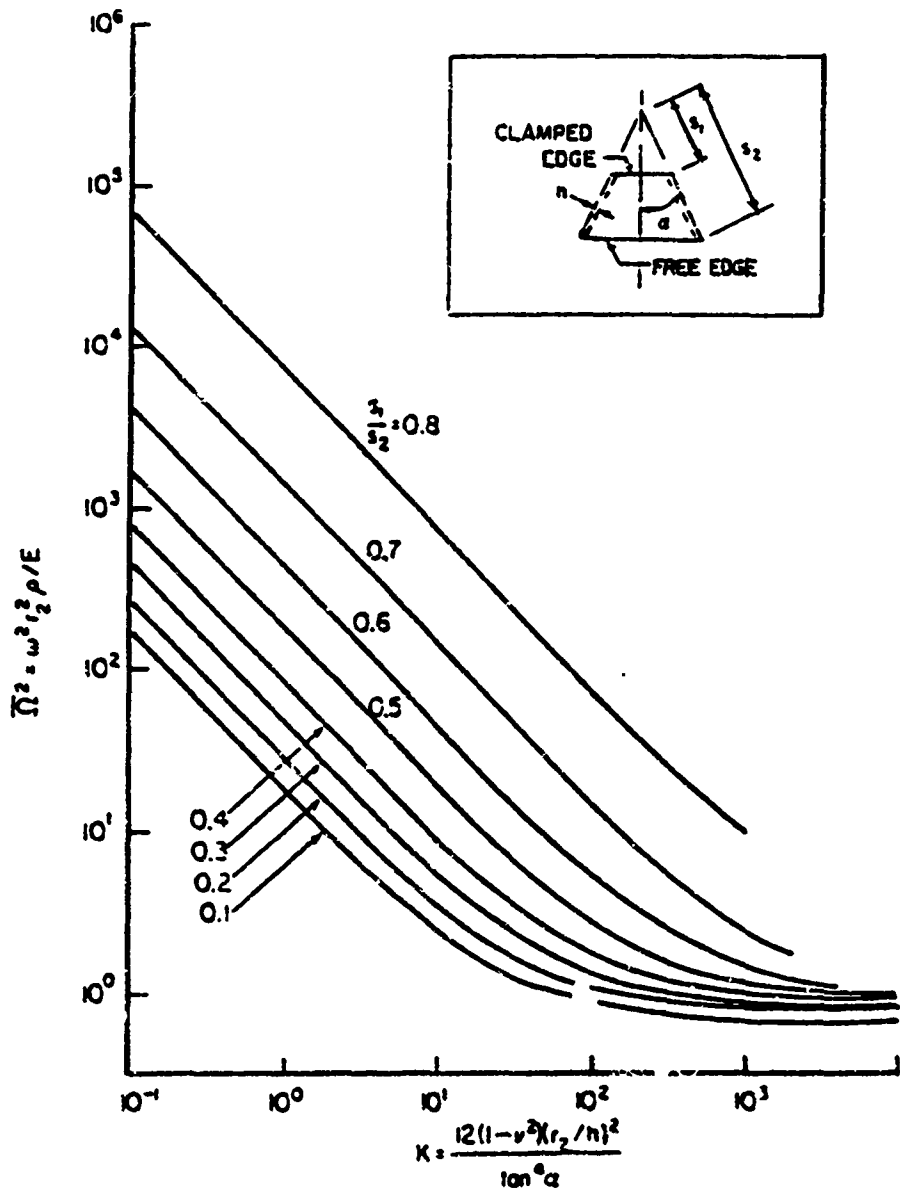


Figure 3.26. Axisymmetric frequency parameters of clamped-free conical shells for various s_1/s_2 ratios.

REFERENCES

- 3.1 Gorman, D., "Free Vibration Analysis of Beams and Shafts," John Wiley and Sons, 1975
- 3.2 Leissa, A.W., "Vibration of Plates," NASA SP-160, 1969
- 3.3 Leissa, A.W., "Vibration of Shells," NASA SP-288, 1973
- 3.4 Ballentine, J.R., et.al., "Refinement of Sonic Fatigue Structural Design Criteria," AFFDL-TR-67-156, 1968
- 3.5 Soovere, J., "Effects of Combined Acoustic and Flight Loads on Crack Growth," AFFDL-TR-76-68, 1976
- 3.6 Szechenyi, E., "Approximate Methods for the Determination of the Natural Frequencies of Stiffened and Curved Plates," Current Developments in Sonic Fatigue, ISVR Conference, July 1970
- 3.7 Rudder, F.F., Jr. and Plumblee, H.E., Jr., "Sonic Fatigue Design Guide for Military Aircraft," AFFDL-TR-74-112, 1975
- 3.8 Pulgrano, J.J. and Ablowitz, M., "The Response of Mechanical Systems to Bands of Random Excitation," Shock and Vibration Bulletin B9, pp. 43, January 1969
- 3.9 Harris, C.M. and Crede, C.E., "Shock and Vibration Handbook, Volume 1 - Basic Theory and Measurements," McGraw Hill, 1961
- 3.10 Miles, J.W., "On Structural Fatigue under Random Loading," Journal of Aeronautical Science Vol. 21 p 753-762, 1954
- 3.11 Sewall, J.L., "Vibration of Cylindrically Curved Panels with Simply Supported and Clamped Edges and Comparison with Some Experiments" NASA TN-D-3791, January 1967
- 3.12 Thomson, A.G.R., "Acoustic Fatigue Design Data, Part I," AGARD-AG-162-Part 1, May 1972
- 3.13 Soovere, J., "Vibration Analysis of Stiffened Honeycomb Panels with Beveled Edges," Journal of Aircraft, Vol. 23, No. 6, pp. 537, June 1986
- 3.14 Sweers, J.E., "Prediction of Response and Fatigue Life of Honeycomb Sandwich Subjected to Acoustic Excitation," Acoustic Fatigue in Aerospace Structures, Syracuse University Press, 1965, pp.389

- 3.15 Rasor, J.E., "Sonic Fatigue Test of 0.045 Lb/Ft² Adhesive for Honeycomb Sandwich Panels," Lockheed Report ER-9028, March 1967
- 3.16 Rasor, J.E., "Sonic Fatigue Tests on Low Density Core Honeycomb Panels," Lockheed Report ER-8601, July 1966
- 3.17 Bozich, W.F., "The Vibration and Buckling Characteristics of Cylindrical Shells under Axial Load and External Pressure," AFFDL-TR-67-28, May 1967

SECTION 4

DAMPING DESIGNS AND DESIGN APPROACH

The purpose of this section is to help the designer select the most appropriate damping concept for his particular problem. It provides general, but brief, information on how to design damping systems. The user is referred to the appropriate sections in Volume I for more detailed information.

4.1 SELECTION OF DAMPING CONCEPT

There are three basic damping concepts: the free layer treatment, the constrained layer treatment, and the tuned damper. The following sections briefly review each concept.

4.1.1 Free-Layer Damping

A free-layer damping system is the simplest method to add damping to a structure. It involves choosing the appropriate damping material and bonding it to the structure (Figure 4.1a). Typical examples of free layer damping are:

- 1) Polymeric coatings on sheet metal bins to reduce impact noise.
- 2) Automotive undercoating.
- 3) Glass coating on turbine blades.

The main drawback with this damping system is that the increased damping is obtained with the greatest weight increase. There is also an optimum free-layer thickness beyond which the damping does not increase significantly with a further increase in the damping layer thickness.

In a free-layer damping design, the principal damping material deformation is due to extension and compression, produced by the deformation of the structure during vibration. The energy dissipated in the damping layer is given by

$$D_S = \pi \int_V \eta E \epsilon^2 dV \quad (4.1)$$

where the integration is taken over the volume, V , of the damping material. Also E and η are the Young's modulus and loss factor of the damping material, respectively.

and ϵ is the localized dynamic strain. This localized strain is determined by the mode shape of the structure. Since the design of the damping treatment offers no way of maximizing the strain other than by location on the structure or through the use of a spacer (Figure 4.1b), the optimum free-layer design is primarily dependent on the damping material properties (see equation 4.1). Spacers, which have a high shear stiffness and a very small or no extension stiffness, increase the strain by increasing the distance from the neutral axis to the free damping layer. This increase in strain is, however, obtained at the expense of increased weight.

A good free-layer damping material must, therefore, have a high modulus and a high loss factor. Generally effective free-layer materials have an extensional loss modulus, the product of the Young's modulus and loss factor, above 10^5 pounds per square inch ($6.9 \times 10^8 \text{ N/m}^2$). The optimum design temperature range for a free-layer material is shown in Figure 4.2.

There are two approaches available to increase the effective temperature range of a free-layer damping system. The first is to use a polymer blend of two or more good free-layer damping materials which results in a new material with multiple transition regions leading to a larger effective damping temperature range. The second approach is to use a multiple layer system as shown in Figure 4.3. The temperature range increase, resulting from a two-layer system, is also shown in Figure 4.3. Note that the high temperature material must be placed next to the structure for two reasons. First, if the low temperature material was next to the structure, it would be too soft at higher temperatures to transmit strains to the higher temperature materials. Second, at the lower temperatures, the higher temperature material would restrict the deformation of the lower temperature material because it is stiffer, which would reduce the low temperature damping.

An important point to remember is that a free-layer damping system will function only if the structural mode shapes to be damped are beam or plate-like and have large areas with significant bending strains.

4.1.2 Constrained Layer Damping

The simplest form of a constrained layer damping treatment is the single constrained layer system illustrated in Figure 4.4. The constraining layer causes the damping material to deform in shear as the structure it is applied to vibrates. The constrained layer damping system has the advantage of being considerably lighter than a free-layer system which would produce the same level of modal damping for a given structure.

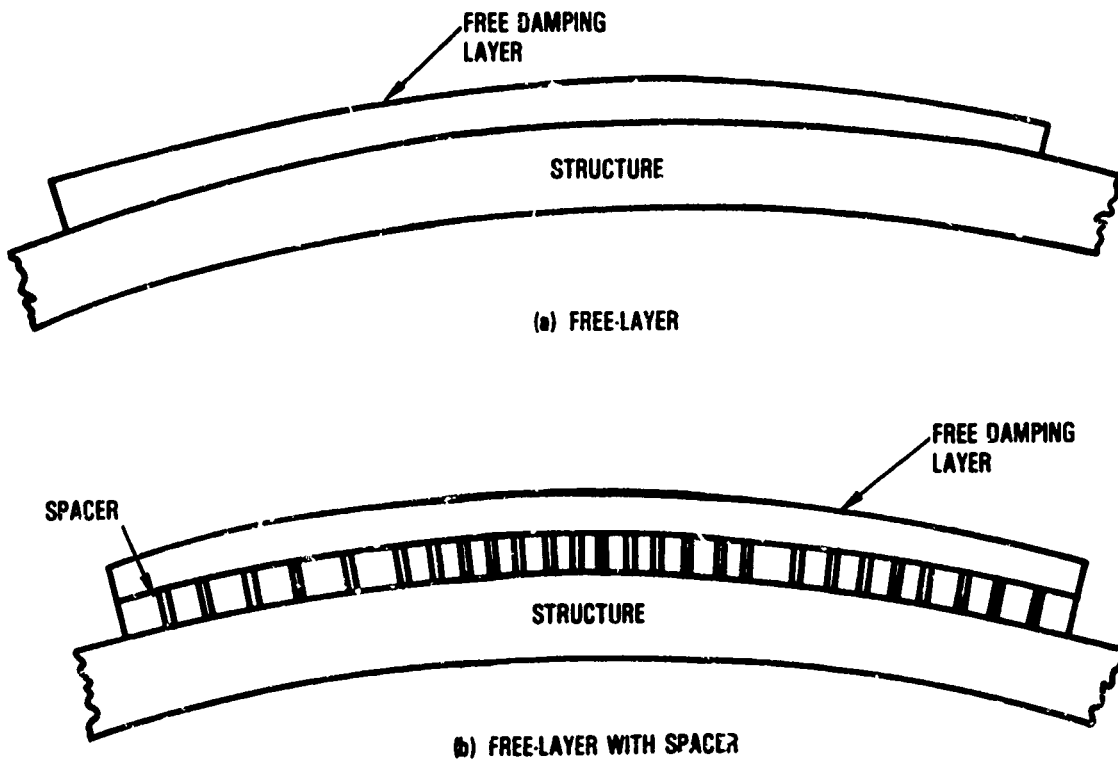


Figure 4.1. - Typical free-layer damping treatment.

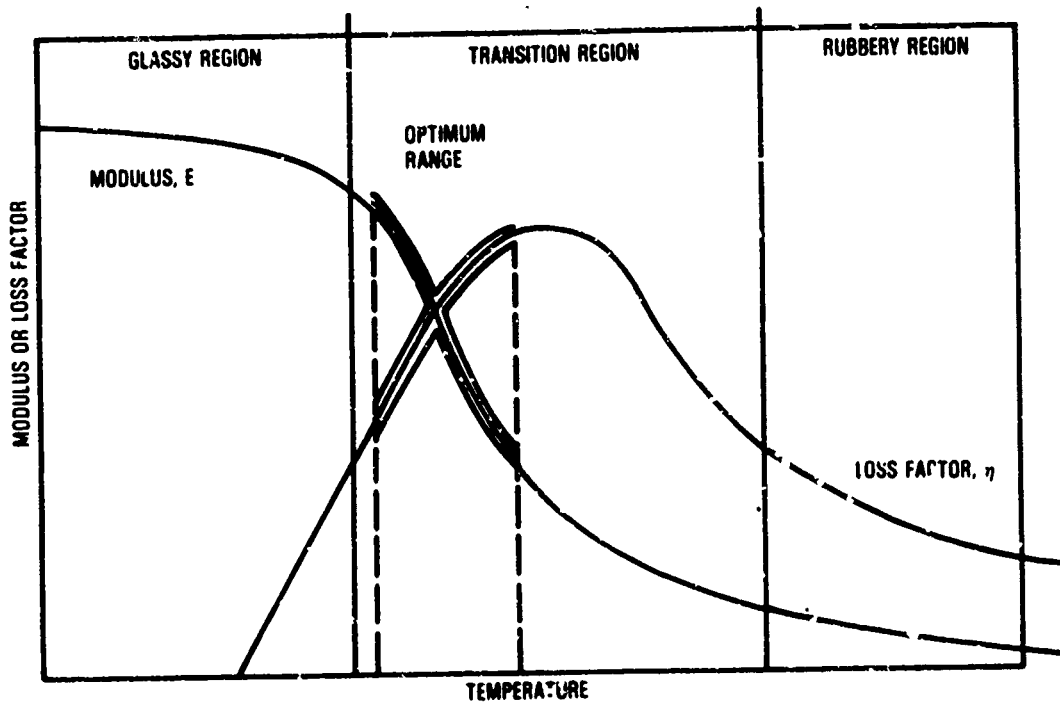
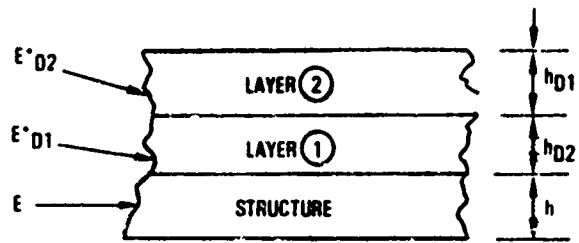


Figure 4.2. - Optimum temperature range for free-layer treatment.



h - THICKNESS
 E^* - COMPLEX MODULUS OF DAMPING MATERIAL
 E - MODULUS OF STRUCTURE
 $D1, D2$ - SUBSCRIPTS DENOTING FIRST AND SECOND LAYER OF DAMPING MATERIAL

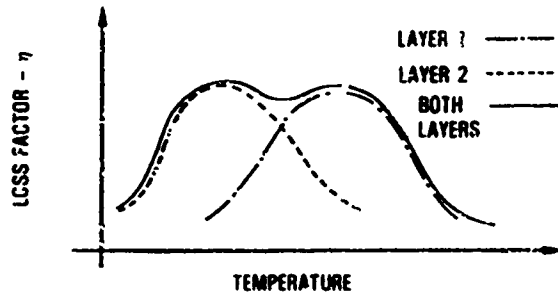


Figure 4.3. - Multiple free-layer broadening effect.

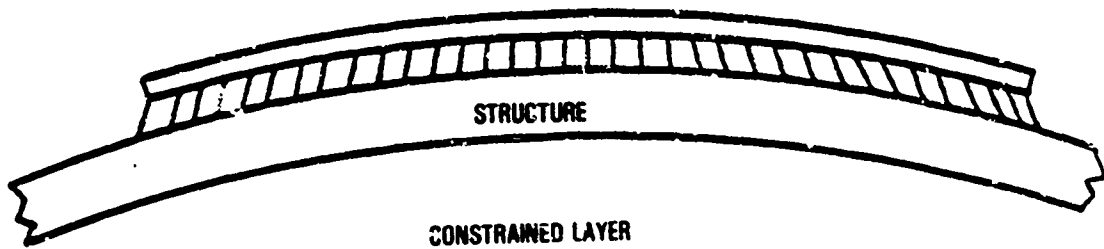


Figure 4.4 - Constrained layer damping treatment.

The damping material may be self adhesive and adhere to both the structure and the constraining layer without the use of an additional bonding agent. The most efficient design of the constrained layer damping involves the use of a viscoelastic damping layer that is sandwiched between two equal thickness structural surfaces. This design introduces the greatest shear into the damping material. Typical examples of constrained layer damping are:

- 1) Adhesive tape applied to aircraft panels to reduce dynamic stress and interior noise
- 2) Sandwich sheet type components in diesel engines to reduce indicated noise
- 3) Wraps applied to jet engine inlet guide vanes
- 4) Damped bolts for mirror supports in space applications.

The main drawback is that the design of an effective constrained layer damping system is considerably more complicated through the free layer system.

The energy dissipated by shear in the damping layer is given by

$$D_S = \pi \int_V \eta C \gamma^2 dV \quad (4.2)$$

where C is the shear modulus and γ is the localized shear strain in the damping layer. The designer now has control of the strain term, γ^2 . By properly matching the geometry, and damping material modulus to the structure under consideration, the design can maximize the strain in the damping material.

The temperature range for obtaining maximum damping from a shear damping material is shown in Figure 4.5. A good shear damping material generally has a maximum loss factor equal to or greater than 1.0. The optimum modulus for a shear damping material is totally dependent on the structure on which the material is being applied, the material of the constraining layer and the geometry of the constrained layer system. Often, an optimum material which would give maximum damping for all the modes of the structure cannot be found. In this case the damping design must be tailored to provide maximum damping for the particular resonant modes of interest.

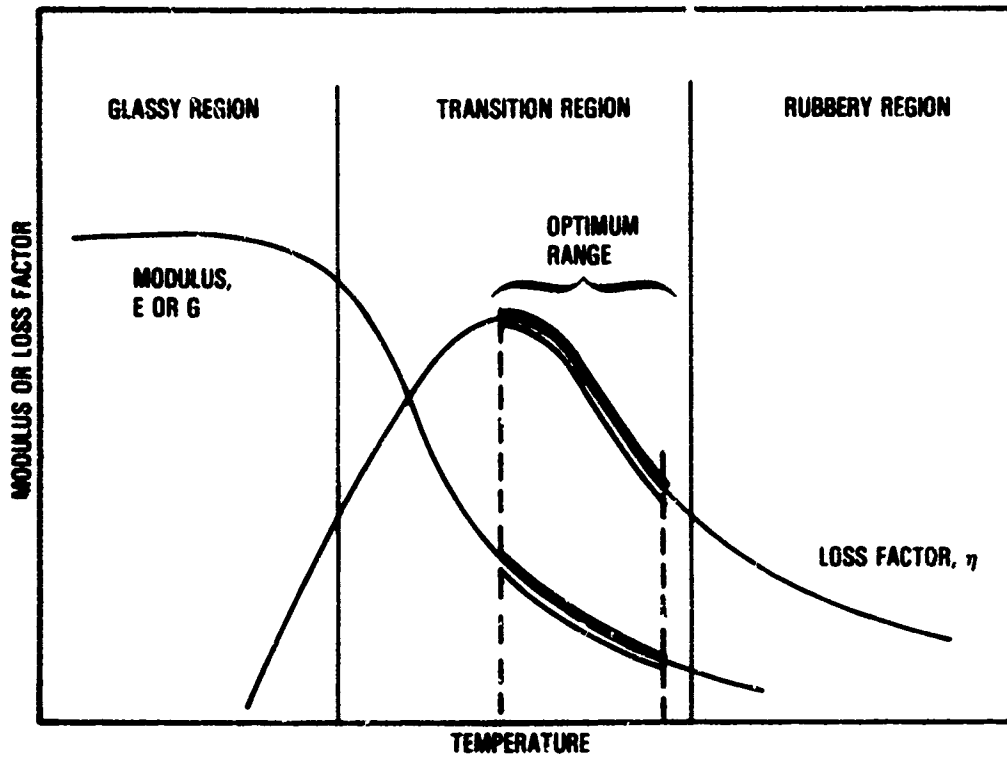


Figure 4.5. - Optimum temperature range for constrained layer treatment.

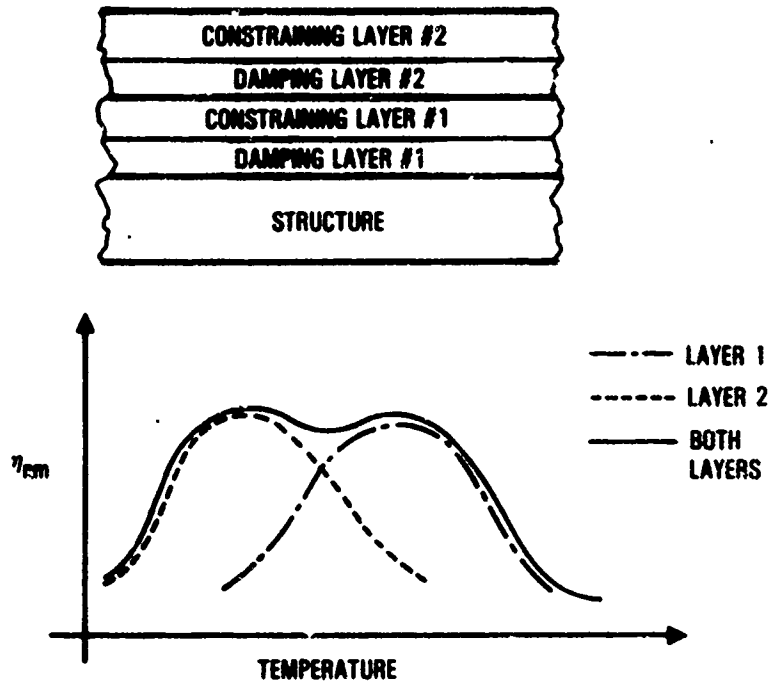


Figure 4.6. - Multiple constrained layer broadening effect.

The effective temperature range of a damping design is sometimes narrower than the required temperature range for high system damping. The standard approach to increase the effective temperature range is to use a multi-layered system as shown in Figure 4.6 where the increased effective damping temperature range is also shown. It is again extremely important to note the order in which the layers must be applied. The highest temperature damping material must be closest to the structure with the lower temperature material (or materials) applied next. The primary reason for this order is that no strain energy would be passed on to the outer damping layers if the lowest temperature material was applied adjacent to the structure as the temperature increases because the low temperature material would be too weak to transmit the energy.

An important point to remember is that a constrained layer damping system will only work if the structural mode shapes to be damped are beam or plate-like and have large areas with significant bending strains.

4.2 TUNED DAMPERS

The dynamic absorber, DA, is a well understood vibration control device and is used when a single frequency excitation is generating a resonant vibration problem. The dynamic absorber and its frequency response effect on a single degree-of-freedom structure is shown in Figure 4.7. The tuned visco-elastic damper, DT, as shown in Figure 4.8, has several advantages over the DA. One advantage is that a properly tuned TD results in two controlled resonant frequency peaks as shown in Figure 4.9 instead of the DA response as shown in Figure 4.7. The second advantage is that the TD can control more than one mode.

Tuned dampers have been applied on:

- 1) Electronic circuit boards to control resonant response
- 2) Jet engine structural components to increase fatigue life
- 3) Aircraft antenna to increase fatigue life
- 4) Aircraft skin panels to increase sonic fatigue life

The major advantage the TD has over the DA is its ability to control more than one vibration mode. The multi-mode control effect is illustrated in Figure 4.10 for various types of structures.

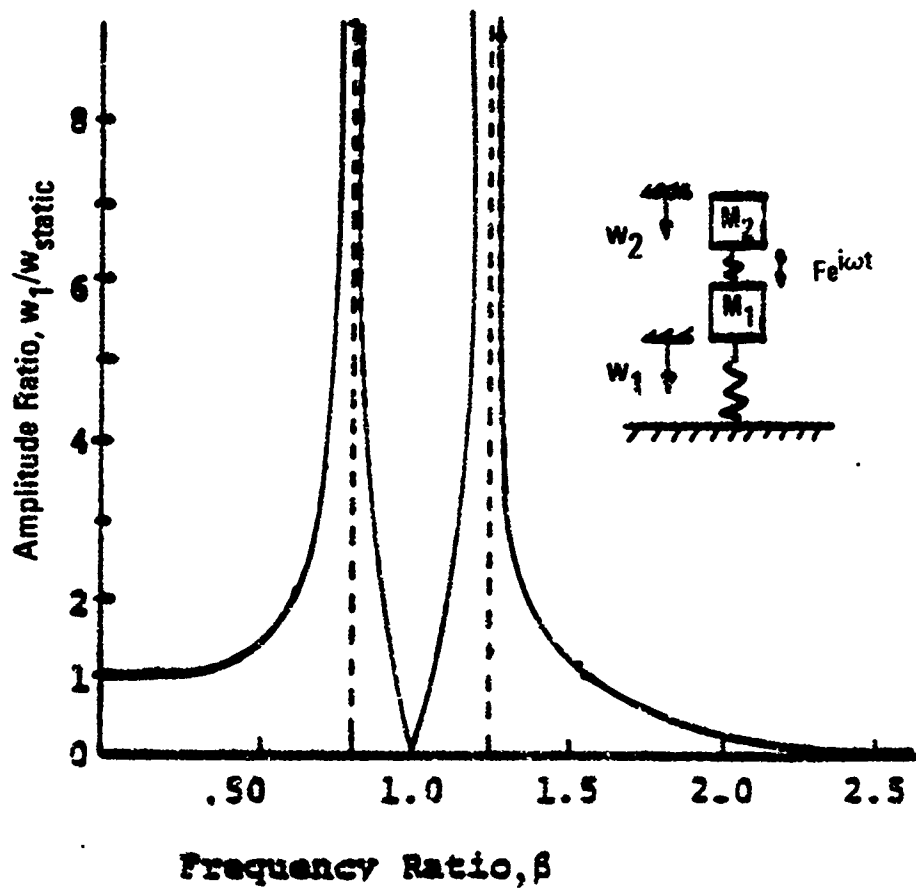


Figure 4.7. - Response of a single degree-of-freedom system with a dynamic absorber.

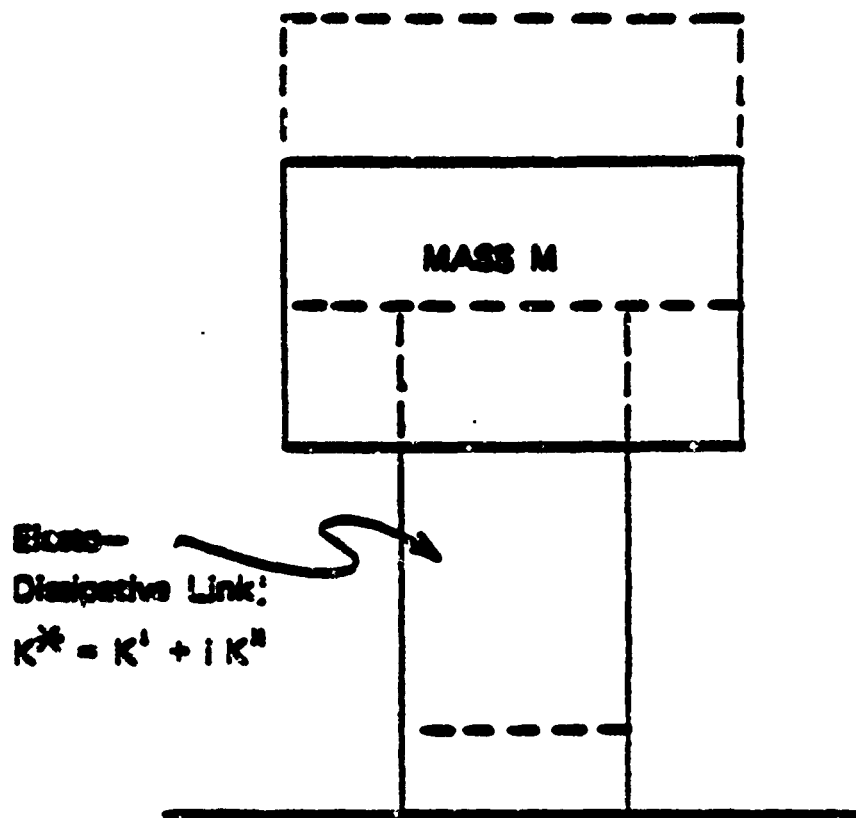


Figure 4.8. - Idealized tuned damper.

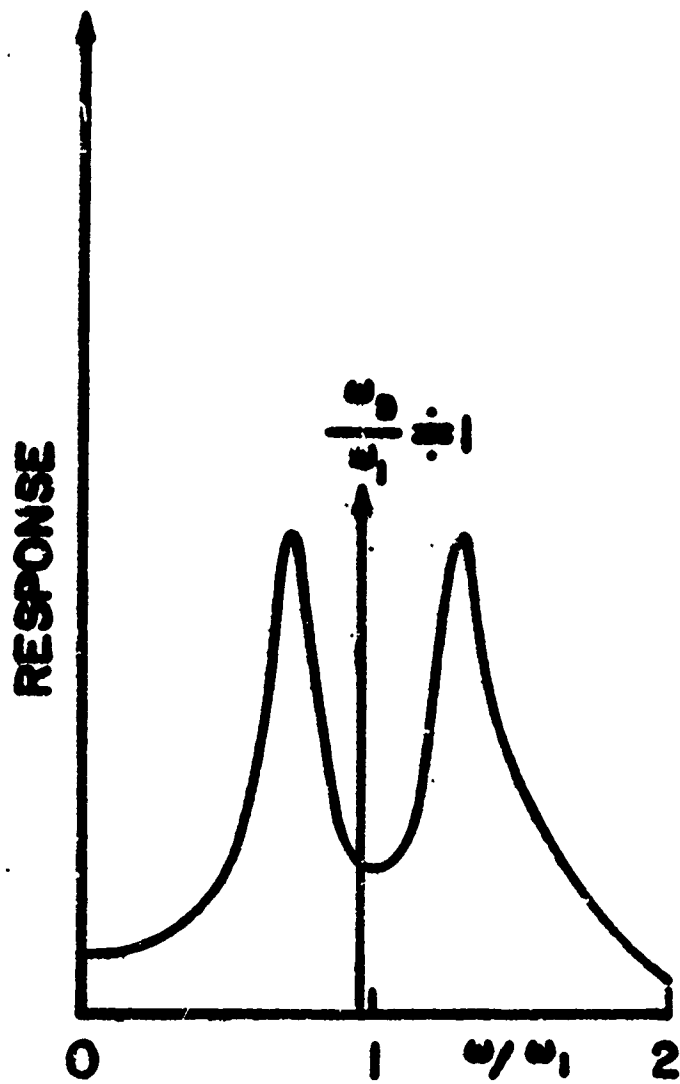
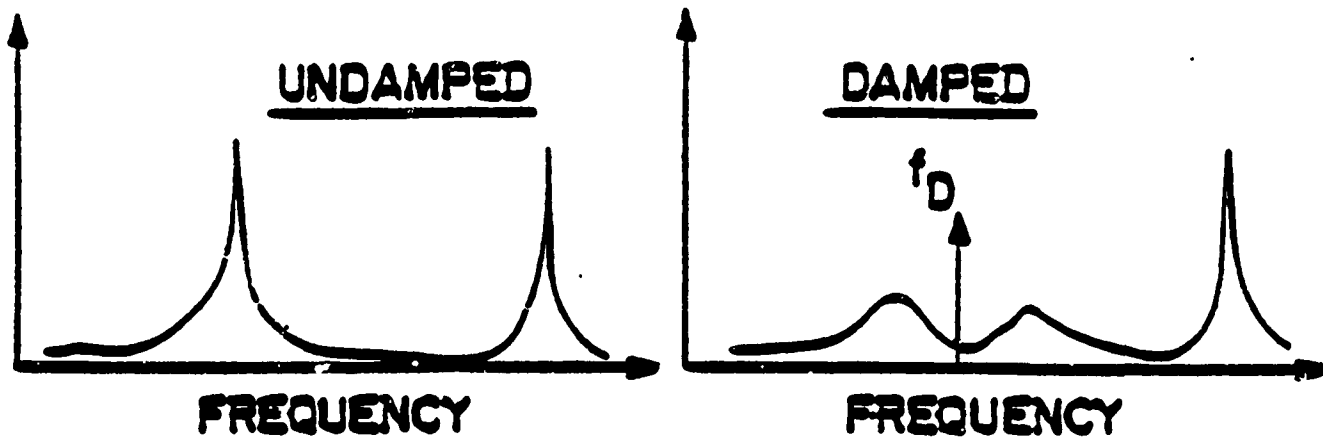
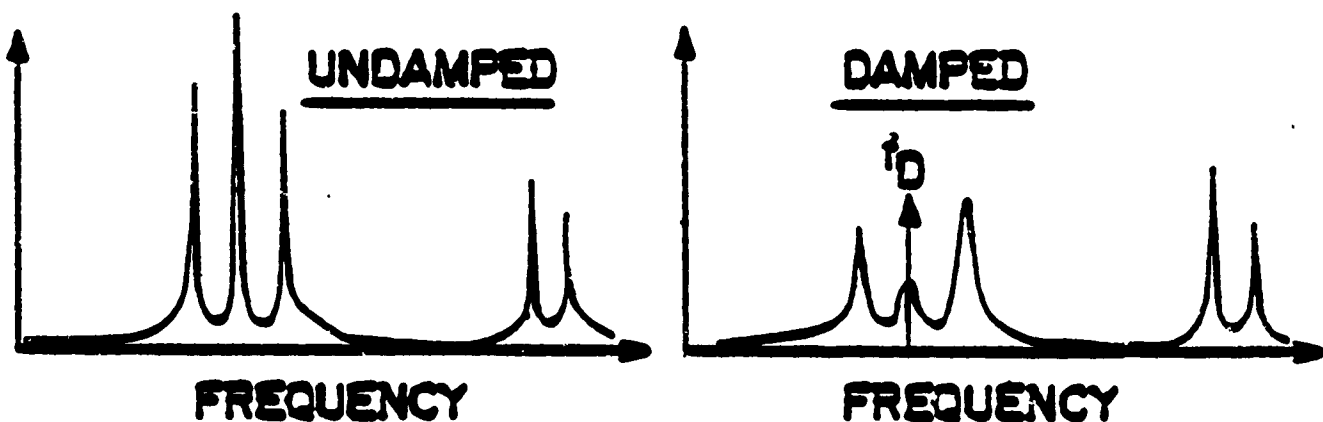


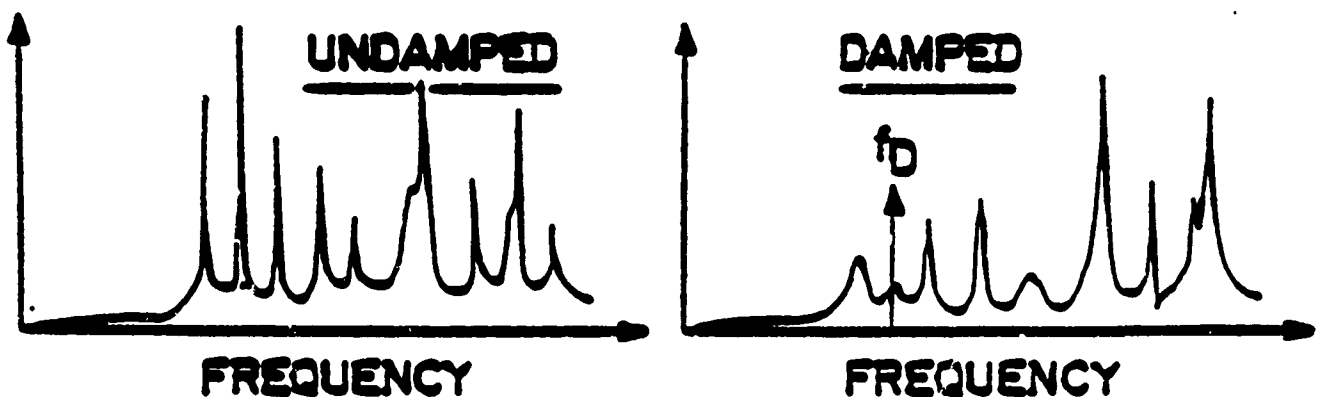
Figure 4.9. - Effect of tuned damper.



STRUCTURE WITH WIDELY SEPARATED RESONANCES



STRUCTURE WITH WIDELY SPACED MODAL BANDS



STRUCTURE WITH VERY WIDE MODAL BAND

Figure 4-10. - Effects of a tuned damper on different types of structures.

There are two major concerns when designing with a TD. First, the TD must be located on the structure at or near an anti-node of the mode or modes to be damped. Second, since the resonant frequency of the TD is extremely important for effective damping, the modulus of the TD material must be relatively constant with temperature. The design temperature range for materials used as TD's is shown in Figure 4.11.

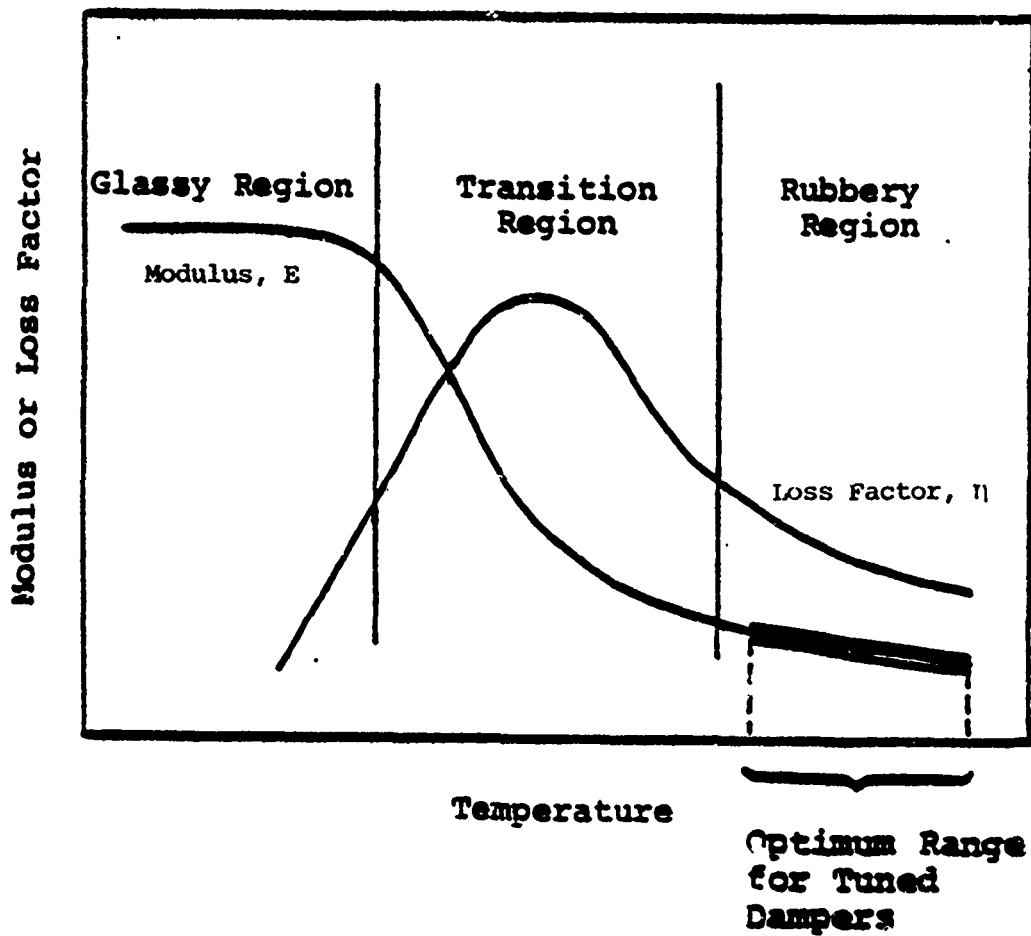


Figure 4.11. - E and η versus temperature for typical elastomer.

4.3 GENERAL APPROACH TO DAMPING DESIGN

The following section covers the general approach to designing damping treatments. The steps in this approach are:

- Verify that the problem is due to resonant vibration.
- Conduct dynamic analysis of the system to determine resonant frequencies, mode shapes, and damping.
- Define the environmental conditions in which the system operates.
- Define the system damping required to eliminate the problem.
- Select the appropriate damping materials and basic damping configuration.
- Develop the required design from the data collected [4.1,4.2].

These steps are discussed in more detail in the following subsections.

4.3.1 Dynamic Problem Identification

The first step in the solution of any problem is to completely define that problem. This is also true when attempting to solve a vibration induced problem through the use of damping technology. Therefore, the very first step in a damping design approach is to assure that the problem is indeed due to structural resonance.

In case of a new design, the designer must obtain the anticipated force input or excitation environment for the system and correlate the frequency content of this information with the results of a natural frequency analysis of the system. If there are natural frequencies occurring within the frequency band of excitation expected, the designer has identified the potential dynamics problem or problems which must be addressed.

If a problem develops in an existing part, the designer might choose one of the following approaches to identify the problem.

In the case of a cracked component, an analysis should be performed to verify that the crack is due to high cycle fatigue. Also, an instrumented operational test of the component should be conducted. This test can be run with strain gages or accelerometers. The data from this test will identify the frequencies and the vibration levels associated with the problem.

If the problem under consideration is a high noise radiation problem, an operational evaluation should be made to determine both the frequencies and magnitudes of the noise being radiated and the source of radiation. An unacceptable vibration level environment problem should be attacked in the basic manner as the noise problem.

As a result of the above investigations, the designer has determined the operational dynamic cause of the problem and the resonant frequencies that are developing the high dynamic response.

4.3.2 Dynamic Characteristics of Structure

A successful damping design can only be developed from a complete understanding of the dynamic behavior of the structural system and the component to be damped. Generally, the frequency range over which dynamic information is needed, is obtained from the analysis completed in the first step. Once a frequency range is chosen for a problem, a complete dynamic investigation must be conducted. All of the resonant frequencies, the corresponding structural mode shapes, and the inherent modal damping values must be accurately determined in this frequency range. If a tuned absorber is to be properly applied, the modal mass and stiffness are also needed. These data can be obtained analytically or experimentally.

In the early design stages, where a prototype is available, the optimum solution for data acquisition is experimental analysis on the prototype structure used to refine analytical models which are then used for further component damping design evaluation [4.3,4.4,4.5].

Often, when added damping is used in redesign, the necessary dynamic characterization can be acquired more efficiently through the use of modern experimental methods than through finite element or other analytical methods. Experimental methods can quickly determine the data needed for a highly complex structural system; however, measurements on operational systems can be extremely difficult and costly.

The Fourier analyzer is the most powerful experimental tool currently available to do the experimental work; however, holographic methods for determining mode shapes and standard sine sweep methods for resonant frequencies and modal damping values are also extremely useful [4.6,4.7,4.8]. The designer must choose the most expedient method to develop the required data.

4.3.3 Environmental Definition

A major data point still needed in the quest for an optimally designed damping application is the definition of the operational environment to which the design will be exposed. This definition, at first thought, might seem to be a rather simple task but the importance of accurate temperature data cannot be over stressed.

The all encompassing approach to temperature such as the standard temperature range for operation of many aircraft components of -65°F (-54°C) to 150°F (66°C) is not the total answer. This may be the maximum range seen by the component; however, it will not generally be necessary to provide high damping over this entire range. The engineer must determine over what specific temperature range the damage can occur and design his application for that range while maintaining a total awareness of the required survivability temperature range. Time related recordings of vibration data and temperature from operational tests can be used to determine the temperature range over which damaging vibration levels occur. Operational tests can also supply the necessary maximum temperature limits to be used in the design. If temperature data from a large number of different operational tests are available, a statistical study of the data will reveal the temperature range in which the majority of operational time is spent. An example of this type of data is shown in Figure 4.12 where minimum and maximum temperatures are shown along with percent of total operational time spent in each temperature range. It is easy to see the value of this type of data, particularly, if vibration level and temperature data cannot be simultaneously obtained for operational conditions.

In the early stages of system design, complete operational temperature data may not be available. In such a case data from similar systems should be reviewed and the best estimates of temperature should be developed and used in the design procedure.

Temperature is not the only environmental factor which must be considered. The engineer must know if the application will come in contact with contaminants such as salt water, gasoline, jet engine fuel, hydraulic fluid, or any other substance which might affect the performance or longevity of the candidate damping materials [4.6,4.7].

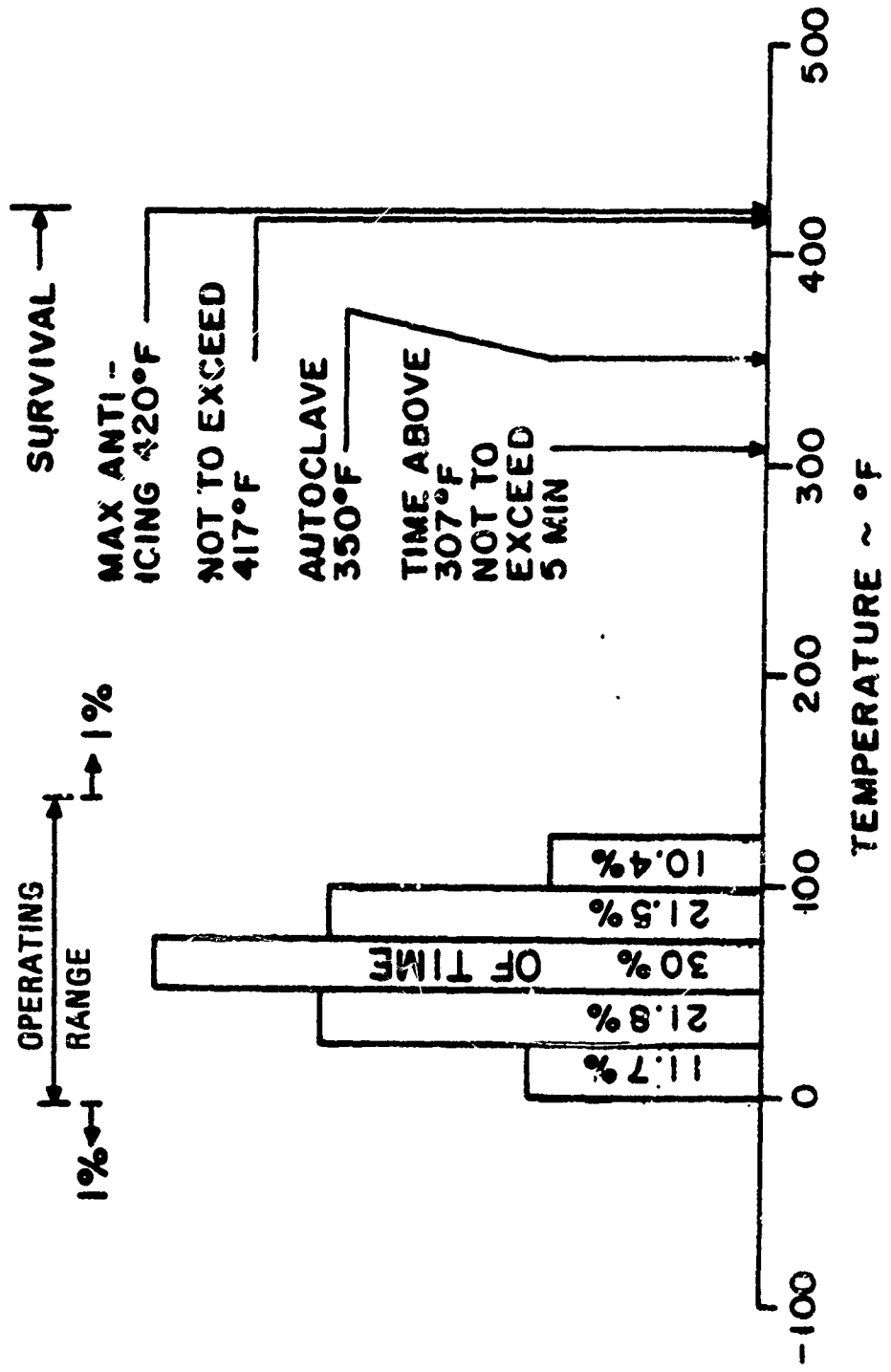


Figure 4.12. - Statistical temperature data.

4.3.4 Required Damping Increase

The remaining question to be answered before a damping design can be started is "How much damping is needed to eliminate the problem?" In the "fix-it" damping business, the general approach found in the literature is to design an optimum damping system and test it in service. If the failures are eliminated the problem is solved. In reality, the designer wants the minimum value of system damping which will eliminate the vibration problem. If the damped design accomplishes just the minimum required damping using an optimum damping system, the design should also be optimized from a weight, size, and cost standpoint.

The method for determining the minimum required system damping will depend on the problem to be solved. From the dynamic characterization, the inherent system damping has been determined. The corresponding vibration problem (high dynamic stress, noise level radiated, high dynamic amplitude response, etc.) is directly related to the inherent damping. Quick calculations can be made to determine the required increase in system damping to eliminate the vibration problem.

In estimating the required damping, account must be taken of the nature of the excitation. If the structure is excited sinusoidally (single frequency) at a resonant frequency, then the damping required, η_D , from the damping material is given by

$$\eta_D = \eta \left(\frac{w_i}{w_D} - 1 \right) \quad (4.3)$$

where η is the damping of the resonant mode before the damping treatment and w_i/w_D is the ratio of the amplitude, strain or acceleration before the application of the treatment to that after the application. After the application of the damping treatment, the total damping, η_s , of the treated structure is given by

$$\eta_s = \eta_D + \eta \quad (4.4)$$

Suppose, for example, that the damping, η , of the structure is 0.01 and it is necessary to reduce the amplitude at resonance by a factor of 3, then w_i/w_D equals 3,

$$\eta_D = 0.01 (3-1) = 0.02$$

and

$$\eta_s = 0.02 + 0.01 = 0.03$$

If the structure is excited by a broad band noise and contains a resonant mode that is being excited, then the damping required from the damping material is given by

$$\eta_D = \eta \left\{ \left(\frac{w_1}{w_D} \right)^2 - 1 \right\} \quad (4.5)$$

If it is necessary to reduce the root mean square amplitude of the structural response to the random excitation by a factor of 3, and the structure has a damping, η , of 0.01, then

$$\eta_D = 0.01 (9-1) = 0.08$$

and

$$\eta_s = 0.09$$

The reason for the increased damping, in the case of random excitation, is that part of the response is nonresonant. Consequently, in order to achieve the necessary reduction in the vibration amplitude, the resonant portion of the response must be reduced much more.

See Section 8 for the values of typical system and material damping for various structural systems and structural materials.

In the literature, most of the successful damping systems currently in use were designed to achieve the maximum possible damping from a given configuration without regard to eliminating the problem with the least required amount of damping.

4.3.5 Damping Materials and Application Design

The primary function of the designer, up to this point, has been to develop an accurate and complete definition of the resonant vibration induced problem. The frequencies at which the problem exists during operation of the component have been defined along with the dynamic characteristics of the component. Thus, the resonant

modes of the component that are creating the vibration problem, which in turn define the frequencies at which damping material is needed to operate, the corresponding resonant mode shapes, the undamped modal loss factors, and the required damped modal loss factor have been determined. This complete set of dynamic data, combined with the environmental conditions, provides the designer with all the data necessary to begin analysis and evaluation of damping materials and their design configurations.

The designer must first look at the temperature range for which damping is needed and the survivability temperature limits to see if either of these temperature ranges eliminates a particular method of damping approach because of no available materials which will meet the temperature requirements. An example would be a damping requirement over the temperature range of 150°F (66°C) to 250°F (121°C) with a survivability to 600°F (316°C). This requirement would eliminate the typical constrained layer or free layer damping approach because there are no effective materials currently available which will meet these requirements.

If the temperature range conditions can be met, the next consideration is the mode shapes of the resonant frequencies which require damping. Tuned dampers require displacements of some magnitude while constrained and free layer applications require large areas of localized bending which can deform the damping material. Highly localized strain distributions will negate the effectiveness of a layered treatment. An example of the localized strain condition is discussed in Reference [4.8]. An antenna mount was incurring high cycle fatigue cracks. The strain distribution was concentrated in the corner areas and therefore a layered damping approach was not feasible. The displacements were such that a properly designed tuned damper was able to eliminate the problem.

From the temperature conditions and the dynamic characteristics, the designer can choose the appropriate class of damping materials and the appropriate type of damping design for the starting point to design the specific application for the structure having the vibration problem. The basic principles of free layer and constrained layer damping applications and tuned dampers have been discussed in

Subsection 4.1. The basic design equations are given in Section 5. Finite element analysis is also discussed in Section 5. More detailed information is contained in Volume I.

Any of these design methods are appropriate for most all problems. However, it is necessary to obtain all the basic information discussed previously to be successful regardless of the analysis procedure used. A flow chart using any of the design analysis techniques is seen in Figure 4.13. The dynamic and temperature data are the input and the output is the structural loss factor. The program loops are continued until the proper η_s is achieved at which time the damping design is complete. Further detailed discussions on the specified design analysis techniques are given in the appropriate section.

4.4 SUMMARY

Restating the importance of the problem definition is appropriate at this point. Inaccurate temperature range formulation can eliminate any beneficial effects from the damping material. This effect can be seen in the reduced temperature nomogram [4.9] in Figure 4.14, where a temperature shift of 100°F, from the maximum loss factor temperature, causes a reduction of more than 50 percent in the loss factor. If the survivability temperature limits are incorrect, the damping application may well provide the necessary reduction in the vibration levels but will be destroyed by an over-temperature condition [4.10]. An assumed set of temperature data will invariably lead to the failure of a damping design.

The other major area where accurate data are necessary is the dynamic characteristics of the system under consideration. The placement of a layered damping design on a portion of the structure which is not undergoing the major motion of a particular mode is as ineffective as placing a tuned damper on a node line of the mode you wish to control.

As with any design project, successful results require accurate information upon which to base the design. Temperature and dynamic characteristics are the two prime factors which must be meticulously measured to obtain good damping design results.

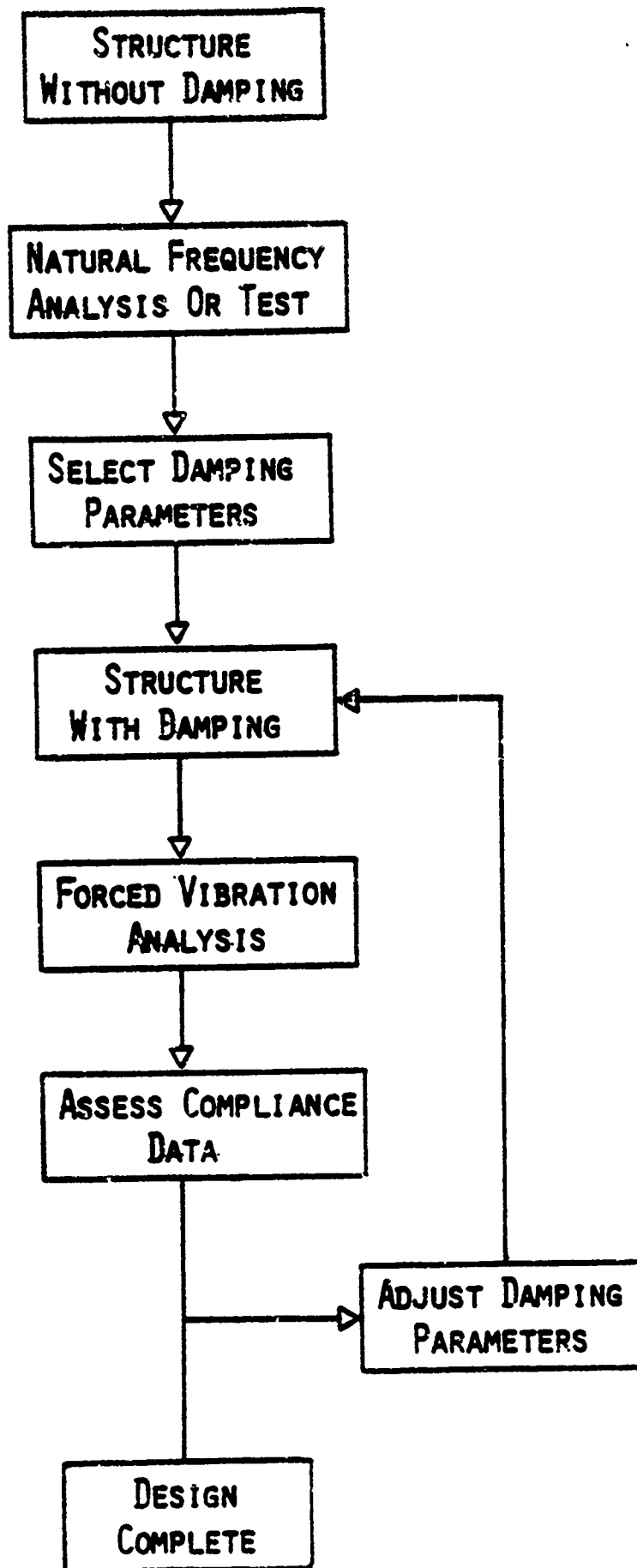


Figure 4.13. - Basic flow chart.

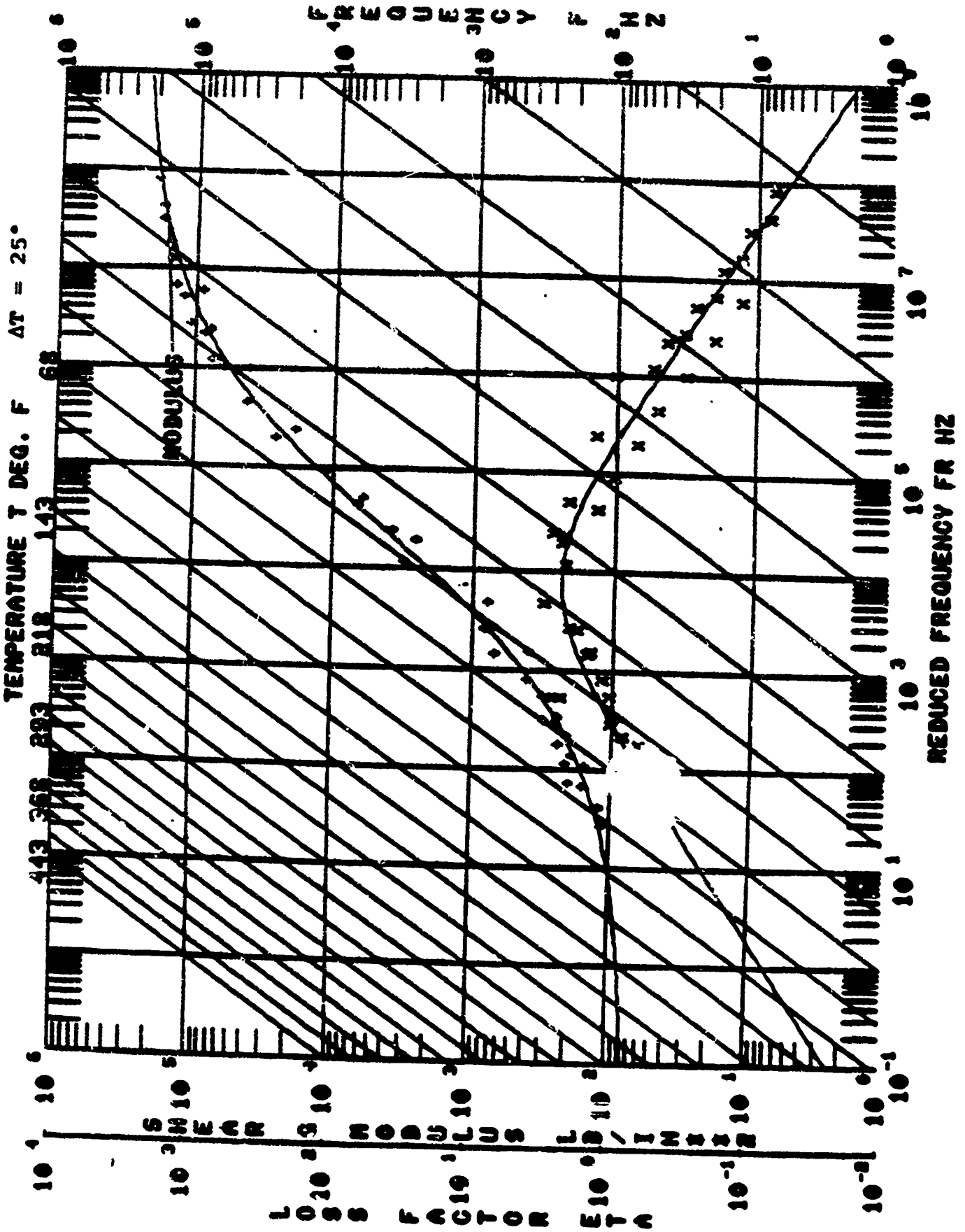


Figure 4.14. - Reduced temperature nomogram.

REFERENCES

- 4.1. Sharp, J.D. and M.L. Drake, "Elimination of Resonant Fatigue Problems for Major Maintenance Benefits," ASME Publication Number 77-DET-135.
- 4.2. Drake, M.L. and J.D. Sharp, "An Example of Additive Damping as a Cost Savings Alternative to Redesign," ASME Publication Number 77-WA/GT-2.
- 4.3. Brown, Dave, Lecture notes - Short Course, "Modal Analysis Theory and Measurement Techniques," sponsored by the University of Cincinnati and Hewlett Packard.
- 4.4. Ramsey, K.A., "Effective Measurements for Structural Dynamics Testing," Sound and Vibration, November 1975, pp 24-35.
- 4.5. Flora, et al, "Dynamic Analysis and Testing of Damped Intermodule Plates for the Sigma Laser Device," ASIAC Report No. 1182 1A, November 1982.
- 4.6. Drake, M.L. and J.P. Henderson, "An Investigation of the Response of a Damped Structure Using Digital Techniques," Shock and Vibration Bulletin 45, Part 5, 1975.
- 4.7. Henderson, J.P. and M.L. Drake, "Investigation of the Effects of Damping Treatments on the Response of Heated Fuselage Structure," NoisEXPO, National Noise and Vibration Control Conference, New York, New York, March, 1976.
- 4.8. Jones, D.I.G., J.P. Henderson, and 1/Lt. G.H. Bruns, "Use of Tuned Viscoelastic Dampers for Reduction of Vibrations in Aerospace Structures," Air Force Materials Laboratory, presented at the 13th Annual Air Force Science and Engineering Symposium at Arnold Air Force Station, Tennessee, September 27-29, 1966.
- 4.9. Jones, D.I.G., "A Reduced Temperature Nomogram for Characterization of Damping Material Behavior," Shock and Vibration Bulletin 48, 1978.
- 4.10. Jones, D.I.G. and C.M. Cannon, "Control of Gas Turbine Stator Blade Vibrations by Means of Enamel Coatings," Journal of Aircraft, Vol. 12, No. 4, pp. 226-230, April 1975.

SECTION 5 DESIGN METHODS

Classical analytical methods for application of viscoelastic damping have been developed, in general, only for simple beam and plate structures because of the complexity of the analysis. The pertinent design equations for these simplified methods are presented in Section 5.1. In many instances, the dynamic response of complex structures can be reduced to that of simple beams or panels, especially if modal test data are available. The simplified analysis methods can then be used in the initial design of the damping treatment. The initial design can, thereafter, be verified and, if necessary, be refined by the use of finite element analysis, as discussed in Section 5.2. Table 5.29 is a list of symbols for Section 5.

5.1 SIMPLIFIED DESIGN EQUATIONS

The basic design equations for beams and plates, and computer programs for these equations, are presented in this section together with worked examples illustrating their use. The derivation of these equations is given in Section 3, Volume I of this design guide.

The suggested approach, in using these equations to analyze the vibration response of more complex structures, is to "adjust" the variables in the undamped frequency equation for the simplified model to obtain a match with the natural frequency of the complex structural mode under study. For example, the thickness of a cantilever beam can be adjusted when modeling the vibration response of a turbine blade with chordwise curvature since the curvature contributes to the bending stiffness of the blade. The density can also be reduced to compensate for over-estimating the blade weight per unit length resulting from the increased blade thickness. The width of a panel stiffened with open section stringers and frames can be reduced when modeling the panel response with a simply supported panel. It is important to develop a model which has approximately the same mode shape and strain energy distribution as the system to be analyzed. An exact frequency is of lesser importance. The adjusted parameters are retained in the loss factor and frequency equations for the damped model structures in this section. Methods for predicting the modal frequencies of complex structures and typical

material properties for some of the more common structural materials are listed in Sections 2 and 9 of this volume, respectively. The damping material properties are listed in Volume III of this design guide.

5.1.1 Cantilever Beam with Free-Layer Damping on One Side

5.1.1.1 Basic Equations

The natural frequency, F_B , of an undamped cantilever beam is given by

$$F_B = \frac{\xi_i}{2\pi L_1} \left(\frac{E_1 I_1 g}{R_1 H_1} \right)^{1/2} \quad (5.1)$$

where

ξ_i is the i^{th} modal eigenvalue

L_1 is the beam's length

H_1 is the beam's thickness

E_1 is the beam's Young's modulus

R_1 is the beam's Density

I_1 is the beam's Moment of inertia and

$$I_1 = \frac{H_1^3}{12} \text{ for a unit width beam)}$$

g is the gravitational constant

The first five eigenvalues of a cantilever beam are listed in Table 5.1.

TABLE 5.1 EIGENVALUES OF CANTILEVER BEAM

MODE NUMBER	ξ
1	3.51602
2	22.0345
3	61.6972
4	120.902
5	199.860

The loss factor, η_s , for a cantilever beam with a free damping layer applied to one side is

$$\eta_s = \eta_D \frac{E_R H_R (2A + 2E_R H_R^3 + E_R^2 H_R^4 - 1)}{(1 + E_R H_R) (1 + 2A E_R H_R + E_R^2 H_R^4)} \quad (5.2)$$

where $E_R = \frac{E_2}{E_1}$; $H_R = \frac{H_2}{H_1}$; $A = 2 + 3 H_R + 2 H_R^2$

η_D is damping material loss factor

E_R is modulus ratio

H_R is thickness ratio

E_1 is beam Young's modulus

E_2 is damping material Young's modulus

H_1 is beam thickness

H_2 is damping material thickness

The corresponding damped cantilever beam modal frequency may be determined from

$$F_s = F_B \left(\frac{1 + 2 E_R H_R (2 + 3 H_R + 2 H_R^2) + E_R^2 H_R^4}{(1 + E_R H_R)(1 + H_R R_R)} \right)^{1/2} \quad (5.3)$$

where F_B is bare beam frequency (Equation 5.1)

R_R is density ratio = $\frac{R_2}{R_1}$

R_1 is beam density

R_2 is damping material density

5.1.1.2 Worked Example

The use of the design equations is illustrated in the following problem for a Haynes Alloy Cantilever beam. It is necessary to calculate the undamped and damped beam second mode frequency and the loss factor at a temperature of 1100°F (593.3°C) using the following parameters:

BEAM MATERIAL: HAYNES ALLOY NO. 188
LENGTH: 10.0 in (254 mm)
THICKNESS: 0.04 in (1.016 mm)
DENSITY: 0.33 lb/in³ (.00913 g/mm³)
YOUNG'S MODULUS: 2.8E7 PSI (1.93E11N/m²) at 1100°F (593.33°C)

MODE: 2

DAMPING MATERIAL: CORNING GLASS NO. 8871
THICKNESS: 0.006 in (.1524 mm)
DENSITY: 0.1387 lb/in³ (.00384 g/mm³)
LOSS FACTOR: 1.2857 at 1100°F (593.3 C) and 73 HZ
YOUNG'S MODULUS: 1.8E5 PSI (1.24E9 N/m²) at 1100°F(593.3°C) and 73 HZ

The undamped cantilever beam frequency from equation 5.1 is

$$F_{B(\text{mode } 2)} = \frac{22.0345}{2(3.1416)(10)^2} \left(\frac{28000000 \left(\frac{(.04)^3}{12} \right) (386.01)}{.33(.04)} \right)^{1/2} = 73.3 \text{ HZ}$$

The modal loss factor for the second mode of the damped beam from equation 5.2 is

$$\eta_s = 1.2857 \frac{(.0064)(.15)[2(2.495)+2(.0064)(.15)^3+(.0064)^2(.15)^4-1]}{[1+(.0064)(.15)] [1+2(2.495)(.0064)(.15)+(.0064)^2(.15)^4]} \\ = .0049$$

The second mode frequency of the damped beam using equation 5.3 is

$$F_s = 73.3 \left(\frac{1+2(.0064)(.15)[2+3(.15)+2(.15)^2]+(.0064)^2(.15)^4}{[1+(.0064)(.15)] [1+(.15)\left(\frac{.1387}{.33}\right)]} \right)^{1/2} \\ = 71.2 \text{ HZ}$$

5.1.1.3 Computer Program For Design Equations

The design equations 5.1 through 5.3 have been combined in a computer program (F1SID) that is listed in Table 5.2. The instructions for using the program and the input and output formats are summarized in Table 5.3. The symbols are defined in Table 5.4.

The example problem in Subsection 5.1.1.2 has also been solved with this computer program. The input and output data for this problem are illustrated below.

TABLE 5.3

USER'S GUIDE FOR CALCULATION OF BARE AND COMPOSITE
FREQUENCIES AND SYSTEM LOSS FACTOR
FOR CANTILEVER BEAM COATED ON ONE SIDE

PROGRAM FISID

Executed program

program will then display:

ENTER HD, RHOD, L1, H1, RH01, E1

for which the user inputs:

the damping layer thickness, HD, the damping layer density, RHOD, the beam length, L1, the beam thickness, H1, the beam density, RH01, and the beam modulus, E1.

program then outputs:

ENTER NO. DATA LINES*

to which user responds:

n

where n is the number of lines of data to be input into program. Program then indicates that it is ready to receive lines of data.

the user inputs:

t_i, M_i, E_i, η_i

for i between 1 and n inclusive, where i is the i^{th} input line, t_i is the temperature, M_i is the mode number, E_i is the modulus of the damping material, and η_i is the loss factor of the damping material.

The program outputs headings for the output data and then the data, including the calculated values of the bare beam frequency and the composite frequency of the damped beam.

*The damping material properties are for the required temperature and at the bare beam frequency. Note, if the damped beam frequency is more than 10% different from the bare beam frequency, the damping material properties should be obtained at the damped beam frequency and the system calculation redone.

TABLE 5.4
 SYMBOLS FOR PROGRAM FISID
 (CANTILEVER BEAM COATED ON ONE SIDE)

SYMBOL	DEFINITION
CH(I)	Eigenvalue for the I th mode where I has been 1-5 inclusive
SF1(J), E1	The modulus of the beam for all J
IT(K), TEMP	The temperature of the K th line of data
IM(K), MODE	The mode of the K th line of data
SF1(K), FB	The calculated bare beam frequency of the K th line of data
SF(K), F	The calculated composite frequency of the K th line of data
SETA(K), ETA	The calculated system loss factor of the K th line of data
SETAD(K), ETA	The material loss factor of the K th line of data
SED(K), ED	The material modulus of the K th line of data
HD	Thickness of the damping layer
RHOD, RD	Density of the damping material
L1, BL1	Beam length
H1	Beam thickness
RH01, R1	Beam density
μ	Beam modulus
N	Number of data lines (maximum of 25)
ER	Modulus ratio
HR	Thickness ratio
RR	Density ratio
A1, A2, A3, A4, A6, A7	Intermediate calculations

INPUT DATA LIST*

HD = .0060 TEMP = 1100 E1 = 28000000
 RHOD = .1387 MODE = 2 ED = 180496
 L1 = 10 H1 = .04 ETAD = 1.2857
 N = 1 RHO1 = .33

OUTPUT DATA LIST*

TEMP MODE ED ETAD E1 ETA F FB
 1100 2 .1805E6 1.286 .2800E8 .005 71.2 73.3

*Program accepts input data and output data in English units only.

5.1.2. Simply Supported Beam with Free-Layer Damping on One Side

5.1.2.1 Basic Equations

The basic equations given in Subsection 5.1.1.1 also apply to the simply supported beam. The eigenvalues in Table 5.1 must be replaced by the eigenvalues in Table 5.5 for a simply supported beam.

TABLE 5.5 EIGENVALUES OF SIMPLY SUPPORTED BEAM

MODE NUMBER	ξ
1	9.86960
2	39.47842
3	88.82624
4	157.91367
5	246.74011

5.1.2.2 Worked Example

The use of the free layer damping coated one side pin-pin beam design equations is illustrated in the following example.

BEAM MATERIAL: HAYNES ALLOY NO. 188
 LENGTH: 10.0 in. (254 mm²)
 THICKNESS: 0.04 in. (1.016 mm)
 DENSITY: 0.33 lb/in³ (.00913 g/mm³)
 YOUNG'S MODULUS: 2.8E7 PSI (1.93E11N/m²) at 1100°F
 (593.3°C)
 MODE: 2

DAMPING MATERIAL: CORNING GLASS NO. 8671
 THICKNESS: 0.006 in. (1.524 mm)
 DENSITY: 0.1387 lb/in³ (.00384 g/mm³)
 LOSS FACTOR: 1.42 at 1100°F(593.3°C) and 127.7
 YOUNG'S MODULUS: 2.494E5 PSI (1.716E9N/m²) at 1100°F(593.3°C)
 and 127.7 HZ

The undamped pinned beam frequency from equation 5.1 is

$$F_{B(\text{mode } 2)} = \frac{39.47842}{2(3.1416)(10)^2} \left(\frac{28000000 \left(\frac{(.04)^3}{12} \right) (386.01)}{.33(.04)} \right)^{1/2} = 131.5 \text{ HZ}$$

The modal loss factor for the second mode of the damped beam from equation 5.2 is

$$\eta_s = 1.42 \left[\frac{.0089(.15) [2(2.495) + 2(.0089)(.15)^3 + (.0089)^2 (.15)^4 - 1]}{[1 + (.0089)(.15)] [1 + 2(2.495)(.0089)(.15) + (.0089)^2 (.15)^4]} \right] = .00751$$

The second mode frequency of the damped beam using equation 5.3 is

$$F_s = 131.3 \left(\frac{1 + 2(.0089)(.15)[2 + 3(.15) + 2(.15)^2] + (.0089)^2(.15)^4}{[1 + (.0089)(.15)][1 + (.15) \frac{.1387}{.33}]} \right)^{1/2} = 127.7$$

5.1.2.3 Computer Program for Design Equations

The same computer program as used in Subsection 5.1.1.3 can be used to analyze the simply supported beam if the CH (I) values given in lines 7 through 11 (Table 5.2) are replaced with those in Table 5.5.

An example of the input and output from the pinned beam program is given below.

INPUT DATA LIST*								
HD	=	.006	TEMP	=	1100	ED	=	249400
RHOD	=	.1387	H1	=	.04	ETAD	=	1.42
L1	=	10	RHO1	=	3.3			
N	=	11	E1	=	28000000			
OUTPUT DATA LIST*								
TEMP	MODE	ED	ETAD	EI	ETA	F	F _B	
1100	2	2.494E5	1.42	.2800E8	.00751	127.7	131.3	

*Program accepts input data and output data in English units only.

5.1.3 Clamped Beam with Free Layer Damping On One Side

The basic equations given in Subsection 5.1.1.1 also apply to the beam clamped at both ends. The eigenvalues in Table 5.1 must be replaced by the eigenvalues in Table 5.6.

TABLE 5.6 EIGENVALUES OF A CLAMPED BEAM

MODE NUMBER	ξ
1	22.373
2	61.673
3	120.903
4	199.859
5	298.556

The computer program given in Subsection 5.1.1.3 can be used to analyze the beam clamped at both ends if the eigenvalues given in Table 5.6 are inserted for the CH(I) values in lines 7 through 11 of the program listed in Table 5.2.

5.1.4 Free Beam with Free Layer Damping on One Side

The basic equations given in Subsection 5.1.1.1 also apply to the beam free at both ends. The eigenvalues in Table 5.1 must be replaced by the eigenvalues in Table 5.7.

TABLE 5.7 EIGENVALUES OF A FREE BEAM

MODE NUMBER	ξ
1	22.373
2	61.673
3	120.903
4	199.859
5	298.556

The computer program given in Subsection 5.1.1.3 can be used to analyze the beam free at both ends if the eigenvalues given in Table 5.7 are

inserted for the CH(I) values in lines 7 through 11 of the program listed in Table 5.2.

5.1.5 Clamped-Pinned Beam with Free-Layer Damping on One Side

The basic equations given in Subsection 5.1.1.1 also apply to the beam clamped at one end and pinned at the other. The eigenvalues in Table 5.1 must be replaced by the eigenvalues in Table 5.8.

TABLE 5.8 EIGENVALUES OF A CLAMPED-PINNED BEAM

MODE NUMBER	ξ
1	15.418
2	49.965
3	104.248
4	178.270
5	272.031

The computer program given in Subsection 5.1.1.3 can be used to analyze the clamped-pinned beam if the eigenvalues given in Table 5.8 are inserted for CH(I) values in lines 7 through 11 of the program listed in Table 5.2.

5.1.6 Cantilever Beam with Free-Layer Damping on Both Sides

5.1.6.1 Basic Equation:

The natural frequency F_B of an unclamped cantilever beam is given by Equation 5.1 which is repeated here for convenience.

$$F_B = \frac{\xi_1}{2\pi L_1^2} \left(\frac{E_1 I_1 g}{R_1 H_1} \right)^{1/2} \quad (5.4)$$

where

ξ_i is the i^{th} modal eigenvalue

L_1 is the beam's length

H_1 is the beam's thickness

E_1 is the beam's Young's modulus

R_1 is the beam's Density

I_1 is the beam's Moment of inertia and

$I_1 = \frac{H_1^3}{12}$ (for a unit width beam)

g is the gravitational constant

The first five eigenvalues of a cantilever beam are listed in Table 5.9.

TABLE 5.9 EIGENVALUES OF CANTILEVER BEAM

MODE NUMBER	ξ
1	3.51602
2	22.0345
3	61.6972
4	120.902
5	199.860

The loss factor (η_s) for a cantilever beam with a free damping layer applied to both sides is

$$\eta_s = \eta_D \left[\frac{E_R (8 H_R^3 + 12 H_R^2 + 6 H_R)}{1 + E_R (8 H_R^3 + 12 H_R^2 + 6 H_R)} \right] \quad (5.5)$$

where $E_R = \frac{E_2}{E_1}$; $H_R = \frac{H_2}{H_1}$

- η_D is damping material loss factor
- E_R is modulus ratio
- H_R is thickness ratio
- E_1 is beam Young's modulus
- E_2 is damping material Young's modulus
- H_1 is beam thickness
- H_2 is damping material thickness

The corresponding damped cantilever beam modal frequency may be determined from

$$F_s = F_B \left(\frac{[8 H_R^3 + 12 H_R^2 + 6 H_R](E_R) + 1}{1 + 2 \frac{R_R}{R_1}} \right)^{1/2} \quad (5.6)$$

where F_B is bare beam frequency (Equation 5.4)

R_R is density ratio = $\frac{R_2}{R_1}$

R_1 is beam density

R_2 is damping material density

5.1.6.2 Worked Example

The use of the design equations is illustrated in the following problem for a Haynes Alloy cantilever beam. It is necessary to calculate the

undamped and damped beam second mode frequency and the composite loss factor at a temperature of 1100°F (593.3°C). The following data form the input:

BEAM MATERIAL: HAYNES ALLOY NO. 188
 LENGTH: 10.0 in (254 mm)
 THICKNESS: 0.04 in (1.016 mm)
 DENSITY: 0.33 lb/in³ (.00913 g/mm³)
 YOUNG'S MODULUS: 2.8E7 PSI (1.93E11 N/m²) at 1100°F (593.3°C)

MODE 2

DAMPING MATERIAL: CORNING GLASS NO. 8871
 THICKNESS: 0.006 in (.1524 mm) each side of the beam
 DENSITY: 0.1387 lb/in³ (.00384 g/mm³)
 LOSS FACTOR: 1.2857 AT 1100°F (593.3°C) AND 73 HZ
 YOUNG'S MODULUS: 1.2049E5 PSI (1.24E9 N/m²) at 1100°F (593.3°C) and 73 HZ

The undamped cantilever beam frequency from equation 5.4 is

$$F_{B(\text{mode } 2)} = \frac{22.0345}{2(3.1416)(10)^2} \left(\frac{(2.8E7) \left(\frac{(0.04)^3}{12} \right) (386.01)}{.33(.04)} \right)^{1/2} = 73.3 \text{ Hz}$$

The modal loss factor for the second mode of the damped beam from equation 5.5 is

$$\eta_s = 1.2857 \left(\frac{.0064 [8(.15) + 12(.15)^2 + 6(.15)]}{1. + .0064 [8(.15)^3 + 12(.15)^2 + 6(.15)]} \right) = .00977$$

The second mode frequency of the damped beam using equation 5.6 is

$$F_s = 73.3 \left(\frac{[8(.15)^3 + 12(.15)^2 + 6(.15)] (.0064) + 1}{1 + 2(.15) \left(\frac{.1387}{.33} \right)} \right)^{1/2} = 69.3 \text{ Hz}$$

5.1.6.3 Computer Program for Design Equations

The design equations 5.4 through 5.6 have been combined in a computer program (F2SID) that is listed in Table 5.10. The instructions for using the program and the input and output formats are summarized in Table 5.11. The symbols are defined in Table 5.12. The example problem is Subsection 5.1.6.2 and has also been solved with this computer program. The input and output data are illustrated below.

INPUT DATA LIST*

HD	=	.006	RHO1	=	.33	MODE	=	2
RHOD	=	.1387	E1	=	2.8E7	ED	=	1.80496E5
L1	=	10	N	=	1	ETAD	=	1.2857
H1	=	.04	TEMP	=	1100			

OUTPUT DATA LIST*

TEMP	MODE	ED	ETAD	E1	ETA	F	FB
1100	2	.1805E6	1.286	.2800E8	.010	69.3	73.3

*Program accepts input data and output data in English units only.

5.1.7 Simply Supported Beam with Free-Layer Damping on Both Sides

5.1.7.1. Basic Equations

The basic equations given in Subsection 5.1.6.1 also apply to the simply supported beam. The eigenvalues in Table 5.9 must be replaced by the eigenvalues in Table 5.13 for a simply supported beam.

TABLE 5.13 EIGENVALUES OF A SIMPLY SUPPORTED BEAM

MODE NUMBER	ξ
1	9.8696
2	39.7842
3	88.83644
4	157.91367
5	246.74011

TABLE 5.10 COMPUTER LISTING FOR PROGRAM F2SID

```

0001      PROGRAM F2SID
0002      DIMENSION CMT(5), IT(25), IN(25), SF(25), SF1(25), SE1(25), SED(25),
0003      1SETA(25), SETA(25)
0004      CMT(1)=2.5E02
0005      CMT(2)=2E+05
0006      CMT(3)=2E+05
0007      CMT(4)=2E+05
0008      CMT(5)=1E0-100
0009      CMT(5)=1E0-100
0010      C
0011      WRITE(1,12E1)
0012      12E FORMAT(//,2X,'ENTER NO. OF NO. L1,M1,M0D1,E1')
0013      READ(1,3I4,2D,2L1,M1,M1,E1)
0014      WRITE(1,12E1)
0015      12E FORMAT(//,2X,'ENTER NO. OF DATA LINES')
0016      READ(1,2I4)
0017      DO 200 J=1,N
0018      SE1(J)=E1
0019      WRITE(1,14M)
0020      14E FORMAT(//,2X,'ENTER',12,' LINES:TEMP,NODE,ED,ETAD')
0021      READ(1,2) IT(L),IN(L),SED(L),SETA(L)
0022      CONTINUE
0023      READ(1,2) N
0024      SF1(N)=CMT(SETA(N)/1E2/1E-12./R1)NCH(IN(N))/EL123006CT(306./M1)/
0025      1E-25
0026      EX=SED(N)/SE1(N)
0027      M=25./M1
0028      M=25./M1
0029      R1=2.5E02+1E-250000+6.2NR
0030      M=1.43.250000
0031      Q2=(Q1+M+1.)/M2
0032      SF(N)=CMT(Q2)/SF1(N)
0033      Q4=(2.5E02+1E-250000+6.2NR)NR
0034      SETA(N)=SETA(N)Q4/(1.+Q4)
0035      CONTINUE
0036      GO TO 200
0037      WRITE(1,15)
0038      15E FORMAT(//,'TEMP, NODE, ED, ETAD, E1, ETA
0039      1 F
0040      15E J=1,M
0041      WRITE(1,25)IT(J),IN(J),SED(J),SETA(J),SF(J),SF1(J)
0042      CONTINUE
0043      25E FORMAT(2I5,2X),E10.4,2X,F6.3,2X,E10.4,2X,F6.3,2X,F6.1,2X,F6.1)
0044      GO TO
0045      END

```

TABLE 5.11

USER'S GUIDE FOR CALCULATION OF BARE AND COMPOSITE
FREQUENCIES FOR CANTILEVER BEAM COATED ON BOTH SIDES

PROGRAM F2SID

Execute program

program will then display:

ENTER HD, RHOD, L1, H1, RHO1, E1

for which the user inputs:

the damping layer thickness, HD, the damping layer density, RHOD,
the beam length, L1, the beam thickness, H1, the beam density,
RHO1, and the beam modulus, E1, followed by a carriage return line
feed.

program then outputs:

ENTER NO. DATA LINES

to which user responds:

n

where n is the number of lines of data to be input into program.
Program then indicates that it is ready to receive lines of data.

the user inputs:

t_i, M_i, E_i, η_i

for i between 1 and n inclusive, where i is the i^{th} input line,
 t_i is the temperature, M_i is the mode number, E_i is the modulus
of the damping material, and η_i is the loss factor of the damping
material.

The program outputs headings for the output data and then the data,
including the calculated values of the bare beam frequency and the
composite frequency of the damped beam.

TABLE 5.12
SYMBOLS FOR PROGRAM F2SID

SYMBOL	DEFINITION
CH(I)	Eigenvalue for the I th mode where I has been limited to 1-5 inclusive
IT(J), TEMP	The temperature of the Jth line of data
IM(J), MODE	The mode of the J th line of data
SF(J), F	The calculated composite frequency of the J th line of data
SF1(J), FB	The calculated bare beam frequency of the J th line of data
SE1(K), E _i	The modulus of the beam for all K
SED(J), ED	The material modulus of the J th line of data
SETA(J)	The calculated system loss factor of the J th line of data
SETAD(J), ETAD	The material loss factor of the J th line of data
HD	Thickness of the damping layer
RHOD, RD	Density of the damping material
L1, BL1	Beam length
H1	Beam thickness
RHO1, R1	Beam density
E1	Beam modulus
N	Number of data lines (Maximum of 25)
ER	Modulus ratio
HR	Thickness ratio
RR	Density Ratio
A1, A2, A3, A4	Intermediate calculations

5.1.7.2 Worked Example

The use of the design equations for free layer damping coated on both sides of a simply supported beam are illustrated in the following example.

BEAM MATERIAL:	HAYNES ALLOY NO. 188
LENGTH:	10.0 in (254 mm)
THICKNESS:	0.04 in (1.016 mm)
DENSITY:	0.33 lb/in ³ (.00913 g/mm ³)
YOUNG'S MODULUS:	2.8E7 PSI (1.93E11 N/m ²) at 1100°F (593.3°C)
MODE	2

DAMPING MATERIAL:	CORNING GLASS NO. 8871
THICKNESS	0.006 in (.1524 mm)
DENSITY	0.1387 lb/in ³ (.00384 g/mm ³)
LOSS FACTOR	1.42 at 1100°F (593.3°C) and 124.4 HZ
YOUNG'S MODULUS	2.45E5 PSI (1.69E9 N/m ²) at 1100°F (593.3°C and 124.4 HZ

The undamped pinned beam frequency from equation 5.4 is

$$F_{B(\text{mode } 2)} = \frac{39.47842}{2(3.1416)(10)^2} \left(\frac{2.8E7 \left(\frac{(.04)^3}{12} \right) (386.01)}{.33(.04)} \right)^{1/2} = 131.3 \text{ HZ}$$

The modal loss factor from equation 5.5 is

$$\eta_s = 1.42 \left[\frac{.0088 [8(.15)^3 + 12(.15)^2 + 6(.15)]}{1 + .0088 [8(.15)^3 + 12(.15)^2 + 6(.15)]} \right] = 0.148$$

The second mode frequency of the damped beam using equation 5.6 is

$$F_s = 131.3 \left(\frac{[8(.15)^3 + 12(.15)^2 + 6(.15)] (.0088) + 1}{1 + 2(.15) \left(\frac{.1387}{.33} \right)} \right)^{1/2} = 124.4$$

5.1.7.3 Computer Program For Design Equations

The same computer program as used in Subsection 5.1.6.3 can be used to analyze the simply supported beam if the eigenvalues (CP(I) values given in lines 5 through 9 in Table 5.10) are replaced with those in Table 5.13.

An example of the input and output from the pinned beam program is given below.

INPUT DATA LIST*

HD	=	.006	RHO1	=	.33	MODE	=	2
RHOD	=	.1387	E1	=	2.8E7	ED	=	2.454E5
L1	=	10	N	=	1	ETAD	=	1.42
K1	=	.04	TEMP	=	1100			

OUTPUT DATA LIST*

TEMP	MODE	ED	ETAD	E1	ETA	F	FB
1100	2	2.45E5	1.42	.2800E8	.0147	124.4	131.3

*Program accepts input data and output data in English units only.

5.1.8 Clamped Beam with Free Layer Damping on Both Sides

The basic equations given in Subsection 5.1.6.1 also apply to the beam clamped at both ends. The eigenvalues in Table 5.9 must be replaced by the eigenvalues in Table 5.14.

TABLE 5.14. EIGENVALUES OF A CLAMPED BEAM

MODE NUMBER	ξ
1	22.373
2	61.673
3	120.903
4	199.859
5	298.556

The computer program given in Subsection 5.1.6.3 can be used to analyze the beam clamped at both ends if the eigenvalues given in Table 5.14 are inserted for the CH(1) values in lines 5 through 9 of the program listed in Table 5.10.

5.1.9 Free Beam with Free-Layer Damping on Both Sides

The basic equations given in Subsection 5.1.6.1 also apply to the beam free at both ends. The eigenvalues in Table 5.9 must be replaced by the eigenvalues in Table 5.15.

TABLE 5.15 EIGENVALUES OF A FREE BEAM

MODE NUMBER	ξ
1	22.373
2	67.673
3	120.903
4	199.859
5	298.556

The computer program given in Subsection 5.1.6.3 can be used to analyze the beam free at both ends if the eigenvalues given in Table 5.15 are inserted for the CH(1) values in lines 5 through 9 of the program listed in Table 5.10.

5.1.10 Clamped-Pinned Beam with Free-Layer Damping on Both Sides

The basic equations given in Subsection 5.1.6.1 also apply to the clamped-pinned beam. The eigenvalues in Table 5.9 must be replaced by the eigenvalues in Table 5.16.

TABLE 5.16 EIGENVALUES OF A CLAMPED-PINNED BEAM

MODE NUMBER	ξ
1	15.418
2	49.965
3	104.248
4	178.270
5	272.031

The computer program given in Subsection 5.1.6.3 can be used to analyze the clamped-pinned beam if the eigenvalues given in Table 5.16 are inserted for the CH(I) values in lines 5 through 9 of the program listed in Table 5.10.

5.1.11 Cantilever Beam with a Single Constrained Layer Damping System

5.1.11.1 Basic Equations

The natural frequency F_B of an undamped cantilever beam is given by

$$F_B = \frac{\xi_i}{2\pi L_1^2} \left(\frac{E_1 I_1 g}{R_1 H_1} \right)^{1/2} \quad (5.7)$$

where

ξ_i is the i^{th} modal eigenvalue

L_1 is the beam's length

H_1 is the beam's thickness

E_1 is the beam's Young's modulus

R_1 is the beam's Density

I_1 is the beam's Moment of inertia and

$$I_1 = \frac{H_1^3}{12} \quad (\text{for a unit width beam})$$

g is the gravitational constant

The first five eigenvalues of a cantilever beam are listed in Table

5.17.

TABLE 5.17 EIGENVALUES OF A CANTILEVER BEAM

MODEL NUMBER	ξ
1	3.51602
2	22.0345
3	61.6972
4	120.902
5	199.860

The loss factor (η_s) for a cantilever beam with a single constrained layer damping system applied is

$$\eta_s = \eta_2 \left(\frac{A}{B} \right) \quad (5.8)$$

where

$$A = 3E_{R3} H_{R3} (1 + 2 H_{R2} + H_{R3})^2 D \quad (5.9)$$

$$B = C(1 + E_{R3} H_{R3}^3) + A[1 + D(1 + E_{R3} H_{R3})(1 + \eta_D^2)] \quad (5.10)$$

$$D = G_2 \left(\frac{E_3 H_3 H_2 \xi_1}{L_1^2} \right)^{-1} \quad (5.11)$$

$$C = (1 + D + D E_{R3} H_{R3})^2 + [D(\eta_D) + D(\eta_D)(E_{R3} H_{R3})]^2 \quad (5.12)$$

$$E_{R3} = \frac{E_3}{E_1} ; H_{R3} = \frac{H_3}{H_1} ; H_{R2} = \frac{H_2}{H_1}$$

E_3 is the Young's modulus of the beam constraining layer

H_3 is the thickness of the constraining layer

H_2 is the thickness of the damping layer

G_2 is the shear modulus of the damping material

η_2 is the loss factor of the damping material

The corresponding damped cantilever beam modal frequency may be determined from

$$F_s = \frac{\xi_i}{2\pi L_1^2} \left(\frac{E_1 H_1^3 B g}{12C (R_2 H_2 + R_1 H_1 + R_3 H_3)} \right)^{1/2} \quad (5.13)$$

where

R_1 = density of the beam

R_2 = density of the damping material

R_3 = density of the constraining layer

5.1.11.2 Worked Example

The use of the design equations is illustrated in the following problem.

STRUCTURE:	CANTILEVER BEAM
MATERIAL:	ALUMINUM
LENGTH:	10.0 in (254 mm)
THICKNESS:	0.20 in (5.08 mm)
DENSITY:	0.10 lb/in ³ (.00277 g/mm ³)
YOUNG'S MODULUS:	1E7 PSI (6.89E10 N/m ²)

DAMPING MATERIAL:	SOUNDCOAT DIAD NO. 606
THICKNESS:	0.01 in (.254 mm)
DENSITY:	0.035 lb/in ³ (.000969 g/mm ³)
CONSTRAINING LAYER:	ALUMINUM
THICKNESS:	0.01 in (.254 mm)
DENSITY:	0.10 lb/in ³ (.00277 g/mm ³)
YOUNG'S MODULUS:	1 E7 PSI (6.89E10 N/m ²)
MODE:	2
TEMPERATURE:	170°F (76.7°C)

The undamped cantilever beam frequency from equation 5.7 is

$$F_B = \frac{22.0345}{2(3.1416)(10)^2} \left(\frac{1E7 \left(\frac{(.2)^3}{12} \right) (386.01)}{.1(.2)} \right)^{1/2} = 397.8 \text{ HZ}$$

For Diad 606 at 400 HZ and 170°F (76.7°C)

$$\eta_2 = .8142 \text{ and } G_2 = 299.17 \text{ PSI (2.06 E6N/m}^2\text{)}$$

The modal loss factor (η_s) for the beam can now be found from Equations 5.8 through 5.12.

$$D = (299.17) \left(\frac{1E7(.1)(.01)22.0345}{(10)^2} \right)^{-1} = .136$$

$$C = [1 + .136 + (.136)(1)(.5)]^2 + [.136 (.8142) + (.136 (.8142)(1)(.5))]^2 = 1.477$$

$$A = 3(1)(.5) [1 + 2(.05) + .5]^2 (.136) = .522$$

$$B = 1.477 [1 + (1)(.125)] + .522 [1 + .136 (1 + (1)(.5)) (1 + (.8142)^2)] = 2.360$$

$$\eta_s = .8142 \frac{.522}{2.360} = .18$$

The second mode frequency of the damped beam using Equation 5.13 is

$$F_s = \frac{22.0345}{2(3.1416)(10)^2} \left(\frac{1E7(.2)^3 (2.360)(386.04)}{12(1.477) [.035(.01) + .1(.2) + .1(.1)]} \right)^{1/2} = 408.2$$

5.1.11.3 Computer Program for Design Equations

The design equations 5.7 through 5.13 and Table 5.17 have been combined in a computer program (PREDY) that is listed in Table 5.18. Instructions for using the program and the input and output formats are summarized in Table 5.19. The symbols are defined in Table 5.20.

The example problem in Subsection 5.1.11.2 has also been solved with this computer program. The input and output data for this problem are illustrated below.

INPUT DATA LIST*

HD = .01	R1 = .1	R3 = .1	ETAD = .8142
RD = .035	E1 = 1E7	N = 1	MODE = 2
L1 = 10	E3 = 1E7	TEMP = 170	ITER = -1
H1 = .2	H3 = .1	GD = 299.17	

OUTPUT DATA LIST*

TEMP	MODE	SHEAR MOD	ETAD	BEAM MOD	ETA	FREQ	SPAR
170	2	.2992E3	.814	1.E7	.180	408.2	.136

*Program accepts input data and output data in English units only.

5.1.12 Simply Supported Beam with a Single Constrained Layer Damping System Applied

5.1.12.1 Basic Equations

The basic equations given in Subsection 5.1.11.1 also apply to the simply supported (pinned-pinned) beam. The eigenvalues in Table 5.17 must be replaced by the eigenvalues in Table 5.21 for a simply supported beam.

TABLE 5.18 COMPUTER LISTING FOR PROGRAM PREDY

```

0001 FTN4
0002 PROGRAM PREDY
0003 DIMENSION CH(5),GD(25),IN(25),IT(25),ETAD(25)
0004 CH(1)=3.51002
0005 CH(2)=22.0345
0006 CH(3)=61.0972
0007 CH(4)=120.002
0008 CH(5)=199.027
0009 5 WRITE(1,8)
0010 8 FORMAT(/'ENTER 1 FOR CANT. BEAM, -1 FOR PP BEAM')
0011 READ(1,8)I1
0012 IF(I1)203,204
0013 203 DO 209 I=1,5
0014 AIA=I
0015 209 CH(I)=(AIA**3.14159)/X12
0016 204 WRITE(1,504)
0017 NND=1
0018 NH3=1
0019 504 FORMAT('ENTER 1-COMPOSITE, -1-BARE BEAM')
0020 READ(1,8)JJ
0021 IF(JJ)505,208
0022 WRITE(1,132)
0023 132 FORMAT(/'ENTER HD, RD, L1, H1, R1, E1, E3, H3, R3')
0024 READ(1,8)HD, RD, BL1, H1, R1, E1, E3, H3, R3
0025 HD1=HD
0026 H31=H3
0027 HB=HD
0028 WRITE(1,18)
0029 18 FORMAT(IX,'ENTER NO. DATA LINES')
0030 READ(1,8)M
0031 WRITE(1,14)M
0032 14 FORMAT('ENTER ',I3,' LINES: TEMP, GD, ETAD, MODE')
0033 DO 207 L=1, M
0034 207 READ(1,8)IT(L),GD(L),ETAD(L),IN(L)
0035 WRITE(1,210)
0036 210 FORMAT('DO YOU WISH TO ITERATE ON GEOM PROPERTIES 1=YES -1=NO')
0037 READ(1,8)ITER
0038 IF(ITER)211,212
0039 WRITE(1,214)
0040 214 FORMAT('ENTER HD1 HD2 DELH2 H31 H32 DELH3')
0041 READ(1,8)HD1,HD2,DELH2,H31,H32,DELH3
0042 NND=(NND-HND1)/NND+1
0043 NH3=(NH3-H31)/NH3+1
0044 IF(NND.EQ.0)NND=1
0045 IF(NH3.EQ.0)NH3=1
0046 211 DO 215 I=1,NH3

```

TABLE 5.18 (CONTINUED)

```

8047 AMI-J-1
8048 N3=H31+DM3RANI
8049 DO 216 L=1,NHD
8050 AMI-L-1
8051 H3=H31+DM3R(AMI)
8052 WRITE(1,17)H3,N3
8053 FORMAT(//, 'DAMPING MATERIAL THICKNESS = ',F8.4,/, 'CONSTRAINING LAY
8054 FOR THICKNESS = ',F8.4,/)
8055 WRITE(1,18)
8056 15 FORMAT(1X, 'TEMP MORE SHEAR MOD ETAD BEAM MOD ETA F
8057 1800 SPAR')
8058 DO 209 J=1,N
8059 SPAR=OB(J)/(E3*DM3SCH(IN(J))/BL1*SB)
8060 A=3.2E3/E1*H3/H1E(1+2.2*H2/H1+H3/H1)*R2*SPAR
8061 C=(1+SPAR+SPAR*E3/E1*H3/H1)*SB+(SPAR*ETAD(J)+SPAR*ETAD(J)*E3/E1*H
8062 12/H1)*SB
8063 B=C*(1+E3/E1*H3*SB/H1*SB)+A*(1+SPAR*(1+E3/E1*H3/H1)*X(1+ETAD(J)
8064 13*SB))
8065 ETA=A/D*ETAD(J)
8066 E1=E1*H3*SB/1800/C
8067 DM3=OH(IN(J))/BL1*SB*SB*ETAD(E1*SB*SB.04/((R2*H2+R1*H1)+R3*H3))
8068 DM3=DM3*SB.3.14159
8069 WRITE(1,20)J,IN(J),OB(J),ETAD(J),E1,ETA,DM3A,SPAR
8070 CONTINUE
8071 16 CONTINUE
8072 15 CONTINUE
8073 14 FORMAT(1X,14,2X,18,2X,E10.4,2X,F6.3,2X,E10.4,2X,F6.3,2X,F8.1,2X,F7
8074 1.3)
8075 WRITE(1,500)
8076 FORMAT(ENTER 1=CONTINUE, -1=END)
8077 17(11)60,204
8078 IF(11)60,204
8079 WRITE(1,20)
8080 FORMAT(ENTER R1,E1,H1,L1,NODE NO. )
8081 READ(1,20)R1,E1,H1,L1,NODE NO.
8082 E1=E1*H1*SB/18.
8083 DM3=OH(IN(1))/BL1*SB*SB*ETAD(E1*SB*SB.04/R1/H1)/3.3.14159
8084 WRITE(1,500)DM3A
8085 FORMAT(//, 'DAMP BEAM FREQ. = ',F8.1)
8086 GO TO 507
8087 CONTINUE
8088 END
8089 ENDS

```

TABLE 5.19
 USER'S GUIDE FOR CALCULATION OF SYSTEM LOSS FACTOR
 FOR A BEAM WITH A CONSTRAINED
 DAMPING LAYER SYSTEM APPLIED

Execute program

Program displays:

ENTER 1 FOR CANT. BEAM, -1 FOR PP BEAM

to which user responds:

1 CR/LF for a cantilever beam prediction or

-1 CR/LF for a pin-pin beam predictor

Program displays:

ENTER 1 = COMPOSITE, -1 = BARE BEAM

to which user responds:

1 CR/LF for a composite prediction or

-1 CR/LF for a bare beam prediction

Program then displays:

ENTER HD, RD, L1, H1, R1, E1, E3, H3, R3

for which the user inputs the damping layer thickness (HD), the damping material density (RD), the beam length (L1), the beam thickness (H1), the beam density (R1), the beam modulus (E1), the constraining layer modulus (E3), the constraining layer thickness (H3), and the constraining layer density (R3).

Program then outputs:

ENTER NO. DATA LINES

to which user responds:

n

where n is the number of data lines to be input into program.

Program then indicates that it is ready to receive lines of data.

the user inputs:

$t_1, G_{D1}, \eta_{D1}, M_1$

TABLE 5.19 (Continued)

for i between 1 and n inclusive, where i is the i^{th} input line, t_i is the temperature, G_{Di} is the shear modulus of the material, η_{Di} is the loss factor of the material, and M_i is the mode number.

program asks:

DO YOU WISH TO ITERATE ON GEOM PROPERTIES 1 = YES -1 = NO

If user does not wish to iterate the geometric properties of the system, the user inputs:

(If "No" go to Part a; if "Yes" go to Part b)

Part a.

Program responds by printing the values of the thicknesses of the damping material and of the constraining layer. It will then print headings for the output data and then the data, including calculated values of the system loss factor, composite frequency, and the shear parameter, g .

Part b.

If user does wish to iterate the geometric properties of the system, the user inputs:

1

Program then outputs:

ENTER HD1 HD2 DELH2 H31 H32 DELH3

for which the user inputs the minimum and maximum thickness of the damping layer, HD1 and HD2, respectively, the size of the increment for the damping layer, DELH2, the minimum and maximum thickness of the constraining layer, H31 and H32, respectively, and the size of the increment for the constraining layer, DELH3.

Program responds by repeating Part a. for each possible configuration of geometric properties.

After completion of predictions, program outputs:

ENTER 1 - CONTINUE, -1 = END

If user wishes to perform more predictions, the user enters:

1

and program returns to beginning of sequence. If not, the user enters:

-1 and program terminates.

TABLE 5.20
SYMBOLS FOR PROGRAM PREDY

SYMBOL	DEFINITION
CH(I)	Eigenvalue for the I th mode where I has been limited to 1-5 inclusive
GD(J)	Shear modulus of the damping layer
IM(J)	Mode number of the beam
IT(J)	Temperature
ETAD(J)	Loss factor of the damping layer
AiA	Intermediate variable
NHD, NH3	Indicators as to whether or not geometric properties are to be iterated
HD	Thickness of the damping layer
RD	Density of the damping layer
L1, BL1	Length of the beam
H1	Thickness of the beam
R1	Density of the beam
E1	Modulus of the beam
E3	Modulus of the constraining layer
H3	Thickness of the constraining layer
R3	Density of the constraining layer
H2	Intermediate variable
N	Number of data lines
ITER	Variable equal to "1" if geometric properties are to be iterated and equal to "-1" if not
HD1	Minimum thickness of damping layer
HD2	Maximum thickness of damping layer
DELH2, DHD	Thickness of damping layer increment
H31	Minimum thickness of constraining layer
H32	Maximum thickness of constraining layer
DELH3, DH3	Thickness of constraining layer increment
AMI, AML	Increment factors
SPAR	Shear parameter
A, B, C, EI	Intermediate calculations
OMEGA	Composite frequency (or bare frequency if prediction is for bare beam)

TABLE 5.21 EIGENVALUES OF SIMPLY SUPPORTED BEAM

MODE NUMBER	ξ
1	9.86960
2	39.47842
3	88.82644
4	157.91367
5	246.74011

5.1.12.2 Worked Example

The use of the single constrained layer damping system equations for a beam pinned at both ends is illustrated in the following example.

PINNED BEAM:

MATERIAL: ALUMINUM
LENGTH: 10.0 in (254 mm)
THICKNESS: 0.20 in (5.08 mm)
DENSITY: 0.10 lb/in³ (.00277 g/mm³)
YOUNG'S MODULUS: 1E7 PSI (6.89E10 N/m²)

DAMPING MATERIAL: SOUNDCOAT DIAD NO. 606
THICKNESS: 0.01 in (.254 mm)
DENSITY: 0.035 lb/in³ (.000969 g/mm³)

CONSTRAINING LAYER:
MATERIAL: ALUMINUM
THICKNESS: 0.10 in (2.54 mm)
DENSITY: 0.10 lb/in³ (.00277 g/mm³)
YOUNG'S MODULUS: 1E7 PSI (6.89E10 N/m²)

MODE: 2
TEMPERATURE: 170°F (76.7°C)

The undamped pinned beam frequency from equation 5.7 is

$$F_B = \frac{39.47842}{2(3.1416)(10)^2} \left(\frac{1E7 \left(\frac{(.2)^3}{12} \right) (386.04)}{.1 (.2)} \right)^{1/2} = 712.7$$

For Diad 606 at 700 HZ and 170°F

$$\eta_2 = .8930 \text{ and } G_2 = 395.83 \text{ PSI } (2.73 \text{ E6 N/m}^2)$$

The modal loss factor (η_2) for the beam can now be calculated from Equations 5.8 through 5.12.

$$D = 395.83 \left(\frac{1E7(.1)(.01) 39.47842}{(10)^2} \right)^{-1} = .1003$$

$$C = [1 + .1003 + .1003(1)(.5)]^2 + [.1003(.893) + .1003(.893)(1)(.5)]^2 = 1.342$$

$$A = 3(1) .5 [1 + 2(.05) + .5]^2 .1003 = .3852$$

$$B = 1.342 [1 + 1 (.5)^3] + .3852 [1 + .1003(1 + (1)(.5))(1 + (.893)^2)] = 1.9991$$

$$\eta_s = \frac{.3852}{1.9991} (.893) = .1721$$

The second mode of the damped beam using Equation 5.13 is

$$F_s = \frac{39.47842}{2(3.1416)(10)^2} \left(\frac{1E7(.2)^3(1.9991)(386.04)}{12(1.342)(.035(.01) + .1(.2) + .1(.1))} \right)^{1/2} = 706.17 \text{ HZ}$$

5.1.12.3 Computer Program for Design Equations

The computer program (PREDY) listed in Table 5.18 has also incorporated Table 5.21 which allows analysis of the design Equations 5.7 through 5.13 for pinned beams. Instructions for using the program including input and output formats are given in Table 5.19. All symbols are defined in Table 5.20. The example problem in Subsection 5.1.12.2 has also been solved

with this computer program. The input and output data for this problem are illustrated below.

INPUT DATA LIST*

HD = .01	R2 = .1	R3 = .1	ETAD = .893
RD = .035	E1 = 1E7	N = 1	MODE = 2
L1 = 10	E3 = 1E7	TEMP = 170	ITER = -1
H1 = .2	H3 = .1	GD = 395.83	

OUTPUT DATA LIST*

TEMP	MODE	SHEAR MOD	ETAD	BEAM MOD	ETA	FREQ	SPAR
170	2	395.8	.893	1E7	.172	706.2	.100

*Program accepts input data and output data in English units only.

5.1.13 Clamped Beam with a Single Constrained Layer Damping System Applied

The basic equations given in Subsection 5.1.11.1 also apply to the beam clamped at both ends. The eigenvalues in Table 5.17 must be replaced by the eigenvalues in Table 5.22.

TABLE 5.22 EIGENVALUES OF A CLAMPED BEAM

MODE NUMBER	ξ
1	22.373
2	61.673
3	120.903
4	199.859
5	298.556

The computer program given in Subsection 5.1.11.3 can be used to analyze the beam clamped at both ends if the eigenvalues given in Table 5.22 are inserted for the CH(I) values in lines 4 through 8 of the program listed in Table 5.18.

5.1.14 Free Beam with a Single Constrained Damping System Applied

The basic equations given in Subsection 5.1.11.1 also apply to the beam free at both ends. The eigenvalues in Table 5.17 must be replaced by the eigenvalues in Table 5.23.

TABLE 5.23 EIGENVALUES OF A FREE BEAM

MODE NUMBER	ξ
1	22.373
2	61.673
3	120.903
4	199.859
5	298.556

The computer program given in Subsection 5.1.11.3 can be used to analyze the beam free at both ends if the eigenvalues given in Table 5.23 are inserted for the CH(1) values in lines 4 through 8 of the program listed in Table 5.18.

5.1.15 Clamped-Pinned Beam with a Single Constrained Layer Damping System Applied

The basic equations given in Subsection 5.1.11.1 also apply to the beam clamped at one end and pinned at the other. The eigenvalues in Table 5.17 must be replaced by the eigenvalues in Table 5.24.

TABLE 5.24 EIGENVALUES OF A CLAMPED-PINNED BEAM

MODE NUMBER	ξ
1	15.418
2	49.965
3	104.248
4	178.270
5	272.03

The computer program given in Subsection 5.1.11.3 can be used to analyze the clamped-pinned beam if the eigenvalues given in Table 5.24 are inserted for the CH(I) values in lines 4 through 8 of the program listed in Table 5.18.

5.1.16 Simply-Supported Plate with a Single Constrained Layer Damping System Applied

5.1.16.1 Basic Equations

The natural frequency F_B of an undamped simply-supported plate is given by

$$F_{B_{i,j}} = \left(\frac{\xi_i}{L^2} + \frac{\xi_j}{W^2} \right) \left(\frac{1}{2h} \right) \left(\frac{E_1 \frac{(H_1)^3}{12} g}{R_1 H_1 (1 - \nu^2)} \right)^{1/2} \quad (5.14)$$

- where
- ξ_i is the eigenvalue for the mode along the length
 - ξ_j is the eigenvalue for the mode along the width
 - L is the length of the plate
 - W is the width of the plate
 - E_1 is the Young's Modulus of the plate
 - H_1 is the thickness of the plate
 - R_1 is the density of the plate
 - ν is the Poissons ratio of the plate
 - g is the gravitational constant

Table 5.25 gives the eigenvalues of a simply supported plate.

TABLE 5.25 EIGENVALUES OF A SIMPLY-SUPPORTED PLATE

MODE NUMBER	ξ
1	9.8696
2	39.4784
3	88.8264
4	157.9137
5	246.7401

The loss factor (η_s) for a simply-supported plate with a single constrained layer damping system applied is

$$\eta_s = \eta_2 \left(\frac{A}{B} \right) \quad (5.15)$$

where

$$A = 3 E_{R3} H_{R3} (1 + 2 H_{R2} + H_{R3})^2 D \quad (5.16)$$

$$D = G_2 (E_3 H_3 H_2)^{-1} \left(\frac{\xi_1}{L^2} + \frac{\xi_j}{W^2} \right)^{-1} \quad (5.17)$$

$$B = C (1 + E_{R3} H_{R3}^3) + A [1 + D(1 + E_{R3} H_{R3})(1 + \eta_2^2)] \quad (5.18)$$

$$C = (1 + D + D E_{R3} H_{R3})^2 + (D\eta_2 + D\eta_2 E_{R3} H_{R3})^2 \quad (5.19)$$

$$E_{R3} = \frac{E_3}{E_1} ; H_{R3} = \frac{H_3}{H_1} ; H_{R2} = \frac{H_2}{H_1}$$

E_3 is the modulus of the constraining layer

H_3 is the thickness of the constraining layer

G_3 is the shear modulus of the damping material

H_2 is the thickness of the damping material

η_2 is the loss factor of the damping material

The damped plate modal frequency can be determined from

$$F_{S_{1j}} = \left(\frac{\epsilon_1}{L^2} + \frac{\epsilon_j}{W^2} \right) \left(\frac{1}{\pi^2} \right) \left(\frac{E_1 \left(\frac{H_1}{12} \right)^3 B (386.04)}{C (1-\nu^2) (R_1 H_1 + R_2 H_2 + R_3 H_3)} \right)^{1/2} \quad (5.20)$$

where

R_2 is the density of the damping material

R_3 is the density of the constraining layer

5.1.16.2 Worked Example

STRUCTURE:	SIMPLY SUPPORTED PLATE
MATERIAL:	ALUMINUM
LENGTH:	10.0 in (254 mm)
WIDTH:	5.0 in (127 mm)
THICKNESS:	0.10 in (2.54 mm)
DENSITY:	0.10 lb/in ³ (.00277 g/mm ³)
YOUNG'S MODULUS:	1E7 PSI (6.89E10 N/m ²)
POISON'S RATIO:	.3
DAMPING MATERIAL:	3M ISD 112
THICKNESS:	0.01 in (.254 mm)
DENSITY:	0.035 lb/in ³ (.000969 g/mm ³)
CONSTRAINING LAYER:	ALUMINUM
THICKNESS:	0.10 in (2.54 mm)
DENSITY:	0.10 lb/in ³ (.00277 g/mm ³)
YOUNG'S MODULUS:	1E7 PSI (6.89E10 N/m ²)

MODE 2
 TEMPERATURE 60°F (15.6°C)

The undamped plate frequency from Equation 5.14 is

$$F_{B_{2,1}} = \left(\frac{39.4784}{(10)^2} + \frac{9.8696}{(5)^2} \right) \left(\frac{1}{2(3.1416)} \right) \left(\frac{1E7 \left(\frac{(.1)^3}{12} \right) (386.04)}{.1(.1) [1-(.3)^2]} \right)^{1/2} = 747.16 \text{ Hz}$$

For ISD-112 at 950 HZ* and 60°F (15.6°C) $\eta_2 = 1.2541$

and $G_2 = 719.29$

The modal loss factor (η_3) can now be computed from Equations 5.15 through 5.19.

$$D = (719.29) [1E7(.1)(.01)]^{-1} \left(\frac{39.4784}{(10)^2} + \frac{9.8696}{(5)^2} \right)^{-1} = .0911$$

$$A = 3(1)(1) [1 + 2(.1) + 1]^2 (.0911) = 1.323$$

$$C = [1 + (.0911) + (.0911)(1)(1)]^2 + [.0911(1.2541) + .0911(1.2541)(1)(1)]^2 = 1.4498$$

$$B = 1.4498 [1 + (1)(1)^3] + 1.323 [1 + .0911(1 + 1(1))(1 + 1.5728)] = 4.8428$$

$$\eta_3 = 1.2541 \left(\frac{1.323}{4.8428} \right) = .3426$$

*950 HZ was chosen because the anticipated damped system frequency is 950 HZ. The designer is reminded that the final damped frequency must be within 10% of the frequency used to choose the damping material properties or the calculations must be recomputed.

The damped frequency of the plate from Equation 5.20 is

$$f_{S_{2,1}} = \left(\frac{39.4784}{(10)^2} + \frac{9.8696}{(5)^2} \right) \left(\frac{1}{2(3.1416)} \right) \left(\frac{1E7 \left(\frac{(.1)}{12} \right)^3 (4.8428)(386.04)}{1.4498(1-(.3)^2)[.1(.1)+.035(.01)+.1(.2)]} \right)^{1/2}$$

= 957.3 Hz

5.1.16.3 Computer Program For Design Equations

The design Equations 5.15 through 5.20 and Table 5.25 have been combined in a computer program (PLATE) that is listed in Table 5.26. Instructions for using the program and the input and output formats are summarized in Table 5.27. The symbols are defined in Table 5.28.

The example problem in Subsection 5.1.16.2 has also been solved with this computer program. The input and output for this problem are given below.

INPUT DATA LIST*

HD = .01	R1 = .1	N = 1	MODE 2 = 1
RD = .035	E1 = 1E7	TEMP = 60	ITER = -1
L1 = .10	E3 = 1E7	GD = 719.29	
L2 = 5	H3 = .1	ETAD = 1.2541	
H1 = .1	R3 = .1	MODE 1 = 2	

OUTPUT DATA LIST*

TEMP	MODE 1	MODE 2	SHEAR MOD	ETAD	BEAM MOD	ETA	SPAR	COMP FREQ
60	2	1	719.29	1.254	1E7	.342	.091	946.6

*Program accepts input data and output data in English units only.

TABLE 5.26 COMPUTER LISTING FOR PROGRAM PLATE

```

0001 FTN4
0002
0003
0004
0005
0006
0007
0008
0009
0010
0011
0012
0013
0014
0015
0016
0017
0018
0019
0020
0021
0022
0023
0024
0025
0026
0027
0028
0029
0030
0031
0032
0033
0034
0035

PROGRAM PLATE
DIMENSION IN1(25),GD(25),IN2(25),IT(25),ETAD(25),CHA(5),CH4(5)
REAL KNE
INH=1
NH3=1
202 WRITE(1,132)
132 FORMAT(//'ENTER HD,RD,L1,L2,H1,R1,E1,E3,H3,R3')
READ(1,3)HD,RD,BL1,BL2,H1,R1,E1,E3,H3,R3
H1=HD
H3=H3
H2=HD
WRITE(1,18)
18 FORMAT('X','ENTER NO. DATA LINES')
READ(1,3)M
201 WRITE(1,14)M
14 FORMAT('ENTER ',13,' LINES: TEMP,GD,ETAD,MODE1,MODE2')
DO 207 L=1,N
207 READ(1,8)IT(L),GD(L),ETAD(L),IN1(L),IN2(L)
WRITE(1,210)
210 FORMAT('DO YOU WISH TO ITERATE ON GEOM PROPERTIES 1=YES -2=NO')
READ(1,3)ITER
IF(ITER)211,212
212 WRITE(1,214)
214 FORMAT('ENTER HD1 HD2 DELH2 H31 H32 DELH3')
READ(1,3)HD1,H2G,DHD,H31,H32,DH3
NH3=(H2G-HD1)/DH3+1
NH3=(H32-H31)/DH3+1
IF(NH3.EQ.0)NH3=1
IF(NH3.EQ.0)NH3=1
DO 215 I=1,NH3
211 NH1=I-1
NH3=NH31+DHTANI
DO 216 L=1,NHD
216 NH1=L-1
216 NH1=L-1

```

TABLE 5.26. (CONTINUED)

```

0036: H2=H21+DMS2(NM2)
0037: WRITE(1,217)H2,H2
0038: C022: FORMAT(//,DAMPING MATERIAL THICKNESS - 'FG.4./',CONSTRAINING LAY
0039: 1ER THICKNESS - 'FA.4./)
0040: WRITE(1,18)
0041: 18: FORMAT(1X,'TEMP: N02E1 N02E2 SHEAR MOD ETAD. BEAM MOD E
0042: 17A: SPAR. CORR. FREQ.')
0043: DO 200 J=1,N
0044: SPAR=00(J)/(E3H3/H229.872((IM1(J)/PL1)222+IIM(J)/2(2)222))
0045: A=3.253/E12H3/H12(1.+2.2IM2/H1+H3/H1)222SPAR
0046: C=(1.+SPAR+SPAR23/E12H3/H1)222+(SPAR2ETAD(J)+SPAR2ETND(J)223/E12H
0047: 13/H1)222
0048: C=02X(1.+E3/C12H3222/H0222)+02(1.+SPAR2(1.+E3/E12H3/H1)22(1.+ETAD(J)
0049: 1222))
0050: ETA=A/B2ETAD(J)
0051: E1=E12H1223/122B/C
0052: GRAY=305
0053: RH=RO222+R12H1+R22H3
0054: PR=0.2
0055: N02E1=IM1(J)
0056: N02E2=IM2(J)
0057: KNS=(FLO2(N02E1)23.1416/2L1)222+(FLO2(N02E2)23.1416/2L2)222
0058: SF=KNS/(2.23.1416)2222(E12GRAY/((1.-PR)22)22H1)
0059: WRITE(1,25)IT(J),IM1(J),IM2(J),09(J),ETND(J),E1,ETA,SPAR,SF
0060: 200: CONTINUE
0061: 215: CONTINUE
0062: 215: CONTINUE
0063: 20: FORMAT(1X,14,3X,18,5X,18,3X,E10.4,2X,F0.3,2X,E10.4,2X,F6.3,2X,F6.
0064: 12,F11.1)
0065: 207: WRITE(1,208)
0066: 208: FORMAT('ENTER 1-CONTINUE , -1= END.')
0067: READ(1,2)I1
0068: IF(I1)203,206
0069: 203: CONTINUE
0070: END
0071: E:200

```

TABLE 5.27

USER'S GUIDE FOR CALCULATION OF SYSTEM LOSS FACTOR
FOR A PLATE WITH A
CONSTRAINED DAMPING LAYER SYSTEM APPLIED

Execute program

program will display:

ENTER HD, RD, L1, L2, H1, R1, E1, E3, H3, R3

for which the user inputs:

the damping layer thickness, HD, the damping material density, RD, the plate dimensions, L1 and L2, the plate thickness, H1, the plate density, R1, the plate modulus, E1, the constraining layer modulus, E3, the constraining layer thickness, H3, and the constraining layer density, R3.

program then outputs:

ENTER NO. DATA LINES

to which user responds:

n

where n is the number of lines of data to be input into program. Program then indicates that it is ready to receive lines of data.

the user inputs:

$t_i, G_{Di}, \eta_{Di}, M_{1i}, M_{2i}$

for i between 1 and n inclusive, where i is the i^{th} input line, t_i is the temperature, G_{Di} is the shear modulus of the material, η_{Di} is the loss factor of the material, and M_{1i} and M_{2i} are the mode numbers.

program asks:

DO YOU WISH TO ITERATE ON GEOM PROPERTIES 1 = YES -1 = NO

if user does not wish to iterate the geometric properties of the system, the user inputs:

(If "No" go to Part a; if "Yes" go to Part b)

TABLE 5.27 (Continued)

Part a.

Program will respond by printing the values of the thicknesses of the damping material and of the constraining layer. It will then print headings for the output data and then the data, including calculated values of the system loss factor and the shear parameter, g.

Part b.

if user does wish to iterate the geometric properties of the system, the user inputs:

1

Program then outputs:

ENTER HD1 HD2 DELH2 H31 H32 DELH3

for which the user inputs the minimum and maximum thicknesses of the damping layer, HD1 and HD2, respectively, the size of the increment for the damping layer, DELH2, the minimum and maximum thicknesses of the constraining layer, H31 and H32, respectively, and the size of the increment for the constraining layer, DELH3.

Program responds by repeating Part a. for each possible configuration of geometric properties.

after completion of predictions, program outputs:

ENTER 1 = CONTINUE, -1 = END

if user wishes to perform more predictions, the user enters:

1

and program returns to beginning of sequence. If not, the user enters:

-1 and program terminates.

TABLE 5.28
SYMBOLS FOR PROGRAM PLATE

SYMBOL	DEFINITION
IM1 (B), MODE 1 } IM2 (B), MODE 2 }	Modes of the plate
GD(C), GD	Shear modulus of the damping layer
IT(D), TEMP	Temperature
ETAD(E), ETAD	Loss factor of the damping material
NHD, NH3	Indicators as to whether or not geometric properties are to be iterated
HD	Thickness of the damping layer
RD	Density of the damping layer
L1, BL1 } L2, BL2 }	Plate dimensions
H1	Plate thickness
R1	Density of the plate
E1	Modulus of the plate
E3	Modulus of the constraining layer
H3	Thickness of the constraining layer
R3	Density of the constraining layer
N	Number of lines of data
ITER	Variable which is equal to "1" if geometric properties are to be iterated and equal to "-1" if not
HD1	Minimum damping layer thickness
HD2	Maximum damping layer thickness
DELHZ, DHD	Damping layer thickness increment
H31	Minimum constraining layer thickness
H32	Maximum constraining layer thickness
DEL H3, DH3	Constraining layer thickness increment
AMI, AMI.	Increment factors
TA	System loss factor
SPAR	Shear parameter
A, B, C, EI	Intermediate variable
KN2	The plate eigenvalue
SF	The damped plate frequency

5.2 FINITE ELEMENT DESIGN EQUATIONS

The following subsections discuss methods of using finite element analysis, FEA, in damped system design. For a detailed discussion of FEA see Volume I, Section 5.

5.2.1 Integration of Finite Element Modeling into the Design Process

The finite element technique provides the designer with an accurate and economical means of predicting the dynamic behavior of either damped or undamped structures. As such, finite element analysis can play an important role at several stages in the design of damping treatments. This section describes a procedure for integrating finite element analysis into the damping design process and gives an example to illustrate the procedure. In References [5.2-5.4] a variety of damping design analysis problems are illustrated.

Analytical Procedure in Damping Design

The procedure may be divided into the following steps:

- o perform an assessment of vibration problems present in a preliminary undamped design,
- o evaluate different damping concepts for specific application,
- o evaluate alternate damping treatment design, and
- o qualify final design configurations.

Each of these steps is discussed in greater detail in the following paragraphs. A schematic of the damping design process with the finite element method is shown in Figure 5.1.

In the preliminary design phase, finite element modeling of a structure is a valuable tool in determining the existence of potential vibration problems. Conclusions can be drawn on the basis of either a natural frequency solution (to identify critical excitation frequencies and

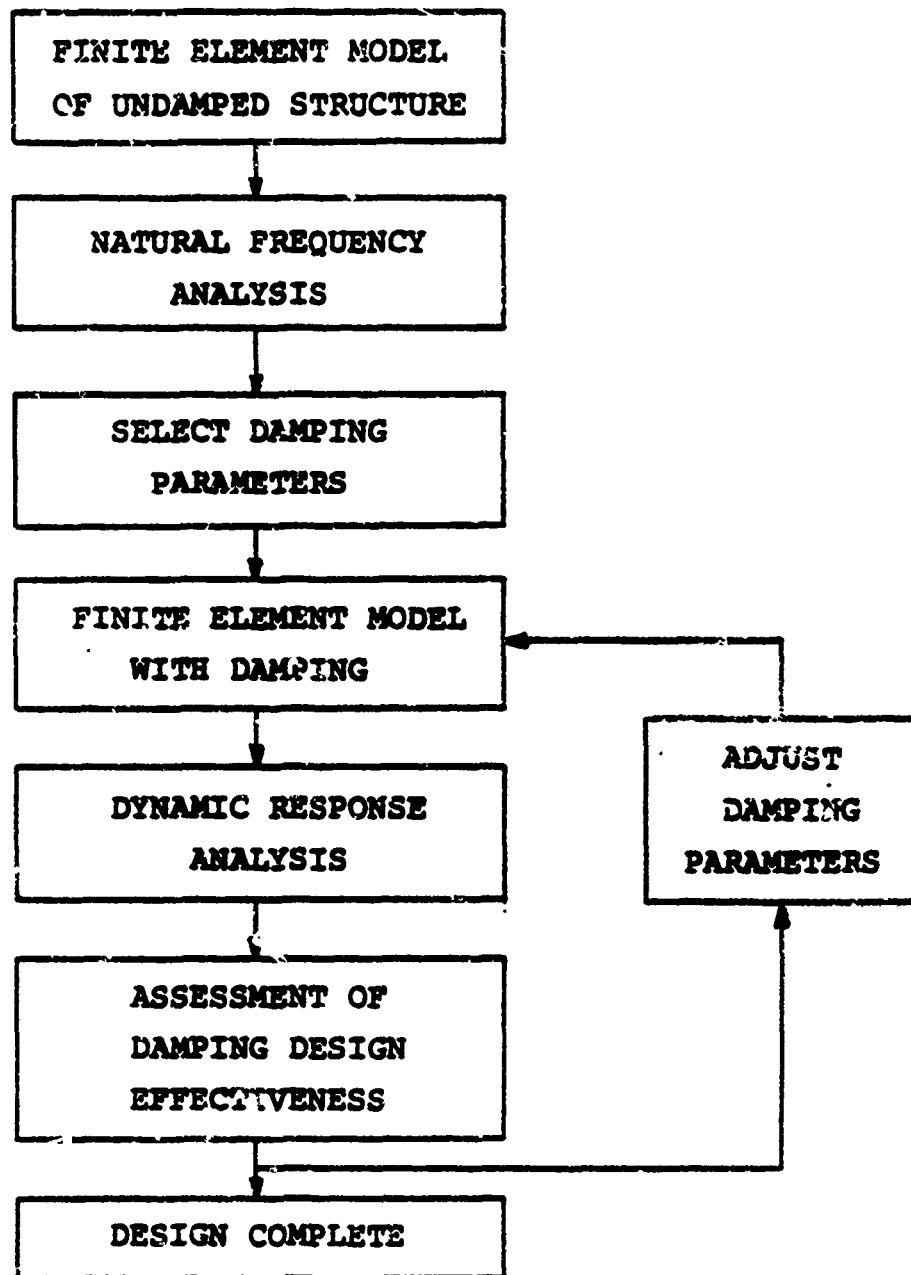


Figure 5.1 Finite element analysis in damping design procedure.

troublesome modes) or a frequency response analysis. Furthermore, examination of the vibration mode shapes will often help to determine those location in which the application of damping treatments will prove most effective.

During the actual design of a damping treatment, a rational choice of the type and location of the treatment can be made much more easily by the use of trial simulations, again performed using finite element methodology. If a model has been developed during the preliminary design stage, simple modifications of such a model will often suffice for identifying the most desirable type of damping treatment to be used. Experience is frequently a sufficient guide to the selection of a damping concept for a particular application. However, in more complex situations, finite element analysis can often provide this same familiarity with the problem, at only modest expenditures of time and money.

Once a damping treatment has been selected (either on the basis of experiments or analytical studies), finite element techniques are readily employed to determine the exact design configuration based upon costs, weight, or performance criteria. A single finite element model can generally serve as a means of evaluating a great number of minor design changes, such as variation in amount and distribution of damping, constraining layer thicknesses, material properties, etc.

Finally, the finite element method can be used for the final qualification of a damping treatment design. The performance of the final design can be assessed accurately and efficiently for a variety of operating environments (temperatures, loading, excitation, frequency). Besides the displacement response, stress information can also be generated in the finite element solution to identify potential fracture or fatigue problems which would not otherwise be anticipated prior to production.

Obviously, the finite element method represents a potentially powerful tool in several stages of the design process. Finite element simulations can, in most instances, be performed more quickly and economically than prototype testing, and can provide the opportunity for modeling the

structural response under operating conditions which may not be easily obtained in laboratory testing.

The recent interest in finite element technology as an aid to the designer has been sparked at least in part, by the development of computer graphics methods which can assist in both the preparation and interpretation of finite element data. The computer graphic processors can aid in

- generation of finite element data,
- model verification, and
- assimilation of analysis results.

An example illustrating the above design analysis procedure is summarized in the following.

Example Damping Analysis

This example illustrates how the finite element method can be used efficiently within the general process of designing a damping treatment to reduce the amplitude of forced vibrations. First, a hypothetical structure is defined which is presumed to have natural frequencies of vibration in the vicinity of the steady-state input frequency. A finite element model of the structure is constructed, and the natural frequencies are determined using a finite element computer program. Structural damping is then assumed in various parts of the structure. The results of the finite element program are used to determine the most effective areas to apply layered damping treatment. Finally, constrained damping is applied strategically, and the finite element program is used to determine the effectiveness of the damping treatment.

A. Problem Definition

The particular problem selected for illustration of the application of finite element analysis in damping treatment design is similar to the engine exhaust duct shown in Figure 5.2.

B. Finite Element Model

Figure 5.3 shows the finite element model used in this demonstration study. A cylindrical shroud with three flat vanes was modeled with variable 8-27 node solid finite elements. The boundary conditions and dimensions are shown in Figure 5.3. Although the full structure is shown, only a symmetric



Figure 5.2 Engine exhaust duct.

Shroud
10" ID
.05" Thick
3" Wide
Steel

Vanes
2.5" Long
.1" Thick
1" Wide
Steel

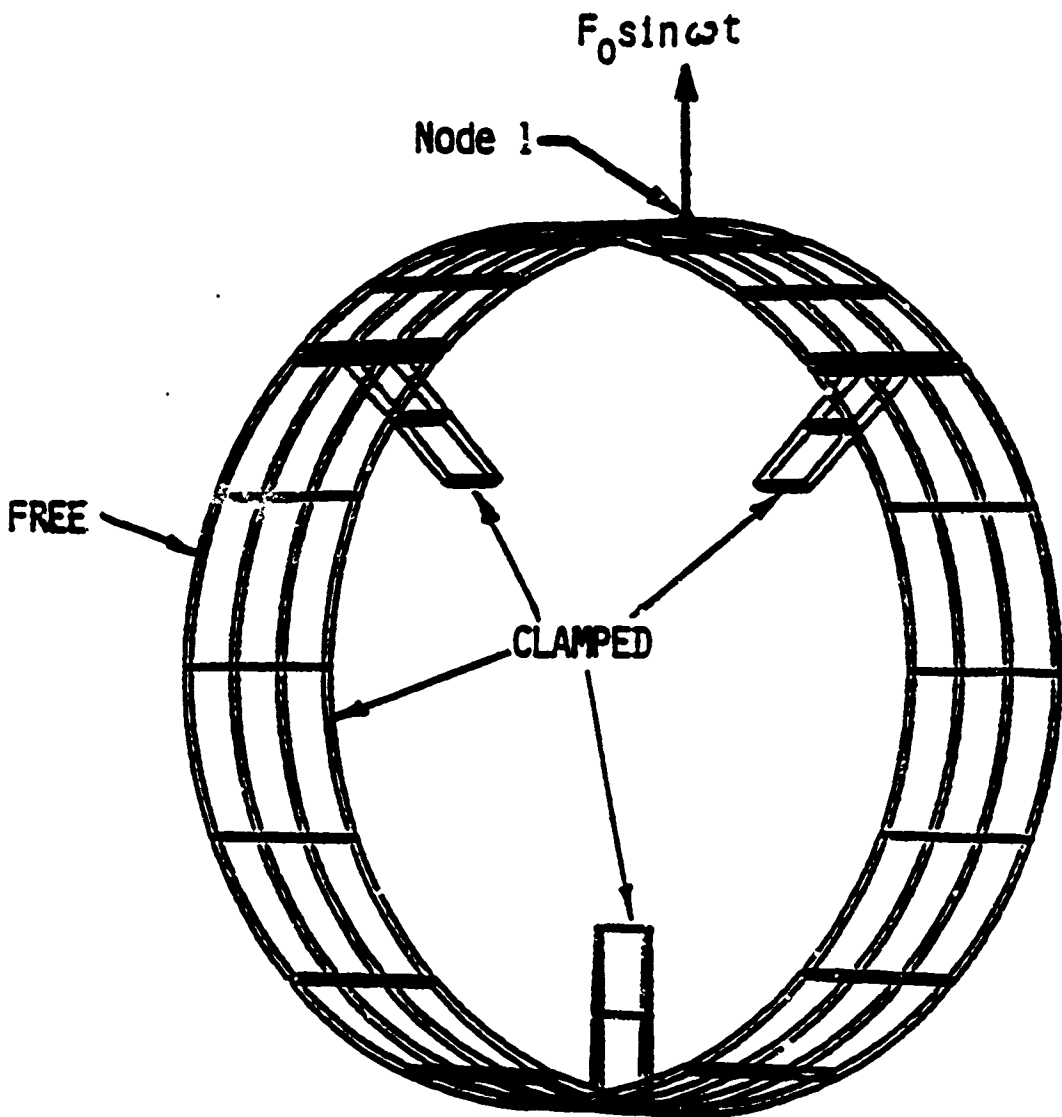


Figure 5.3 Finite element model.

half of the structure on one side of a plane of symmetry through the bottom vane was actually modeled for computation.

C. Natural Frequency Analysis

The finite element program of Reference [5.5] was used to compute the natural frequencies and mode shapes of the model of Figure 5.3. Perspective plots of the first three vibration modes are shown in Figure 5.4 and end-on views of the same modes are shown in Figure 5.5.

D. Preliminary Damping Analysis

In practice, damping treatment is applied to one or more exposed surfaces of a structure. A complete finite element model containing multiple added layers would be quite complex and relatively expensive to analyze. Therefore, a preliminary damping analysis can be performed in which the elements of the original finite element model are assumed to be internally damped. In this case, four different cases are considered:

1. no damping,
2. the vane elements have 5 percent damping,
3. the shroud elements have 5 percent damping, and
4. both the vane elements and the shroud elements have 5 percent damping.

The results of the four cases for mode 2 are shown in Figure 5.6. In this case the amplitude and phase angle for the displacement of No. 1 (see Figures 5.5 and 5.6) are plotted versus input frequency. Figure 5.6 indicates that considerable reduction in amplitude can be obtained if damping is present.

E. Final Damping Design Analysis

The preliminary damping analysis of the preceding section provides the designer valuable information which can be used along with other data to select a damping treatment. After the damping treatment has been designed, another finite element analysis can be performed. This time the damping treatment is modeled separately in order to obtain an accurate representation of the effectiveness of the damping design. Figure 5.7 shows a detailed finite element model of the structure under consideration having a hypothetical damping treatment. In this case, for illustration, the shroud has a constrained damping layer applied to the outside diameter, while the

EXHAUST DUCT MODE SHAPES

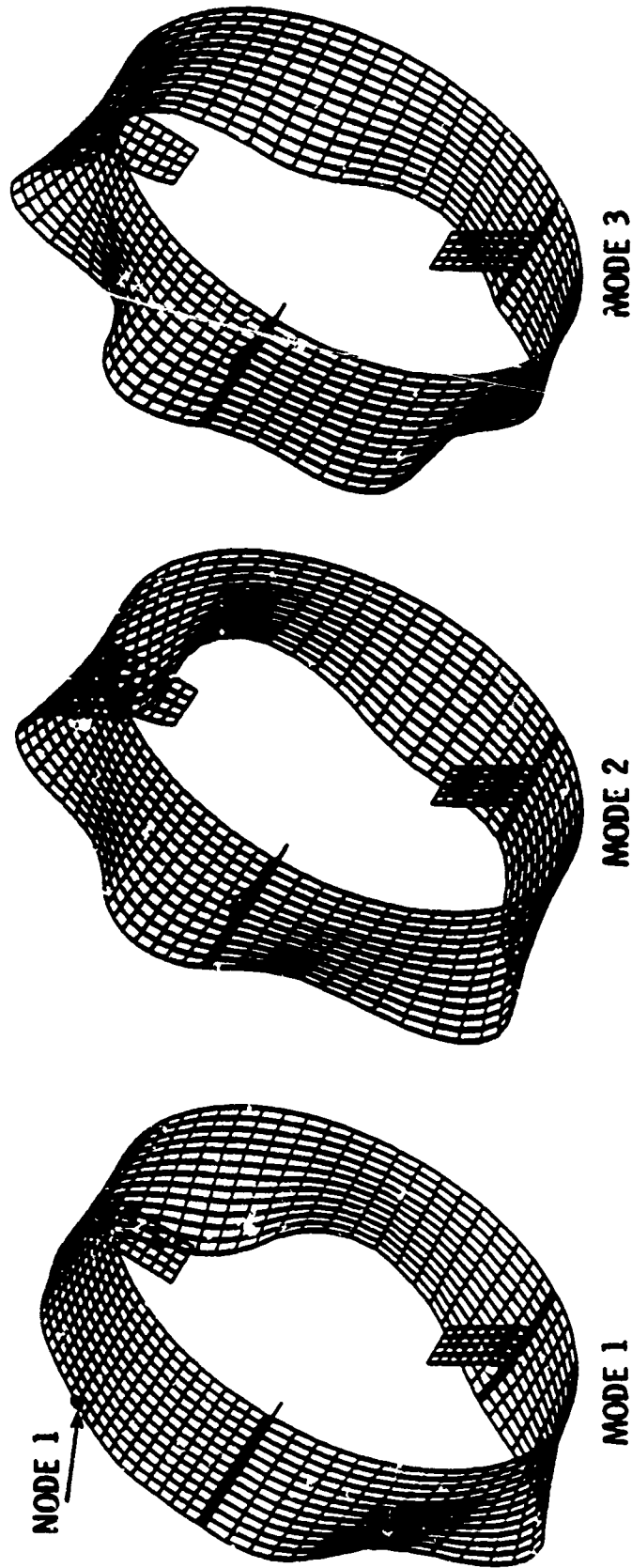


Figure 5.4 Mode shapes of engine exhaust duct (perspective view).

MODE 1
3421 cps

MODE 2
3793 cps

MODE 3
3854 cps

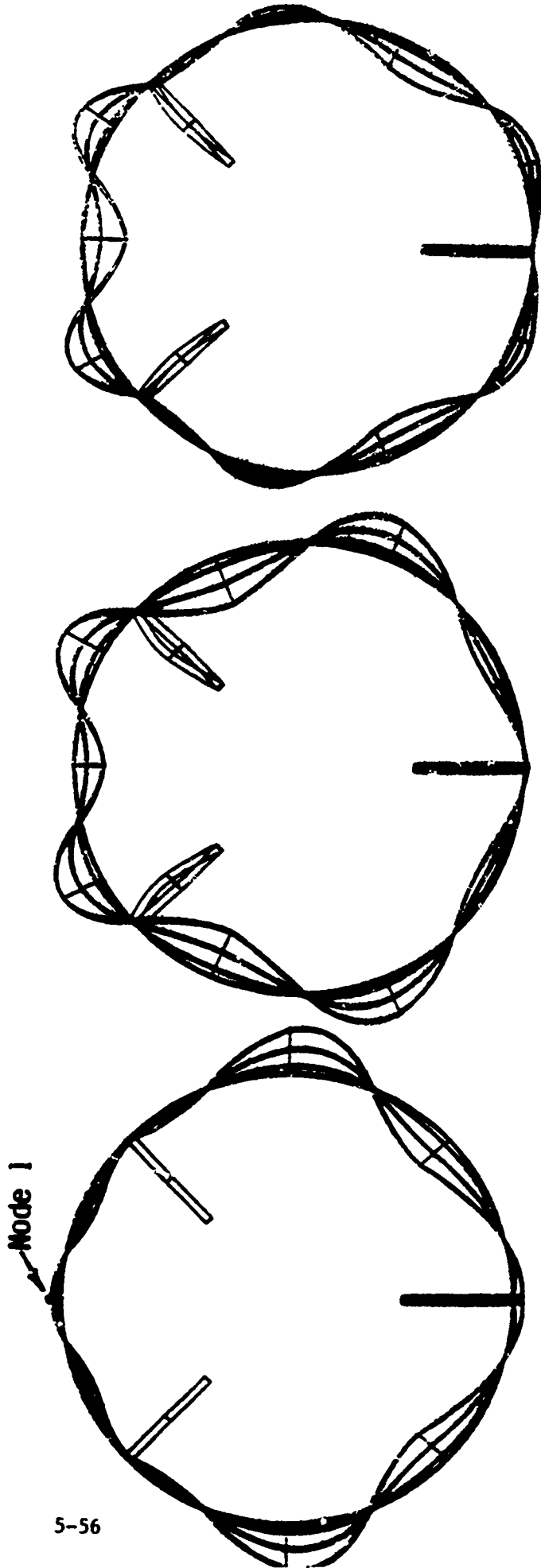
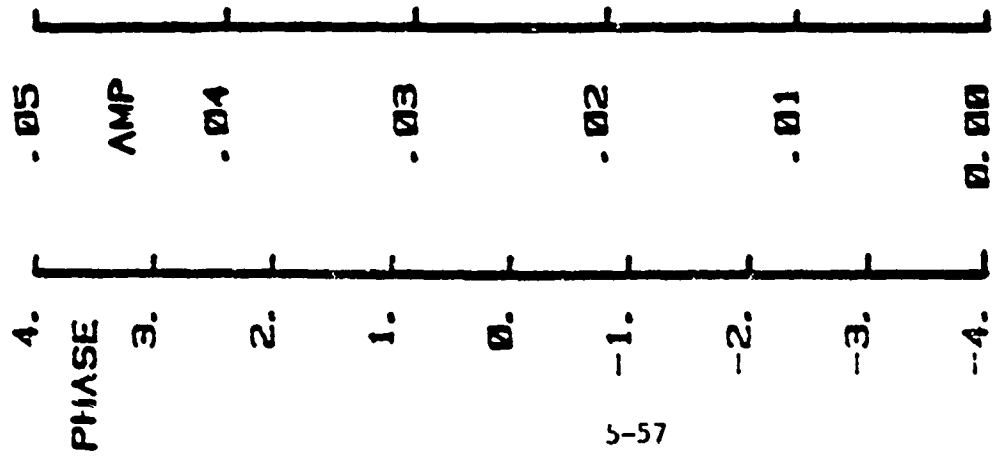


Figure 5.5 Mode shapes of engine exhaust duct (end-on view).

SYSTEM DAMPING

1	0
2	.02
3	.03
4	.05



MATERIAL DAMPING

.05

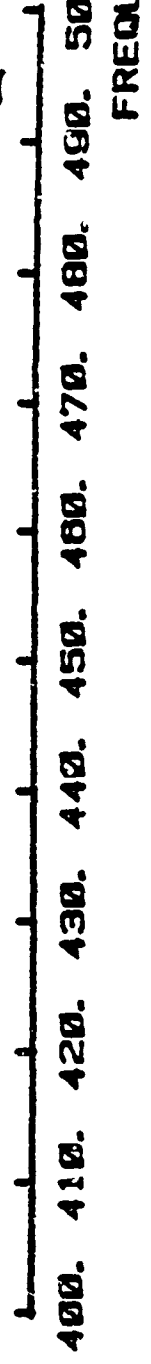


Figure 5.6 Engine exhaust duct: effect of damping treatment on the amplitude-frequency response of the Second Mode of Forced Vibrations,
 1. no damping 2. vanes only 3. shroud only 4. shroud and vanes only.

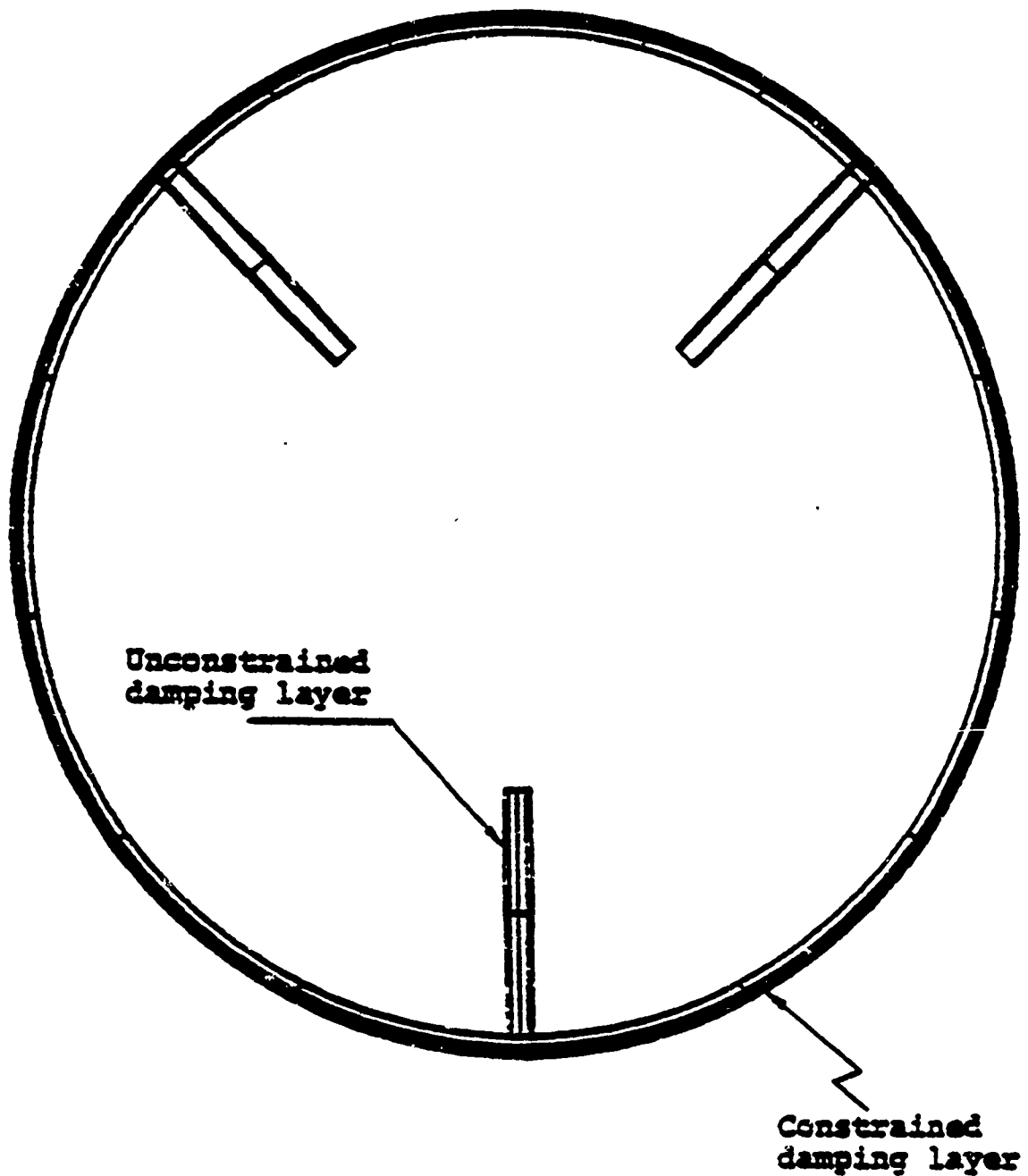


Figure 5.7 Detailed model with damping layer and constraining layer.

vanes have an unconstrained damping layer applied to both sides. The detailed model can be used to proof-check the final design or used at each stage of an iterative design process.

5.2.2 A Note on Finite Element Discretization of Layered Damping Designs

Finite element analysis, because of its flexibility in modeling general structures, is ideally suited for modeling passive damping configurations on integrally damped structures. However, the modeling of layered damping designs on complex structures poses two problems. First, the thin damping layers result in high aspect ratios (length ÷ thickness) of the 3D solid elements representing the damping system. Secondly, if a multi-layered damping system is being modeled, there are a large number of degrees-of-freedom. This section discusses ways to reduce the number of elements representing the damping system and the accuracy of the damping prediction using high aspect ratios. The recommendations made in the following paragraphs are based on a very limited number of practical applications [5.6].

Results Using High Aspect Ratios

The construction of an FE model for dynamic analysis is usually governed by giving consideration to the number and type of modes that are to be determined from the model. The length and width of the elements in the base structure are thus determined by accepted modeling practice. If a constrained layer damping system is then modeled on the structure and if the damping and/or constraining layers are thin relative to the base structure, the damping and/or constraining layers may have high aspect ratios (length ÷ thickness).

Experimental tests and corresponding FEA evaluation [5.6] of a cantilever plate with a double constrained layer system showed that aspect ratios up to 1000:1 yield very good analytical results. The undamped FE model of the plate is shown in Figure 5.8. Figure 5.9 shows the cross section of one of the damping configurations tested and analyzed. This configuration, referred to as Plate 1, consisted of the 0.25-inch plate with 0.002-inch 3M ISD-110, damping material, 0.007-inch stainless steel middle constraining layer, 0.003-inch

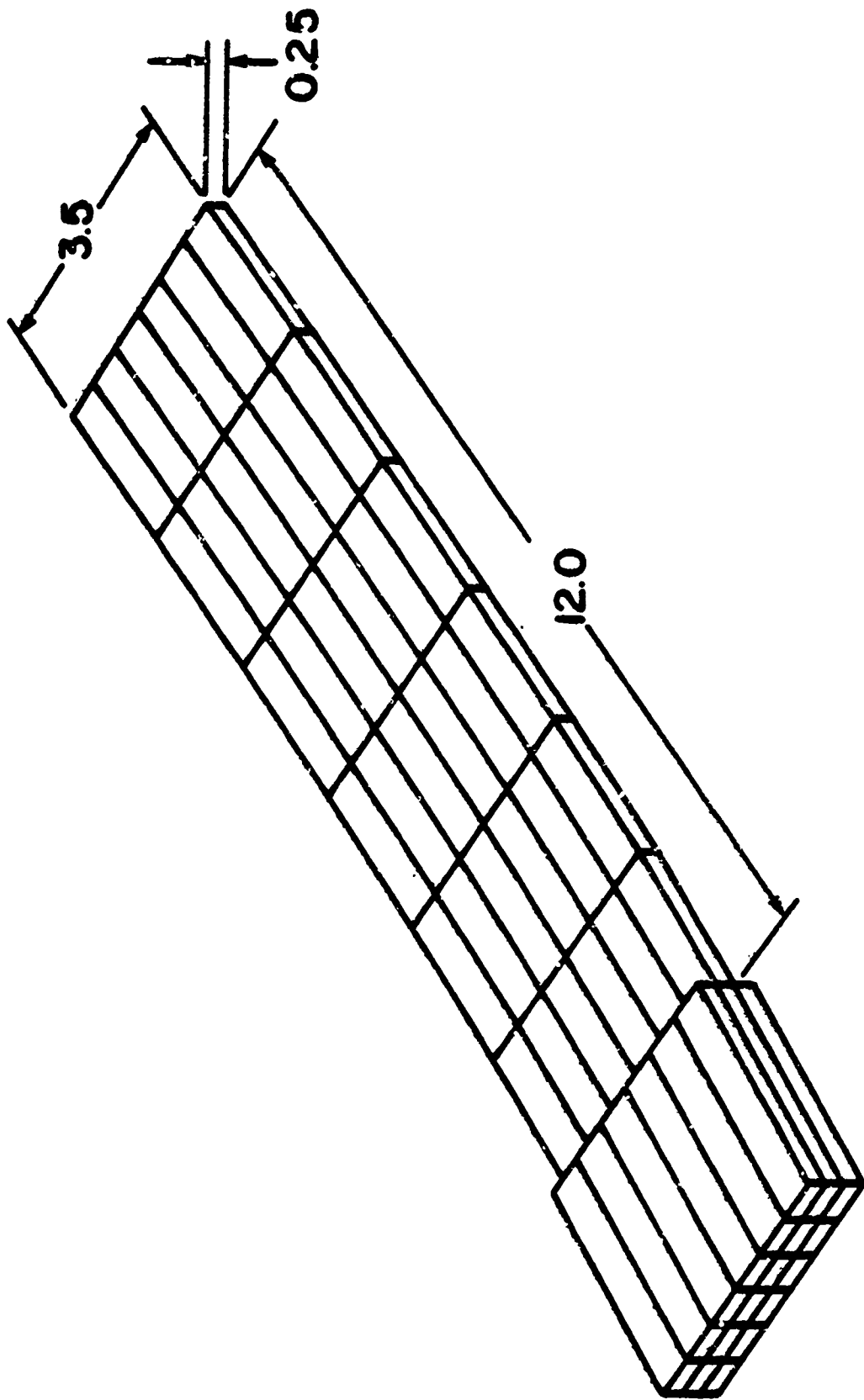


Figure 5.8 Finite element model of a cantilever plate.

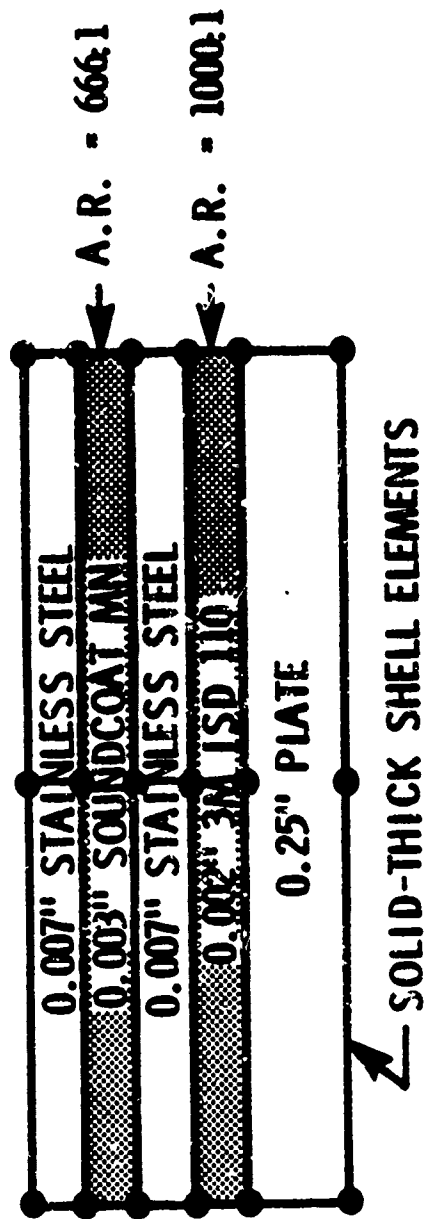


Figure 5.9 Cross section of plate 1 damping system.

Soundcoat MN damping material, and 0.007-inch stainless steel outer constraining layer. All layers in the FE model are modeled with 3D solid-thick shell elements. Since the elements are 2 inches long and some elements are as thin as 0.002 inch, the aspect ratio on some elements are 1000 to 1.

The results of the FEA and test of Plate 1 are shown in Figure 5.10, for the second bending mode. It can be seen that there is very good agreement between the test results and the FE forced vibration results. The results from the FE normal mode are considerably higher than the test results. It is felt, in this case, that the strain energy method using the forced response more closely matches the test. In both the test and the forced response analysis the plate was subjected to a small tip load. Another cause of the discrepancy could be that the tip load does not excite a pure mode. Indeed damping couples mode together. Perhaps if the test had been conducted with the clamped end of the cantilever mounted on a shaker the mode shape of the cantilever plate may have been more nearly a pure mode than exciting the cantilever at the tip. Then perhaps the normal mode method would closely match the shaker test.

A second damping configuration evaluated, referred to as Plate 2, is shown in cross section in Figure 5.11. This damping system has two layers of the same damping material, 0.002-inch 3M ISD-112, separated by a 0.003-inch middle constraining layer. The outer constraining layer is 0.007-inch stainless steel. All layers are modeled with 3D solid-thick shell elements. The aspect ratios of the damping layers are 1000 to 1.

The results of the FEA and test of Plate 2 are shown in Figure 5.12 for the second bending mode. Again there is very good agreement between the test results and the FE forced vibration results. As for the Plate 1, the normal mode results are higher than the test results; the same explanation given for Plate 1, holds here as well.

Results for the first torsion mode are shown in Figure 5.13. The forced vibration results agree well with the test results, as do the normal

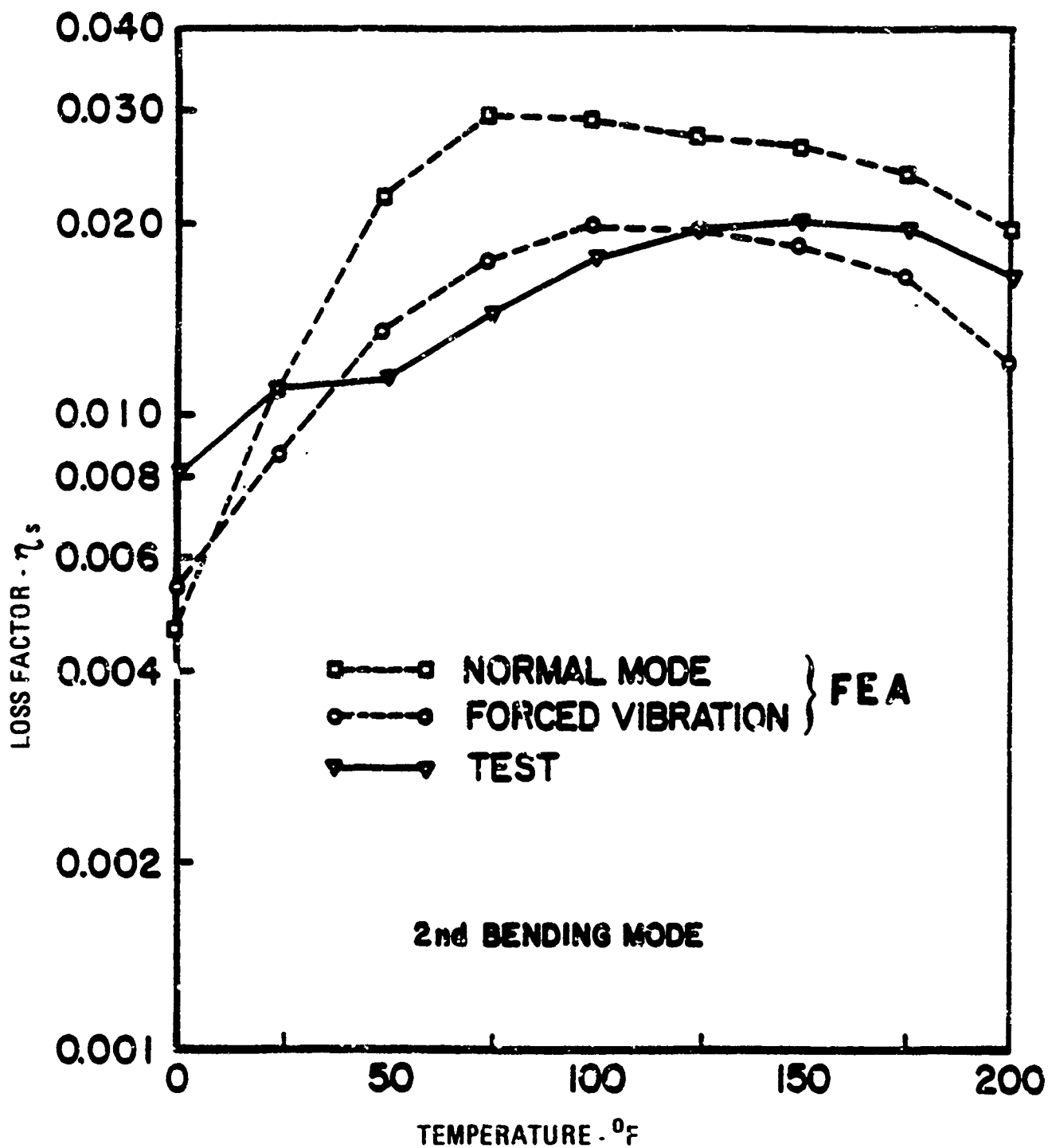


Figure 5.10 Analytical and experimental results for plate 1, 2nd bending mode.

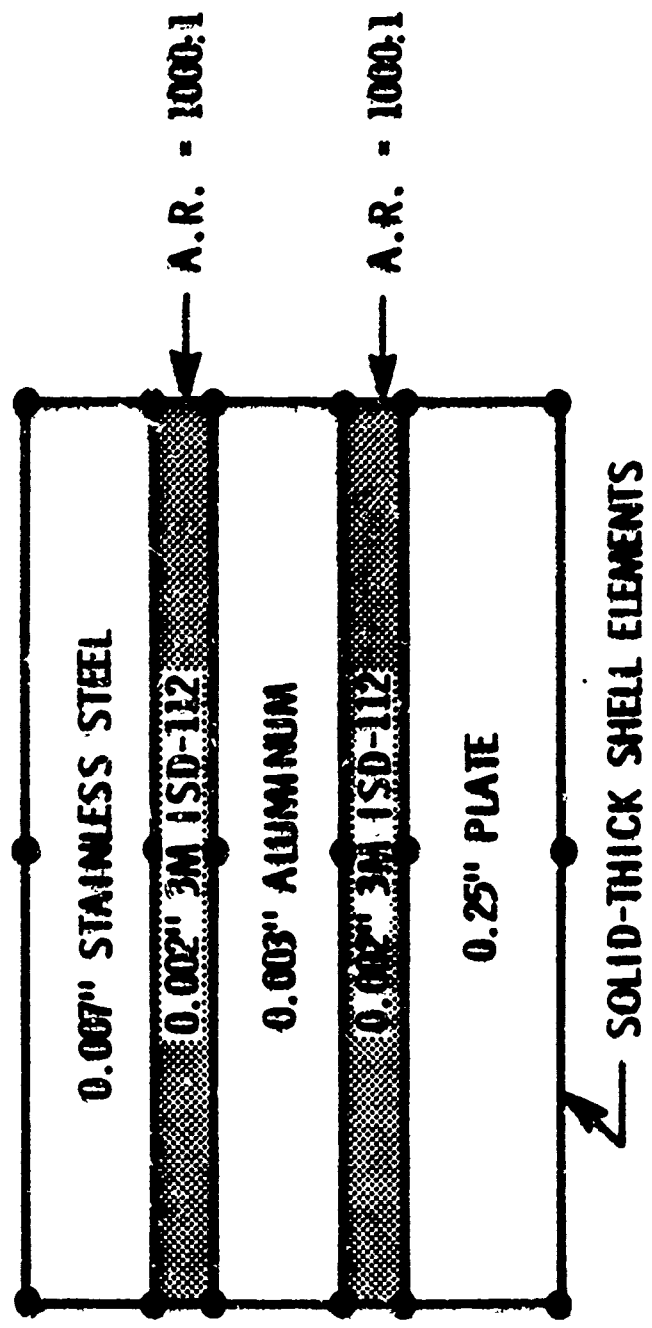


Figure 5.11 Cross section of plate 2 damping system.

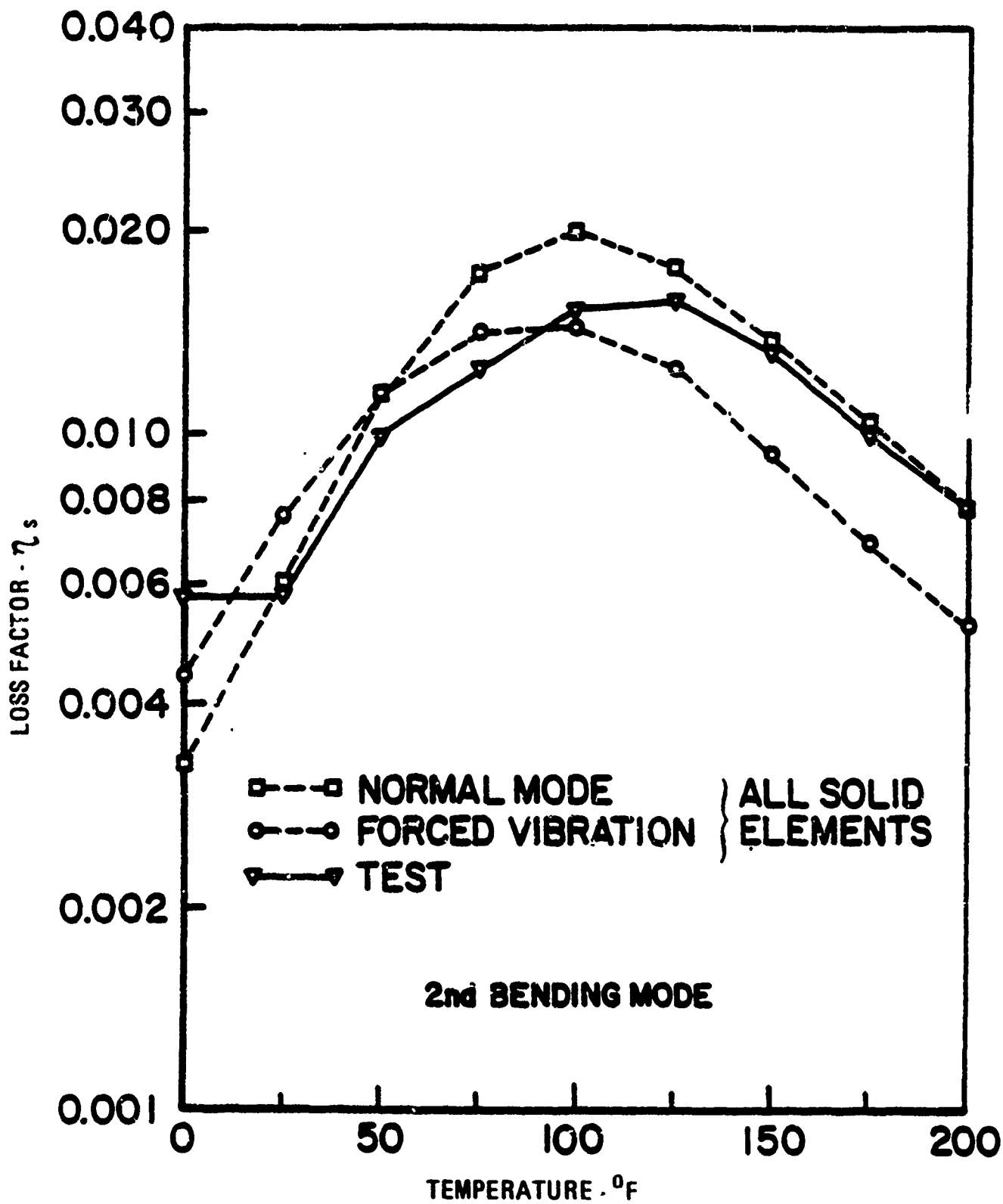


Figure 5.12 Experimental and analytical results for plate 2, 2nd bending mode.

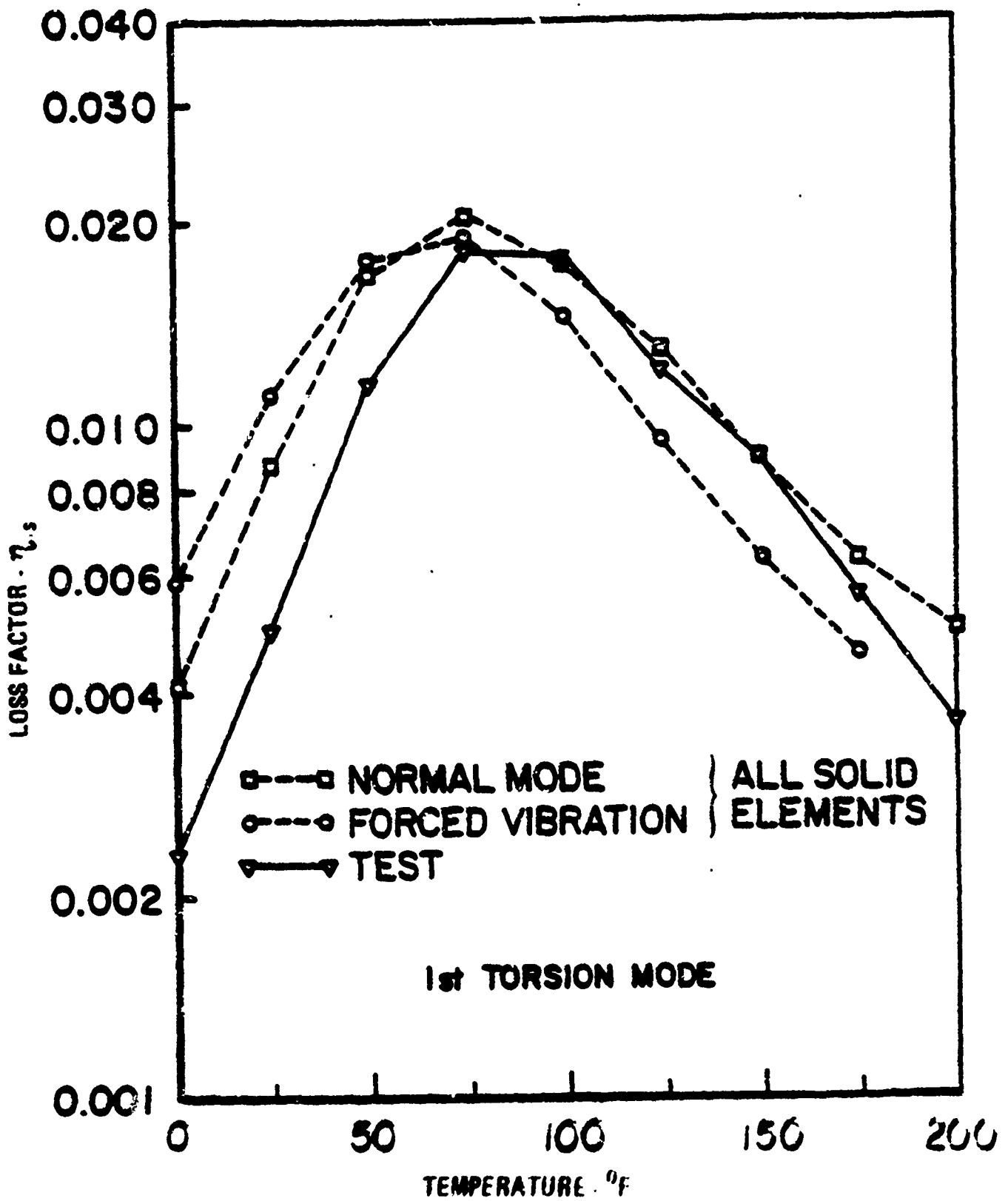


Figure 5.13 Experimental and analytical results for plate 2, 1st torsional mode.

mode results. In this instance, driving at the tip of the cantilever for the forced response (and test results) yields approximately the same results as the normal mode.

It should be noticed that in the Plate 1 and Plate 2 results presented so far, that although the magnitude of the peak damping and the shape of the loss factor curve predicted by the FE forced vibration is nearly identical to the test results, the forced vibration curve is shifted 25° to the left of the test data. This temperature shift could be due to two causes. The finite element model of the cantilever plate may be stiffer than the actual specimen; this is in fact the case, with the second bending mode frequency approximately 8 percent high. The other cause could be that the actual damping material is stiffer than the properties being input into the FE model. It is likely that the cause is a combination of the above two factors.

The results presented so far have been for aspect ratios up to 1000 to 1. To see if the prediction of loss factors could be improved, the FE model was changed. Twelve elements were used in the length of the cantilever instead of six and the aspect ratio was correspondingly cut by a factor of two. The change in the results due to the lower aspect ratio were insignificant. Therefore, the use of aspect ratios up to 1000 to 1 was acceptable. The use of aspect ratios greater than 1000 to 1 needs further investigation.

Modeling Techniques to Reduce the DOF

Even a simple structure with a multi-constrained layer damping system can have a large number of DOF. As an example, the cantilever plate discussed previously has 1300 DOF.

Therefore, two means of reducing the number of DOF are investigated. The first method involves the use of membrane elements to model the constraining layers. The second approach is to replace several layers in the damping system by an "equivalent" element.

A. Use of Membrane Elements for Constraining Layers

The purpose of the constraining layer in a constrained layer damping system is, as its name implies, is to constrain the damping material. During bending the constraining layer places the damping material in a state of shear stress and thus dissipates energy. The constraining layer being stiff, and usually very thin, undergoes very little shear deformation and is subjected to in-plane loading. Thus it has the characteristics of a membrane and can be represented by a membrane element. The damping layer on the other hand undergoes considerable shear deformation and therefore must be modeled with shear deformable elements such as 3D solid-thick shell (solid) element.

The use of membrane elements for constraining layers as applied to the Plate 1 damping configuration is shown in Figure 5.14. The nodes of the membrane elements are coincident with the nodes on the upper surface of the damping layers. Therefore, the membrane elements do not add any DOF to the three solid elements used for the damping layers and plate. Thus the damping system shown in Figure 5.9 which was modeled by five solid elements through the thickness is modeled by three solid elements and two membrane elements, resulting in a 33 percent reduction in DOF.

Figure 5.15 shows the FE forced vibration results using the membrane and solid elements model. Also shown are the FE forced vibration results using all solid elements, previously shown in Figure 5.10. It is seen that the two methods compare very favorably. Notice that the damping predicted by the use of the membrane elements is nearly uniformly lower than the results using all solid elements. This is probably due to the fact that the outer damping material and outer constraining layer are not as far away from the neutral bending axis because the membrane elements have no physical thickness.

For structures with constraining layers that are thin relative to the base structure, such as Plate 1, a small error is introduced. Thick constraining layers would result in more error. Caution should be exercised in using the membrane elements on curved surfaces as the membrane bending coupling is neglected, and the effect of its absence cannot be generalized.

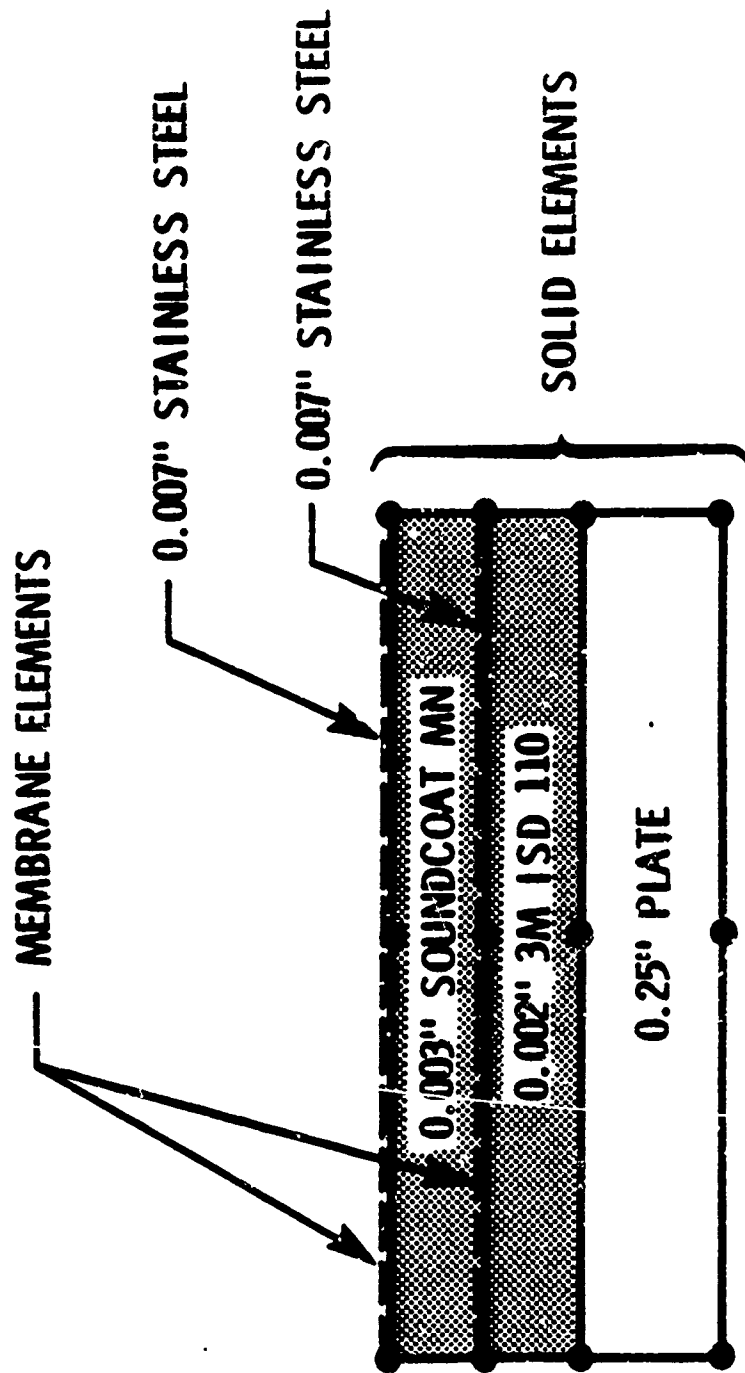


Figure 5.14 Plate 1 modeling scheme using membrane elements.

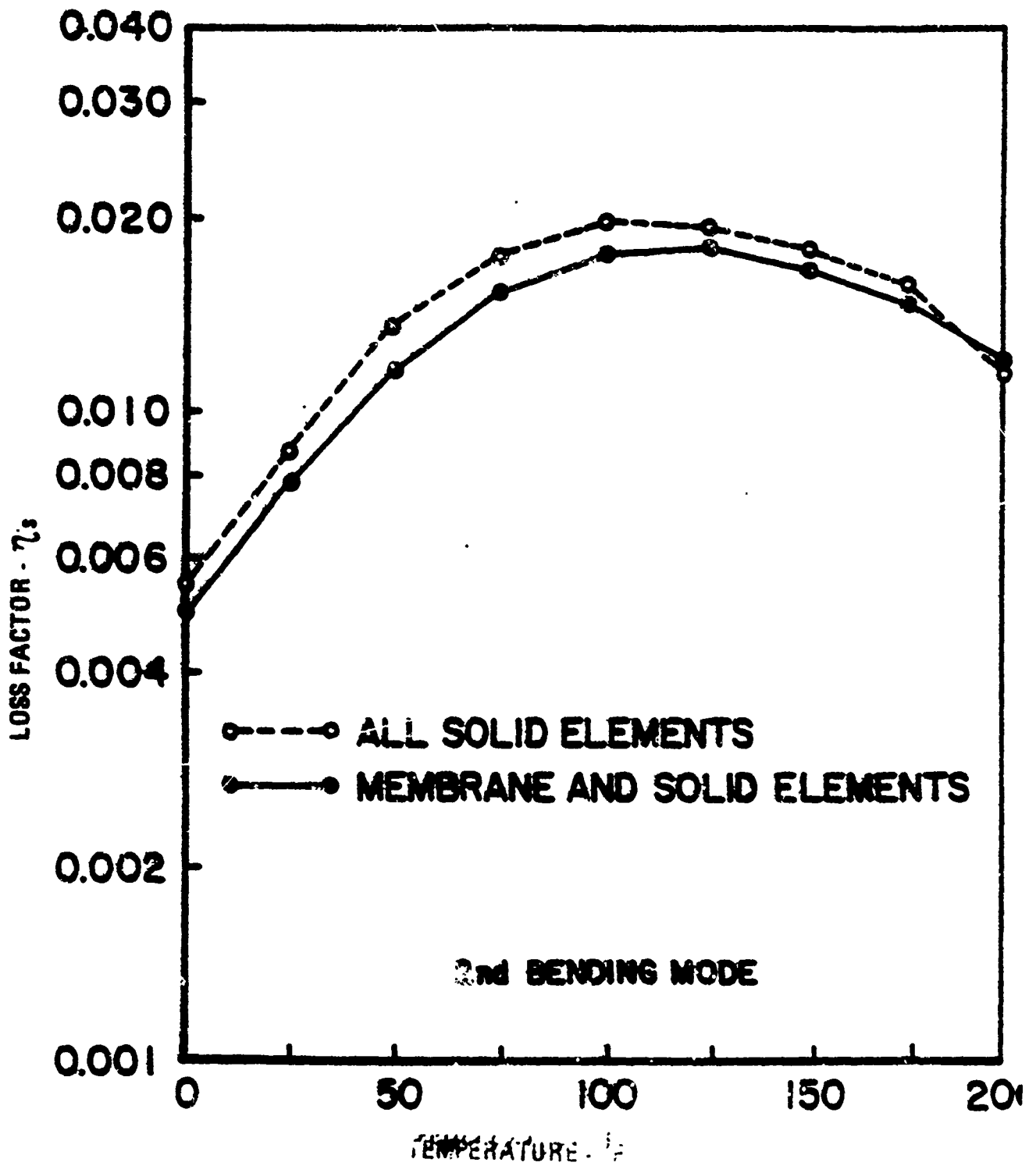


Figure 5.15 FEA results comparing all solid model to membrane model.

B. Use of Equivalent Solid Element

The other means of reducing the number of DOF becomes apparent by studying the Plate 2 configuration (see Figure 5.11). Since the two damping layers are the same thickness, of the same material and are separated by a thin middle constraining layer, it seems that the overall behavior of the three layer system could be governed by the soft damping materials. Furthermore, it seems that the three layers could be represented by a single "equivalent" layer. It only remains to determine the dynamic properties of the three layers. The properties are determined from a symmetric sandwich beam test. Usually to determine the properties of a constrained layer damping material the material is placed between symmetric sandwich beams and tested over a broad temperature and frequency range, as discussed in Volume I, Section 2. In the present case, the three layer system is placed between symmetric sandwich beams, as shown in Figure 5.16, and tested as if it was a typical damping material. The properties could also be determined analytically thus avoiding the test procedure.

The application of this modeling technique to the Plate 2 configuration is shown in Figure 5.17. Figure 5.18 shows the second bending mode FE forced vibration results using all solid elements (previously shown in Figure 5.12) and the equivalent solid element. The results are nearly identical. The same is true for the first torsion mode shown in Figure 5.19.

To summarize, the modeling techniques for reducing the DOF are found to be accurate. The use of membrane elements for constraining layers predicts a slightly lower value of damping than the standard approach and reduces computer costs 44 percent in the analyses shown. An equivalent solid element replacing the two damping materials and middle constraining layer gave nearly identical results as the standard modeling approach. This technique reduces computer costs 60 percent.

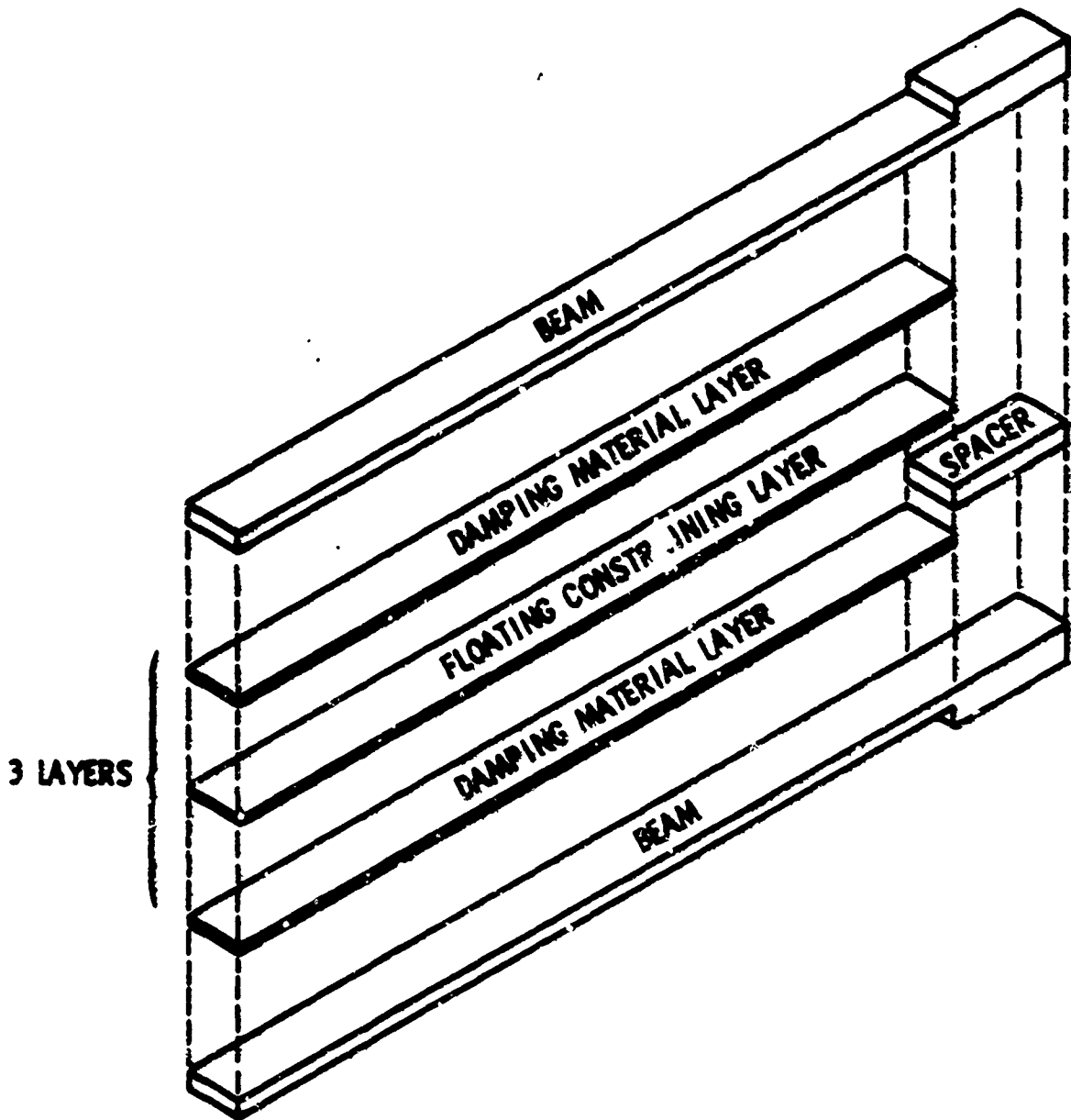


Figure 5.16 Equivalent solid beam test specimen.

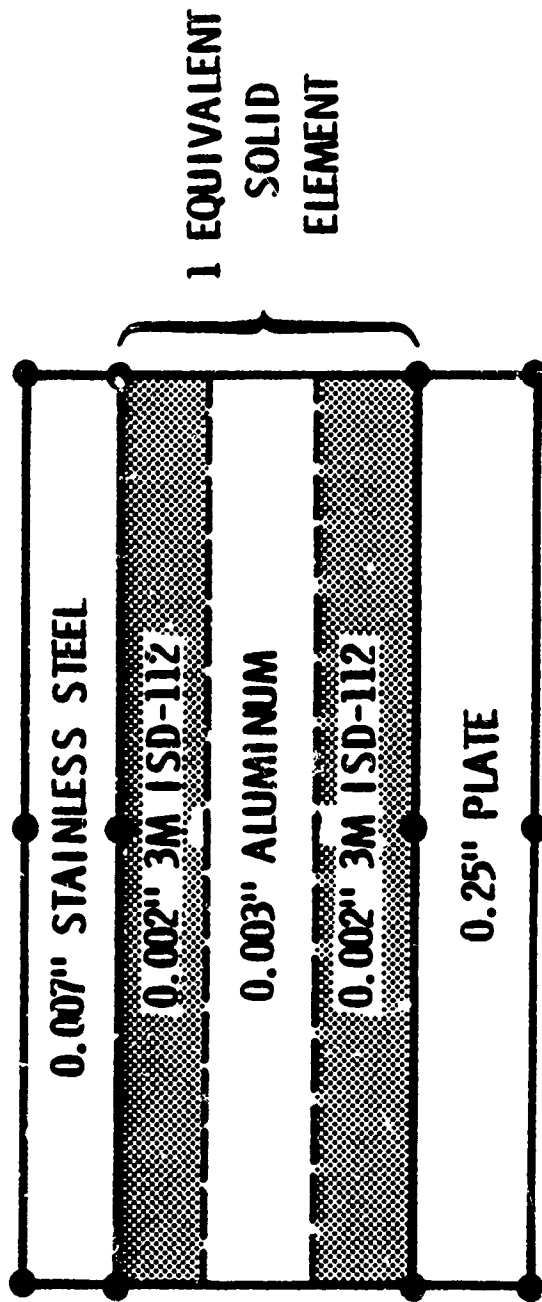


Figure 5.17 Plate 2 modeling scheme using the equivalent solid element approach.

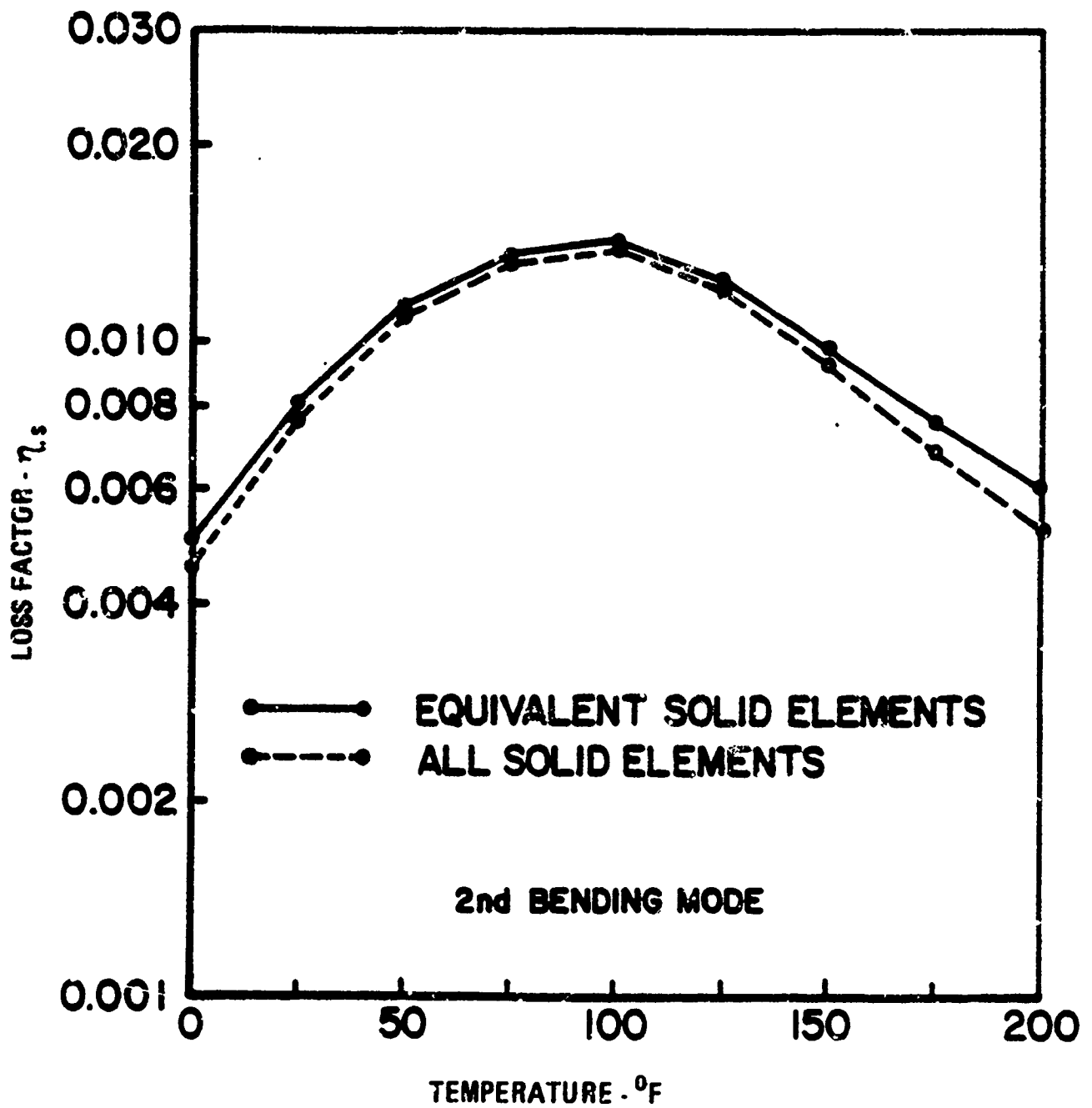


Figure 5.18 Analytical results comparing the all solid model to the equivalent solid model for the second bending mode.

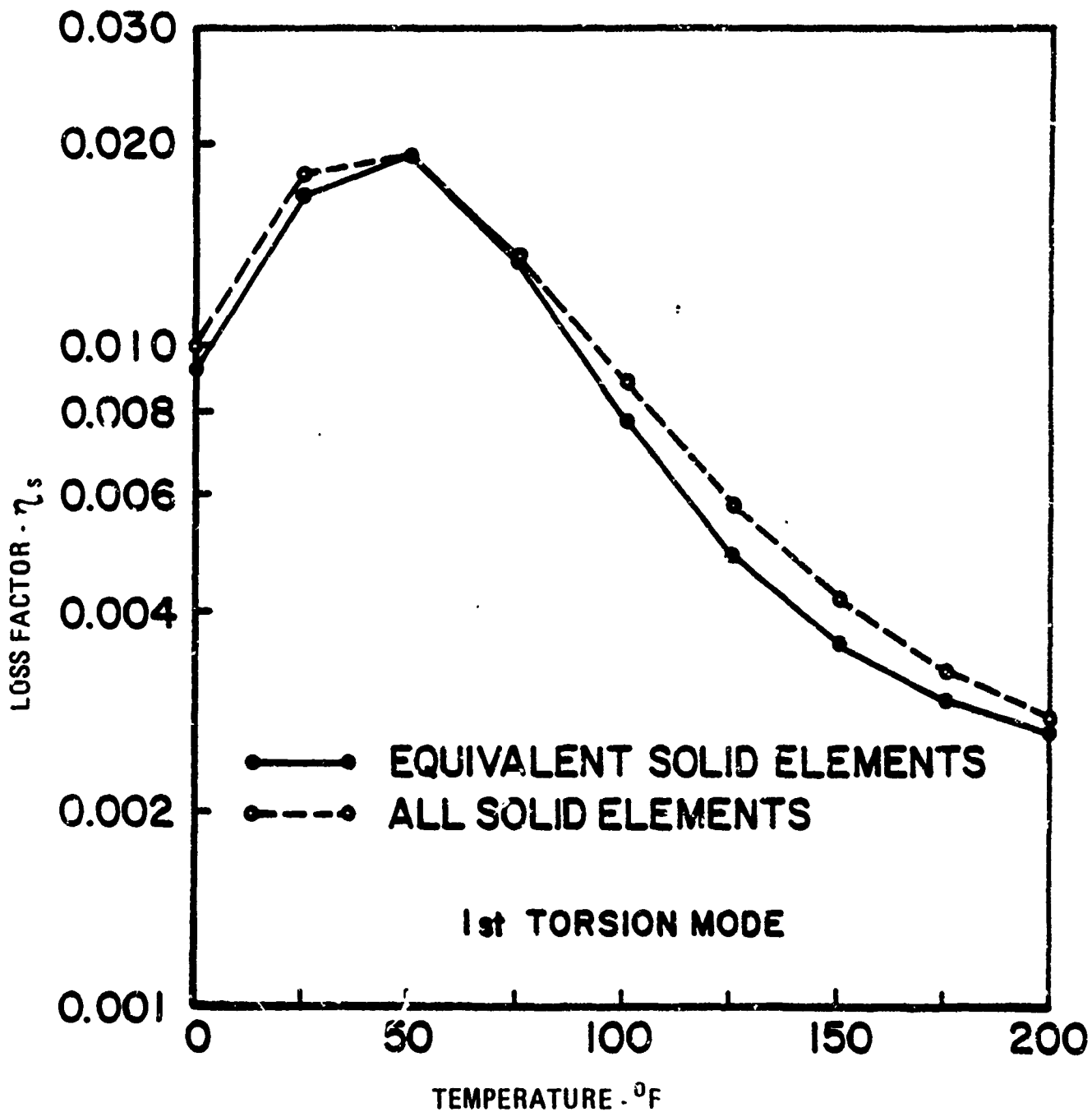


Figure 5.19 Analytical results comparing the all solid model to the equivalent solid model for plate 2 first torsion mode.

TABLE 5.29 SYMBOLS FOR SECTION 5

SYMBOL	DEFINITION
F_B	Natural frequency of an undamped cantilever beam
ξ_i	i^{th} modal eigenvalue
L_1	Beam length
H_1	Beam thickness
E_1	Young's modulus of the beam
R_1	Beam density
I_1	Moment of inertia of beam
g	Gravitational constant
η_s	Loss factor of beam
η_D	Damping material loss factor
E_R	Modulus ratio
H_R	Thickness ratio
E_2	Young's modulus of the damping material
H_2	Damping material thickness
F_s	Frequency of a damped cantilever beam
R_R	Density ratio
R_2	Damping material density
E_3	Young's modulus of the beam constraining layer
H_3	Thickness of constraining layer
G_2, G_3	Shear modulus of the damping material
η_2	Loss factor of damping material
R_3	Density of the constraining layer
ξ_i	Eigenvalue for mode along plate length
ξ_j	Eigenvalue for mode along plate width
L	Plate length
W	Plate width
γ	Poisson's ratio of the plate

REFERENCES

- 5.1 Bishop, R.E.D., Johnson, D.C., *The Mechanics of Vibration*, Cambridge University Press, 1960.
- 5.2 Kluesener, M. F., Drake, M. L., "Damped Structures Design Using Finite Element Analysis," *The Shock and Vibration Bulletin*, 51, Part 5, May 1982, pp. 1-12.
- 5.3 Holman, R. E., Liu, C. P., Bauer, J. L., "Damping of Precision Pointing Systems and the Use of Finite Element Computational Program for Performance Prediction," Hughes Aircraft Company, Air Force Weapons Laboratory Contract No. F29604-80-C-0015.
- 5.4 Kienholz, D. A., Johnson, C. D., Parekh, J. C., "Design Methods for Viscoelastically Damped Plates," Paper No. 83-0904, 24th Structures, Structural Dynamics and Materials Conference, Lake Tahoe, Nevada, May 2-4, 1983, pp. 334-343.
- 5.5 Brockman, R. A., "MAGNA Computer Program User's Manual," University of Dayton Report UDR-TR-80-107, November 1980.
- 5.6 Kluesener, M. F., "Practical Methods of Applying Finite Element Analysis to the Design of Complex Damped Structures," AIAA Paper No. 84-0971-CP.

SECTION 6

EXAMPLE PROBLEM, DESIGN EXAMPLES, AND CASE HISTORIES

There are many options open to a designer to solve a resonant vibration problem (stiffening, damping, isolation, source modification, etc.). The point of the following paragraphs is to discuss design approaches using viscoelastic damping as the solution to a vibration problem. It is not the intent to leave the impression that viscoelastic damping is a "cure-all," but only that it is a viable alternative. The designer must decide which method of vibration control should be used for each problem encountered.

The work in this section consists of a detailed example problem in Subsection 6.1, a number of design examples in Subsection 6.2 and a number of case histories in Subsection 6.3.

6.1 EXAMPLE PROBLEM

The following example problem demonstrates the use of the design procedure discussed in Section 4. The example is quite detailed and intended to help a designer gain further understanding of the design procedure.

6.1.1 A Solution to a Noise and Vibration Problem [6.1]

Background

The increasing emphasis on fuel efficient ground transportation has caused system designers to become conscious of both size and weight requirements. An example is the redesign of an automobile radiator cooling fan's electric motor. If a functional redesign could be found, the front end of a car could be shortened approximately two inches. Obviously, an overall vehicle weight reduction would be realized which would result in increased fuel economy. With these goals in view, the quest was to find an optimum motor design combining the required power outputs with minimum size and weight requirements.

These redesign efforts were successful; however, the new motor design developed an objectionable noise and vibration problem. Operational tests revealed two large noise peaks. One peak occurred in the range of 200 to 300 Hz, while the other occurred in the range of 1100 to 1200 Hz. The new motor was in production when this problem was discovered.

An investigation to pinpoint the source of these problems and to locate a probable damping solution was initiated. The investigation was divided into the following sections:

- (1) Dynamic analysis of the motor and mount system to identify system resonant frequencies and mode shapes
- (2) Comparison of the frequency spectrum of the operational noise to system frequencies to identify noise generating modes
- (3) Design, optimization, and laboratory evaluation of a damping system to reduce the radiated noise
- (4) Full scale automotive system test.

A general approach to developing a damping design will be discussed in the following paragraphs and developed with this case history used as the example [6.2].

General Approach

Damping design like any other design procedure requires a basic core of data. The approach has seven basic steps.

- (1) Problem and Environmental Definition. - Damping is successful only in controlling resonant vibration related problems. It is futile to attempt to solve a problem through the use of damping when the problem is not resonance related. The temperature sensitivity of the damping material for both useful damping and survivability is extremely important. Contaminants which may come in contact with the damping design must also be considered.

(2) Structural Dynamics Characterization. - A damping design is totally dependent on the resonant frequency, modal damping, and mode shape of the problem modes(s) [6.3, 6.4]. Proper damping design cannot be done without an adequate definition of the dynamic characteristics of the system being studied.

(3) Damping Material Selection. - The environment is the primary factor which dictates the material chosen for use in a design. The damping material for a specific design depends on: (a) the type of damping application to be used (i.e., free layer, constrained layer, or tuned damper); (b) frequency of vibration; (c) the contaminants that the design will be exposed to; and (d) the temperature at which the design must operate.

(4) Damping System Selection and Design. - The type of damping system (i.e., free layer, constrained layer, tuned damper, damped line to ground, etc.) is prescribed by the materials available for use in the given environment and the dynamic properties of the structure system. The actual design analysis can be done using simple fourth order beam theory [6.5], or can be as detailed as complete finite element analysis [6.6, 6.7].

(5) Laboratory Mock-up and Evaluation Test - A proof-of-design test should be conducted in a laboratory. This test should evaluate damping performance under all phases of system operation and also evaluate problems in manufacturing the damped system [6.3, 6.8].

(6) Full-Scale Application and Field Evaluation. - Full-scale application and field evaluations should be conducted. Here, service problems will be discovered and solved and the transition from prototype application to production line application should begin [6.3, 6.8, 6.9].

(7) Development of Tooling and Methods for Manufacture. - The final phase of the implementation of a new design is its incorporation into the product [6.3, 6.9]. If step 6 has been properly completed, the primary emphasis of this effort will be to manufacture the required installation tools and train the production line personnel in the new assembly procedures.

The Fan System

The system studied in this case history is a low profile electric radiator cooling fan motor. The motor and mounting bracket are sketched in Figure 6.1.1. The motor case is constructed from 0.060 inch (1.52 mm) steel and is approximately 4 inches (101.6 mm) in diameter. The motor mount frame is constructed from 0.5 inch (12.7 mm) metal tube. The motor is bolted into the frame at three locations.

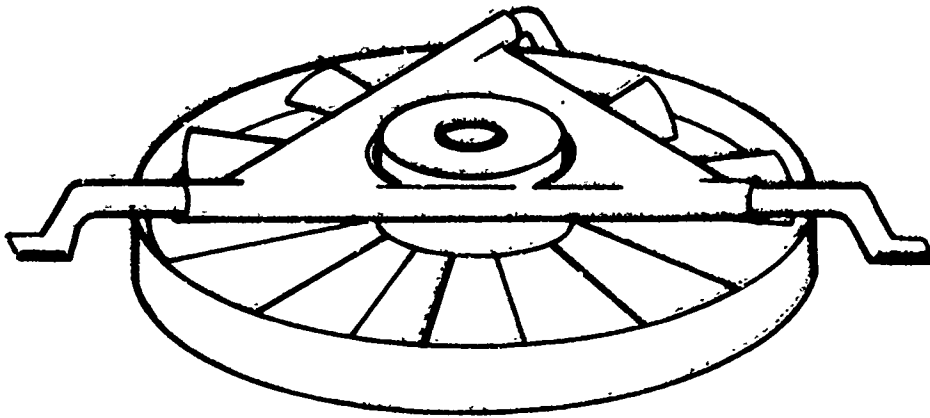


Figure 6.1.1. - Motor and mounting bracket.

Problem and Environmental Definition

The first step is to substantiate the fact that the problem is indeed resultant from structural resonance.

The problem definition is accomplished through the collection of microphone data near the motor and of vibration response data from the motor. The microphone data revealed high noise peaks occurring near 250 Hz and 1200 Hz. The acceleration response of the motor case has a peak which matches the 1200 Hz noise peak; however, there is no such corresponding structural response for the 250 Hz noise peak. The correspondence at 1200 Hz in both the noise and vibration data is a strong indication that the 1200 Hz noise is due to structural resonance. The 250 Hz noise has some other cause. The 250 Hz noise peak has been identified as being generated from the aerodynamic interaction between the pressure wave from the fan blades and the strut supports of the motor.

At first thought, defining environmental temperature criteria might seem to be a simple task. It might be thought that since in Alaska it gets down to -65°F (-54°C), and in Death Valley the thermometer rises to 120°F (49°C), this temperature range is an approximate one for automotive parts. This situation is not actually the case. A radiator cooling fan will not run when the outside temperature is -65°F (-54°C). Also, when the outside air temperature is 120°F (49°C), the motor case will be considerably warmer due to the heat generated by the engine. Even though the maximum temperature range seen by the component may generally be easy to define, the temperature range over which high damping is needed is often considerably smaller than the total operational temperature range. The designer must determine over what specific temperature range the problem occurs and design his application for that range, while keeping in mind the maximum temperature range over which the material must survive.

If the material will come in contact with contaminants such as salt water, gasoline, hydraulic fluid, cleaning solvents, or other substances which might affect the performance or longevity of the candidate damping materials [6.10], the designer must take these into account when selecting materials.

In this instance, the actual operational environment was not determined because a proof-of-concept design was the goal of the effort. However, in a complete design, an environmental definition is extremely important.

Dynamic Characteristics

Damping design needs to be based on the dynamic behavior of the structural system [6.3, 6.4, 6.8]. The frequency range over which the dynamic information is needed is usually known from operational data. A dynamic investigation must be conducted to determine all the resonant frequencies, corresponding structural mode shapes, and modal damping in this range.

If damping is considered in the early design stages of a system, the best approach usually consists of experimental analysis on a prototype structure. This analysis is used to refine analytical models, which in turn are used for further component damping design evaluations [6.11, 6.12].

If damping is considered as a redesign approach the necessary dynamic data can often be obtained much better by experimental modal analysis than through finite element or other analytical methods.

In this particular study, the required dynamic characteristics were determined using digital modal analysis. The fan was removed and the motor and mounting bracket were impact tested and the data analyzed with a fast Fourier analyzer. Figure 6.1.2 is a computer representation of the test model where point A indicates the impact point. Figure 6.1.3 is a typical frequency response from the test.

Modal analysis identified several modes of vibration in the frequency range of testing (0 to 2,500 Hz). The response at 1150 Hz was the strongest, with high response also noted at 820 Hz and 1280 Hz.

The primary motion of the assembly at 1150 Hz resonance was a 2-nodal diameter breathing mode of the motor housing as illustrated in Figure 6.1.4. The dashed lines indicate the undeformed model of the motor with the solid lines indicating the deformed modal shape. Figure 6.1.5 illustrates the accompanying modal response in the mounting bracket. The principle motion at 1150 Hz is in the motor housing; therefore, it was decided to add damping to only the motor housing and not to the mounting bracket.

Damping Material Selection

The designer must consider both the temperature range for which damping is needed and the survivable temperature limits to see if either of these ranges eliminates a particular method of damping approach due to the unavailability of a suitable damping material. An example would be a damping temperature range of 150°F to 250°F (66°C to 121°C) with survivability to 600°F (316°C) which would eliminate a constrained layer or free layer damping design because there are no effective materials currently available to meet these requirements. If these had been the temperature requirements for this case history, another vibration control approach would have to have been used.

MOTOR HOUSING
AND
MOUNTING BRACKET

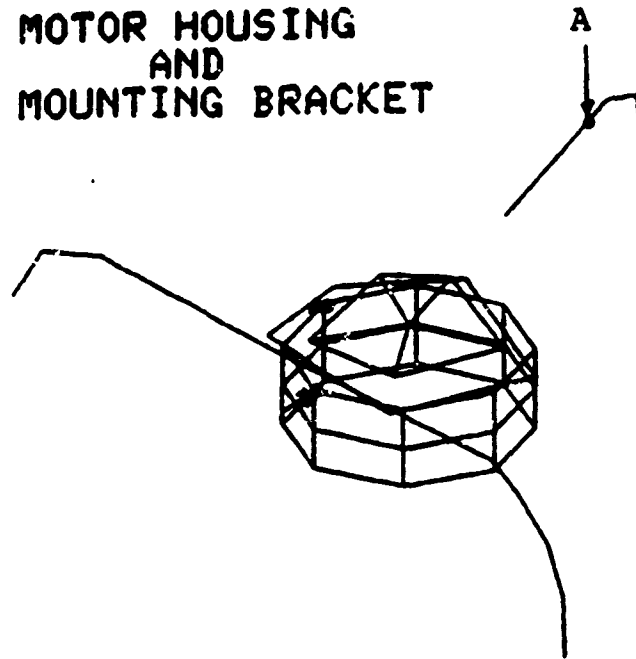


Figure 6.1.2. - Computer representation of impact test geometry.

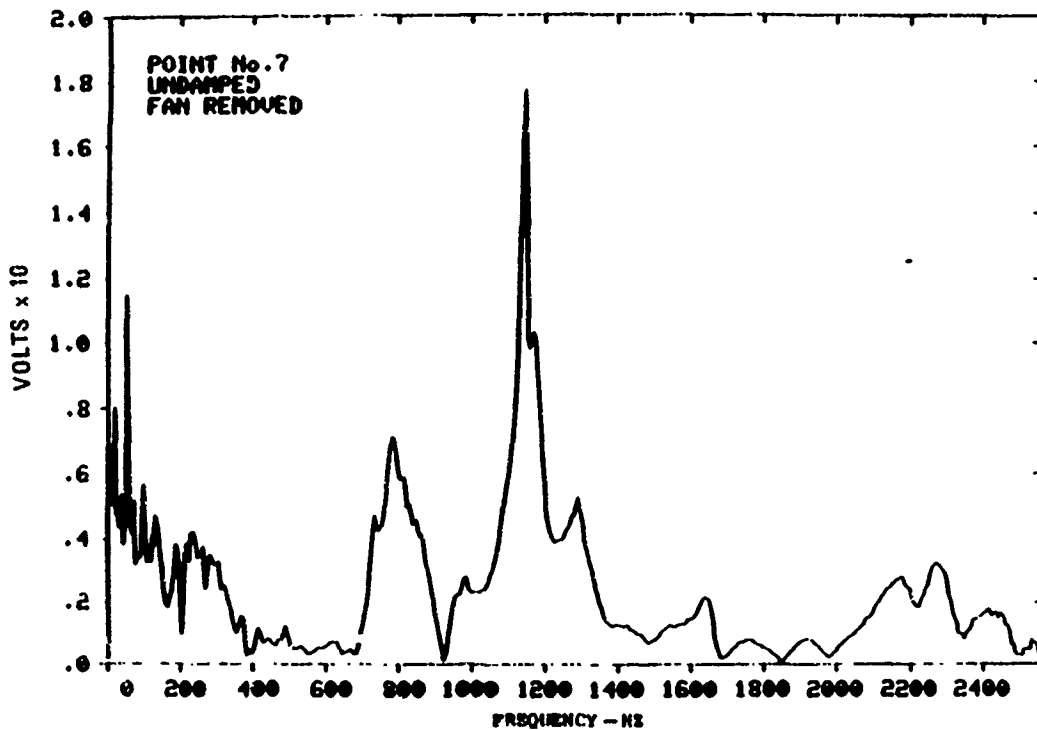


Figure 6.1.3. - Typical impact response on motor.

MOTOR HOUSING

**FREQUENCY
1150 HERTZ**

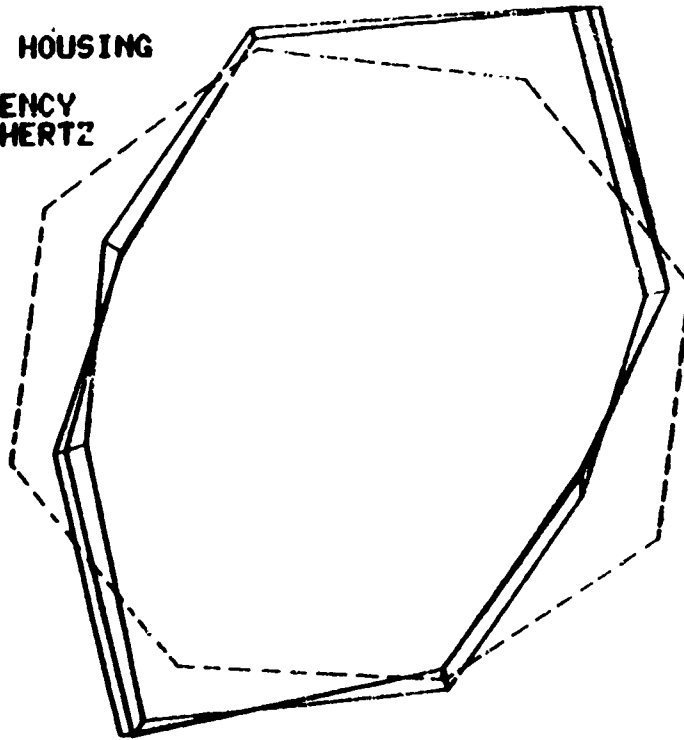


Figure 6.1.4. - Mode shape at 1150 Hz of motor housing (top view).

MOUNTING BRACKET

**FREQUENCY
1150 HERTZ**

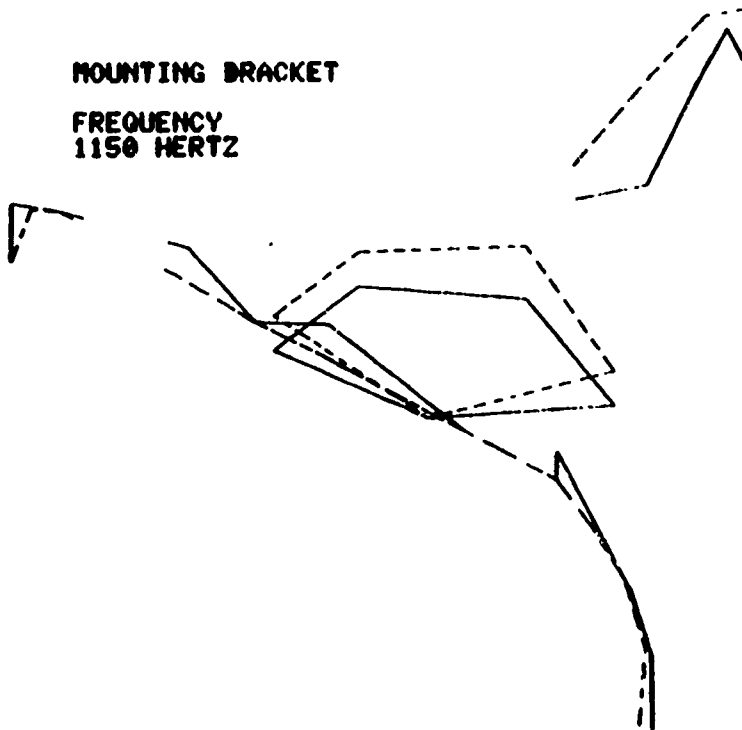


Figure 6.1.5. - Mode shape at 1150 Hz of mounting bracket.

Fortunately, the design temperature was 70°F (21°C) for the laboratory evaluation. There are several available commercial materials which meet this requirement [6.13]. The particular material chosen was 3M's ISD-112.

Damping System Selection and Design

Assuming a sufficient number of materials are available, the first consideration in selecting the type of damping system to be designed is the mode shapes of the resonant frequencies to be damped. Tuned dampers require displacements of some magnitude while constrained and free layer applications require large areas of localized bending which can deform the damping material. Highly localized strain distributions will negate the effectiveness of a layered treatment [6.14].

A review of Figure 6.1.4 shows that a good candidate damping system for this problem is a layered damping approach. Specifically, a constrained layer system was chosen because it would provide higher damping with less added weight and the constraining layer would enhance the durability of the damping design.

The actual damping design effort can be conducted using a number of analysis methods such as: (1) 4th order beam theory analysis (i.e., the Ross, Ungar, and Kerwin equations) [6.5]; (2) finite element codes capable of using complex modulus data [6.2]; (3) finite element analysis using modal strain energy approaches [6.7]; and (4) classical strain energy design methods and modal strain energy.

During this particular project, the 4th order beam theory analysis was chosen for the design analysis of the damping system. The 4th order beam analysis is discussed in detail in Volume I Section 3. The specific design equations used on this project are given in Volume II Subsection 5.1.16. An analytical model was developed to simulate the response of the motor housing. Using the mode shape and symmetry conditions, the motor housing was modeled as a flat plate with the length equal to one-half the circumference of the motor.

The thickness and width of the model were the same as the motor. It should be noted that the assumption of taking a 4-inch (102 mm) diameter cylinder and modeling it as a flat plate affects the accuracy of the predicted results. This is illustrated in Figure 6.1.6 where the flat plate predictions are compared to a finite element analysis of the actual motor case. It can be seen that the peak damping is lower for the more exact finite element analysis and that the temperature of peak damping is shifted considerably higher. The trend shown here has been seen many times before when working with flat models of curved surfaces. Keeping these facts in mind, this "quick but dirty" approach will rapidly and inexpensively allow the designer to get into the right design area. This simplified model and analysis is often used as an initial step leading into a more complicated design analysis.

The physical properties of the simplified model and material properties of the ISE 112 form the inputs to a computer program which predicts the damped dynamic response of the model. The first output generated by the program is

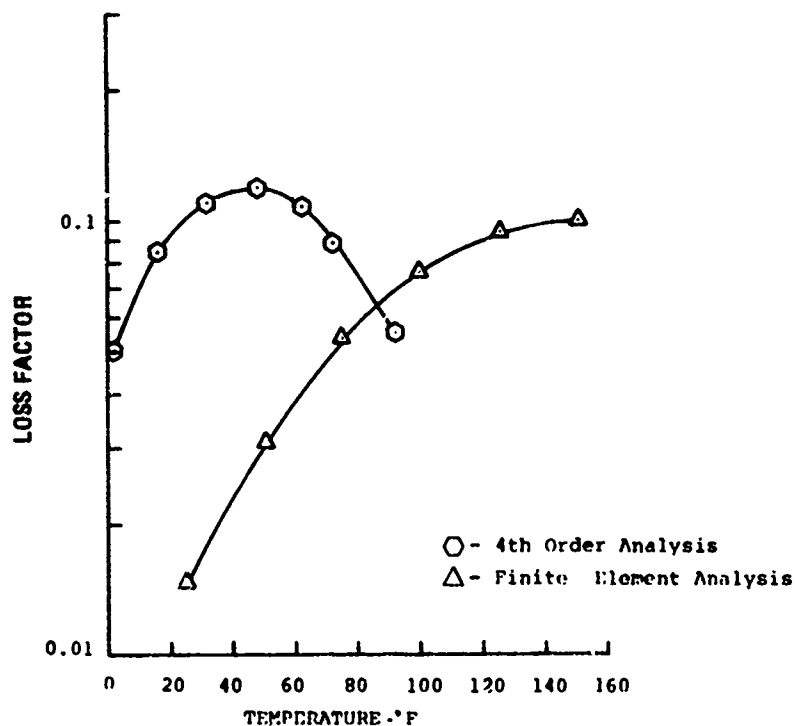


Figure 6.1.6. - Loss factor versus temperature for 4th order analysis and finite element analysis.

a plot as seen in Figure 6.1.7. The plot in Figure 6.1.7 shows the system loss factor as a function of temperature for a specific damping design. The designer can vary the geometry of the damping design and generate a multitude of plots similar to Figure 6.1.7 until a satisfactory design is found. Another approach is to add a graphics option to your computer program and generate a carpet plot. To develop the carpet plot, the designer selects a range of thicknesses for both the damping and constraining layers, and a temperature range over which the program evaluates the model's damped response. The carpet plot charts the peak loss factor for each specific combination of damping layer and constraining layer evaluated versus temperature. A typical carpet plot is shown in Figure 6.1.8.

The damping design chosen for this problem has a damping layer thickness of 0.002 inch (0.051 mm) with a constraining layer thickness of 0.030 inch (0.76 mm) steel. The damped response system for this combination is shown in Figure 6.1.7. As is seen in Figure 6.1.7, the chosen damping design has peak damping at 57°F (14°C). This predicted peak damping temperature is 20 to 30°F (11 to 17°C) lower than the anticipated test evaluation temperature because the analysis assumed a flat plate model. The complete computer input data set is given in Figure 6.1.7. Combining the input data with the design equations and computer program in Volume II, Section 5, the system response data can be generated which also is given in Figure 6.1.7.

Laboratory Mock-up and Evaluation Test

For a convenient proof test of the proposed design, the 0.030-inch (0.76 mm) thick constraining layer was constructed from three 0.010-inch (0.254 mm) thick layers. The total damping system consisted of three layers with each layer composed of 0.002-inch (0.051 mm) thick ISD-112 and 0.010 inch (0.254 mm) thick steel. (A multi-layer damping system possesses practically the same properties as a single layer system with a total constraining layer thickness equal to the sum of the constraining layer in the multi-layer system [6.2].)

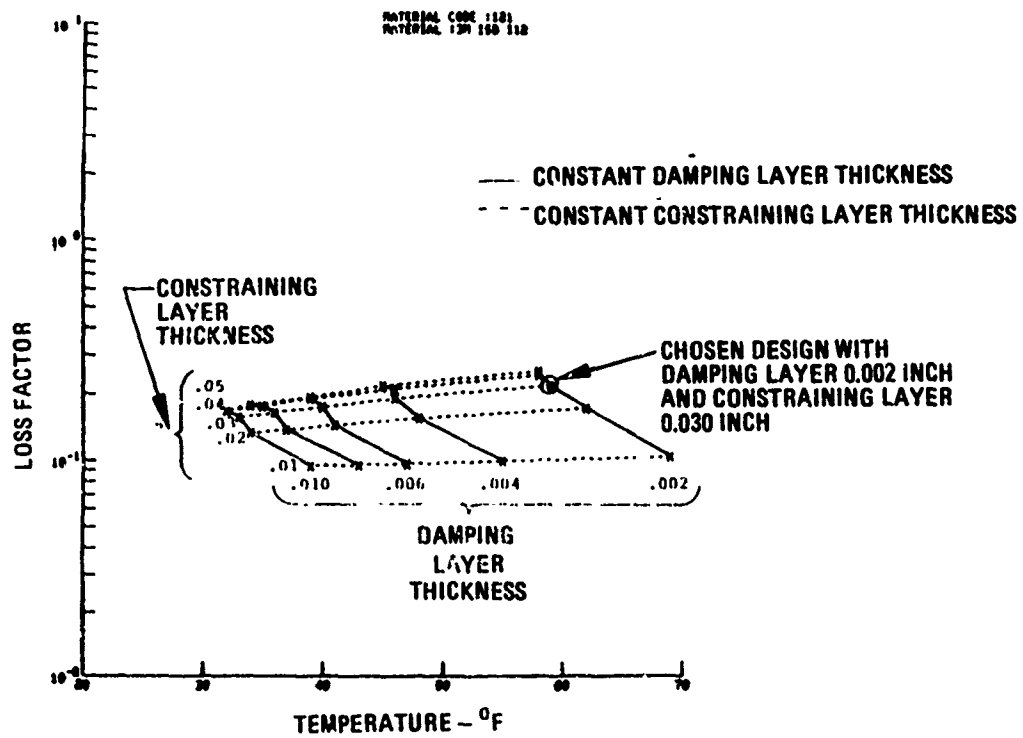


Figure 6.1.8. - Carpet plot from which damping was chosen.

The layers of damping material were applied one at a time. Each layer was applied using a vacuum bag to eliminate entrapped air and to apply pressure. With the vacuum bag attached, the motor was placed in an oven and heated to 200°F (93°C) to enhance the bonding of the ISD-112 to the motor.

Prior to the full damping wrap application, the assembly was impact tested at five locations on the motor bracket as shown in Figure 6.1.9. The impact tests were conducted between the application of each layer. These tests showed that the damping treatments consisting of two and three layers reduced the response of the assembly by a factor of two for frequencies between 1000 Hz and 1300 Hz. Figure 6.1.10 illustrates a typical frequency response, both damped and undamped. Figure 6.1.11 shows the effects of the damping treatment on the structural response with a constraining layer thickness of 0.030 inch (0.76 mm).

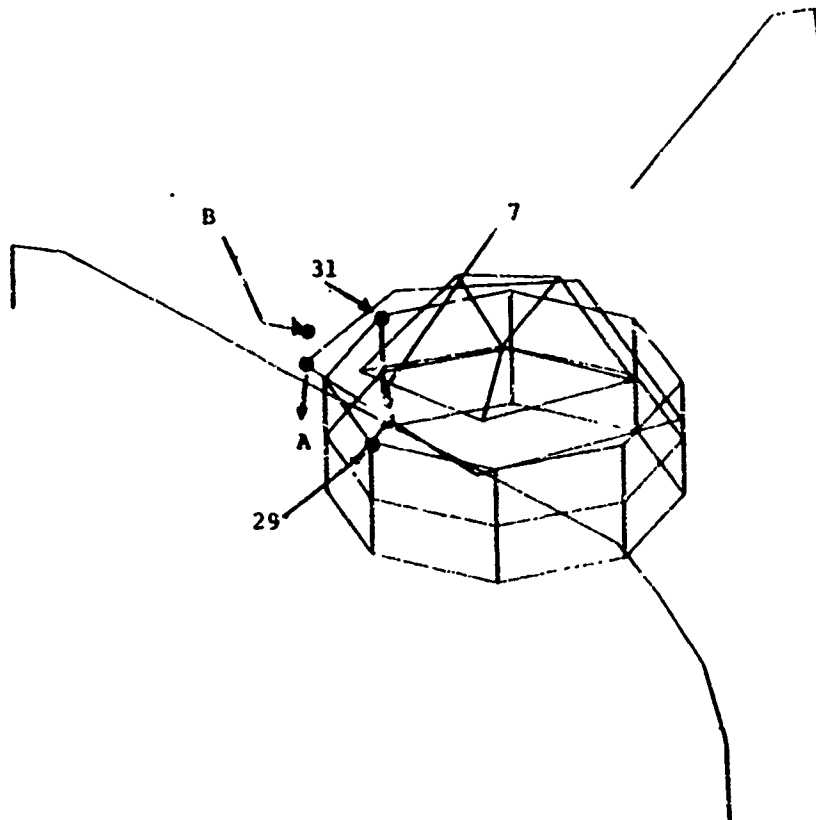


Figure 6.1.9. - Impact locations for damping wrap evaluation
(Note: point B is on the lip of the motor housing bracket).

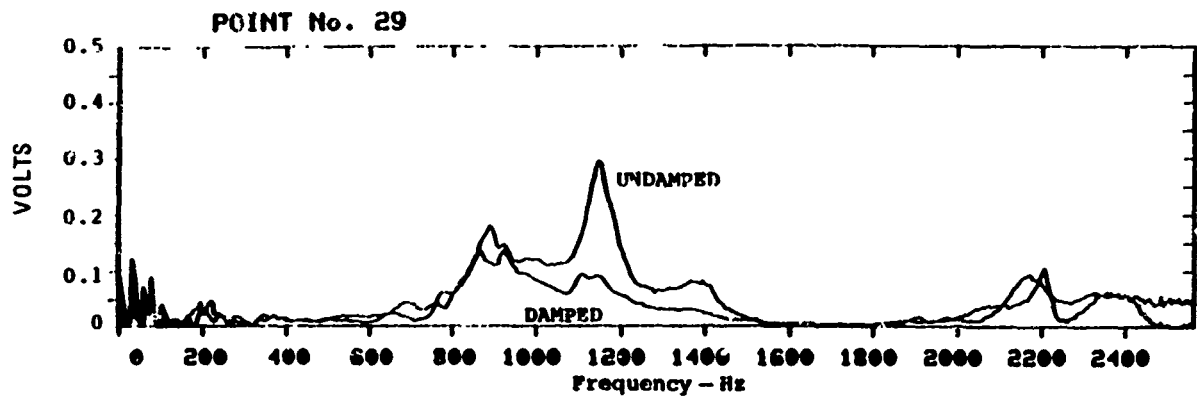


Figure 6.1.10. - Point 29 frequency response; damped and undamped.

The final proof-of-concept test was operational. The damped fan motor was mounted in an automobile and noise measurements were made. A substantial noise reduction was measured, but specific data were not released by the manufacturer of the fan.

Summary

A general approach to the design of a damping system was demonstrated through the solution of a noise and vibration problem with an electric motor. The basic steps in the general approach are:

- (1) Problem and Environmental Definition;
- (2) Structural Dynamics Characterization;
- (3) Damping Material Selection;
- (4) Damping System Design;

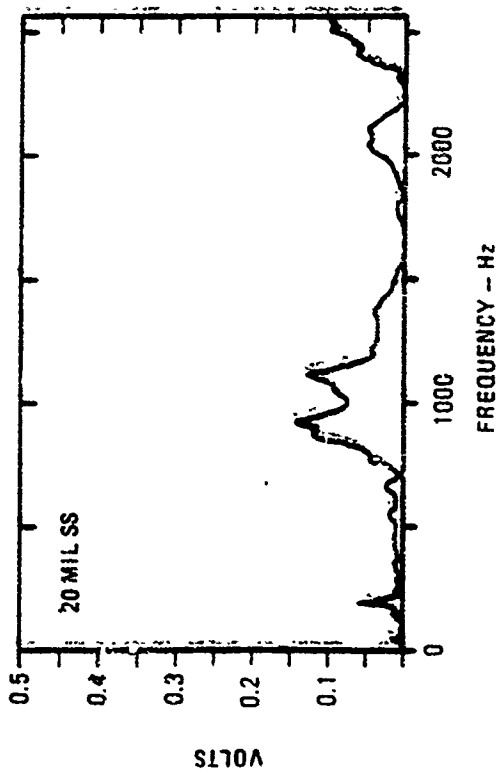
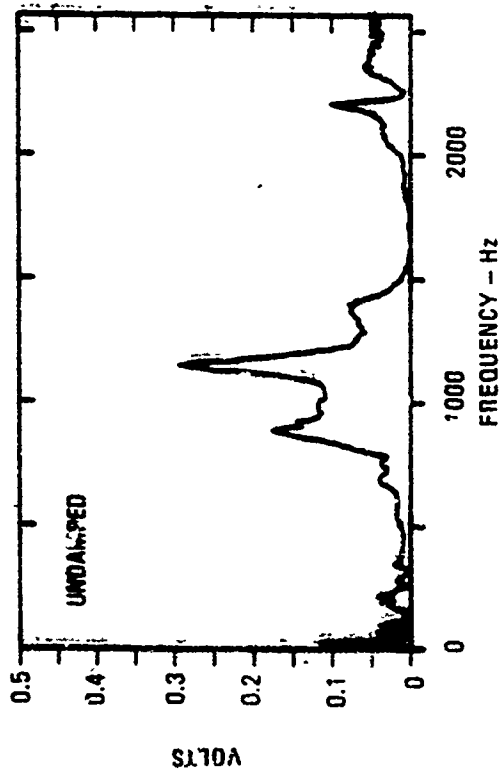
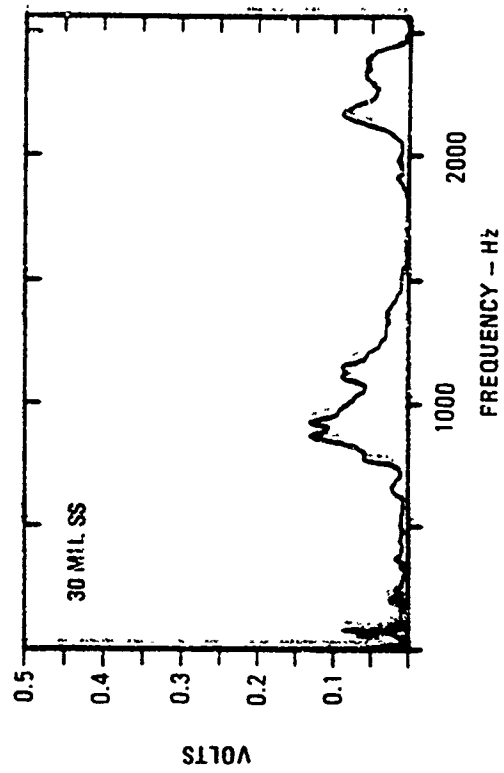
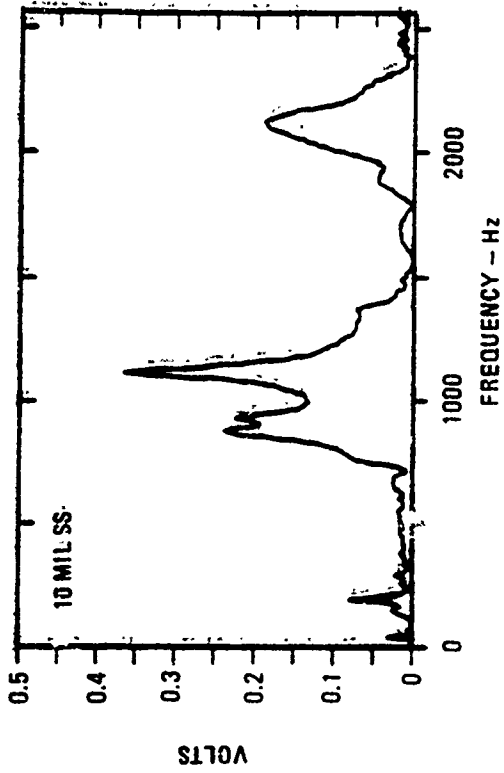


Figure 6.1.11. - Point 29 frequency response; undamped 10 mil, 20 mil, and 30 mil stainless steel constraining layers.

- (5) Laboratory Mock-up and Evaluation Test;
- (6) Full-Scale Application and Field Evaluation;
- (7) Development of Tooling and Methods for Manufacture.

A brief summary of the program is given below.

Modal analysis identified a strong vibration mode at 1150 Hz. The primary motion of the motor assembly at 1150 Hz was a two nodal diameter breathing mode of the electric motor housing. The 1150 Hz mode was selected as the design point for the damping treatment. The design incorporated a visco-elastic constrained layer additive damper to reduce the breathing mode of the 1150 Hz mode.

An analytical model of the motor housing was developed to simulate the motor housing response. Several damping treatments were developed using analytical methods. Two wraps were most effective at the single test temperature. Both wraps incorporated a two mils (0.051 mm) thick layer of damping material constrained by either a 30 mils (0.76 mm) thick stainless steel layer or a 20 mils (0.508 mm) thick stainless steel layer.

A prototype of the damping treatment was developed and applied to the outer diameter of the motor housing. Impact tests showed an approximate two-to-one ratio decrease in the structural response for frequencies in the 1000 Hz to 1300 Hz range.

Operational tests on the motor, with the damping design applied, indicated a substantial reduction in high frequency noise levels.

6.2 DESIGN EXAMPLES

The following sections present damping design efforts in brief detail illustrating various techniques designers should consider and typical problems to be avoided.

6.2.1 A Damped Cantilever Beam

Problem

Select damping material to provide a specified level of damping for the fourth mode of a sandwich cantilever beam.

Structural Constraints

The sandwich beam is 7 inches (177.8 mm) long and constructed from two 0.08 inch (2.03 mm) thick aluminum beams bonded together with a 0.006 inch (0.152 mm) damping layer (See Figure 6.2.1.1).

Temperature Data

The minimum system loss factor (η_s) is to be greater than 0.1 for the temperature range 0°F to 100°F (-18°C to 38°C).

Approach to the Problem

The first step is to calculate the bare beam resonant frequency. This is accomplished using equation 5.7, Subsection 5.1.11. Using a Young's modulus of 1×10^7 psi (6.9×10^{11} N/m²), a density of 0.101 lb/in³ (2.8 g/cm³), a thickness of 0.166 inches (4.22 mm) and an eigenvalue of 120.902 for the fourth mode of the aluminum beam, the resonant frequency of the base beam is calculated at approximately 3697 Hz.

Knowing the temperature range (0°F (-18°C) to 100°F (38°C)) and having determined the frequency region (3697 Hz) of interest, the designer can now begin to evaluate the damping materials which might be used to solve the problem. The loss factor properties of four commercially available damping materials - 3M ISD 112 and ISD 113, and Soundcoat MN and M are given in

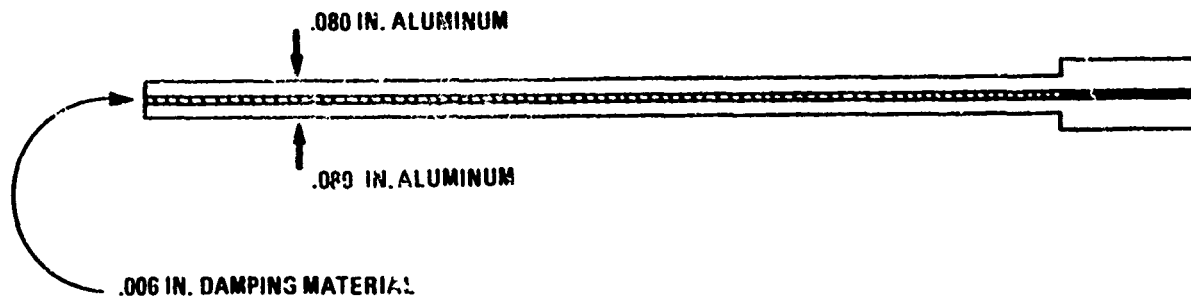


Figure 6.2.1.1. - Illustration of damped system.

Figure 6.2.1.2. The complex modulus data for all four materials are listed in Table 6.2.1.1. From Figure 6.2.1.2, it can be seen that the loss factors of MN and ISD 113 are the best suited for this particular problem. Examination of Table 6.2.1.1 reveals a difference in the shear modulus of these two materials. The final choice of the proper damping material must be made by comparing the system loss factor for each of these two damping material incorporated into the damped beam design.

These two damping designs are evaluated using equations 5.8 and 5.13 in Sub-section 5.1.11, for a constrained layer cantilever beam. All of the required geometric and material data for input into the design equation and the computed results for both the MN material design and the ISD 113 material design are listed in Table 6.2.1.2. The calculated results for both materials are plotted in Figure 6.2.1.3. The data illustrates that both materials meet the system loss factor requirements at 0°F (18°C); however, only the MN design

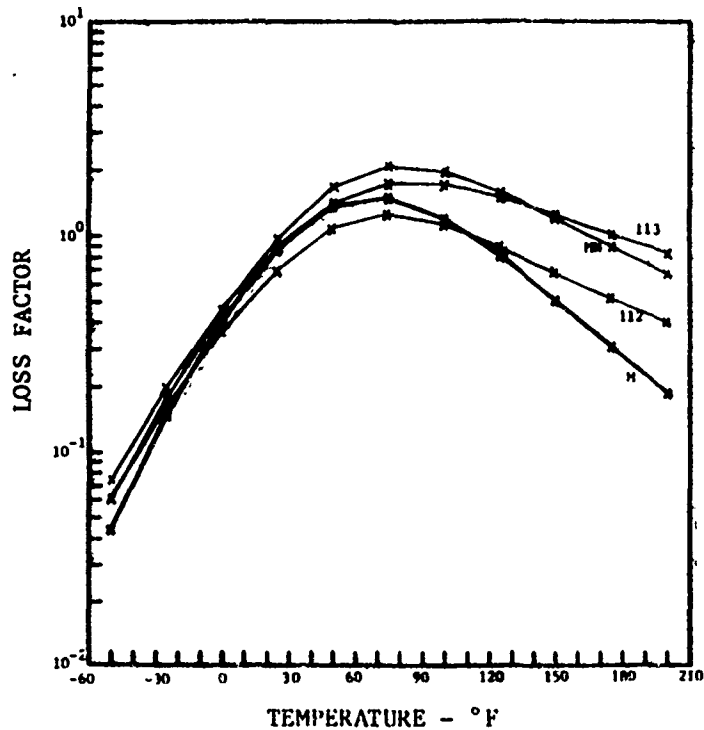


Figure 6.2.1.2. - Loss factor versus temperature for ISD 112, ISD 113, MN, and M damping materials.

also meets the system loss factor requirements at 100°F (38°C). From the analysis, the damping design chosen is the one incorporating the MN material.

Figure 6.2.1.4 shows the comparison of the predicted system loss factor to the experimentally measured system loss factor. The predicted and measured results are also listed in Table 6.2.1.3. The comparison is seen to be quite good.

TABLE 6.2.1.1. - COMPLEX MODULUS DATA FOR ISD112, ISD113, MN, AND M DAMPING MATERIALS

Damping Material	Temperatures Degrees F	Modulus Loss Factor	Modulus PSI
ISD 112	-50.0	0.0628	9.76992E+04
	-25.0	0.1637	5.85706E+04
	0.0	0.3660	2.56155E+04
	25.0	0.6987	8.56500E+03
	50.0	1.0846	2.58963E+03
	75.0	1.2597	8.56816E+02
	100.0	1.1265	3.47155E+02
	125.0	0.8922	1.75632E+02
	150.0	0.6830	1.07384E+02
	175.0	0.5222	7.57628E+01
200.0	0.4035	5.91999E+01	
ISD 113	-50.0	0.0753	3.47765E+04
	-25.0	0.2036	1.83755E+04
	0.0	0.4642	6.63939E+03
	25.0	0.8530	1.83483E+03
	50.0	1.4131	5.13900E+02
	75.0	1.7360	1.63858E+02
	100.0	1.7136	7.03196E+01
	125.0	1.5053	3.73899E+01
	150.0	1.2536	2.47053E+01
	175.0	1.0372	1.84346E+01
200.0	0.8410	1.58759E+01	
MN	-50.0	0.0604	6.16409E+04
	-25.0	0.1786	2.97844E+04
	0.0	0.4539	1.18308E+04
	25.0	0.9732	4.14298E+03
	50.0	1.6894	1.46874E+03
	75.0	2.1344	5.08521E+02
	100.0	1.9987	2.06589E+02
	125.0	1.5968	9.67124E+01
	150.0	1.2064	5.20596E+01
	175.0	0.9004	3.17119E+01
200.0	0.6751	2.14103E+01	
M	-50.0	0.0438	2.43291E+04
	-25.0	0.1428	1.77944E+04
	0.0	0.4087	9.75486E+03
	25.0	0.8744	3.87097E+03
	50.0	1.3636	1.28735E+03
	75.0	1.4853	4.62821E+02
	100.0	1.1995	2.11934E+02
	125.0	0.8127	1.25244E+02
	150.0	0.5690	3.98393E+01
	175.0	0.3100	7.31803E+01
200.0	0.1900	6.44716E+01	

TABLE 6.2.1.2. - INPUT DATA AND COMPUTED RESULTS FOR DAMPED SYSTEM FOR BOTH ISD 113 AND MN DAMPING MATERIALS

Temperatures Degrees F	ISD 113		MN	
	Predicted Composite Loss Factor	Predicted Frequency Hz	Predicted Composite Loss Factor	Predicted Frequency Hz
-50.0	0.00423	3595.9	0.00854	3504.9
-25.0	0.02269	3478.5	0.03675	3351.7
0.0	0.10144	3237.2	0.14165	2974.7
25.0	0.28969	2841.9	0.29691	2340.3
50.0	0.44214	2302.8	0.22328	1932.8
75.0	0.28645	1940.4	0.10204	1819.2
100.0	0.11672	1830.6	0.04478	1787.4
125.0	0.04489	1795.1	0.02249	1776.7
150.0	0.01931	1781.4	0.01288	1772.1
175.0	0.00926	1775.0	0.00822	1769.9
200.0	0.00492	1771.6	0.00568	1768.7

*Input data; damping material loss factor and modulus are in Table 6.2.1.1.

Beam	Damping Layer	Constraining Layer
Length 7.00 in	Thickness 0.0060 in	Thickness 0.0800 in
Thickness 0.0800 in	Density 0.0350 lb/in ³	Density 0.1010 lb/in ³
Density 0.1010 lb/in ³		Modulus 1.000E+07 psi
Modulus 1.000E+07 psi		

TABLE 6.2.1.3. - PREDICTED AND MEASURED FREQUENCY AND LOSS FACTOR FOR CANTILEVER BEAM WITH MN DAMPING MATERIAL.

Temperatures Degree F	Predicted System Loss Factor	Predicted Frequency Hz	Measured System Loss Factor	Measured Frequency
-50.0	0.00423	3595.9	0.0113	3507.9
-25.0	0.02269	3478.5	0.0269	3399.8
0.0	0.10144	3237.2	0.0686	3210.0
25.0	0.28969	2841.9	0.2444	2777.3
50.0	0.44214	2302.8	0.4809	2163.1
75.0	0.28645	1940.4	0.1556	1848.1
100.0	0.11672	1830.6	0.0489	1774.1
125.0	0.04489	1795.1	0.0233	1748.8
150.0	0.01931	1781.4	0.0151	1737.3
175.0	0.00926	1775.0	0.0083	1724.5
200.0	0.00492	1771.6	0.0056	1715.6

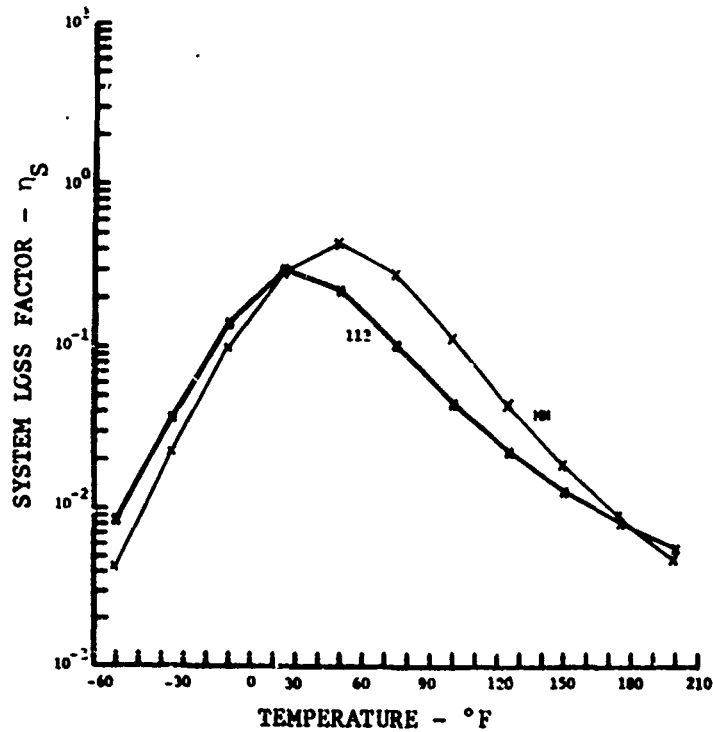


Figure 6.2.1.3. - Predicted damped system response for both the ISD 113 and MN damping materials.

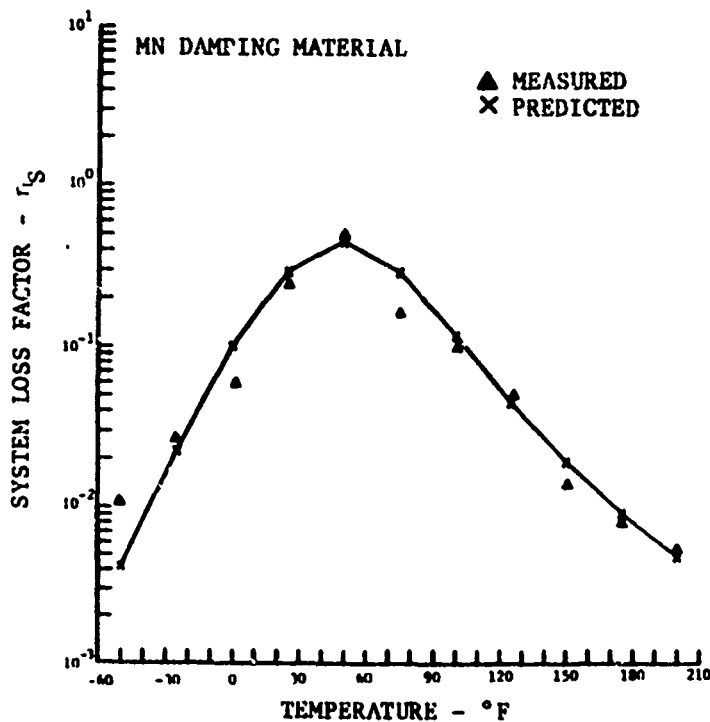


Figure 6.2.1.4. - Comparison of predicted and measured beam composite loss factor.

6.2.2 Turbine Ground Power Component Design Example [6.15]

Problem

Premature failure of inlet guide vanes (IGV) on the GG4 ground power turbine engine. Failure was due to cracking of the vane in the transition areas from the vane to the inner and/or outer hub. Failure was assumed to be caused by resonant fatigue.

Primary Function of System

Provide power at remote sites or assist in providing power during peak demand periods for cities.

Part

Solid cast aluminum inlet guide vane case. Cast in net form.

Location of Component

The IGV case is the front most portion of the turbine engine.

Type of Loading

Primary sources of excitation would be:

- a) Out-of-balance forces from rotor,
- b) pressure waves from the first stage fan impinging on the IGVs.

Temperature Data

Due to the system function, the operational environment must be -65°F (-54°C) to 150°F (66°C). Damping is needed across the entire range.

Approach to the Problem

I. Problem Identification

a) Evaluate operational strain gage data with a spectrum analyzer to determine which frequencies have the highest strain levels.

The results of this evaluation showed the high strain levels were occurring at approximately 1200 Hz.

b) Experimentally or analytically conduct a modal analysis to determine which resonant modes are generating the high strain levels. The results of this effort was the identification of the second bending mode and the second torsional mode, both in the 1200 Hz range.

c) Determine temperature range that the damping system must survive and also the temperature range where damping is required. This effort identified the operational temperature as -65°F (-54°C) to 150°F (66°C) with significant system damping required for the entire range.

II. Analysis

a) The vane has an airfoil shape, with considerable twist along the length and a nonconstant cross section.

b) Fourth-order plate analysis was used to design the damping system. The equations are discussed in Volume II, Subsection 5.1.16. The damping system chosen was a constrained layer system because the constraining layer would provide protection for the damping material in the engine inlet environment and also because the constrained layer system would provide higher modal damping at a lower increase in blade thickness.

c) The vane was modeled as a flat rectangular plate with pinned edges. The length and width dimensions of the plate model were identical to that of the vane. The thickness was adjusted to 0.6 inch (15.2 mm) in order to get the second bending mode frequency for the model to equal the measured frequency of the vane, i.e., 1200 Hz.

d) With the model matched to the system, an interactive design procedure can be utilized. The designer must now evaluate various damping materials (material data in Volume III) and constraining layers and geometric combination in order to develop an appropriate damping system. In this case the

temperature range is so large that the damping system will require more than one material. A possible solution is to start by designing a lower temperature damping system with optimum damping $1/4$ to $1/3$ of the total temperature range above the minimum temperature and a higher temperature damping system with optimum damping $1/4$ to $1/3$ of the total temperature range below the maximum temperature. The actual damping design could be done over the entire temperature range at one time if the designer has programmed the multilayer multi-material design equations given in Volume I, Section 3.2. However, a simpler approach is to use the single layer equations and computer program given in Volume II, Subsection 5.1.16 and design the low temperature and high temperature systems independently. This particular problem was solved with the latter approach. The model data, material data, and computer results are given in Figure 6.2.2.1. Test data from a vane test are also given in Figure 6.2.2.1 for comparison with the predicted results.

e) Practical considerations include: (1) the ease of application which required that the wrap be applied in the field with the case on the engine; (2) long-term durability to the erosion environment in the front of the engine; (3) relatively low cost; and (4) no decrease in engine performance due to increased thickness of the vane.

III. Results

a) Final design of the damping system is shown in Figure 6.2.2.2. Figure 6.2.2.1 shows the measured system damping and the calculated damping.

b) The damping system was applied to an IGV. An instrumented engine test demonstrated 70 to 90 percent stress reduction.

c) A one-year durability test on several engines revealed no durability problems caused by erosion or degradation of the damping materials.

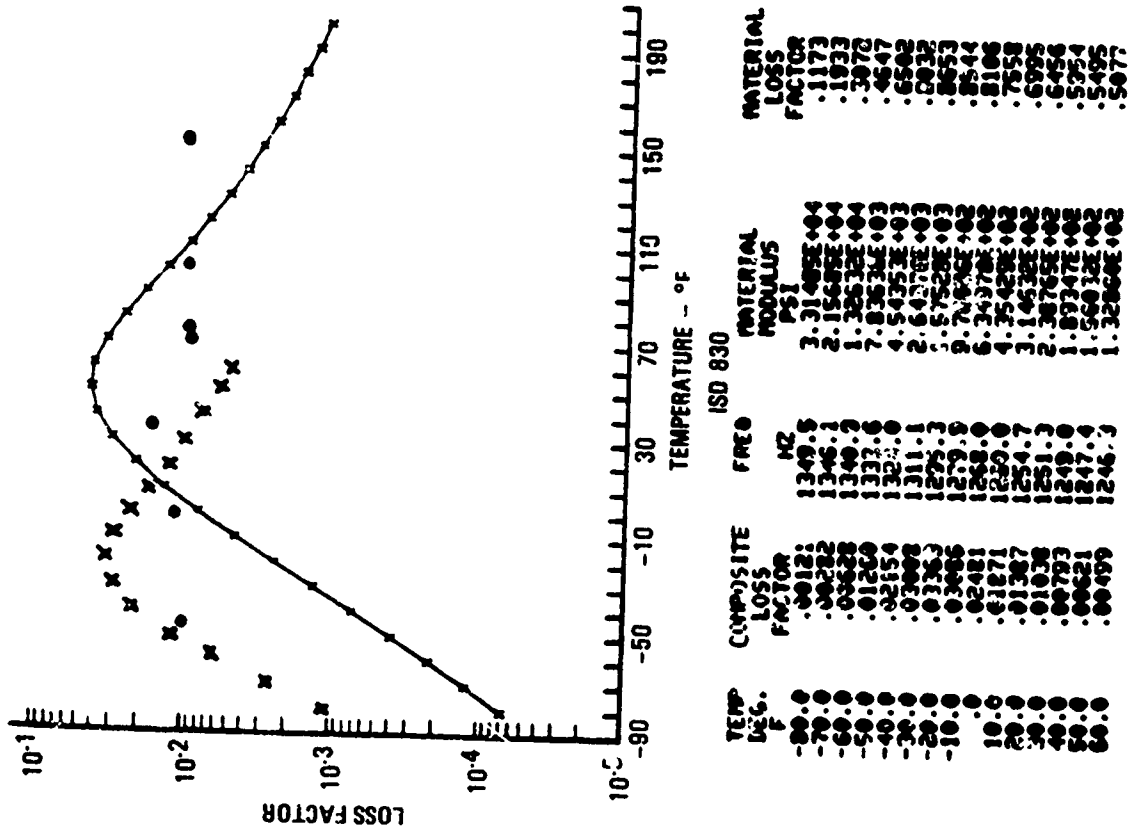
d) The application procedure developed required eight man-hours to install all 18 vane dampers. The installation procedure is given in Table 6.2.2.1.

OUTPUT LISTED IN ENGLISH
PLATE
CONSTRAINED LAYER

PLATE 2 1
SIMPLY SUPPORTED 1
RIN. 13.00 5.50
THICKNESS .5000
DENSITY .4500
MODULUS 1.000E+07
DAMPING LAYER
DENSITY .0150
THICKNESS .0350
CONST. LAYER
THICKNESS .0100
DENSITY .2700
MODULUS .300E+08
TEMP RANGE
BASE FREQ-1248.8

MAX DELTA
.0150 9999.00
.0100 9799.00
200.50 10.00

NOTE: THE EQUATIONS USED TO
GENERATE THIS DAMPING DESIGN
UNITS ARE GIVEN IN VOLUME II
SUBSECTION 5.1.16

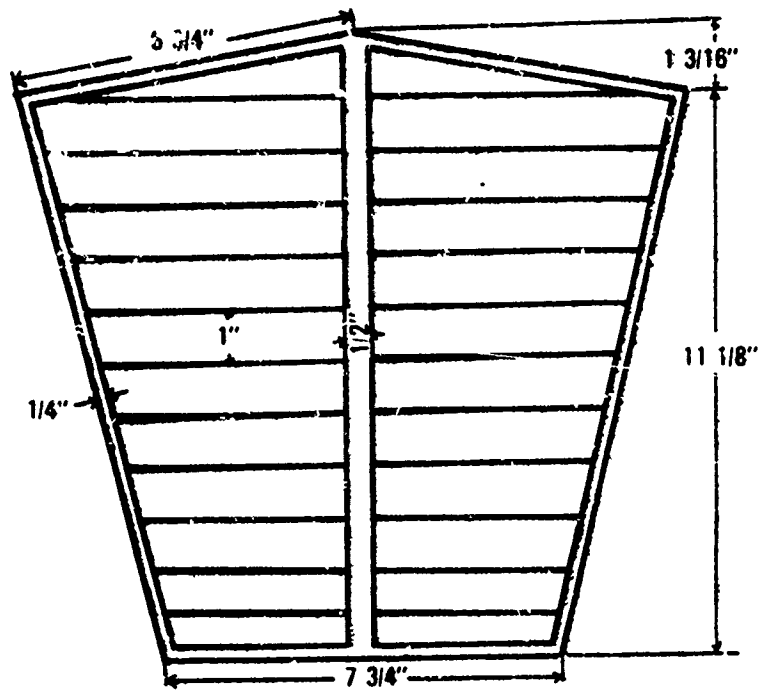


MATERIAL LOSS FACTOR
.5438
.6548
.9219
.9901
1.1351
1.2302
1.2596
1.2278
1.1535
1.0577
.9553
.8554
.7625
.6785
.6037
.5377
.4787
.4289
.3845
.3455
.3113

MATERIAL MODULUS PSI
1.5843E+04
3.7948E+03
9.9147E+03
3.5457E+03
2.1431E+03
1.3234E+03
8.4333E+02
5.5888E+02
3.8476E+02
2.7644E+02
2.0677E+02
1.6033E+02
1.2063E+02
9.0399E+01
6.9195E+01
5.0233E+01
3.6907E+01
2.7692E+01
2.0654E+01
1.5192E+01

ISD 112
COMPOSITE LOSS FACTOR
TEMP DEG. F
10.0
20.0
30.0
40.0
50.0
60.0
70.0
80.0
90.0
100.0
110.0
120.0
130.0
140.0
150.0
160.0
170.0
180.0
190.0
200.0

Figure 6.2.2.1. - Damped system response data.



DAMPING WRAP LOOKING AT ADHESIVE SIDE



EDGE VIEW OF DAMPING WRAP

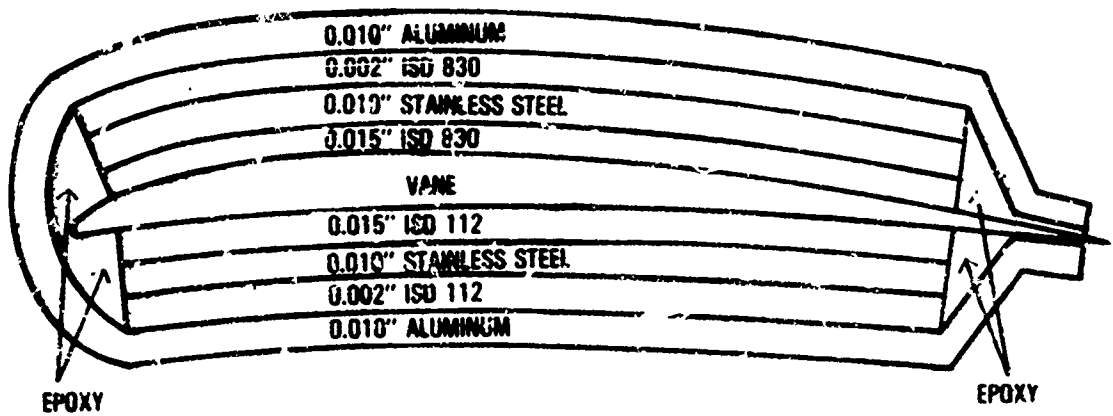


Figure 6.2.2.2. - Final damper design.

TABLE 6.2.2.1. - WRAP APPLICATION PROCEDURE

- Clean guide vane
- Apply tape primer
- Mix and apply epoxy
- Remove backing paper
- Position damping treatment
- Apply wrap working from L.E. to T.E.
- Avoid entrapped air
- Roll wrap surface
- Wipe off excess epoxy

6.2.3 F-15 Rudder Fairing Damper [6.16]

Problem

High-cycle resonant fatigue cracking occurred in the leading-edge fairing of the F-15 rudder. Resonance was induced by turbulent air flow across the fairing.

Structure

The fairing is a sheet metal structure riveted and bonded to the advanced composite rudder (see Figure 6.2.3.1).

Undamped Structure Response

Figure 6.2.3.2 shows the undamped response of the fairing. The primary modes of interest were at 213, 260, and 509 Hz with amplification factors, Q , of 28.8, 36.4, 84.8, respectively. The mode shapes for 213 Hz and 509 Hz are shown in Figures 6.2.3.3 and 6.2.3.4. The large deformations caused high bending stresses which in turn caused fatigue cracking. Such deformations are, however, well-suited for layer damping treatments.

Damping Treatments

Since the operational temperature range of the fairing is broad (0°F (-18°C) to 125°F (52°C)), no single damping material can provide adequate damping across this range. The treatment design (see Figure 6.2.3.5) consisted of a layer of 3M ISD-830, an aluminum constraining layer, a layer of 3M ISD-112,

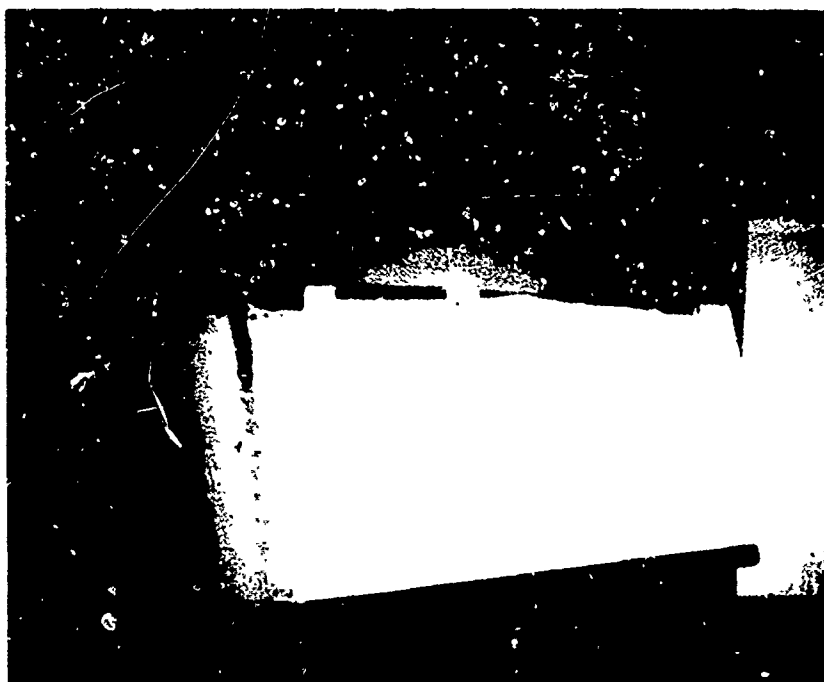


Figure 6.2.3.1. - Rudder and fairing.

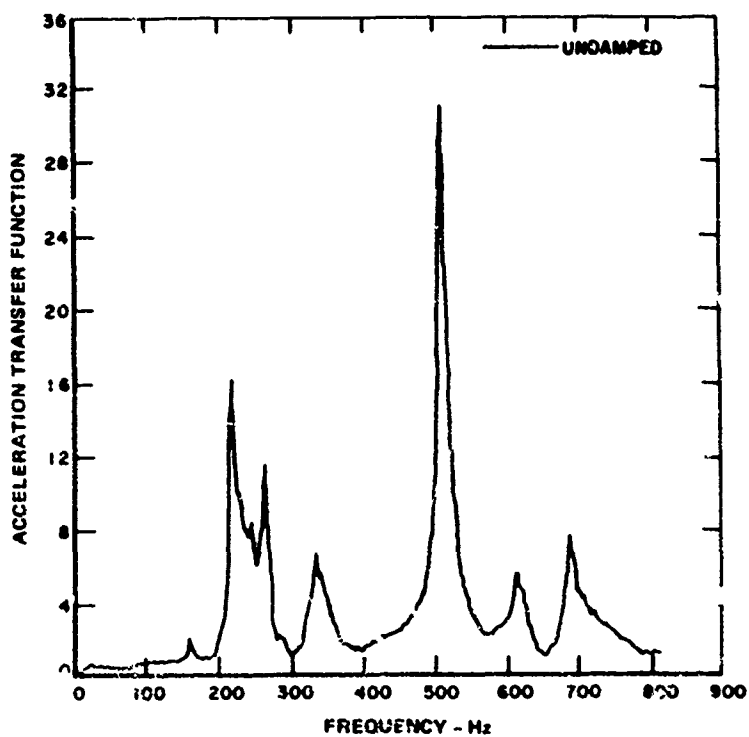


Figure 6.2.3.2. - Undamped fairing response.

UNDEFORMED ○
DEFORMED ▲

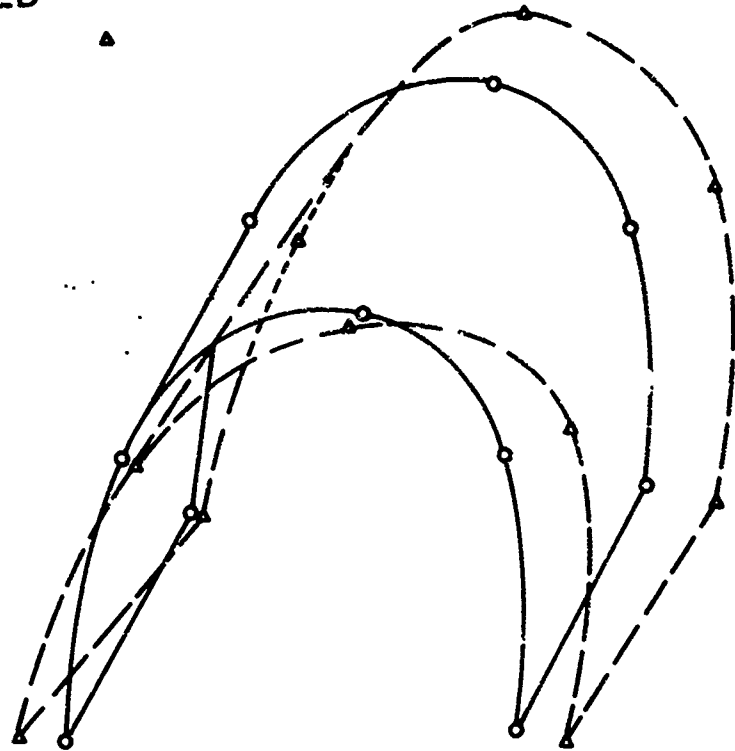


Figure 6.2.3.3. - Fairing mode shape at 213 Hz.

UNDEFORMED ○
DEFORMED ▲

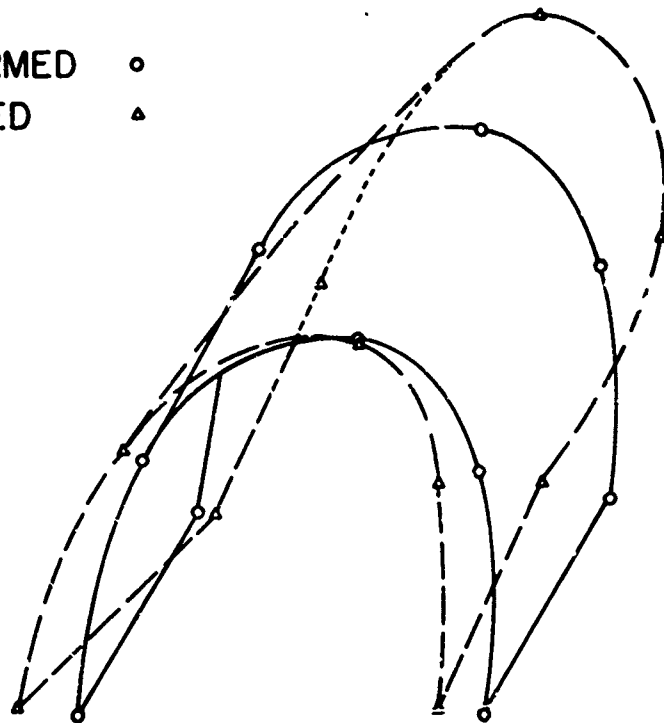


Figure 6.2.3.4. - Fairing mode shape at 509 Hz.

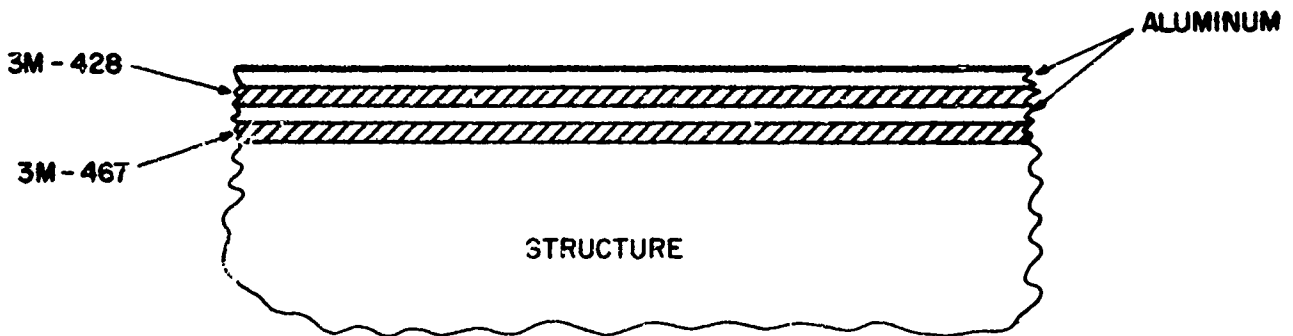
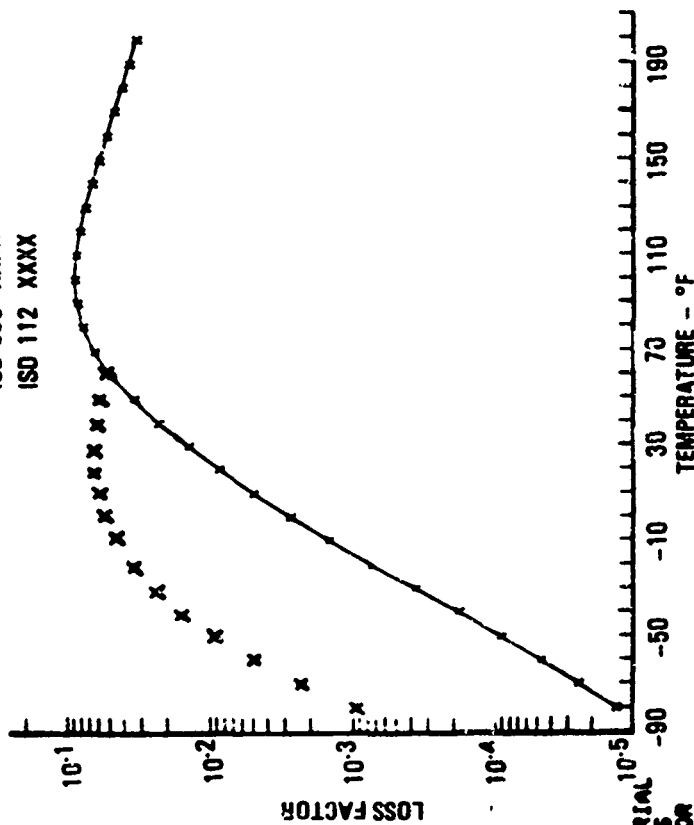


Figure 6.2.3.5. - Final damping configuration.

and another aluminum constraining layer. The 3M ISD-830 provided peak damping in the 0°F (-18°C) to 60°F (16°C) range, while the 3M ISD-112 provided peak damping in the 60°F (16°C) to 125°F (52°C) range. The design tool used to develop this specific damping system was the flat plate constrained layer damping equations and computer program given in Subsection 5.1.16. The design approach was to optimize the ISD-830 design and then optimize the ISD-112 design independently. Figure 6.2.3.6 presents the system loss factor versus temperature for both the ISD-830 and ISD-112 designs. Also included in Figure 6.2.3.6 is all the required computer mode and input data and computer results. The designer can use his computer program to verify the results

ISD 830 XXXX
ISD 112 XXXX



OUTPUT LISTED IN ENGLISH
PLATE
CONSTRAINED LAYER

PLATE
NODE 2
SIMPLY SUPPORTED 2
BIN. 16.00 6.75
THICKNESS .0250
DENSITY .1000
MODULUS 1.000E+07
BASE LAYER
THICKNESS .0020
DENSITY .0350
CONST. LAYER
THICKNESS .0050
DENSITY .1000
MODULUS 1.000E+07
TEMP RANGE
BASE FREQ= 241.5

MAX DELTA
.0020 9999.00
MAX DELTA
.0050 9999.00
200.00 10.00

TEMP DEG. F	COMPOSITE LOSS FACTOR	FREQ HZ	MATERIAL MODULUS PSI	MATERIAL LOSS FACTOR	TEMP DEG. F	COMPOSITE LOSS FACTOR	FREQ HZ	MATERIAL MODULUS PSI	MATERIAL LOSS FACTOR
0	.00275	302.4	7.06257E+03	.7026	-80	.00096	302.5	1.22104E+04	.3295
10	.00423	302.2	4.05205E+03	.0472	-70	.00279	302.2	6.80720E+03	.5118
20	.00845	301.8	2.33478E+03	1.1130	-60	.00504	301.9	3.72020E+03	.7137
30	.01397	301.1	1.37473E+03	1.2249	-50	.00936	301.2	2.06835E+03	.8439
40	.02206	300.0	8.30735E+02	1.2546	-40	.01590	300.0	1.19375E+03	.8651
50	.03303	298.2	5.34616E+02	1.2214	-30	.02541	299.0	7.23837E+02	.8254
60	.04915	295.3	3.50090E+02	1.1350	-20	.04506	296.0	4.66954E+02	.7874
70	.06316	291.2	2.51724E+02	1.0364	-10	.07577	291.2	3.23500E+02	.7047
80	.07589	286.1	1.85390E+02	.9136	0	.09450	286.9	2.37300E+02	.5443
90	.08391	280.5	1.42584E+02	.8064	10	.09450	282.5	1.83700E+02	.5086
100	.08648	274.3	1.12402E+02	.7037	20	.05450	274.5	1.47463E+02	.5362
110	.08405	269.6	9.22545E+01	.6141	30	.03319	271.5	1.24620E+02	.4900
120	.07873	265.3	7.85800E+01	.5305	40	.02191	268.3	1.07853E+02	.4470
130	.07159	261.6	6.81207E+01	.4716	50	.01549	265.5	9.67820E+01	.4109
140	.06443	258.7	6.07374E+01	.4160	60	.01036	262.5	8.86300E+01	.3786
150	.05751	256.3	5.50060E+01	.3683					
160	.05077	254.2	5.04761E+01	.3243					
170	.04409	252.6	4.70619E+01	.2887					
180	.03800	251.3	4.43070E+01	.2578					
190	.03260	250.1	4.20000E+01	.2310					
200	.03187	249.2	4.05546E+01	.2076					

Figure 6.2.3.6. - Damped system response.

presented. A more accurate evaluation of the total damping system could be obtained if the multilayer-multimaterial design equations given in Volume 1, Section 3 are used.

Damp Structure Response

The response of the fairing was reduced an order of magnitude as a result of the multilayer damping treatment, as shown in Figure 6.2.3.7.

Field Survivability Evaluation

Six aircraft had the damping design installed and a one year flight test revealed no fatigue cracks or durability problems.

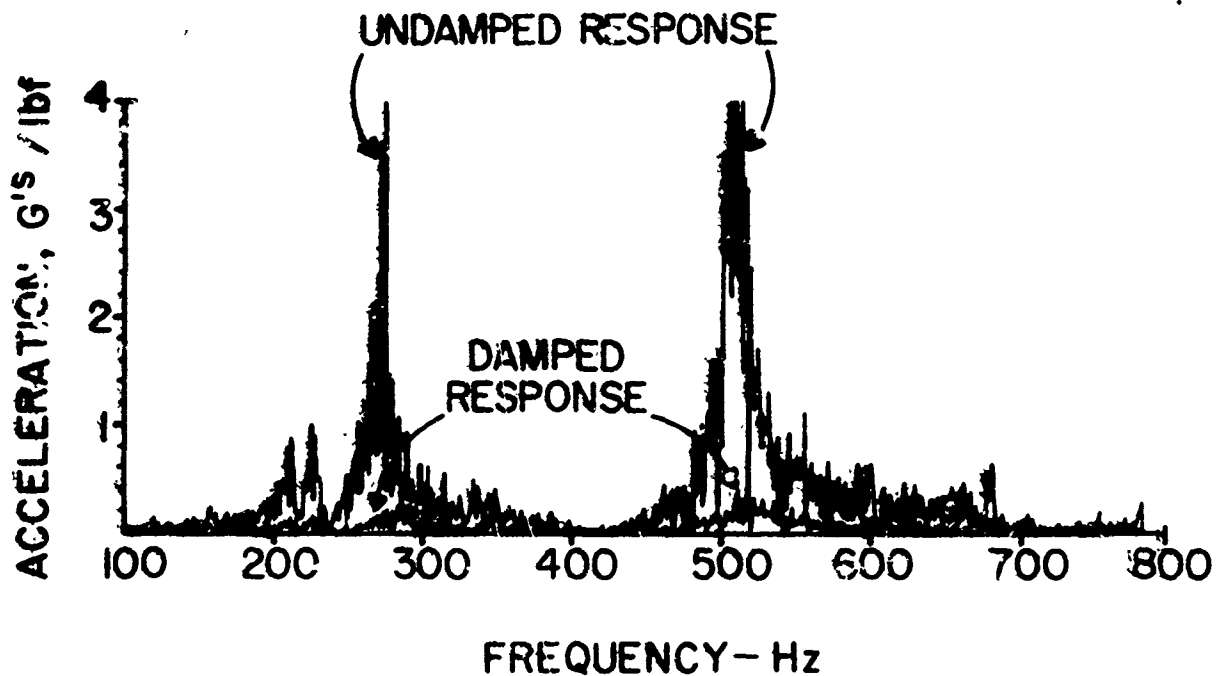


Figure 6.2.3.7. - Comparison of damped and undamped response.

6.2.4 TF-41 Engine Inlet Extension Damper [6.17]

Problem

Passage of the first stage fan blades caused high amplitude resonant response in the inlet extension from 2000 to 3500 Hz resulting in high-cycle fatigue cracking of TF-41 engine inlet extensions. The fiberglass/epoxy wrap, applied to the extension to prevent fatigue cracking, failed due to delamination and disbonding. As a result, the epoxy wrap was eliminated from consideration. In order to avoid a costly redesign of the extension to eliminate the problem, an effort was undertaken to develop an additive damping design to replace the fiberglass wrap.

Structure

The inlet extension is an 8 inch (203 mm) wide ring of sheet steel with 1 inch (25.4 mm) wide flanges welded to each side. The entire assembly is shaped into a truncated cone, as shown in Figure 6.2.4.1.

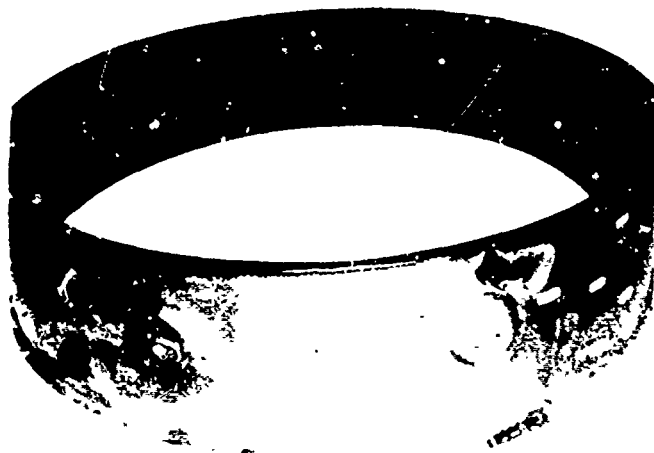


Figure 6.2.4.1. - TF-41 inlet extension.

Undamped Structure Response

A typical response of the bare extension is shown in Figure 6.2.4.2. The peak at 3140 Hz occurs in the operational rotor speed of the engine and is therefore the mode of interest. Modal analysis revealed the mode shape to be a circumferential bending wave with node lines spaced six to eight inches apart.

Damping Design

During 90 percent of its flight time, the extension is exposed to temperatures from 50°F (10°C) to 200°F (93°C). No single damping material can provide appreciable damping across this entire temperature range, so a multi-layer system was designed. The final design is shown in Figure 6.2.4.3. The 3M ISD-112 plus constraining layer provided peak damping at 80°F (27°C) while the 3M ISD-110 plus constraining layer resulted in peak damping at 175°F (79°C). The design tool used to develop this specific damping system was the flat plate constrained layer damping equations and computer program given in Subsection 5.1.16. The design approach was to optimize the ISD-112 design and the ISD-110 design independently. See Figure 6.2.4.4 for the predicted damped system response. Also contained in Figure 6.2.4.4 is all the required computer model and input data and the computed results. The designer can use his computer program to verify the results presented.

Damped Structure Response

A damped and undamped section of an inlet extension were tested in the laboratory to verify the multilayer treatment's effectiveness. The damping treatment increased the loss factor by an order of magnitude (Figure 6.2.4.5). Engine test cell runs of full-scale extensions, one with a fiberglass wrap and one with a damping wrap, were then conducted. The response obtained with these two treatments are illustrated in Figures 6.2.4.6 and 6.2.4.7, respectively. Overall, the response levels of the damped extension were lower than those of the fiberglass extension by a factor of five to six.

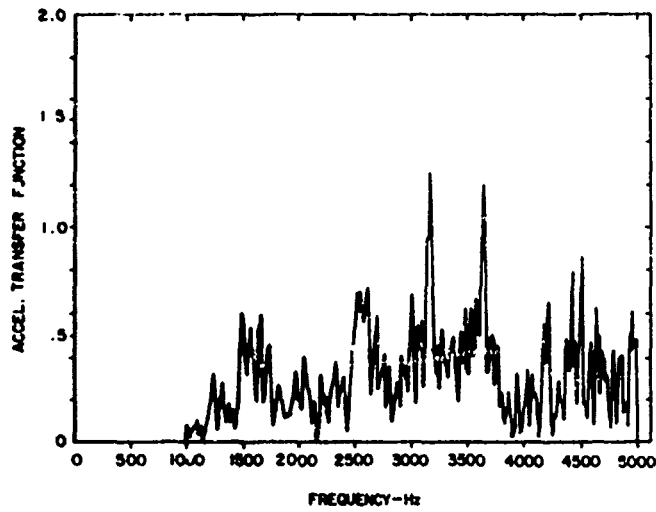


Figure 6.2.4.2. - Typical measured undamped frequency response of the inlet extension.

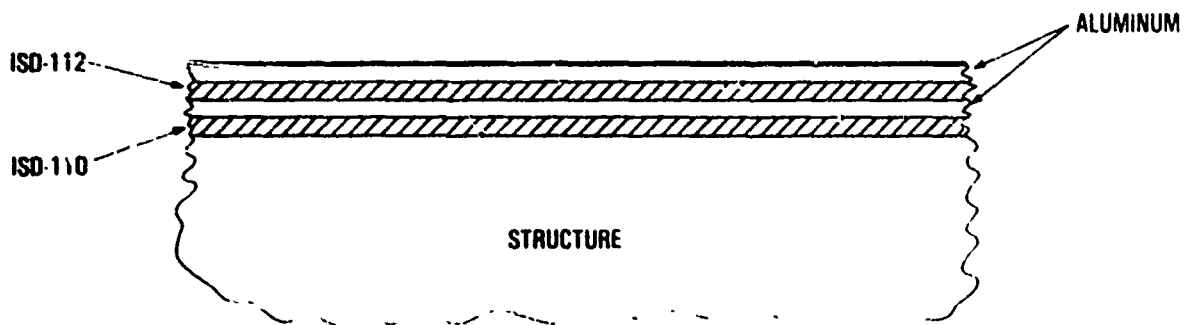


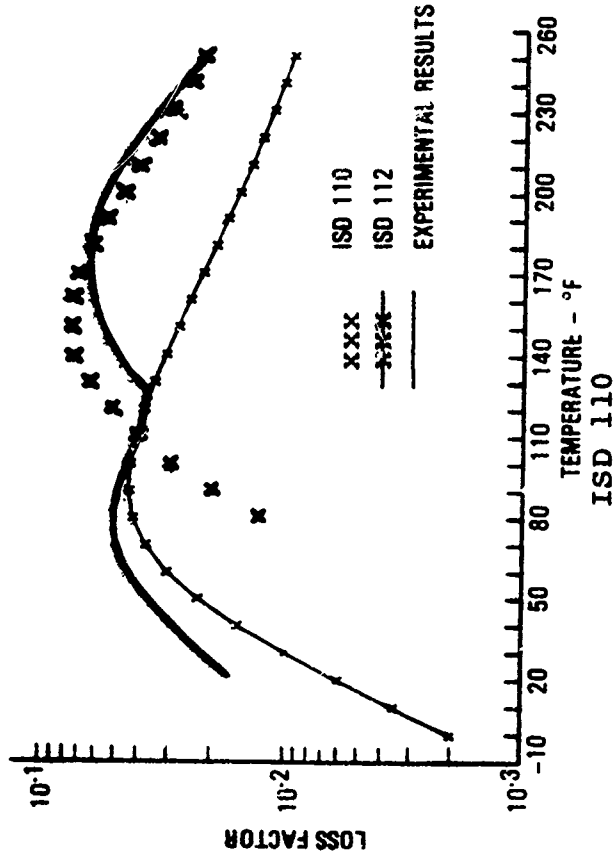
Figure 6.2.4.3. - Damping design.

OUTPUT LISTED IN ENGLISH
 PLATE
 CONSTRAINED LAYER

PLATE
 POSE 1
 SIMPLY SUPPORTED
 DIM. 8.00 8.00
 THICKNESS .0400
 DENSITY .2830
 MODULUS .283E+08
 DAMPING LAYER
 THICKNESS .0000
 DENSITY .0350
 CONST. LAYER
 THICKNESS .0100
 DENSITY .1000
 MODULUS 1.000E+07
 TEMP RANGE .00
 FREQ RANGE 116.1

NOTE: EQUATIONS USED TO PREDICT
 THE DAMPED RESPONSE ARE
 GIVEN IN SUBSECTION 5.1.16

MAX DELTA
 .0000 9999.00
 .0100 9999.00
 100.00 10.00



ISD 112		ISD 110							
TEMP DEG. F	COMPOSITE LOSS FACTOR	FREQ HZ	MATERIAL MODULUS PSI	MATERIAL LOSS FACTOR	TEMP DEG. F	COMPOSITE LOSS FACTOR	FREQ HZ	MATERIAL MODULUS PSI	MATERIAL LOSS FACTOR
0	.00001	133.7	4.20001E+03	.00005	20.0	.01754	132.9	5.01378E+02	1.0437
10.0	.00365	133.6	2.40044E+03	1.10075	30.0	.00015	132.5	2.05120E+02	1.1000
20.0	.00504	133.5	1.37878E+03	1.3247	143.0	.00314	132.0	2.51330E+02	1.2535
30.0	.00900	133.3	8.26531E+02	1.26993	110.0	0.4954	131.1	1.07584E+02	1.2027
40.0	.01247	132.9	5.13370E+02	1.2147	120.0	.05345	129.9	1.15007E+02	1.3020
50.0	.02258	132.3	3.10745E+02	1.1107	130.0	.00501	128.3	8.17933E+01	1.2057
60.0	.03082	131.4	2.35787E+02	1.0036	140.0	.07496	126.4	6.07000E+01	1.2023
70.0	.04170	130.3	1.78643E+02	1.0053	150.0	.07004	123.4	4.00483E+01	1.1210
80.0	.04170	129.0	1.32261E+02	1.0036	160.0	.07161	122.6	3.04590E+01	1.0304
90.0	.04358	127.7	1.00000E+02	1.0036	170.0	.07191	120.9	2.04590E+01	.8411
100.0	.04305	127.4	8.74110E+01	1.0036	180.0	.06444	119.6	1.07331E+01	.7512
110.0	.04005	127.4	7.44970E+01	1.0036	190.0	.06504	118.7	8.09330E+01	.6014
120.0	.03772	127.4	6.51170E+01	1.0036	200.0	.04846	117.7	6.09330E+01	.5175
130.0	.03485	127.0	5.81470E+01	1.0036	210.0	.04170	116.7	4.09330E+01	.4064
140.0	.03077	126.0	5.20300E+01	1.0036	220.0	.03000	116.3	3.09330E+01	.3000
150.0	.02733	125.5	4.65410E+01	1.0036	230.0	.02000	115.8	2.09330E+01	.2000
					240.0	.01000	115.5	1.09330E+01	.1000
					250.0	.00500			
					260.0	.00250			

Figure 6.2.4.4. - Predicted damped system response.

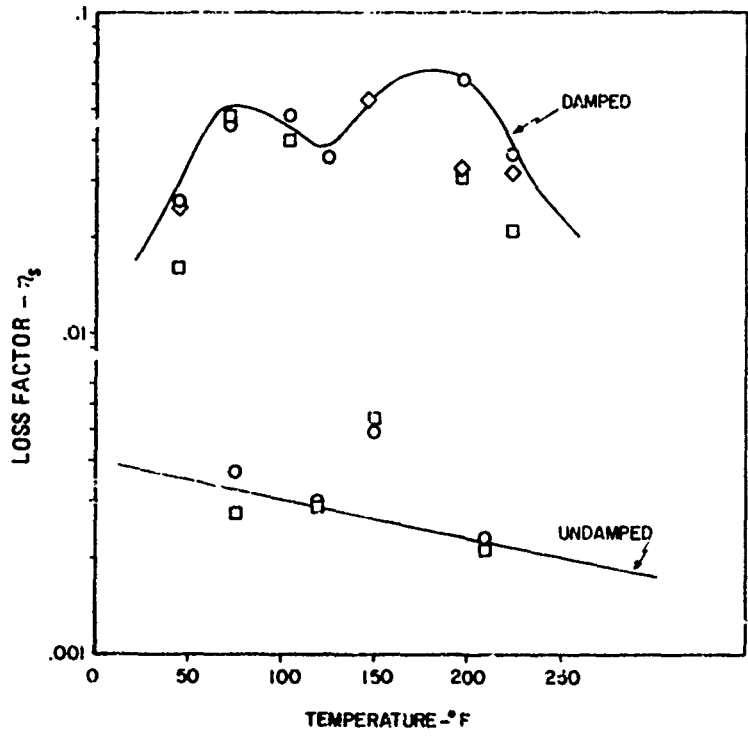


Figure 6.2.4.5. - Measured inlet extension loss factor.

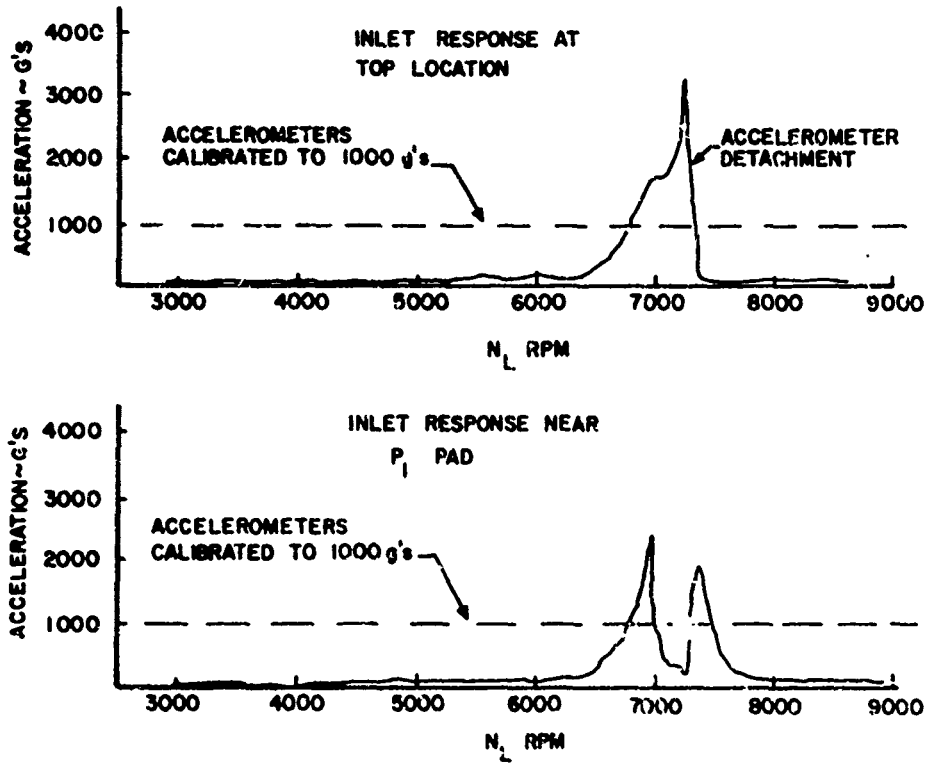


Figure 6.2.4.6. - Fiber glass wrapped response.

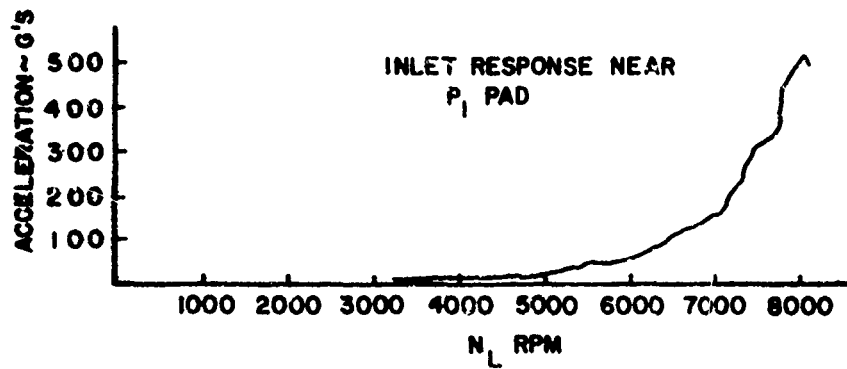
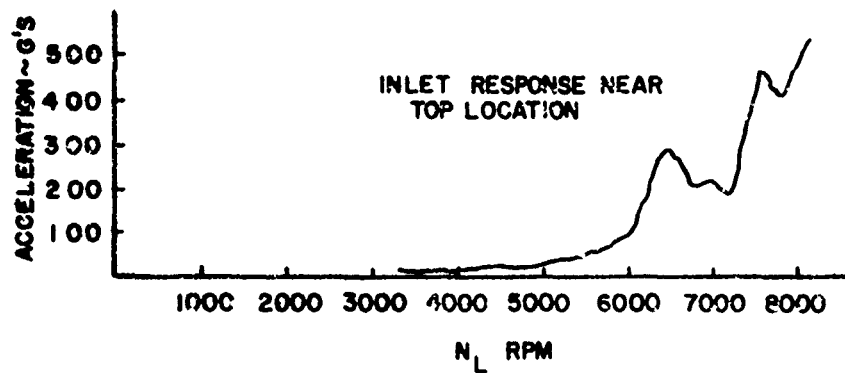


Figure 6.2.4.7. - Response of damped extension.

Engine Test Cell Durability Study

A damped inlet ran for over 1000 hours of test cell operation with no cracking or durability problems. An instrumented engine test after the 1000 hour test revealed the same level of modal damping as was measured before the durability test. Therefore there was no damping material deterioration.

6.2.5 OSTA-1 Shelf Damper [6.18]

Problem

High levels of vibration were expected to be transmitted to the OSTA-1 experiment support shelf because of high acoustic and vibration levels generated during launch of the space shuttle.

Structure

The shelf was used to support various experiments aboard the shuttle (see Figure 6.2.5.1). It is approximately 39 inches (991 mm) wide and 113 inches (2870 mm) long, and consists of an aluminum honeycomb core sandwiched between two aluminum face sheets.

Undamped Structure Response

Experimental modal analysis of the shelf had not been conducted. Analytical finite element analysis, however, revealed the probable resonant frequency to be 30 Hz; with an assumed inherent damping of 0.2.

Damping Treatments

The optimum design temperature was 70°F (21°C), with a design temperature range of 50°F (10°C) to 90°F (32°C). The design frequency was 30 Hz with a design frequency range of 15 Hz to 400 Hz. The design maximum structural loss factor was 0.3. Carpet plots of structural loss factor versus temperature at the design frequency were output for a number of materials, showing the effect of varying materials and geometries in a constrained layer damping configuration (see Figure 6.2.5.2). The resulting damping treatment was a 0.08 inch (2.032 mm) thick layer of 3M LSD-110 viscoelastic damping material constrained by a 0.12-inch (3.05 mm) thick layer of graphite. The design tool used was the flat plate constrained layer damping equations and computer program given in Subsection 5.1.16. The carpet plots were generated by plotting the maximum system damping for various damping configurations at the temperatures the maximums occurred. As can be seen from Figure 6.2.5.2 this allows the designer to choose rapidly the geometry of the damping design which will provide the required damping at the specified temperature of the problem to be solved.

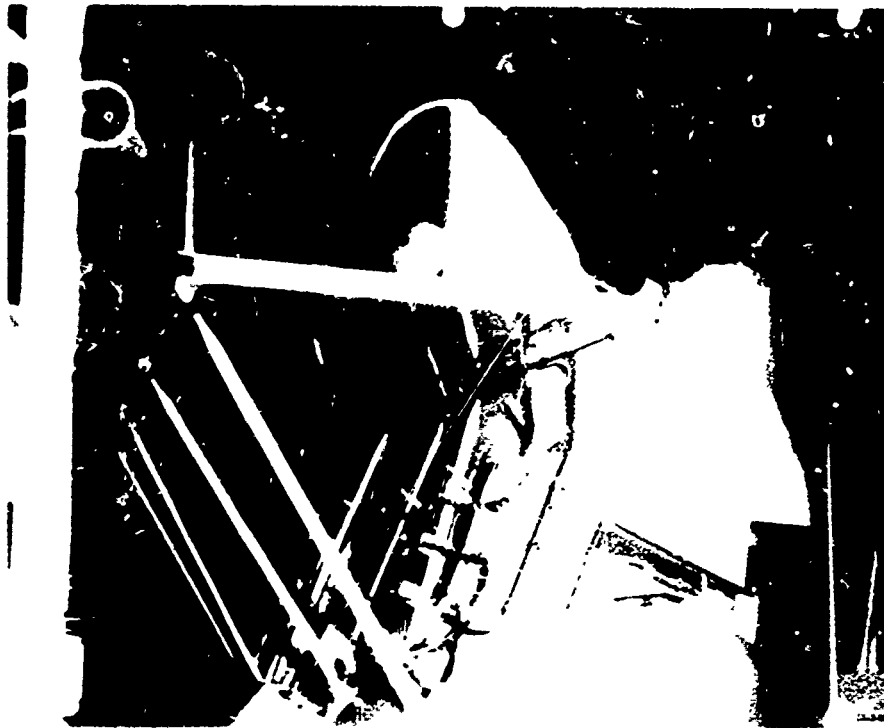


Figure 6.2.5.1. - OSTA-1 shelf.

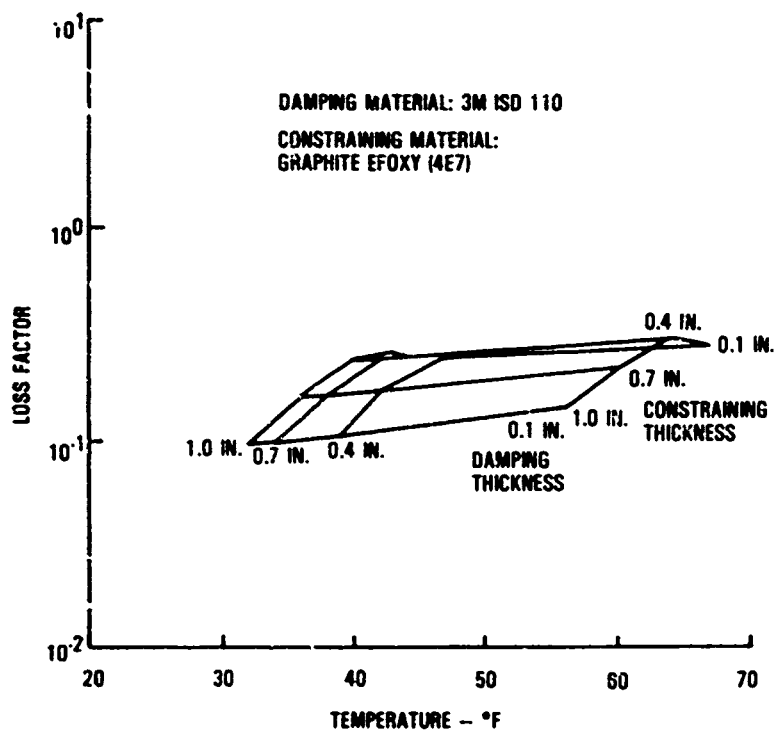


Figure 6.2.5.2. - Typical carpet plot.

Once the geometry has been chosen, the designer can run the appropriate computer program from Section 5.1.16 to generate the data for the system loss factor as a function of temperature as shown in Figure 6.2.5.3. This plot allows the designer to determine the effective temperature of the damping design as well as the maximum damping level and temperature of peak damping. The computer model, all required input data and the computer generated results are contained in Figure 6.2.5.3 so that the designer can use his own program to obtain the results.

Damped Response

The predicted structural damping over the temperature range of interest at the design frequency is shown in Figure 6.2.5.3. The maximum structural loss factor is 0.29458 at 70°F (21°C). No experimental investigations had been undertaken to verify this prediction.

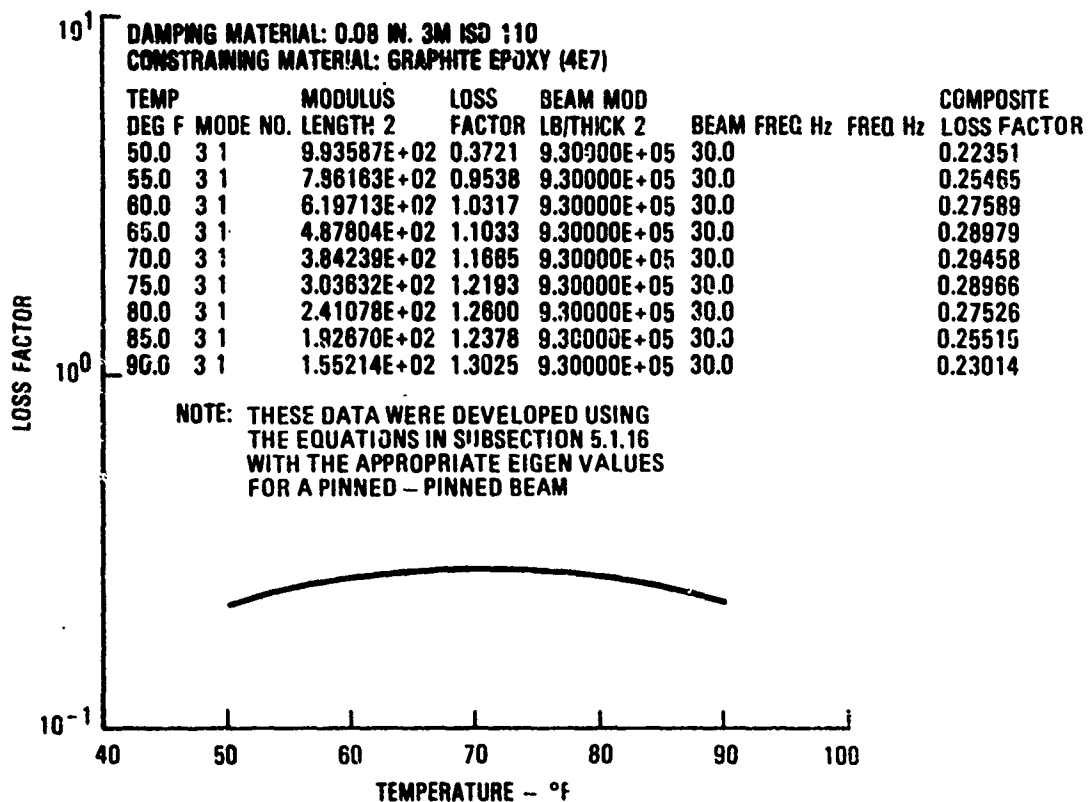


Figure 6.2.5.3. - Loss factor versus temperature for shelf with 0.08 inch thick ISD 110 and 0.12 inch graphite constraining layer.

6.2.6 RF-33-P3 Turbojet Engine Component Design Example [6.19, 6.20]

Problem

High cycle fatigue cracking was occurring in both the vanes and the shrouds of the inlet guide vane (IGV) case of the TF-33-P3 turbojet aircraft engine. The end result of the cracking was high repair and replacement costs for IGV cases to keep the engines in service and operationally ready.

Part Description

The IGV case is a titanium weldment consisting of 28 hollow vanes supported between two hollow cylindrical shrouds. Deicing air is routed through the vanes as necessary by way of the shrouds. The inner diameter shroud serves also as the support for the front bearing of the engine rotor system. The vanes serve to react the front bearing loads and to align the airflow for the first stage fan, which is located immediately downstream of the vanes.

Type of Loading

Primary sources of excitation were:

1. pressure waves from the first stage fan blades impinging on the vanes,
2. out-of-balance forces from the rotor, and
3. inlet airflow turbulence.

Temperature Data

Available temperature test data showed the operational temperature range of the IGV was -25°F (-32°C) to 150°F (66°C) for 99 percent of the operational time with occasional deicing air heating of the vanes to 425°F (218°C).

Additional Background

Considerable effort and expense had been expended in installing supplementary stiffeners through the vanes near their outboard end and through the two walls of the outer shroud because most cracks occurred at or near the vane outer shroud welded joint. Those structural modifications did not alleviate

the situation. The problem also had been one of the drivers of extensive studies of titanium fabrication and repair welding procedures.

Approach to the Problem

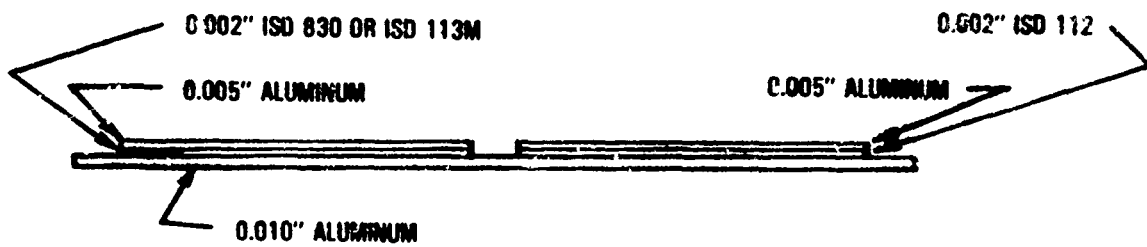
I. Problem Identification

Investigation of the problem began with a modal analysis of an ICV case mounted on a test stand engine. The analysis showed significant modal deflections of the vanes and outer shroud walls in the range from 300 to 4500 Hz. That range included the first four torsional modes of the vanes. The shroud-vane joint area would be involved in reacting out the dynamic loads induced by these vibratory modes. The first stage fan blade passage impulses would excite the higher modes of the vane. The lower modes would be excited by the unbalance and turbulence forces, and by the sum and difference frequencies of all excitation sources and their harmonics. It was expected, however, that fan blade passage pulses, in the frequency range of 2500 to 4500 Hz, were causing the most damaging vibrations, similar to the situation of the TF-30 engine IGV for which engine run strain gage data had been analyzed.

II. Analysis

a) The Ross-Kerwin-Unger equations were used to model the vane on the computer with a constrained layer damping systems, such a system being capable of producing maximum damping for a minimum of added thickness to the vane. Fourth order equations from Subsection 5.1.12 were used. The vane was modeled as a flat plate beam with pinned ends and the beam geometry was adjusted to approximate the resonance modes of the vane.

b) With the mode matched to the vane, an interactive design procedure was used to obtain a two-material constrained layer damping system that provided high damping over the operational temperature range in the frequency range of interest. The damping system is shown in Figure 6.2.6.1



VIEW A-A

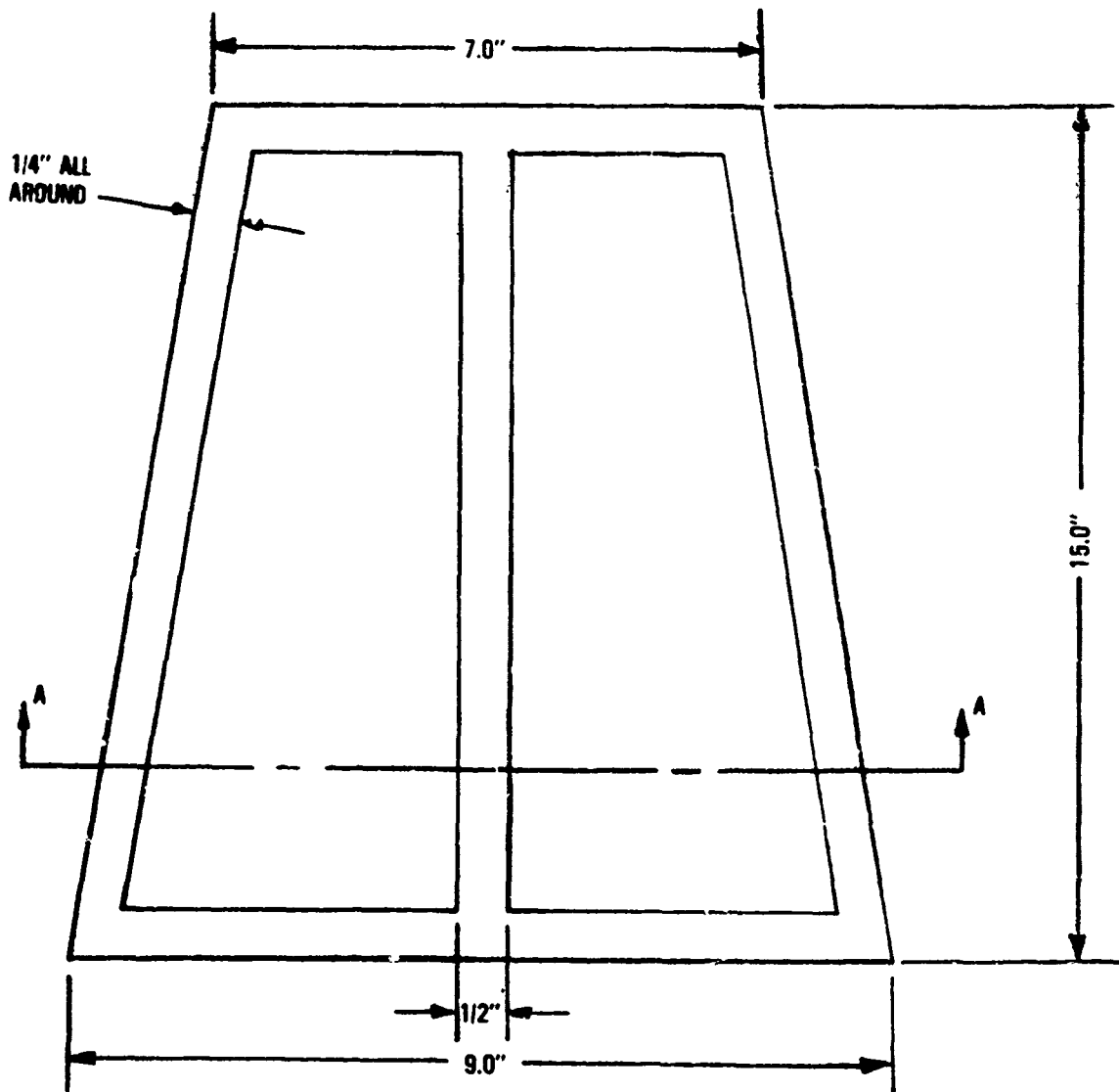


Figure 6.2.6.1. - TF-33-P3 IGV case damping wrap configuration.

III. Laboratory Testing

A three vane segment of the IGV case was obtained and was bolted to heavy aluminum plates at the inner and outer shroud sections to simulate the fixity of the case in an engine. A modal analysis, performed on the center vane and the adjacent outer shroud area of that specimen, showed the same resonance mode characteristics as previously measured on an IGV case, mounted in the engine. Vane and outer shroud baseline damping then were established by measuring the loss factor using swept sine wave excitation and the half-power-point method, over the temperature range of -25°F (-31°C) to 250°F (121°C), for all the major resonance modes between 1000 and 5000 Hz. The constrained layer damping treatment, shown in Figure 6.2.6.1, was then installed on all three vanes with structural epoxy adhesive using the vacuum bag process with an autoclave temperature and pressure curing cycle. The loss factor measurements, with the swept-sine excitation, were then repeated in the temperature chamber. The results of these tests, shown in Figure 6.2.6.2 and 6.2.6.3, were so favorable that a demonstration case was obtained in late 1979, all the vanes were wrapped, and the case was installed in an engine in the operational B-52H aircraft fleet. Room temperature loss factor values measured before and after the vane damping wraps were installed on that case are also shown in Figures 6.2.6.2 and 6.2.6.3

IV. Results

The wrapped demonstration case has been in use on an operational engine for more than four years and no fatigue cracking or durability problems with the damping wraps have been encountered. About a year after its installation a goose passed through the engine and caused damage the size of a pencil eraser to the wrap on one vane. The damage spot was repaired with room temperature setting epoxy and has caused no problems.

A cost analysis based on 1978 dollars and repair and replacement costs then showed a 10.5 million dollar savings could be effected on the TF-33-P3 engine inventory by a time point five years after all IGV case vanes were wrapped (total time frame eleven years with 896 cases wrapped in six years). Unfortunately, this effort has been delayed during attempted development of a new epoxy bonding installation process which encountered unexpected problems.

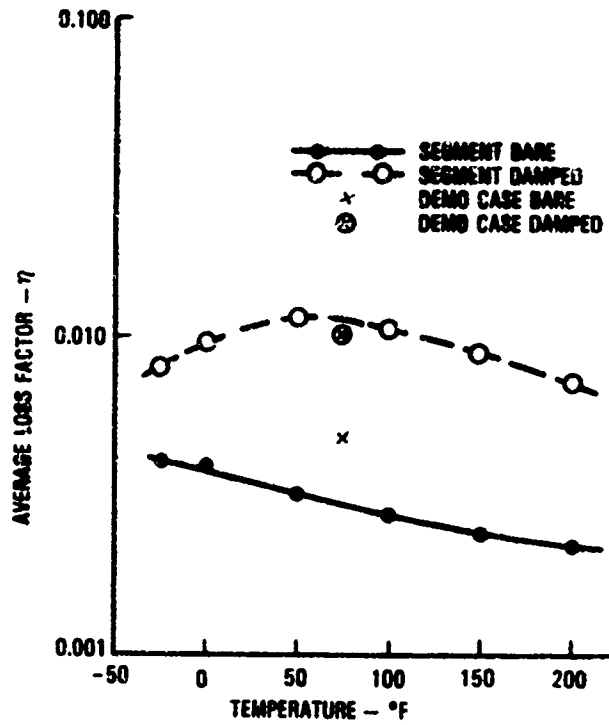


Figure 6.2.6.2. - TF-33-P3 IGV vane loss factor for the range 1 - 5 kHz versus case temperature.

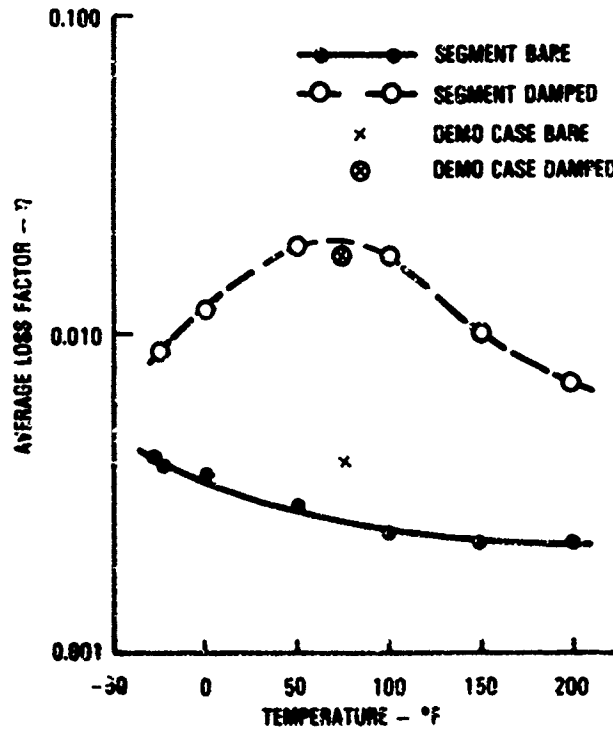


Figure 6.2.6.3. - TF-33-P3 IGV outer shroud loss factor for the range 1 - 5 kHz versus case temperature.

6.2.7 Radar Antenna Tuned Damper Design Example

Problem

Low cycle fatigue caused premature failure of an aircraft radar antenna. Failure involved the cracking of the antenna near the rim.

Primary Function of System

The antenna is used as part of an IFF system.

Part

The antenna is a circular, brass stamping with an electrical connector at its center (see Figure 6.2.7.1).

Location of Component

As shown in Figure 6.2.7.2, the antenna was mounted just forward of the aircraft's nose cannon.

Type of Loading

The high vibration levels are induced by nose cannon fire, transmitted by the airframe to the antenna.

Temperature Data

The operational temperature range of the antenna was estimated to be 80°F (27°C) to 170°F (77°C).

Approach to the Problem

1. Problem Identification

a) Evaluate in-flight vibration records to characterize the structural vibrations. The analysis indicated the vibration field to be broad band and suggested that random noise vibration (rather than sinusoidal) would best simulate gunfire in laboratory testing.

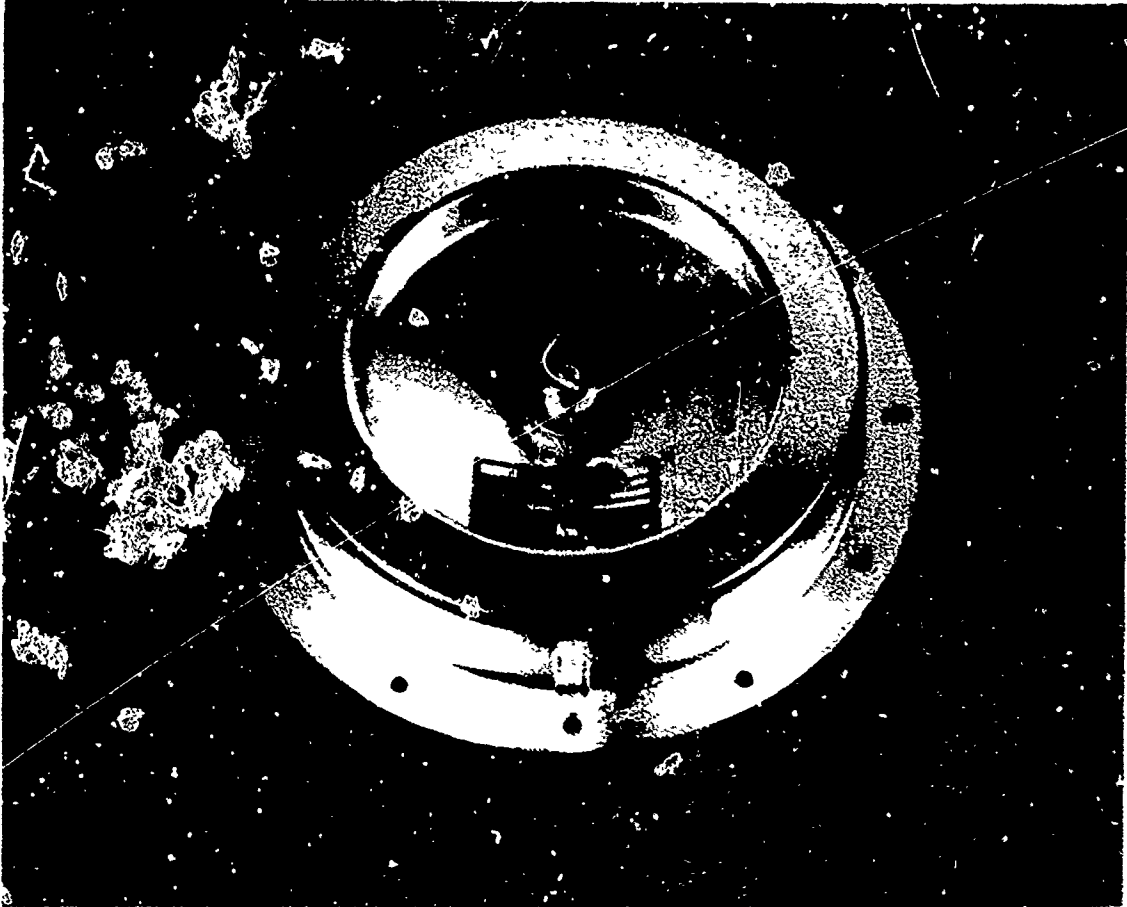


Figure 6.2.7.1. - Radar antenna.

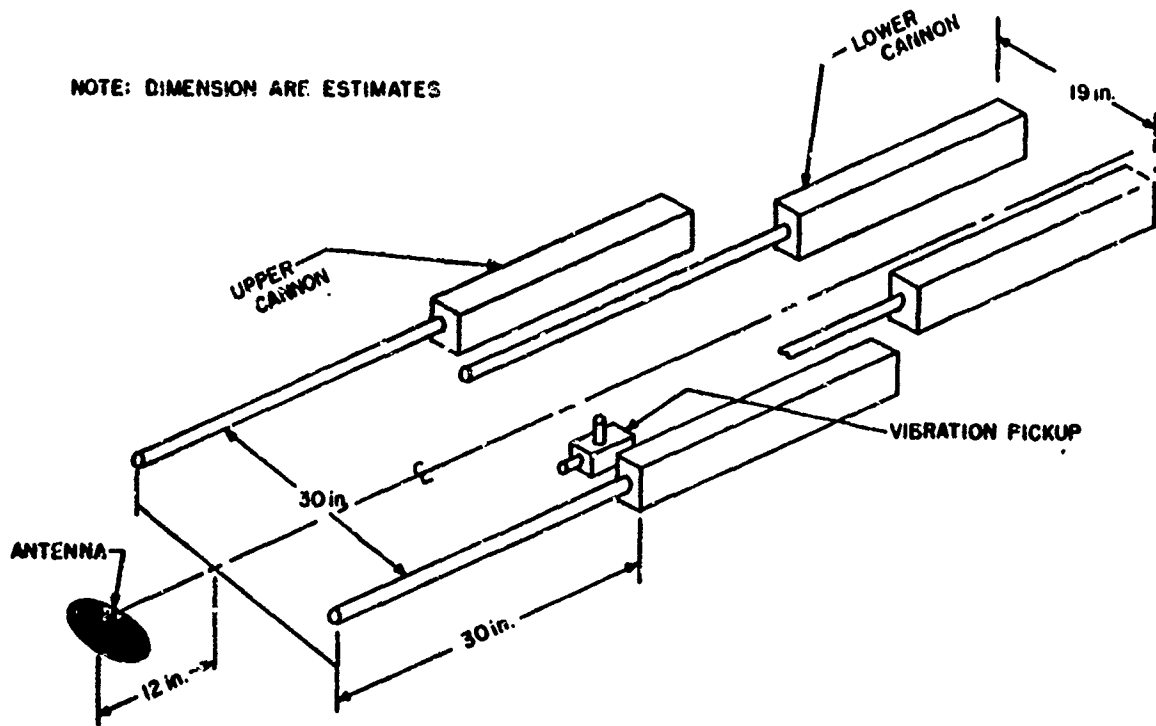


Figure 6.2.7.2. - Relative locations of cannon, pickups, and antenna.

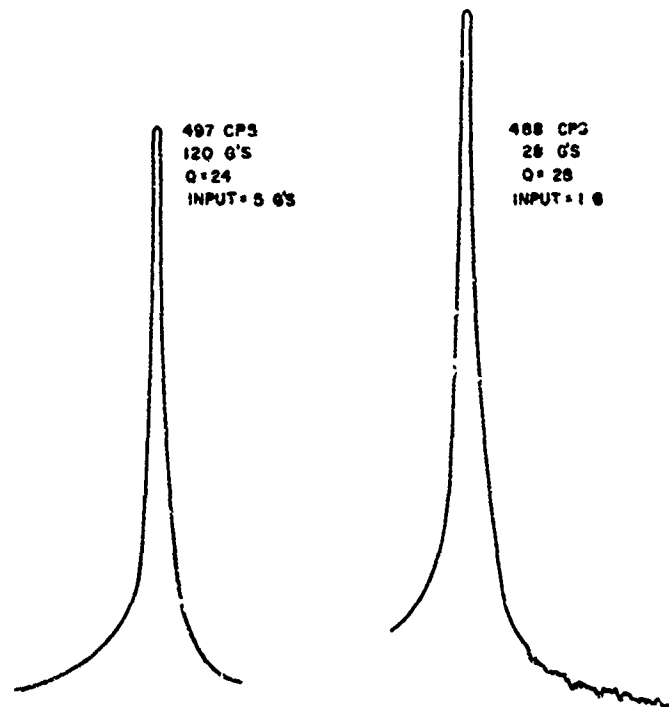


Figure 6.2.7.3. - Typical response spectra for undamped antenna.

b) Perform experimental modal analysis to identify the damage-causing mode. The resonant frequency, as shown in Figure 6.2.7.3, was 490 Hz. The motion was diaphragmatic, with the center of the antenna experiencing the greatest displacement. The average amplification factor (Q) of the mode was 30.

c) Determine the operational and survivability temperature ranges. From available information the operational and survivability temperature ranges were determined to be 80°F (27°C) to 170°F (77°C).

11. Analysis

a) Stiffening of the antenna structure had been tried but was discarded because the broad band excitation made it impossible to shift resonances out of the range of excitation frequencies.

b) Surface damping treatments depend for their effectiveness on the existence of large areas of high cyclic strain on the surface. In this instance, since the mode of vibration was predominantly diaphragmatic, no large strains existed anywhere apart from the small region near the rim where failure occurred. For this reason, no surface damping technique was usable.

c) Because the only significant response occurred at the center of the antenna, an effective damping treatment had to utilize this amplitude of vibration. The development of a tuned viscoelastic damper, attached around the electrical connector at the antenna's center, was therefore made the aim of the investigation.

d) An experimental design procedure was employed to develop a suitable tuned damper. A candidate damping material was chosen, a damper geometry was developed, prototype dampers were fabricated, and then the dampers were tested and evaluated. The procedure was repeated as necessary until an acceptable design was found.

e) Testing was conducted in two phases. Sinusoidal shaker excitation at various input levels at the resonant frequency determined the damping resulting from a given viscoelastic material and tuning mass. Intermittent random shaker excitation, which represented gunfire vibration, tested the durability of the damper and provided a means of correlating results with in-flight observations.

f) Candidate damping materials had to meet the following qualifications: high loss factor (≥ 0.2) over the temperature range of interest and nearly constant shear modulus over the temperature range of interest. The operational temperature range (80°F (27°C) to 170°F (77°C)) would thus have to correspond to the rubbery phase of a candidate material. The material finally chosen was Panacril-BJ with 25 PIR super abrasive furnace carbon black added for strength. Without the added carbon the material was found to fail rapidly during testing despite adequate damping. Figure 6.2.7.4 shows the material properties.

g) Figure 6.3.8.5 shows the final geometry of the tuned damper. The cross-hatched areas represent the viscoelastic damping material. The outer circular areas are the tuning masses for the damper. The bonding surfaces are radiused to provide additional bond area and to reduce stress concentrations. The damper was attached to the electrical connector at the center of the antenna.

III. Results

a) The final design of the damper is shown in Figure 6.2.7.5

b) Sinusoidal shaker testing showed the modal damping (loss factor) to be 0.14. This is more than a four-fold reduction in resonant amplitude (from $Q = 30$ to $Q = 7$). Figure 6.2.7.6 shows the amplification factor as a function of temperature and input level.

c) Random shaker testing showed that the damper and antenna could survive at least 30 minutes of gunfire vibration excitation, compared with one to four minutes for the undamped antenna during in-flight conditions.

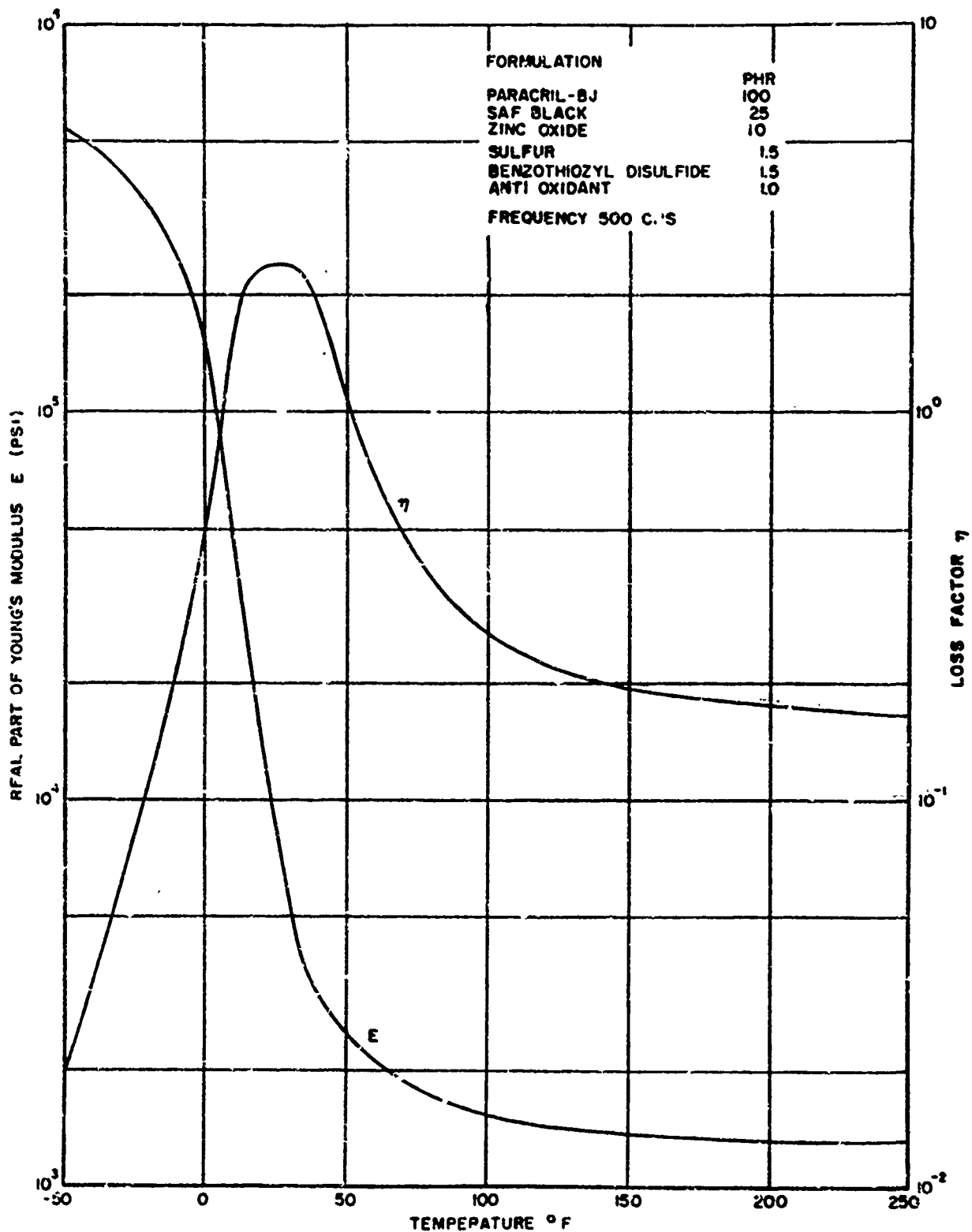


Figure 6.2.7.4. - Damping properties of panacril-BI with 25 PIR carbon.

MATERIAL: QQ-B-626 BRASS

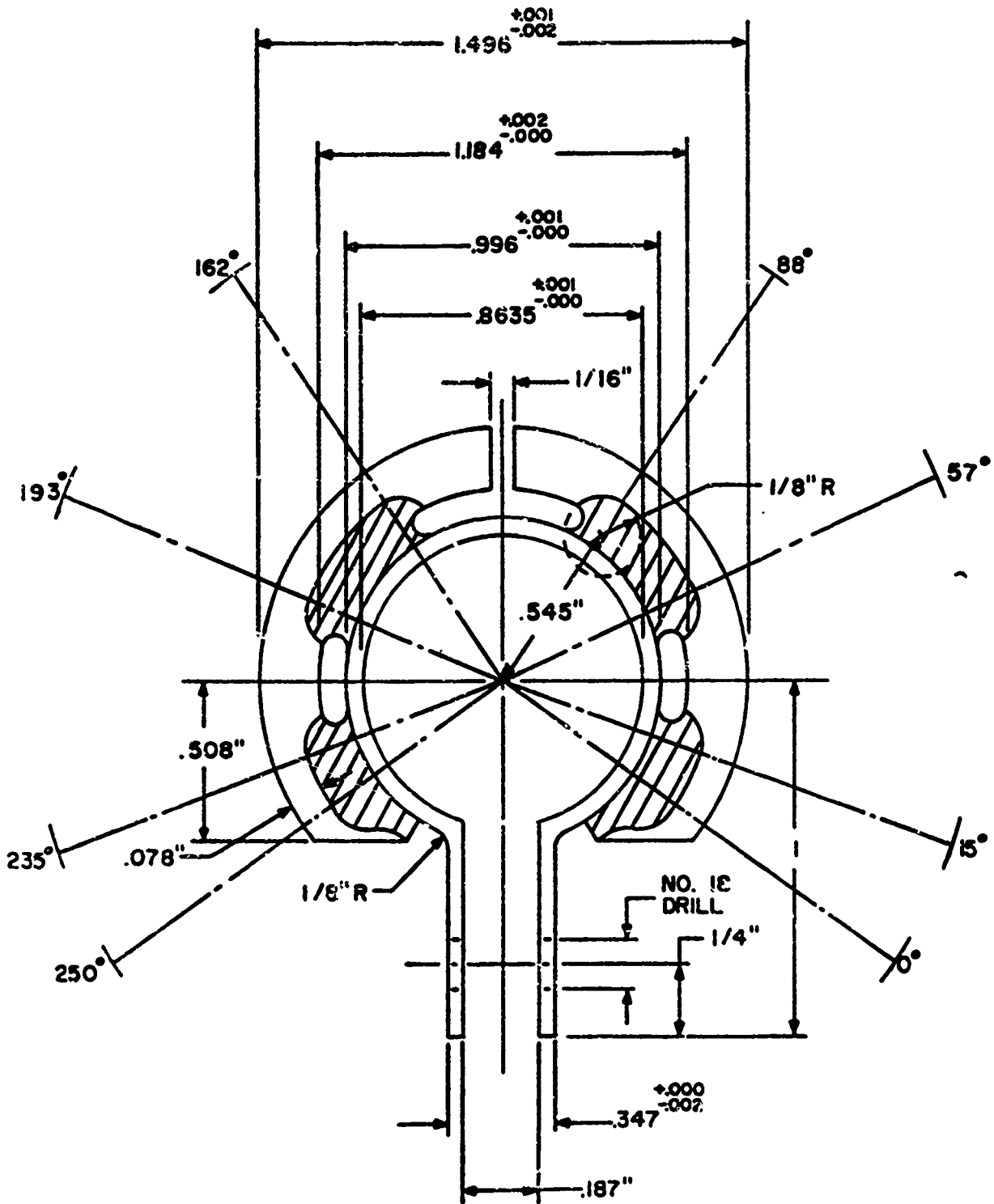


Figure 6.2.7.5. - Final geometry of prototype.

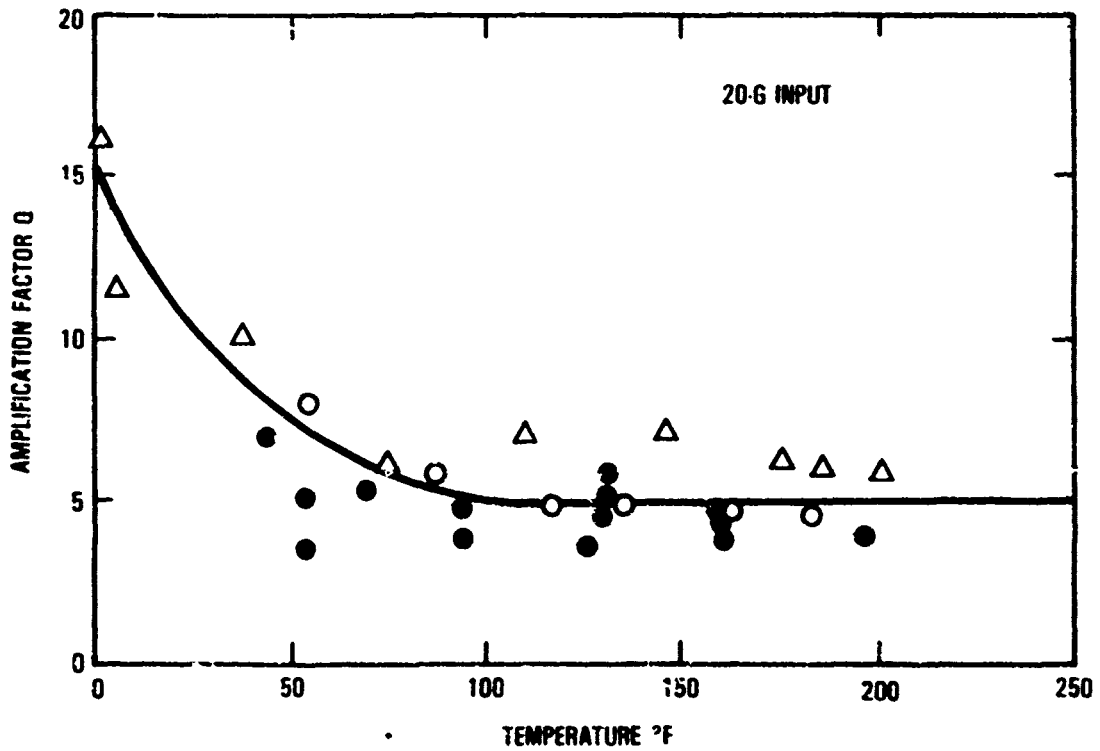
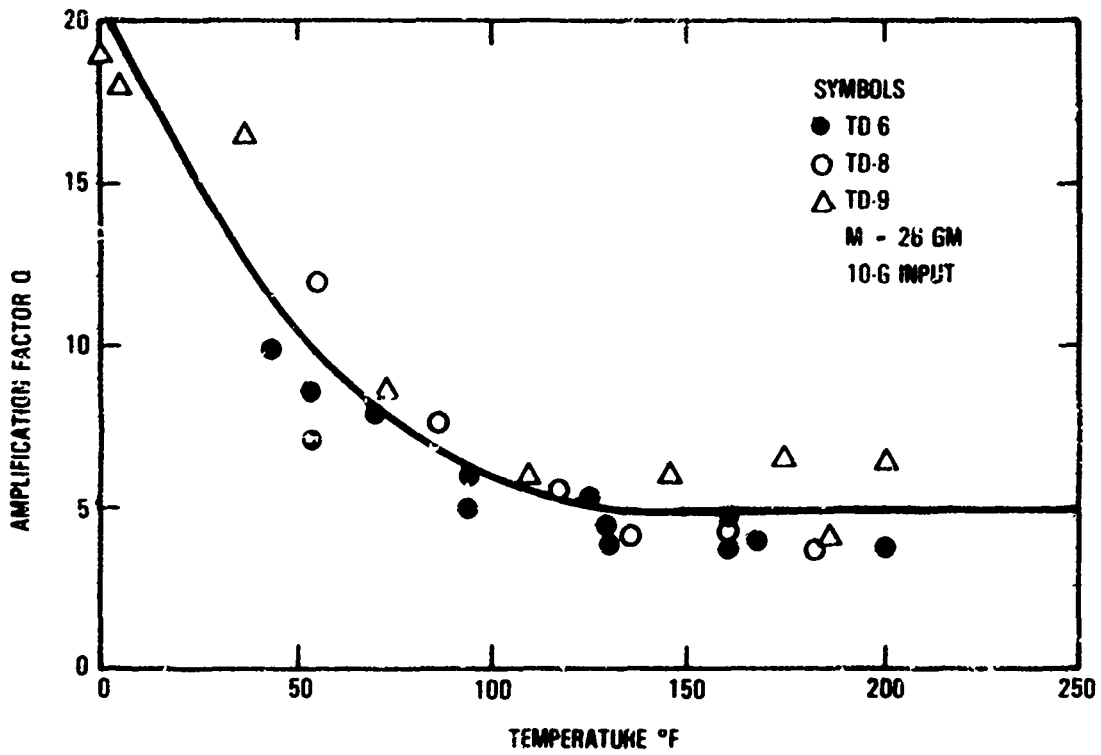


Figure 6.2.7.6. - Graphs of amplification factor against temperature for antenna with prototype 8 attached.

d) Field testing of five damped antennas over a three month period showed a durability life of 41.6 hours to 105.5 hours.

6.2.8 Laser Component (Ring Mirror) Design Example [6.21]

Problem

Potential existed for a resonant yawing vibration of the annular reference mirror (ring mirror) of a laser. This would produce beam jitter during operation.

Part

Annular disk supported by an axle on a graphite-epoxy yoke (see Figure 6.2.8.1).

Type of Loading

Primary sources of excitation would be:

- a) Acoustic excitation from the environment around the laser assembly.
- b) Structural vibrations transmitted through the laser mounting assembly.

Temperature Data

The operational and damping temperature range are the same, namely, 55°F (13°C) to 75°F (24°C).

Approach to the Problem

1. Problem Identification

a) Using experimental modal analysis, identify any modes in the vicinity of 140 Hz (believed to be the location of possible resonance problem). A rough modal analysis had been performed earlier for other purposes. This analysis revealed a rotational mode about the mirror pivot axis at 135 Hz.

b) The temperature range of operation, over which damping must be effective, was a cool room temperature of approximately 55°F (13°C) to 75°F (24°C).

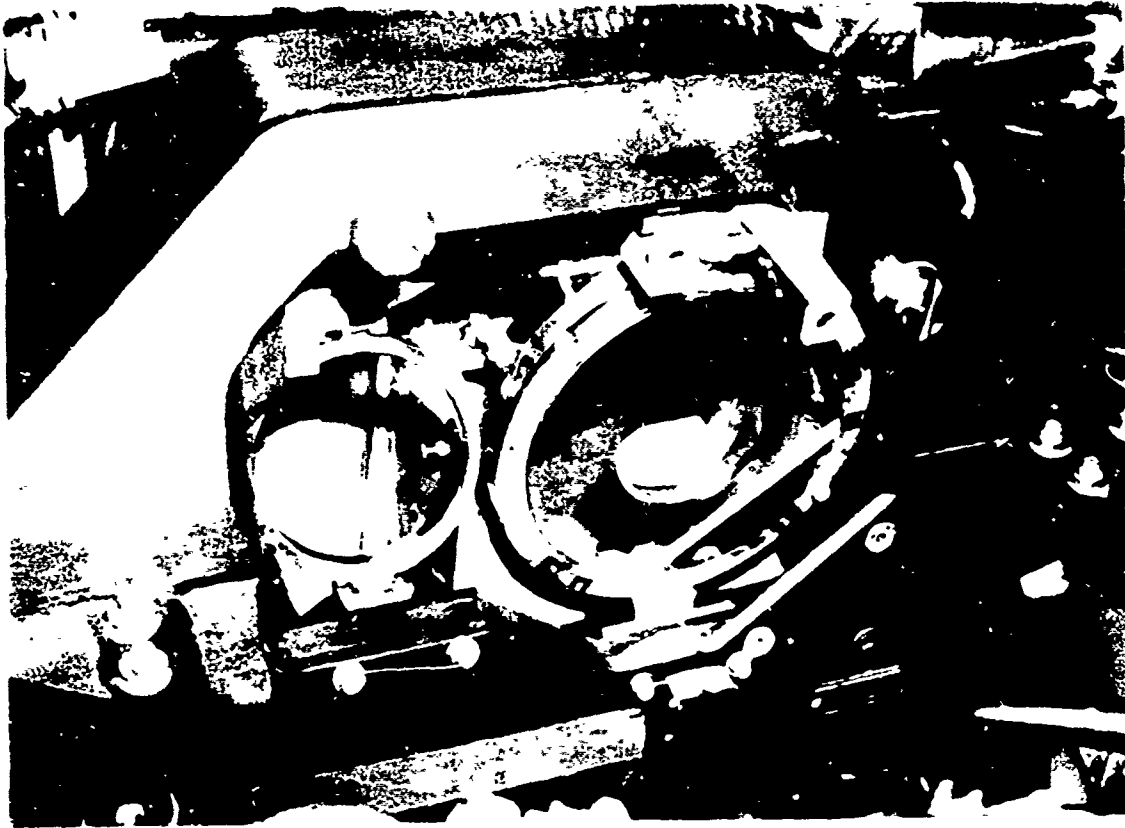


Figure 6.2.8.1. - Annular reference mirror on the bench.

II. Analysis

a) A damping design concept is determined. A steel strap mounted between the base structure and mirror could stiffen the mirror assembly about the yawing axis and increase the frequency. Using a split strap with damping material could also damp out the resonant vibration. Experimental frequency response analysis reveals that the solid steel strap causes undesirable cross-coupling of responses. The damped strap is, therefore, the concept chosen for solution of the problem.

b) NASTRAN finite element models (see Volume I, Section 5) of the mirror/yoke assembly and the damped strap are developed. The mirror, a portion of the yoke, and an adjustment bracket (to which the strap would be fastened) are modeled as shown in Figure 6.2.8.2. Because the modal analysis shows the mode shape to be rotation of the mirror only, the mirror pivot points are modeled as fixed in space and the surrounding portions of the yoke left

out. The torsional stiffness at the pivot points is adjusted to give a frequency of 135.4 Hz for the mode of interest. Figure 6.2.8.3 gives the resulting mode shapes.

The damped strap is modeled with the configuration shown in Figure 6.2.8.4. HEXA isoparametric solid elements are used to represent the viscoelastic solid elements using membrane-bending coupling.

c) The modal strain energy method with normal modes finite element analysis (see Volume I, Section 5) is used to optimize the loss parameter. The loss parameter is the strain energy in the viscoelastic material (VEM), divided by the total system strain energy or

$$\text{loss parameter} = \frac{V_v}{V} \quad (6.1)$$

where V_v is the strain energy in the VEM and V is the total strain energy in the mirror/support structural damped strap assembly. Maximizing the loss parameter also maximizes the amount of energy that will be dissipated by the VEM and therefore, by definition, the system damping.

For this damping design, the VEM parameter G/t (where G = shear modulus and t = thickness) determines the loss parameter. Two thicknesses, 0.020 inch (0.508 mm) and 0.060 inch (1.52 mm), are chosen and then a variety of values for G are tried to determine the combination which maximizes the loss parameter. The mode shape is similar throughout, and is shown in Figure 6.2.8.5. The frequency and loss parameter results are presented in Table 6.2.8.1. The maximum loss parameter is obtained when $G = 600$ psi (4.14×10^6 N/m²) and $t = 0.060$ inch (1.52 mm) or when $G = 200$ psi (1.38×10^6 N/m²) and $t = 0.020$ inch (0.508 mm). For both these cases, the design parameter G/t is 10,000 psi/in (2.71×10^6 N/m²/mm). The 0.020 inch (0.508 mm) treatment was chosen for fabrication.

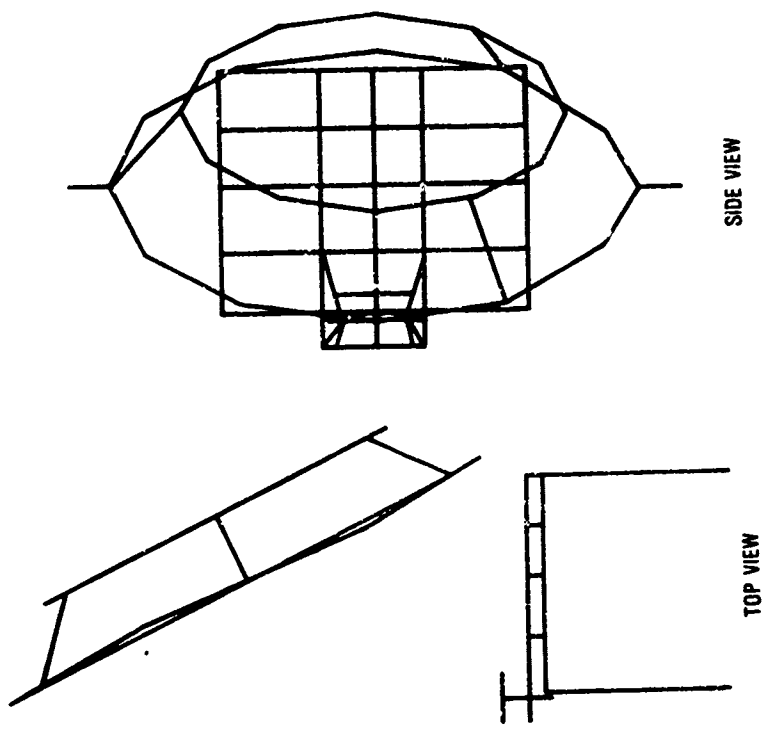


Figure 6.2.8.2. - Top and side view of flute element model of the ring mirror.

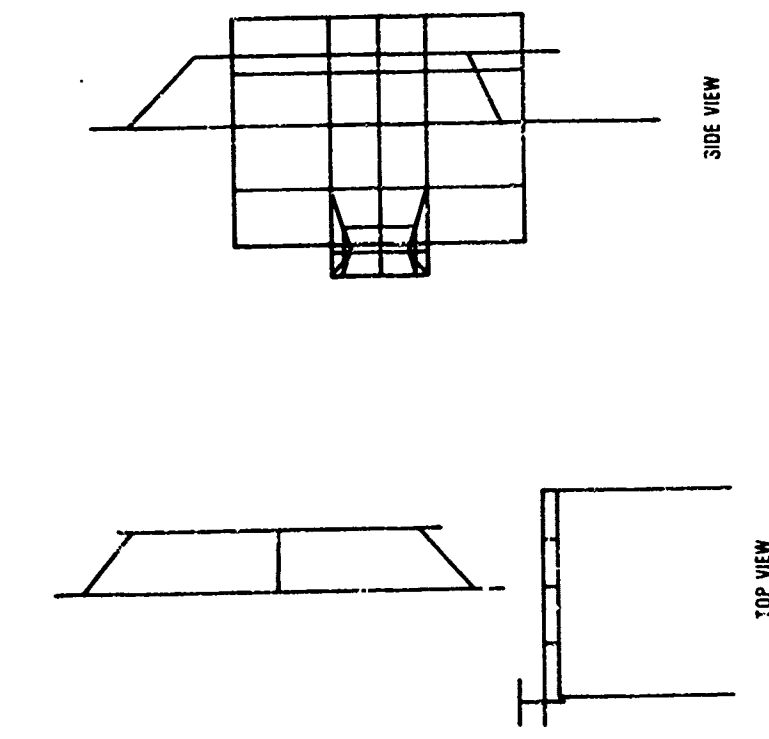


Figure 6.2.8.3. - Modal deformation plot of ring mirror at 135 Hz.

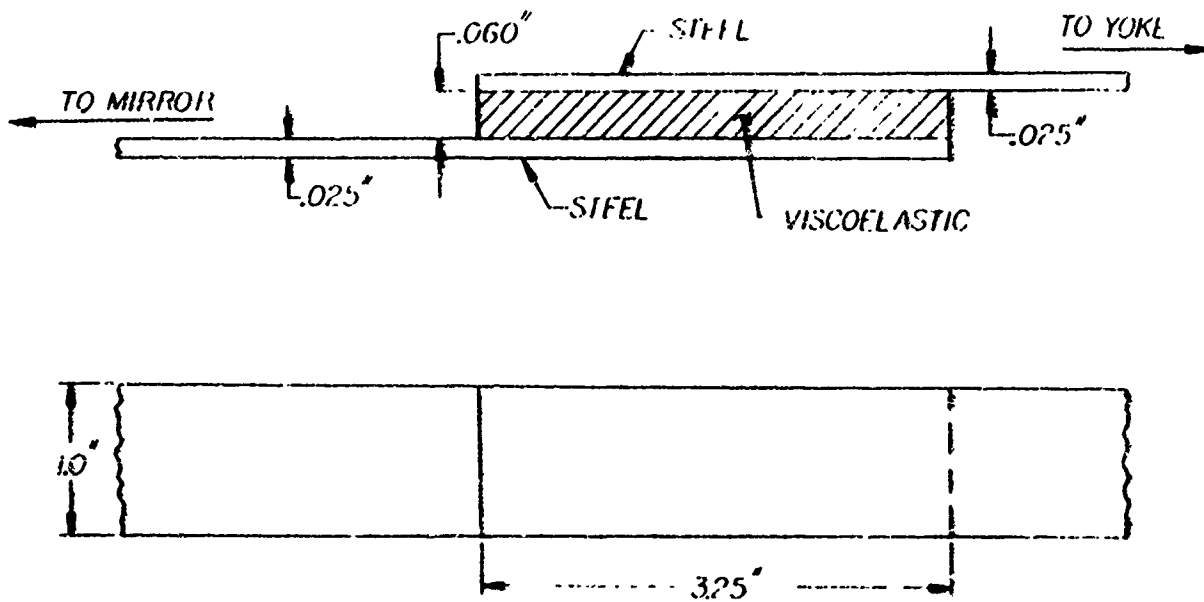
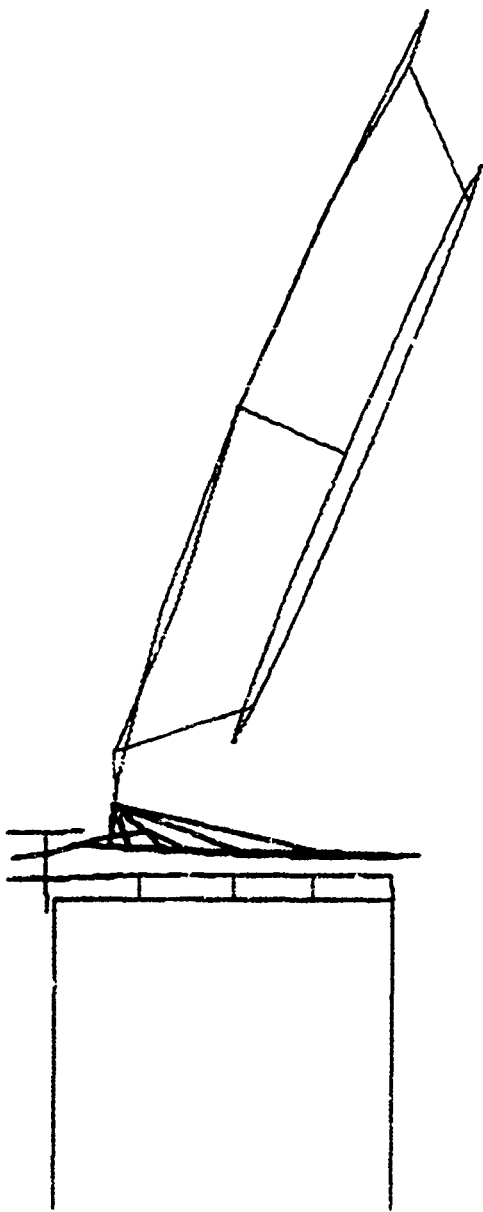


Figure 6.2.8.4. - Schematic drawing of the damped strap.

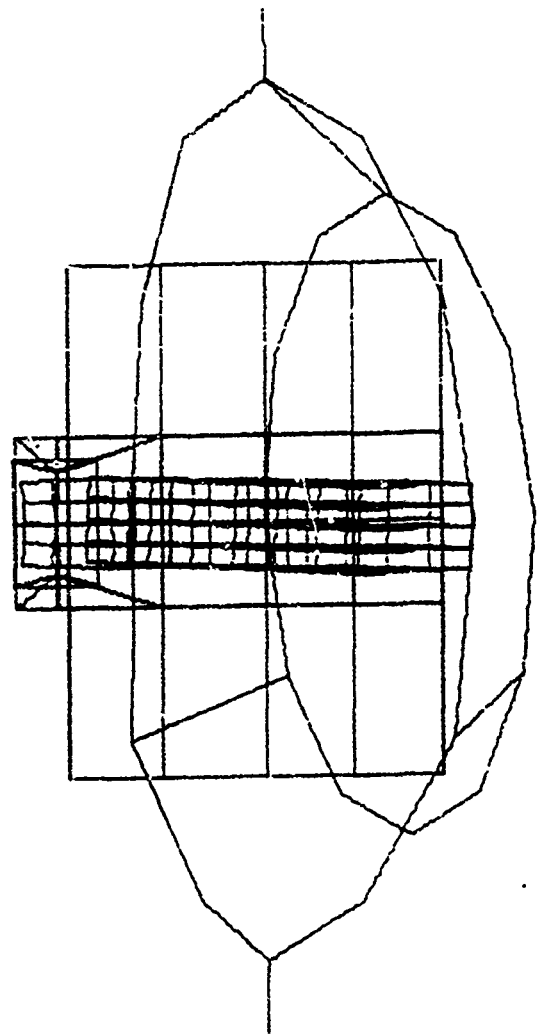
Both pinned and fixed strap boundary conditions were investigated. Table 6.2.8.1 shows that nearly the same results are obtained for each. The mode shapes are also unchanged.

d) Selection of a suitable viscoelastic material. It was assumed in the analysis of c) that the temperature was 65°F (18°C). Thus the material selection criteria are: $G = 200$ psi (1.38×10^6 N/m²), frequency = 172 Hz, and temperature = 65°F (18°C) with maximum loss factor near this point. The material ISD-112, manufactured by 3M Company, has properties which meet these criteria (see Figure 6.2.8.6). The shear modulus is approximately 200 psi (1.38×10^6 N/m²) while the loss factor is 0.99 for the frequency and temperature of interest. The modal (structural) loss factor is estimated by the MSE method to be

$$\eta_s = \eta_v \frac{V_v}{V} \quad (6.2)$$



Top View



Side View

Figure 6.2.8.5. - Modal deformation plot of ring mirror with damped strap at 172.6 Hz.

TABLE 6.2.8.1. FREQUENCY AND LOSS PARAMETERS OF RING MIRROR

Analysis Case	Mode 1	
	Frequency	Loss Parameter
No Strap	135.4	N.A.
0.025 Inch Steel Strap	205.5	N.A.
0.060 Inch Viscoelastic Layer G = 200 psi	152.7	0.203
0.060 Inch Viscoelastic Layer G = 600 psi	172.6	0.219
0.060 Inch Viscoelastic Layer G = 1000 psi	181.8	0.180
0.060 Inch Viscoelastic Layer G = 17,729 psi	202.4	0.019
0.020 Inch Viscoelastic Layer G = 200 psi Pinned on End	172.3	0.220
0.020 Inch Viscoelastic Layer G = 200 psi Fixed on End	173.2	0.225

where η_s = structural loss factor, η_v = VEM loss factor, and V_v/V is the loss parameter discussed earlier. From Table 6.2.8.1 V_v/V is 0.219, so

$$\eta_s = 0.99 \times 0.219 = 0.216$$

e) The finite element analysis results are experimentally verified. The damped strap is fabricated and installed based on the finite element analysis design. Frequency response analysis shows the resonant frequency to be 150 Hz, well below the predicted frequency of 172 Hz. With the strap removed, a detailed modal analysis of the ring is performed. Two modes are identified at 135 Hz rather than the one mode that is determined from the original coarse modal survey. In addition to the rotation of the mirror about its pivot points, a front-to-back translation of the mirror and yoke assembly occurs. The two motions are out of phase at the bottom of the mirror where the strap is

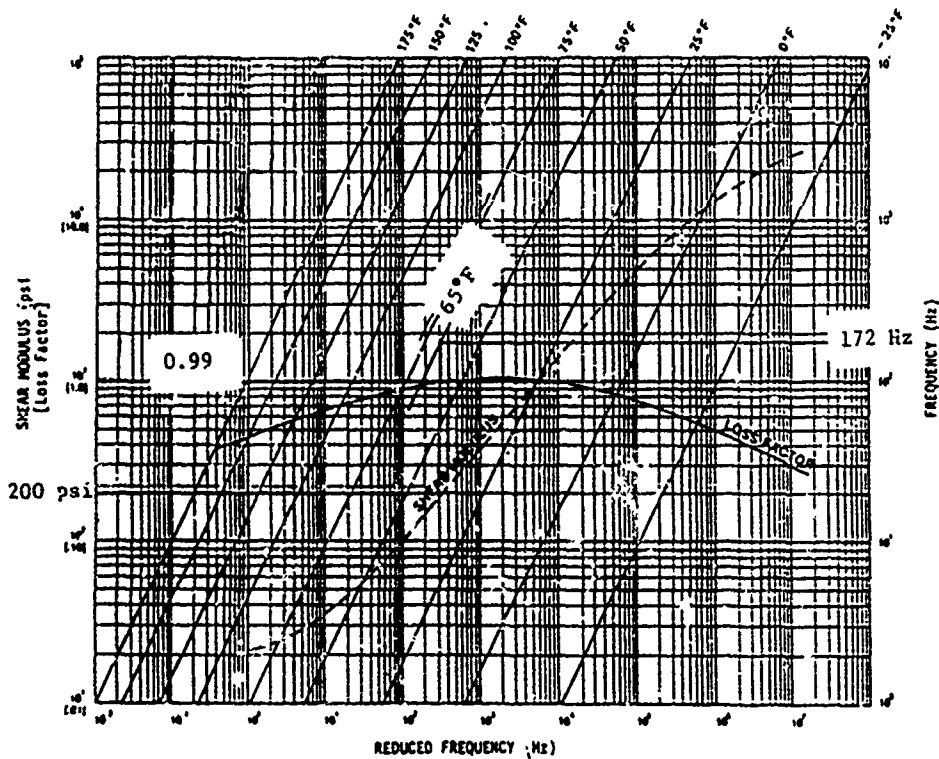


Figure 6.2.8.6. - Material properties for 3M, type 112 viscoelastic.

attached, so that almost no net motion of the strap occurs (see Figure 6.2.8.7). As a result, little VEM deformation occurs, so that the increase in jamping of the assembly is minimal.

f) Practical considerations include: 1) minimizing weight addition to the laser assembly, and 2) simple installation without modification to the existing structure.

III. Results

a) Final design of the strap damping system is shown in Figure 6.2.8.8. The predicted structural loss factor of the mirror/strap assembly is 0.216.

b) Results of frequency response analysis do not agree with the finite element analysis. Subsequent modal analysis revealed that an additional mode is present at the frequency of interest which is not included in the finite element model.

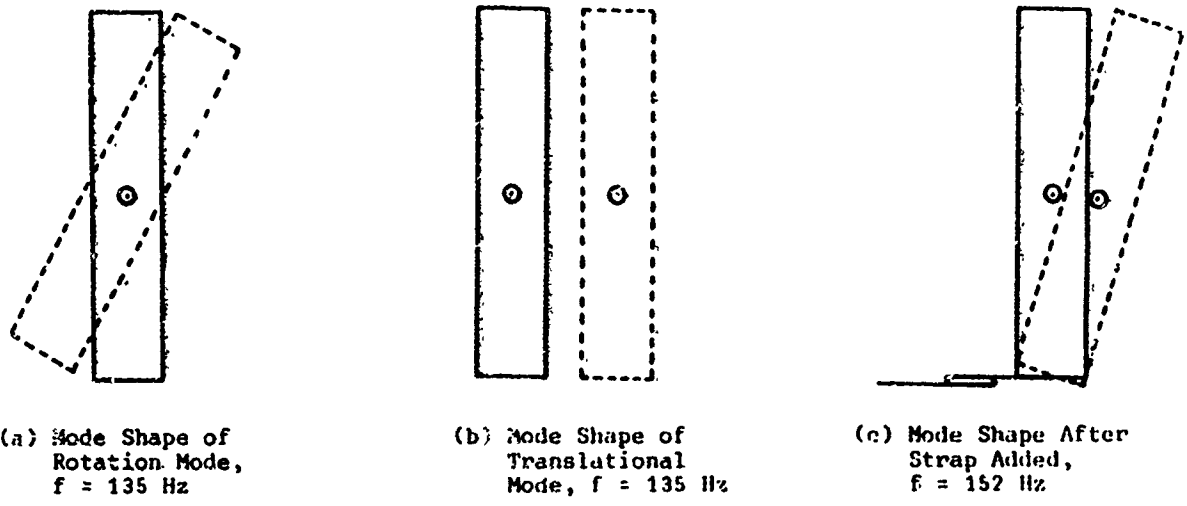


Figure 6.2.8.7. - Schematic of measured mode shapes of ring mirror.

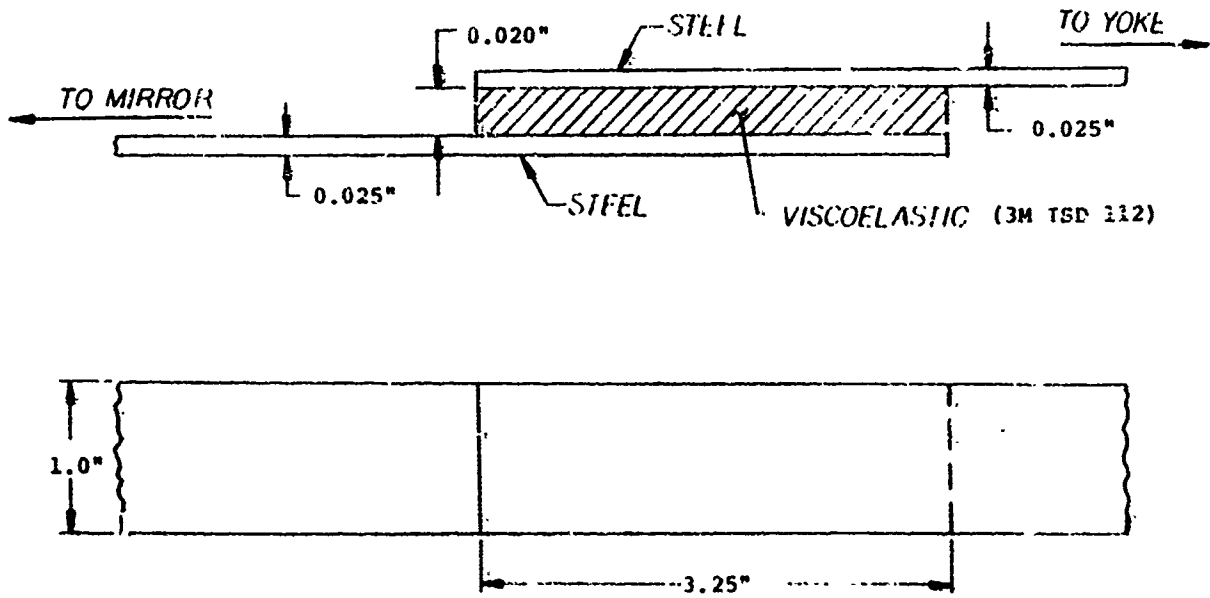


Figure 6.2.8.8. - Schematic drawing of the damped strap.

c) The lesson to be learned from this investigation is that system dynamics must be accurately understood before a representative analytical model can be constructed and an appropriate damping concept chosen. In this case the yoke assembly should have been modeled, so that the transitional mode can be present in the finite element model.

6.2.9 Aeroelastic Flutter Design Example [6.22]

Problem

Aeroelastic flutter at the lips of the intermodular plate.

Primary Function of System

Air discharge flow channel.

Part

Plate 0.3-inches (7.62 mm) thick and 19.3 inches (490 mm) in diameter, as shown in Figure 6.2.9.1.

Type of Loading

Self-excited vibration induced by unsteady cooling gas flow interacting with the intermodular plate lips.

Temperature Data

Damping required from 75°F (24°C) to 460°F (204°C), with ability to survive short-term exposures to 650°F (343°C).

Approach to the Problem

I. Problem Identification

a) Analytical normal mode and flutter analyses of the undamped plate determined that the important vibration modes for flutter are local, out-of-phase bending modes of the lips.

b) Experimental modal analysis to determine precisely the mode shape and frequency of the lowest-frequency out-of-phase bending mode is performed. The mode is found to have a frequency of 2140 Hz and damping (loss factor) of 0.0012. The mode shape is shown in Figure 6.2.9.2.

c) Temperature ranges over which damping is required and over which the damping material must survive are determined. The operational temperature

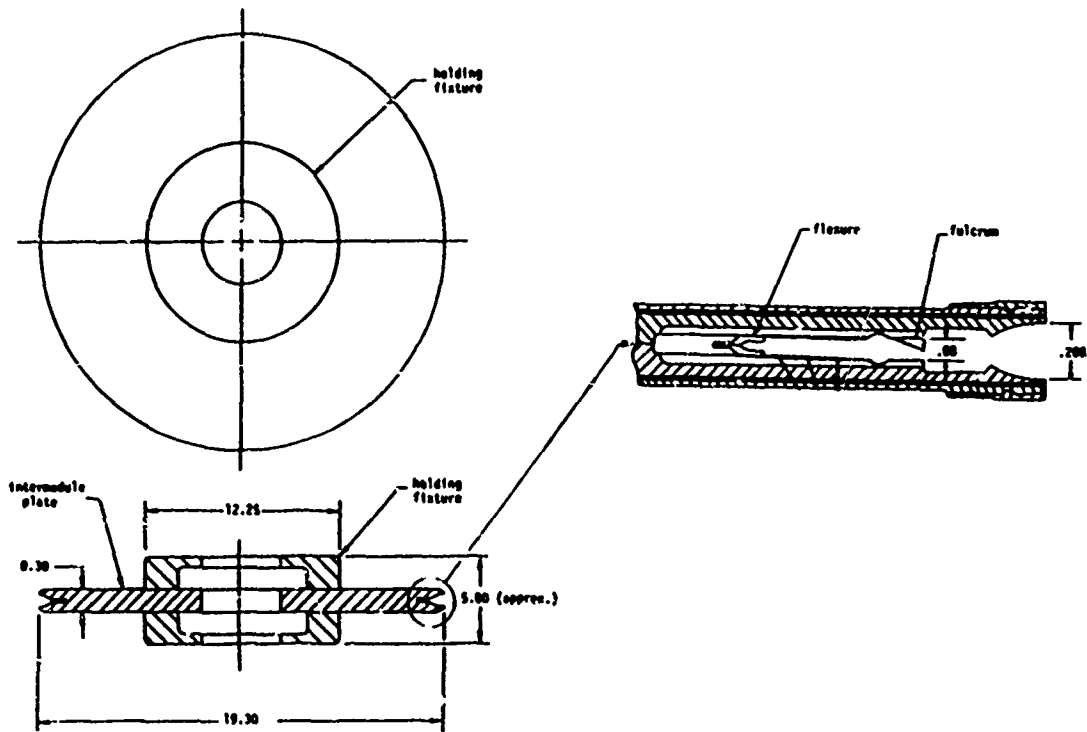


Figure 6.2.9.1. - Plan and cross-sectional views of intermodule plate in holding fixture for experimental modal testing (not to scale).

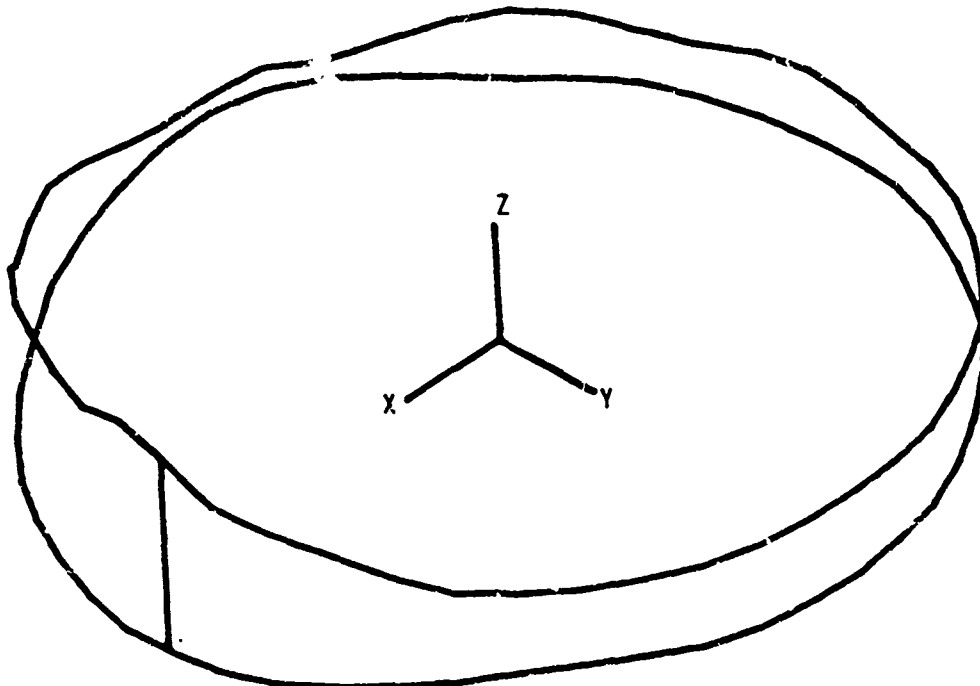


Figure 6.2.9.2. - First out-of-phase mode at 2140 Hz.

range is found to be 75°F (24°C) to 400°F (204°C), while the survivability temperature range is 75°F (24°C) to 650°F (343°C).

II. Analysis

a) A damping design concept is determined. Practical considerations dictate an O-ring of damping material inserted into the cavity formed by the plate lips (Figure 6.2.9.3).

b) A NASTRAN finite element model is developed (see Volume I, Section 5) to evaluate and optimize the O-ring damper. The plate model is a 10.21 degree azimuthal sector of one of the two lips (Figure 6.2.9.4) consisting entirely of solid (HEXA and PENTA) elements. The model is constrained axially and circumferentially to suppress all but the out-of-phase lip bending modes. The modulus of elasticity is decreased and density increased to tune the model frequency to match the experimental frequency (2146 Hz). The O-ring model, composed of HEXA elements, is then added to the plate model (Figure 6.2.9.5). The O-ring is modeled to retain its cross-sectional area under deformation.

c) Normal mode (natural frequency) finite element analyses are performed (see Volume I, Section 5) to determine the maximum allowable stiffness (shear modulus) of the O-ring. System requirements dictate that the maximum increase in static stiffness due to the O-ring is 10 percent. The analyses showed that this maximum limit is obtained for an O-ring shear modulus of approximately 500 psi.

d) An appropriate damping material is selected. The requirements are a static shear modulus of 500 psi ($3.45 \times 10^6 \text{ N/m}^2$) at 75°F (24°C), highest possible damping from 2000 Hz to 3000 Hz, significant damping from 75°F (24°C) to 400°F (204°C), and short-term survivability to 650°F (343°C). A fluorosilicone rubber (Down Corning LS-63) is identified which possesses these properties (see Figure 6.2.9.6).

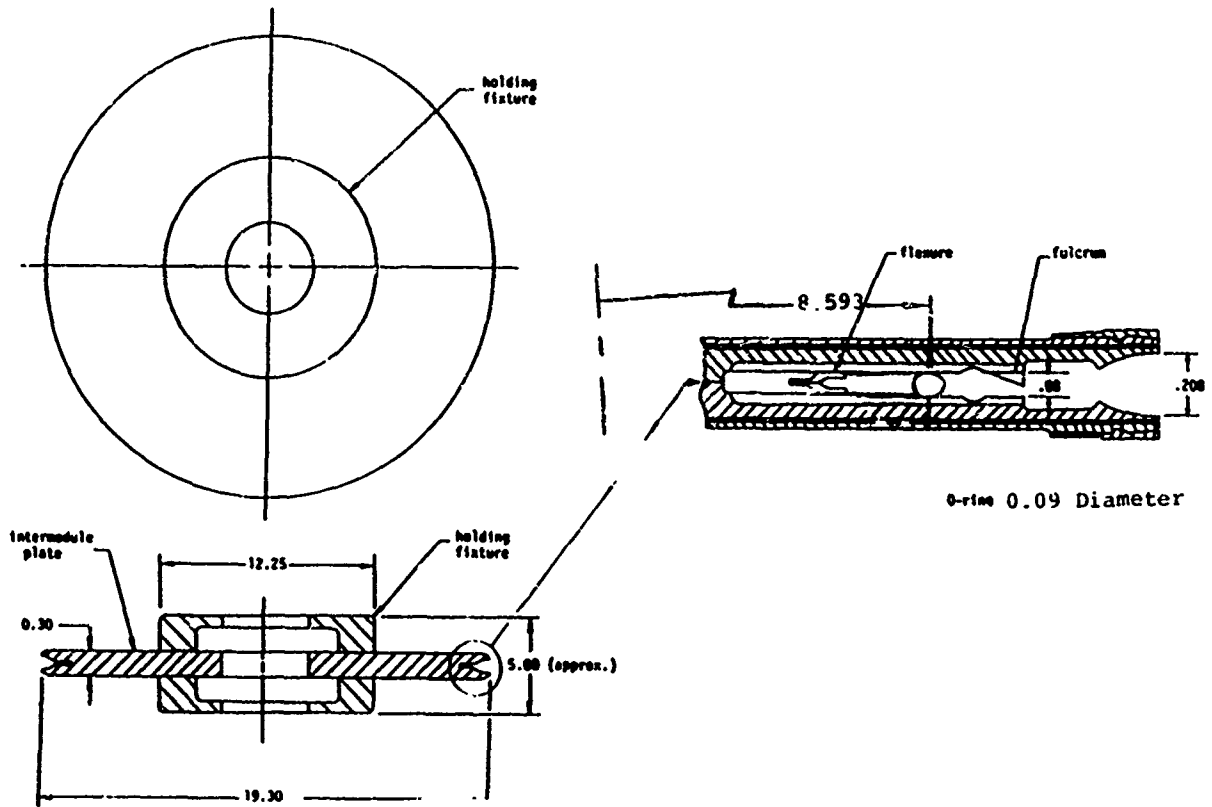


Figure 6.2.9.3. - Plan and cross-sectional views of intermodule plate with O-ring in holding fixture for experimental modal analysis (not to scale).



Figure 6.2.9.4. - NASTRAN model of undamped plate.

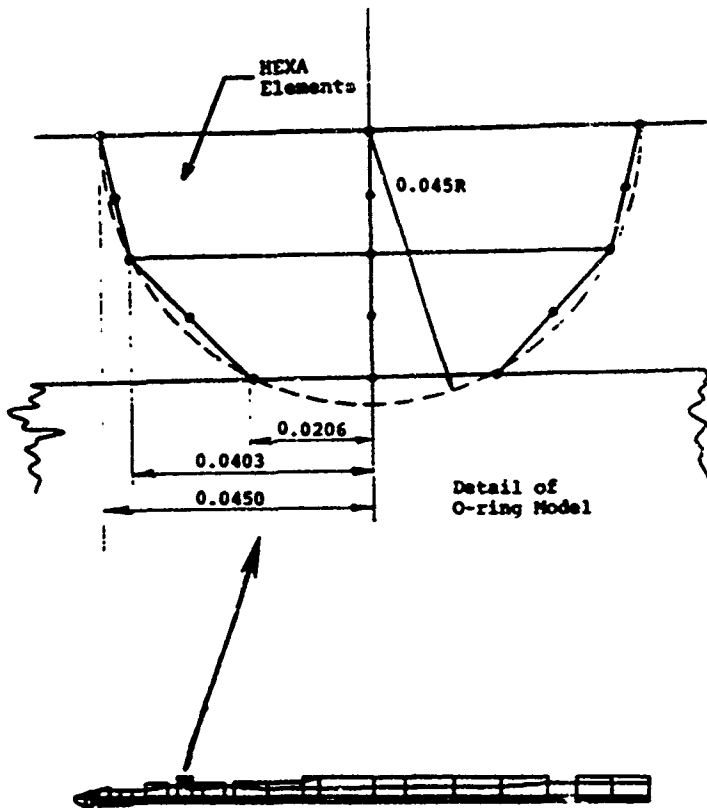


Figure 6.2.9.5. - NASTRAN model of plate with O-ring damper.

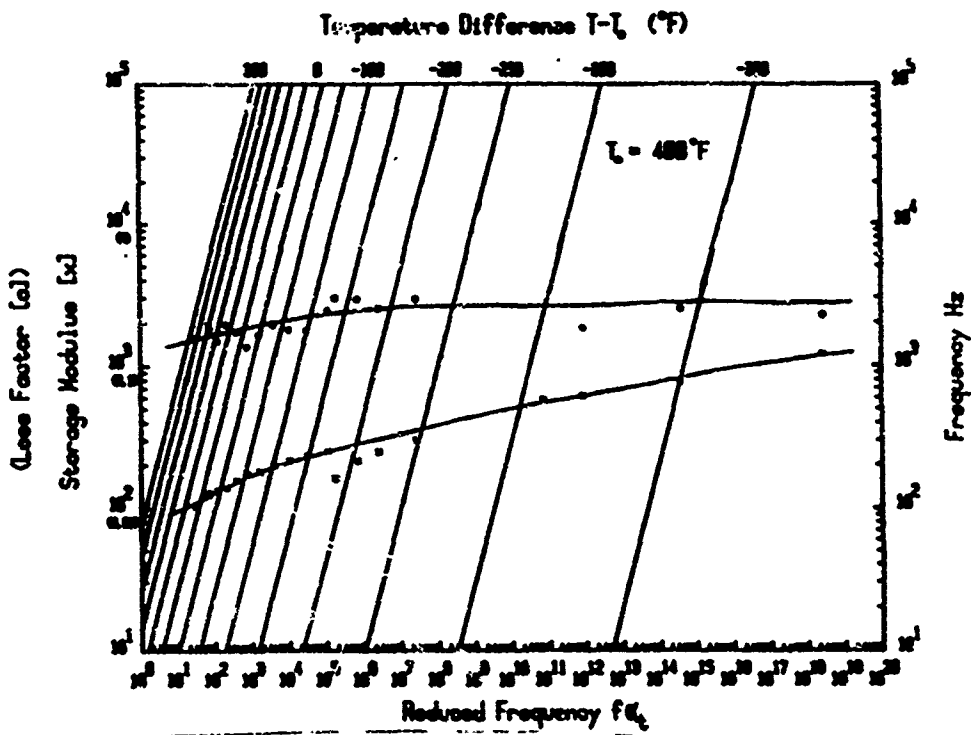


Figure 6.2.9.6. - Damping properties of O-ring (Dow Corning IS-63) material.

e) Damping material properties are incorporated in the finite element model and the system damping is determined at various temperatures and frequencies. The modal strain energy method is used with the normal modes analysis to compute structural loss factor. From the MSE method, (see Volume I, Section 5),

$$\begin{aligned} \eta_{\text{structure}} &= \frac{\text{Total Strain Energy Dissipated}}{\text{Total Strain Energy in Structure}} \\ &= \frac{\sum (\eta_i V_i)}{\sum V_i} \end{aligned} \quad (6.3)$$

where

η_i = loss factor of *i*th element

V_i = strain energy in *i*th element

Figure 6.2.9.7 is a summary of the results. A system loss factor of at least 0.01 was required to prevent flutter. The analyses showed the system loss factor to range from 0.012 to 0.043 through a 75°F (24°C) to 400°F (204°C) temperature range.

f) The finite element analyses results are verified by experimental modal analysis of an actual damped plate. Excellent correlation of system damping is obtained at the two verification temperatures 75°F (24°C), 200°F (93°C), as shown in Figure 6.2.9.7.

g) Practical considerations include:

- 1) Ease of fabrication, which rules out a damping treatment consisting of a high temperature viscoelastic plus constraining layer;
- 2) Static stiffness limitations, which rules out filling the lip cavity with damping material and limits the static shear modulus of the O-ring treatment to 500 psi ($3.45 \times 10^6 \text{ N/m}^2$), and
- 3) Weight restrictions, which dictates only minimal increases in the assembly weight.

III. Results

a) The final design is shown in Figure 6.2.9.3.

b) Experimental modal analysis and finite element normal mode analysis show the loss factor of the damped intermodule plate to be 0.012 to 0.048 over the entire temperature range of interest, exceeding the system loss factor of 0.01 needed to prevent flutter. Figure 6.2.7.6 is a summary of the findings.

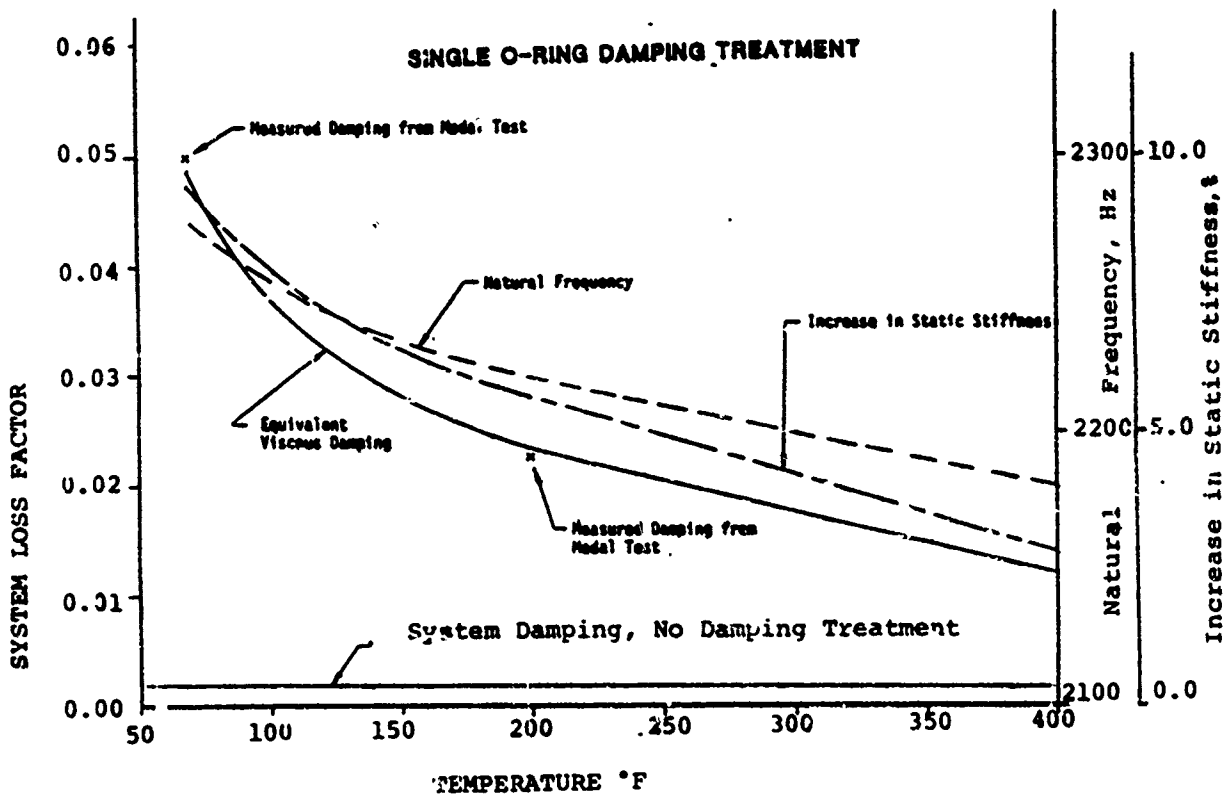


Figure 6.2.9.7. - Properties of the intermodule plate with single O-ring damper.

6.3 CASE HISTORIES

The following case histories describe various problems which have been solved through the use of damping technology.

6.3.1 B-52 TRU 82/A Pitot-Static Tube Damper [6.23]

Problem

High-cycle fatigue cracking occurred in the TRU 82/A pitot-static tube assembly used on B-52H aircraft. The failures are attributed to resonance vibration induced by turbulent boundary layer airflow over the assembly and adjacent fuselage skin.

Structure

The pitot-static tube assembly consists of a beryllium copper casting carrying pressure lines through the fuselage skin from the pitot and static ports to the aircraft's airspeed and altitude transducers. The assembly supports the tube and their ports outside the turbulent boundary layer flow near the fuselage skin. The assembly is supported by a mounting ring which attaches to a reinforced skin area with six screws threaded into nutplates (see Figures 6.3.1.1 and 6.3.1.2). The assembly contains appropriate anti-icing heaters for the ports and tubes.

Undamped Structure Response

Failures were occurring near the mount ring at the root of the cantilevered structure. Flight test strain gage and accelerometer data shows that first bending mode resonance vibration of the cantilevered assembly at 94 Hz exceeds the endurance limit of the structure because of a stress concentration at the failure location. A typical frequency response plot of a flight test data segment is shown in Figure 6.3.1.3.

Damping Treatment Development

The flight test data shows a constant ratio of strain at the failure location to acceleration at a selected acceleration mounting site. Accelerometer data from that site is used to assess the effectiveness of proposed



Figure 6.3.1.1. - Instrumented pitot-static tube mounted to aircraft.



Figure 6.3.1.2. - View of pitot-static tube mount inside aircraft.

damping treatments studied in laboratory tests of a TRU 82/A assembly and suitable mount structure attached to an electromagnet shaker. The damping treatment selected consisted of two 0.006-inch (0.152-mm) thick layers of elastomeric damping material, one applied to each side of the plastic seal used between the mount ring and the fuselage skin, as shown in Figure 6.3.1.4.

Damped Structure Response

A comparison of the damped to undamped structure response is shown in Table 6.3.1.1. Reduction of the stress level at the failure location is accomplished to the extent that uncracked assemblies do not crack and that the crack growth rate is reduced in structures with existing cracks.

6.3.2 Aircraft Fuselage Damper [6.24]

Problem

The possibility for sonic fatigue of the aft fuselage structure of the B-1 aircraft existed. The potential cause of the fatigue is high sound pressure levels (exceeding 168 dB) resulting from the jet engines.

Structure

The basic construction consists of titanium skin stiffened by perpendicular frames, with the inside frame caps interconnected by straps. Figure 6.3.2.1 illustrates the structure.

Undamped Structure Response

Figure 6.3.2.2 shows a typical transfer function for the structure, revealing high modal density between 250 Hz and 300 Hz. Figure 6.3.2.3 shows a few of the modes present, plotted with the undeformed geometry.

Damping Treatments

Both constrained layer treatments and tuned dampers are successfully used in a room-temperature environment. The constrained layer treatments are multilayered, with each layer consisting of 0.002-inch (0.051-mm) thick 3M ISD-112 and 0.005-inch (0.127-mm) thick aluminum backing. The tuned

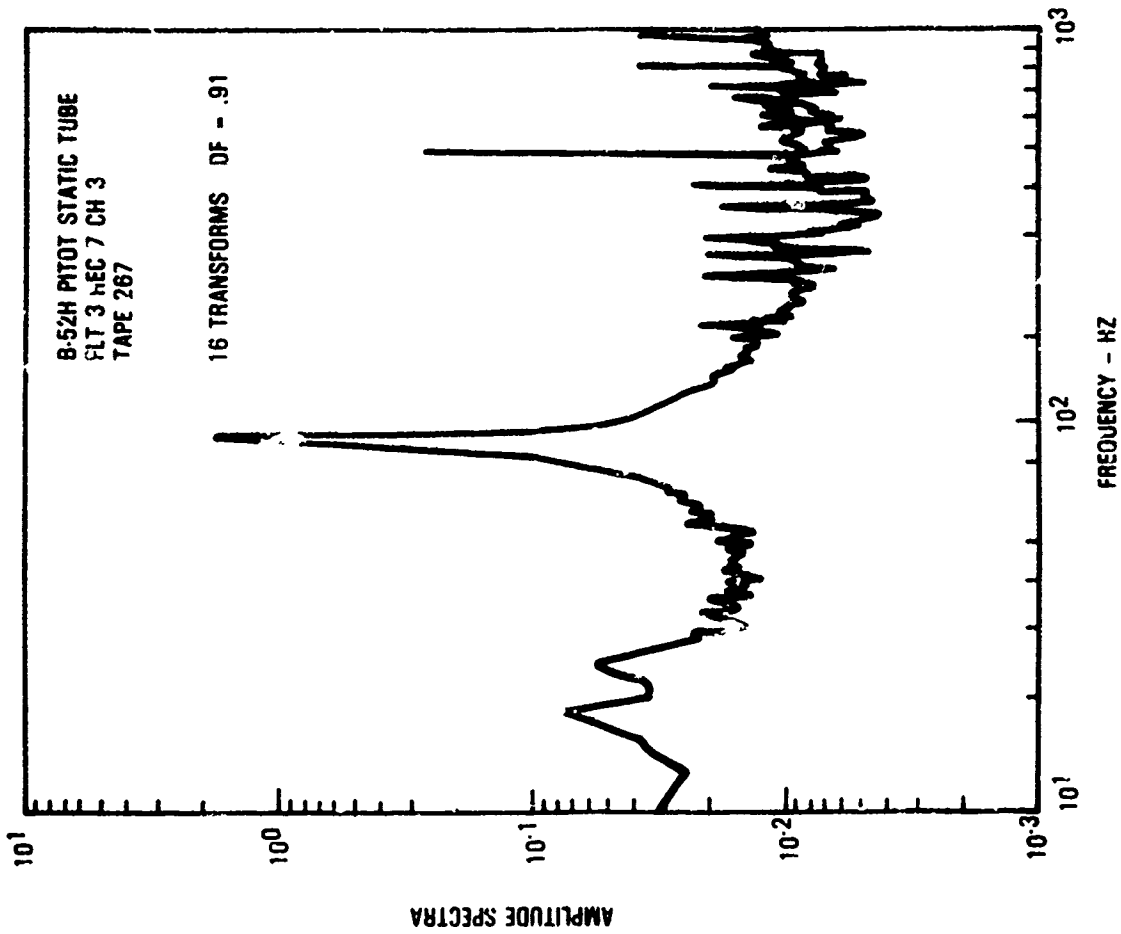


Figure 6.3.1.3. - Typical response plot obtained from flight test data.

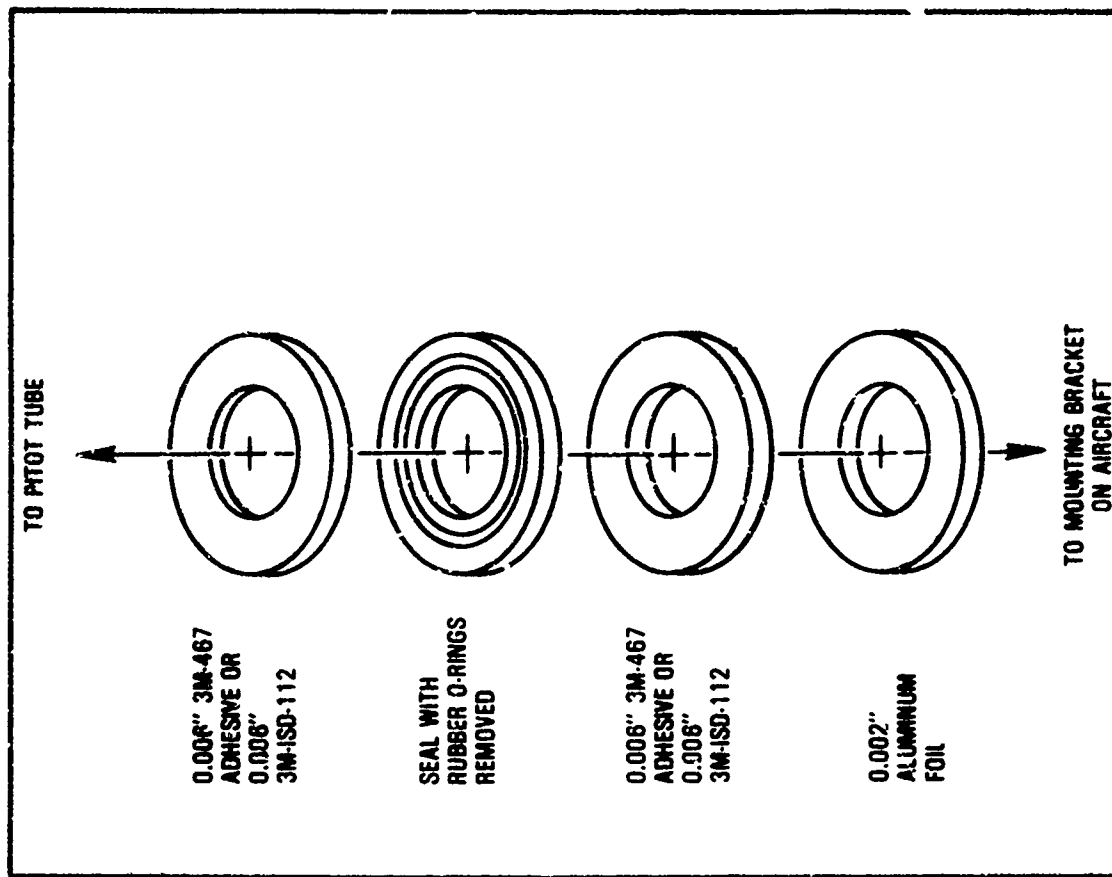


Figure 6.3.1.4. - Exploded view of damping fix assembly to control fatigue failures of the B-52H AIMS TRU pitot tube.

TABLE 6.3.1.1. LABORATORY TEST DATA

Pitot Tube Configuration	Input at Base (G's RMS)	Horizontal Acc. of Bracket (G's RMS)	Vertical Acc. on Cannon Plug (G's RMS)	Resonant Freq. (Hz)	Loss Factor (Ms)	Maximum Normal Stress	Maximum Shear Stress
1972 Production	0.1	1.2	1.9	85.1	0.007	4096	1758
Model - No Damping	0.2	2.25	3.8	84.9	---	6226	2462
Treatment-Rosette	0.3	3.2	5.5	85.2	0.007	9889	4789
Strain Gage	0.4	3.9	6.9	85.0	0.008	11675	5604
	0.5	4.6	8.4	84.9	0.008	13519	6234
	1.0	7.5	15.0	84.4	0.011	21264	10153
1972 Production	0.1	0.23	0.88	84.1	0.067	1175	477
Model with Damping	0.2	0.41	1.3	84.0	0.038	1855	744
Fix - Rosette	0.3	0.56	1.75	83.9	0.036	2674	1156
Strain Gage	0.4	0.71	2.2	83.7	0.036	3180	1267
	0.5	0.85	2.65	83.6	0.038	3702	1517
	1.0	1.5	4.8	82.6	0.039	6279	2636

dampers are single degree-of-freedom spring-mass systems with Dow Corning fluorosilicone sealant as the viscoelastic spring (see Figure 6.3.2.4). The resonance frequency is designed to be 280 Hz, which corresponds to one of the structural resonances. The tuned dampers are positioned as shown in Figure 6.3.2.5. Table 6.3.2.1 is a compilation of the damping treatment configurations and their locations.

Damped Structure Response

Table 6.3.2.2 presents the changes in maximum resonance amplitude due to each treatment. The constrained layer treatment applied to the skin and frame proved to be the most effective treatment in terms of reducing amplitude at resonance.

6.3.3 Boeing 747 Upper Deck Noise Suppression Damper [6.25]

Problem

During flight, excessive noise was occurring in the upperdeck passenger cabin of the Boeing 747 aircraft. Resonant vibration of the fuselage skin

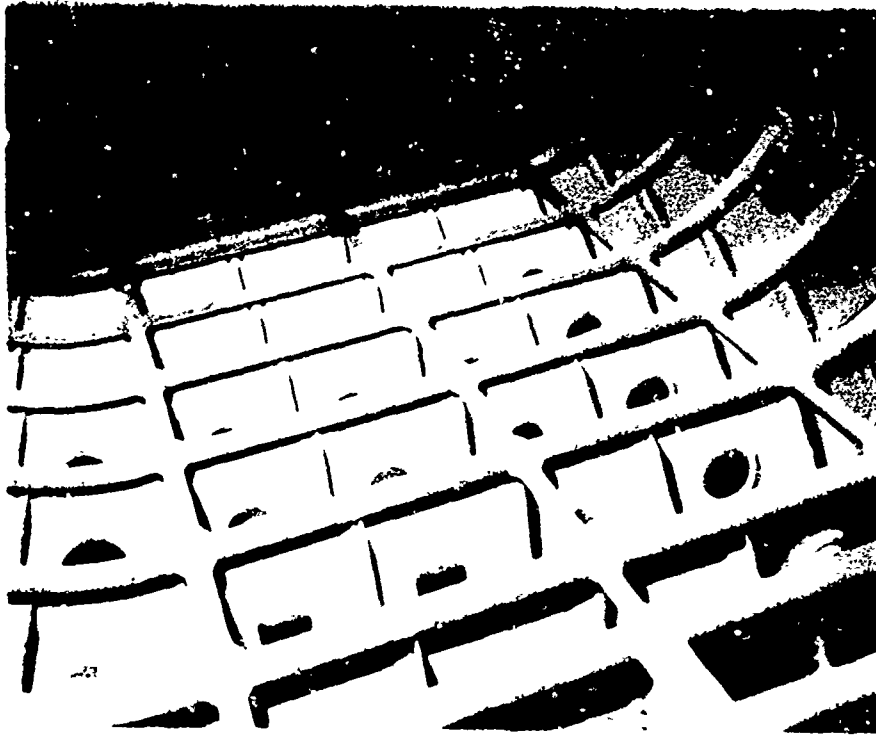


Figure 6.3.2.1. - Internal view of test specimen.

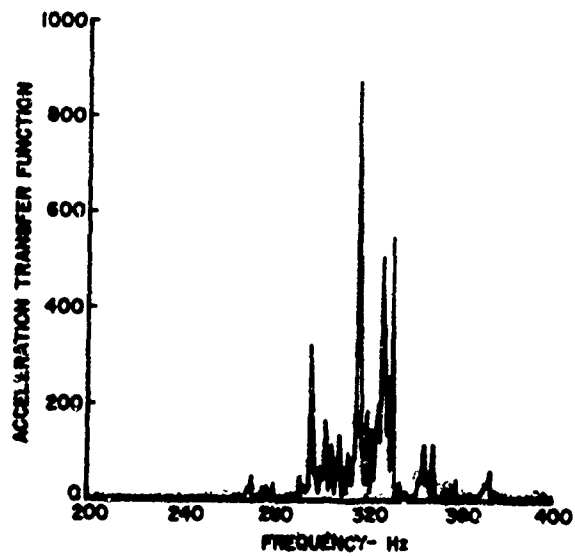
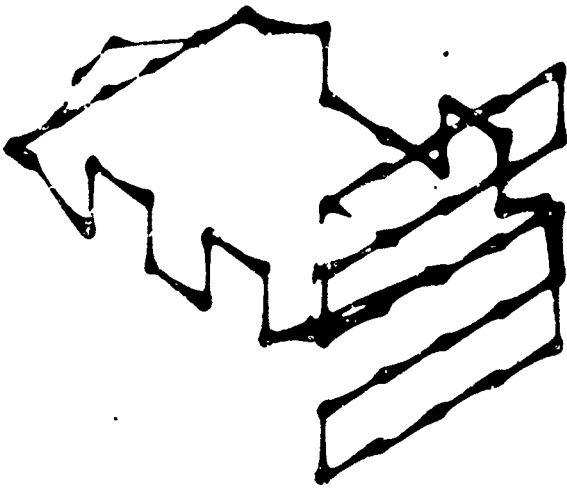


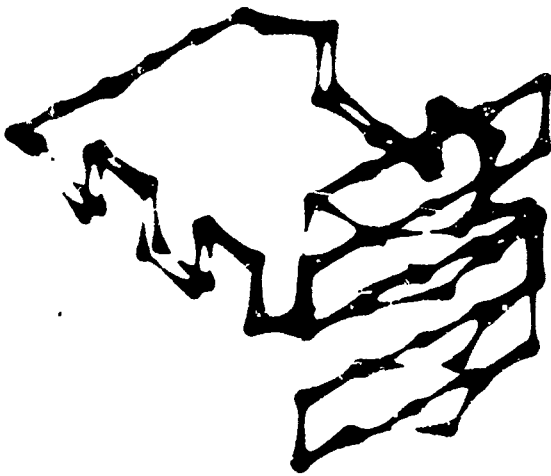
Figure 6.3.2.2. - Undamped transfer function.



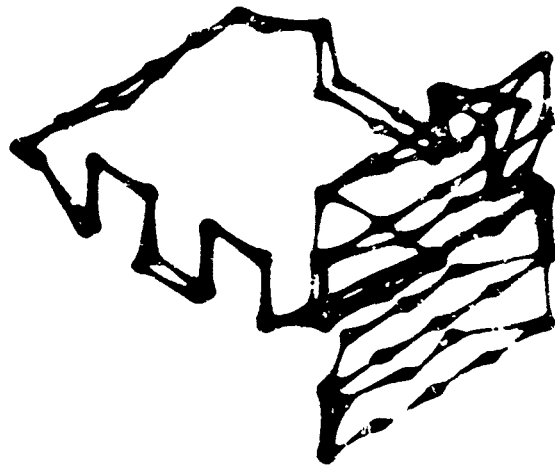
First Bending Mode of the Strap at 237 Hz



Edge View of Skin and Strap Mode at 295 Hz



Mode Shape at 295 Hz



Mode Shape at 354 Hz

Figure 6.3.2.3. - Structure mode shapes.

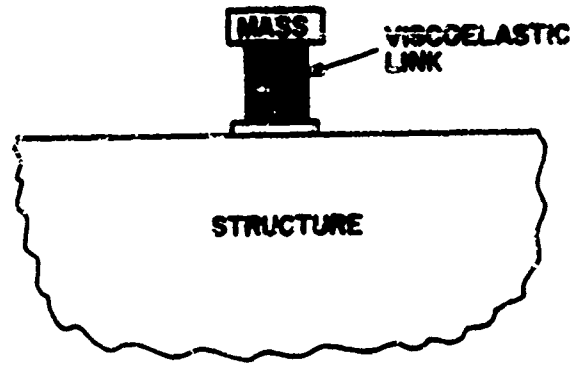


Figure 6.3.2.4. - Configuration of damping treatments applied.

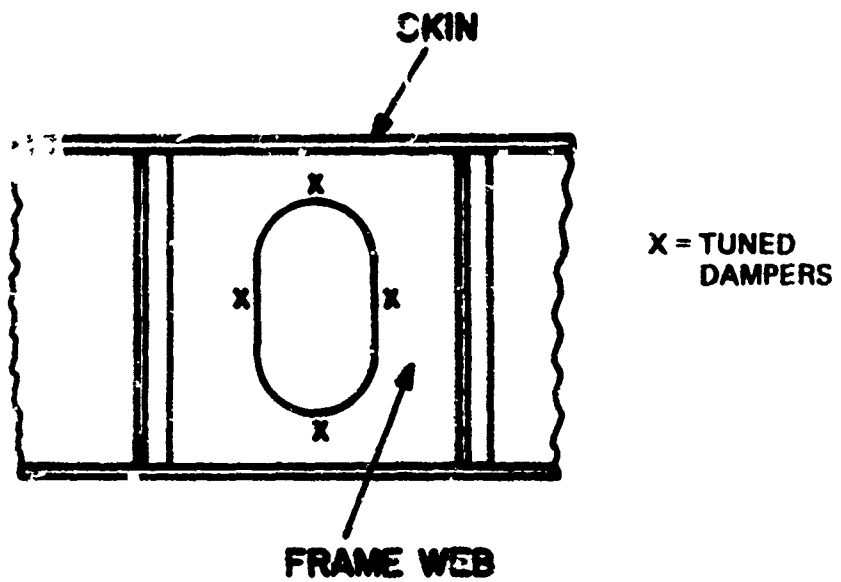


Figure 6.3.2.5. - Placement of tuned dampers.

TABLE 6.3.2.1. TYPES OF DAMPING TREATMENTS AND THE PART OF STRUCTURE TO WHICH IT IS APPLIED

Treatment No.	Type of Treatment and Part of Structure to Which it is Applied
0	Undamped
1	Six layers of the constrained layer treatment applied to frame web only
2	Three layers of the constrained layer treatment applied to skin panels and adjacent to web
3	Six layers of the constrained layer treatment applied to frame web and adjacent skin panels
4	Four tuned dampers applied to the frame web. (See Figure 6.3.2.5 for location on frame.)

TABLE 6.3.2.2. TREATMENT NUMBER AND PEAK TRANSFER FUNCTION RESULTS

Location of Pickup	Treatment Number* and Relative Amplitude of Maximum Peak in Transfer Function Below 350 Hz				
Skin	0-320	1-112	2-63	3-11	4-90
Skin	0-650	1-118	2-20	3-11	4-540
Frame	0-1400	1-100	2-520	3-110	4-500

*See Table 6.3.2.1

(due to randomly varying pressure waves caused by the turbulent boundary layer surrounding the fuselage) is responsible for the high noise levels.

Structure

The structure consists of thin aluminum skin reinforced by interconnecting longitudinal stringers and circumferential frames, as shown in Figure 6.3.3.1.

Undamped Response

Figure 6.3.3.2 shows the resonant vibration spectrum of the fuselage skin along with the corresponding cabin noise spectrum. Major resonant peaks of the structure occur at 335 Hz, 490 Hz, and 630 Hz, coinciding exactly with the major noise peaks. Figure 6.3.3.3 illustrates the shapes of the three problem modes, revealing them to be low-order plate bending modes.

Damping Treatments

Two layers of 3M Y436 Sound Damping Tape are applied to the inside fuselage skin. Modal testing showed only slight damping of the modes of interest, with significant damping for frequencies of 700 Hz and greater. The modes of interest are not damped since the damping tape is not designed for the dynamics of the fuselage structure.

The final damping treatment chosen appears in Figure 6.3.3.4. Two Kevlar I-beam constraining layers are bonded to one layer of 3M Y436 damping tape on each skin panel using 3M ISD-113.

The high bending stiffness of the beam constraining layers causes thickness as well as shear deformation of the 3M ISD-113 and the damping tape viscoelastic material (see Figure 6.3.3.5). Damping of low-order modes, such as the modes of interest, is therefore significantly enhanced.

Damped Response

Figure 6.3.3.6 shows that large reductions in the response of the modes of interest are obtained. The corresponding cabin noise levels are comparable to those that had been obtained with a system of stiffness weighing nearly 150 percent more than the beam damper system (see Figure 6.3.3.7).

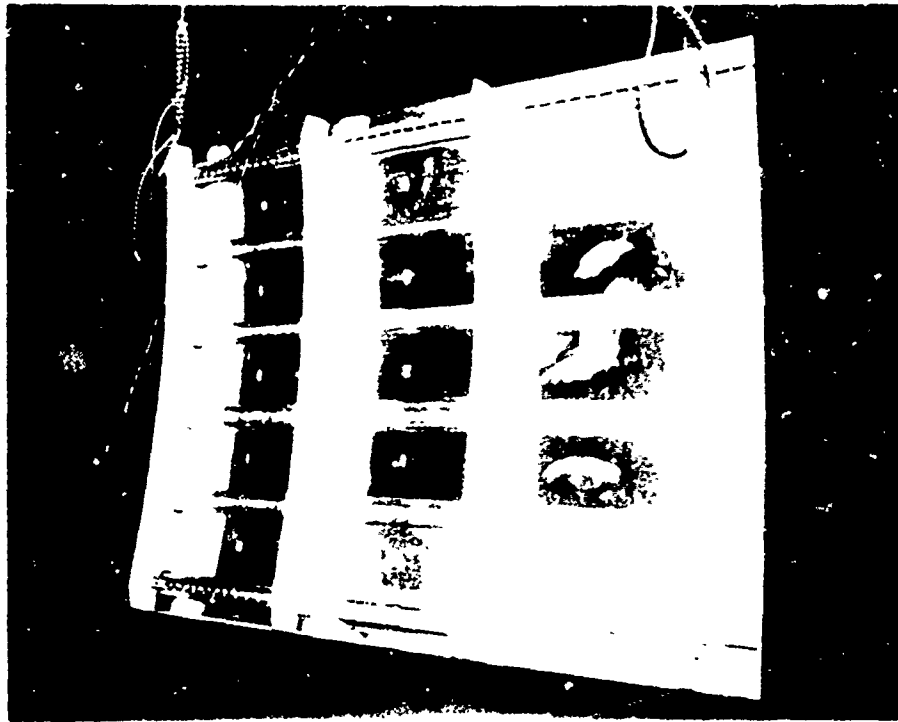


Figure 6.3.3.1. - Fuselage skin panel structure.

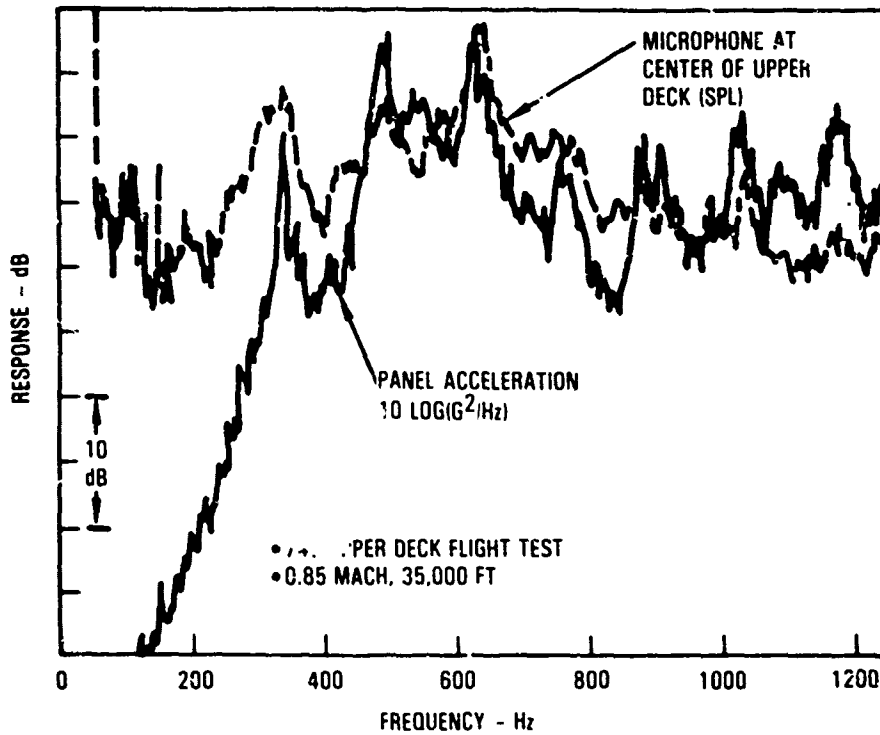


Figure 6.3.3.2. - Comparison of skin panel response and cabin sound pressure.



Figure 6.3.3.3. - Skin panel mode shapes.

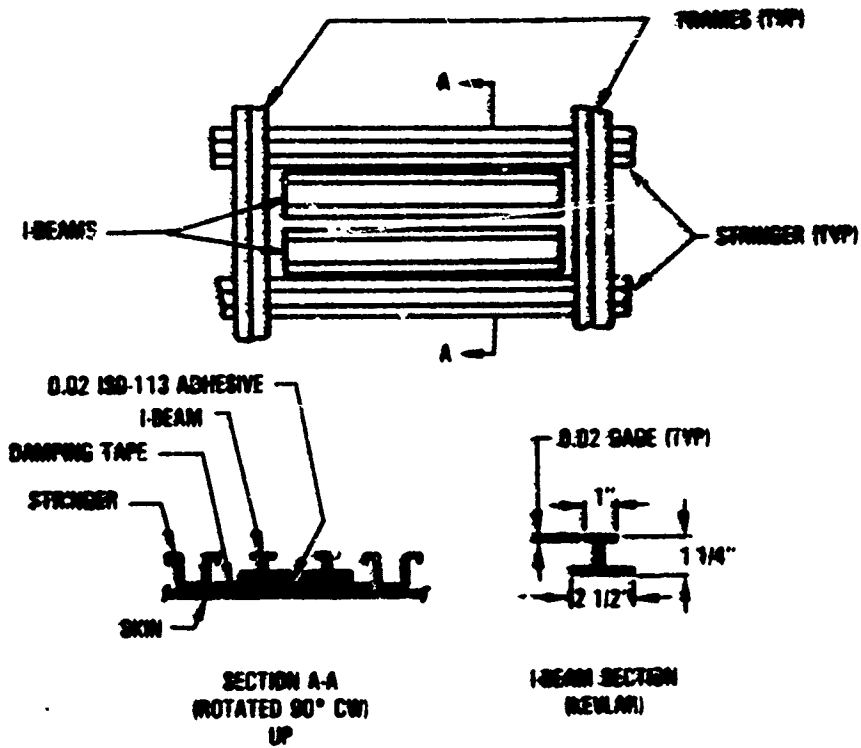


Figure 6.3.3.4. - Damping treatment configuration.

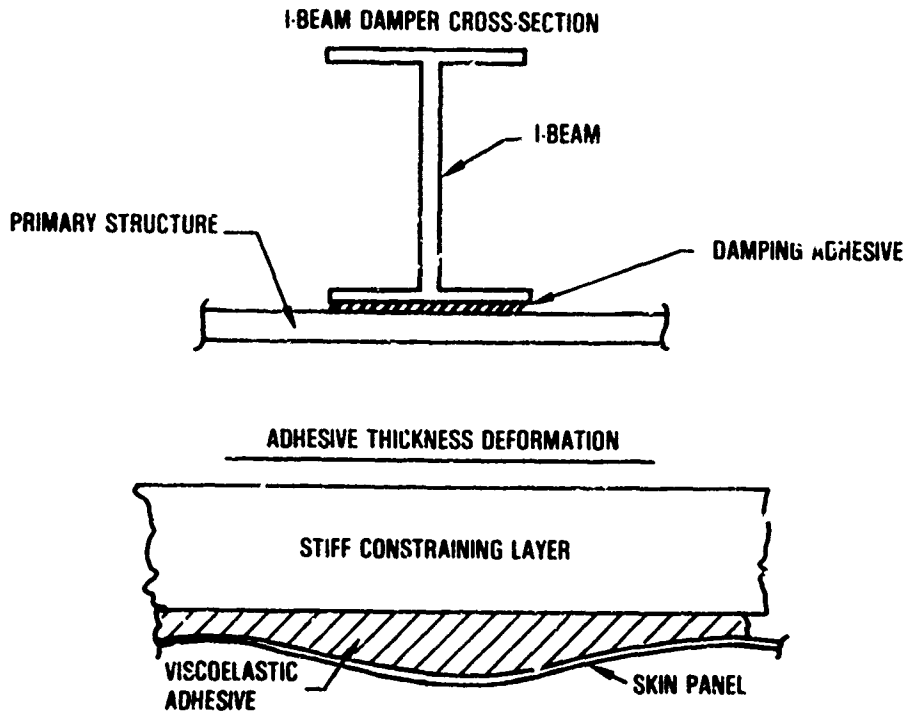


Figure 6.3.3.5. - Thickness deformation in stiff constrained layer dampers.

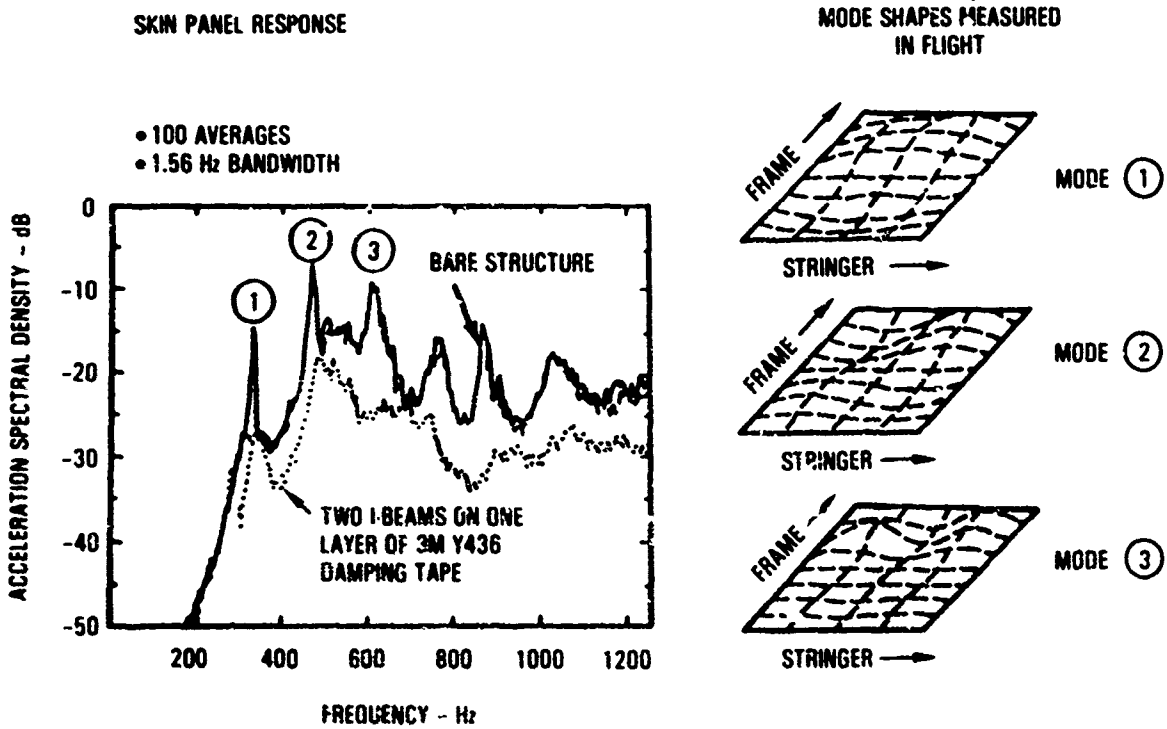


Figure 6.3.3.6. - Effect of beam damping system on structure frequency response.

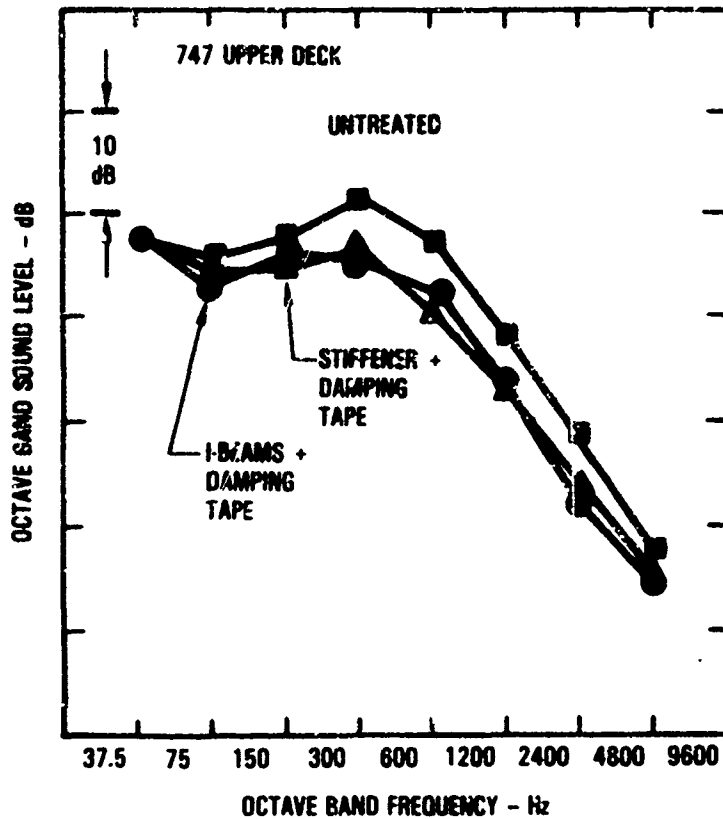


Figure 6.3.3.7. - Effect of beam damping system on cabin noise levels.

6.3.4 Distribution Manifold Damper

Problem

Analytical data indicated a high cycle fatigue problem in the distribution manifold of a laser system. The manifold is being excited by combustor instabilities which generates pressure gradients in the frequency and wavelength range which match the resonances in the manifold.

Structure

The manifold is shown in Figure 6.3.4.1. The circular portion is nine inches (228.6 mm) in diameter and the actual manifold length is 90 inches (2286 mm). The manifold is made from INCOL 903.

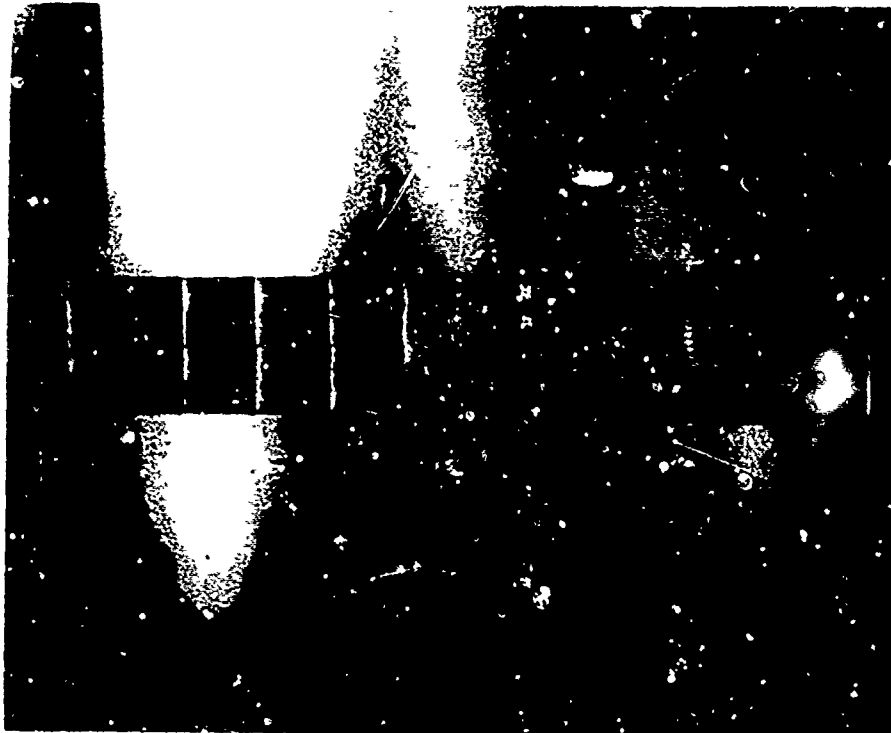
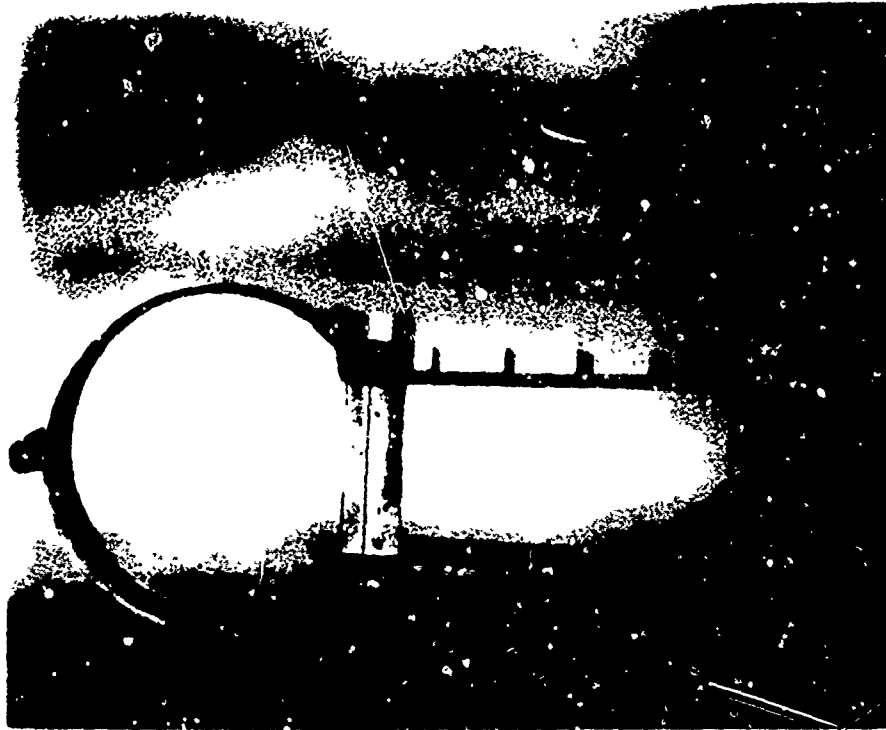


Figure 6.3.4.1. - Section of distribution manifold.

Undamped Structural Response

The resonant modes of concern are in the frequency range of 300 Hz to 4000 Hz. The mode at approximately 3300 Hz is of particular interest. Table 6.3.4.1 lists the specific modes and their amplification factors, Q . The general displacements for all the modes are plate-like in nature which lend themselves to good layered damping designs.

Damping Design

The operational temperature of the manifold was 64°F (17.8°C) due to internal cooling flow. Fourth order plate analysis shows that sufficient damping can be obtained from an 0.002-inch (0.051-mm) thick layer of ISD-112 with an 0.050-inch (1.27-mm) thick aluminum constraining layer. The 0.050-inch (1.27-mm) thick aluminum layer is difficult to apply to the manifold. The modified design consists of five layers of both 0.002-inch (0.051-mm) thick ISD-112 and 0.010-inch (0.254-mm) thick aluminum. The combined function of the five layer treatment is approximately the same as the single layered 0.050-inch (1.27-mm) thick aluminum treatment.

Damped Structure Response

The Q of the modes is reduced an average of about 50 percent. The damped data is shown in Table 6.3.4.2.

Operational Data

The damping design reduced the operational stresses and no failures occurred. In limited operation, no durability problem is evident; however, getting a good bond between the substrate and the damping material is difficult.

6.3.5 Engine Mount Ring Tuned Damping [5.26]

Problem

High cycle fatigue cracks occurred on a jet engine mounting ring. The excitation forces are engine caused vibrations exciting the lower frequency resonant modes of the mount ring.

TABLE 6.3.4.1. UNDAMPED MODAL FREQUENCIES AMPLIFICATION FACTORS

Frequency (Hz)	Amplification Factor, Q
374	134
403	152
903	110
1172	168
1396	134
3515	126
4325	103

TABLE 6.3.4.2. DAMPED MODAL FREQUENCIES AND AMPLIFICATION FACTORS

Frequency (Hz)	Amplification Factor, Q
374	64
403	95
871	58
1172	93
1368	70
3436	48
4299	75

Structure

The engine mount ring is a one piece metal structure shown in Figure 6.3.5.1. It is approximately four feet (1219 mm) in diameter. Figure 6.3.5.2 illustrates the mount ring's location on the engine.

Undamped Structural Response

Figure 6.3.5.3 shows the undamped response of the mount ring. The primary modes of interest are those up to 200 Hz. The mode shapes are typical of the lower order modes of circular plate with a hole cut in the middle. All the modes have deformation patterns which are amenable to layered damping treatments. The three primary modes also produce strain patterns which can account for the crack patterns which are occurring.

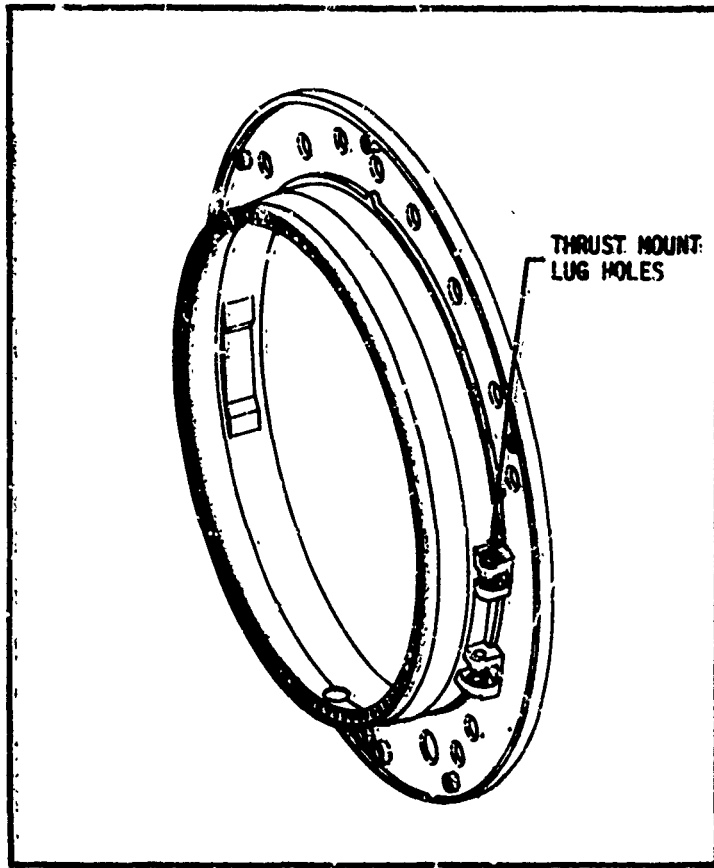


Figure 6.3.5.1. - Mount ring.

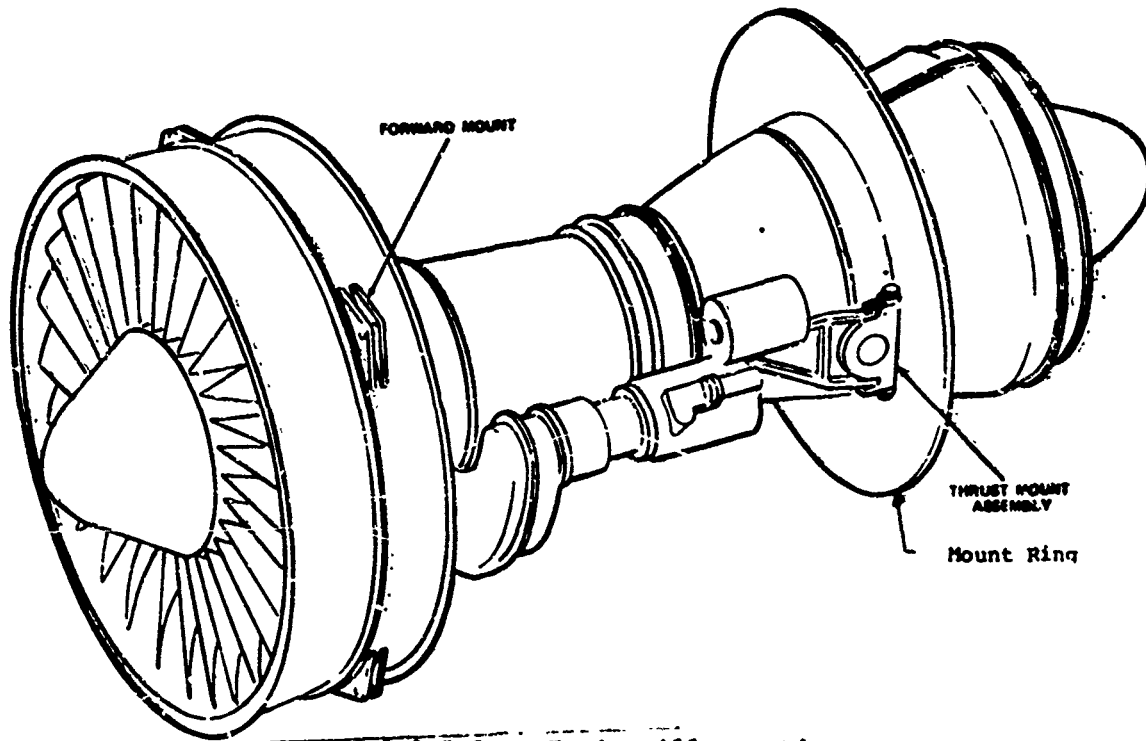


Figure 6.3.5.2. - Engine illustration.

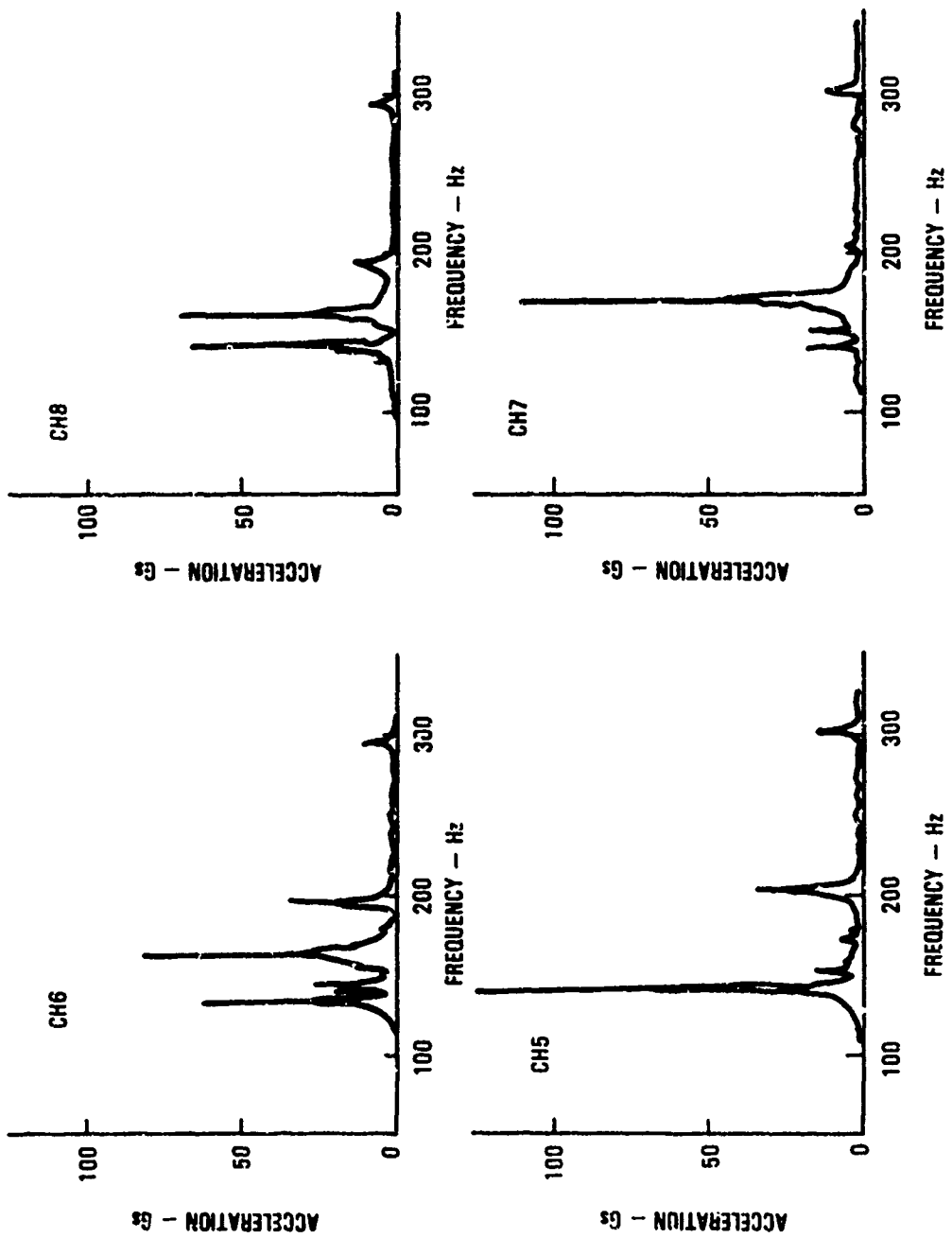


Figure 6.3.5.3. - Typical undamped acceleration response of mount ring to 0.5 g's input.

Damping Design

The operational temperature of the mount ring is 150°F (66°C) to 300°F (149°C), which is in the range of layered damping materials. Unfortunately, the survival temperature is 650°F (343°C) which no current layered damping material can survive while providing damping in the 150°F (66°C) to 300°F (149°C) range. A functional solution is the use of tuned dampers. There are materials which can function as the damped spring at temperatures between 150°F (66°C) and 300°F (149°C) and survive 650°F (343°C). To prove the concept, tuned dampers are designed to operate at room temperature. The design methods are discussed in Volume I, Section 3. Once the concept is proven, it remains to define the proper material for operational use.

Damped Structure Response

The placement of the tuned dampers on the mount ring is illustrated in Figure 6.3.5.4. Note that the size of the tuned dampers is larger than true scale for clarity. Figure 6.3.5.5 shows the damped response of the mount ring. Comparison of Figure 6.3.5.5 and Figure 6.3.5.3 demonstrates an order of magnitude reduction in the dynamic response of the mount ring as a result of placing five tuned dampers on the structure.

6.3.6 Design of a Damped Acoustic Enclosure [6.27]

Problem

High levels of structural vibration can cause failures within electronic packages of experiments carried on board the Space Shuttle. Such vibrations may be encountered because of the high level noise (greater than 145 dB) from the rocket engines, which are in close proximity to the payload bay. As an alternative to modifying the payload bay or the payloads themselves, this investigation is performed to evaluate small acoustic enclosures to protect the experiments.

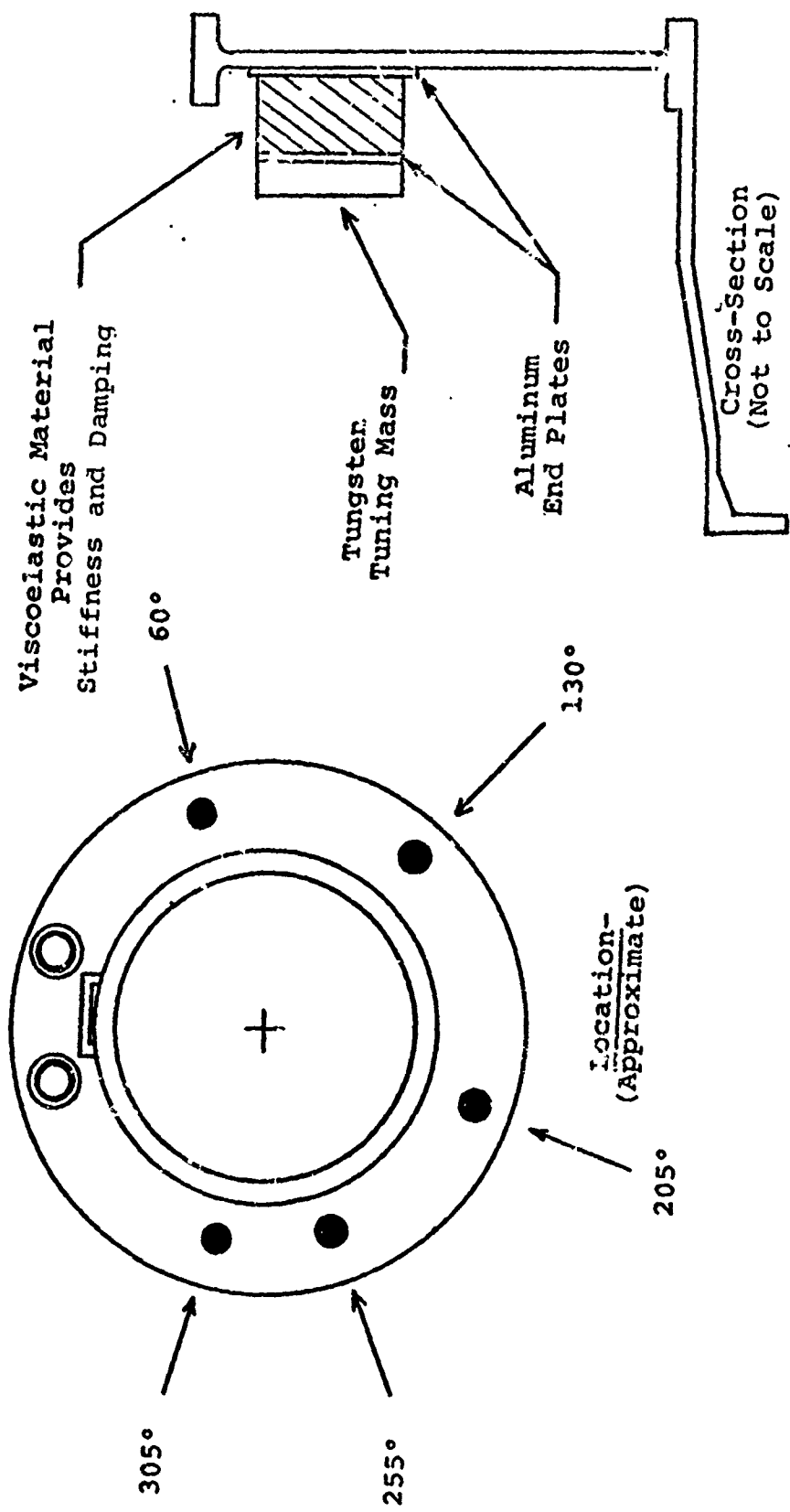


Figure 6.3.5.4. - Sketch of mount ring illustrating how and where the tuned viscoelastic damper units are attached.

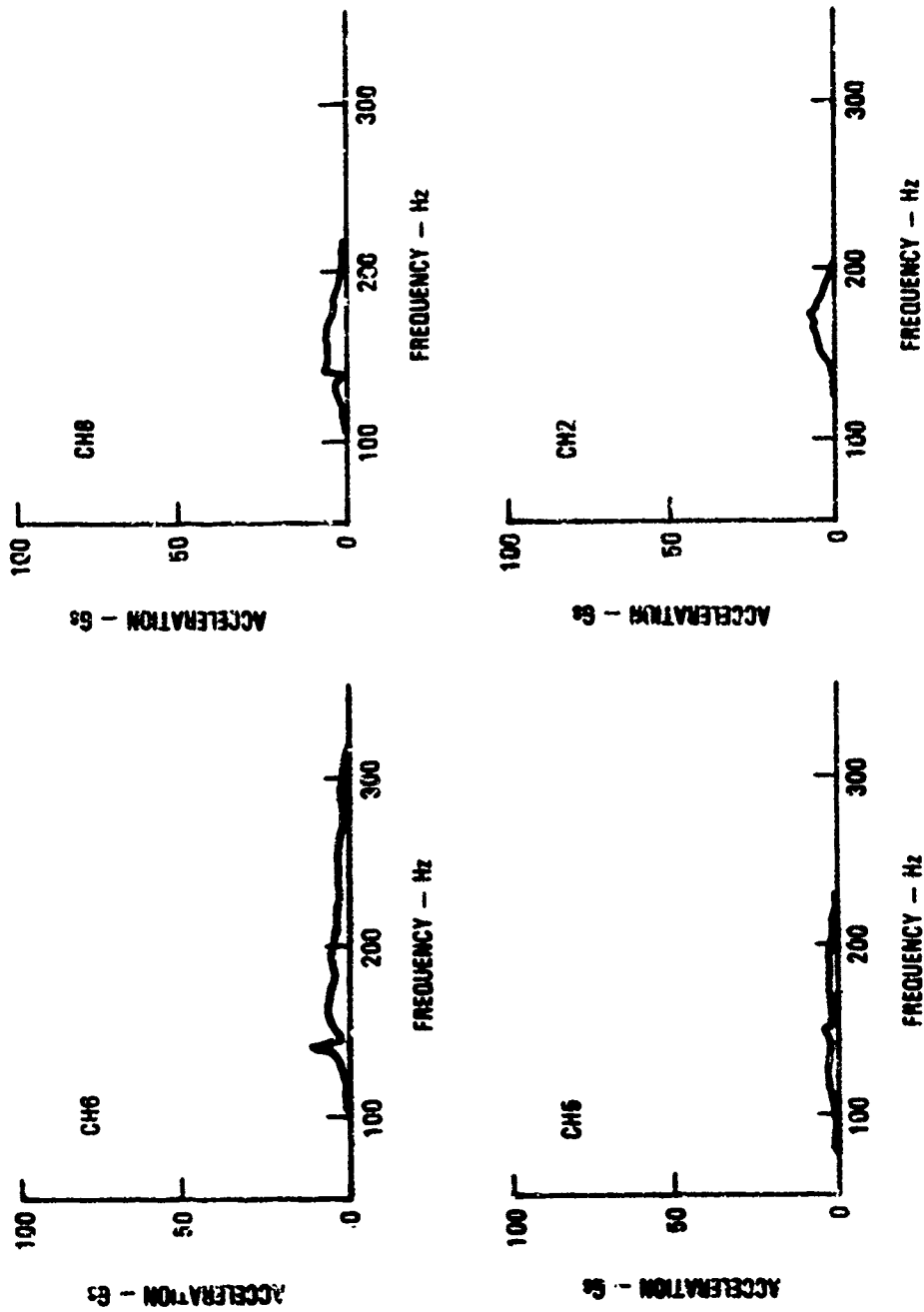


Figure 6.3.5.5. - Typical damped acceleration response of mount ring to 0.5 g's input.

Structure

The basic enclosure is a double-sheathed capped cylinder, three-feet (914.4 mm) in diameter and length. The walls and bulkheads are formed from strong, light-weight materials such as aluminum, magnesium, or graphite composite. An interconnecting series of frames and stringers joins the inner and outer walls together, providing lightweight, stiff construction.

Undamped Response

Little damping would be present in such a construction and little acoustic attenuation would be achieved. No specific results are available since only the damped configuration is analyzed and tested.

Damping Treatments

In the low frequency range (less than 500 Hz for the configuration under consideration), the noise transmitted into the enclosure can be significantly decreased if the enclosure is very stiff and highly damped. High damping viscoelastic epoxy materials (SMRD) provide these desired properties for the temperature and frequency ranges of interest. The stringers and frames are fashioned from the SMRD. The test enclosure consists of 0.020-inch (0.508-mm) thick aluminum wall sheets joined by 0.25-inch (6.35-mm) by 0.5-inch (12.7-mm) SMRD stringers and frames on 5-inch (127-mm) centers. In addition, wedges of SMRD are joined to the conical shaped bulkheads on 15-degree centers. A fiberglass liner is inserted to prevent reverberation inside the enclosure.

Damped Response

Computer analysis of the damped enclosure indicates a minimum resonant frequency of 500 Hz with a corresponding loss factor of 0.66. Figure 6.3.6.1 shows the predicted and actual (from acoustic chamber testing) noise reduction for an external sound pressure level of 150 dB. The overall noise reduction is 18 to 29 dB, with as much as 30 to 40 dB at frequencies below 125 Hz. This reduction represents over an order of magnitude reduction in acoustic pressures. Vibration levels on the enclosure walls range from 20 to 70 μ rms.

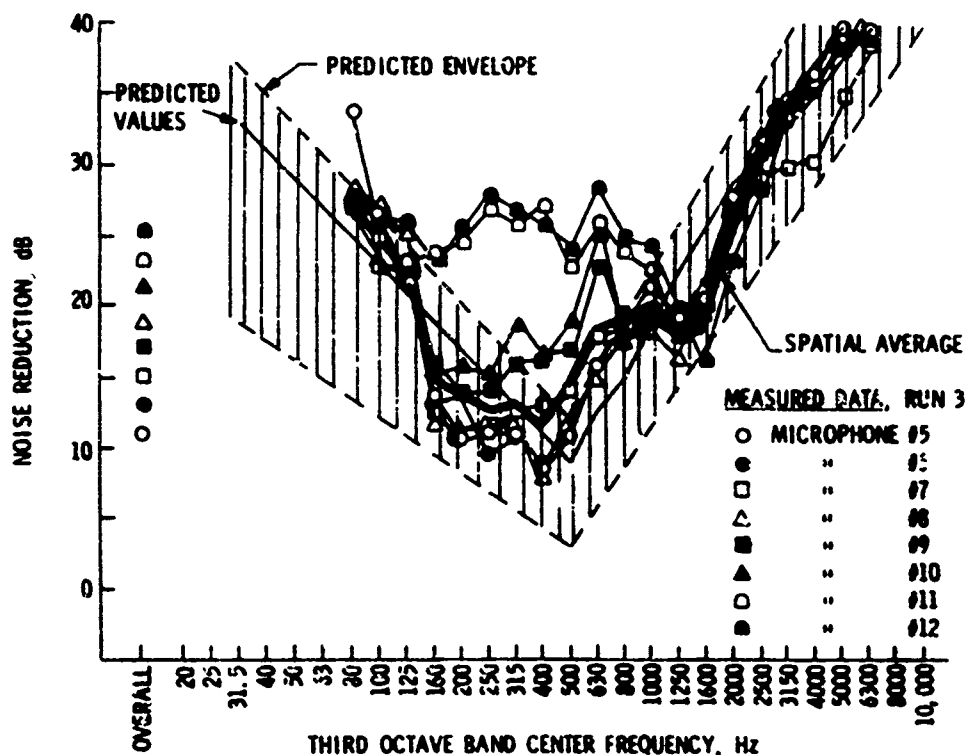


Figure 6.3.6.1. - Acoustic cover, measured noise reduction comparison to predicted values, with acoustic liner (OA external SPL = 150 dB).

6.3.7 Printed Wiring Board Damper No. 1 [6.28]

Problem

Structural or electrical failure of a printed wiring board (PWB) onboard a spacecraft occurred when resonance is induced in the board by vibrations transmitted from the booster engines.

Structure

The PWB is a 0.063-inch (1.6-mm) thick rectangular plate 7.5 inches (191 mm) by 7.5 inches (191 mm), on which electrical wiring and electronic components are attached. The PWB is mounted in the chassis.

Undamped Response

The first mode of vibration of the PWB occurs at 65 Hz with an amplification factor, Q , of approximately 35. This mode is independent of the chassis response.

Damping Treatment

The basic treatment consists of a 0.094-inch (2.4-mm) thick strip of viscoelastic material with or without a 0.315-inch (0.8-mm) thick graphite-epoxy constraining layer strip. The viscoelastic material is chosen to provide maximum damping in the operational temperature range of the PWB. The constrained layer strips are arranged in cruciform fashion on the PWB to correspond with the locations of maximum deflection and/or strain of the first mode of vibration. This includes a strip on the connector area to suppress rocking modes. The use of strips rather than sheets of damping treatment add appreciable damping to the PWB without covering the entire surface, which would hinder modification and maintenance.

Damped Response

Figure 6.3.7.1 shows that the damping treatment shifts the frequency of the first mode to 115 Hz and reduces the amplification at resonance by a factor of 7 (from $Q = 35$ to $Q = 5$).

Field Survivability Evaluation

No failures have been encountered during qualification testing at 12.5 g rms.

6.3.8 Printed Wiring Board Damper No. 2 [6.28]

Problem

Resonant vibration of a spacecraft printed wiring board (PWB) caused structural or electrical failure. Resonance resulted from engine vibrations transmitted to the PWB.

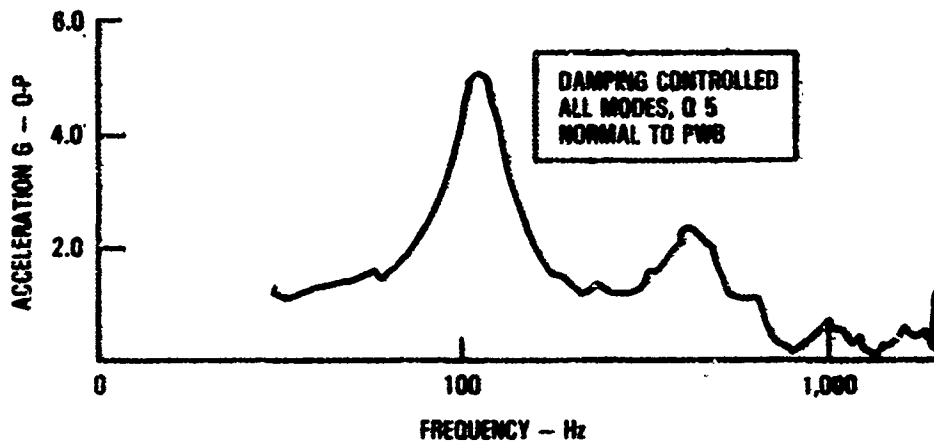


Figure 6.3.7.1. - Worst PWB response to Y-sweep.

Structure

The PWB is a very thin rectangular 3.5-inch (89-mm) by 4.6-inch (117-mm) panel upon which wiring and electronic components are attached.

Undamped Response

Figure 6.3.8.1 shows the undamped response of the PWB, both measured and predicted, using a flat plate response prediction program. Two major resonances are apparent between 0 and 1000 Hz, with the first mode having a frequency of 165 Hz and an amplification factor, Q , of 22.

Damping Treatments

Several damping treatments of various configurations are tried. The basic treatment consists of a 0.031-inch (0.8-mm) thick graphite-epoxy constraining layer strip bonded to a 0.094-inch (2.4-mm) thick viscoelastic damping material strip. The strips are placed in different locations on the PWB as shown in Table 6.3.8.1. The use of strips allows for appreciable additive damping without covering the structure, which would inhibit maintenance and modification.

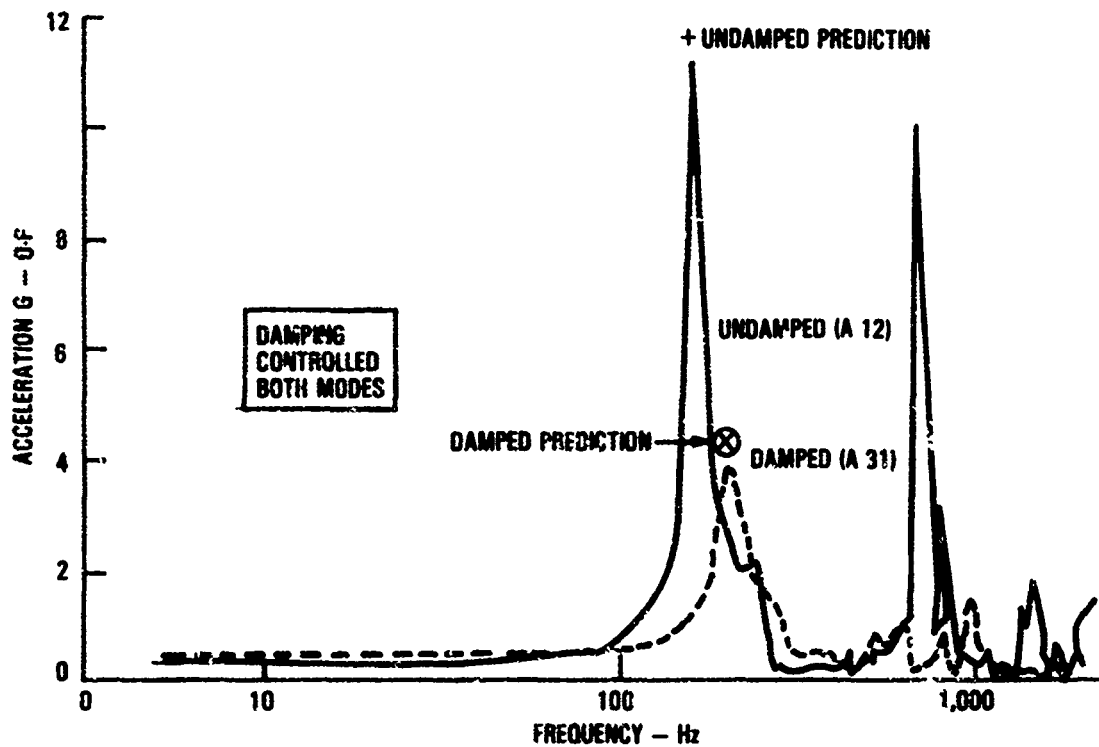
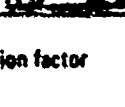


Figure 6.3.8.1. - Effect of edge strip on sine vibration response.

TABLE 6.3.8.1. SUMMARY OF PREDICTION AND MEASUREMENTS

Article A

Board	Configuration	Sine				Comment
		Predicted		Measured		
		f*	Q**	f*	Q**	Predictions by Single Degree-of-Freedom Theory
A-12	Undamped 	100-200	30	165	22	First Mode Good; Higher Mode Uncontrolled
A-31		165-258	8.7 - 7.95	200	7.6	Good
A-14		209-297	8.3 - 7.4	240	6.8	First Mode Good; Higher Mode Poorly Controlled
A-13		258-305	7.95 - 6.25	285	8.2	Good
A-32		205-284	5.6 - 5.3	220	7.2	First Mode Good; Higher Mode Uncontrolled Edge Strip Too Stiff to Participate in 2nd Mode

*Frequency
**Amplification factor

Damped Response

Figure 6.3.8.1 shows a typical response function for the A-31 damped configuration along with the undamped response. Table 6.3.8.1 summarizes the first mode responses for the various damping configurations. Amplitude at resonance is reduced by a factor of three for each of the configurations. Configurations A-31, A-14, A-13 also suppressed the second mode. However, due to the excessive stiffness of the edge strip and the shape of the second mode of vibration, configuration A-32 could not control the second mode.

Field Survivability Evaluation

The percentage of failures encountered during qualification testing at 25 g rms is reduced from about 40 percent to less than 10 percent.

6.3.9 Vibration Damping Compound as a Means to Reduce Steel Noise Barrier Cost [6.29]

Problem

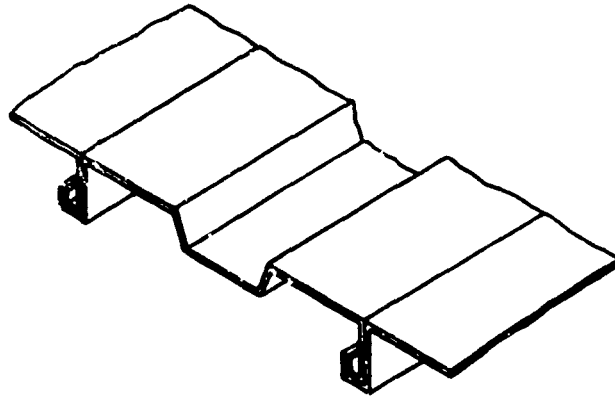
This study is performed to investigate the feasibility of reducing the costs associated with the construction of highway noise barriers through the use of thin steel panels coated with a viscoelastic damping material.

Structure

The highway noise barriers are formed steel panels, Figure 6.3.9.1, which are situated along congested highways near residential or business areas. The panels used in this study are 0.035-inch (0.138-mm) thick galvanized steel with both faces coated with silicone alkyd, 0.001-inch (0.025-mm) thick.

Undamped Structural Response

Table 6.3.9.1 shows the sound transmission loss (dB) as a function of frequency. The traffic noise frequency that most influences the sound level is 2000 hertz.



DIMENSIONS IN MM

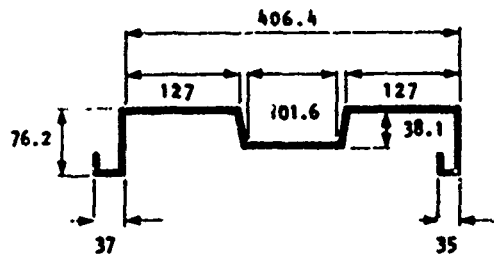


Figure 6.3.9.1. - Profile of the panel tested (WRT-168, ARMC0, Canada).

TABLE 6.3.9.1. TRANSMISSION LOSS (TL) OF THE SAMPLE WITH AND WITHOUT DAMPING COMPOUND (AQUAPLAS)

Frequency (kHz)	0.125	0.160	0.200	0.250	0.315	0.400	0.500	0.630	0.800	1	1.25	1.6	2	2.5	3.14	4	STC*
TL "with" (dB)	19	17	16	17	21	22	25	27	30	30	34	32	32	35	37	40	29
TL "without" (dB)	19	17	15	17	19	20	23	26	28	27	32	27	26	30	30	37	26
TL increment (dB)	0	0	1	0	2	2	2	1	2	3	2	5	6	5	7	3	3

*Sound Transmission Class - See Ref. 6.29

Damping Treatments

The damping compound used is Aquaplas DL10 from Blackford Ltd. The compound is applied at a surface density of 0.52 lb/ft² (2.54 kg/m²).

Damped Structural Response

The damped response is also shown in Table 6.3.9.1. At 2000 Hertz the transmission loss is 32 dB with the damping treatment applied, and 26 dB without the damping treatment applied. Figure 6.3.9.2 illustrates the reduction in sound level (dB) over a frequency range of 200 to 2000 hertz. The noise recorded at the edge of the pavement of a large highway is 97.6 dB(A). For a barrier without damping it is reduced to 63.2 dB(A); and for a barrier with damping it is reduced to 60.0 dB(A).

Conclusion

A cost analysis is provided showing that a savings between 7 and 23 percent could be realized by reducing the thickness of the steel barrier panel and coating the panel with a viscoelastic damping layer.

- A Typical A - weighted noise recorded at the edge of pavement of a large highway: 97.6 dB(A)
- B Through barrier noise obtained by subtraction of transmission loss spectrum of the barrier sample without damping: 63.2 dB(A)
- C Same as before with damping: 60.0 dB(A).

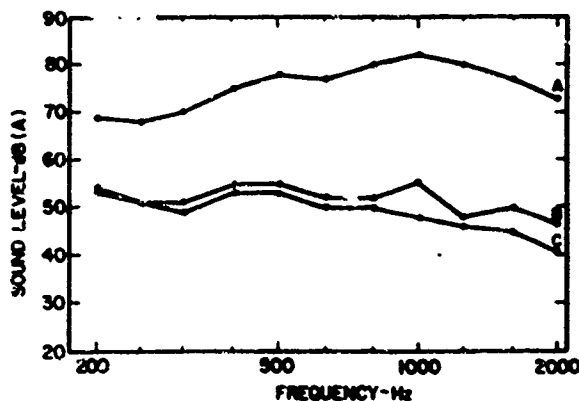


Figure 6.3.9.2. - Reduction of highway noise transmitted through a barrier with and without damping compound (Aquaplas).

6.3.10 Damping to Eliminate Rocket "Pogo" Problem [6.30]

Problem

The appearance of low frequency longitudinal vibrations during the initial stages of a rocket launching is commonly referred to as the "Pogo" effect. This phenomenon was observed during the first five launchings of the DIAMANT B satellite launch vehicle.

Structure

The structure enduring the "Pogo" effect is the 1st stage of the DIAMANT B launch vehicle. To examine the applicability of the viscoelastic damping treatment to the DIAMANT B launch vehicle, a suitable tank model is constructed which can simulate the "Pogo" effect. A 0.039-inch (1-mm) thick cylindrical tank, with a diameter of 34.6 inches (879 mm) and a length of 58.3 inches (1481 mm), is made of AG5 aluminum alloy. It is filled with water to simulate the liquid fuel.

Undamped Structural Response

The mode shapes of the tank are determined experimentally with point excitation. Strong radial mode coupling is obtained. Radial reinforcement is applied to the tank structure to reduce the effect of the radial modes. As a result, it is possible to obtain the longitudinal vibration mode in the desired frequency range.

Damping Treatment

The area to be treated with the viscoelastic material is the rear section of the tank. Two damping treatments are examined: a coating of Lord Manufacturing type L D 400 material, 0.063-inch (1.6-mm) thick, and a constrained layer treatment using a 0.02-inch (0.5-mm) thick Hoechst VP 71 damping layer with an 0.004-inch (0.1-mm) thick aluminum constraining layer.

Damped Structural Response

For the two damping treatments both pressure and displacement amplitudes are measured. The maximum dynamic pressure in the fluid at the modal frequency is reduced by 78 percent and 83 percent for the single damping layer and constrained layer, respectively. The ratio of radial to longitudinal displacement is reduced by 27 and 33 percent for the single damping layer and constrained layer, respectively. These results are shown on Figures 6.3.10.1 and 6.3.10.2. Damping of the actual DIAMANT B launched vehicle tank is extrapolated from the tank mock-up; and a single layer damping treatment is chosen for the launch test. Two DIAMANT B launchings took place on February 6, 1975 and May 17, 1975 with the damping treatments applied. The low frequency longitudinal vibration, "Pogo" effect, had successfully been eliminated.

Conclusion

The successful use of viscoelastic damping layers to reduce the high acceleration loading factors which occur during the "Pogo" phenomenon, eliminated the need to redesign the DIAMANT B satellite launch vehicle.

6.3.11 Damping for Rapid Transit Structures [6.31]

Problem

The noise radiated from rapid transit bridge structures has attracted recent attention. In this example the effect upon the noise level radiated from the box bridge girder are examined, when a viscoelastic damping layer is applied.

Structure

A low bridge girder is the main horizontal support of the rapid transit bridge. Two scale models of the bridge girder are evaluated. The first is an all concrete design, and the second is a composite steel/concrete design. A full scale composite steel/concrete bridge girder is also examined.

- NON-DAMPED TANK
- TANK DAMPED WITH LD 400
- TANK DAMPED WITH THICKNESS VP 71

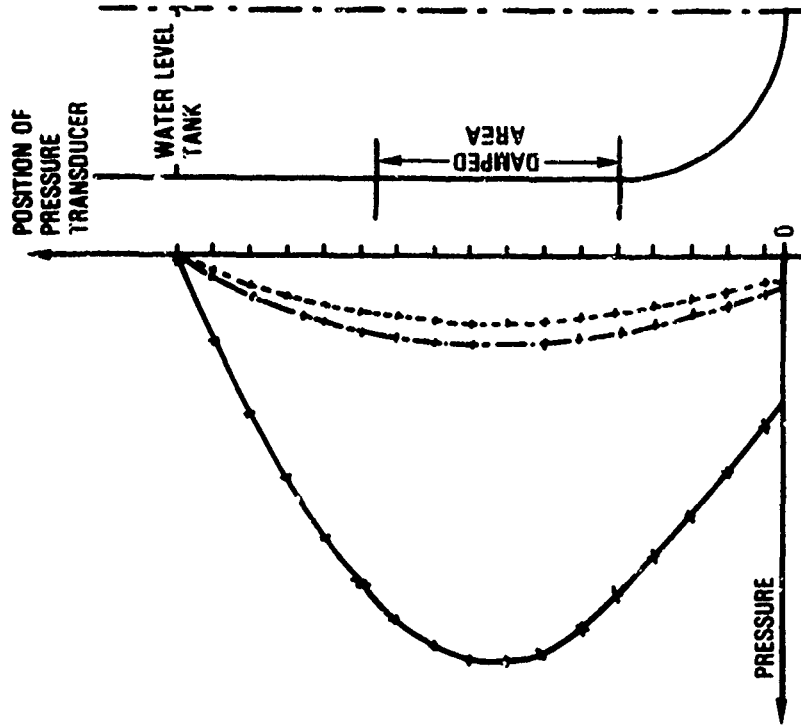
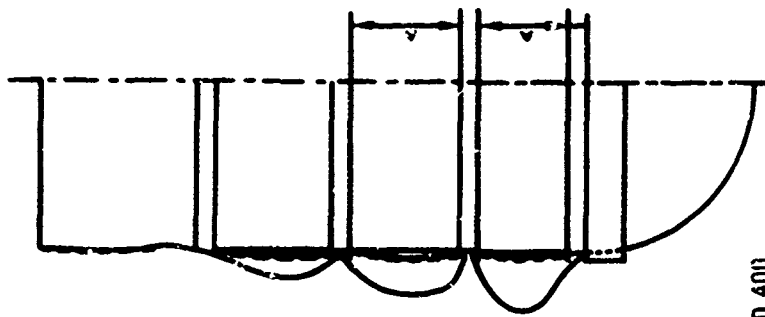


Figure 6.3.10.2. - Comparison of dynamic pressure in liquid with and without added damping.



LONGITUDINAL DISPLACEMENT IS NOT REPRESENTED
 VALUES ARE: 19.3 μ RAS FOR 1
 2.6 μ RAS FOR 2
 3.6 μ RAS FOR 3

10 μ RAS

- 1— NON-DAMPED
- 2, 3--- DAMPED WITH VP 71 AND LORD LD 400
- A : AREAS TREATED WITH VISCOELASTIC COATINGS

Figure 6.3.10.1 - Radial distortion of tank with and without added damping.

Undamped Structural Response

Noise levels (dB) as a function of excitation frequency are determined for the scale model of the concrete bridge girder having no prestressing, 575 psi ($3.96 \times 10^6 \text{ N/m}^2$) prestressing, and 1150 psi ($7.93 \times 10^6 \text{ N/m}^2$) prestressing. A peak noise level of 80 dB occurs at an excitation frequency of 1200 hertz for the 1500 psi ($1.03 \times 10^7 \text{ N/m}^2$) prestressed bridge girder. Lowering the magnitude of prestressing reduces the noise level at all excitation frequencies, see Figure 6.3.11.1. The noise level emitted from the scale model of the composite steel/concrete bridge girder, Figure 6.3.11.2, increased to a level higher than the 1150 psi ($7.93 \times 10^6 \text{ N/m}^2$) prestressed concrete bridge girder. The noise level emitted from the full scale composite steel/concrete bridge girder is shown in Figure 6.3.11.3.

Damping Treatments

The damping treatment applied to both the scale and full scale composite steel/concrete bridge girder consists of a viscoelastic material bonded to the steel portion of the bridge girder. The viscoelastic material used for the damping treatment has a loss factor of 0.4 and an elastic modulus of 1.45×10^6 psi ($1 \times 10^{10} \text{ N/m}^2$) over the frequency range of 100 to 4000 hertz.

Damped Structural Response

Noise level reductions of from 10 to 16 dB are observed for the scale model composite steel/concrete bridge girder. The damped noise level of the scale model decreased to that of the concrete bridge girder with no prestressing (Figures 6.3.11.1 and 6.3.11.2). For the full scale composite bridge girder the noise level is typically reduced by 12 to 26 dB as shown in Figure 6.3.11.3.

Conclusion

A composite steel/concrete bridge girder, which will need no prestressing, can effectively be used to construct rapid transit bridges without the addition of an excessive noise level to the surrounding environment.

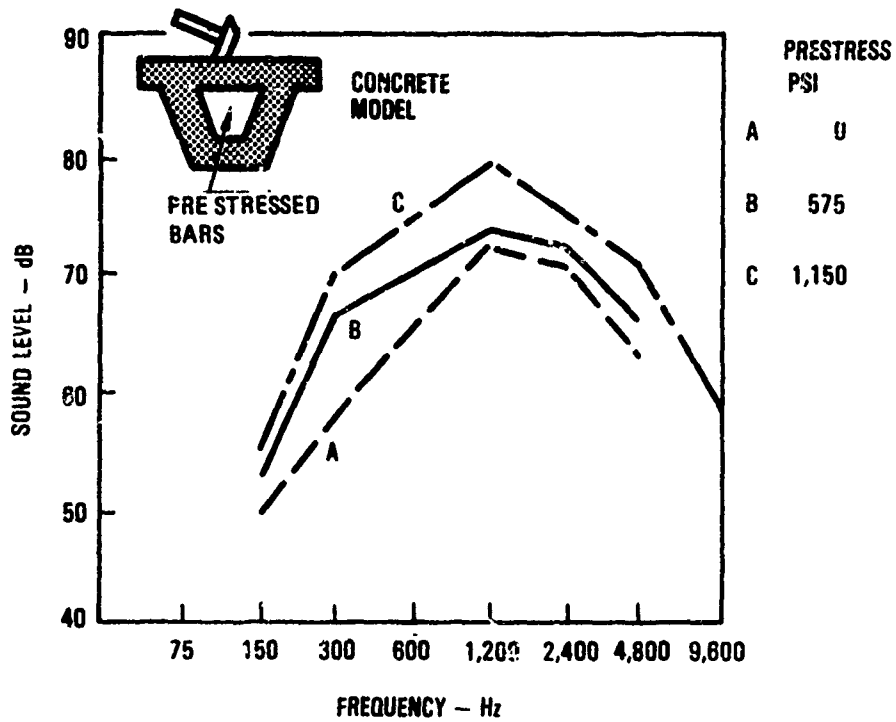


Figure 6.3.11.1. - Impact sound octave band level as a function of prestress.

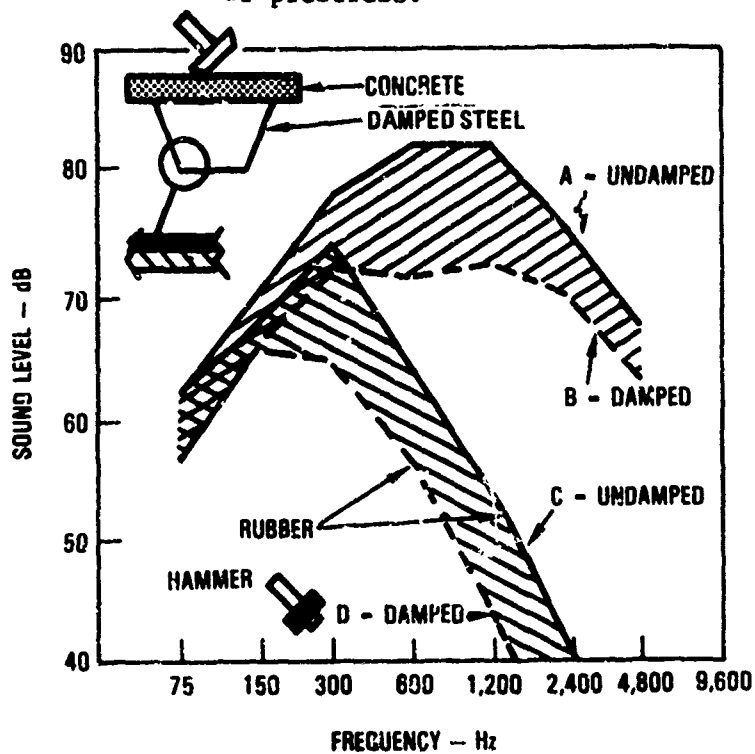


Figure 6.3.11.2. - Model composite concrete-steel bridge girder.

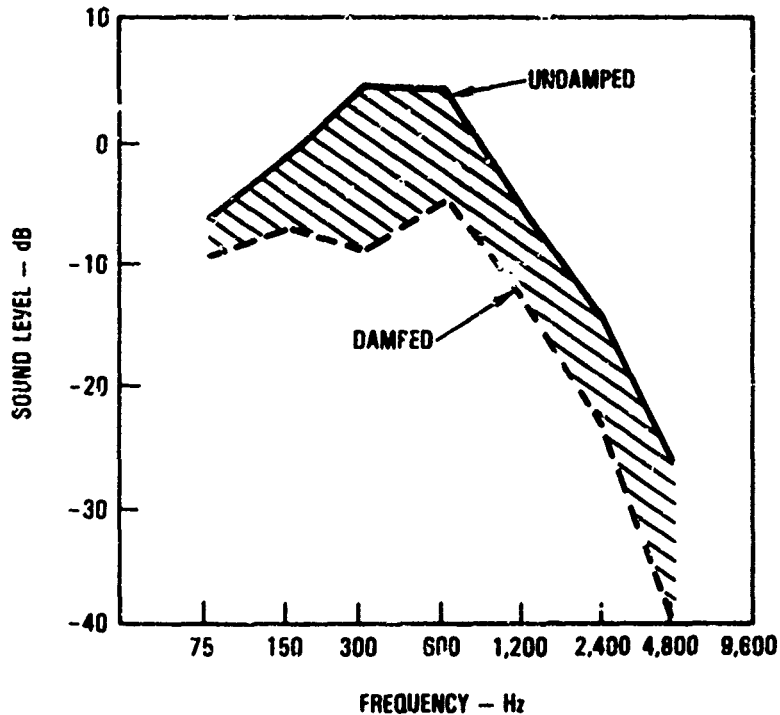


Figure 6.3.11.3. - Full scale composite concrete-steel bridge girder.

6.3.12 Damping for a Diesel Engine Oil Pan [6.32]

Problem

Recent federal legislation has resulted in a considerable effort to reduce the noise levels of on-highway vehicles. One of the major contributors to the noise level is the diesel engine. Specifically, the oil pan comprises a major source of the diesel engine noise level.

Structure

The oil pan is made of sheet steel and stamped to the desired shape. It is bolted to the bottom of the diesel engine.

Undamped Structure Response

Noise and vibration data are taken for a number of operational conditions to correlate the effects of resonance to the generation of excessive noise.

levels on the highway. An example is shown in Figure 6.3.12.1. The resonant frequency of interest occurs in the neighborhood of 500 hertz as shown in Figure 6.3.12.2. The mode shapes are determined. Figure 6.3.12.3 illustrates the fundamental bending mode which is excited at 467 hertz.

Damping Treatments

To design the proper damping treatment the following items are considered; the frequency to be damped is 500 Hz, the operational temperature range is between 175°F (79°C) and 250°F (121°C), the material must be resistant to oil contamination and long term heat exposures, and the oil pan, with its damping treatment, must be manufactured in a cost effective manner. Typical material characteristics are shown in Figure 6.3.12.4. A viscoelastic material sandwiched between two steel layers of equal thickness is the oil pan configuration chosen. The damping material is bonded securely to the steel outer ply using a 0.0002-inch (0.005 mm) thick adhesive.

Damped Structural Response

The damping performance of the layered oil pan configuration using the damping material properties of Figure 6.3.12.4 is shown in Figure 6.3.12.5. Figure 6.3.12.6 illustrates the improved damped response of the oil pan at 210°F (99°C). Figures 6.3.12.7 and 6.3.12.8 illustrate the noise level and vibration reduction, respectively, for the operational conditions.

Conclusions

The application of viscoelastic material can effectively be used to solve noise problems. If the damping design is performed in a systematic way the noise problem can be solved in a cost effective manner.

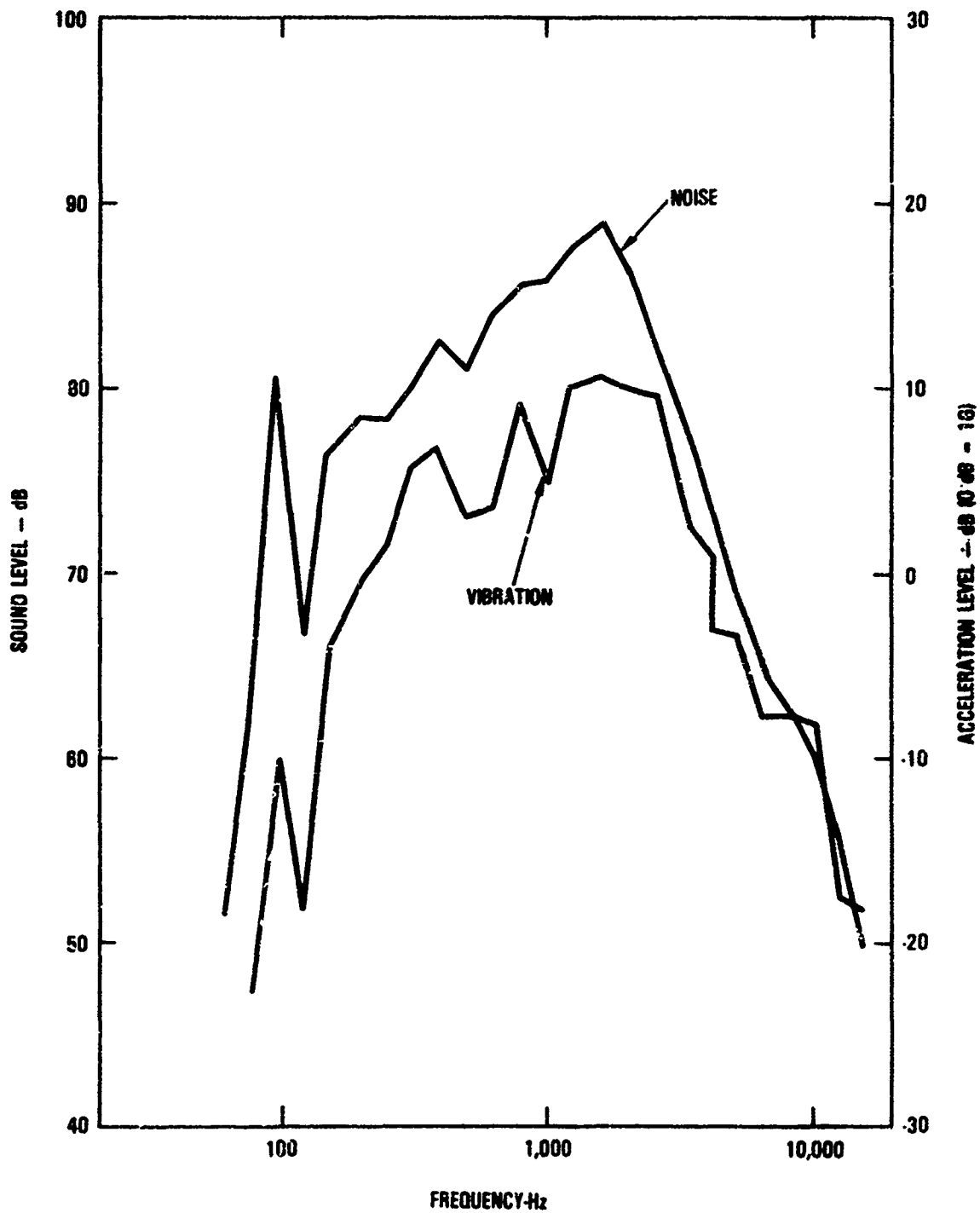


Figure 6.3.12.1. - Variation of the noise and vibration of the oil pan with frequency for a typical operating condition.

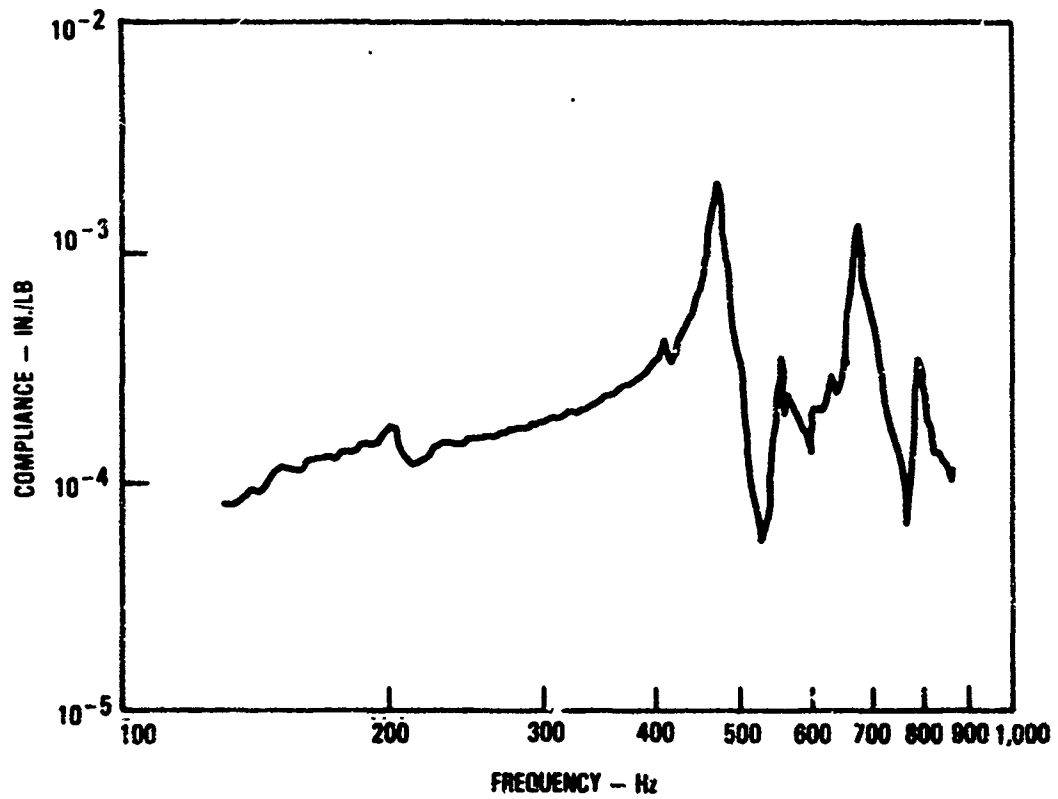


Figure 6.3.12.2. - Driving point frequency response on the left side of the undamped oil pan.

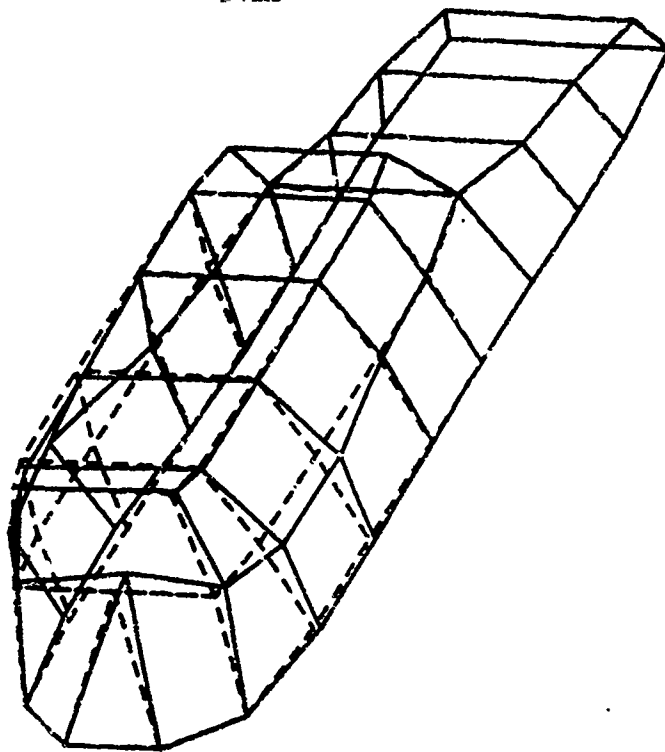


Figure 6.3.12.3. - Mode shape of vibration of the oil pan at 467 Hz.

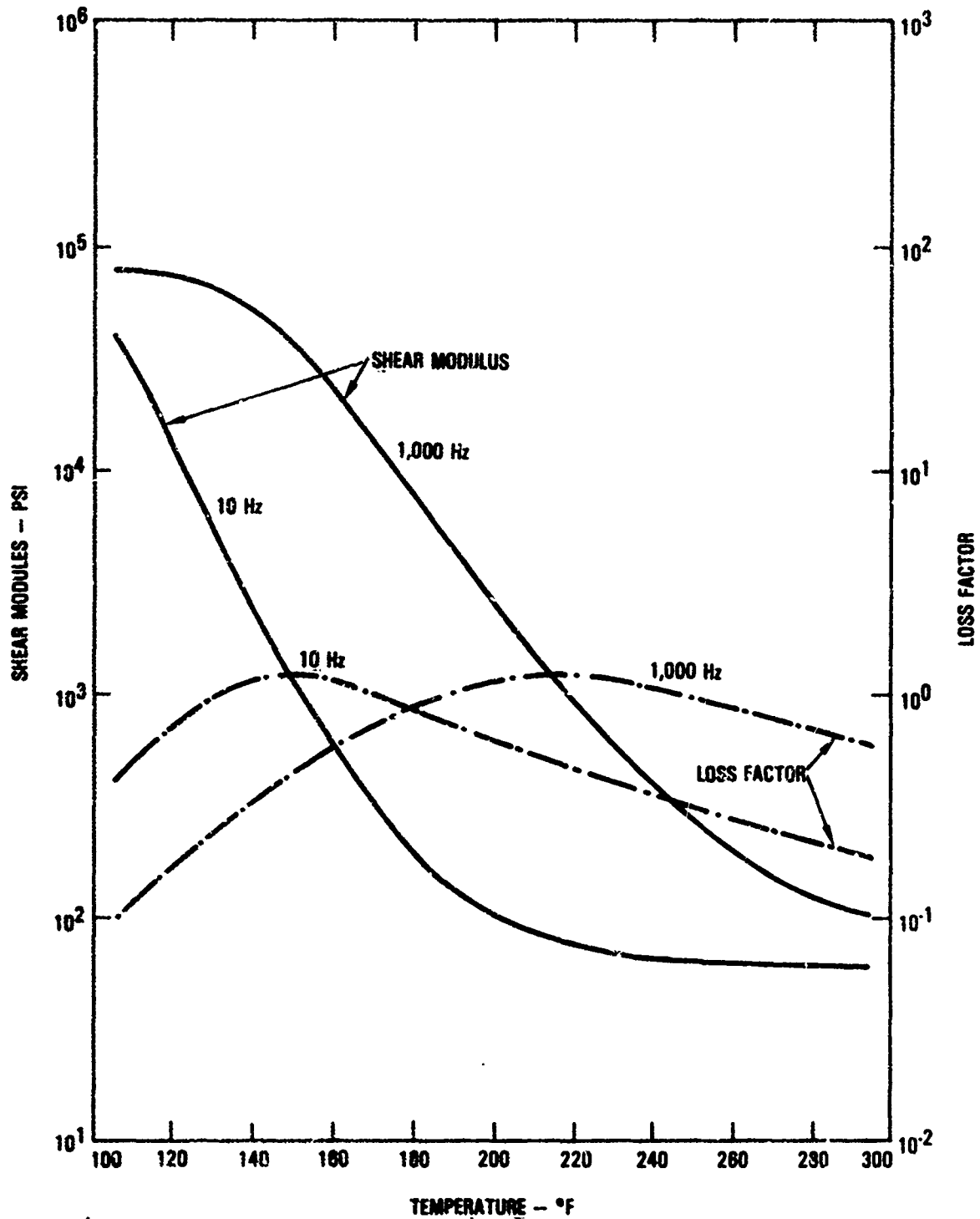


Figure 6.3.12.4. - Variation of the damping properties of a high temperature damping material.

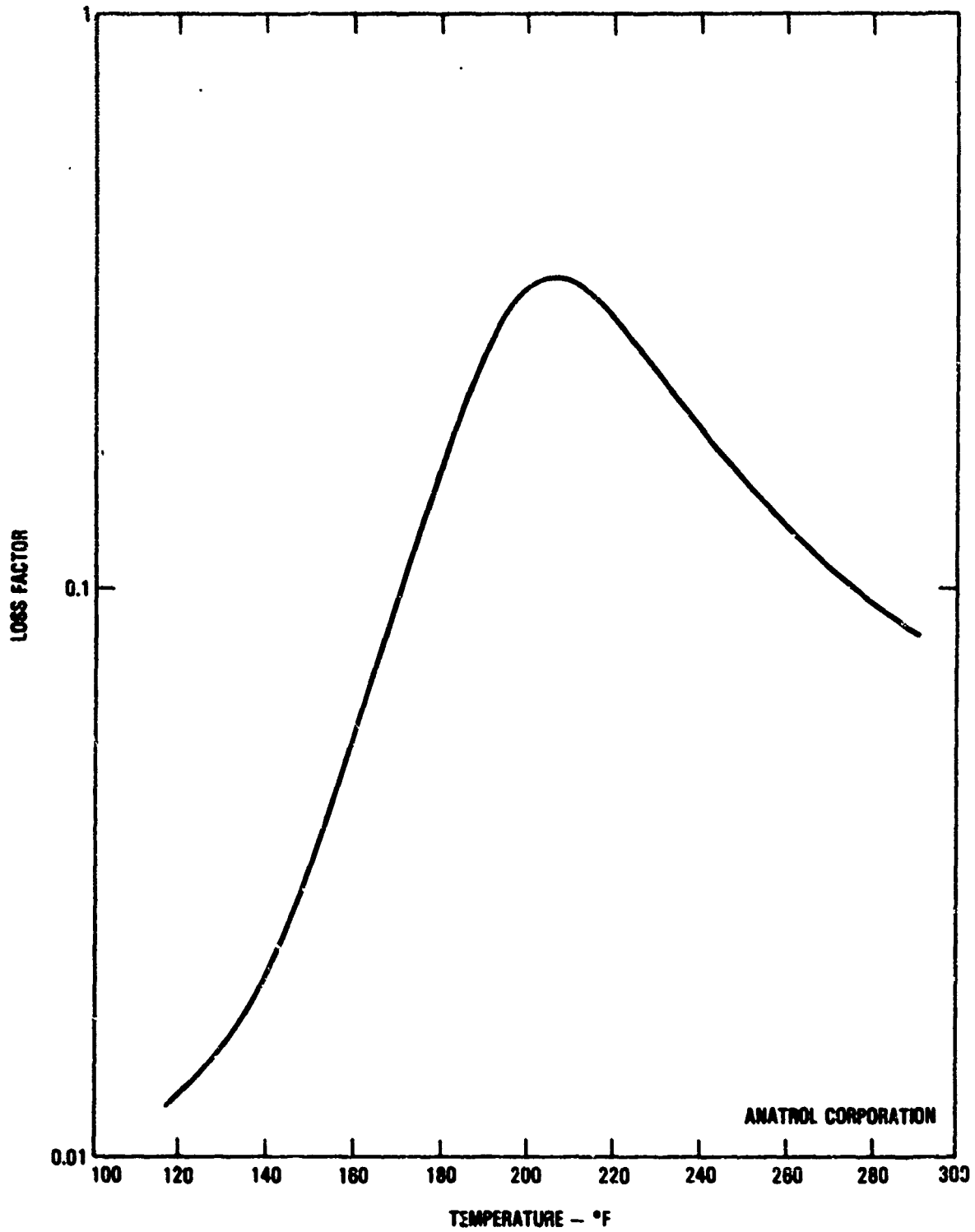


Figure 6.3.12.5. - Predicted values for damped oil pan.

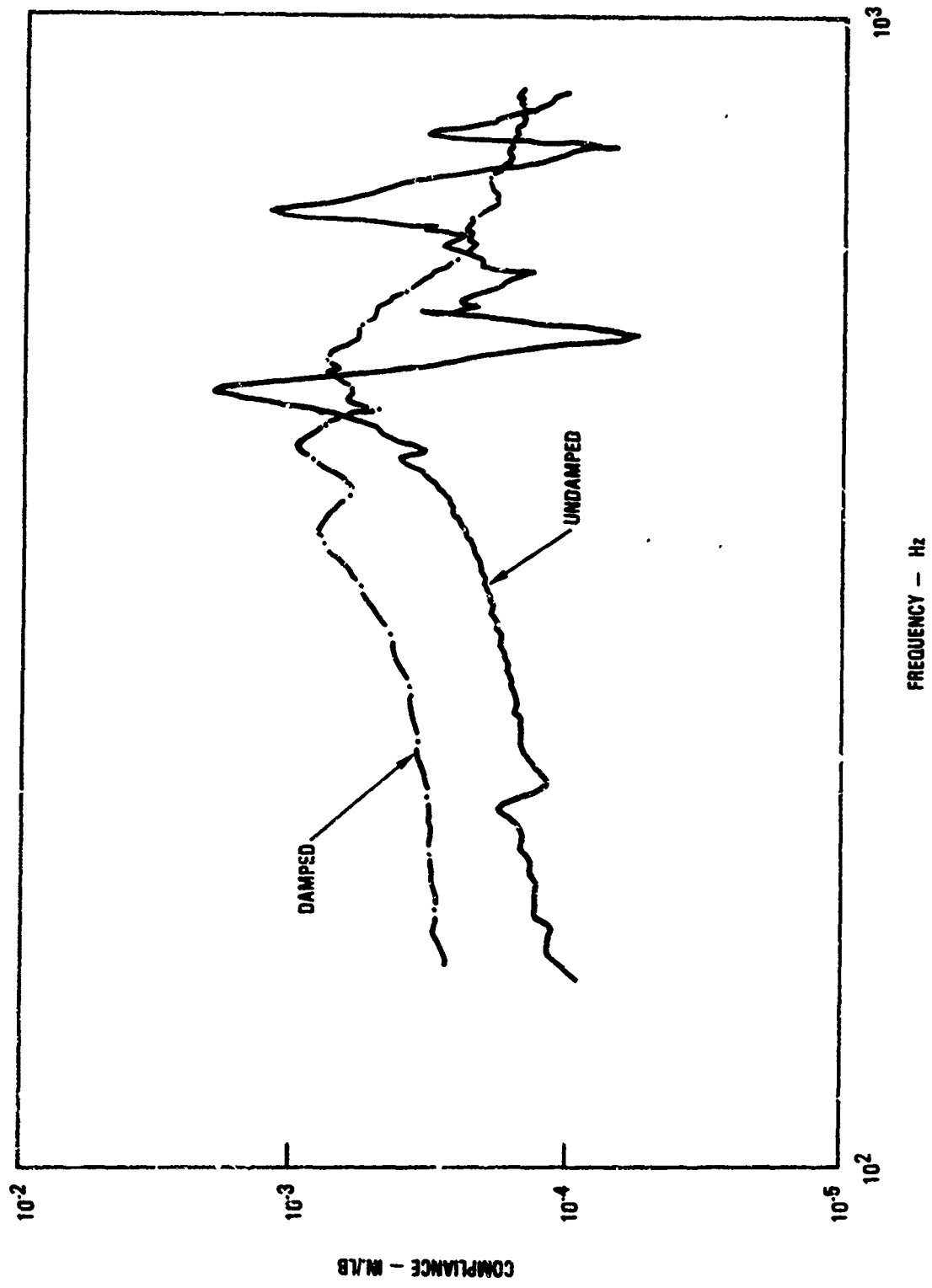


Figure 6.3.12.6. - Comparison of the damped and undamped oil pan response at 210°F.

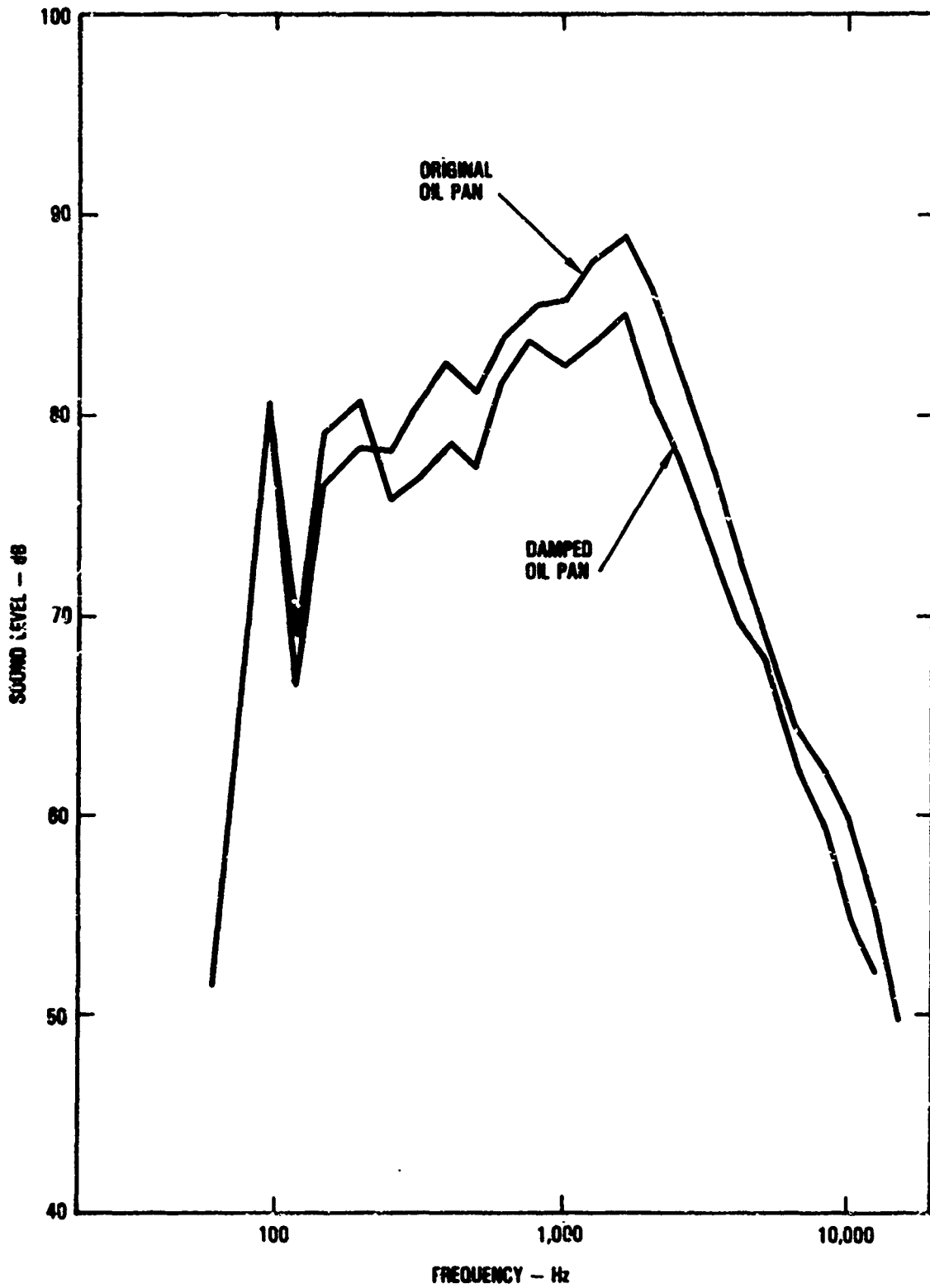


Figure 6.3.12.7. - Effects of damping on reducing the oil pan noise for a typical operating condition.

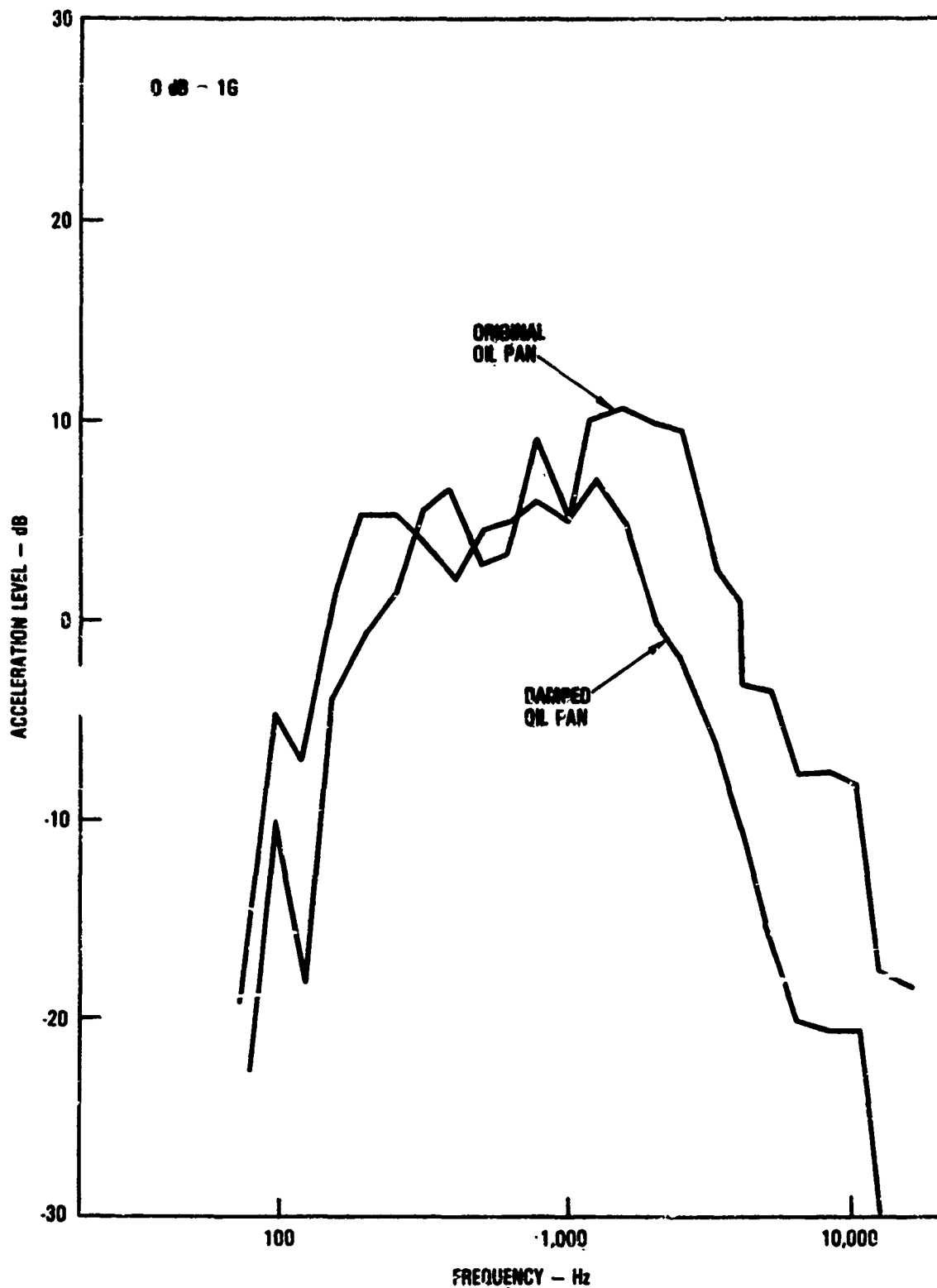


Figure 6.3.12.8. - Effects of damping and reducing the oil pan vibration for a typical operating condition.

6.3.13 Jet Engine Inlet Vane Damper [6.33]

Problem

High cycle fatigue cracks are occurring in the vanes and shrouds of the TF-30 Engine inlet guide vane, IGV, cases. The fatigue cracking leads to extremely high refurbishment/replacement costs because it occurs at much less than the estimated lifetime of the part.

Structure

The TF-30 IGV case is a titanium weldment consisting of a set of hollow vanes welded to vane stubs on a pair of cylindrical shrouds. Deicing air is routed through the vanes by way of the shrouds. The inner shroud structure supports the front bearing of the engine rotor system. The vanes align the inlet airflow for the first stage fan blades, located immediately downstream aft, and react the front bearing loads.

Undamped Response

Engine test stand and flight test strain gage data shows damaging vibratory stress cycles at the higher order vane bending and vane torsion modes due to the first stage fan blade passage frequency at the 28th engine order, 28E, and similar but less severe cyclic stresses at lower vane modes due to lower engine order shaft and case vibrations. Some wideband excitation is caused by inlet air turbulence. The Campbell diagram shown in Figure 6.3.13.1 is generated from test stand data. It clearly shows the first bending mode of the vane at 350 Hz and the first torsion mode at 850 Hz. However, higher cyclic stresses are measured at the higher order modes in the 3000 to 4000 Hz range and the higher cyclic stress rate leads to much more rapid accumulation of fatigue damage due to vibration in these modes. It is shown that the high frequency stress cycles exceeded the endurance limit defined by the Goodman diagram for the IGV case material.

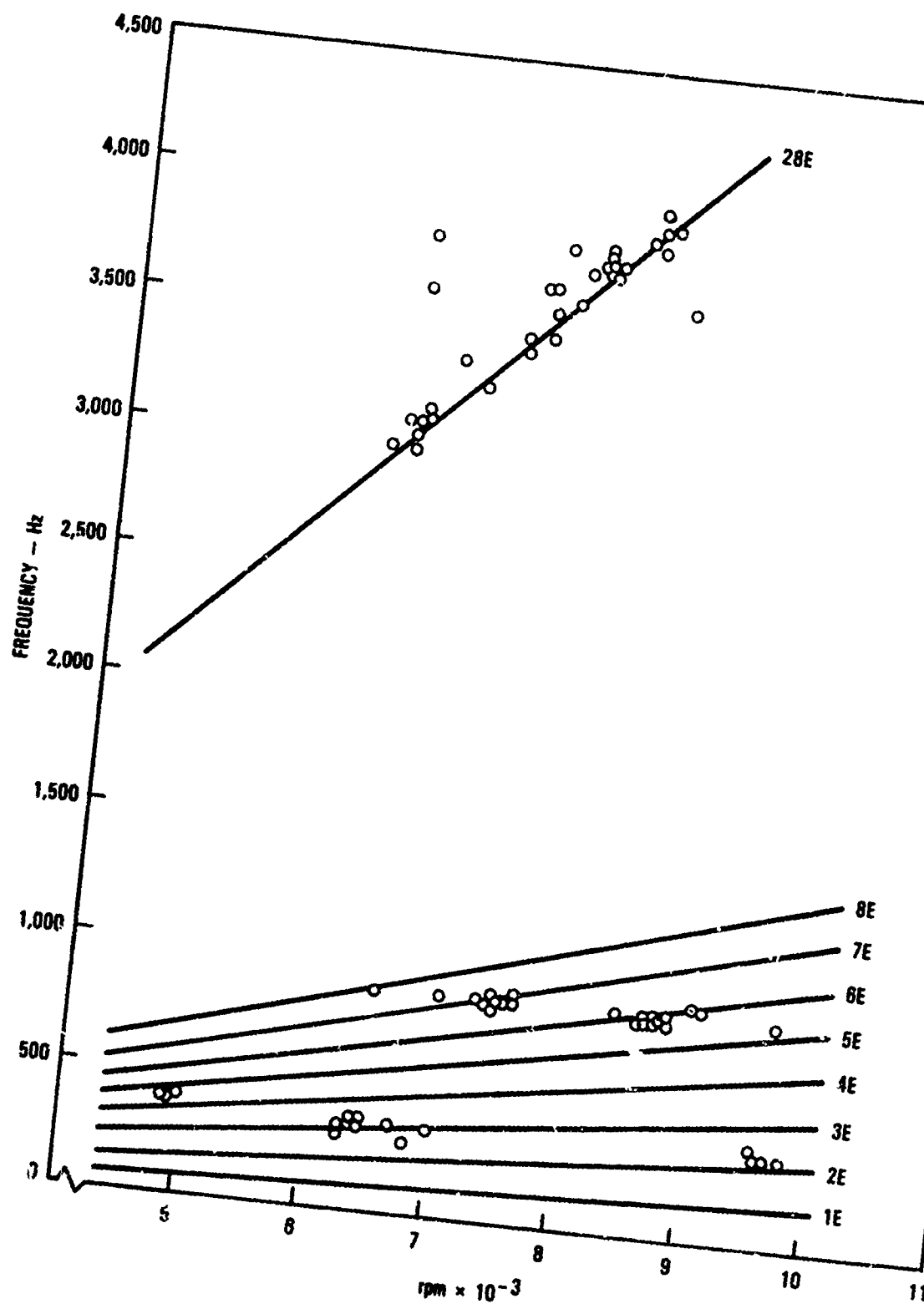


Figure 6.3.13.1. - Frequency and rpm of peak stresses.

Damping Treatment

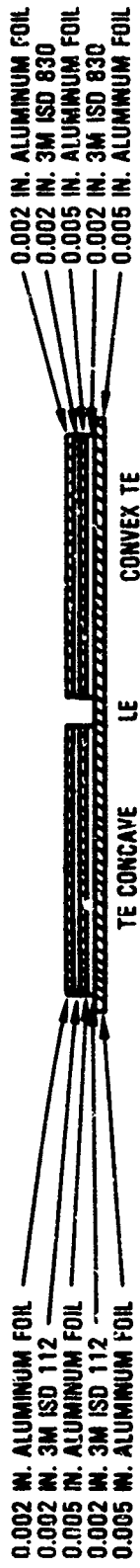
A multilayer constrained-layer damping treatment, as shown in Figure 6.3.13.2, is designed to reduce the IGV response to the vibratory excitation. Viscoelastic damping materials with different damping effectiveness temperature ranges are chosen for use on the two sides of the vanes to cover the IGV case operational temperature range from 0°F (-18°C) to 150°F (66°C), which accounts for 98 percent of the operational time of the engine. The damping wraps and their attachment to the vanes also have to survive anti-icing during which the vane surface reaches 400°F (204°C). The damping wraps are bonded to the vanes in an autoclave with AF 453 epoxy adhesive manufactured by 3M.

Damped Response

The loss factor versus temperature is shown in Figure 6.3.13.3 for the damped and undamped configuration of the TF-30 IGV case vane for the fourth torsional mode at 4000 Hz. The percentage operational time at temperature is shown also on the figure. The loss factor data is measured during laboratory vibration tests. Similar data is measured for the other vibration modes of the vane. Test cell runs of engines with and without damped vanes shows vibratory stress peaks are reduced from 50 to 80 percent in the vanes and from 41 to 61 percent in the standup stubs on the shrouds, to which the vanes are welded. Analysis shows that the reduced cyclic stresses are well below the endurance limit for the IGV case material. Test stand operational evaluations shows that addition of the damping wrap thickness to the vanes did not affect significantly any of the operational parameters of the engine.

Field Survivability

A demonstration IGV case used on an operational aircraft shows no adverse effects from inlet air flow erosion or de-icing cycles over 540 hours of operation. Minor FOD damage occurs on some vanes but is easily repaired with quick-setting epoxy, and no impact on maintenance or flight schedules occurs. Likewise, no fatigue cracks occur. A damping wrap installation program is instituted for replacement cases at the fabrication site and for repairable



VIEW A-A

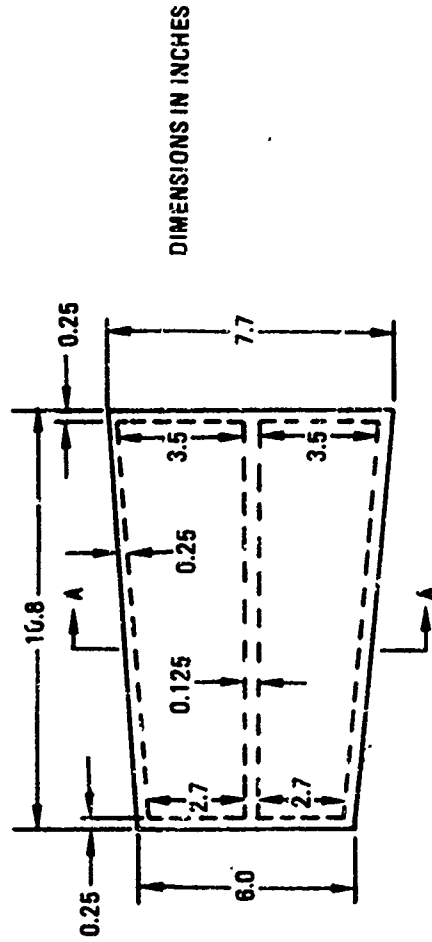


Figure 6.3.13.2. - IF-30 IGV damper wrap.

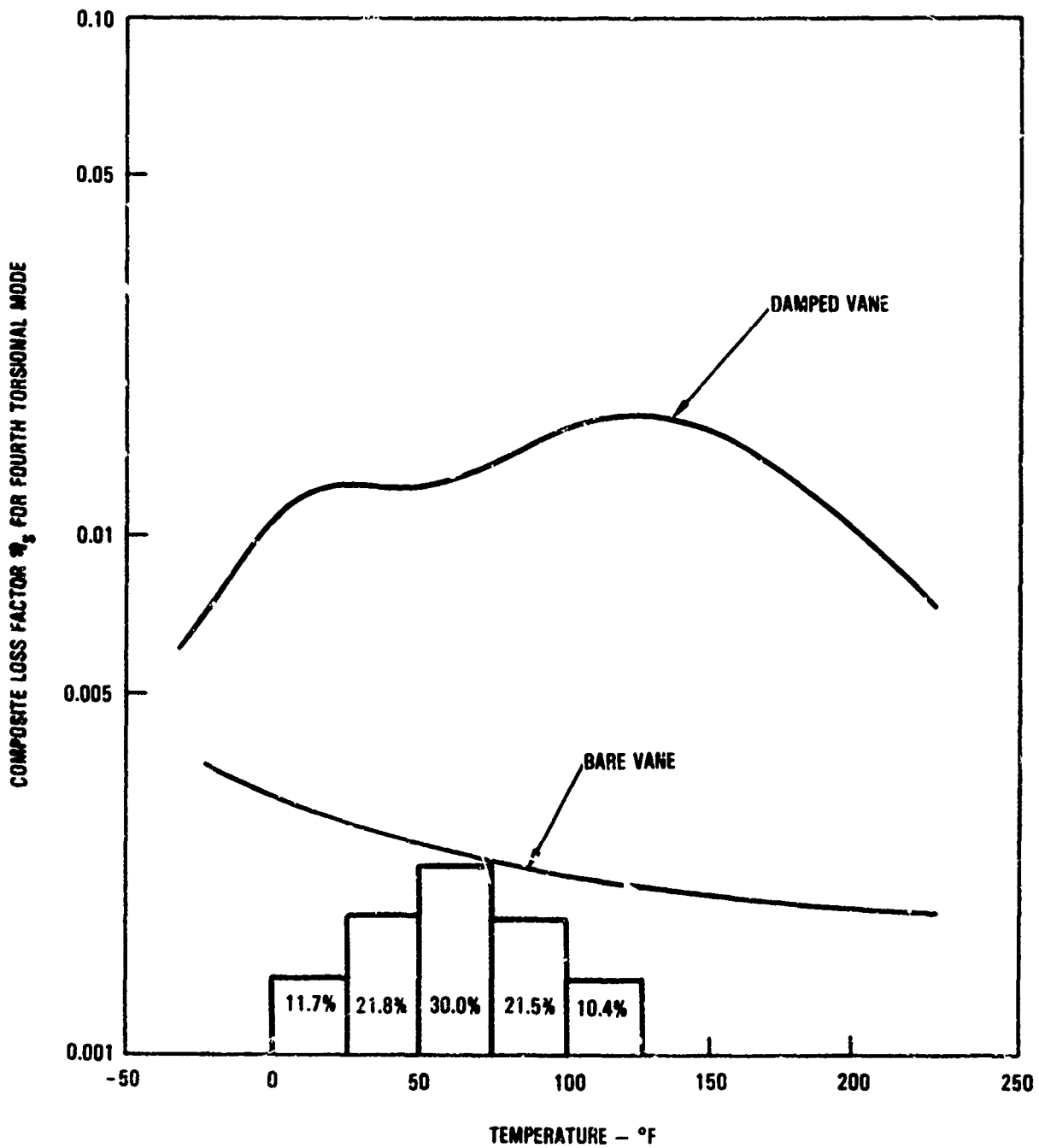


Figure 6.3.13.3. - loss factor and percentage of time at temperature for the damped and undamped TF-30 IGV case vane.

cases at the engine overhaul site. Most engines are now operating with damped vanes in their IGV cases and the fatigue cracking problem and its attendant repair costs have been eliminated by the use of damping wraps at a much lower cost including the design, fabrication, and installation.

6.3.14 Skin Stringer Structure Dampers [6.34, 6.35]

Problem

High-cycle resonant fatigue caused by acoustic loading or high interior cabin noise levels radiated by fuselage vibration, both generate problems which can be reduced through the use of passive damping techniques.

Structure

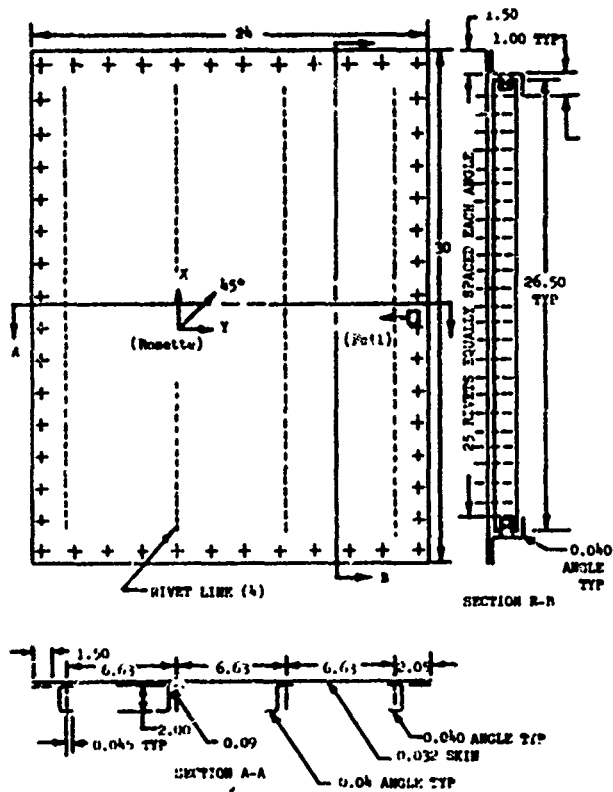
Typical skin-stringer structure is shown in Figure 6.3.14.1.

Undamped Structural Response

A typical response function from an undamped skin-stringer structure is shown in Figure 6.3.14.2. As can be seen there is a band of modes in the frequency range from 280 Hz to 360 Hz. If the frequency limit of the test is expanded, a second band of modes will be seen near 600 Hz. This type of bands of resonant modes is quite typical. The usual system damping on a skin-stringer structure is on the order of 0.010 to 0.001. (Q's of 100 to 1000.) It is the low values of damping that generate the problems.

Damping Treatments and Damped Structural Response

Since this is a generic discussion, several damping designs will be discussed without regard to specific frequencies or temperatures. In Reference [6.34] the use of tuned dampers to control panel resonances is discussed. Figure 6.3.14.3 illustrates the types of dampers used. The results of the testing in reference [6.34] indicate that the tuned dampers work well over a limited frequency range reducing the strain by as much as 9 dB; however, the overall response to random excitation is reduced only by 0.5 dB to 4 dB.



NOTE: DIMENSION IN INCHES

Figure 6.3.14.1. - Skin-stringer panel.

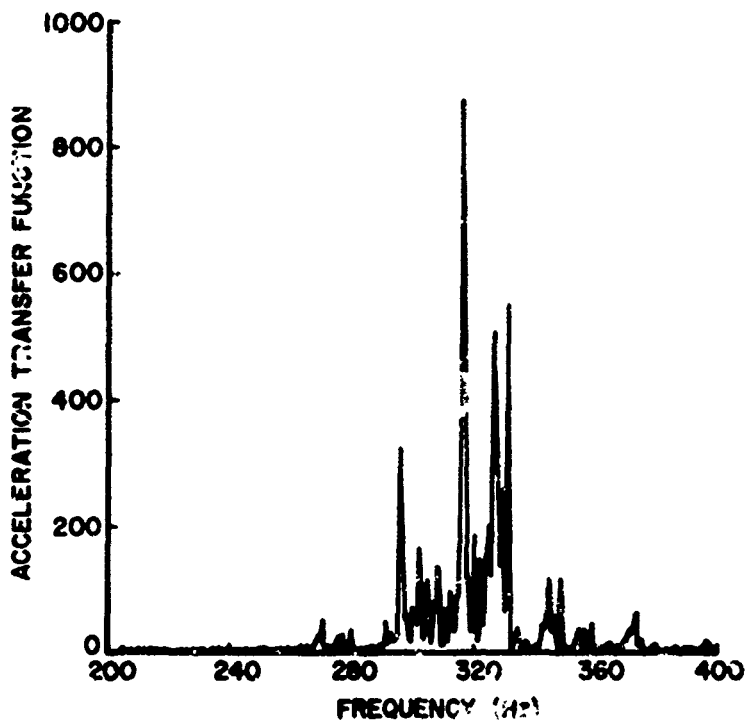


Figure 6.3.14.2. - Typical skin-stringer structural response.

In Reference [6.35], three sandwich skin configurations are evaluated to see their effects on acoustic fatigue life. The configurations are shown in Figure 6.3.14.4. The laminate material is described as a polyurethane material with no material characteristics given. The typical undamped response of the control panel is given in Figure 6.3.14.5 with the damped response shown in Figure 6.3.14.6. The conclusion drawn from this study is that the viscoelastic damped panel, which is equal in weight to the control panel, has a fatigue life at least three times longer than the control panel.

6.3.15 Mirror Mount Dampers [6.36]

Problem

Damping of laser mirrors is critical because of the requirements for minute surface deflection allowables, stringent line of sight, fatigue life, and jitter requirements.

Structure

Damping of the laser mirror mounts is attained using either of the mounts shown in Figure 6.3.15.1. The structure consists of a bolt (spring) and a viscoelastic damping material (damper) assembled in a manner that leaves the spring and damper in a parallel configuration.

Damping Treatments

Several configurations of the spring and damper are investigated. The objective of the study is to attain a system loss factor of 0.2. For a round bolt and using 3M-468 damping material a loss factor of 0.14 is attained. Using a square bolt and the identical damping material a loss factor of 0.22 is attained.

Damped Structural Response

The frequency and loss factor temperature dependence for the square bolt design are shown in Figure 6.3.15.2. The maximum loss factor is 0.22 which will occur at a temperature of 70°F (21°C) and a frequency of 580 hertz. Two test results, one frequency and one system loss factor are shown in Figure 6.3.15.2. The test results agree quite well with the analytical results.

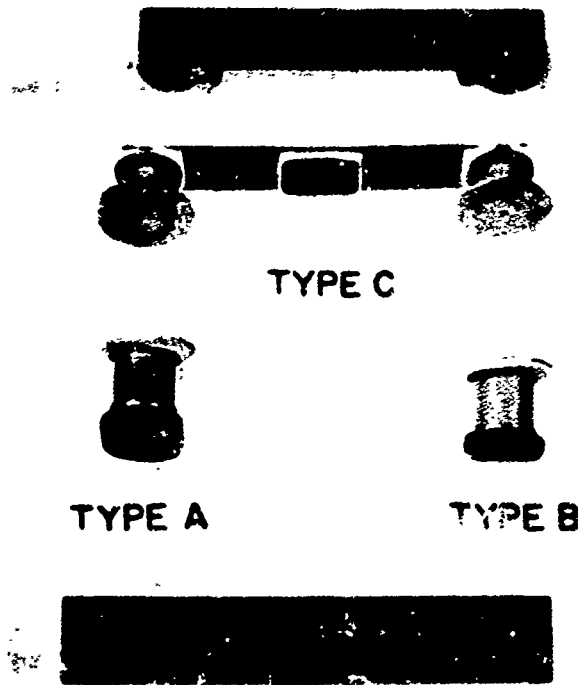


Figure 6.3.14.3. - Close-up of dampers used for tests.

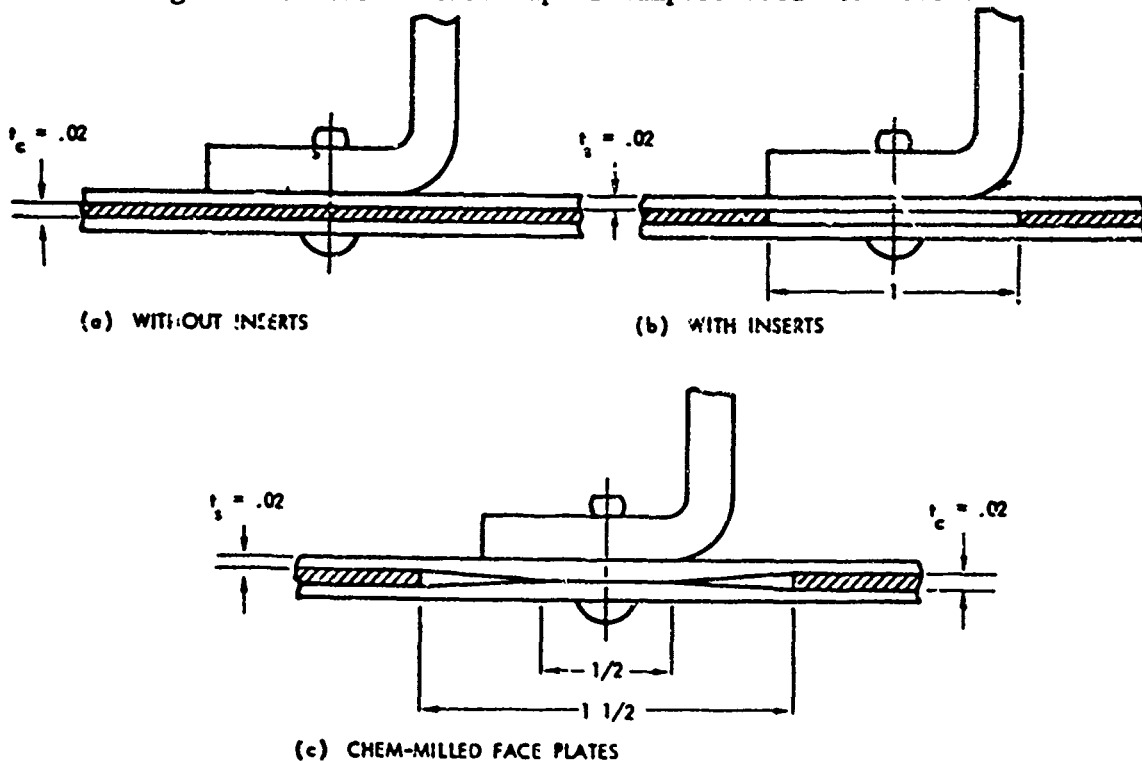


Figure 6.3.14.4. - Joint designs of sonic fatigue test specimens with polyurethane cone.

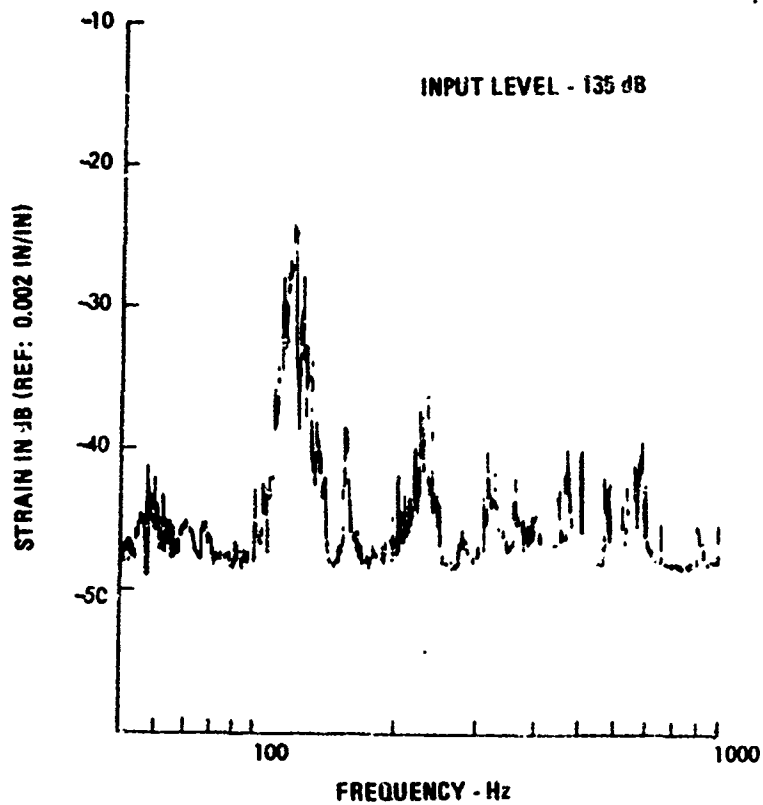


Figure 6.3.14.5. - Typical response of control panel, sinusoidal sweep test.

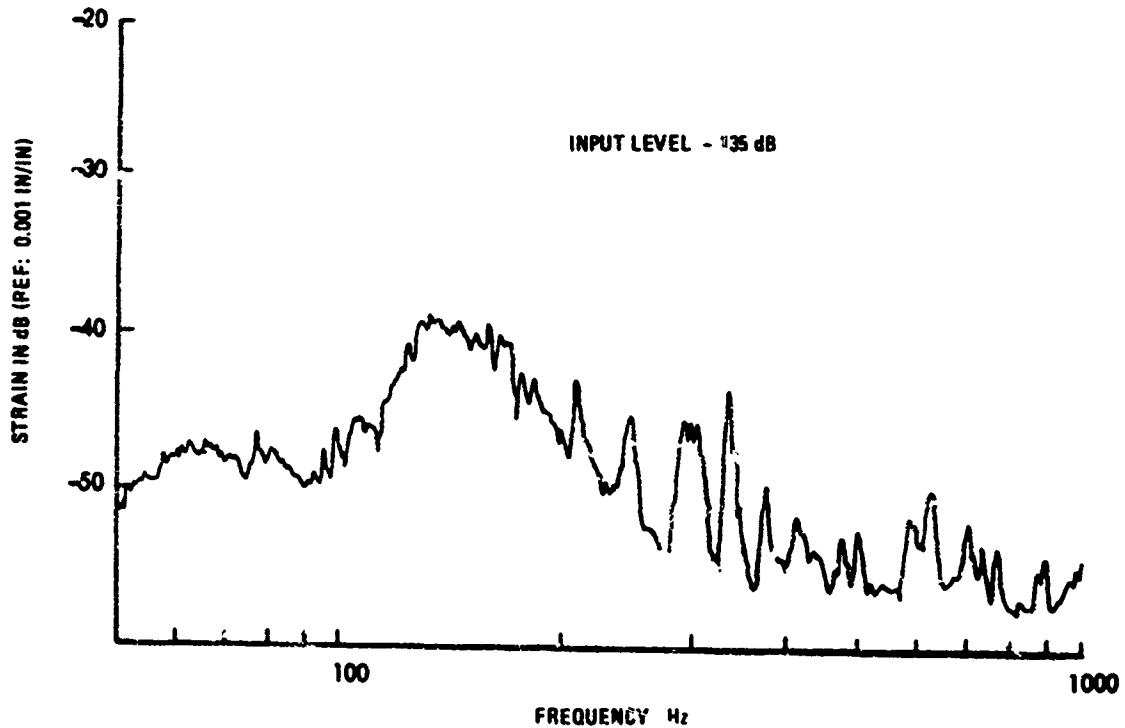


Figure 6.3.14.6. - Typical response of viscoelastic panel, sinusoidal sweep test.

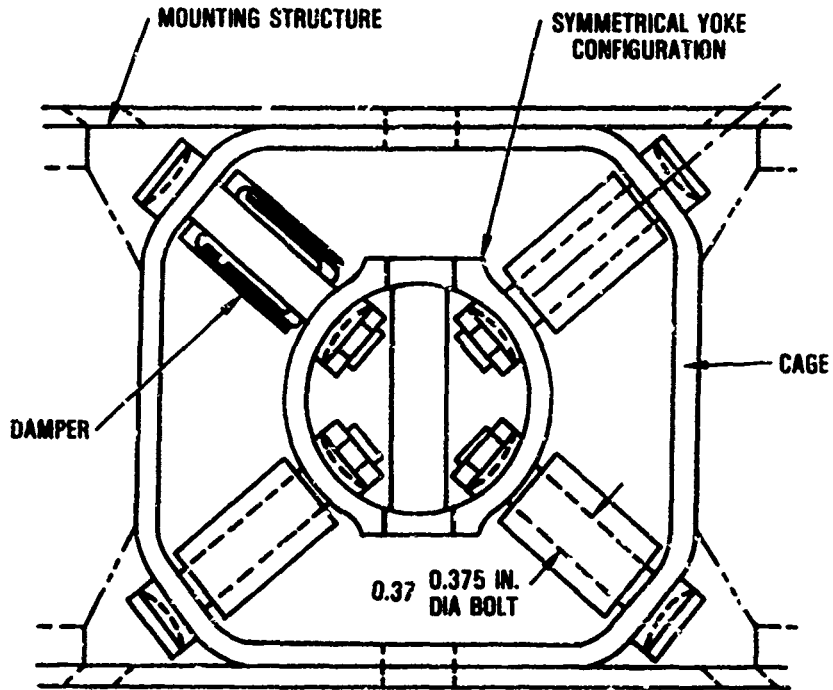


Figure 6.3.15.1. - Torsionally compliant main mount.

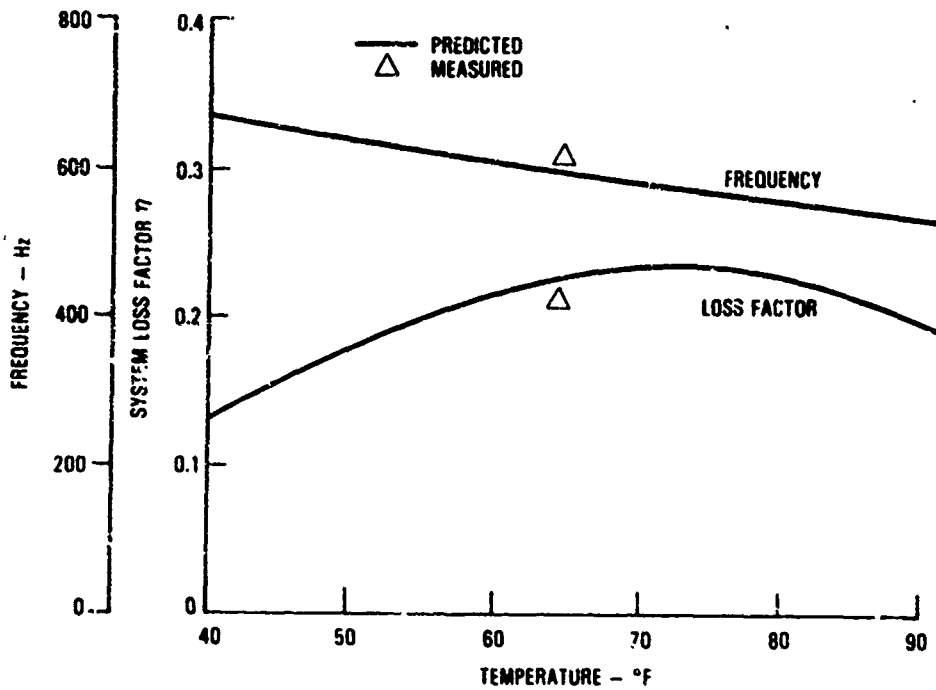


Figure 6.3.15.2. - Comparison of measured and predicted loss factor and frequency.

6.3.16 Composite Beam Damper [6.37]

Problem

The viscoelastic damping of a composite beam is investigated to support the requirement of a properly damped laser mirror mount.

Damped Structural Configuration

The graphite/epoxy test beams (3 total) are shown in Figure 6.3.16.1. The undamped beam is constructed by bonding two pieces of graphite/epoxy together using Eastman EA-934 adhesive. The damped beam is constructed by bonding two pieces of graphite/epoxy together using 3M-468 viscoelastic damping material.

Structural Response

The response of the two beams is determined by mounting them as cantilevered beams and deflecting them, then quickly releasing the free end of the beam. The undamped beam had a loss factor of 0.025 and the damped beam had a loss factor of 0.226 (see Figure 6.3.16.2).

The deflection of the beams of typical laser mirror mount structures is in the micro-inch range. The damped response for this small deflection is determined using a cantilevered configuration and exciting the beam by hitting the free end with a rubber band. The maximum tip deflection which occurred is 27 micro-inches (6.86×10^{-4} mm). The system loss factor for the undamped composite beam is 0.008 and the system loss factor for the damped composite beam is 0.2. Thus damping is maintained even at these extremely small deflections.

6.3.17 Floor Damping

Problem

The design and analysis of shock isolated floors is studied by examining the effect of additive damping upon the dynamic characteristics of the structure.

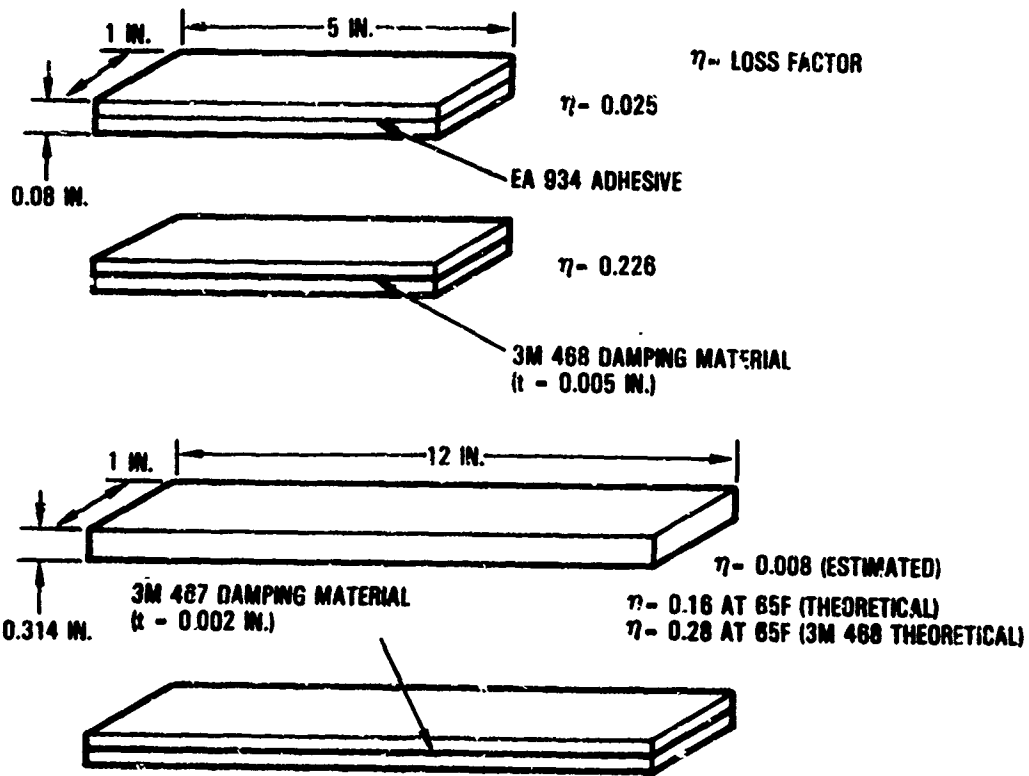


Figure 6.3.16.1. - Graphite/epoxy test beams.

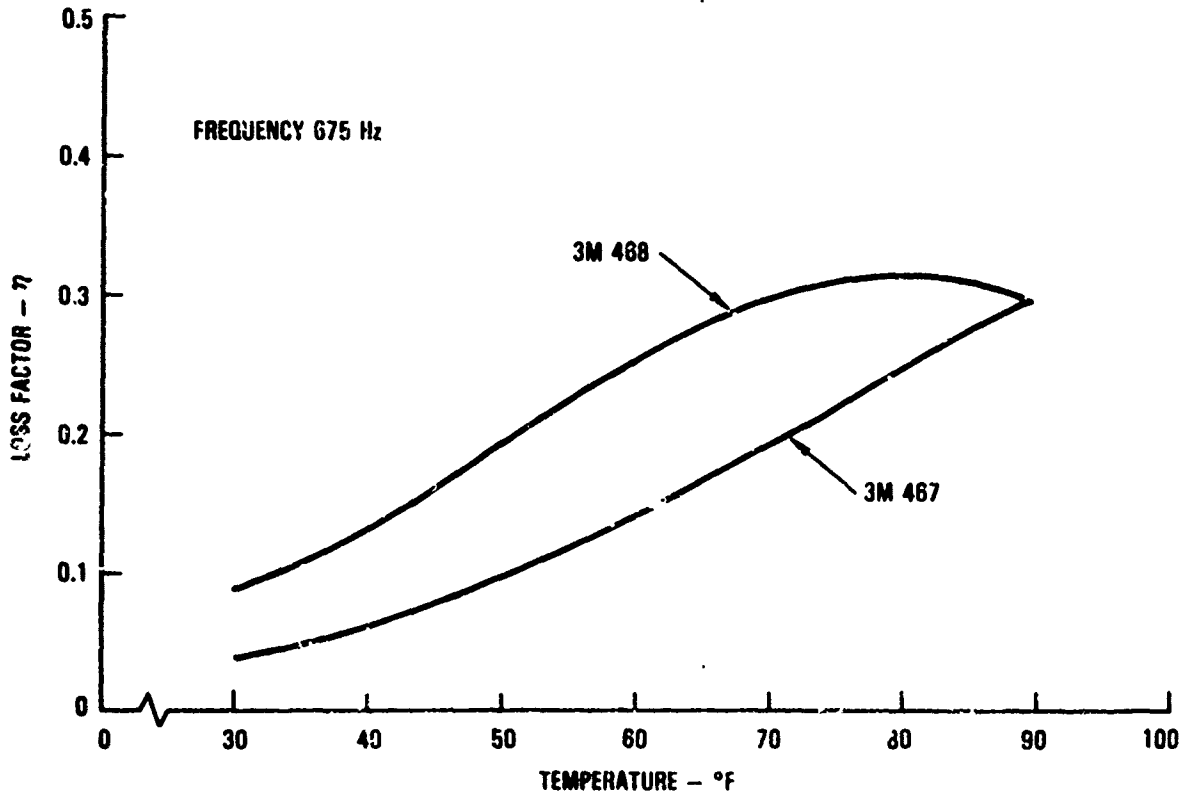


Figure 6.3.16.2. - Variation of loss factor with temperature of graphite/epoxy beam.

Structure

Two steel structures are studied. One a stiff floor specimen, the other a flexible floor specimen. The stiff floor specimen is constructed using a 3/8 inch (9.53 mm) thick floor plate with ST7WF17 wide flange T-beam stiffeners. The flexible specimen is constructed using a 1/4 inch (6.35 mm) thick floor plate with ST318.625 T-beam stiffeners. The two specimens are shown in Figure 6.3.17.1.

Damping Treatment

The flexible specimen is tested and analyzed using three different damping configurations. The first configuration consists of a free layer damping treatment in which the bottom surface of the floor plates, the T-beam flanges and one side of the T-beam web are covered by Class II Navy tile manufactured to MIL-P-23653B. The second configuration is a combined free layer and constrained layer damping treatment. This configuration is obtained by replacing the free layer damping treatment on the bottom flange of the T-beams with a 25-mil (0.635-mm) thick layer of 3M SJ2003X viscoelastic damping material and a 1-inch (25.4-mm) thick steel constraining layer. The third configuration is a constrained layer damping treatment obtained by removing the remaining free layer damping treatment from the bottom surface of the floor plate and the T-beams; see Figure 6.3.17.2.

The stiff specimen is tested and analyzed using two different damping configurations. The first configuration is a constrained layer damping treatment, which consists of a 100-mil (2.54-mm) thick layer of 3M SJ2003X viscoelastic damping material with a 3/4-inch (19.05-mm) thick steel constraining layer applied to the upper and lower surface of the bottom flange of the wide flange T-beams. The second configuration is a spaced constrained layer damping treatment, which consists of a 3/4-inch (19.05-mm) thick layer of Class II Navy tile constrained by a 1/2-inch (12.7-mm) thick plate offset from the bottom flange of the wide flange beams. The offset consists of U-section spacers welded to the bottom flange of the T-beams, see Figure 6.3.17.3.

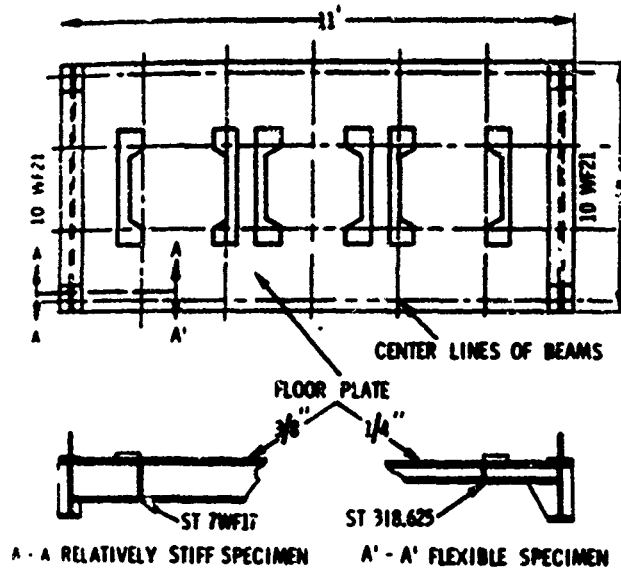


Figure 6.3.17.1. - Schematic of floor test specimens.

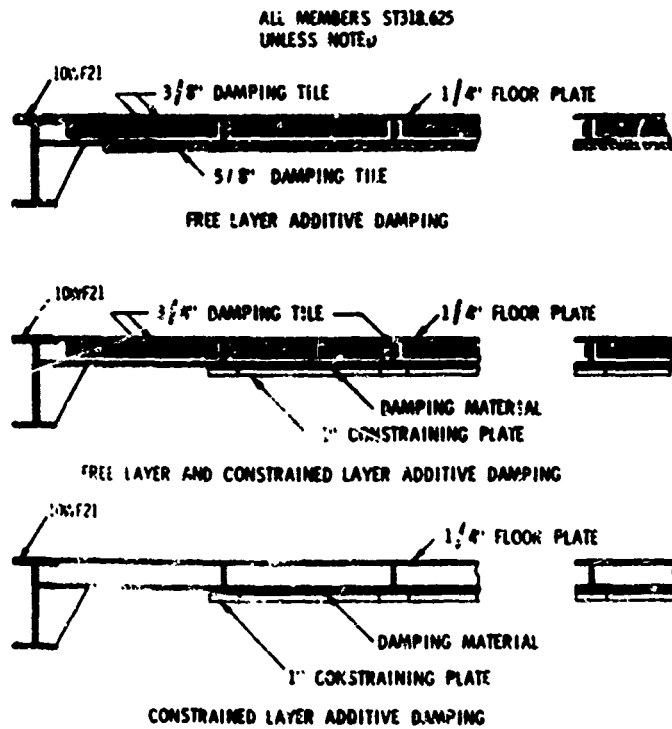


Figure 6.3.17.2. - Additive damping configurations for flexible steel specimen.

Structural Response

The structural response of the specimens is shown as acceleration transfer function magnitude versus frequency plots. The acceleration transfer function magnitude is a combination of the inherent damping, the viscoelastic damping, and the airbag damping of the structural system. The airbags are used in the test program to reduce rigid body frequencies below 2 hertz.

The effectiveness of the three damping treatments upon the flexible specimens to a low level transient shock are shown in Figures 6.3.17.4 through 6.3.17.6. Figure 6.3.17.4 shows that the free-layer damping treatment does not reduce the transfer function magnitudes until the local plate resonant frequencies are suppressed. Figure 6.3.17.5 compares the response of the free-layer damping treatment to the combined free/constrained layer damping treatment. In general, the response of the combined system is less than the free-layer system. Figure 6.3.17.6 compares the damped and undamped response of the constrained layer damping treatment. The constrained layer treatment does not seem to be as effective as the free-layer damping treatment.

The effectiveness of the two damping treatments upon the stiff specimen exposed to a low level transient shock are shown in Figures 6.3.17.7 and 6.3.17.8. Figure 6.3.17.7 compares the response of the undamped system to the constrained layer damped system. The magnitude of the response is reduced in the 20-30 hertz range and above 800 hertz; although the areas beneath the two curves are essentially the same. This fact indicates that the constrained layer damping treatment is ineffective in reducing transient responses. Figure 6.3.17.8 compares the response of the undamped system to the spaced constrained layer damped system. The magnitude of the response is reduced above 300 hertz.

Conclusions

Some important conclusions of this study are:

- 1) Stiff specimens appear to be far more difficult to damp than flexible specimens;

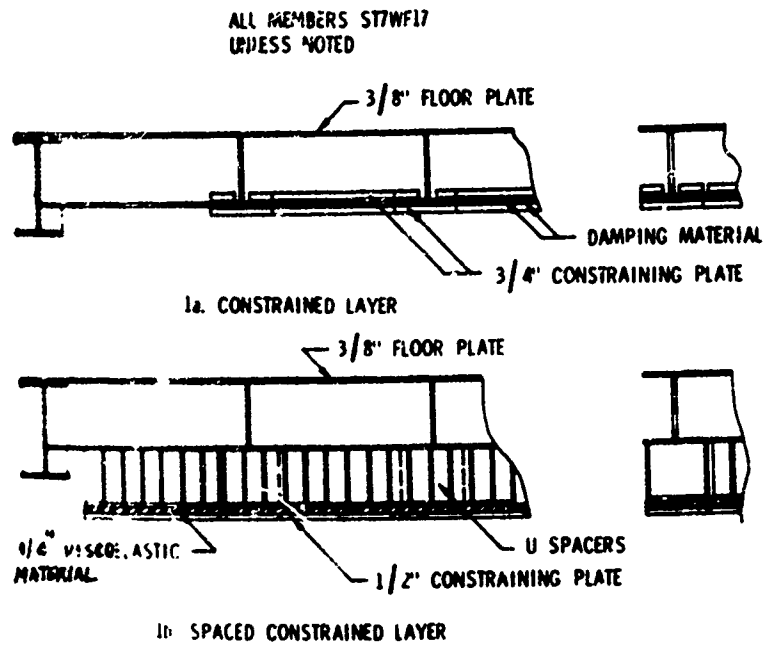


Figure 6.3.17.3. - Relatively stiff steel floor additive damping configurations.

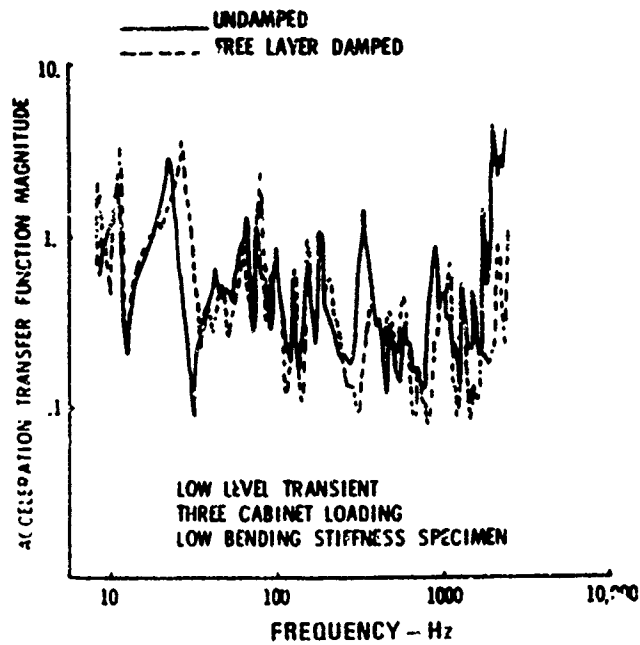


Figure 6.3.17.4. - Comparison of low bending stiffness specimen transfer function magnitudes undamped to free-layer damped at cabinet base near input.

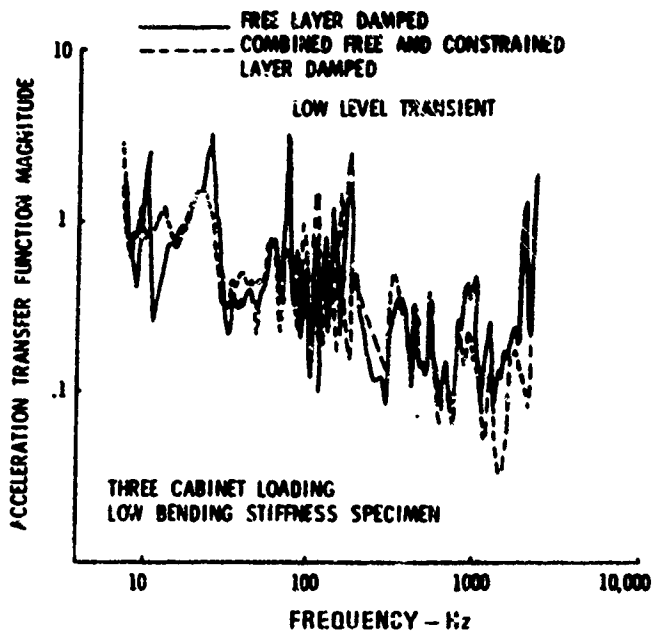


Figure 6.3.17.5. - Comparison of low bending stiffness specimen transfer function magnitude free-layer damped to combined free-layer and constrained layer damped at cabinet base near input.

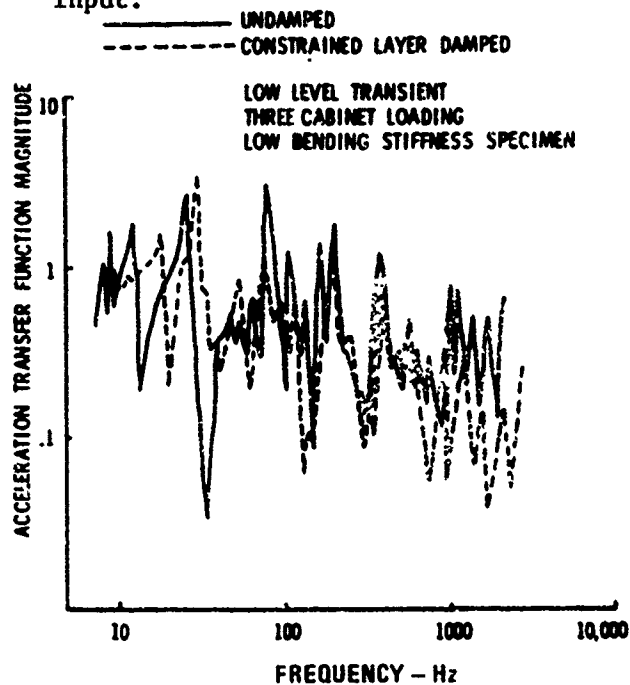


Figure 6.3.17.6. - Comparison of low bending stiffness specimen transfer function magnitude undamped to constrained layer damped at cabinet base near input.

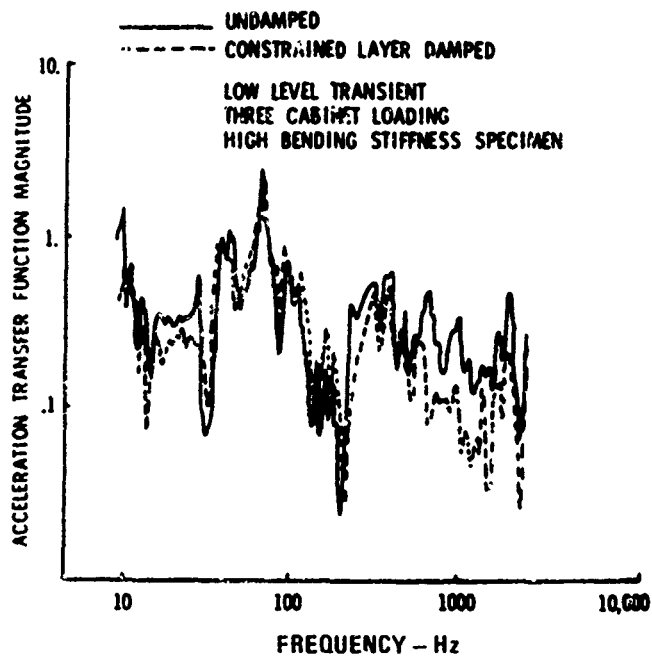


Figure 6.3.17.7. - Comparison of high bending stiffness specimen transfer function magnitude undamped to constrained layer damped at cabinet base furthest from input.

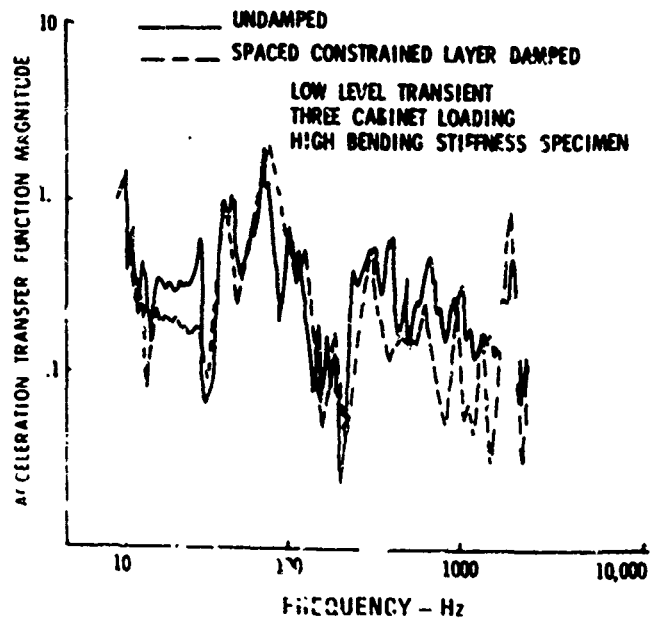


Figure 6.3.17.8. - Comparison of high bending stiffness specimen transfer function magnitude undamped to spaced constrained layer damped at cabinet base furthest from input.

- 2) Free layer damping is ineffective in reducing the overall response of the system, although it provides excellent attenuation of local resonant frequencies;
- 3) Although additive damping always reduces the harmonic response, it may not reduce transient response because of increases in area under the transfer function magnitude plot, as the peaks are lowered, the valleys are increased.

6.3.18 Turbine Engine Exhaust Stack Damper [6.38]

Problem

The fatigue life of helicopter engine exhaust extensions are of great concern. To increase the fatigue life, a coating of vitreous enamel damping material is applied. This damping treatment significantly reduces the vibrational amplitudes which causes the fatigue life problems.

Structure

The helicopter engine exhaust extension is of metal construction and is bolted to the engine exhaust tailpipe.

Undamped Structural Response

The undamped structural response is determined using two experimental techniques. A Digital Fourier Analyzer (DFA) is used to study driving point frequency response plots (Figures 6.3.18.1 and 6.3.18.2) and to obtain the animated mode shapes. A Transfer Function Analyzer is used as an aid in determining the exhaust stack loss factors. Typical loss factors are in the range of 0.001 and 0.91. The maximum operational temperature range of the exhaust extension is determined to be 700°F (371°C) to 800°F (427°C).

Damping Treatment

A room temperature damping treatment is used to study the damped response of the engine exhaust extension. Choosing damping properties of the high temperature damping treatment that are similar to the room temperature damping treatment ensured correspondence between the two configurations (see Figures 6.3.18.3 and 6.3.18.4). The high temperature damping treatment used

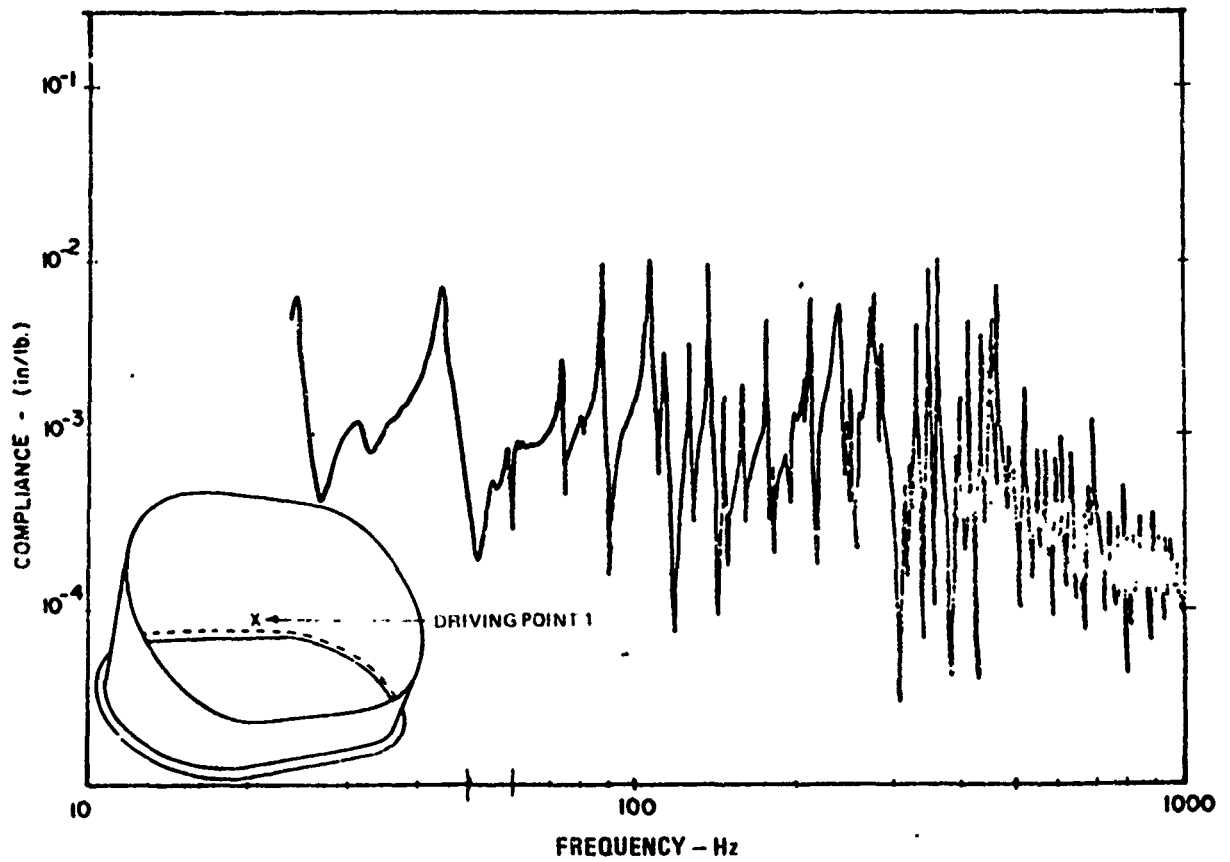


Figure 6.3.18.1. - Driving point 1 frequency response of undamped exhaust extension.

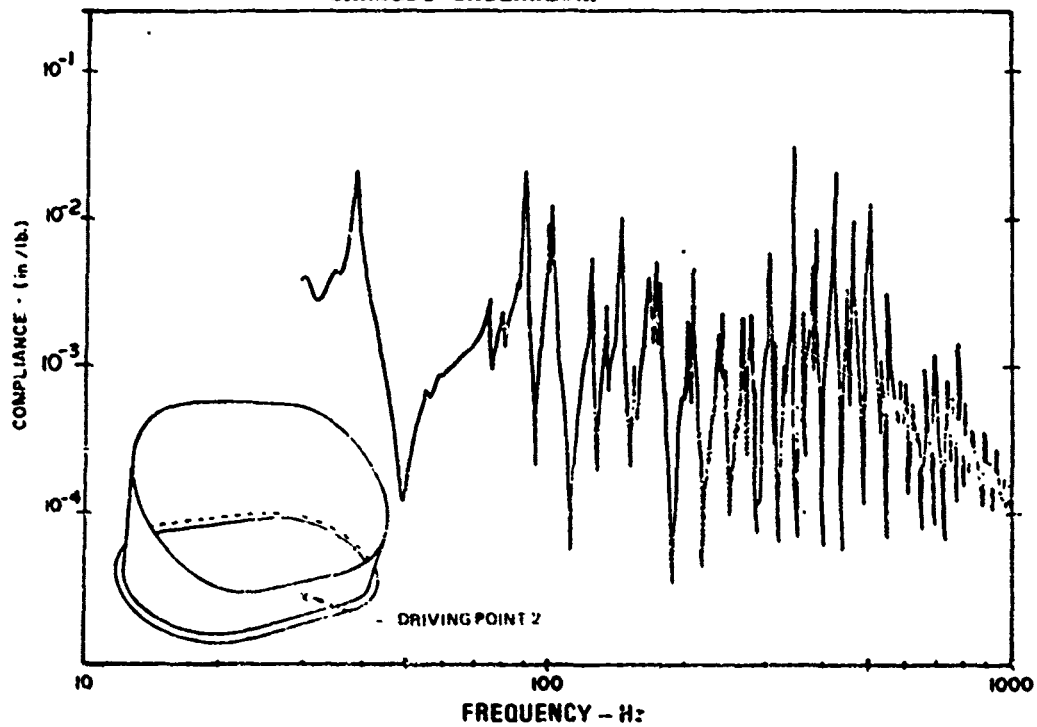


Figure 6.3.18.2. - Driving point 2 frequency response of undamped exhaust extension.

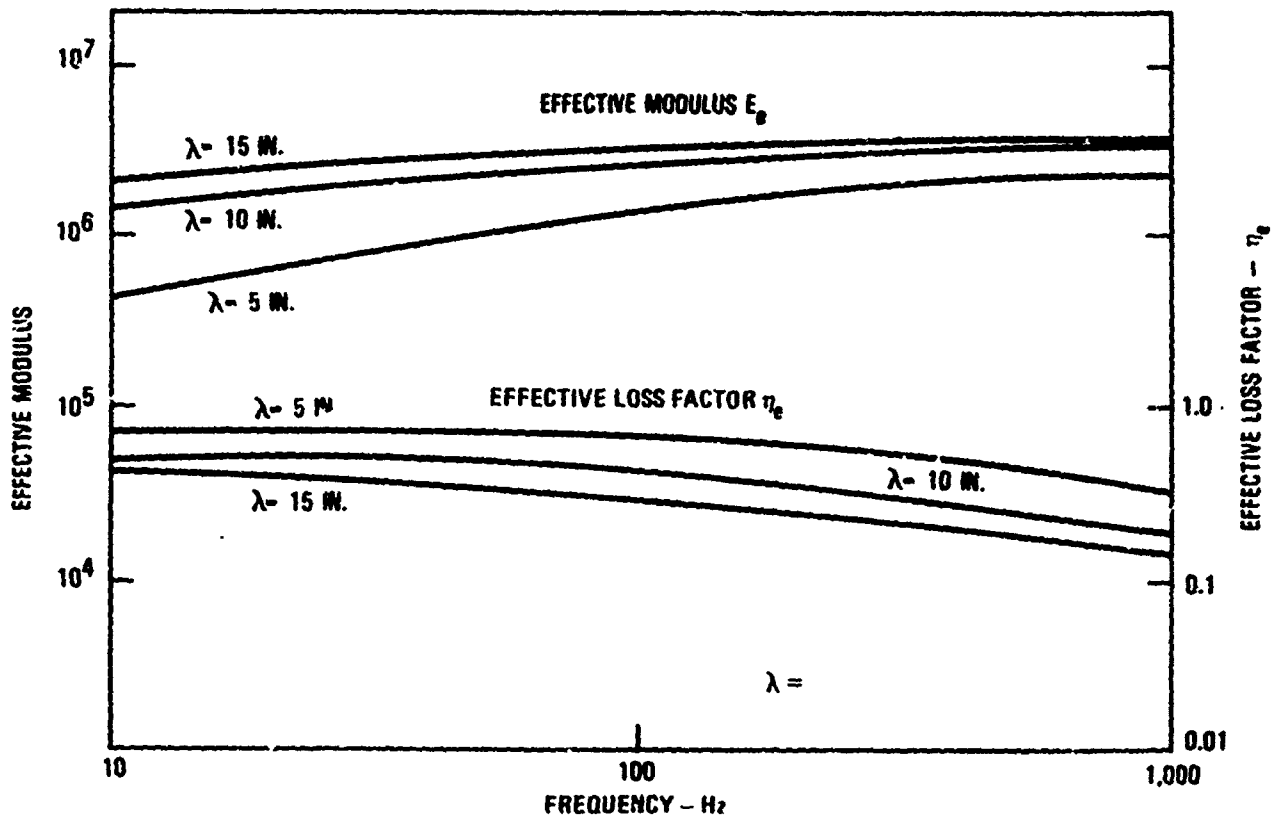


Figure 6.3.18.3. - Equivalent damping properties of the room temperature damping treatment.

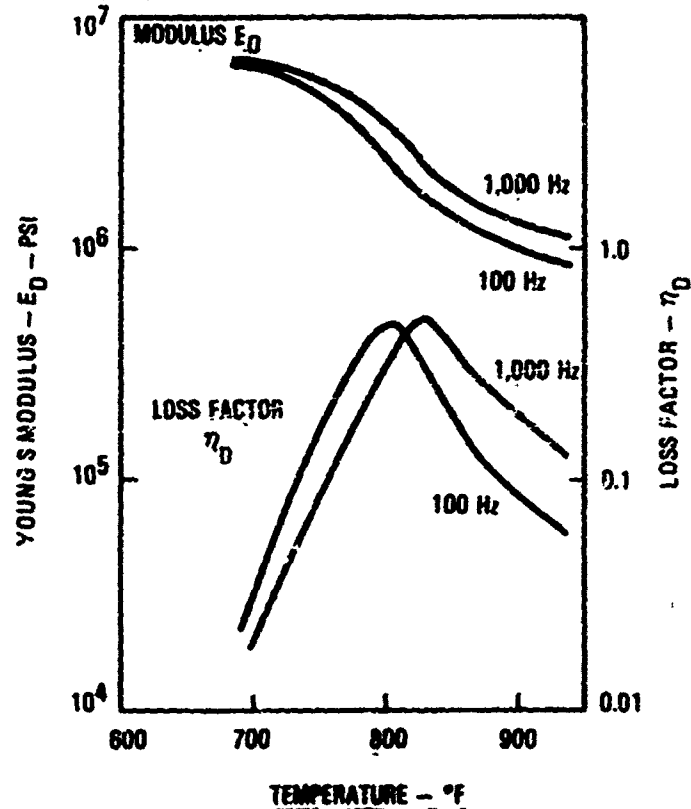


Figure 6.3.18.4. - Damping properties of Corning glass no. 8363.

for the helicopter engine exhaust extension was a 0.010 inch (0.254 mm) thick layer of Corning Glass No. 8363 enamel applied to each side of the structure.

Damped Structural Response

The damping values for the room temperature damping treatment are increased by a factor of 10 (see Figures 6.3.18.5 and 6.3.18.6). Additional testing revealed that no significant change in damping capacity occurs with 15 percent of the damping treatment removed as shown in Figure 6.3.18.7. This is significant because flaking of the enamel was encountered during field tests.

Field Survivability Evaluations

A 100 hour flight test using a CH-54 helicopter (A/C 18470) is performed to verify the integrity of the damped engine exhaust extension. After 30 hours, flaking of the enamel material occurs on the inside portion of the exhaust extension. After further investigation, it is found that an adequate damping capability can be maintained by coating the outer surface only. After the completion of the 100 hours of flight testing the exhaust extension inspection reveals no metal fatigue.

6.3.19 High Temperature Damper for an Afterburner Liner [6.39]

Problem

The purpose of the project is to develop a porcelain enamel high temperature vibration damping application to reduce the vibratory stresses in the front and midfront sections of the J85-21 afterburner liner.

Structure

The afterburner liner is a perforated four section cylindrical structure designed to attenuate the energy generated by the acoustics of combustions. (See Figure 6.3.19.1.)

Damping Material Requirement

The vibration damping coating should possess good damping characteristics for the temperature range of from 1200°F (649°C) to 1500°F (816°C) and survive exposure to 1650°F (899°C). The damping treatment is designed to damp a resonance

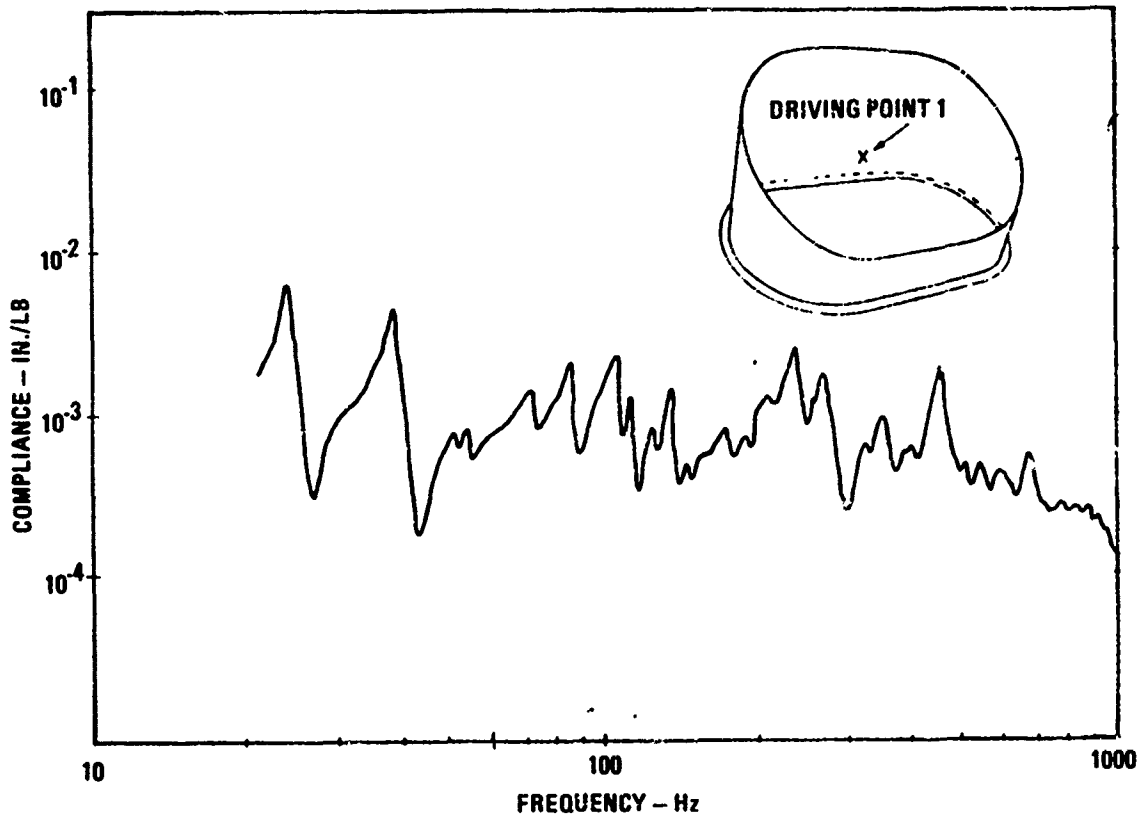


Figure 6.3.18.5. - Driving point 1 frequency response of the damped exhaust extension.

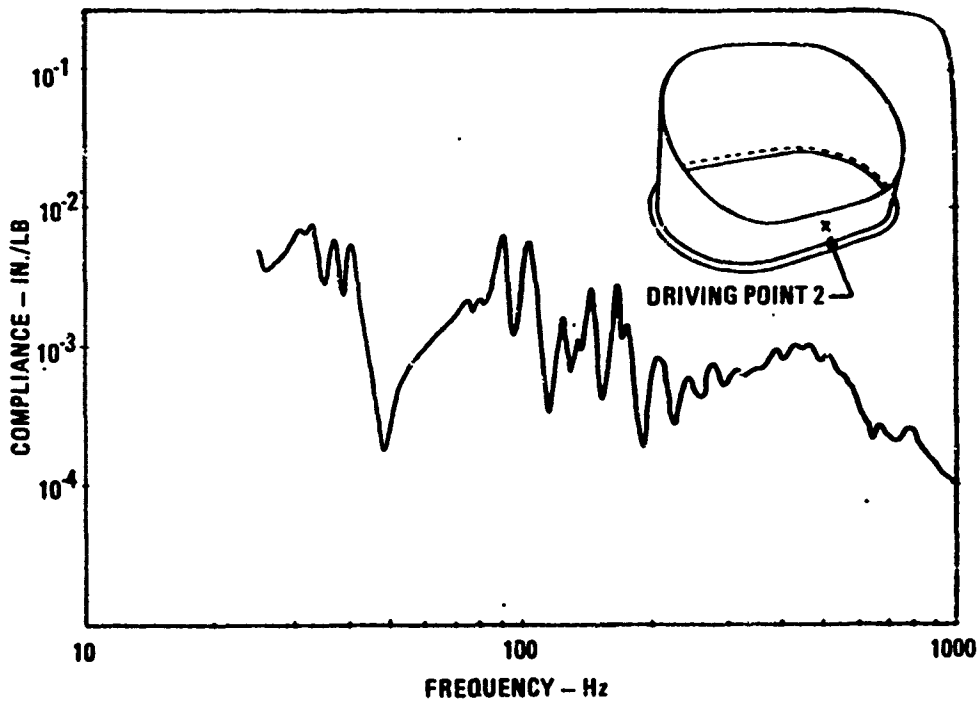


Figure 6.3.18.6. - Driving point 2 frequency response of the damped exhaust extension.

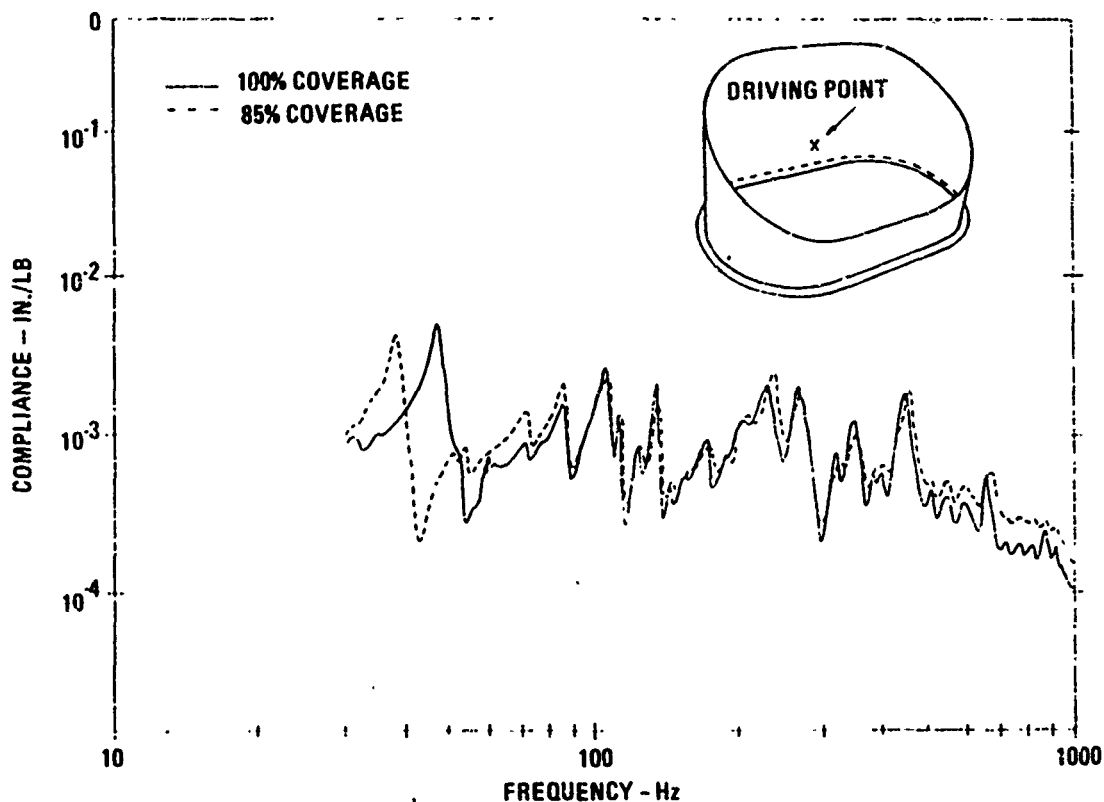


Figure 6.3.18.7. - Driving point frequency response of the damped exhaust extension showing 100% and 85% coverage.

of 145 Hertz. The damping characteristics of the porcelain coating must also remain constant for a long time exposure (300 hours) at 1600°F (871°C) temperature.

Damping Treatment Design

Using standard cantilever beam testing, sixteen materials and three multi-layer systems are evaluated for vibration damping properties. Four materials successfully meet the design criteria. Two materials are chosen to be evaluated with a nichrome protective coating applied to the beam. The damping material system is chosen but when applied to the liner it does not adhere. The damping treatment is redesigned using an O'Hommel refractory glass as the protective coating and is applied to the liner. See Figure 6.3.19.2 for damping characteristics of the damping system.

Test Cell Endurance Testing

The coated afterburner liners are engine tested for 400 cycles of advanced mission testing. During the test cracks developed at two locations on the liner. The damping treatment provided no favorable effect in reducing high cycle fatigue induced cracks as compared to the undamped liner.

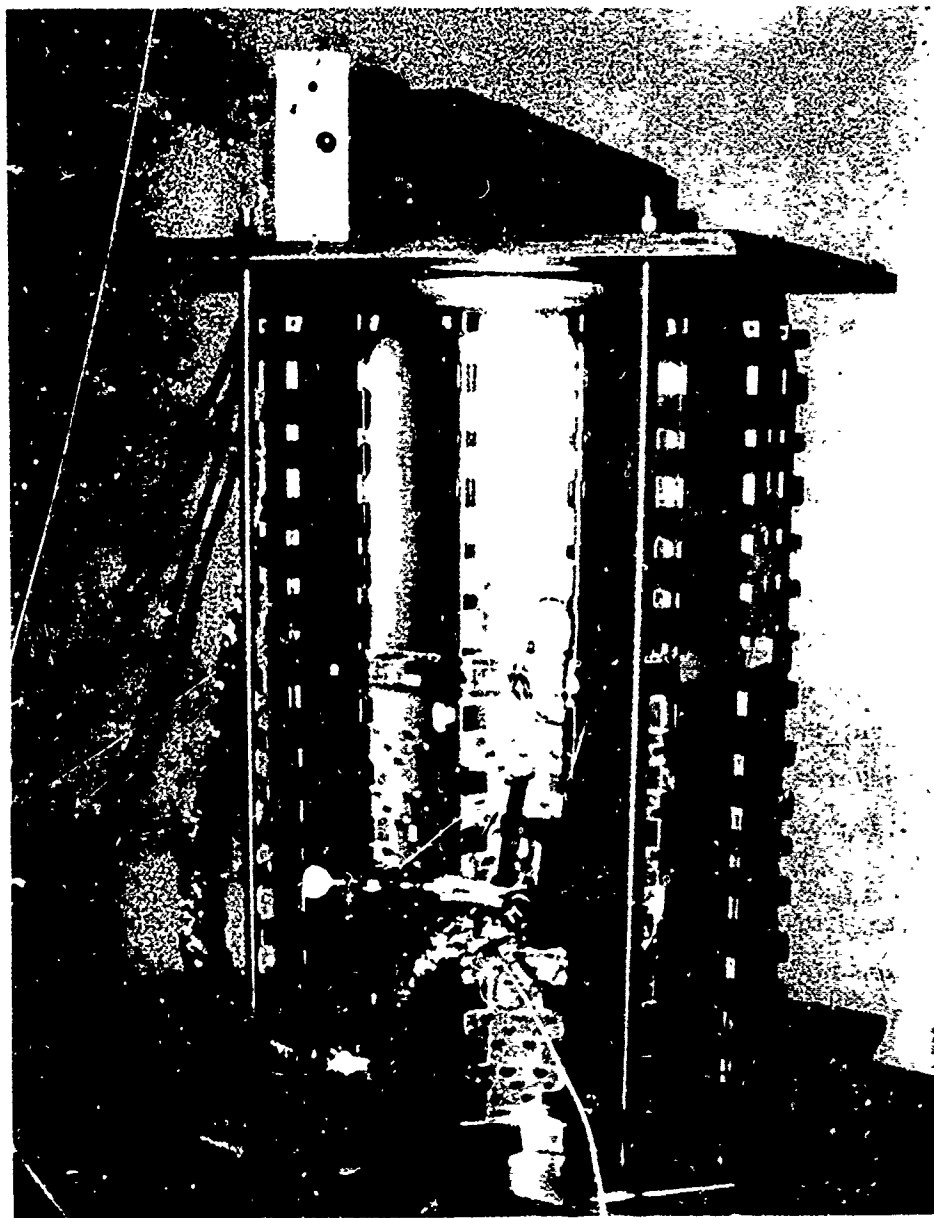


Figure 6.3.19.1 - Front two sections of the J-85 afterburner liner.

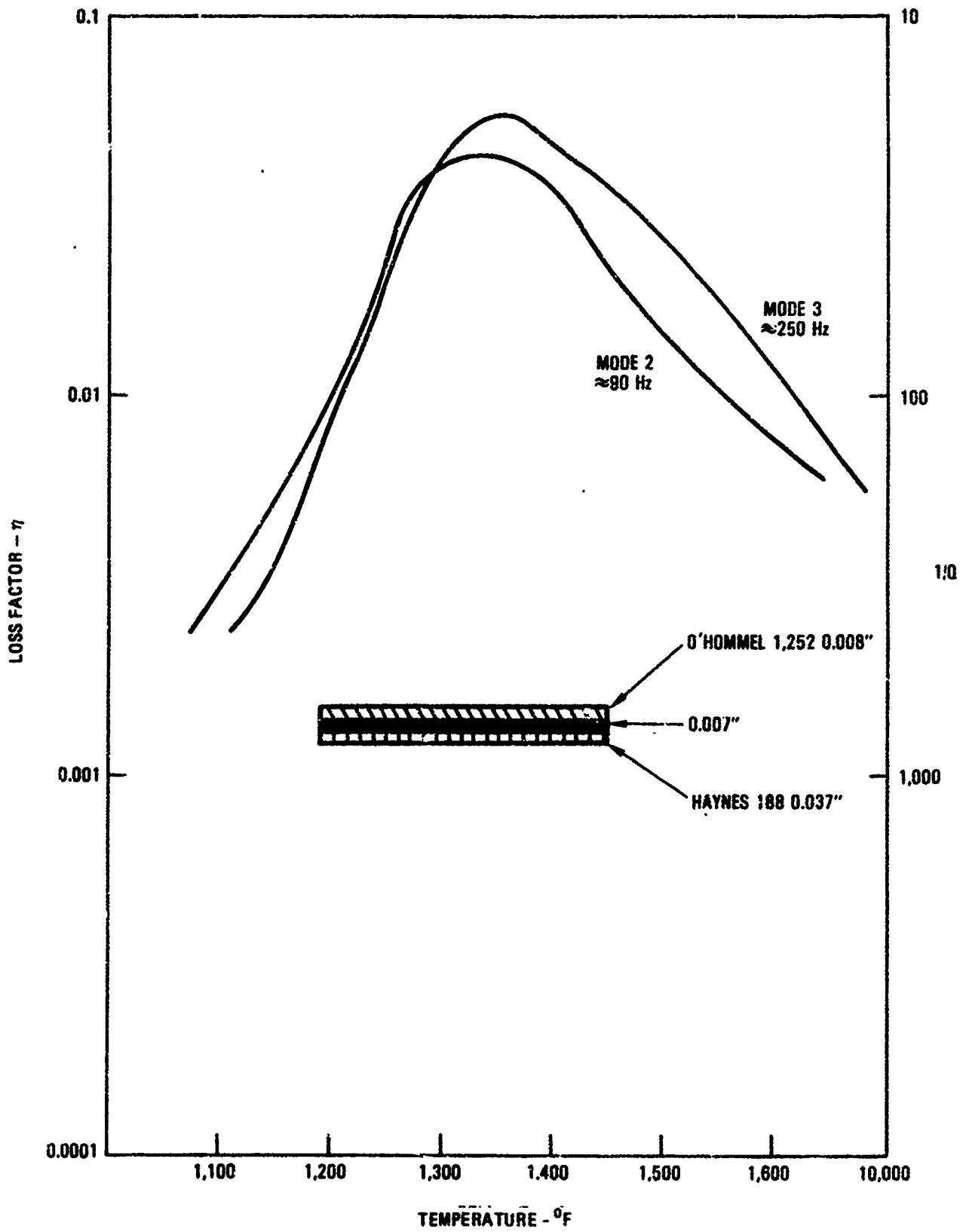


Figure 6.3.19.2. - Enamel number 21 as fired, modes 2 and 3.

Past Engine Testing Evaluation

Analysis indicated that the porcelain enamel devitrified due to exposure to a high sulphur environment in the afterburner, which caused the material to lose its good damping characteristics.

Recommendations

The enamel coating must be protected from sulphur attack by an impervious refractory overcoat. Glasses used in this type of application must be less sensitive to sulphur attack.

6.3.20 Noise Damper for the HH-53C Helicopter [6.40]

Problem

Noise levels in the cabin of the HH-53C helicopter are found to be at an unacceptable level. An acoustic intensity survey of the middle of the cabin near station 342 (Figure 6.3.20.1) showed high sound pressure levels at three frequency peaks (Figure 6.3.20.2) corresponding to gear clash frequencies in the transmission. Frequently an important part of the noise in a system is secondary noise radiation from resonating structural surfaces. An investigation is conducted to evaluate the effectiveness of the application of layered damping treatments to the skin panels of the skin-stringer structure to reduce specific peaks in the noise spectrum caused by resonant vibrations of the skin panels.

Structure

The cabin structure of the HH-53C is typical skin-stringer structure. The section of the cabin selected for investigation is illustrated in Figure 6.3.20.3. Since only a small portion of the aircraft is investigated flanking paths for noise radiated from other sources are reduced with fiberglass blankets.

Undamped Structure Response

Ground tests, in which the transmission supporting frame is excited by an electromagnetic shaker applying constant amplitude harmonic force, and flight test of the undamped structure shows structural resonances peaking at

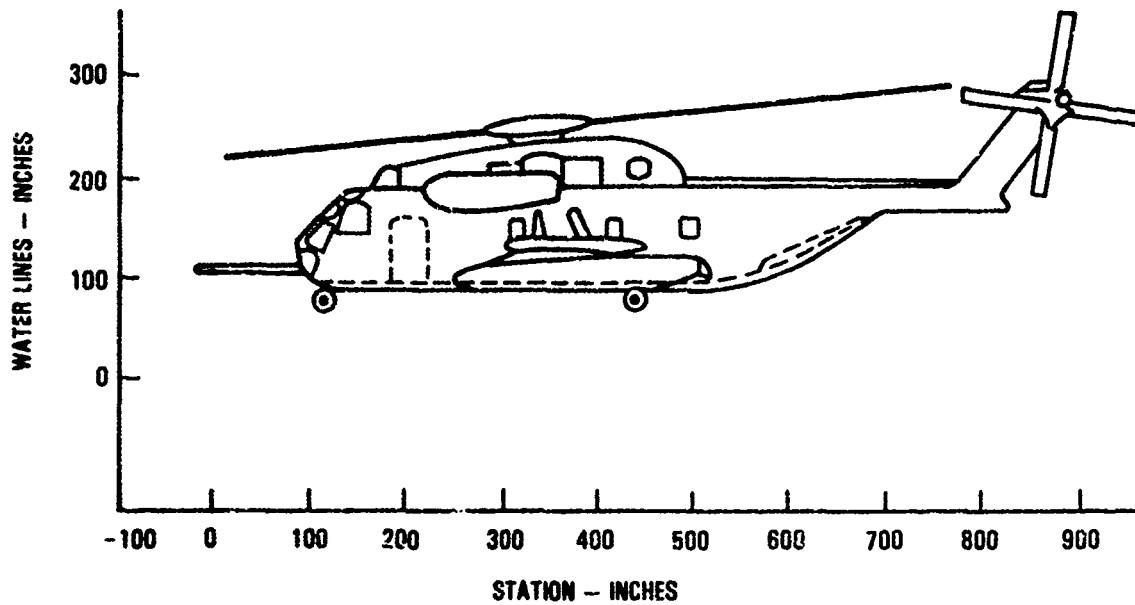


Figure 6.3.20.1. - Sideview of HH-53 helicopter.

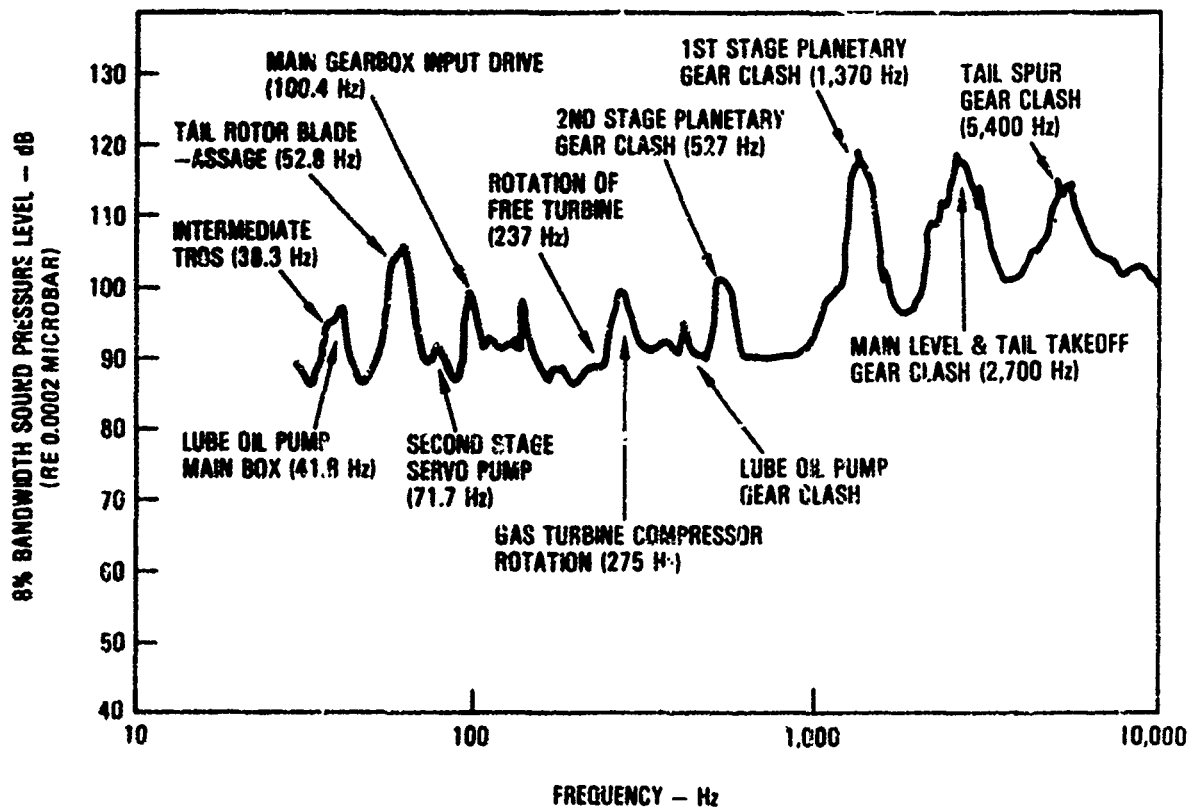


Figure 6.3.20.2. - Eight percent bandwidth sound pressure level data.

approximately 1370, 2700, and 5400 Hz corresponding to the transmission gear clash frequencies found in the previous acoustic survey. Skin panel resonances occurs at all three peaks with the heavier support structure resonances contributing to the 2700 and 5400 Hz peaks.

Damping Treatments

The damping material selected is a pressure sensitive adhesive having optimum damping near room temperature (Figure 6.3.20.4). The complex shear modulus properties as a function of temperature are shown in Figure 6.3.20.5. The layered damping treatment is illustrated in Figure 6.3.20.6. The effective temperature range can be expanded by selecting damping materials with transition regions at different temperatures (Figure 6.3.20.7).

Damped Structure Response

Narrow band (50 Hz) analysis of a small portion of the flight test data on the undamped (Flight 1) and treated (Flight 3) structure are shown in Figures 6.3.20.8 and 6.3.20.9 and summarized in Table 6.3.20.1. Keep in mind that large reductions in noise level are not expected because of the limited area treated. During ground tests, resonances are excited by an electromagnetic shaker through an impedance head. Comparative results of responses to harmonic excitation during ground tests are presented in Figure 6.3.20.10. The reductions in peak response at the frequencies of interest compared favorably with those observed in the flight test data.

Conclusion and Implementation

This study demonstrated the effectiveness of layered damping treatments to skin panels in the HH-53, VH-3, and SH-3H helicopters. In the Air Force HH-53 helicopters, approximately 150 square feet (13.9 square meters) of coverage is used adding only 37 pounds per aircraft. Installation time is about 24 man-hours per aircraft.

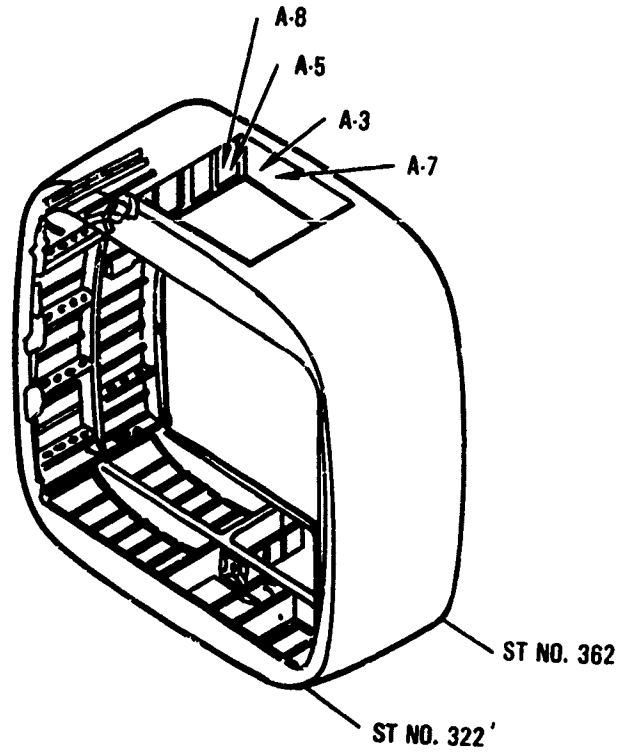


Figure 6.3.20.3. - Isometric view of center cabin structure where damping is applied.

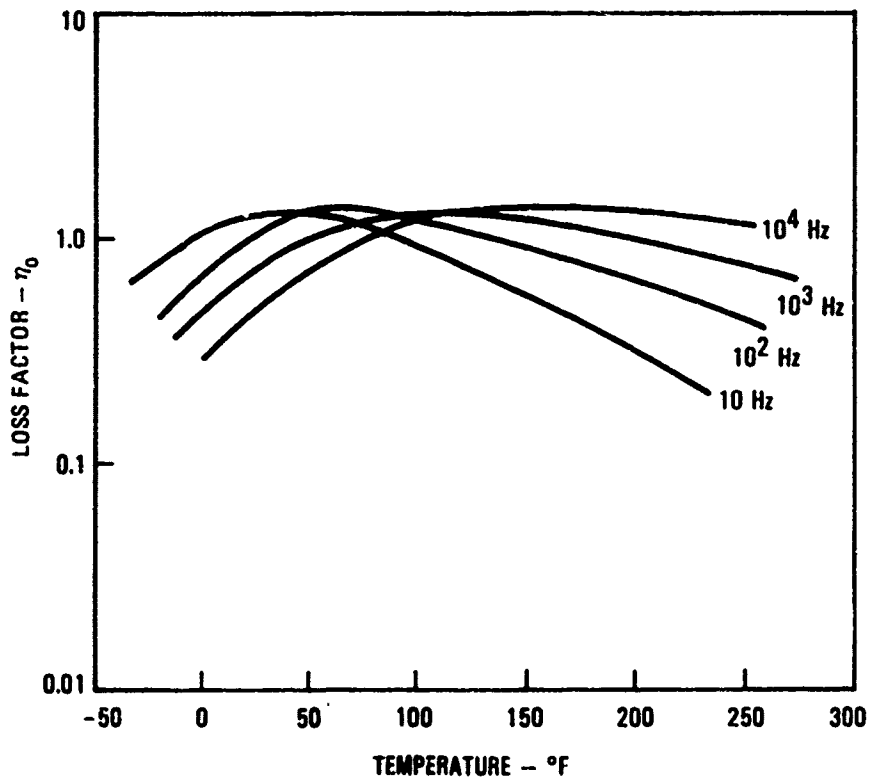


Figure 6.3.20.4. - Variations of the loss factor with temperature and frequency.

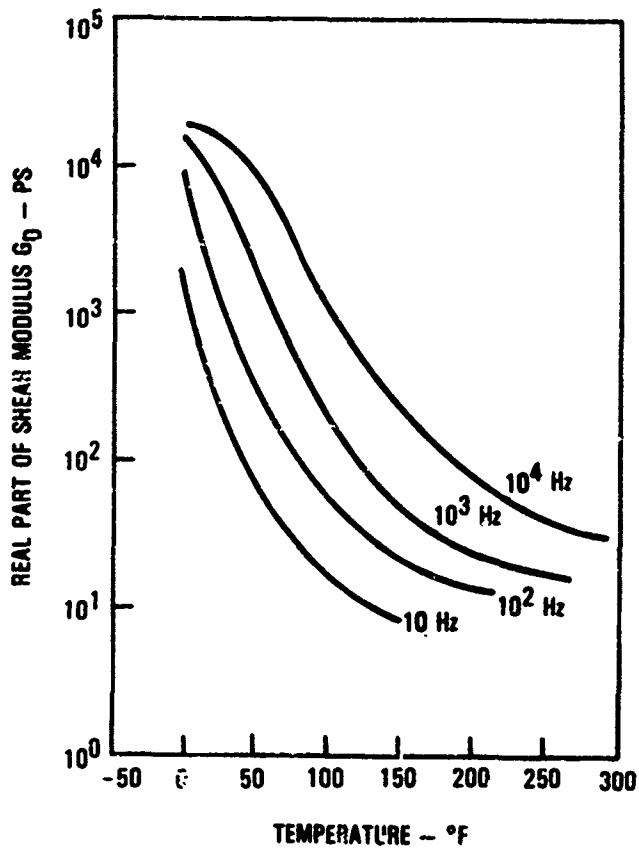


Figure 6.3.20.5. - Variations of the real part of shear modulus with temperature and frequency.

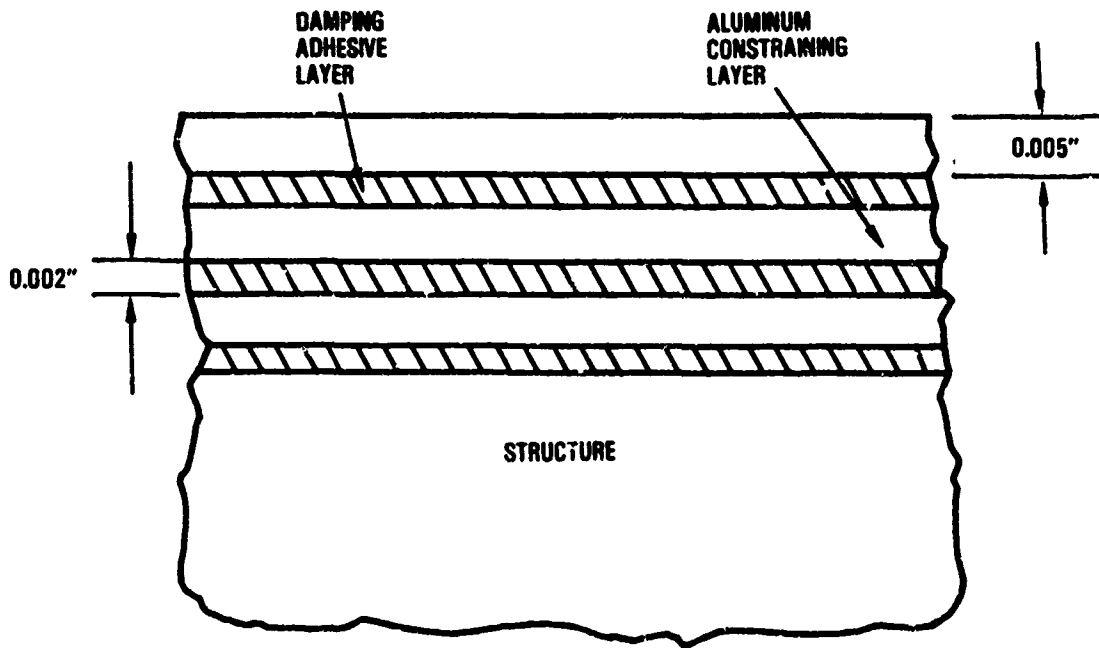


Figure 6.3.20.6. - Layered damping treatment.

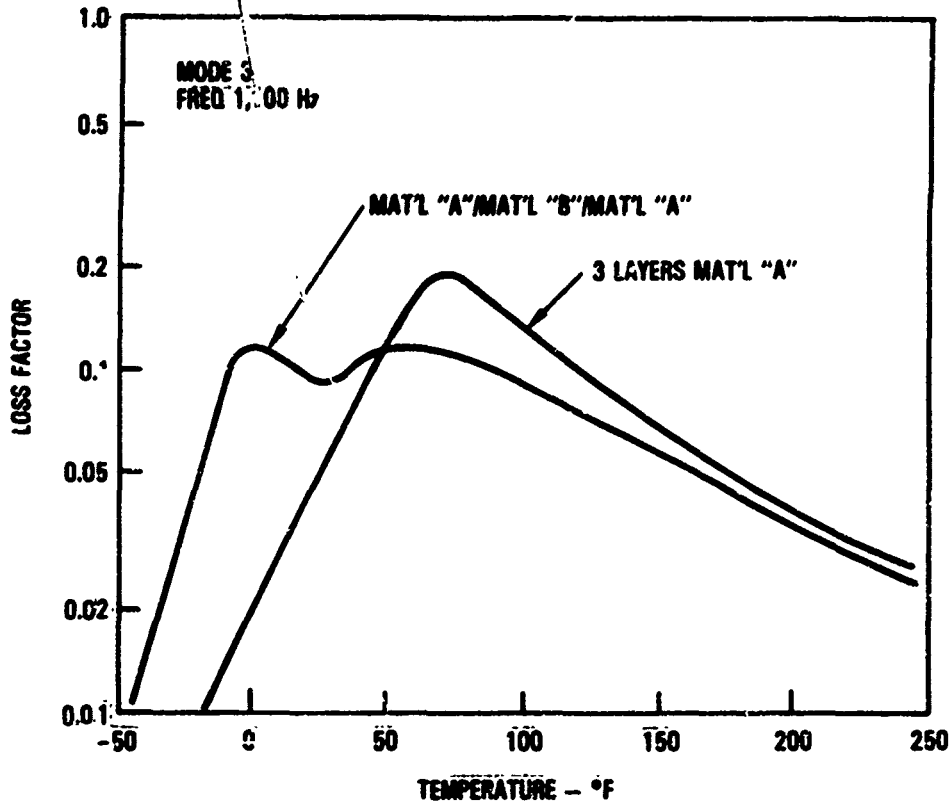


Figure 6.3.20.7. - System loss factor of a clamped-clamped beam with multiple layer damping treatments.

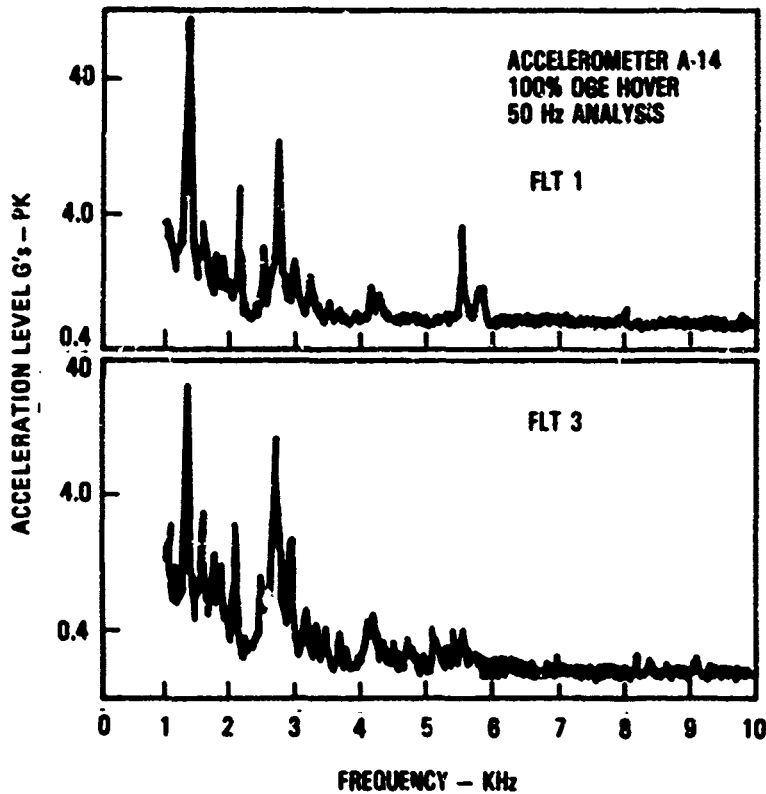


Figure 6.3.20.8. - Acceleration - 100% OGE hover.

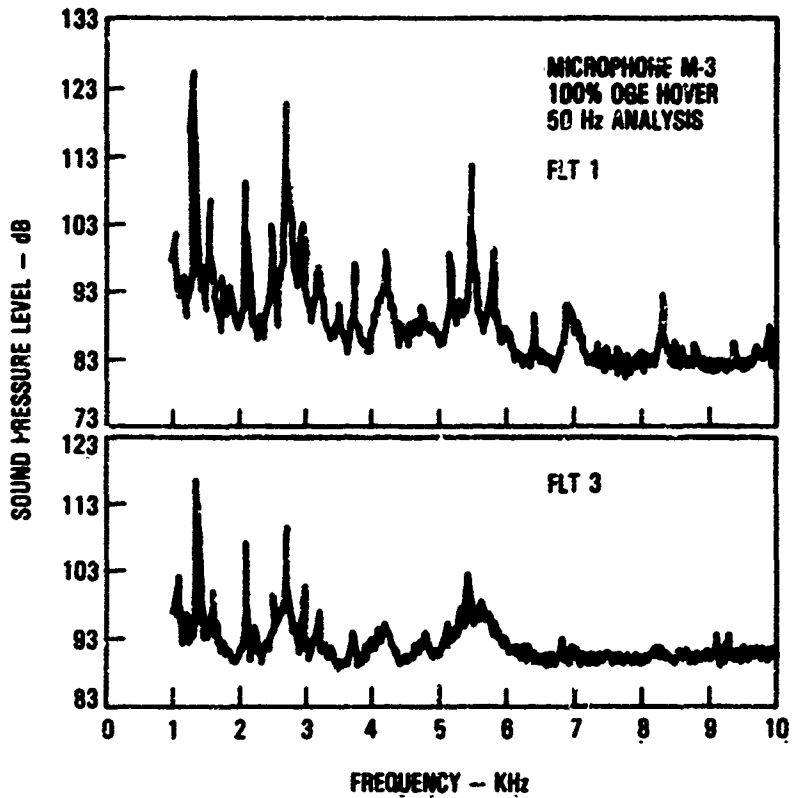


Figure 6.3.20.9. - Microphone data - 100% OGE hover.

TABLE 6.3.20.1. NARROW BAND ACCELERATION AND ACOUSTIC LEVELS OF FLIGHT 3 COMPARED WITH FLIGHT 1.

Acceleration (A-14); dB Ref. Flight 1			
	1370 Hz	2700 Hz	5400 Hz
O.G.E. Hover 95%	-11 dB	-9 dB	0 dB
O.G.E. Hover 100%	-13	-2	-10
O.G.E. Hover 105%	-2	-5	-9
Sound Pressure Level - O.G.E. Hover 100%			
M-3	-10	-12	-9
M-5	-11	-17	-7

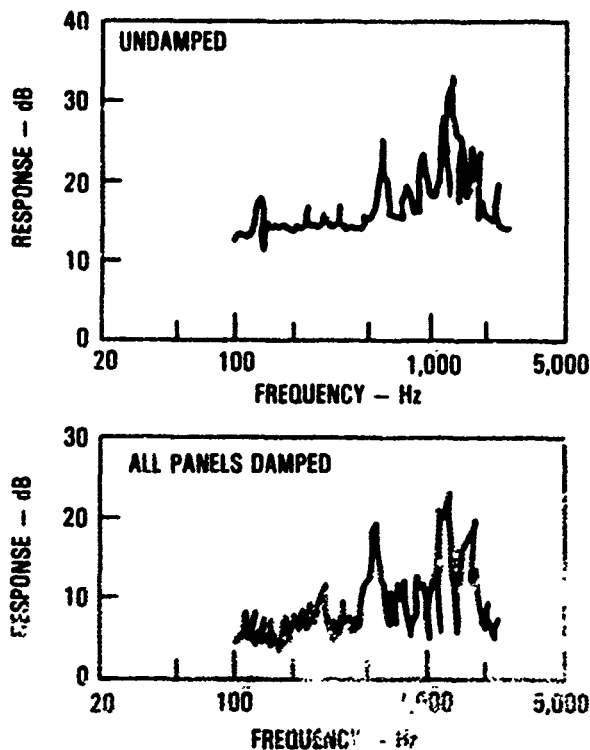


Figure 6.3.20.10. - Typical ground vibration test spectra.

6.3.21 Turbine Blade High Cycle Fatigue Control Methods [6.41]

Problem

High cycle resonant fatigue occurs quite often in jet engine turbine blades. The primary mode of failure is the first bending mode of the blade.

Structure

The turbine blades are made from high temperature super alloys. The construction varies considerably depending on the size of the engine and the particular stage the blade is in. A typical blade is shown in Figure 6.3.21.1.

Undamped Structural Response

Figure 6.3.21.2 shows the room temperature undamped response of a particular turbine blade. The first bending mode occurs at 746 Hz (see Figure 6.3.21.3). The first torsional mode occurs at 824 Hz (see Figure 6.3.21.4). Figure 6.3.21.5 shows typical modal loss factor versus temperature for turbine blades.

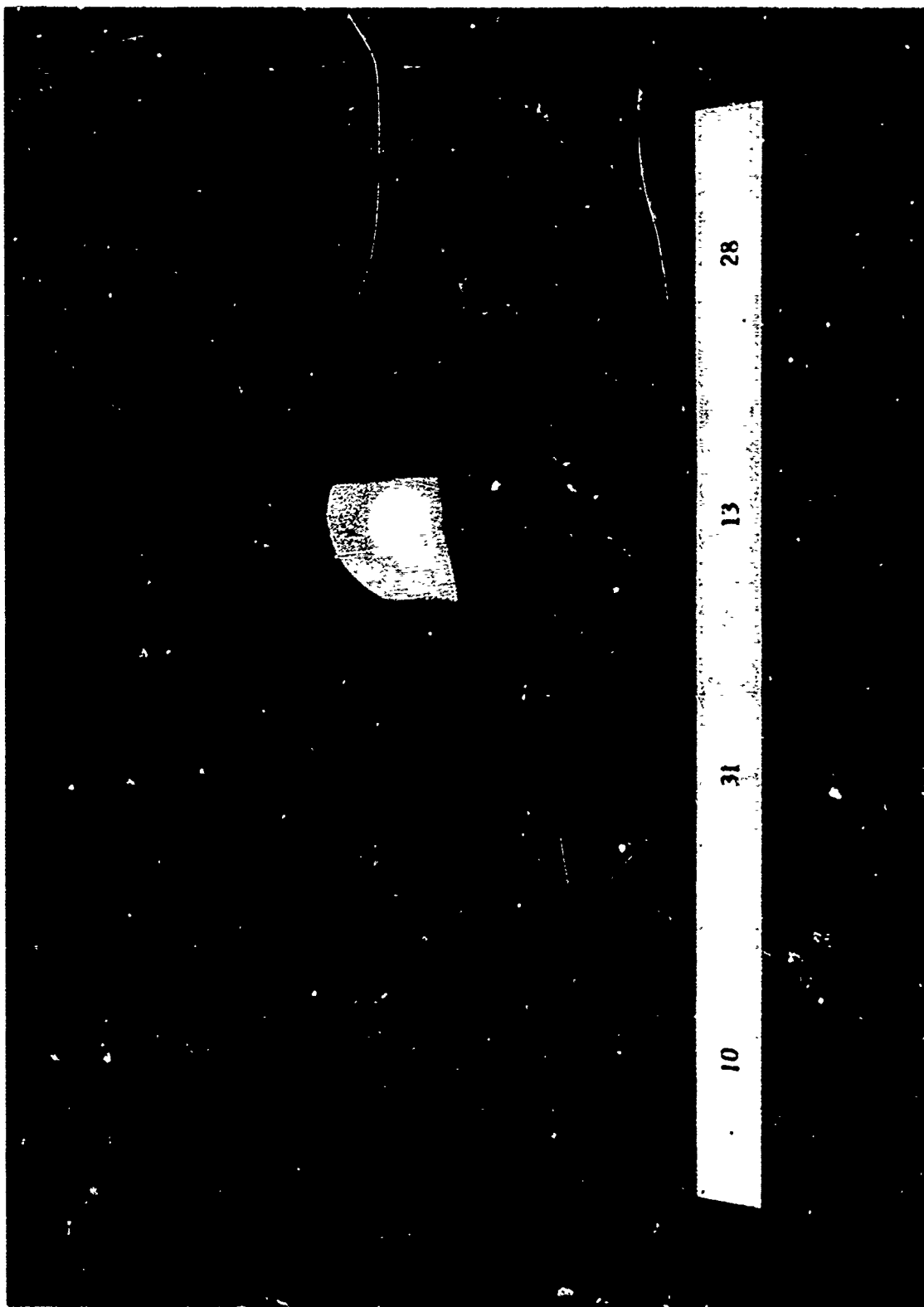


Figure 6.3.21.1. - Typical turbine blade. (Note: Half blade damping coatings applied.)

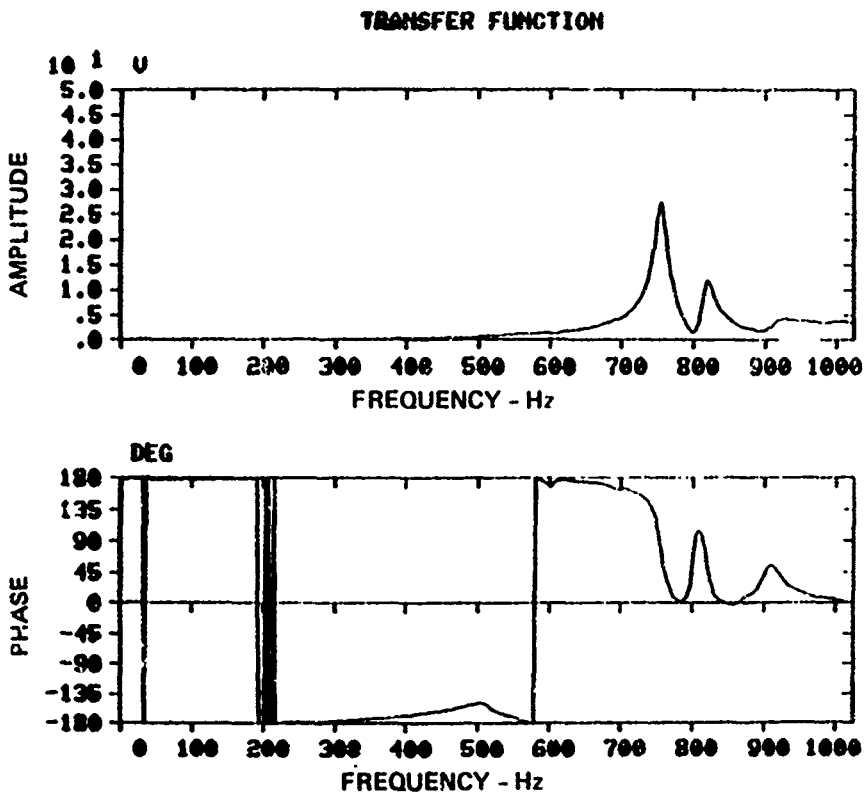


Figure 6.3.21.2. - Transfer function taken at point 4 on blade.

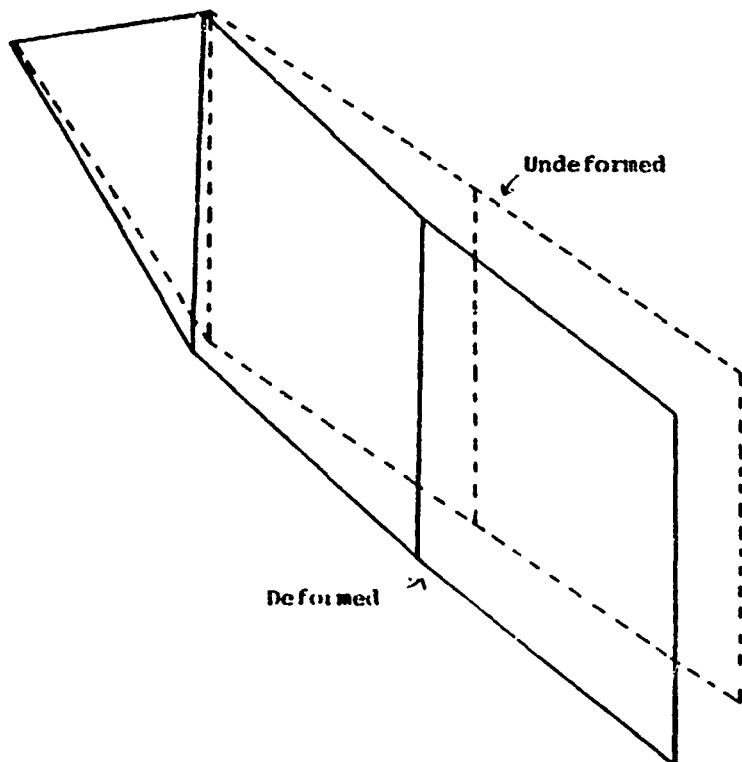


Figure 6.3.21.3. - First bending mode, 746 Hz, deformed mode shape superimposed on undeformed mode shape.

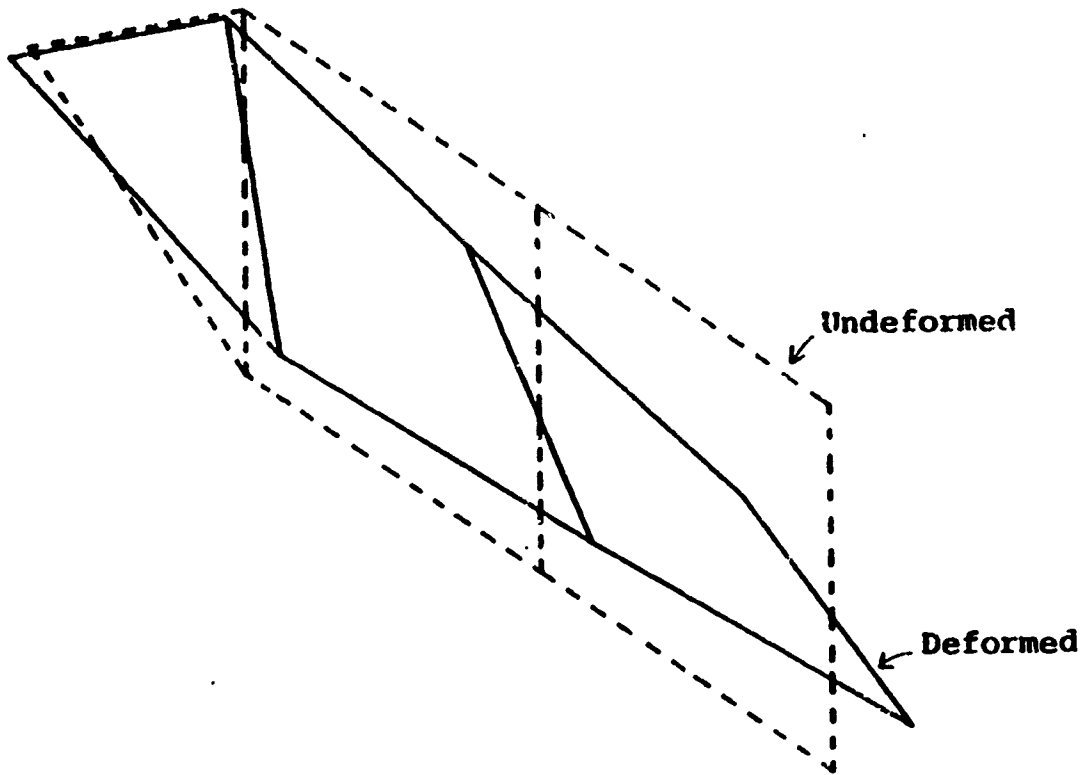


Figure 6.3.21.4. - First torsional mode, 824 Hz, deformed mode shape superimposed on undeformed mode shape.

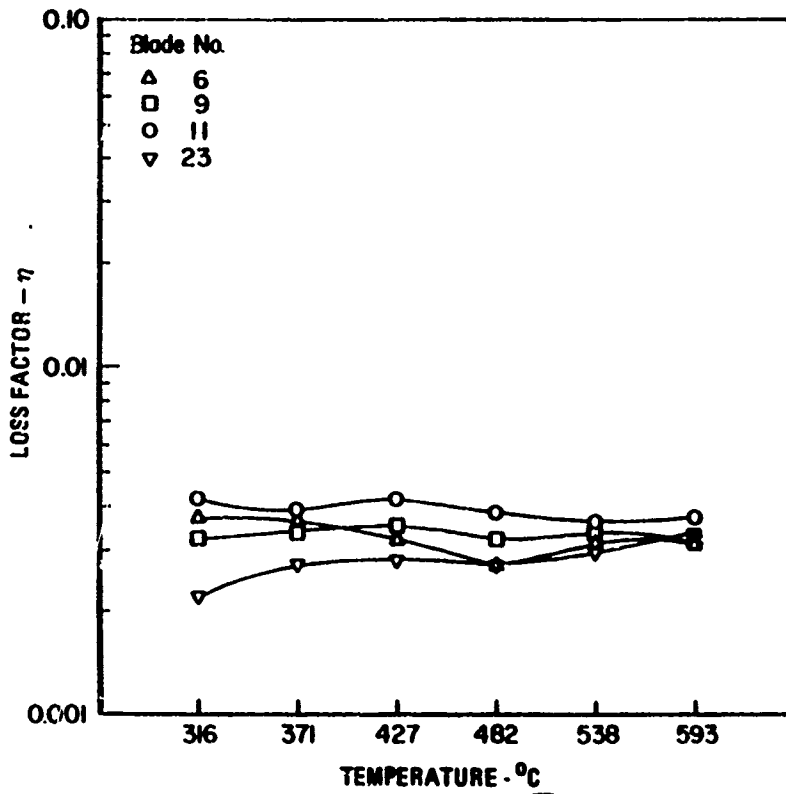


Figure 6.3.21.5. - Loss factor measurement for undamped blades.

Damping Treatments

The operational temperatures of turbine blades vary from over 2000°F (1093°C) to below 1000°F (538°C). For this particular test series, the design temperature varies from 750°F (399°C) to 1000°F (538°C). The damping materials used are enamels (see Volume III). The configurations evaluated are:

- 1) Whole Blade Coating (free-layer damping)
- 2) Half Blade Coating (free-layer damping)
- 3) Half Blade Constrained Layer Damping
- 4) Root Coating

The free and constrained layer damping designs functioned normally. The root coating is a deliberate attempt to replace the friction damping (slip) in the dove tail root section with viscoelastic material damping.

Damped Structural Response

The damping coatings are tested in the laboratory and in a heated spin pit. Figure 6.3.21.6 shows the modal loss factor versus temperature for several damping configurations. As can be seen, the blade damping is significantly improved. The spin pit results indicated that the root coatings produced the maximum strain reduction.

Damping System Durability

The high temperature, high centrifugal load environment destroyed the damping designs during the tests (see Figure 6.3.21.7). The blade coatings with a protective covering shows promise for providing the required durability. Free-layer materials are spun off the blade. The root coatings also showed promise as a feasible design, particularly if the design of the root attachment area is modified to more readily accommodate a damping coating.

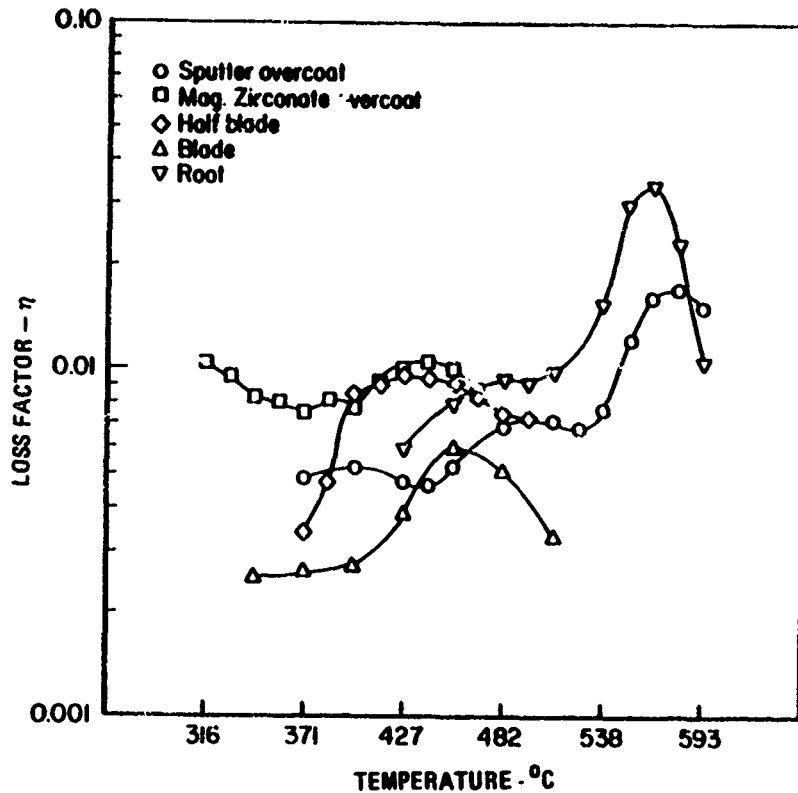


Figure 6.3.21.6. - Results of damping material 8463 tested in all five damping configurations.

6.3.22 Exducer-Turbine Assembly Damper

Problem

Resonant fatigue cracking occurs in the exducer-turbine assembly of the C-5 cooling turbine. The cracks are developing across the exducer blade tips. Resonance is induced by turbulent airflow through the assembly.

Structure

The structure consists of the exducer and turbine mounted on a common shaft, the downstream face of the exducer mates with the upstream face of the turbine. (See Figure 6.3.22.1.)

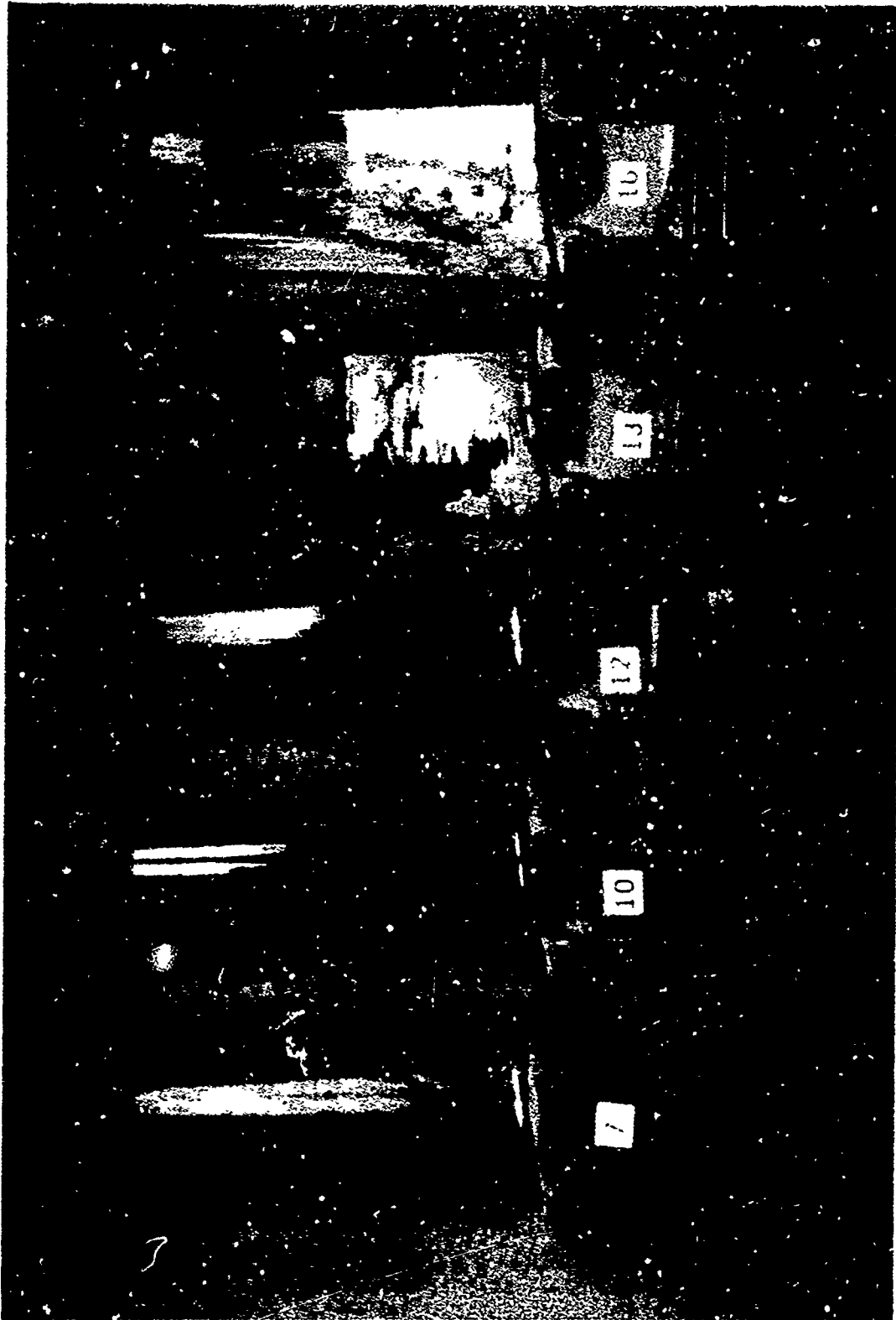


Figure 6.3.21.7. - Damping coatings after spin testing.

Undamped Structure Response

The structure is excited by an electromechanical shaker inducing harmonic oscillating motion of constant acceleration amplitude about the axis of rotation of the assembly. Responses are measured with a low mass accelerometer mounted at the tips of exducer and turbine blades. The experimental apparatus is illustrated in Figure 6.3.22.1.

The laboratory tests of the structure identified resonances at 5300 Hz and 8500 Hz. Laser holography is used to photographically identify the lower resonance to be the first bending mode of the exducer blade and the 8500 Hz resonance to be one of the bending modes of the turbine blade. The acceleration spectra for the tips of the undamped exducer and turbine blades are presented in Figures 6.3.22.2 and 6.3.22.3, respectively. The scale, in these figures, is proportional to g, the acceleration due to gravity.

Damping Treatments

Two damping mechanisms are evaluated for relative effectiveness in reducing damaging response amplitudes. The first is a mid-span steel damper wire, the other being a laminated viscoelastic treatment sandwiched between the mating surfaces of the exducer and turbine (Figure 6.3.22.4). The multi-layer configuration was selected to give flexibility in expanding the temperature range of effective damping.

Damped Structure Response

Response spectra of the tip acceleration amplitudes of the assembly treated with the midspan wire damper are presented in Figures 6.3.22.5 and 6.3.22.6 and the spectra of the assembly treated with the viscoelastic sandwich are presented in Figures 6.3.22.7 and 6.3.22.8.

Curves of the modal loss factor, η_g , for the three configurations are given in Figures 6.3.22.9 and 6.3.22.10.



Figure 6.3.22.1. - Exducer turbine assembly with electromechanical shaker attached.

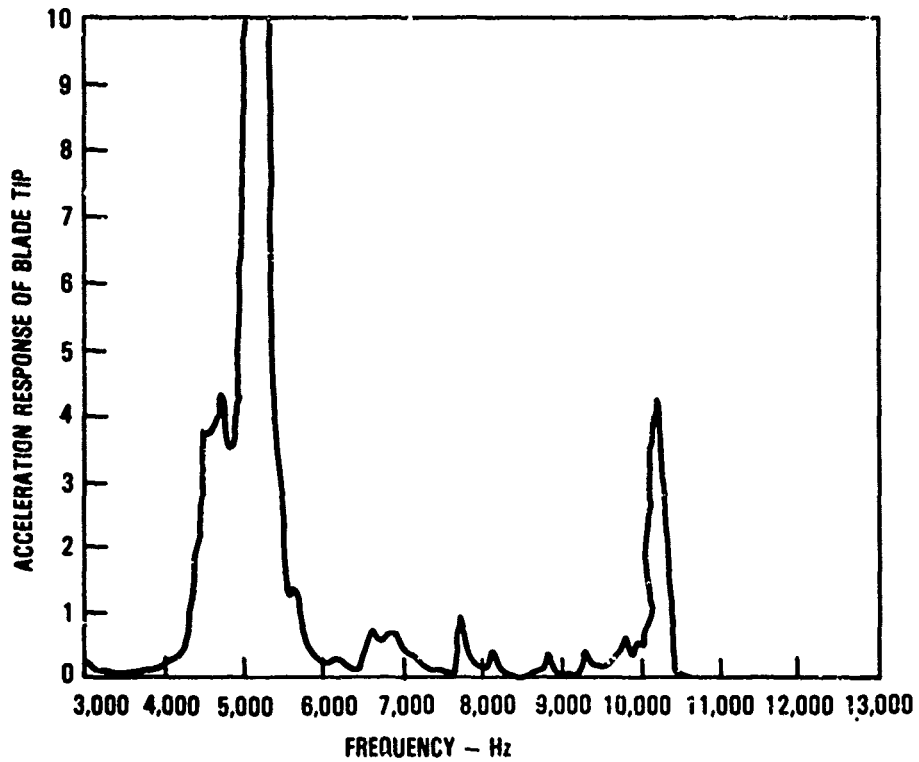


Figure 6.3.22.2. - Tip vibration response of an exducer blade for the undamped C-5 cooling turbine.

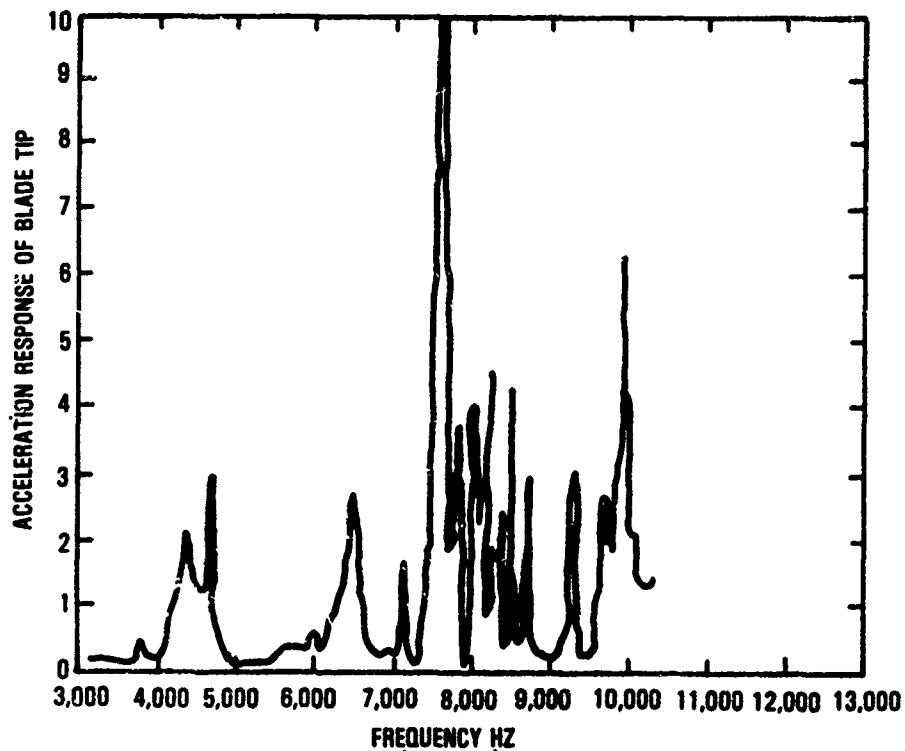


Figure 6.3.22.3. - Tip vibration response of a turbine blade for the undamped C-5 cooling turbine.

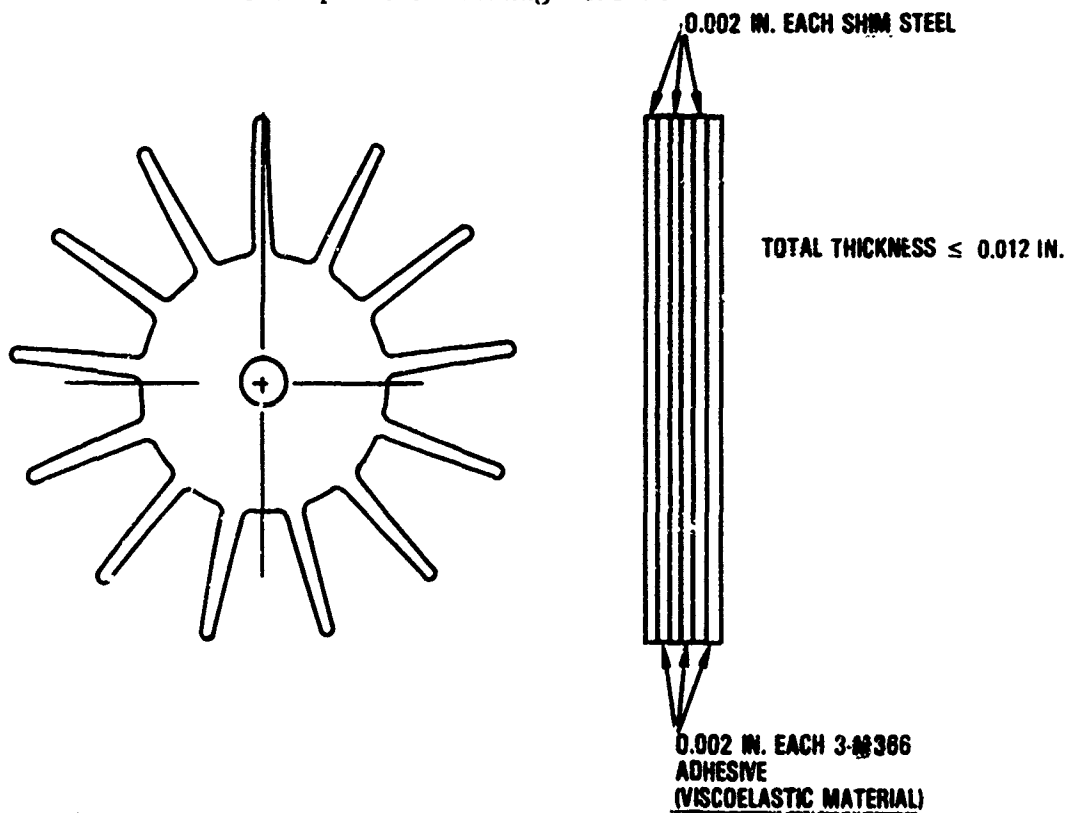


Figure 6.3.22.4. - Configuration of viscoelastic damping treatment placed between exducer and turbine section of C-5 cooling turbine.

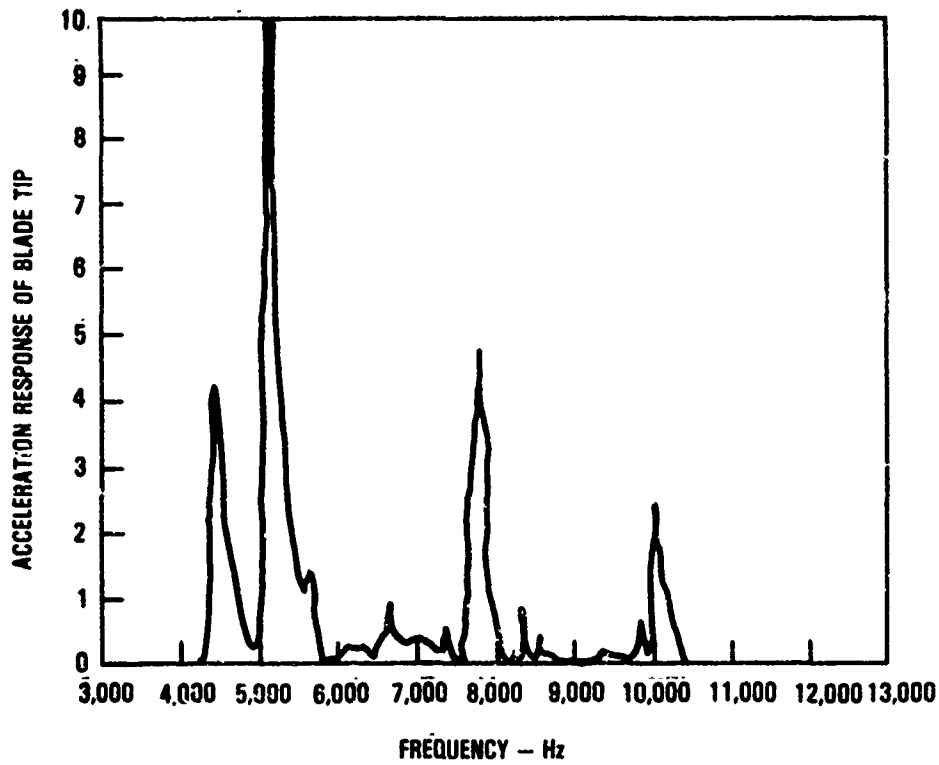


Figure 6.3.22.5.- Tip vibration response of an exducer blade of the C-5 cooling turbine damped with the midspan wire damper.

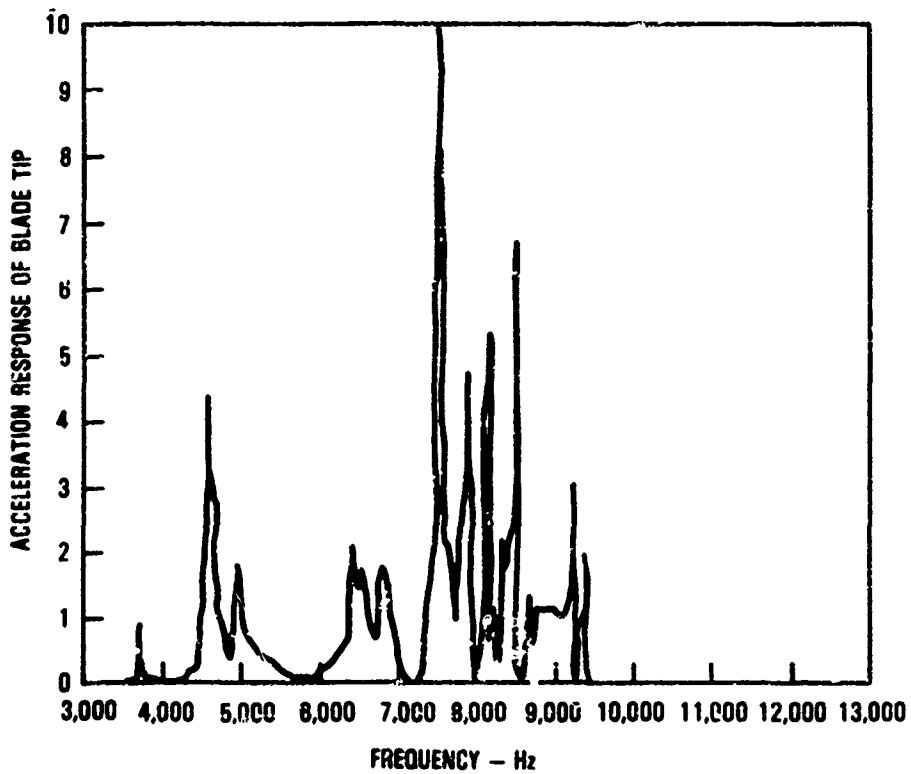


Figure 6.3.22.6. - Tip vibration response of a turbine blade of the C-5 cooling turbine with the midspan wire damper.

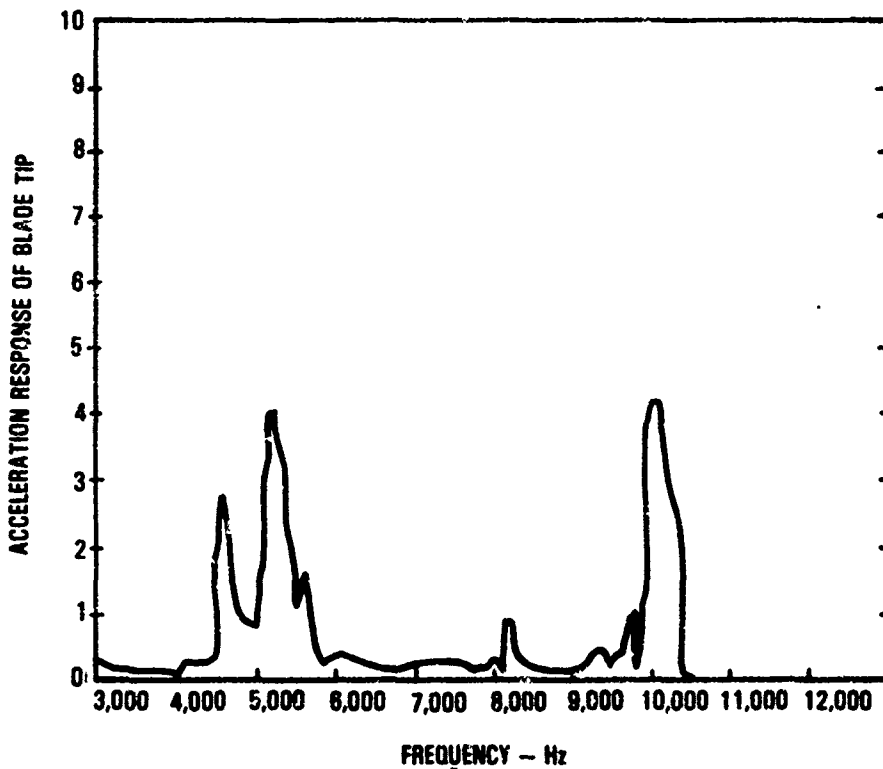


Figure 6.3.22.7. - Tip vibration response of an exducer blade of the C-5 cooling turbine damped with a viscoelastic treatment between exducer and turbine.

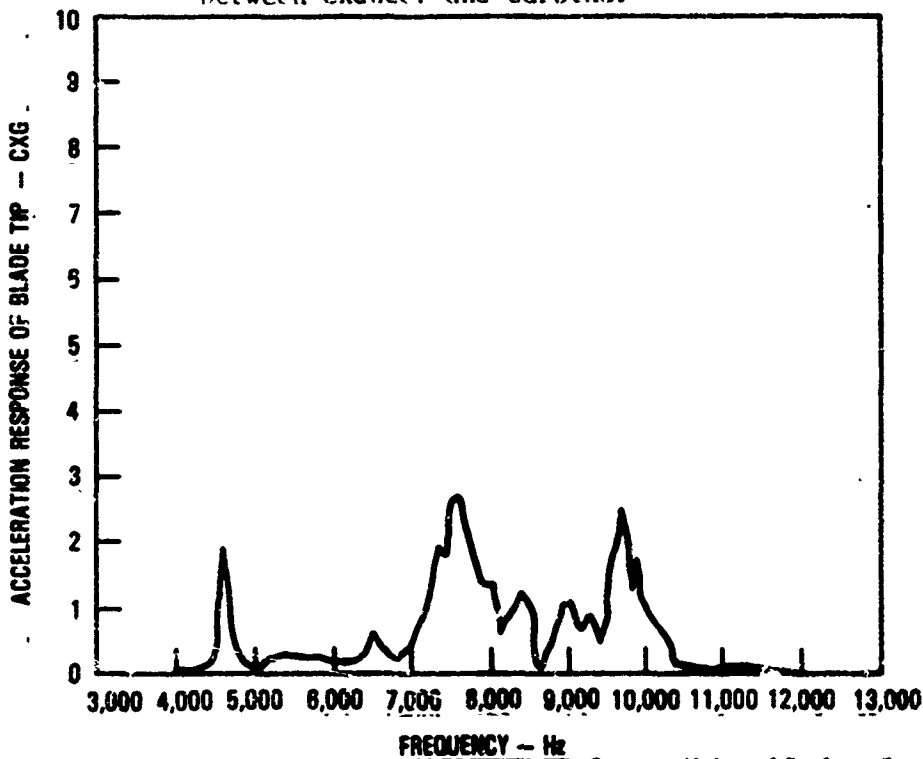


Figure 6.3.22.8. - Tip vibration response of a turbine blade of the C-5 cooling turbine damped with a viscoelastic damping treatment between exducer and turbine

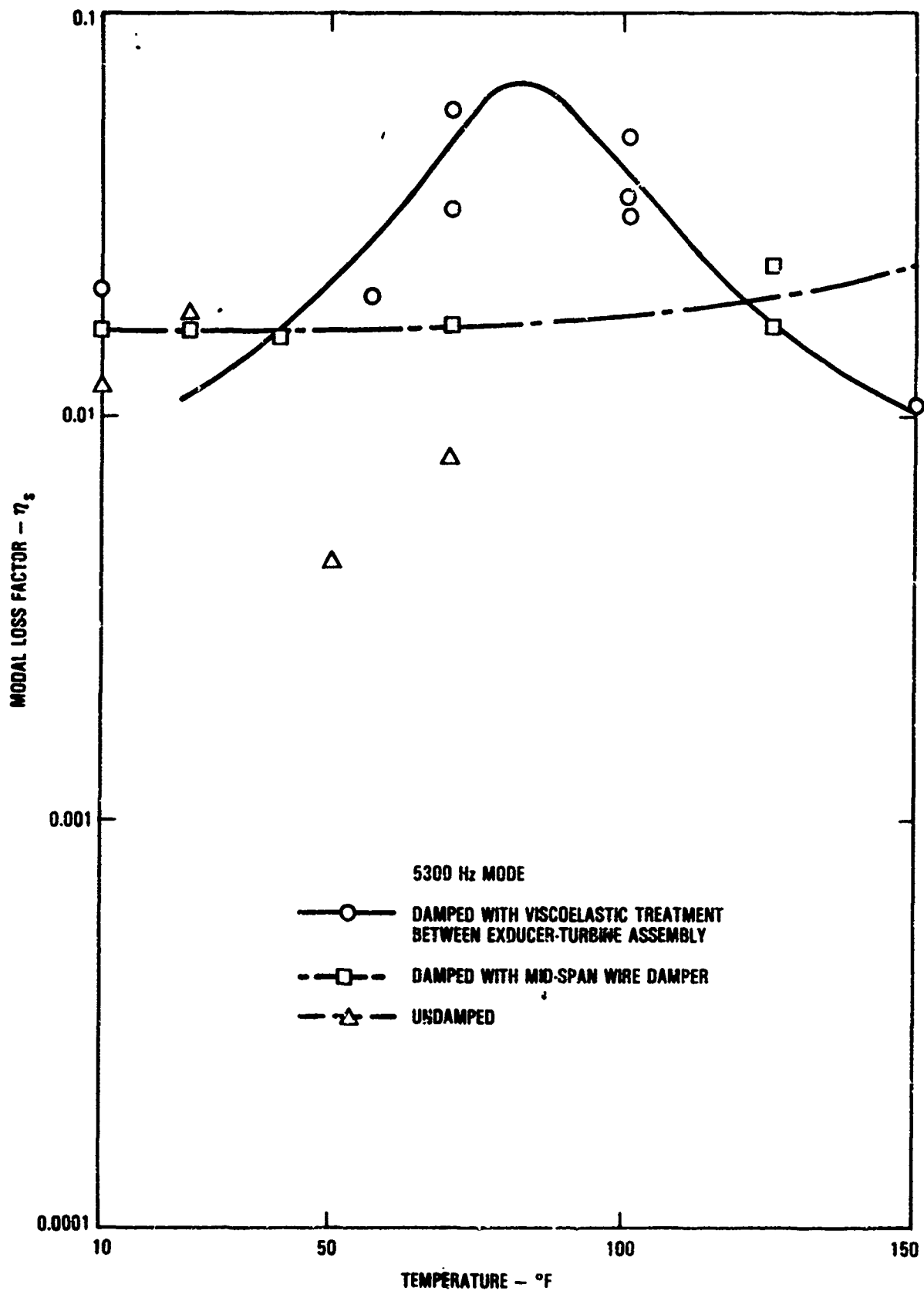


Figure 6.3.22.9. - Modal loss factor versus temperature for three configurations of the C-5 cooling turbine.

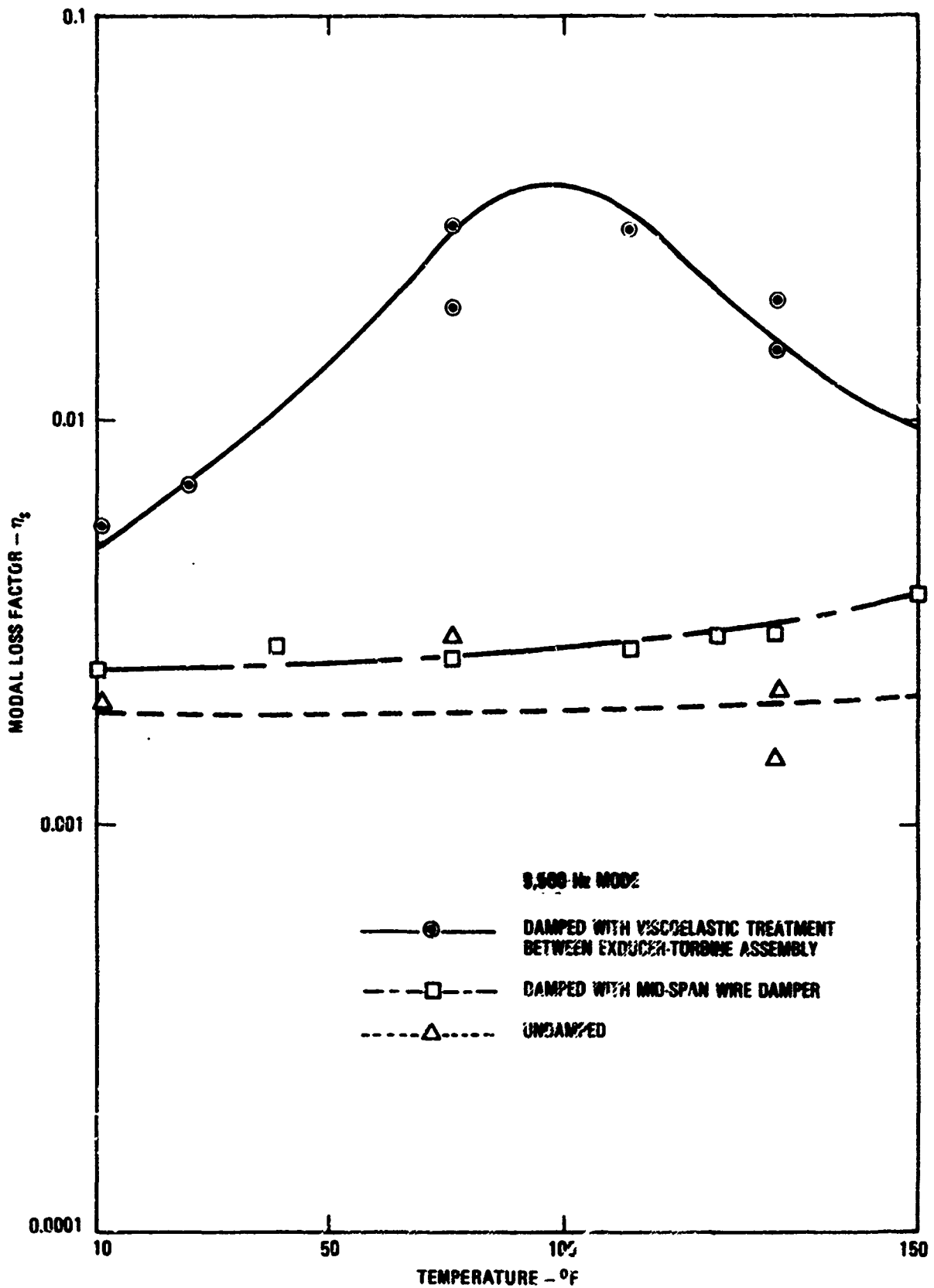


Figure 6.3.22.10. - Modal loss factor versus temperature for three configurations of the C-5 cooling turbine.

These illustrations show a slight increase in modal damping affected by the midspan wire damper and a significant increase in peak modal damping resulting from the viscoelastic treatment at approximately 80°F (27°C). The temperature range over which improved damping is demonstrated varies from approximately 40°F (4°C) to 120°F (49°C).

Recommendations

It is recommended, if the need to reduce vibratory stress levels continues to be critical, design a viscoelastic treatment similar to the one evaluated that would be effective over the operating temperature range of the exducer turbine assembly and also survive the high centrifugal load that it would experience in an operating system.

6.3.23 Shear Damper for Micro-Inch Deflections [6.42]

Problem

Vibrations in the long magnetometer and heavy RTG booms are induced from the rotation of the TV camera on the Mariner Jupiter/Saturn 1977 (MJS77) spacecraft. The vibrations cause jitter in the TV transmission.

Structure

The joints and overall construction are typical of spacecraft materials and construction.

Undamped Structural Response

Slowing of the TV camera generated a disturbance along the science boom which excited structural resonances in the support arms of the experiments. The structural damping is very low; and therefore, the settling time is quite long. The vibration results in blurry TV. Figure 6.3.23.1 shows the undamped settling time.

Damping Treatment

The damper design has two critical requirements. First, the damper has to function in a displacement range of 0.0025 inches (0.0635 mm) to

100 micro-inches (2.54×10^{-3} mm). Secondly, it had to operate in the frequency range of 1.28 to 0.16 Hz. The temperature range over which damping is required is 50°F (10°C) to 85°F (29°C). The required damping is achieved by incorporating shear dampers in the joints at the base of the booms that need damping. The shear damper provides constrained layer damping by sandwiching the damped washer between the inner and outer flanged sleeves (see Figure 6.3.23.2). The damper stiffness is designed to insure at least a 0.1% shear in the damper during any vibration.

Damped Structural Response

Figure 6.3.23.1 shows the greatly reduced settling time with the damper installed.

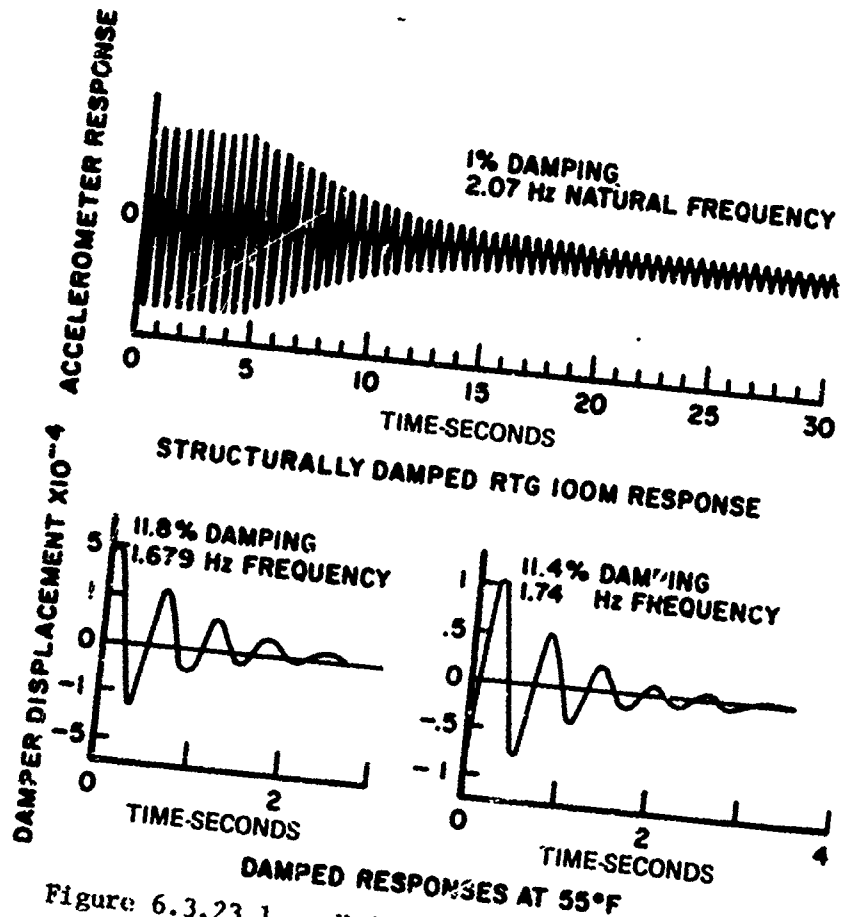


Figure 6.3.23.1. - Undamped and damped response.

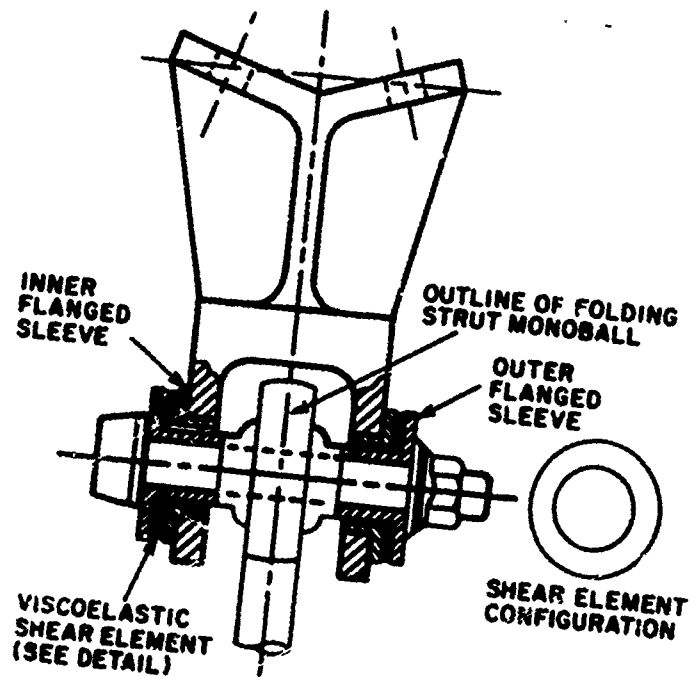


Figure 6.3.23.2. - Damping design.

REFERENCES

- 6.1 Drake, Michael L., "A Damping Technology Solution to an Automotive Vibration Problem," *Sound and Vibration*, September 1983, pp. 20-24.
- 6.2 University of Dayton Research Institute Vibration Damping Short Course Notebook, 1982.
- 6.3 Drake, M.L. and J.D. Sharp, "An Example of Additive Damping as a Cost Savings Alternative to Redesign," ASME Publication Number 77-WA/CT-2.
- 6.4 Drake, M.L. and J.P. Henderson, "An Investigation of the Response of the Damped Structure Using Digital Techniques," *Shock and Vibration Bulletin* 45, Part 5, 1975.
- 6.5 Ross, E., E.E. Ungar, and E.M. Kerwin, "Damping of Plate Flexural Vibrations by Means of Viscoelastic Laminates," *Proc. Colloq. Struc. Damping ASME*, 1959, pp. 49-87.
- 6.6 Soni, M.L., "Finite Element Analysis of Initially Stressed Viscoelastic Solids," University of Dayton Research Institute, UDR-TR-79-113, November 1975.
- 6.7 Rogers, L.C., C.D. Johnson, D.A. Keinholtz, "The Modal Strain Energy Finite Element Analysis Method and Its Application to Damped Laminated Beams," 51st Shock and Vibration Symposium, October 21-23, 1980, San Diego, California.
- 6.8 Sharp, J.D. and M.L. Drake, "Elimination of Resonant Fatigue Problems for Major Maintenance Benefits," ASME Publication Number 77-DET-135.
- 6.9 Rogers, L.C. and M.L. Parin, "A Thoroughly Engineered Application of Damping Technology to Jet Engine Inlet Guide Vanes," (L. Rogers, ed.) from Conference on Aerospace Polymeric Viscoelastic Damping Technology for the 1980's. AFFDL-TM-780 78-FBA, July 1978.
- 6.10 Henderson, J.P. and M.L. Drake, "Investigation of the Effects of Damping Treatments on the Response of Heated Fuselage Structure," *NoisEXPO*, National Noise and Vibration Control Conference, New York, New York, March 1976.
- 6.11 Brown, Dave, Lecture notes - short course, "Modal Analysis Theory and Measurement Techniques," sponsored by the University of Cincinnati and Hewlett-Packard.
- 6-12 Ramsey, K.A., "Effective Measurements for Structural Dynamics Testing," *Sound and Vibration*, November 1975, pp. 24-35.

REFERENCES (Continued)

- 6.13 Drake, M.L. and G.E. Terborg, "Polymeric Materials Testing Procedures to Determine the Damping Properties and the Result of Selected Commercial Materials," University of Dayton Research Institute, UDR-TR-80-40, 1980.
- 6.14 Jones, D.I.G., J.P. Henderson, and 1st/Lt. G.H. Bruns, "Use of Tuned Viscoelastic Dampers for Reduction of Vibrations in Aerospace Structures," Air Force Materials Laboratory, presented at the 13th Annual Air Force Science and Engineering Symposium at Arnold Air Force Station, Tennessee, September 27-29, 1966.
- 6.15 Drake, Michael L., "Design Evaluation and Field Qualification of a Damping System for an Auxiliary Power Unit," presented at Vibration Damping Workshop, sponsored by Air Force Wright Aeronautical Laboratories, Long Beach, California, February 27-29, 1984.
- 6.16 Sharp, J.D. and Drake, M.L., "Elimination of a Resonant Fatigue Problem for Major Maintenance Benefits," presented at ASME Design Engineering Technical Conference, Chicago, Illinois September 26-30, 1977.
- 6.17 Drake, M.L. and Sharp, J.D., "An Example of Additive Damping as a Cost Savings Alternative to Redesign," presented at Winter Annual Meeting ASME Turbine Division, Atlanta, Georgia, November 27-December 2, 1977.
- 6.18 Drake, M.L. and M.F. Kluesener, "OSTA-1 Modal Analysis Test Plan and Damping Design Study," UDR-TM-80-47, University of Dayton Research Institute, Dayton, Ohio, December 1980.
- 6.19 Dominic, R.J., "TF-33-P3 Inlet Guide Vane Damping Wrap Program," UDR-TR-80-17, University of Dayton Research Institute, February, 1980, Dayton, Ohio.
- 6.20 Dominic, Robert, "Evaluation of TF-33 Inlet Guide Vane Damping Wraps Installed by the Elastomeric Method," Final Report, UDP-TR-83-53, University of Dayton Research Institute, Dayton, Ohio, June 1983.
- 6.21 "Analysis of the Damped Ring Mirror," Aerospace Structures Information and Analysis Center, Report No. 1182.1B, November 1982.
- 6.22 "Dynamic Analysis and Testing of Damped Intermodule Plates for the Sigma Laser Device," Aerospace Structures Information and Analysis Center, Report No. 1182.1A, November 1982.
- 6.23 Cannon, Charles M. and Michael L. Drake, "Design and Evaluation of a Damping Treatment to Eliminate Fatigue Failure on the B-52 AIMS T&U-82 Pitot Static Tube," Presented at the 47th Shock and Vibration Symposium, Albuquerque, New Mexico, 19-21 October 1976.

REFERENCES (Continued)

- 6.24 Drake, M.L. and Henderson, J.P. "An Investigation of the Response of a Damped Structure Using Digital Techniques," Shock and Vibration Bulletin 45, Part 5, June 1975.
- 6.25 Miles, R.N., "Beam Dampers for Skin Vibration and Noise Reduction in the 747," presented Vibration Damping Workshop sponsored by Air Force Wright Aeronautical Laboratories, Long Beach, California, February 27-29, 1984.
- 6.26 "Reducing the Vibration Amplitudes of the TF-34-100 and -400 Mount Rings with Tuned Viscoelastic Dampers," UDR-TM-80-01, January, 1980, University of Dayton Research Institute, Dayton, Ohio.
- 6.27 Ferrante, M., Stahle, C.V., and On F.J., "Feasibility Study of an Acoustic Enclosure for Shuttle Payloads," NASA, Goddard Space Flight Center, Contract No. NAS5-24021.
- 6.28 Medaglia, J.M., "Dynamic Integrity Methods Including Damping for Electronic Packages in Random Vibration," General Electric Space Division.
- 6.29 Behar, A. and May, D.N., "Vibration Damping Compound as a Means to Reduce Steel Noise Barrier Cost," Ministry of Transportation and Communications, Acoustics Office, Research and Development Division, Ontario, Canada, November, 1978, 78-AC-11.
- 6.30 Poizat, M., Vialatoux, P., Cochery, P., and Vedrenne, "Viscoelastic Damping System Use as a Remedy for Pogo Effect on the Diamant Satellite Launch Vehicle," Centre National D'Etudes Spatiales, Tour Lorraine, Boulevard de France, 91000 Evry-France.
- 6.31 Kirschner, Francis; Salmon, Vincent; Oleson, Stanley K.; "Viscoelastic Damping for Rapid Transit Structures," 5th Congres International D'Acoustique, Liege 7-14 September 1965.
- 6.32 Nashif, Ahid D., "Application of Damping for Noise Control," AnatroI Corporation, presented at University of Dayton Short Course, Dayton, Ohio.
- 6.33 Rogers, Lynn C., Parin, Michael L., "A Thoroughly Engineered Application of Damping Technology to Jet Engine Inlet Guide Vanes." presented at Conference on Aerospace Polymeric Viscoelastic Damping Technology for the 1980's, Dayton, Ohio, 7-8 February 1978.
- 6.34 "Test Report on the Effects of Dampers on the Response of Skin-Stringer Panels Excited by Random Noise," Vehicle Dynamics Division, Air Force Flight Dynamics Laboratory Wright-Patterson Air Force Base, Ohio, Report No. FDD-A-4-68, May 21, 1968.

REFERENCES (Continued)

- 6.35 Lamoree, M.D., and LaBarge, W.L., "Sonic Fatigue Resistance of Structures Incorporating a Constrained Viscoelastic Core," Shock and Vibration Bulletin 40 Part 5, 1969.
- 6.36 Peller, R.C., "Damping in Mirror Mounts and Composite Structure," Internal Report General Dynamics Convair Division.
- 6.37 Vail, Curtis F., "Effect of Additive Damping on Transfer Function Characteristics of Structures," General Motors Research Laboratories, GMR-1255, Vehicle Research Dept. October 2-5, 1972.
- 6.38 DeFelice, John J. and Ahid D. Nashif, "Damping of an Engine Exhaust Stack," Shock and Vibration Bulletin 48, Part 4, September 1978.
- 6.39 Drake, Michael L., Binod Kumar, and David M. Hopkins, "High Temperature Damping System Development for the J-85-21 Afterburner Liner," UDR-TR-80-79, University of Dayton Research Institute, Dayton, Ohio, August 1980.
- 6.40 Henderson, John P. and Ahid D. Nashif, "Reduction of Interior Cabin Noise Levels in a Helicopter through Additive Damping," Shock and Vibration Bulletin 44, Part 5, August 1974.
- 6.41 Drake, Michael L., Robert J. Dominic, and Binod Kumar, "Evaluation of High Temperature Damping Applications to Increase Fatigue Life in Rotating Jet Engine Components," AFWAL-TR-80-4174, Final Report for Material Laboratory, Wright-Patterson Air Force Base, Ohio. September, 1980.
- 6.42 Otth, David, "Shear Dampers for Deflections of Micro-Inch Magnitudes," Jet Propulsion Laboratory, California Institute of Technology, sponsored by NASA, contract No. NAS7-100.

SECTION 7

OTHER DESIGN CONSIDERATIONS

7.1 INTRODUCTION

In this section other considerations which may affect the design of the damping treatment are briefly discussed. The topics addressed include the nature of the damping materials, how their characteristics may influence the design, and potential installation problem areas.

7.2 NATURE OF DAMPING MATERIALS

There are basically two types of damping materials that have been used in the temperature range below 300°F (151°C). These are the linear polymers and the cross-linked polymers. The linear polymers consist of atoms linked in long chains sliding over similar atomic chains. The cross-linked polymers consist of a lattice work of coiled atomic chains that do not readily slide over each other.

The linear polymers tend to develop the highest damping values, usually between a loss factor of one to three, due to the high energy loss produced by the sliding action. These polymers retain their high damping values down to the lowest shear strain levels [7.1]. The high damping is, however, maintained only over a limited temperature range. Because of the high damping and relative insensitivity to strain, the linear polymers represent the more commonly used class of damping materials. However, these linear polymers creep out under sustained static load. Consequently, when used in a constraining layer treatment, the constraining layer must be prevented from picking up any static load, such as peel loads. If, for example, the constraining layer has some flexural stiffness, and there is a mismatch in the curvature between the constraining layer and the surface of the structure being damped, the constraining layer will, in time, lift off the structural surface. The linear polymeric

damping materials are often used in the form of damping tape, in which the thin metal foil constraining layer conforms readily to the surface contours, thereby overcoming the above problem. Alternatively, the constraining layer must itself be constrained in a manner to prevent separation without restricting the shearing motion within the damping layer that is necessary for producing the damping.

Cross-linked polymers are form stable, which means that the damping materials return, essentially, to their undeformed state on removal of the load. The damping, obtained from these cross-linked polymers, is generally lower than that from linear polymers with a loss factor usually below one. This loss factor is, generally, retained over a broad temperature range. Examples of cross-linked polymers are silicone rubber and structural adhesives. Actually, rubber exhibits various degrees of cross-linking which can be determined by such methods as discussed in Reference [7.2]. The silicone rubber, however, is strain sensitive [7.3, 7.4]. There appears to be a lower threshold of shear strain below which the damping falls off quite rapidly to a lower damping level as illustrated in Figure 7.1. This reduction in the loss factor is, generally, accompanied by an increase in the shear modulus. The shear sensitivity was first discovered in 1958 with BRT elastomer [7.3] and later with Sylgard 188 [7.4]. Unpublished data [7.5], obtained by means of the low shear strain (below 0.001) sandwich beam test on the same batch of Sylgard 188 damping material, indicated that the low strain damping plateau is around a loss factor of 0.3. However, damping data obtained from fluorinated silicone rubber [7.6] did not contain such a shear strain threshold (Figure 7.1) between the measured shear strains of 0.001 to 0.01, but did exhibit a somewhat erratic behavior within the above limits. Fillers added to the rubber [7.6] can improve the damping values to a certain extent and influence the degree of cross-linking in the rubber.

It is recommended that the type and the characteristics of the damping materials be established by testing prior to their use.

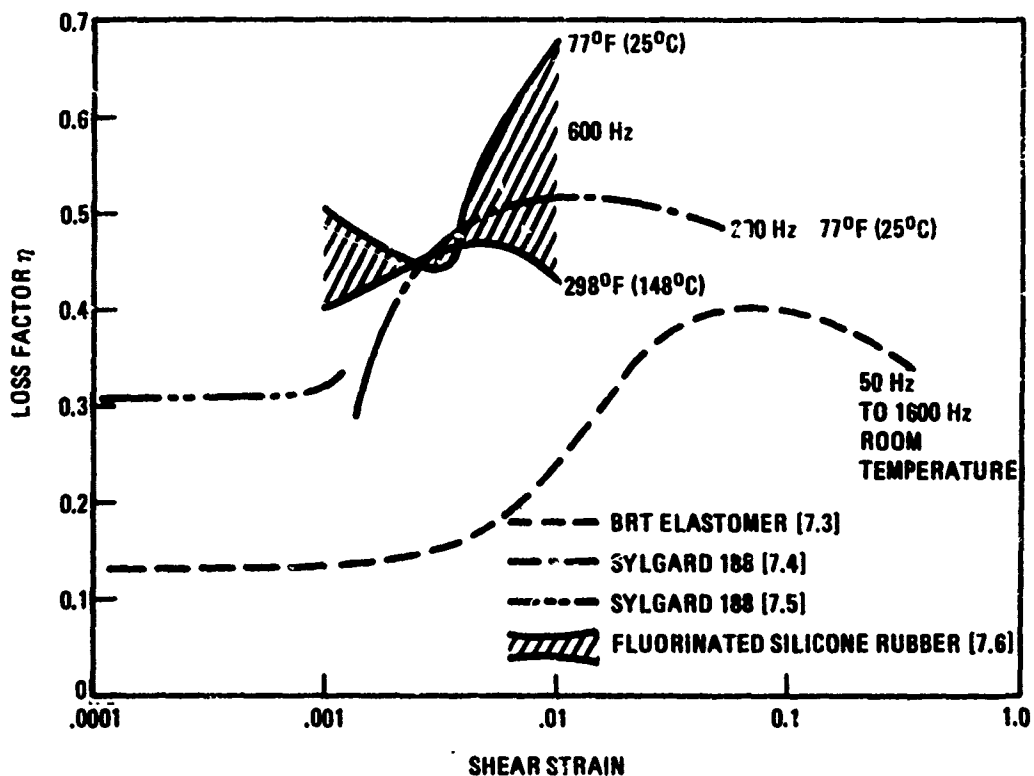


Figure 7.1. Variation of loss factor with shear strain for silicone rubber.

7.3 ENVIRONMENTAL CONSIDERATIONS

Some of the damping materials are adhesives and may not require an additional adhesive layer. Others, such as the silicone rubber, usually require both a primer and an adhesive to attach the damping material to the structure. The adhesive used must be compatible in strength with the damping material over its operating temperature range.

The primer, adhesive and the damping material must not produce a corrosive reaction with the structure that they are attached to. In areas of high moisture, these materials must prevent moisture from being trapped adjacent to the structure. These aspects are of concern when the damping material is applied to the interior fuselage shell of aircraft. The fuselage shell needs also to be inspected for cracks throughout the aircraft's life. Consequently, the ease of removal as well as of installation becomes a design consideration. Because of the condensation present in aircraft avionics boxes containing circuit boards, damping treatments applied over the surface of the circuit board's conformal coating could trap moisture which will penetrate the conformal coating with time and produce electrical failures. Application of the conformal coating over the damping treatment could short circuit the performance of the damping treatment.

In space applications, the moisture aspects are not a problem. However, most materials outgas in space to various degrees. Outgassing from the damping layers must be kept to a minimum to prevent coating of optical instruments. In these applications it is important to use space qualified materials. Silicone rubber type damping materials tend to exhibit the least amount of outgassing. The damping materials could also deteriorate with time in the space environment.

7.4 STRUCTURAL ASPECTS

The optimum design of a constrained layer damping treatment involves a configuration where the damping material is sandwiched between two sheets of equal thickness structural material. However, care must be exercised when this type of construction is used in load carrying structures. Under compression load, the buckling strength of such a panel could be as low as sixty percent [7.7] of the buckling strength of the same weight of solid panel because of the relatively low shear stiffness of the damping material. For this reason, it is more common to use this type of construction in low load carrying structures, such as control surfaces and leading edge slats, that are subjected to high acoustic or fluctuating pressure environments.

Heavier structural members such as aircraft frames are more difficult to damp than panel type structures because of their high stiffness. The performance of a constrained layer damping treatment, designed for these structures, can be improved by the use of a constraining layer with a much higher modulus than the metal of the frame. Ultra-high modulus graphite/epoxy composites lend themselves readily for such applications [7.4], not only because of their high modulus, but also because of their low density, just over half that of aluminum. Typical damping, that can be obtained with a damping material of relatively low loss factor (maximum of 0.7), is illustrated in Figure 7.2. The ultra high modulus constrained layer damping treatment was applied to a 6 inch-deep channel section aluminum beam, 65 inches-long, supported at both ends on flexures. The test was designed to address the loss in performance obtained by the use of a non-symmetric frame that was both supported and excited in a manner to provide a high degree of coupling between the frame bending and torsional modes. The loss factor was reduced by thirty-three percent below the theoretical optimum, as predicted by the single mode symmetric beam analysis in Reference [7.8], by such a coupling. The effects of such a coupling on the loss factor (Figure 7.2) and frequency (Figure 7.3) could be predicted by coupled mode theory [7.4]. The results indicate that heavy members can be successfully damped and that, for the highest damping, the members should be symmetrical to minimize coupling with the other frame modes. Asymmetric frame sections can still be damped effectively, provided that the viscoelastic damping treatment is designed to also increase the damping in the modes which couple up with the bending mode.

When the viscoelastic damping material, used in the above application, is a cross-linked polymer, static loads can be transferred from the heavy frame or structure to the constraining layer. In this event, the strain capabilities of the constraining layer and the heavy frame must be taken into account. The stress buildup in the ultra-high modulus graphite/epoxy constraining layer due to a tension load applied at both ends of the frame, is illustrated in Figure 7.4 as a function of the damping material shear modulus. The damping material shear modulus was assumed to be sufficiently low so as to be fully

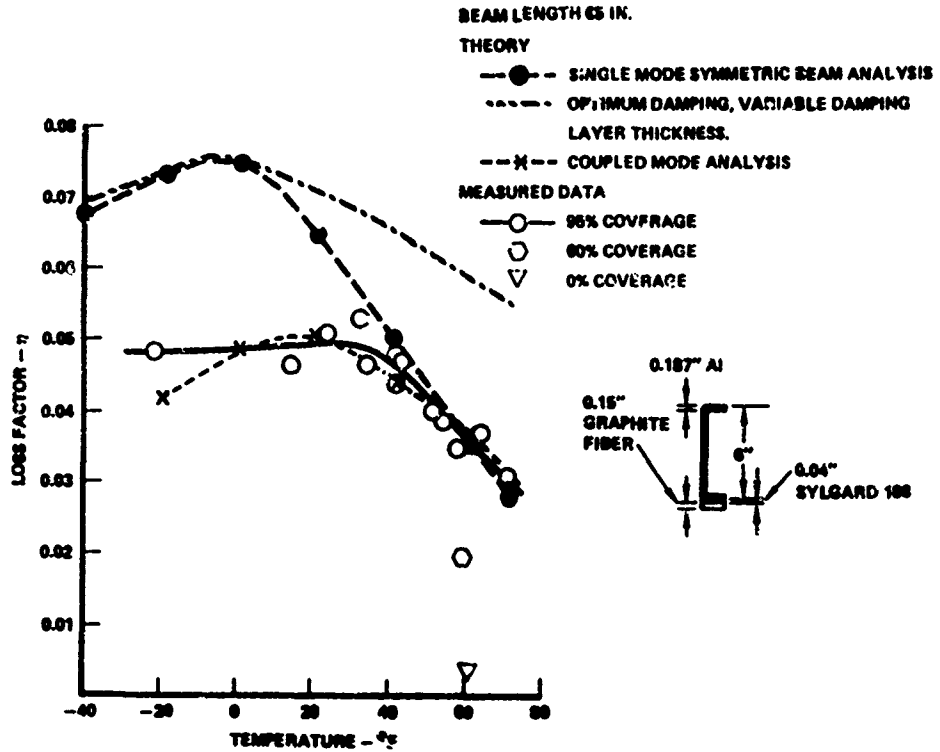


Figure 7.2. Variation of test beam loss factor with temperature.

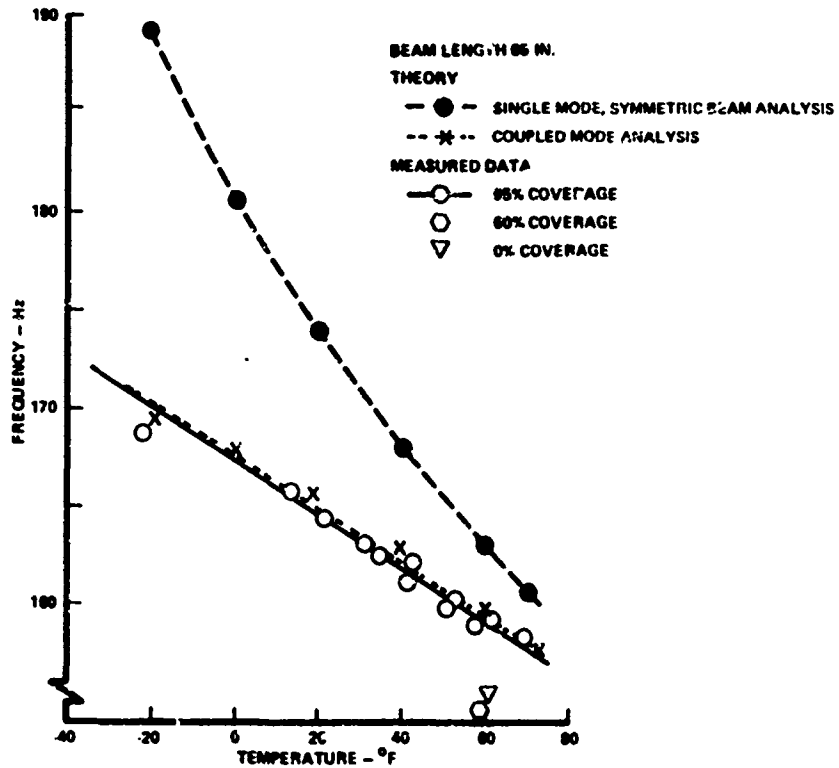


Figure 7.3. Variation of test beam frequency with temperature.

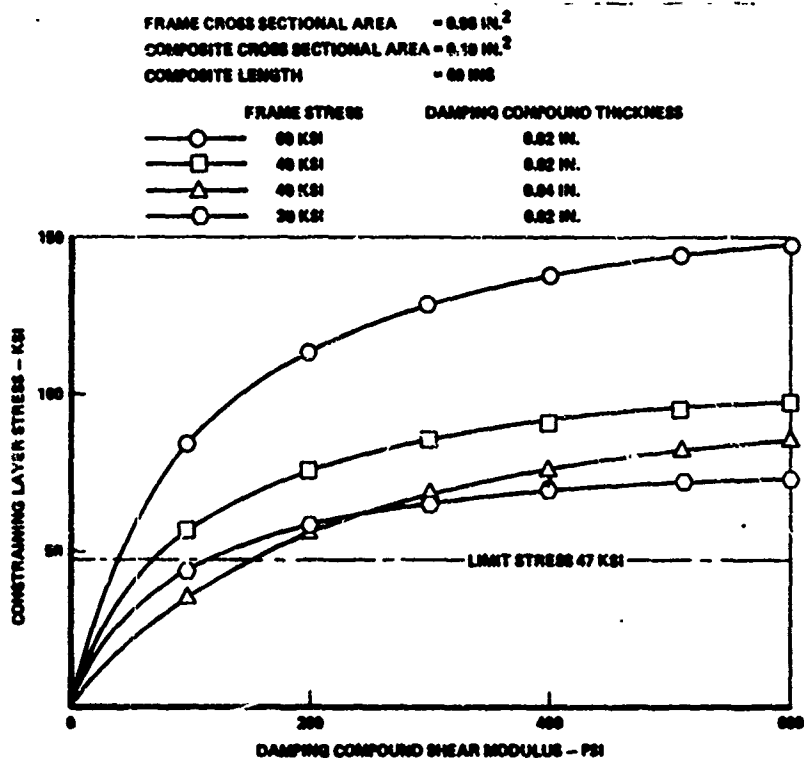


Figure 7.4. Composite constraining layer stress variation with damping compound shear modulus.

effective in shear. The constraining layer was taken as 60 inches long in the analysis. In reality, the variation of the strain along the constraining layer is not linear with length, but a function of the shear parameter, KL , as illustrated in Figure 7.5. The shear parameter, KL , is given by

$$KL = \left\{ \frac{GL^2}{Eth} \right\}^{1/2}$$

where G and h are the static shear modulus and thickness of the damping material, respectively, and E , t and L the Young's modulus, thickness and length of the constraining layer, respectively. For a damping material with a high shear modulus, the strain is concentrated at the edge of the constraining layer. In this event it will be necessary to cut up the constraining layer into many segments or to use partial coverage. The use of partial

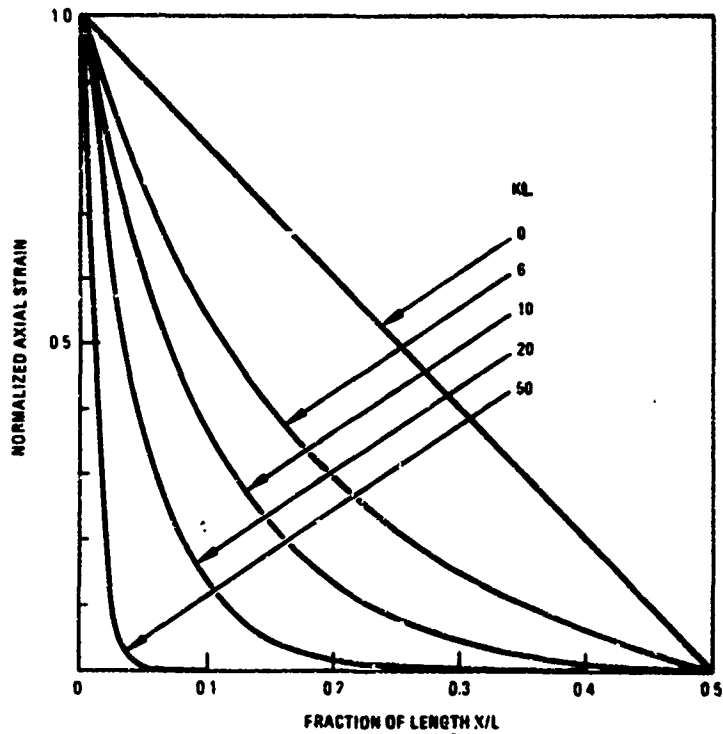


Figure 7.5. Variation of constraining layer normalized axial strain as a function of the shear parameter, KL , over its semi-span.

coverage [7.9] or segmentation of the constraining layer [7.10] could increase the damping of the treatment under these circumstances. The shear stiffness of the damping material, used in the previously described beam test [7.4], was too low to benefit from partial coverage (Figure 7.2).

REFERENCES

- 7.1 Lagnese, T. J. and Jones, D. I. G., "Complex Modulus Behaviour of a Viscoelastic Adhesive Measured at Harmonic Strain Amplitudes of 10^{-10} ", Vibration Damping 1984 Workshop Proceedings (Dr. L. C. Rogers, Editor), AFWAL-TR-84-3064, November 1984.
- 7.2 Fedors, R. F., "Estimating the Degree of Cross-Linking in Rubber", NASA Tech. Brief, Vol. 7, No. 2, Item #31, July 1983.
- 7.3 Painter, G. W., "Dynamic Properties of BRT Elastomers", presented at SAE National Aeronautics Meeting, Los Angeles, California, 29 September - 4 October 1958.
- 7.4 Soovere, J., "High Modulus Graphite Fiber Constrained Layer Damping Treatment for Heavy Aerospace Structures", Conference on Aerospace Polymeric Viscoelastic Damping Technology for the 1980's, L. C. Rogers, Editor, AFFDL-TM-78-78-FBA, July 1978.
- 7.5 Jones, D. I. G., Unpublished test data on Sylgard 188, sent to J. Soovere on 17 May, 1978.
- 7.6 Coote, C. T., "Measurement of the Damping Properties of Silicone-Based Elastomers Over Wide Temperature Range", Journal of Sound and Vibration, Vol. 12, No. 2, 1972, pp 133-147.
- 7.7 Lamoree, M. D., LaBarge, W. L., Prydz, R. A., "The Development, Fabrication and Evaluation of Sonic Fatigue Resistance of Aerospace Structures Utilizing Viscoelastic Materials", AFML-TR-69-140, June 1969.
- 7.8 Ruzicka, J. E. et al, "Damping of Structural Composites with Viscoelastic Shear - Damping Mechanisms", NASA CR-742, March 1967.
- 7.9 Nokes, D. and Nelson, F., "Constrained Layer Damping with Partial Coverage", The Shock and Vibration Bulletin, 38, 1968, pp 5-12.
- 7.10 Plunkett, R. and Lee, C. T., "Length Optimization for Constrained Viscoelastic Layer Damping", The Journal of the Acoustical Society of America, Vol. 48, No. 1 (Part 2), 1970.

SECTION 8

SUMMARY OF DAMPING IN AEROSPACE MATERIALS AND STRUCTURES

The typical damping levels in aerospace materials and the more common structures are summarized in this section. The levels quoted are not to be treated as absolute values, but more as an indication of the expected average damping values. In reality, there is considerable scatter in the measured damping data, especially for built up structures. A deviation from the quoted damping value of a factor of two, either way, is quite possible for these structures. A more detailed discussion on the nature of damping and the damping levels in the materials and some more common aerospace structures is contained in Section 7, Volume I of the design guide. A large list of references is also provided in that section for further study. This list also includes references for material damping in nonmetallic materials. Methods for measuring material damping are also discussed in some detail in that section since the damping values are generally very low and can be easily contaminated by the test method or the test apparatus.

All of the damping data in this section are presented in terms of the viscous damping ratio, ζ . The relationships between the more common damping expressions used in representing material damping are the loss factor (or structural damping), η , the logarithmic decrement, δ , the specific damping capacity, ψ , and the amplification factor, Q . These are related by

$$\eta = \frac{\psi}{2\pi} = \frac{\delta}{\pi} = \frac{1}{Q} = 2\zeta.$$

The damping data for aerospace metals are presented first followed by composites, metal matrix composites and aerospace structures. Much of the damping in stiffened panel type structures has been measured only for the fundamental mode. A method is provided by which the damping in the higher order modes can be estimated from the frequency and damping of the fundamental

mode. The commonly used one-over-the-frequency type variation of the damping with frequency is valid only if higher modes are included in such data. The damping in the fundamental mode of stiffened panel type structures is essentially constant with frequency. This behaviour has only recently been discovered [8.1] and verified by careful experiment [8.2].

Acoustic radiation damping also plays a greater role in the damping of riveted aluminum panels than originally thought. It is the dominant source of damping in stiffened aluminum and composite honeycomb panels [3.5]. Acoustic radiation is the only source of damping in integrally stiffened graphite/epoxy panels [8.3, 8.4] on account of the very low damping in graphite/epoxy material. The damping in these panels can now be predicted by theory [8.1, 8.5]. These developments are discussed in more detail both in Section 8.2 and in Section 7, Volume I of the design guide.

8.1 MATERIAL DAMPING IN AEROSPACE METALS AND COMPOSITES

8.1.1 Material Damping in Metals

The typical damping levels in the more common metals are listed in Table 8.1. In some of the metals, the material damping varies with dynamic stress amplitude [8.6, 8.7] as illustrated in [8.7] Figures 8.1 and 8.2. In some metals such as aluminum, the damping remains constant with stress level but is dependent on frequency, with maximum damping occurring at the relaxation frequency (see Section 7, Volume I). Some metals have especially high material damping values. These materials [8.8] are indicated in Figure 8.3 as a function of their Young's modulus for quick reference. Typical material damping values for steel and aluminum are included for comparison.

8.1.2 Material Damping in Composites with Epoxy or Polyester Matrix

The material damping in graphite, boron, Kevlar and glass fiber reinforced composites in, primarily, an epoxy matrix are presented in this section. The material damping is the lowest in unidirectional composite layups, with the fibers running parallel to the axial direction. Typical damping values are

listed in Table 8.2. The boron and graphite epoxy composites have the lowest material damping and Kevlar has the highest.

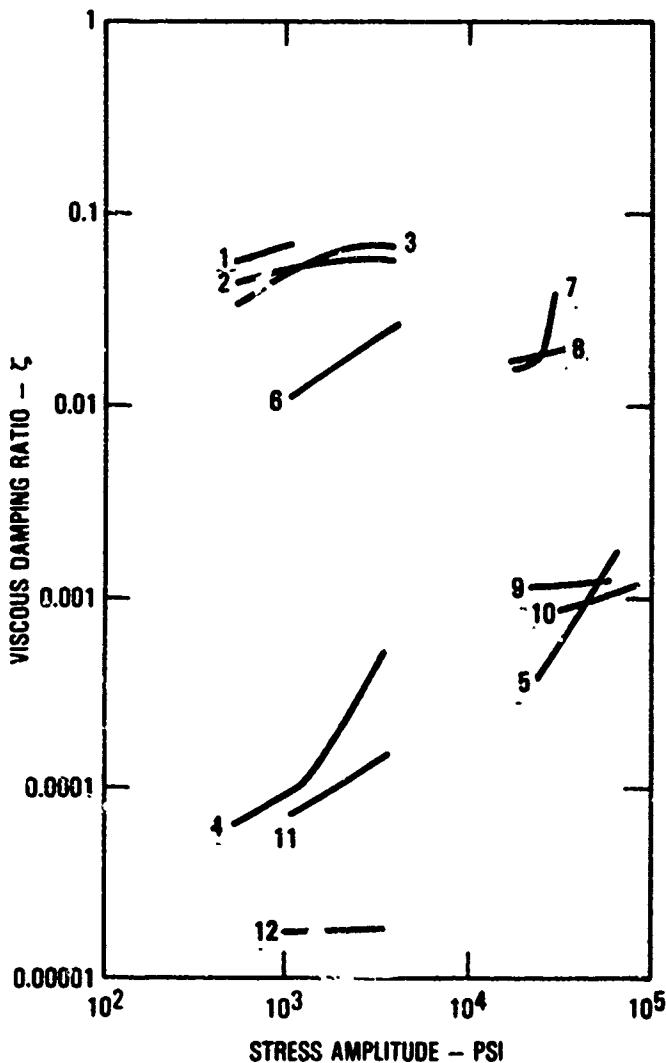
TABLE 8.1. TYPICAL MATERIAL DAMPING LEVELS IN METALS

MATERIAL	VISCOUS DAMPING RATIO ζ
Mild steel	0.0025 - 0.005
Alloy steel	0.0005 - 0.004
Aluminum alloy	0.00005 - 0.0012
Titanium alloy	≈ 0.0009

The damping in composites varies both with fiber volume as illustrated [8.9] in Figure 8.4 and with fiber orientation as illustrated in Figures 8.5 and 8.6 for graphite/epoxy [8.10] and Kevlar [8.2, 8.5], respectively. The material damping in composites, including the uniaxial composites, is derived entirely from the material damping in the matrix, as indicated in Table 8.3, in this instance for uniaxial aligned chopped fiber composites [8.11]. The damping in the uniaxial composites is not affected significantly by temperature [8.10]. For other fiber orientations, it follows the damping behaviour of the epoxy with temperature [Figure 8.7]. The shear (torsion) damping in composites is also high because of its dependence on the resin damping. The damping in axially aligned chopped fiber composites [8.11, 8.12, 8.13] can be increased by the use of progressively smaller fibers at the expense of a progressively reduced modulus. The variation of the damping in the composites with fiber orientation is predictable by theory [8.14, 8.15] based on the measured axial, transverse and shear damping values and the corresponding Young's moduli of uniaxial composites.

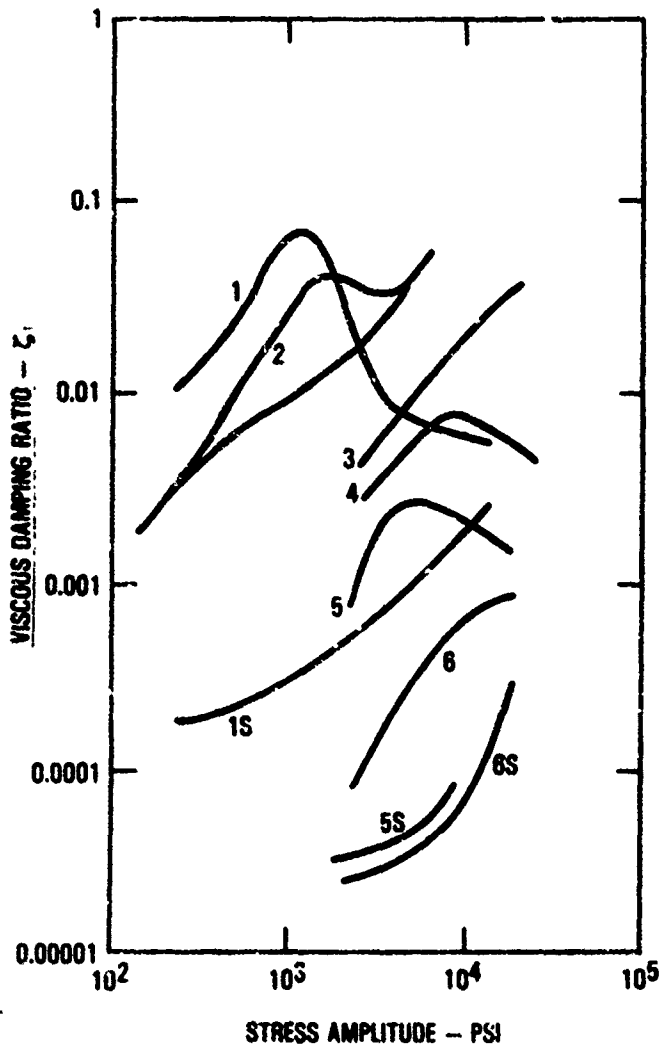
8.1.3 Metal Matrix Composites

The measured material damping in metal matrix composites is summarized in Table 8.4. A number of types of reinforcing fibers are used in, basically, an aluminum or magnesium matrix. The damping appears to be reasonably constant with frequency but does vary with both stress amplitude and temperature [8.16].



No.	MATERIAL
1	CAST MAGNESIUM 99.9% PURE
2	Mg - 0.6% Zn
3	Mg - 0.8%
4	Mg - 8.1% Al, 0.5% Zn, 0.2% Mn
5	AUSTENITIC STEEL OIL QUENCHED FROM 1000°C, 16 HOURS, 660°C
6	Mn - 35.9% Cu, 0.24% Fe, HEAT 1 HR, 790°C, QUENCH 2 HR, 450°C
7	N - 155 ALLOY, Fe 21.7% Cr, 1.9% W, 0.15% C, 19.4% Ni, 1.74% Mn, 19% Co, 0.78% Co, 2.75% Mo, 0.37% Si QUENCHED, AGED
8	STELLITE CO - 0.48% C, 1.4% Fe, 0.42% Mn, 24.8% Cr, 0.93% Si, 10.4% Ni, 7.28% W AS CAST
9	Ti - 3.9% Al, 4.3% Mn, 0.1% C ANNEALED
10	SANDVIK STEEL Fe - 1% Cr, 0.2% Si, 1% C, 0.28% Mn, 0.24% Mo, QUENCHED TEMPERED
11	Al - 5.5% Cu, 0.5% Fe, 0.5% Bi
12	Al - 4% Cu, 0.5% Mg, 0.5% Mn

Figure 8.1. Variation of the material damping in metals with dynamic stress amplitude.



No.	MATERIAL
1	Fe - 3.3% Si, ANNEAL 5.5 HR AT 1200°C
1S	SAMPLE 1 SATURATION MAGNETIC FIELD
2	PURE NICKEL
2S	SAMPLE 2 SATURATION MAGNETIC FIELD
3	INVC0 73.5% Co, 22.5% Ni, 1.8% Ti, 1.1% Zr
4	403 STEEL ALLOY Fe - 12% Cr, 5% Ni
5	MILD STEEL 0.28% C, 0.2% Si, 0.76% Mn, 0.12% Cu, 0.14% Ni, 0.1% Cr, ANNEALED 18 HRS AT 625°C
5S	SAMPLE 5 SATURATION MAGNETIC FIELD
6	CARBON STEEL 0.42% C, 0.32% Si, 0.99% Mn, 0.09% Ni, 0.06% Cr, NORMALIZED
6S	SAMPLE 6 SATURATION MAGNETIC FIELD

Figure 8.2. Variation of the material damping with dynamic stress amplitude in metals.

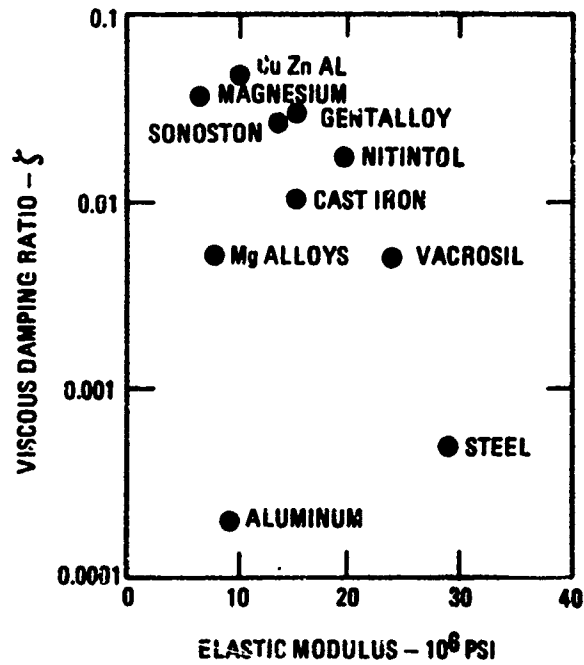


Figure 8.3. Typical damping ratio for various alloys at a stress level equal to one tenth of the yield stress as function of the elastic modulus.

TABLE 8.2 TYPICAL DAMPING VALUES IN UNIDIRECTIONAL COMPOSITES WITH AXIAL FIBERS

Material	Fiber Volume Fraction V_f	Flexural Modulus MSI	Viscous Damping Ratio ζ
Fiberglass/Epoxy	0.72	7.79	0.0005
	0.50	5.48	0.0007
Fiberglass/Polyester	0.66	6.2	0.0009
	0.54	4.95	0.0012
Kevlar/Epoxy	0.65	9.75	0.0018
HM Graphite/Polyester	0.54	25.8	0.0011
	0.61	33.6	0.0012
HT-S Graphite/LY558 Epoxy	0.60	17.9	0.00015*
	0.70	19.7	0.00012*
HT-S Graphite/F-HNA Epoxy	0.70	20.5	0.00012*
HT-S Graphite/PLA 4517 Epoxy	0.60	19	0.00053
AS1 Graphite/3501-6 Epoxy	-	-	0.0005
Celion 3000 Graphite/5208 Epoxy	-	21.1	0.00033
Celion 3000 Graphite/5213 Epoxy	-	19.7	0.00024
CY-70 Graphite/934 Epoxy	-	42.3	0.00046
HM-S Graphite/CY209 - HT972 Epoxy	0.5	22.3	0.00049
Boron/Epoxy	0.55	27.6	0.00064

*Lowest values ever measured.

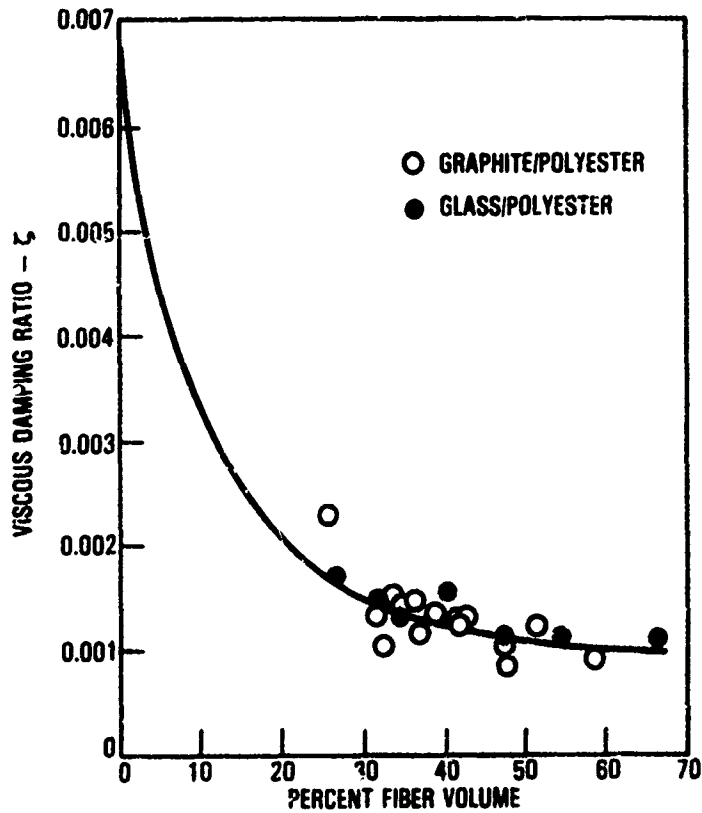
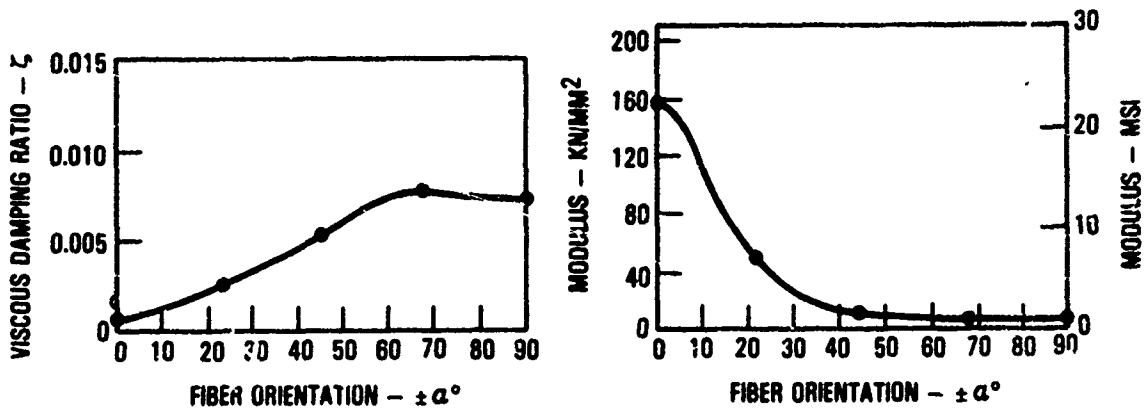


Figure 8.4. Variation of viscous damping ratio with fiber volume in early beam tests.



(b) VARIATION OF DAMPING AND YOUNG'S MODULUS WITH FIBER ORIENTATION IN THE FIRST MODE [7.75]

Figure Figure 8.5. Measured Young's modulus and damping for graphite/epoxy composite at ambient temperature.

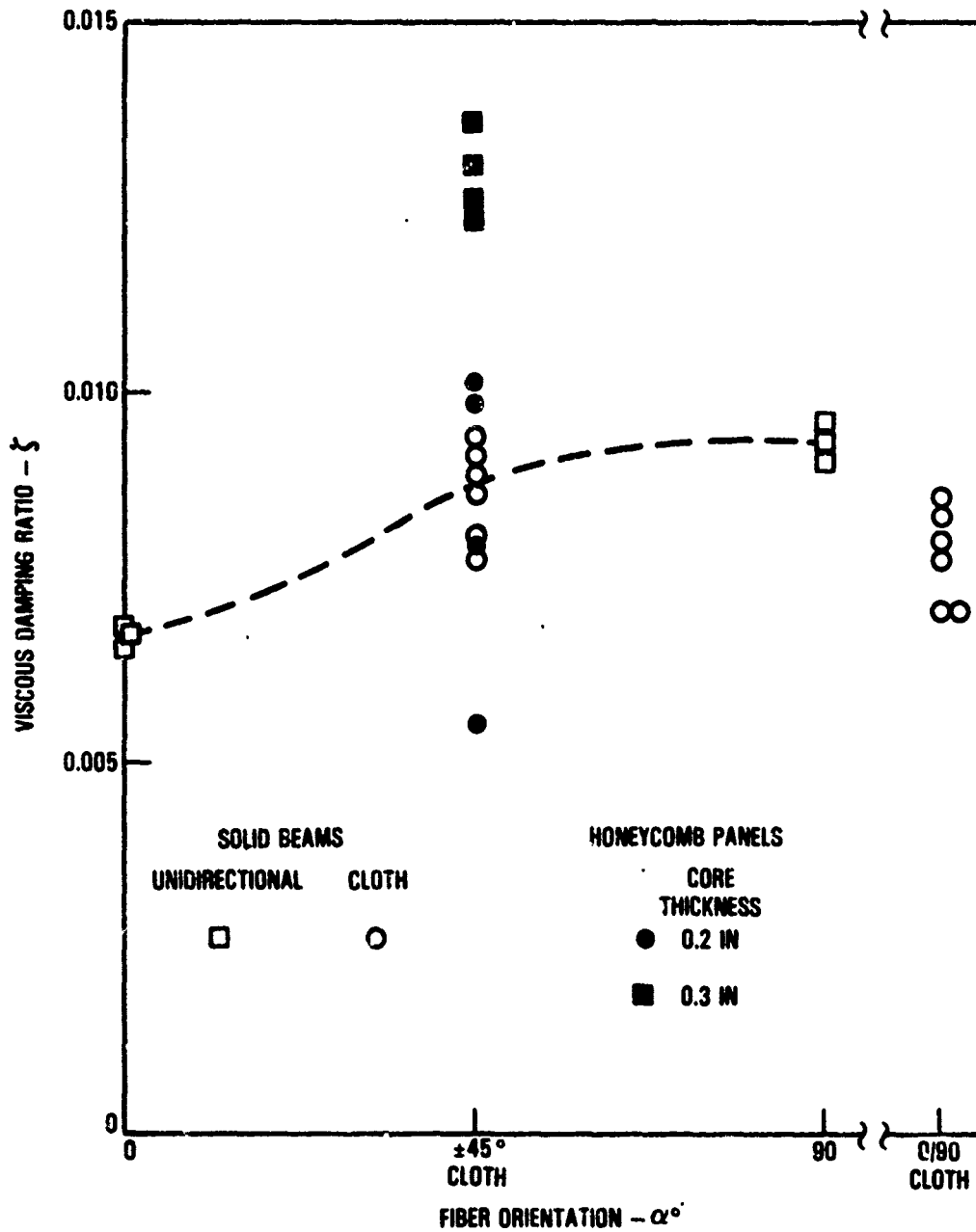


Figure 8.6. Measured damping in free-free Kevlar honeycomb panels and beams.

TABLE 8.3. EFFECT OF RESIN DAMPING ON THE DAMPING OF CHOPPED ALIGNED GRAPHITE FIBER COMPOSITE

Material Identified by Resin Number Only [8.11]	Resin		Chopped Fiber Composite ($V_f^* = 0.6$)	
	Modulus MSI	Viscous Damping Ratio, δ	Modulus	Viscous Damping Ratio, δ
1	0.144	0.075	13.25	0.004
5	0.475	0.0035	17.62	0.00025
6	0.249	0.075	16.69	0.005

*Fiber volume fraction

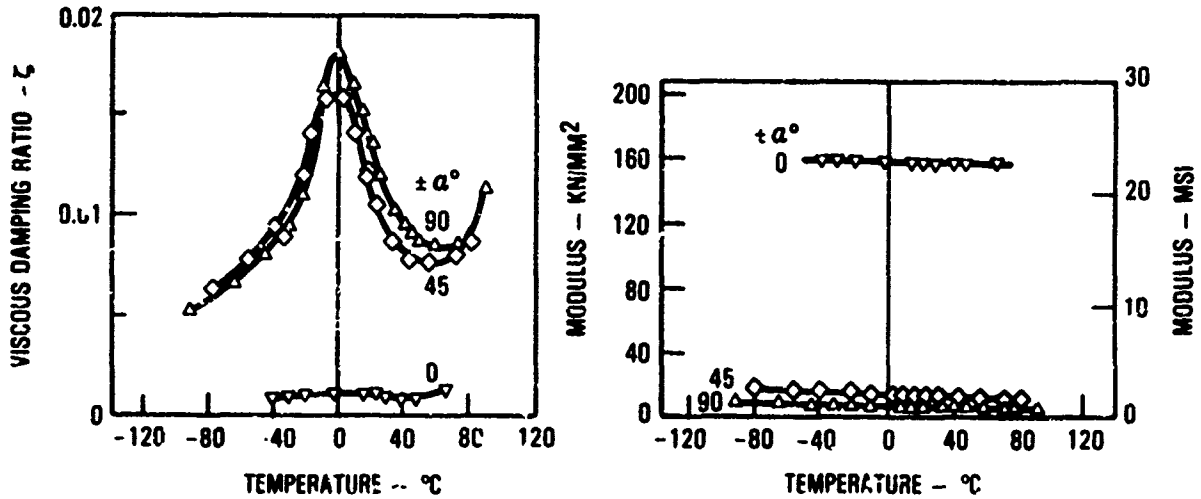


Figure 8.7. The behavior of graphite/epoxy composite, as a function of temperature.

TABLE 8.4 MATERIAL DAMPING IN METAL MATRIX COMPOSITES

Material	Fiber Volume Fraction V_f	Flexural Modulus MSI	Viscous Damping Ratio ζ
Boron BR4C/6061 Al	0.57	34.1	0.00038
P55 Graphite/6061 Al	-	26.4	0.00088
P100 Graphite/6061 Al	-	42.5	0.00085
P55 Graphite/ZE41A Mg	-	23.1	0.00070
P100 Graphite/ZE41A Mg	-	40.8	0.00065
P55 Graphite/AZ91C-Ti	-	-	0.0004
P100 Graphite/AZ91C-Ti	-	-	0.0004
P100 Graphite/AZ91C-Mg	-	-	0.0010
FP-Al ₂ O ₃ /Li Al	-	32	0.00045
FP-Al ₂ O ₃ /C.P. Mg	-	30	0.00045
FP-Al ₂ O ₃ /Ze41A Mg	-	30	0.00045
Particulate SiC/6061 Al	0.45	22	0.0002*- 0.001
Whiskers SiC/6061 Al	0.20	14.1	0.0002*- 0.001

*Damping decreases with frequency, with lower damping value at higher frequency (6000 Hz) and the higher damping value at low frequency (10 Hz).

8.2 DAMPING IN STIFFENED HONEYCOMB AND STIFFENED MULTI-BAY COMPOSITE AND METAL PANELS

8.2.1 Nature of the Damping

Stiffened multi-bay panels and stiffened honeycomb panels are typically used in secondary aircraft structures, which can also be exposed to high level acoustic loading. As a consequence, these types of structure are used in acoustic fatigue tests which represent the major source of information on the damping of these structures. A nine-bay panel, with a larger center bay, is typically used to represent the multi-bay panel. The intent is to ensure that failures occur in the periphery of the center bay and not along the test frame edges where the interpretation of the results becomes difficult. However, multi-bay panels with even stiffener spacings and even number of panels in the array have also been used. This variety of panel configurations has lead to difficulties in both identifying and interpreting the panel modes since many "fundamental" modes can exist with frequencies dependent on which adjacent panels combine in the vibration. The situation can be even more confusing for the higher modes. In contrast, stiffened honeycomb panels are tested singly on account of their large size. Modes, and damping trends of these modes, can be readily identified. Testing of stiffened honeycomb panels [8.2, 8.5] provided the conclusive experimental evidence of the near constant damping behaviour [8.1] in the fundamental mode (Figure 8.8). More recently, the trend has been towards the greater use of composites, employing fastener attached large-bay minisandwich skin construction [8.17], bonding [8.18, 8.19] or integrally stiffened construction [8.3, 8.20]. Bonding has also been used with aluminum panels [8.21, 8.22].

The highest damping is generally obtained in the fundamental mode. The damping usually falls off in level, in the higher modes of the panel, with increasing mode number. Acoustic radiation damping behaves in a similar manner. The reduction in the higher mode damping is produced by the cancellation effect. Since acoustic radiation is proportional to the area of each panel in the panel array, cancellation effect can also be obtained in a panel array in which the adjacent panels are vibrating out-of-phase with each other.

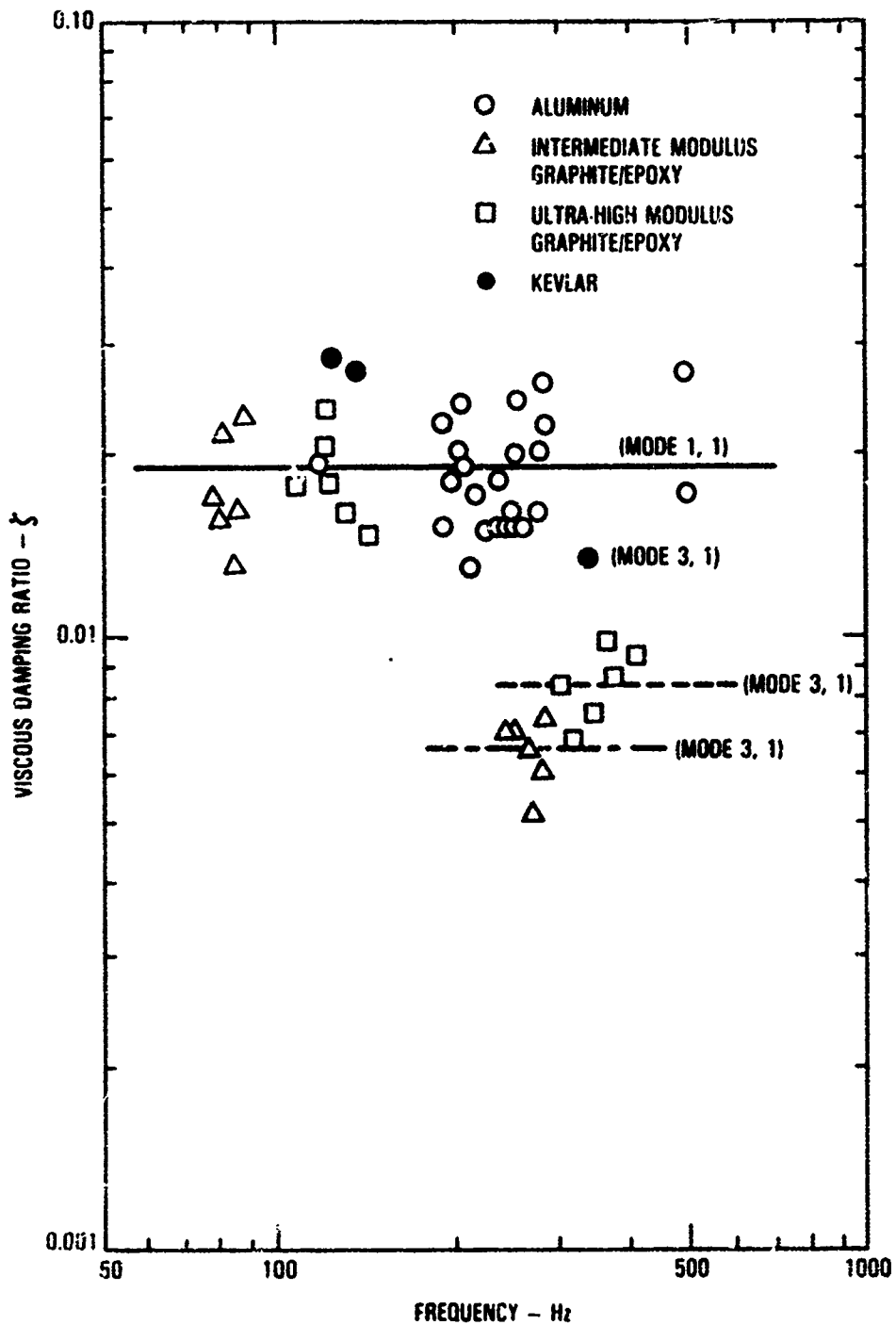


Figure P.8. Actual measured variation of fundamental mode damping with frequency for stiffened honeycomb panels.

The acoustic damping in this instance would be the acoustic damping of a single panel divided by the number of panels vibrating out-of-phase. If the panels are all vibrating in-phase then the acoustic damping is the same as that of a single panel in the array. The panels obviously have to have equal stiffener spacing for this type of response to occur.

Basically, there should be no significant difference in the damping of identical bonded metal, bonded composite or integrally stiffened metal or composite panels since the dominant source of damping is due to acoustic radiation. Kevlar composites have a significant material damping, with a viscous damping ratio of approximately 0.008 or more, which must be added to the acoustic radiation damping. Also, the friction damping at the fastener line, in fastener attached panels, must be added to the acoustic radiation damping. Even then the acoustic radiation damping still dominates. This result [8.1] is illustrated in Figure 8.9 by comparing the fundamental mode damping in multi-bay riveted panels [8.23] with that in multi-bay bonded panels [8.21]. The average damping is slightly lower for the bonded panels. The constant fundamental mode damping with frequency is also evident in the figure. The main difference is obtained in the higher panel modes where the damping at the fastener line becomes the dominant source of damping. In integrally stiffened or bonded panels, the damping level continues to drop down towards the material damping level for the layup used in the composite skin, as illustrated in Figure 8.10, or to that provided by the bonding. The material damping of a quasi-isotropic graphite/epoxy panel, with a $(0^\circ, \pm 45^\circ, 90^\circ)_s$ layup in the skin, has a viscous damping ratio around 0.0015. There is virtually no difference in the fundamental mode damping of fastener attached graphite/epoxy and aluminum panels (Figure 8.8) of similar size, although the smaller Kevlar honeycomb panels did exhibit a higher damping due to the significant contribution from the material damping. The most encouraging result is that the damping in these panels are predictable (Figures 8.10 and 8.11), subject to the usual scatter in the test data.

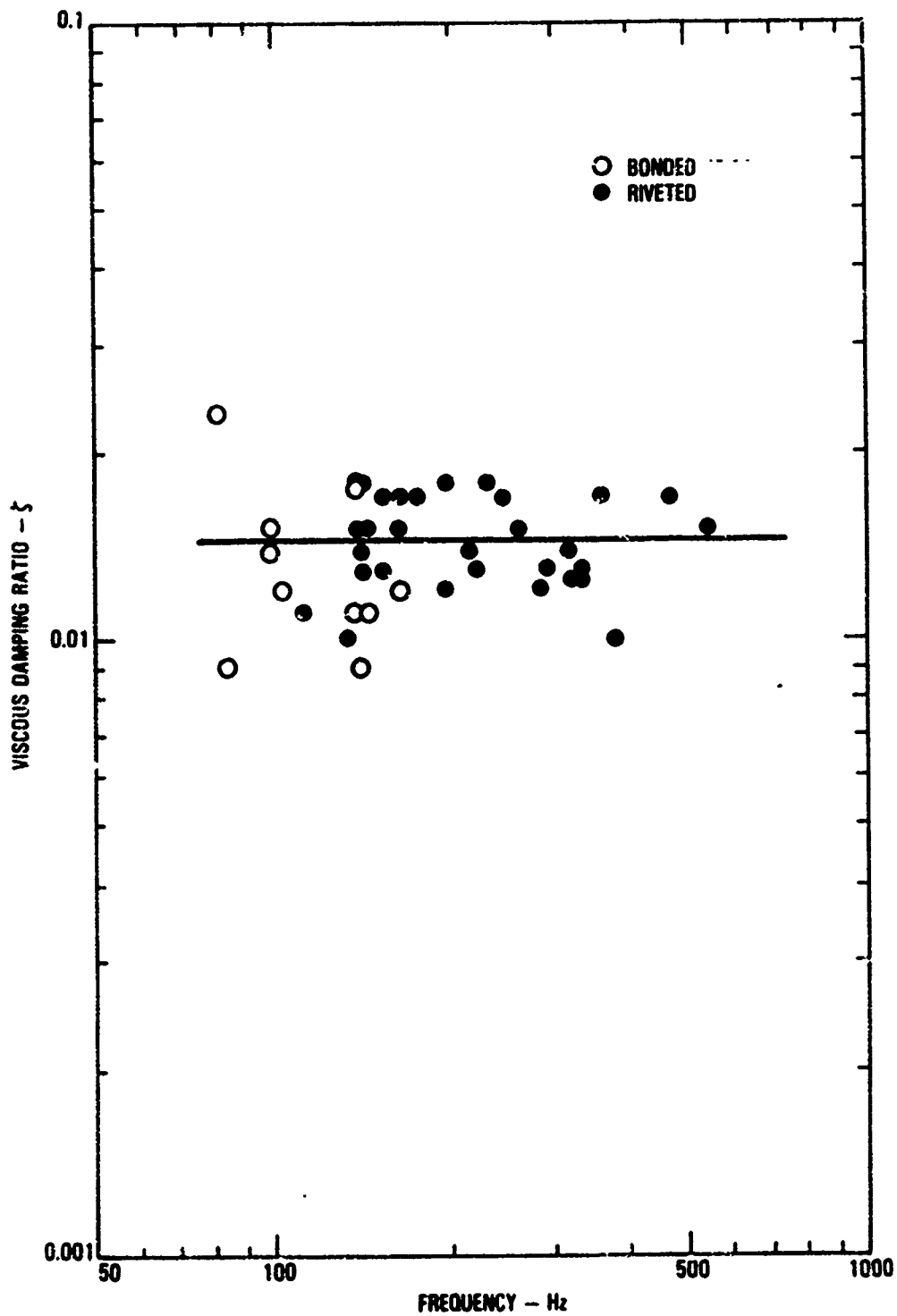


Figure 8.9. Variation of the measured damping in the fundamental mode of riveted and bonded multi-bay skin-stringer aluminum panels with frequency.

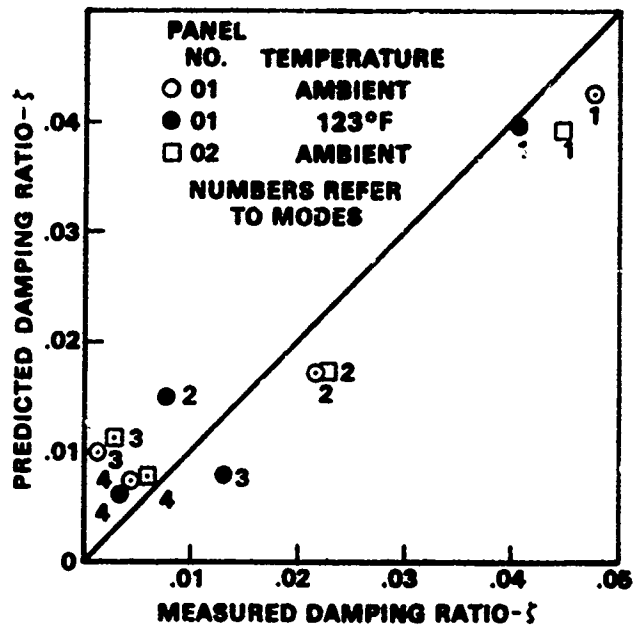


Figure 8.10. Comparison of theoretically predicted and measured viscous damping ratios of blade stiffened mini-sandwich graphite/epoxy panel.

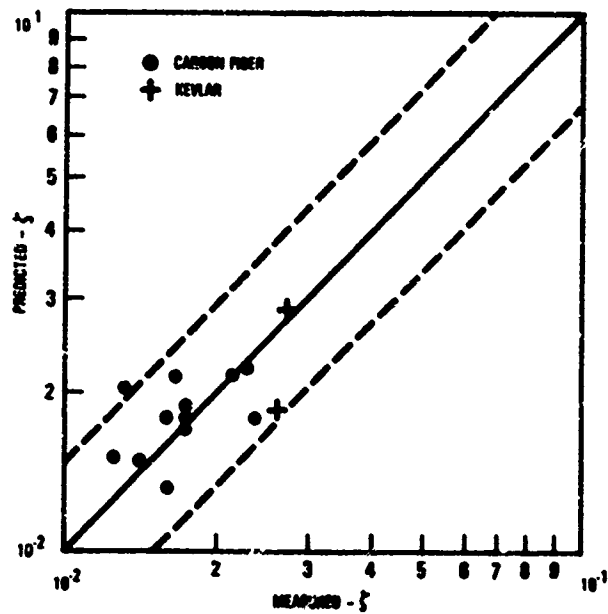


Figure 8.11. Comparison of theoretically predicted and measured viscous damping ratios for fundamental mode of stiffened composite honeycomb panels.

8.2.2 Damping Levels

The damping levels for the fundamental mode of a range of stiffened panel type structures are summarized in Table 8.5. These are the average measured damping levels. The actual damping can vary by a factor of two or more above and below this value due to scatter in the data as illustrated in Table 8.5. The damping data are least defined for multi-bay composite panels. The data that are available [8.3, 8.20, 8.21] range from a low viscous damping ratio of 0.0042 to a high value of 0.047 in the fundamental mode. Since the high damping values are generally for panels with a large center bay, these damping values are generally predictable. It is the low damping values that are least predictable. Consequently, based on the discussion in the previous section, the bonded and integrally stiffened graphite/epoxy panels are assumed to have the same average damping as the bonded aluminum skin-stringer panels. The average damping for the fundamental mode of integrally stiffened Kevlar cloth panels has been obtained by adding the average material damping from the ± 45 degree layup in Figure 8.6 to the bonded aluminum skin-stringer panel damping.

The actual measured damping for the graphite/epoxy box structure (the NASA L-1011 composite aileron) is quoted in Table 8.5. The mini-sandwich panel sizes used in the NASA L-1011 composite aileron are much larger than used in the corresponding aluminum design. Thus, a direct comparison between the damping of the aluminum box structure in Table 8.5 and that from the composite aileron is probably not valid.

Chemical milling has the effect of increasing the resonant frequency of the panel relative to a panel with the unmilled skin. Since the fundamental mode damping of a stiffened panel is, basically, unaffected by frequency, the damping in the chemically milled panel is assumed (Table 8.5) to be the same as that of a conventional skin-stringer panel.

8.2.3 Method for Predicting the Damping of Skin-Stringer Type Panels

The method for predicting the damping of the skin-stringer panels is the same as that described in Reference [8.1]. For simplicity, the panel array

**TABLE 8.5 FUNDAMENTAL MODE VISCOUS DAMPING RATIO FOR METAL
AND COMPOSITE STIFFENED PANEL TYPE STRUCTURES**

Structures	Average Viscous Damping Ratio ζ	Typical Range of Measured Data	
		Minimum ζ	Maximum ζ
Riveted aluminum skin-stringer panels both flat and curved with and without seaiaant	0.0145	0.005	0.05
Riveted titanium skin-stringer panels	0.0145	0.008	0.03
Riveted aluminum box structure	0.0145	0.008	0.04
Bonded aluminum skin-stringer panels	0.0125	0.009	0.022
Bonded and integrally stiffened graphite/epoxy panels	0.0125	0.0042	0.047
Bonded and integrally stiffened Kevlar cloth panels	0.020*	0.012*	-
Graphite/epoxy box structure assembled with fasteners	0.004	Only one tested	
Fastener attached stiffened metal and graphite/epoxy honeycomb panels	0.019	0.013	0.027
Fastener attached stiffened Kevlar honeycomb panels	0.027	Only two tested	
Corrugated and closely spaced hat stiffened aluminum panel structure	0.017	0.014	0.019
Built-up aluminum structures with integrally machined skins	0.0057	0.0019	0.0145
Riveted chemically milled aluminum panels (expected to be the same as skin-stringer panels but at higher frequency).	0.0145*	-	-

*Estimated.

is assumed to have a large center bay which produces the dominant vibration response and, therefore, the highest rms strain level to excitation such as random acoustic loading. In the most general panel, the damping is composed of three parts. These are the acoustic radiation damping, the fastener-like friction damping and the material damping represented by the viscous damping ratios ζ_a , ζ_F and ζ_M , respectively. The viscous damping ratio, ζ_{mn} , in the m, n^{th} mode of a skin-stringer type panel is given by

$$\zeta_{mn} = \zeta_a + \zeta_F + \zeta_M \quad (8.1)$$

The material damping is obtained from previously described beam tests for the particular layup used in the composite panel. It is usually taken as zero for graphite/epoxy and aluminum panels. The material damping for a Kevlar panel with a $\pm 45^\circ$ cloth layup is given approximately by $\zeta_M = 0.008$.

The viscous damping ratio due to acoustic radiation can be calculated from the equation

$$\zeta_a = \frac{64}{\pi} \frac{\rho}{4} \frac{f_n}{c} \frac{1}{M} \frac{a}{m} \frac{b}{n} \quad (8.2)$$

where

ρ = density of air

c = speed of sound in air

f_n = natural frequency of the m, n^{th} mode

M = panel surface density

a, b = panel length and width

m, n = mode number in the length and width direction respectively

The viscous damping ratio due to friction at the fastener line is given approximately by [8.1]

$$\zeta_F = 0.0253 \frac{s(a+b) - \frac{n}{s} - \frac{m}{s}}{ab} \quad (8.3)$$

where s is the number of fasteners per inch and the other dimensions are

also given in inches. The above equation is based on a viscous damping ratio of 0.0085 measured on a particular panel array under near vacuum conditions. A viscous damping ratio of only 0.0034 has been measured on a large unbaffled curved panel array. The friction damping is considered to produce the greatest scatter in the data due to variability in the fabrication of the panels. Consequently, the constant term in equation 8.3 can be adjusted to reflect actual measured friction damping levels. For bonded aluminum and composite panels, and integrally stiffened composite panels, $\zeta_F = 0$. The degree of correlation achieved by this method is illustrated in Figure 8.12 and in Figure 8.13 for the fundamental mode of two typical panels.

The damping in the higher order modes of a panel can be predicted using the average fundamental mode viscous damping ratio in Table 8.5 for the appropriate stiffened structure, the fundamental mode resonant frequency of the panel and the resonant frequency of the higher mode. The viscous damping ratio for the m,n^{th} mode is given by

$$\zeta_{mn} = (\zeta_{11} - \zeta_M - \zeta_F) \left(\frac{f_{mn}}{f_{11}} \cdot \frac{1}{m^2 n^2} \right) + \zeta_M + \zeta_F \quad (8.4)$$

where

- ζ_{mn} = m,n^{th} mode viscous damping ratio
- ζ_{11} = fundamental mode viscous damping ratio
- ζ_M = contribution from material damping
- ζ_F = contribution from friction damping of the rivet line (equation 8.3)
- f_{mn} = m,n^{th} mode resonant frequency
- f_{11} = fundamental mode resonant frequency

Typical higher mode viscous damping ratios predicted by equation 8.4 are illustrated in Figure 8.13.

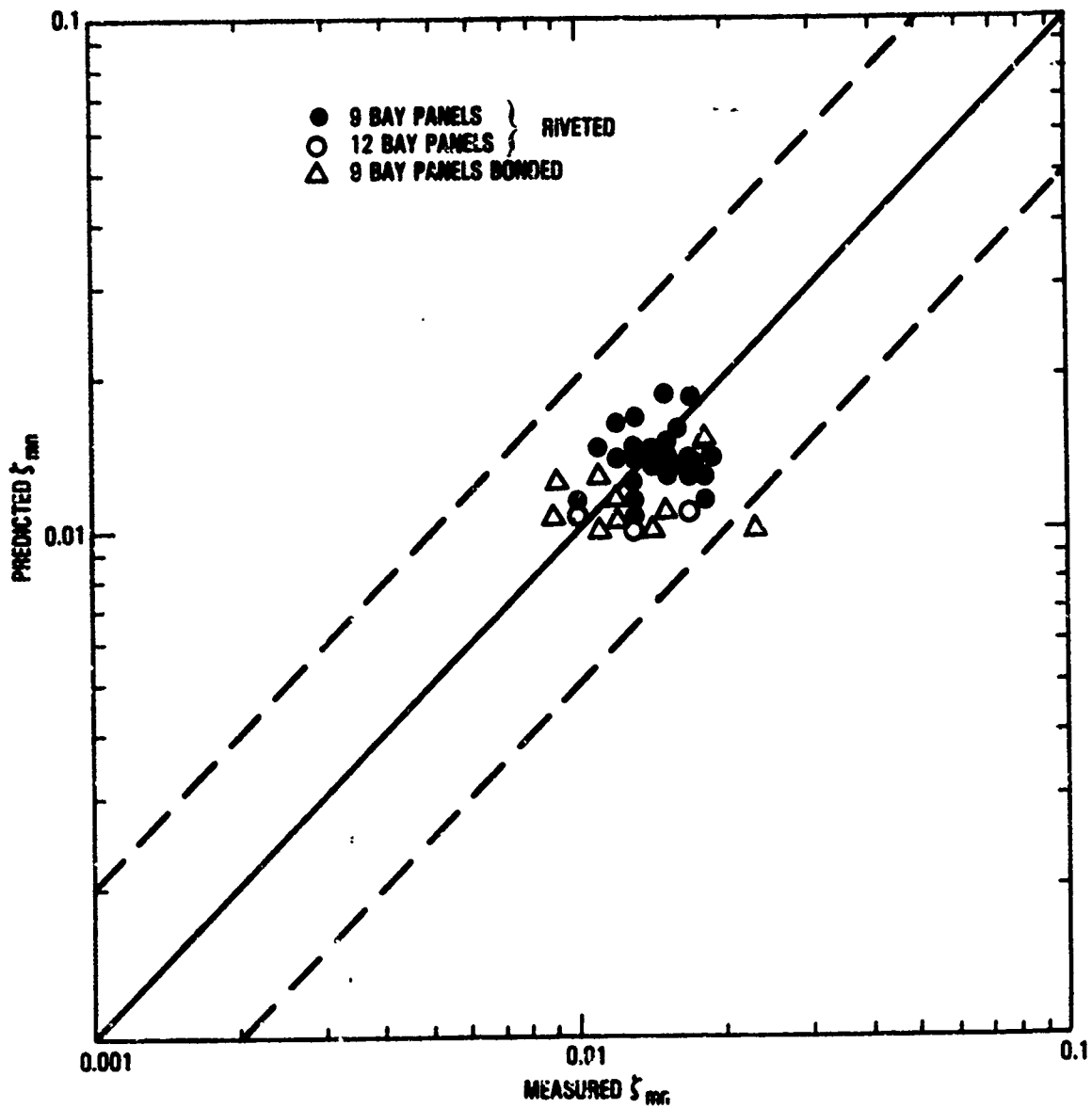


Figure 8.12. Comparison of measured and predicted damping in the fundamental mode of riveted and bonded multi-bay skin-stringer aluminum panels.

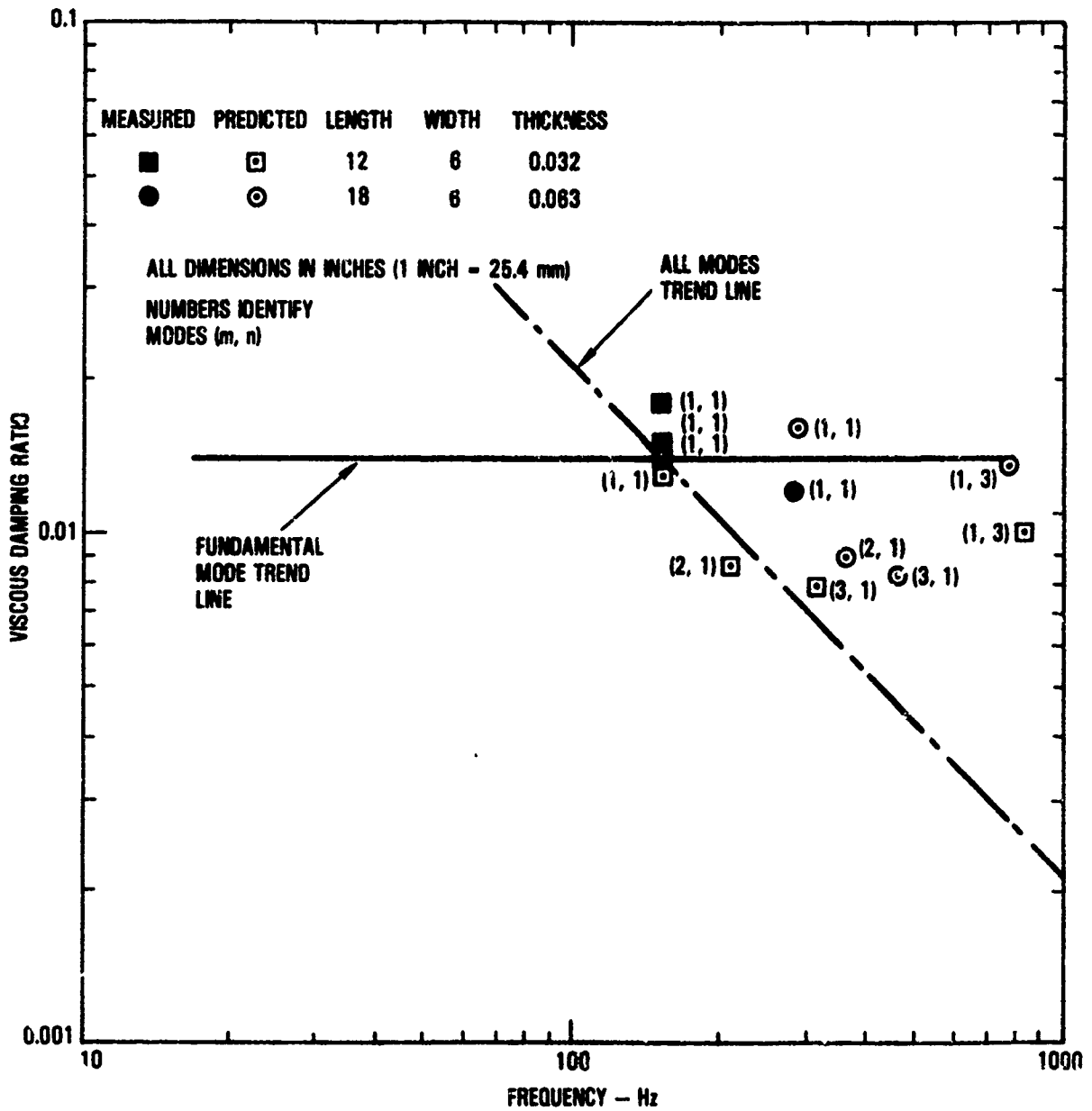


Figure 8.13. Comparison of measured and predicted damping of riveted multi-bay aluminum panels with predictions for higher mode damping.

8.2.4 Effect of Axial and Shear In-Plane Loads on Stiffened Panels Damping

The damping of stiffened panels under axial in-plane loading [8.24] remains constant with axial tension load, but increases with compression on approaching buckling. The damping of the panel becomes nonlinear on approaching buckling as indicated by a change in the rate of the free decay response with amplitude. The damping of the stiffened panel also increases with in-plane shear load on approaching panel buckling [8.25], as illustrated in Figure 8.14 for an integrally J-stiffened mini-sandwich panel. The damping in noncritical modes also increases on approaching shear buckling. Typical variation of the modal frequencies with shear load is illustrated in Figure 8.15.

8.2.5 Effect of Fluid Loading on Stiffened Panel Damping

The effect of fluid loading on the damping of stiffened steel panels [8.26] with welded T-section stiffeners is illustrated in Figure 8.16. There is virtually no difference in the damping of the panel when in air or when in contact, on one side, with water. There is a shift in frequency due to a combination of mass loading and hydrodynamic pressure. The one-over-the-frequency type trend line is due to the presence of higher order modes.

8.3 DAMPING IN STIFFENED SHELLS

The viscous damping ratios measured on two untrimmed aircraft fuselage shells [8.27, 8.28] and on a small diameter stiffened cylinder [8.29], both with and without acoustic trim, are illustrated in Figure 8.17. The damping data for all three of the untrimmed shells appear to collapse onto a single curve. The interior acoustic trim, even when not in contact with the shell skin, does appear to increase the damping approximately by a factor of four over the bare shell damping. The one-over-the-frequency trend line is again due to the presence of higher order modes.

8.4 DAMPING IN SPACECRAFT AND ROCKETS

Typical damping data measured during ground vibration tests on unmanned spacecraft [8.30, 8.31] are illustrated in Figures 8.18 and 8.19. The limited damping data [8.30] measured on a spinning satellite indicate that

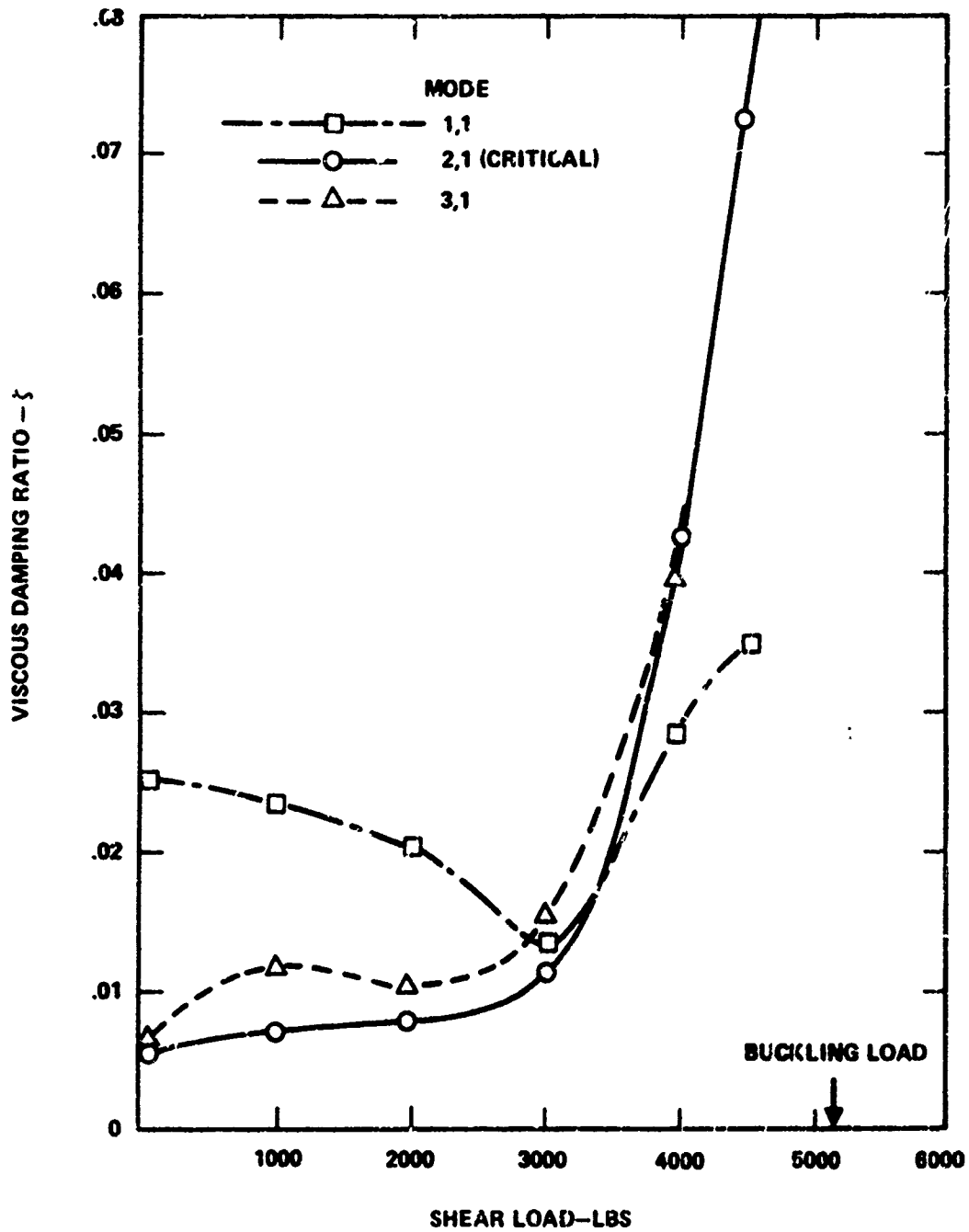


Figure 8.14. Variation of damping with Jack load for J-stiffened mini-sandwich panel.

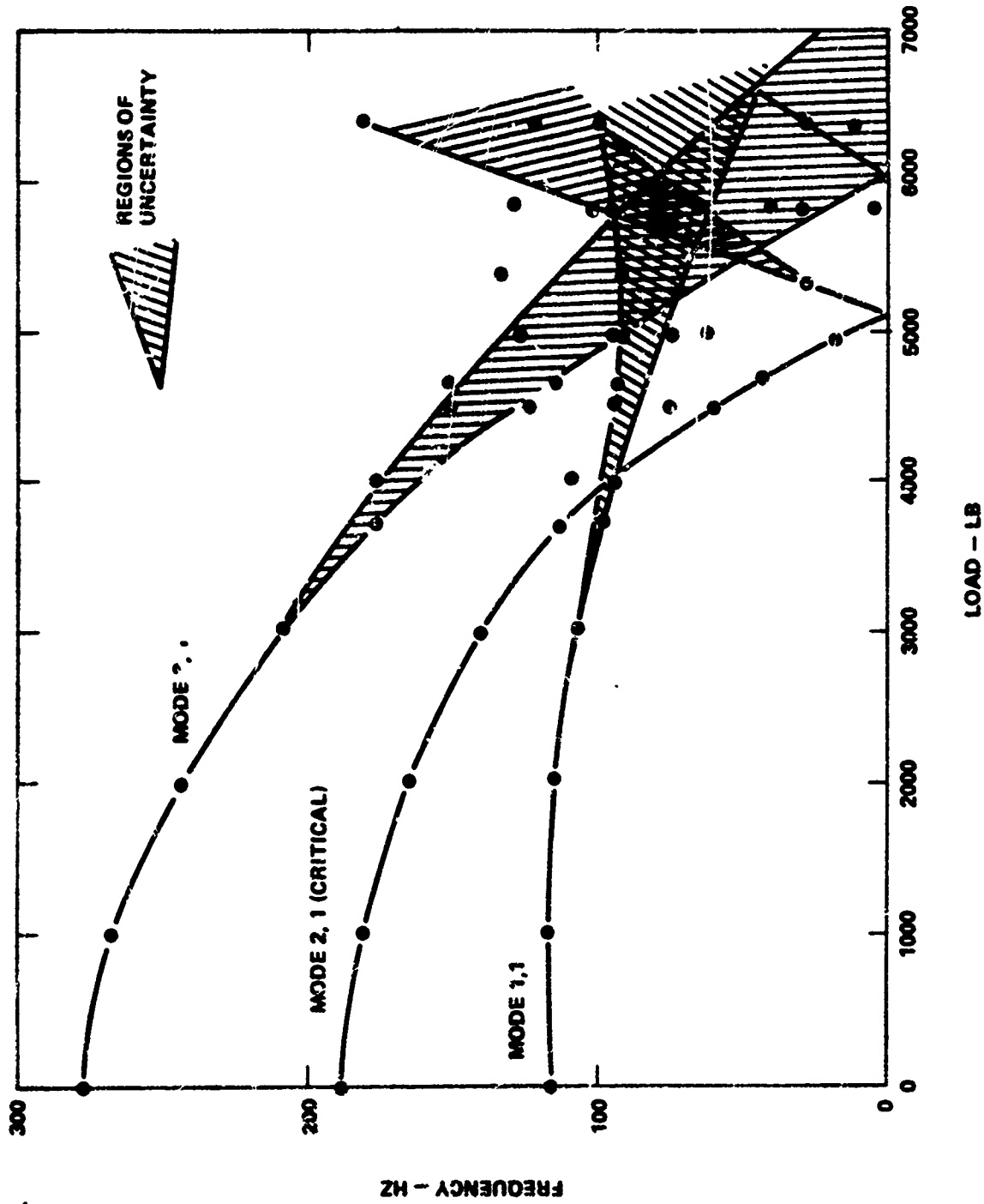


Figure 8.15. Variation of the J-stiffened mini-sandwich panel resonant frequencies with Jack load.

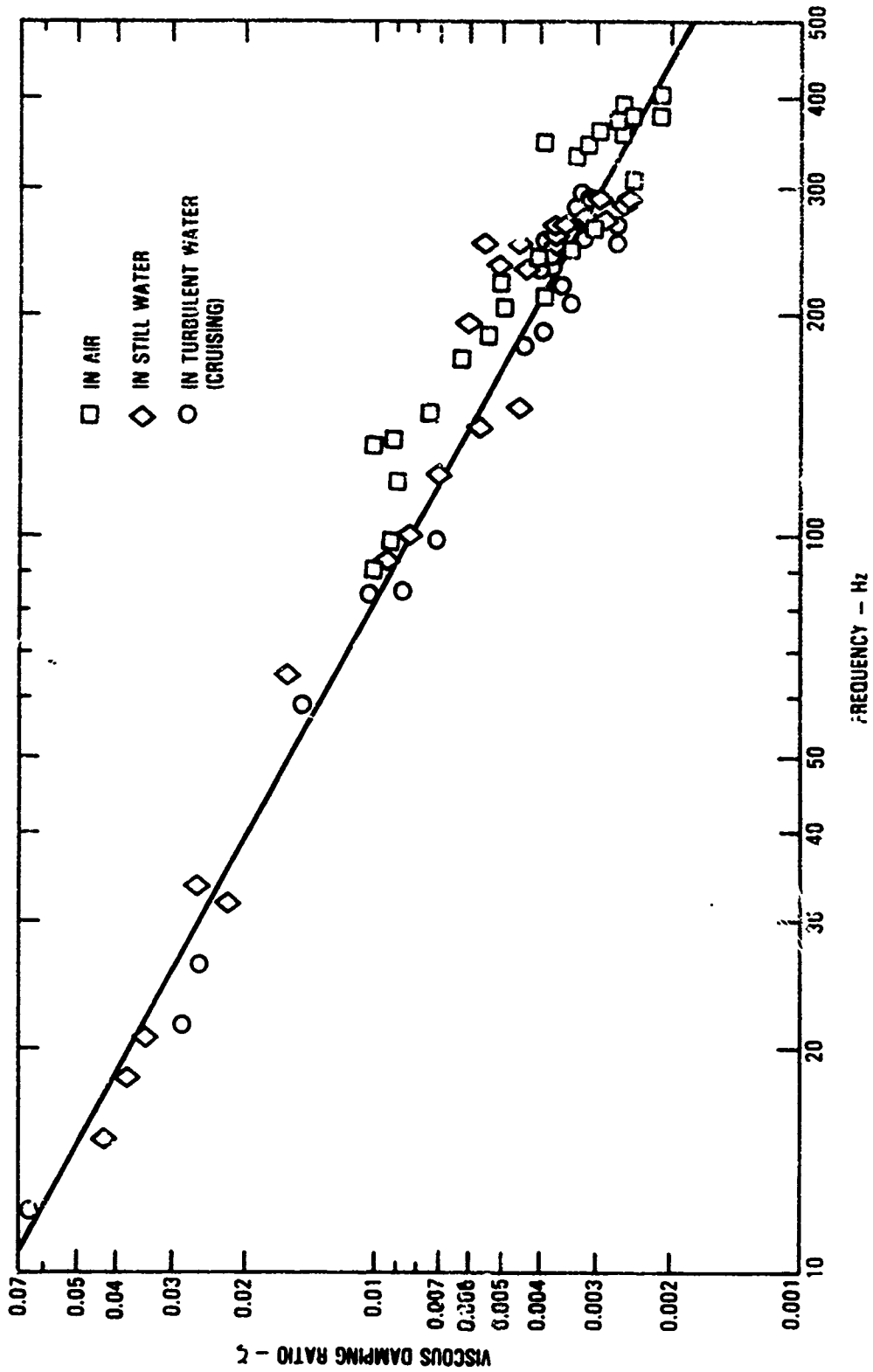


Figure 8.16. Damping measured on a welded stiffened steel structure in air and immersed in water.

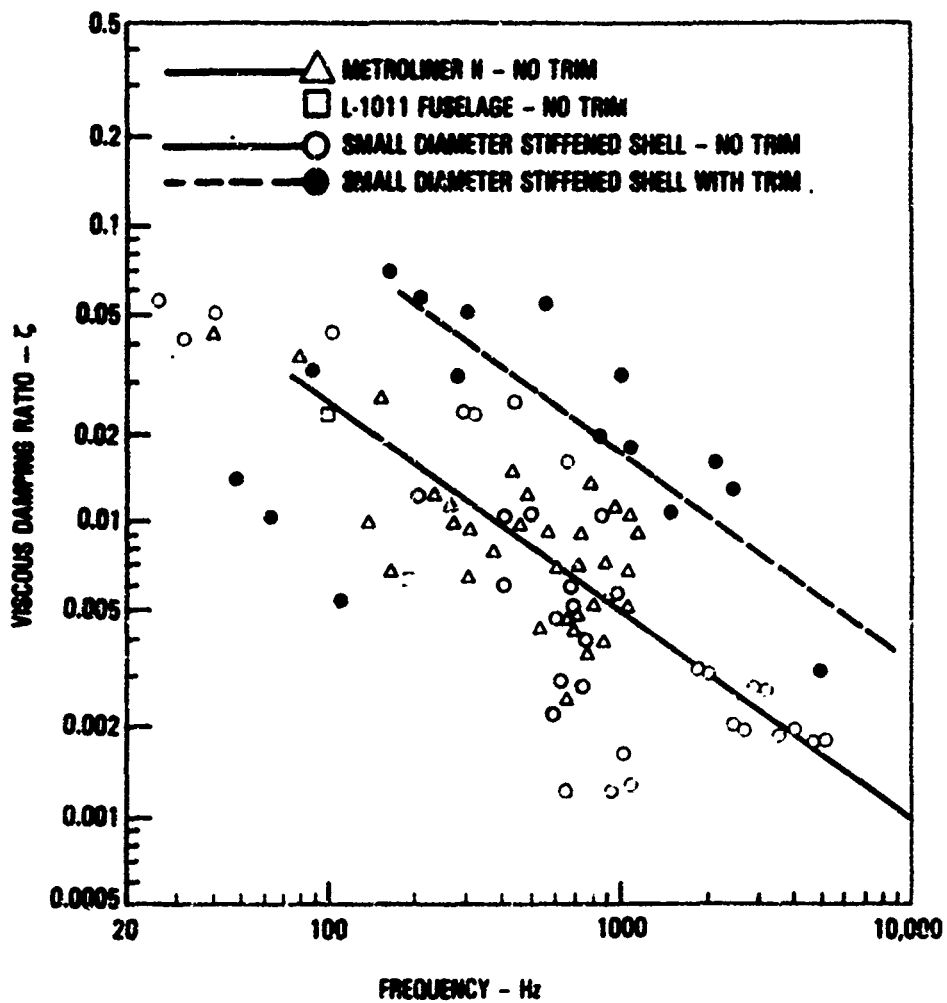


Figure 8.17. Damping measured on bare stiffened shells and a trimmed stiffened shell as a function of frequency.

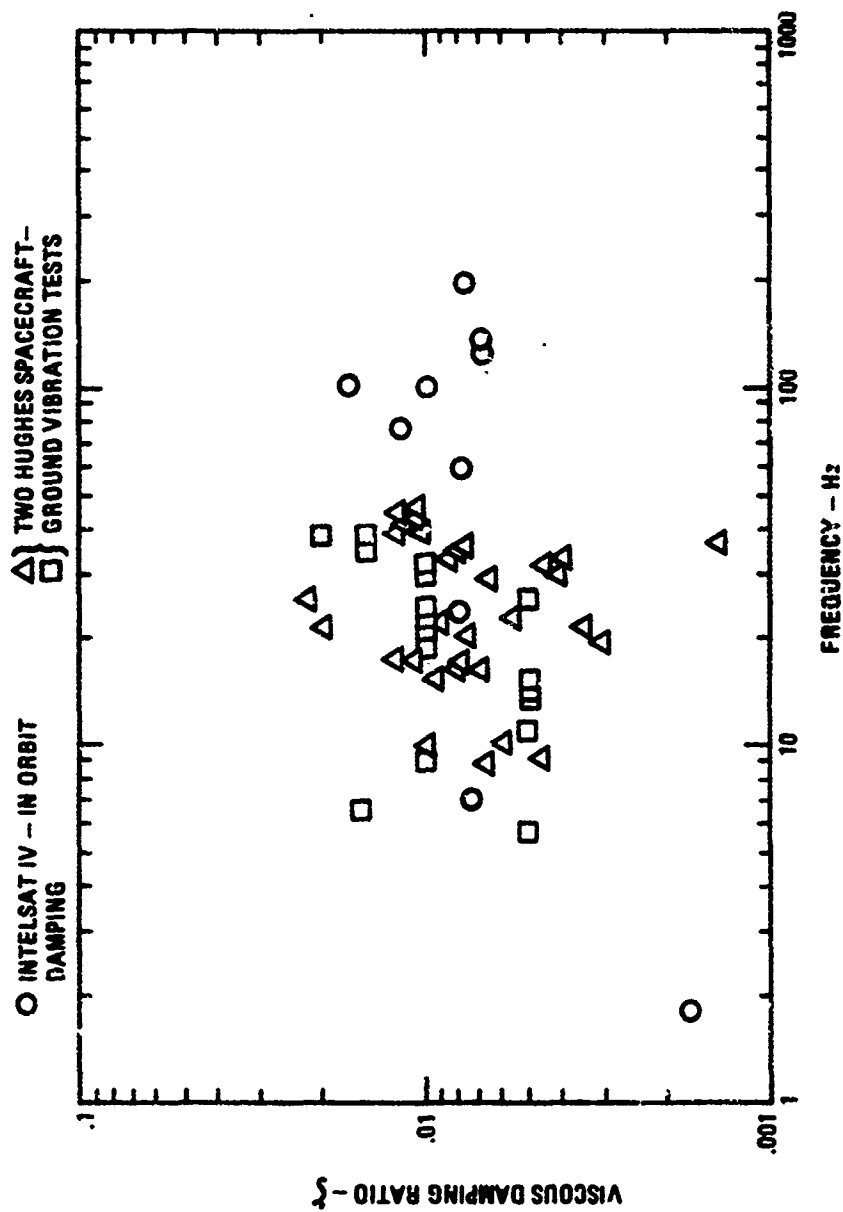


Figure 8.18. Comparison of typical damping levels measured on the ground and in orbit.

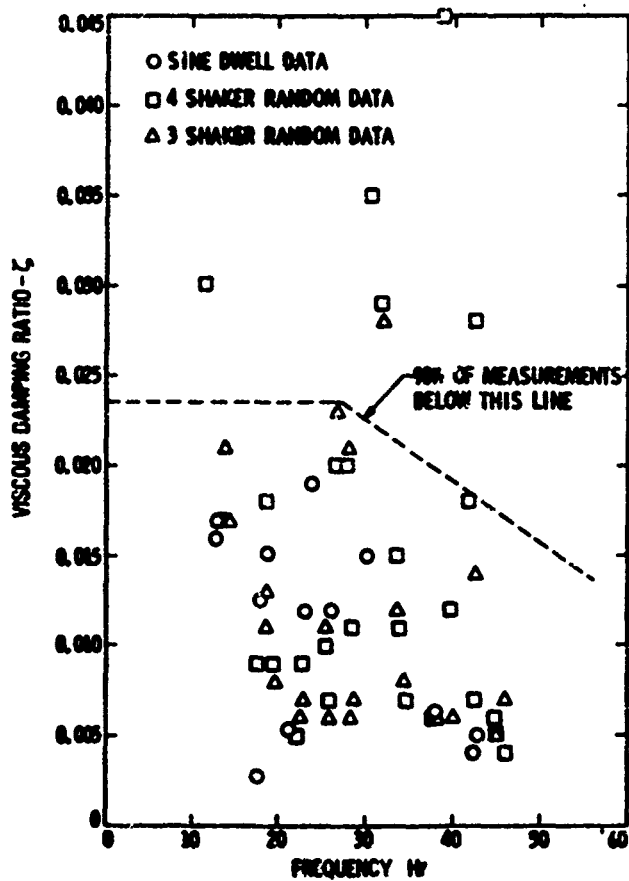


Figure 8.19. Typical damping levels measured during Galileo spacecraft modal tests.

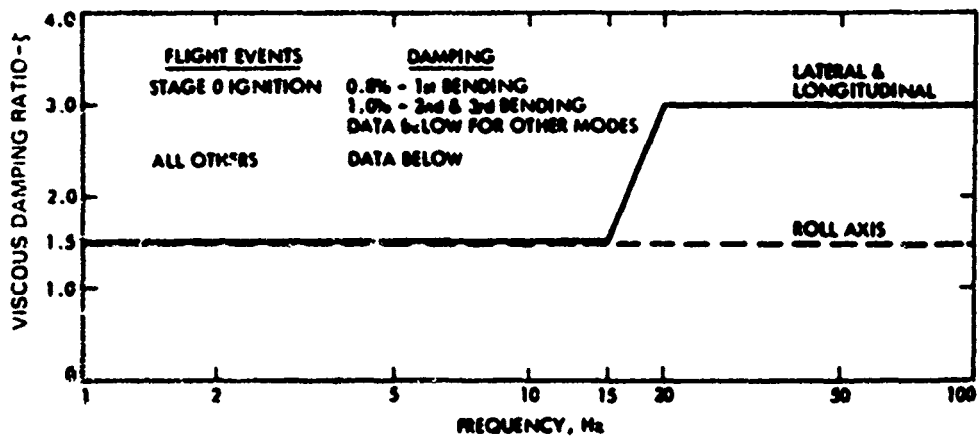


Figure 8.20. Damping schedule for Titan launch vehicle.

similar damping levels (Figure 8.18) are also obtained in orbit. Friction damping in the joints is the main source of damping in these spacecraft, both on the ground and in orbit.

Typical damping schedule [8.30] of a rocket, used to launch some of the unmanned spacecraft, is illustrated in Figure 8.20. Damping levels measured on the space shuttle ascent vehicle [8.32] currently used to launch unmanned spacecraft, are illustrated in Figure 8.21.

8.5 DAMPING IN JET ENGINE COMPONENTS

Typical damping levels in jet engine components taken from Section 6 of this volume are summarized in Table 8.6.

8.6 DAMPING IN PRINTED CIRCUIT BOARDS

Typical measured damping in printed circuit boards [8.33, 8.34] is summarized in Table 8.7. A method for predicting the circuit board damping [8.33] is also contained in the table.

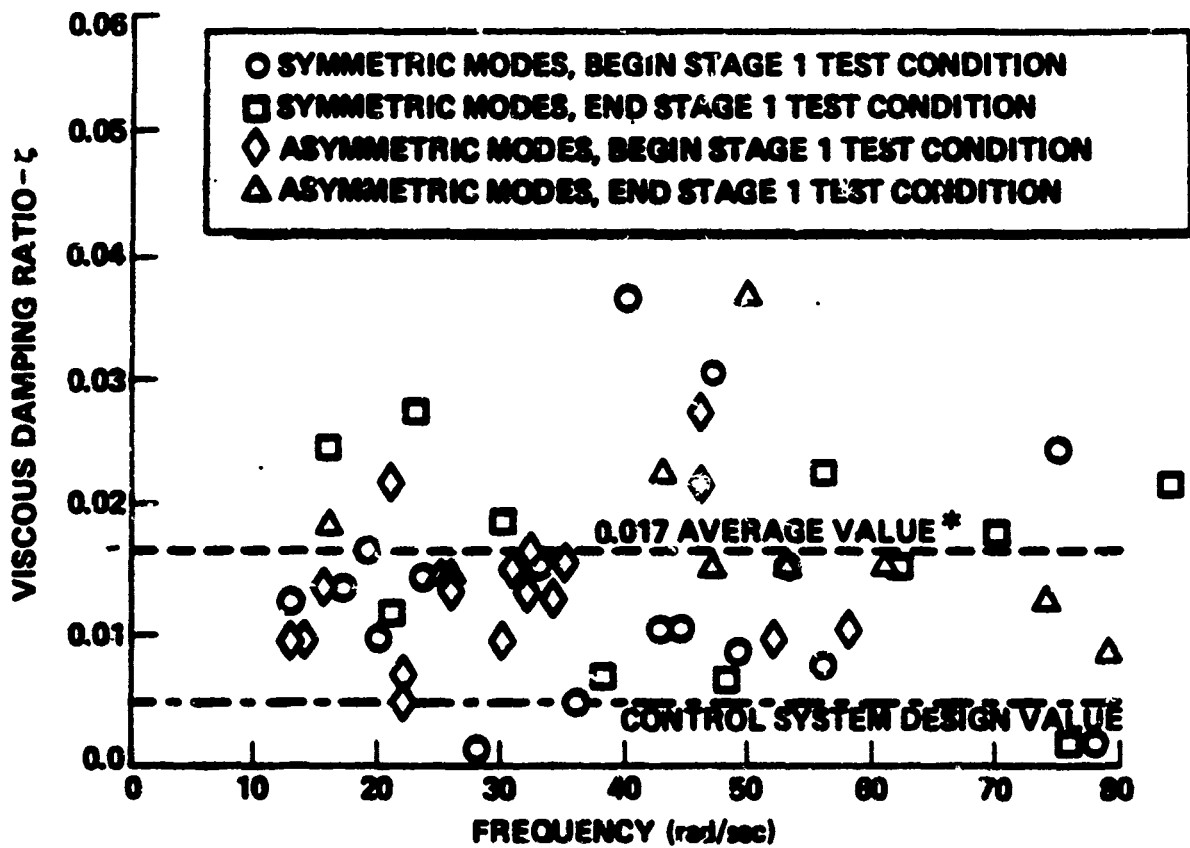


Figure 8.21. Equivalent viscous damping ratios measured during space shuttle ascent vehicle Stage 1 vibration test.

TABLE 8.6. MEASURED DAMPING VALUES FOR ENGINE COMPONENTS

Description of Structure	Frequency Hz	Viscous Damping Ratio - ζ
TF-41 Jet Engine Inlet Extension	3140	0.0011 to 0.0027*
RF-33-P3 Turbojet Engine Welded Inlet Guide Vanes (IGV) and Shrouds	1000 to 5000	0.0012 to 0.0023*
Engine Rear Mount Ring	374 403 903 1172 1396 3515 4325	0.0037 0.0033 0.0045 0.0030 0.0037 0.0040 0.0049
TF-30 Jet Engine Welded Titanium Guide Vanes	3000 to 4000	0.0009 to 0.0018*
Helicopter Turbine Engine Exhaust Stacks	50 to 500	0.0005 to 0.005
Jet Engine Turbine Blade	746 Bending } 824 Torsion }	0.001 to 0.002
Exducer - Turbing Blade Assembly	5300 8500	0.0022 to 0.0039* 0.0009 to 0.0014

*Damping varies with temperature

TABLE 8.7. TYPICAL RANGE OF MEASURED PRINTED CIRCUIT BOARD DAMPING VALUES

Frequency f_n Hz	ζ	Q	K	Reference
65	0.0142	35	4.3	8.34
165	0.023	22	1.71	8.34
215 (2g's input)	0.033	15	1.023	8.33
182 (5g's input)	0.045	11.2	-	
161 (10g's input)	0.061	8.2	-	
<p>Empirical relationship [8.33]</p> $Q \approx K (f_n)^{1/2}$ $\zeta = \frac{1}{2Q}$ <p style="text-align: right;">K \approx 0.5 \rightarrow 2 Typical Input 2g's and less</p>				

REFERENCES

- 8.1 Soovere, J., "Method for Predicting the Damping in Stiffened Structures", Paper to be Presented at the Vibration Damping Workshop II, Las Vegas, 5-9 March 1986.
- 8.2 Soovere, J., "Dynamic Properties of Graphite Fibre Honeycomb Panels", AIAA Dynamics Specialists Conference, Williamsburg, Virginia, March 1973, Paper No. 73-326.
- 8.3 Soovere, J., "Effect of Acoustic/Thermal Environments on Advanced Composite Fuselage Panels", Journal of Aircraft, Volume 22, No. 4, April 1985.
- 8.4 Soovere, J., "Dynamic Response and Acoustic Fatigue of Stiffened Composite Structures", Proceeding of the Second International Conference on Recent Advances in Structural Dynamics, M. Petyt and H.F. Wolfe Editors, University of Southampton, 9-13 April, 1984, p. 775.
- 8.5 Soovere, J., "Dynamic Response of Acoustically Excited Stiffened Composite Honeycomb Panels", Ph.D. Thesis, Institute of Sound and Vibration Research, Southampton University, England, March 1984.
- 8.6 Lazan, B.J., "Damping of Materials and Members in Structural Mechanics", Oxford: Pergamon Press, 1968.
- 8.7 Birchak, J.R., "Damping Capacity of Structural Materials", Published After 1976 - Babcock and Wilcox, Lynchburg Research Center.
- 8.8 Vandeurzen, U., "Identification of Damping in Materials and Structures - Optimization of the Dynamic Behavior of Mechanical Structures", A University of Leuven Report, Leuven, Belgium.

- 8.9 Adams, R.D., Fox, M.A.O., Flood, R.J.L., Friend, R.J. and Hewitt, R.L., "The Dynamic Properties of Unidirectional Carbon and Glass Fiber Reinforced Plastics in Torsion and Flexure", J. Composite Materials, Vol. 3, October 1969, p. 594.
- 8.10 Georgi, H., "Dynamic Damping Investigations on Composites", Damping Effects in Aerospace Structures, AGARD-CP-277, October 1979.
- 8.11 White, R.G. and Palmer, T.A., "Control of the Material Properties and Structural Application of Carbon Fiber-Reinforced Plastics", 24th Structures, Structural Dynamics and Materials Conference, Lake Tahoe, Nevada, May 2-4, 1983, Paper No. 83-859.
- 8.12 White, R.G., "Some Measurements of the Dynamic Properties of Mixed Carbon Fiber Reinforced, Plastic Beams and Plates", Aeronautical Journal, July 1975, p. 318.
- 8.13 Gibson, R.F., Suarez, S.A. and Deobald, L.R., "Improvement of Damping in Fiber-Reinforced Polymer Composites", Vibration Damping 1984 Workshop Proceedings, Dr. Lynn Rogers Editor, AFWAL-TR-84-3064, November 1984, p. S-1.
- 8.14 Ni, R.C. and Adams, R.D., "The Damping and Dynamic Moduli of Symmetric Laminated Composite Beams - Theoretical and Experimented Results", J. Composite Materials, Vol. 18, March 1984.
- 8.15 Bert, C.W. and Sin, C.C., "Sinusoidal Response of Composite - Material Plates with Material Damping", Journal of Engineering for Industry, May 1974, p 603.

- 8.16 Timmerman, N.S. and Doherty, J., "Loss Factors Measured in Metal Matrix Composite Materials", AMMRC-TR-84-22, June 1984.
- 8.17 Soovere, J. "Sonic Fatigue Testing of the NASAL-1011 Composite Aileron", The Shock and Vibration Bulletin, No. 50, Part 4, September 1980.
- 8.18 Holehouse, Ian, "Sonic Fatigue Design Techniques for Advanced Composite Aircraft Structures", AFWAL-TR-80-3019, April 1980.
- 8.19 Jacobson, M.J., "Advanced Composite Joints: Design and Acoustic Fatigue Characteristics" AFFDL-TR-71-127.
- 8.20 Jacobson, M.J.. "Fatigue of V/STOL Composite Fuselage Panels Under Acoustic-Thermal Environments", NADC-81045-60, March 1981.
- 8.21 Jacobson, M.J., "Sonic Fatigue Design Data for Bonded Aluminum Aircraft Structures", AFFDL-TR-77-45, June 1977.
- 8.22 Wolfe, H.F. and Holehouse, I., "Durability of Adhesively Bonded Structures Subjected to Acoustic Loads", AGARD Report No. 701, December 1981.
- 8.23 Ballentine, J.R., Rudder, F.F., Mathis, J.T. and Plumblee, H.E., "Refinement of Sonic Fatigue Structural Design Criteria", AFFDL-TR-67-156, January 1968.
- 8.24 Soovere, J. and Chiu, S.T., "Effect of Combined Acoustics and Flight Loads on Crack Growth", AFFDL-TR-76-68, July 1976.
- 8.25 Soovere, J., "Dynamic Response of Flat Integrally Stiffened Graphite/Epoxy Panels Under Combined Acoustic and Shear Loads", Recent Advances in Composites in the United States and Japan, J.R. Vinson and M. Taya Editors, ASTM Special Technical Publication 864, July 1985.

- 8.26 White, R.G., "The Application of a Transient Test Technique to the Study of the Local Vibration Characteristics of Ship Structures", I.S.V.R. Technical Report No. 31, May 1970.
- 8.27 Prydz, R.A., Revelle, J.D., Hayward, J.L. and Balena, F.J., "Evaluation of Advanced Fuselage Design Concepts for Interior Noise Control on High Speed Propeller-Driven Aircraft", NASA Contractor Report 165960, September 1982.
- 8.28 Socvere, J., "High Modulus Graphite Fiber Constrained Layer Damping Treatment for Heavy Aerospace Structure", AFFDL-TM-78-78-FBA, July 1978.
- 8.29 Pope, L.D. and Wilby, E.G., "Analytical Prediction of the Interior Noise for Cylindrical Models of Aircraft Fuselages for Prescribed Exterior Noise Fields (Part II), NASA Contractor Report 165869, April 1982.
- 8.30 Wada, B.K., "Spacecraft Damping Considerations in Structural Design", AGARD-CP-277, October 1979, pp. 6-1.
- 8.31 Chen, J.C., "Evaluation of Modal Test Methods", AIAA Dynamics Specialists Conference, Palm Springs, California, May 1984, Paper No. 84-1071.
- 8.32 Jensen, D.L., "Structural Damping of the Space Shuttle Orbiter and Ascent Vehicles", Vibration Damping 1984 Workshop Proceedings, Dr. Lynn Rogers Editor, AFWAL-TR-84-3064, p. Z-2.
- 8.33 Steinberg, D.S., "Vibration Analysis for Electronic Equipment", John Wiley and Sons, 1973.
- 8.34 Medaglia, J.M., "Dynamic Integrity Methods Including Damping for Electronic Packages in Random Vibration", General Electric Space Division.

SECTION 9

MATERIAL DATA FOR COMPOSITES AND METALS, U.S./METRIC CONVERSION TABLES

Typical material data for composite materials and metals used in the aerospace industry are summarized in Tables 9.1 and 9.2, respectively.

All of the unidirectional lamina data and the Kevlar cloth data for the 0.69 fiber volume fraction, in Table 9.1, have been taken from Reference [9.1]. The unidirectional lamina and fabric data for Kevlar at the 0.5 fiber volume fraction, are based on test data developed by Dupont and Lockheed-California Company in the early 1970s.

The crossplied laminate data, in Table 9.1, have been extracted from the carpet plots in Volume I of Reference [9.1]. These data indicate that the elastic properties of composite structures are highly dependent on the fiber orientations used in the laminate. The carpet plots, in Reference [9.1], can be used to obtain the elastic properties for laminates with other fiber orientations. These crossplied laminate elastic properties are average values for use with axial loading. These average values can be used to estimate the flexural stiffness of symmetric laminates with reasonable accuracy, provided the laminates have eight or more plies.

The material data, in Table 9.2, have been taken from References [9.2] and [9.3]. The 1984 Material Selector in Material Engineering [9.3] is a good source of data for a wide range of metallic and nonmetallic materials.

A list of the more common metric units, used in dynamics, is provided in Table 9.3. The corresponding conversion table from U.S. units to metric units is contained in Table 9.4. The more commonly used prefixes are listed in Table 9.5 and the Greek alphabet in Table 9.6.

TABLE 9.1. TYPICAL ROOM TEMPERATURE COMPOSITE MATERIAL PROPERTIES

Material	Fiber Volume - V_f	Nominal Thickness in.	Density lb/in ³ ρ	Modulus - Msi			Poisson's Ratio ν_{LT}	Coefficient of Thermal Expansion $\mu\text{in/in/}^\circ\text{F}$	
				Longitudinal E_L	Transverse E_T	Shear G_{LT}		Longitudinal α_L	Transverse α_T
UNIDIRECTIONAL LAMINA									
Boron/Epoxy	0.5	0.0052	0.073	30	2.7	0.7	0.32	2.3	10.6
Boron/Aluminum	0.5	0.007	0.098	32	21.5	9.3	0.26	3.2	10.6
Graphite/Epoxy High Strength*	0.6	0.005	0.056	21	1.7	0.65	0.3	-0.21	16.0
High Modulus	0.6	0.005	0.056	30	1.2	0.65	0.3	-0.3	19.5
Ultra High Modulus	0.64	0.005	0.063	50	0.92	0.69	0.32	-0.45	13.0
Kevlar-49	0.5	0.005	0.050	10.6	0.7	0.29	0.33	-0.28	32.0
CROSSPLIED LAMINATE ($90^\circ/\pm 45^\circ/90^\circ$)_s**									
Boron/Epoxy	0.5	0.042	0.073	11.3	11.3	4.2	0.33	3.2	3.2
Graphite/Epoxy High Strength*	0.6	0.040	0.056	8.0	8.0	3.1	0.32	1.2	1.2
High Modulus	0.6	0.040	0.056	10.8	10.8	4.2	0.32	1.3	1.3
Ultra High Modulus	0.64	0.040	0.063	17.6	17.6	6.5	0.32	0.8	0.8
CROSSPLIED LAMINATE ($0^\circ/\pm 45^\circ$)_s**									
Boron/Epoxy	0.5	0.031	0.073	12.0	5.2	5.4	0.76	2.1	4.8
Graphite/Epoxy High Strength*	0.6	0.030	0.056	8.5	3.8	3.8	0.74	-0.4	4.0
High Modulus	0.6	0.030	0.056	12.0	4.6	5.3	0.82	0.3	3.4
Ultra High Modulus	0.64	0.030	0.063	18.5	6.8	3.6	0.88	0.4	1.6
FABRIC - 181 STYLE WEAVE									
Kevlar-49	0.5	0.09	0.05	4.56	4.7	0.35	0.15	-	-
	0.69	0.08	0.049	5.2	5.2	0.36	0.12	2.3	3.3

*Ultimate Tensile Strength 180 KSI

**Subscript s Denotes a Symmetric Layup

TABLE 9.2. TYPICAL ROOM TEMPERATURE MATERIAL PROPERTIES FOR METALS

Material	Density lb/in ³ ρ	Modulus Msi E	Poisson's Ratio ν	Thermal Expansion Coefficient $\mu\text{in/in}^{\circ}\text{F}$ α
Aluminum Alloy				
2024	0.10	10.6	0.33	12.9
7075	0.101	10.4	0.33	13.1
Beryllium	0.067	42.0	0.081 (Sheet)	6.2
Cobalt Alloy 188	0.33	33.6	0.31	9.9
Magnesium Alloy	0.065	6.5	0.35	14.0
Molybdenum	0.37	47.0	0.32	2.9
Steel Alloy				
AISI 4130	0.283	29.0	0.32	6.3
5CR-MG-v	0.281	30.0	0.32	7.1
9NI-4CO	0.284	28.5	0.32	6.4
17-7PH	0.276	29.5	0.32	6.9
Titanium Alloy				
6AL-4V	0.16	16.2	0.31	5.2
8AL-1MO-1V	0.158	17.7	0.32	5.6

TABLE 9.3. METRIC UNITS AND SYMBOLS

Quantity	Unit	Symbols
Length	meter centimeter millimeter	m cm (= 0.01 m) mm (= 0.001 m)
Area	square meter square millimeter	m ² mm ² (= 10 ⁻⁶ m ²)
Volume	cubic meter cubic millimeter	m ³ mm ³ (= 10 ⁻⁹ m ³)
Time	seconds	.
Velocity	meters per second	m/s
Acceleration	meter per second squared	m/s ²
Frequency	hertz	Hz
Mass	kilogram gram	kg g
Density	kilogram per cubic meter gram per cubic millimeter	kg/m ³ g/mm ³
Inertia	kilogram - meter squared	kg - m ²
Force	newton	N
Pressure, Stress or Modulus	newton per square meter or pascal	N/m ² Pa (= 1 N/m ²)
Temperature	degrees centigrade or degrees kelvin	°C °K (= 273.16 + °C)
Noise	decibel	dB
Sound Power	watts	W

TABLE 9.4. U.S.-TO-METRIC CONVERSION

To Convert From	To	Multiply By
Length		
foot	meter (m)	3.0480×10^{-1}
inch	meter (m)	2.5400×10^{-2}
inch	centimeter (cm)	2.5400
inch	millimeter (mm)	2.5400×10
Area		
square foot	square meter (m ²)	9.2903×10^{-2}
square inch	square meter (m ²)	6.4516×10^{-4}
square inch	square millimeter (mm ²)	6.4516×10^2
Volume		
cubic foot	cubic meter (m ³)	2.8317×10^{-2}
cubic inch	cubic meter (m ³)	1.6387×10^{-5}
cubic inch	cubic millimeter (mm ³)	1.6387×10^4
Velocity		
foot per second	meter per second (m/s)	3.0480×10^{-1}
inches per second	millimeter per second (mm/s)	2.5400×10
Acceleration		
foot per second squared due to gravity (32.174 foot per second squared)	meter per second squared (m/s ²) meter per second squared (m/s ²)	3.0480×10^{-1} 9.8067
Mass		
pound-mass	kilogram (kg)	4.5359×10^{-1}
slug	kilogram (kg)	1.4594×10
Density		
pound-mass per cubic foot	kilogram per cubic meter (kg/m ³)	1.6018×10^1
pound-mass per cubic inch	kilogram per cubic meter (kg/m ³)	2.7680×10^4
pound-mass per cubic inch	gram per cubic millimeter (g/mm ³)	2.7680×10^2
Inertia		
pound-mass-foot squared	kilogram-meter squared (kg-m ²)	4.2143×10^{-2}
slug-foot squared	kilogram-meter squared (kg-m ²)	1.3558
Force		
pound-force	newton (N)	4.4482
Force per Unit Length		
pound-force per inch	newton per meter (N/m)	1.7513×10^2
Pressure, Stress, Modulus		
pound-force per square foot	newton per square meter (N/m ²)	4.7880×10
pound-force per square inch	newton per square meter (N/m ²)	6.8948×10^3
Temperature		
degrees Fahrenheit (°F)	degrees centigrade (°C)	(1) subtract 32°F from °F (2) then multiply by 5/9

TABLE 9-5. COMMONLY USED PREFIXES AND THEIR SYMBOLS

Amount	Factor	Prefix	Symbol
1 000 000 000 =	10^9	giga	G
1 000 000 =	10^6	mega	M
1 000 =	10^3	kilo	k
0.001 =	10^{-3}	milli	m
0.000 001 =	10^{-6}	micro	μ

TABLE 9.6. GREEK ALPHABET

Upper Case	Lower Case		Upper Case	Lower Case	
A	α	Alpha	N	ν	Nu
B	β	Beta	Ξ	ξ	Xi
Γ	γ	Gamma	O	\omicron	Omicron
Δ	δ	Delta	Π	π	Pi
E	ϵ	Epsilon	P	ρ	Rho
Z	ζ	Zeta	Σ	σ	Sigma
H	η	Eta	T	τ	Tau
Θ	θ	Theta	Υ	υ	Upsilon
I	ι	Iota	Φ	ϕ	Phi
K	κ	Kappa	X	χ	Chi
Λ	λ	Lambda	Ψ	ψ	Phi
M	μ	Mu	Ω	ω	Omega

REFERENCES

- 9.1 "DOD/NASA Advanced Composites Design Guide", July 1983.
- 9.2 MIL-HDBK-5.
- 9.3 Materials Engineering, 1983